Mitteilungen des Bundesamtes
für Kartographie und Geodäsie
Band 48

# Proceedings of the 17th International Workshop on Laser Ranging

## Extending the Range

**May 16 – 20, 2011**
**Bad Kötzting, Germany**

Verlag des Bundesamtes für Kartographie und Geodäsie
Frankfurt am Main 2012

Druck:
Bonifatius GmbH
Paderborn

## Extending the range

Almost immediately after the first successful demonstration of the functions of a laser, the technology was used to carry out satellite and lunar laser ranging experiments at a level of accuracy measured in metres. Of course, the technique continues to develop and to reinvent itself; the powerful concept of a two-way range estimate via a time-of-flight measurement of ultra short laser pulses has turned LR into a standard tool of modern global geodesy. Extending the capabilities and accuracy of this powerful technique is therefore an on-going process within the International Laser Ranging Service.

The 17th International Workshop on Laser Ranging was held in Bad Kötzting near the Geodetic Observatory Wettzell in Germany between 16th and 20th May 2011. The growing technical diversity within the SLR technology, that already marked earlier workshops, continued also through this meeting. The implementation of new technologies, including high repetition rate lasers, single-photon avalanche photodetectors, and new epoch timing systems have increased ranging systems' precision and data yield. It is now common for Satellite Laser Ranging (SLR) systems to interleave passes of several satellites at a time thereby increasing temporal and special coverage. Systems are now routinely ranging to satellites at GNSS and geosynchronous altitudes helping to link the GNSS and SLR reference frames and enhancing time transfer capability. Laser Ranging is one of the space geodesy techniques that defines the International Terrestrial Reference Frame, an essential standard for measurement of global change, and provides a tool for precision orbit determination and instrument calibration and validation of space-borne metric systems that measure dynamic properties of the Earth and the Earth-Moon system.

One-way laser ranging to the Lunar Reconnaissance Orbiter, for example, demonstrated impressively how this technique can be utilized in interplanetary satellite missions and precision inter-continental time transfer. New mission concepts like Time Transfer by Laser Link (T2L2, on the Jason-2 altimeter satellite) are pioneering, complex additions to the well-established retroreflector space segment. Several new mission proposals for planetary exploration of the recent years are built on optical ranging concepts. This gives rise to the expectation that this trend will continue into the future.Lunar laser ranging, the branch of space geodesy that has the longest time series available, is one of the science fields where close constraints are put on tests of general relativity in fundamental physics. Furthermore, lunar exploration programmes also build on laser ranging technology.

As well as these emerging fields of ranging application, a large variety of technological aspects such as advances in lasers, timers and signal detectors were discussed and it became obvious that the momentum of improvement that has taken laser ranging from a resolution of several meters only four decades ago to range resolutions of about 2 mm today is still continuing. As a consequence, strategic considerations like the geographic distribution of the station network and the need for the combination of laser ranging measurements with those of the other major space geodetic techniques are gaining more and more importance. The emergence of the IAG's Global Geodetic Observing System, with its goal of definition and maintenance of a global reference frame at a level of accuracy of 1mm, ensures that the laser ranging technique continues to face challenges both technologically and in data analysis. As measurement techniques address these challenges, they push the world of geoscience model development and enhance our understanding of our Earth environment.

On behalf of the Organizing Committee we wish to thank all participants for their contributions.Your effort has made this workshop a great success. Furthermore we are gratefulto the city of Bad Kötzting for the outstanding support. Without this generous help this meeting would not have happened. Finally we wish to extend our gratitude to the local Organizing Committee and the numerous helping hands, which made this workshop a pleasantand efficient experience.

Bad Kötzting, May 17, 2011

Ulrich Schreiber, Michael Pearlman, Graham Appleby

# Table of contents

# 17th International Workshop on Laser Ranging

## Extending the Range

Bad Kötzting, Germany
May 16 – 20, 2011

## PROGRAM

### SUNDAY, MAY 15

| | |
|---|---|
| 15:00 | Registration |
| 17:00 | Ice Breaker |
| 18:00 | Program Committee Meeting |

### MONDAY, MAY 16

| | |
|---|---|
| 9:00 | Opening Ceremony |
| 9:30 | Invited Keynote Talk:<br>GOCE and its challenging gravimetric sensor system<br>*Reiner Rummel (Technical University Munich)* |
| **10:00 – 10:30** | **COFFEE BREAK** |
| **Session 1:** | **Science Session (10:30 – 12:30 / 14:00 – 14:30)**<br>*Session Chairs: G. Appleby, P. Bianco* |
| 10:30 | LARETS Laser Relativity Satellite<br>*I. Ciufolini, A. Paolozzi, E. Pavlis, R. Koenig, J. Ries, R. Matzner, R. Neubert, D. Rubincam, D. Arnold, V. Slabinski, G. Sindoni, C. Paris, M. Ramiconi, D. Spano, C. Vendittozzi, H. Neumayer.* |
| 10:45 | Benefits of SLR in epoch reference frames<br>*Mathis Bloßfeld, Horst Müller, Manuela Seitz, Detlef Angermann* |
| 11:00 | The SLR monitoring crustal movement in South America<br>*Yin Zhiqiang, Han Yanben, Liu Weidong, R.Podesta, A. Pacheco, A.Ester* |
| 11:15 | Assessment of the non gravitational forces acting on the Lageos satellites, and impacts on gravitational parameters<br>*Florent Deleflie, Jean-Michel Lemoine, Franck Reinquin, Gilles Métris, François Barlier, Pierre Exertier* |
| 11:30 | Constraining spacetime torsion with Lunar Laser Ranging, Mercury Radar Ranging, LAGEOS, next lunar surface missions and BepiColombo<br>*R. March, G. Bellettini, R. Tauraso, S. Dell'Agnello* |
| 11:45 | On the Calibration of TanDEM-X Precise Baselines via SLR<br>*R. Koenig, Y. Moon, L. Grunwaldt* |

12:00 The Global Geodetic Observing System:
Space Geodesy Networks for the Future
*Michael Pearlman, Erricos Pavlis, Zuheir Altamini, Chopo Ma, David Stowers, and Carey Noll*

**12:30 – 14:00 - LUNCH -**

14:00 The Vector Approach to the Problem of Physical Libration of the Moon: the Linearized Problem
*Kondratyev Boris Petrovich*

14:15 New version of EPM –ERA Lunar theory
*Krasinsky G.A.,Prokhorenko S.O., Yagudina E.I.*

**Session 2: Operations: Spatial and Temporal Coverage (14:30 – 15:30)**
*Session Chairs: M. Pearlman, H. Müller*

14:30 Introduction: Where do we stand and what do we need?
*Michael Pearlman*

Statistical Analysis of SLR tracking in 20xx
*Horst Mueller*

14:45 The Contribution of Korean Side to the International Laser Ranging Service
*Jong Uk Park, Hyung-Chul Lim, Sungki Cho and Jae-Cheol Yoon*

15:00 Current situation and future of cooperative San Juan SLR station between China-Argentina
*Liu Weidong et al.*

15:15 Hazards and Risk @ SLR Network, A Preliminary Overview
*del Pino, Jorge*

**15:30 – 15:45 COFFEE BREAK**

**Session 3: Atmospheric Refraction Correction: Hardware and Modeling (15:45 – 17:00)**
*Session Chairs: Stefan Riepl, F. Koidl*

15:45 Introduction: Multi Color Laser Ranging for Refraction Remote Sensing
*E.Pavlis, S.Riepl*

16:00 Atmospheric range correction for two-frequency SLR measurements
*Dudy D. Wijaya and Fritz K. Brunner*

16:15 Atmospheric Refraction Correction Using Multiple Wavelength Laser Ranging
*Ben Greene, Craig Smith, Jizhang Sang and Nasr A. Al-Sahhaf*

16:30 The Photoconductive Antenna - A new device for Spacegeodetic Applications
*S.Riepl, Christian Plötz, Reinhard Zeitlhöfler, Axel Nothnagel*

16:45 Multi Color Activities at 7405
*M. Häfner*

**Session 4 : SLR Techniques (17:00 – 18:15)**
*Session Chairs: U. Schreiber, K. Arsov, J. Garate*

17:00 Co-optical Path KHz SLR at Kunming Station
*Li Zhulian, Fu Honglin, He Shaohui, Zheng Xiangming,Li Rongwang, Li Yuqiang, Zhai Dongsheng, Xiong Yaoheng*

17:15 Experimental Laser System for Monitoring of GLONASS Time/Frequency Synchronization
*Sadovnikov M.A., Fedotov A.A., Shargorodskiy V.D.*

17:30 Graz 10 kHz SLR
*Georg Kirchner, Franz Koidl, Farhat Iqbal*

17:45 High-energy picosecond laser systems between 10 Hz and 2 kHz for next-generation laser ranging
*M. Schmidt, N. Graf, H. Huber,R. Kelnberger, J. Aus der Au*

18:00 New KHz-capable SLR software in Metsähovi
*Arsov K.*

**18:15 – 19:15 Data Formats & Procedures Working Group Meeting**
*Chair: R. Rickleffs*

## TUESDAY MAY, 17

**Session 6: Modeling and Bias issues (9:00 – 11:30)**
*Session Chairs: T. Otsubo, D. Thaller, C. Luceri*

09:00 Introduction: Introduction to Modeling and Bias Issues: Keynote Paper
*Toshimichi Otsubo, Daniela Thaller, and Vincenza Luceri*

09:15 Improvements in Understanding Systematic Effects in Laser Ranging Observations
*Graham Appleby, Vincenza Luceri and Toshimichi Otsubo*

09:30 Improving ILRS products after an in-depth characterization of station biases
*V. Luceri, G. Bianco, C. Sciarretta*

09:45 GNSS satellites as co-locations for a combined GNSS and SLR analysis
*D. Thaller, K. Sosnica, R. Dach, A. Jäggi, G. Beutler, M. Mareyen, B. Richter*

10:00 Spin of Ajisai: influence of Solar Irradiation on the spin period and precession of the spin axis measured by the Graz 2kHz SLR system
*Daniel Kucharski, Georg Kirchner, Toshimichi Otsubo, Franz Koidl, Mihoko Kobayashi*

**10:15 – 10:45 COFFEE BREAK**

10:45 A New Approach for the Spin Axis Determination of LAGEOS
*D. G. Currie*

11:05 BLITS: spin parameters and its optical response measured by the Graz 2 kHz SLR system
*Daniel Kucharski, Georg Kirchner, Hyung-Chul Lim, Franz Koidl*

**Session 7: Improving Ranging Accuracy, Calibration and Local Ties I. (11:30 – 12:30)**
*Session Chairs: I. Prochazka, Y. Artyukh, L. Grunwaldt*

11:30 Introduction: Alternative approach to the SLR data precision
*I. Prochazka*

11:45 ILRS Standardization of Hardware, Software, and Procedures
*Randall L. Ricklefs*

12:00 Event Timer A033-ET: Curent State and Typical Performance Characteristics
*Artyukh Yu., Bespal'ko V., Boole E., Vedin V.*

12:15 Main Directions of Riga Event Timer Development and Current Results
*Boole Eugene, co-autors: Artyukh Yu., Bespal'ko V., Stepin V., Stepin D., Vedin V.*

**12:30 – 14:00 WPLTN - Meeting**

**12:30 – 14:00 - LUNCH -**

**Session 8: Improving Ranging Accuracy, Calibration and Local Ties II. (14:00 – 15:30)**
*Session Chairs: I. Prochazka, Y. Artyukh, L. Grunwaldt*

14:00 New technologies for sub – millimeter laser ranging
*Ivan Prochazka, Jan Kodet, Josef Blazej, Petr Panek*

14:20 Studies on system stability and calibrations of H-SLR station
*Makram Ibrahim*

14:40 Ground Survey and Local Ties at the Geodetic Observatory Wettzell
*Thomas Kluegel, Swetlana Maehler, Christian Schade*

15:00 Can Continuous Cartesian Connections realize local ties at 0.1 mm level?
*Sten Bergstrand*

**Session 9:** **Introduction to the Observatory Excursion (15:30 – 16:00)**
*Coordinator: U. Schreiber*

15:30 Recent Progress in Sagnac Interferometry
*Robert Hurst (Univ. of Canterbury, Christchurch, NZ)*

15:45 Introduction to the VLBI 2010 TWIN Telescopes
*Gerhard Kronschnabl (Bundesamt fuer Kartographie und Geodaesie)*

**16:00 – 17:00** **COFFEE BREAK**

17:00 **Transfer to Wettzell by bus**
*Self guided tour around the observatory, Wettzell-Poster, Discussions + Buffet*

≈21:00 **Transfer to hotels by bus**

## WEDNESDAY MAY, 18

**Session 10:** **Improving support for GNSS and other challenging missions (9:00 - 11:30)**
*Session Chairs: G. Kirchner, M. Wilkinson, Zhang Zhongping*

9:00 Introduction: Beam Divergence: Introduction, results of measurements
*M. Davis*

Tracking many GNSS targets: Introduction
*M. Wilkinson*

9:15 Measuring sub-mm range differences caused by polarization effects
*Georg Kirchner, Franz Koidl*

9:30 The achievements of the dedicated Compass SLR system with 1m aperture telescope: GEO satellite daylight tracking and laser time transfer (LTT)
*Zhang Zhongping, Yang Fumin, Zhang Haifeng, Meng Wendong,Chen Juping, Chen Wenzhen, Wu Zhibo*

09:45 Comparative verification of return rate on GNSS LRA
*Shinichi Nakamura, Ryo Nakamura, Takahiro Inoue, Hiroyuki Noda, and Motohisa Kishimoto*

**10:00 – 10:30** **COFFEE BREAK**

10:30 Improvements at NASA's NGSLR in Support of GNSS Ranging
*Jan McGarry, Thomas Zagwodzki*

10:50 Direction of the light displacement vector in laser ranging of the artificial Earth satellites
*Yu.V. Ignatenko, I.Yu. Ignatenko, A.A. Makeev and V.N. Tryapitsyn*

11:10 Polarisation at SGF, Herstmonceux
*Matthew Wilkinson, Toby Shoobridge,* Vicki Smith

**Session 11:** **Satellite Subsystems: Retroreflector Arrays (11:30 – 15:15)**
*Session Chairs: R. Neubert, S. Wetzel, T. Otsubo*

11:30 Introduction: Retroreflector and Retroreflector Array: Keynote Paper
*Toshimichi Otsubo, Reinhart Neubert,Scott Wetzel*

11:45 Design of LRA for Compass GEO and IGSO satellites and observations
*Chen Wanzhen,Yang Fumin,Zhang Zhongping,Wang Yuanming,Li Pu*

12:00 GNSS array performance prediction using ZEMAX
*Mark Davis*

12:15 Considerations for the next GNSS Array
*Scott Wetzel, Ed Aaron*

**12:30 – 14:00 - LUNCH -**

14:00 ETRUSCO-2: an ASI-INFN Project of Development and SCF-Test of GNSS Retroreflector Arrays (GRA) for Galileo and the GPS-3
*S. Dell'Agnello, G. O. Delle Monache, D. G. Currie, R. Vittori, C. Cantone, M. Garattini, A. Boni, M. Martini, C. Lops, N. Intaglietta, R. Tauraso, D. A. Arnold, M. R. Pearlman, G. Bianco et al*

14:15 World first SCF-Test of the NASA-GSFC LAGEOS Sector and Hollow Retroreflector
*A. Boni, S. Berardi, M. Maiello, M. Garattini, S. Dell'Agnello, G. O. Delle Monache, C. Lops, C. Cantone, N. Intaglietta,G. Patrizi, J. F. McGarry, M. R. Pearlman,G. Bianco, D. A. Arnold, T. W. Zagwodzki, M. Ruggieri*

14:30 Far-field diffraction pattern analysis of cube corner reflectors
*A.L.Sokolov, M.A.Sadovnikov, V.D.Shargorodsky, V.P.Vasiliev*

14:45 Single Open Reflector for MEO/GNSS Type Satellites. A Status Report
*Reinhart Neubert, Ludwig Grunwaldt, Christian Schopf, Engelbert Hofbauer, Jost Munder, Mark Herding, Rolf Sand*

15:00 BLITS: The first autonomous zero-signature satellite in orbit
*V.P. Vasiliev,V.D. Shargorodskiy, N.N. Parkhomenko*

**15:15 – 15:45 COFFEE BREAK**

**15:15 – 18:00 Poster Session**

**17:15 – 18:00 Missions Working Group Meeting**
*Chair: G. Appleby*

**18:30 – 20:00 Governing Board Meeting**

## THURSDAY MAY, 19

**Session 12: Interaction between Data-User and Stations (9:00 - 10:00)**
*Session Chairs: M. Torrance, K. Arsov, L. Combrinck, S. Schillak*

09:00 Introduction: "Setting the Stage"
*Ludwig Combrinck*

09:15 The estimation of the SLR data
*Stanislaw Schillak*

09:30 New Performance Assessment "Hit Rate" for Laser Ranging Stations
*Toshimichi Otsubo, Mihoko Kobayashi*

09:45 Measures of Network Performance
*P. Dunn, M. Torrence*

10:00 A Second Look at Engineering Data Files
*K.Salminsh*

**10:15 – 10:45** **COFFEE BREAK**

**Session 13:** **New Laser Ranging Technologies and Capabilities that must be developed to support future missions (10:45 – 12:30)**

*Session Chairs: J. Degnan, U. Schreiber*

10:45 Introduction: Introduction to laser transponders for precise interplanetary ranging and time transfer
*J. Degnan*

Introduction to One-Way Ranging Technique (confirmation pending)
*E. Samain*

The First ILRS Laser Transponder Mission: Laser Ranging to NASA's Lunar Reconnaissance Orbiter
*Jan McGarry, Christopher Clarke, Julie Horvath, Dandan Mao, Mark Torrence*

11:15 Laser Ranging Experiment on Lunar Reconnaissance Orbiter: Timing Determination and Orbit Constraints
*Dandan Mao, Jan McGarry, Mark Torrence, Gregory Neumann, Erwan Mazarico, Michael Barker, Xiaoli Sun, David Rowlands, James Golder, Thomas Zagwodzki, John Cavanaugh, Maria Zuber, David Smith*

11:30 Simulation of Two-Way Laser Transponder Links – The Wettzell Experience
*K. U.Schreiber, P. Lauber, A. Schlicht, I. Prochazka, J. Eckl, G. Herold, H. Michaelis*

11:45 GETEMME – An ESA Mission Proposal to Explore the Martian Satellites and the Fundamentals of Solar System Physics
*J. Oberst et al.*

12:00 The European Laser Timing Experiment (ELT) and Data Centre (ELT-DC)
*Schlicht A., Schreiber U., Prochazka I., Luigi Cacciapuoti*

**Session 14:** **Lunar Laser Ranging (13:30 – 15:00)**

*Session Chairs: J. Müller, E. Samain*

12:15 Simulation of optical response for next-generation single-reflector LLR targets
*Toshimichi Otsubo, Hiroo Kunimori, Hirotomo Noda, Hideo Hanada, Hiroshi Araki*

**12:30 – 13:30** **- LUNCH -**

13:30 Introduction: Lunar Laser Ranging – recent activities at Institut für Erdmessung (IfE)
*J. Müller*

13:45 Recent progress at APOLLO (tentative title)
*T. Murphy (presented by U. Schreiber)*

14:00 Lunar Laser Ranging Retroreflector for the 21st Century
*D. G. Currie, S. Dell'Agnello & G. O. Delle Monache*

14:15 Development of pulse detection IC for LIDAR on planetary lander
*Takahide MIZUNO, Hirokazu IKEDA, Kousuke KAWAHARA*

14:30 Ground Stations for the Next Generation Lunar Retroreflectors
*D. G. Currie*

14:45 Lunar Laser Ranging: Support Tools for observers
*Sebastian Bouquillon et al.*

**15:00 – 15:30** **COFFEE BREAK**

**Session 15:** **In-Sky-Laser-safety (15:30 – 17:00)**
*Session Chairs: H. Donovan, G. Appleby, F. Pierron*

15:30 Introduction: What are stations doing and what should we be doing?
*H. Donovan, G. Appleby, F. Pierron*

15:45 Ranging Jason2 from Paris Observatory for Time transfer experiment in summer 2010, operations and security achievements
*F. Pierron*

16:00 Implementation of the LASER Traffic Control System at the Haleakala Observatories
*D. O'Gara, E. Kiernan-Olson, C. Giebink, D. Summers*

16:15 Skyguide and Flarm - 2 in-sky-laser-safety systems used at Zimmerwald Observatory
*Martin Ploner, Adrian Jaeggi, Johannes Utzinger*

16:30 WLRS: In-Sky Laser Safety
*Johann Eckl, Martin Ettl, Alexander Neidhardt, Andreas Leidig, Uwe Hessels, Günter Herold*

16:45 Air traffic patterns near SLR site Riga and In-Sky laser safety
*K.Salminsh*

**17:00 – 18:00** **Transponder WG Meeting**
*Chair: J. Degnan, U. Schreiber*

**19:30 ≈ 22:30** **Banquet (Haus des Gastes)**

## FRIDAY MAY, 20

**Session 16:** **System Automation (9:00 – 10:15)**
**Session Chairs: A.Neidhardt, C. Moore, M. Ploner**

9:00 Introduction: Introduction to the session about automation
*Alexander Neidhardt, Chris Moore, Martin Ploner*

SLR Station Automation - Factors to Consider
*Chris Moore*

9:15 Automated Data Management of SLR Data and Products at the EUROLAS Data Center (EDC)
*Christian Schwatke*

9:30 Controlling Laser Ranging with RTAI-based Real-Time Linux
*Evan Hoffman, Randall Rickleffs*

9:45 SLR Automation for the New Space Geodesy Multi-Technique Sites
*J. McGarry et al.*

10:00 SLR-2.0: An overview about the new SLR/LLR Control software from Wettzell
*Martin Ettl, Alexander Neidhardt, Pierre Lauber, Johann Eckl, Martin Riederer, Lea Schreiber, Andreas Leidig, Reiner Dassing*

Automation and remote control as new challenges on the way to GGOS
*Alexander Neidhardt, Martin Ettl, Pierre Lauber, Andreas Leidig, Johann Eckl, Martin Riederer, Reiner Dassing, Matthias Schönberger, Christian Plötz, Ulrich Schreiber, Iain Steele*

**10:15 – 10:45** **COFFEE BREAK**

**10:45 – 11:30** **Workshop Summary**

**11:30 – 13:00** **General Assembly**

**13:00** **Adjourn**

**14:00 – 16:00** **Analysis Working Group**
*Chair: Cinzia Luceri*

# Session 1:
# Science Session

# LARES Laser Relativity Satellite

*I. Ciufolini, A. Paolozzi, E. Pavlis, R. Koenig, J. Ries, R. Matzner, R. Neubert, D. Rubincam, D. Arnold, V. Slabinski, G. Sindoni, C. Paris, M. Ramiconi, D. Spano, C. Vendittozzi, H. Neumayer.*

ABSTRACT

After almost three decades since the first idea of launching a passive satellite to measure gravitomagnetism, launch of LARES satellite is approaching. The new developed VEGA launcher will carry LARES in a nominally circular orbit at 1450 km altitude. This satellite, along with the two LAGEOS satellites, will allow to improve a previous measurement of the Lense-Thirring effect by a factor of 10. This important achievement will be a result of the idea of combining orbital parameters of a constellation of laser ranging satellites along with a specific design of LARES satellite. Other key points of the experiment are: the ever improving knowledge of the gravitational field of Earth, in particular the lower degree even zonal harmonics with GRACE satellites, and an accurate estimate of all the classical perturbations such as atmospheric drag and solar radiation pressure. In the paper both the scientific aspects as well as the design consideration will be described.

## 1. Introduction

The Italian Space Agency supported the LARES space experiment, in occasion of the foreseen qualification launch of the new launch vehicle VEGA. LARES (LAser RElativity Satellite),is a new laser ranged satellite, it will have an altitude of about 1450 km, and orbital inclination of about 70° and nearly zero eccentricity. The achievement of reaching a few percent uncertainty of Lense-Thirring effect will be the combination of several aspects. The first one is the combined use of three satellites LAGEOS (NASA) LAGEOS 2 (NASA and ASI) and LARES; the second one is the use of the new and ever improving gravitational field of Earth provided by the team of the GRACE (NASA-CSR and DLR-GFZ) satellites. The third one is an optimized design of LARES satellite and relevant orbit.

The original idea of measuring the Lense-Thirring effect dates back to 1984 and required the use of the nodes of two laser ranged satellites in supplementary orbit, one of which (LAGEOS) was already orbiting.

An excellent occasion to materialize that idea was offered by the LAGEOS II satellite in 1992. However it was not possible at that time to launch it in the optimal orbit that should have been supplementary to the one of LAGEOS. Neverthelss Ciufolini and Pavlis were able to obtain an accurate measurement of the Lense-thirring effect at the level of about 10%. The optimal orbit would have allowed a complete cancellation of the static Earth's spherical harmonics secular effects on the satellite nodes in order to measure the much smaller Lense-Thirring effect. Later, Ciufolini proposed a third satellite called LAGEOS III but the weight of about 400 kg (same mass as the LAGEOS satellites) and especially the high altitude of its orbit (about 6000 km) would have required an expensive launch vehicle. In response to a call for proposal of ASI, in year 1998 it was proposed for the first time LARES satellite that was an economic evolution of the predecessor LAGEOS satellites. The satellite orbit should have been supplementary to the one of LAGEOS I and the weight much lower (about 100 kg). But later, aside the difficulty of finding a launch for that altitude, new factors have changed the need of such a high altitude orbit for LARES: in 2002 GRACE spacecraft was launched, making possible the publication of a new generation of very accurate Earth's gravity field models; the idea to use the nodes of N laser-ranged satellites was proposed, to cancel the uncertainty due to the first N-1 even zonal harmonics responsible of the error higher than 1% on the measure of Lense-Thirring effect.

# 2. LARES orbit.

The node motion of a satellite in polar orbit will not be affected by the even zonal harmonics, making in principle possible to measure the Earth's gravitomagnetic field and the Lense-Thirring effect, since those are not canceled at that particular inclination i.e., the Earth will drag its orbit anyway. However, it was pointed out in the 1989 LAGEOS III NASA/ASI study that the uncertainty in the $K_1$ tide (tesseral, $m$=1, tide) is too high to make such an orbit useful for the measurement of the Lense-Thirring effect. Furthermore this consideration is confirmed by Peterson calculation (1997). Finally, to impose a small orbital injection error, as far as inclination goes for the polar orbit, would be too demanding for the launch vehicle. In fact it can be shown that, a quasi-polar orbit would have a nodal precession, due to its departure from 90 degrees of inclination, that would make the measurement of Lense-Thirring effect almost unrecoverable unless a combination with a second satellite is considered. The analysis of the effects of the tides has actually been done with the LAGEOS I and LAGEOS II and it is shown that it is the largest periodical amplitude observed in the combined residuals. If one considers also LARES satellite, the combinations of the three satellites provides as an error in the measurement of the Lense-Thirring effect due to the inclination, the results reported in Fig. 1 for an altitude of 1500 km, i.e., a LARES semimajor axis of about 7880 km (under reasonable assumptions such as zero eccentricity for the LARES orbit).

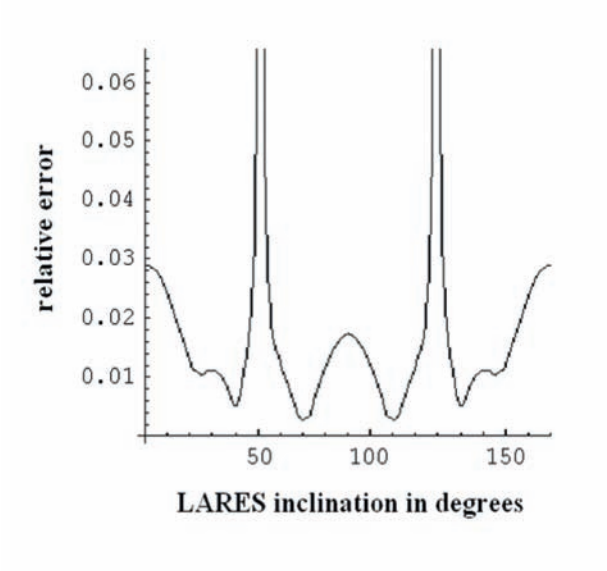


**Figure 1: Uncertainty in the measurement of the Lense-Thirring effect, due to the even zonal harmonics uncertainties, as a function of the inclination of LARES, using LARES, LAGEOS and LAGEOS II. The altitude of LARES is here 1500 km.**

The error sources of gravitational origin, i.e., those due to the uncertainties in the Newtonian gravitational field, are by far larger than the uncertainties of non-gravitational origin, i.e. radiation pressure, both from Sun and Earth, thermal thrust and particle drag; indeed the LAGEOS satellites and especially the LARES satellite are extremely dense spherical satellites with very small cross-sectional-to-mass ratio.

In consideration of the results shown in Fig.1 it was proposed for LARES an inclination at nearly 70 degrees. That would allow a total error in the measurement of the Lense-Thirring of just a few percent.

# 3. The LARES satellite.

As mentioned earlier, the go to the LARES mission has been given by the availability of a qualification flight of the VEGA launcher, developed by an ASI-AVIO joint venture (ELV S.p.A.) under the European Space Agency (ESA). Since the altitude foreseen for the qualification flight could not exceed 1500 km the design of LARES was quite demanding because it should have been optimized for reducing the surface perturbations such as atmospheric drag. Salento and Sapienza

University had a major role in the development of LARES mission and satellite since those were in charge of the design and main tests of both LARES satellite and separation systems. Also the construction of the Mechanical Ground Support Equipments and of some prototypes have been under the responsibility of the universities. The prime contractor for LARES system is CGS. In Fig. 2 is reported a drawing of the LARES system, whose main parts are indicated.

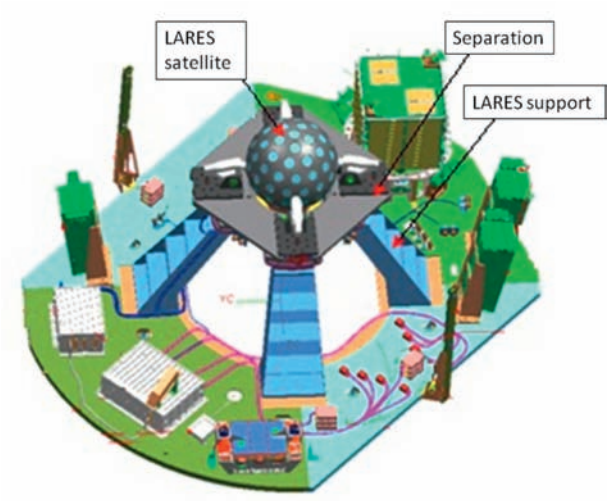


**Figure 2: LARES System. Image taken from reference "Objectives of LARES Satellite".**

The key decision to achieve a surface-to-mass ratio 2.7 times smaller than the one of LAGEOS was that one of using a high density material: a tungsten alloy with 18000 kg/m$^3$ making it the densest known single object in the solar system. The alloy chosen was not-magnetic to avoid unknown effects on LARES orbit due to the interaction with the magnetic field of Earth that even if small could affect the accuracy expected for the experiment. LARES has a radius of only 182 mm with a mass of about 400 kg. Also thermal thrust perturbation needed to be reduced as much as possible. For this reason the main body of LARES was therefore conceived as a single piece (differently from the LAGEOS satellites). The reduction of components will reduce the number of contact conductances that in turn are the main cause of temperature gradients on the surface of a satellite.

One of the most important components of LARES satellite are the Cube Corner Reflectors (CCRs) that provide the return signal of the laser pulses sent by the laser ranging ground stations. The 102 CCRs were positioned on the surface of the satellite in such a way to allow an easier attitude determination that is useful to a better estimate of thermal thrust. Spin axis determination can be performed using for instance the Sun glints, that is sun flashes at the observer location obtained when Sun, CCR front face and observer have a geometrical position which fulfill the law of reflection.The material used for the CCRs is Suprasil 311 with excellent property of homogeneity and isotropy. Surface finish of CCRs were the same as the ones used for LAGEOS satellites: the three back faces are 1/10$^{th}$ of the light wavelength while for the front face is 1/8$^{th}$, resulting in a reflected wavefront 1/4$^{th}$ of wavelength (Peak-to-valley, not RMS). As well known a dihedral angle offset is required to compensate for the satellite motion. Being LARES at lower altitude than LAGEOS this value has been set for all the three back faces to: 1.5 arcsec +/- 0.5 arcsec, while for the two LAGEOS it was 1.25 arcsec.

The effect of thermal condition in orbit on the CCRs was tested in a thermal vacuum facility of Sapienza University. A breadboard simulating the satellite material, carrying a CCR, was positioned inside a thermal vacuum chamber. Temperature of the breadboard was controlled using resistive heaters. The wall of the chamber were cooled by a liquid nitrogen shroud to simulate irradiation toward deep space; a window allowed to illuminate the CCR with a Sun simulator (AM0 spectrum), while a black disk maintained at 250 K simulated the infrared irradiation from Earth. An optical circuit outside the chamber collects the Far Field Diffraction Pattern (FFDP) of the CCR; the laser beam from the optical bench passes through a high quality optical window (λ/20 surface flatness) to reach the CCR inside the chamber. The FFDP acquired in simulated space environment is then compared to the FFDP collected at room temperature (T=20° +/- 5°C) to verify that the pattern shape and the intensity will not significantly change. In Fig. 3 are reported, as an example the results of the CCR exposed to the simulated deep space. In the horizontal axis are reported the velocity aberrations expressed in microradians. The two vertical lines in the bottom figure delimitate the range of interest (30-50 microrad).

The figure shows that in the range of interest, the minimum value of energy is about 60% of the one that the CCR would return if it would be in steady state condition at room temperature. Considering that LARES is much lower altitude than LAGEOS this value is completely acceptable. Similar results were obtained with the CCR pointing towards the sun simulator or towards the Earth. The tests have therefore proven that LARES CCR can work even in the worst cases of thermal conditions.

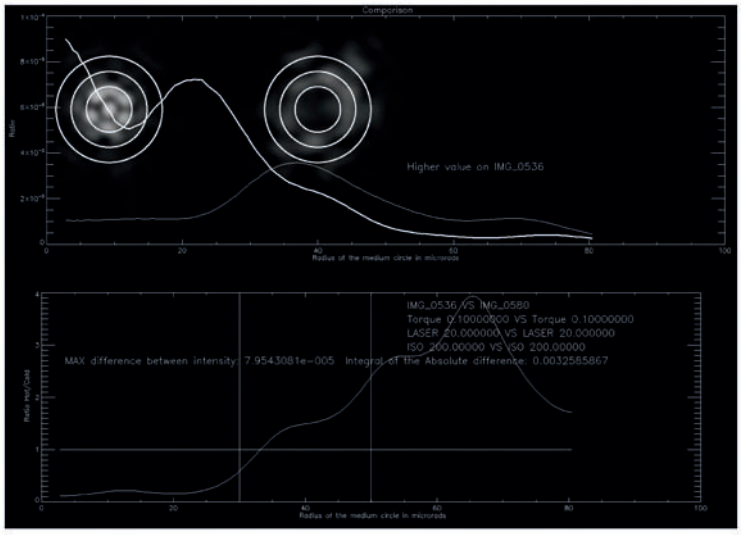


**Figure 3: FFDP comparison during one test in Thermal Vacuum Chamber.**
**FFDP at Room Temperature (RT) (top left). FFDP in simulated space environment (SPE) (top center). Thick curve is relevant to FFDP at RT. The lower curve is the ratio between the intensity of the two FFDPs.**

## References


*Ciufolini, I.,* 1984: Theory and Experiments in General Relativity and other Metric Theories, Ph.D. Dissertation, Univ. of Texas, Austin (Ann Arbor, Michigan).

*Ciufolini, I., Pavlis, E. C.,* 2004: A confirmation of the general relativistic prediction of the Lense-Thirring effect. Nature, 958-960 (2004).

*Ciufolini, I.,* 1986: Measurement of the Lense-Thirring drag on high-altitude laser-ranged artificial satellites. Phys. Rev. Lett., 278-281 (1986).

Ciufolini, I., 1986: On A New Method to Measure the Gravitomagnetic Field Using Two Orbiting Satellites. Nuovo Cimento, 1709-1720 (1996).

*Ciufolini, I., Paolozzi, A., Pavlis, E. C., Ries, J. C., Koenig, R., Matzner, R. A., Sindoni G. and Neumayer, H.,* 2009: Towards a One Percent Measurement of Frame-Dragging by Spin with Satellite Laser Ranging to LAGEOS, LAGEOS 2 and LARES and GRACE Gravity Models. Space Science Reviews, 71-104 (2009).

*Tapley, B., Ries, J.C., Eanes, R.J., and Watkins, M.M.,* 1989: NASA-ASI Study on LAGEOS III, CSR-UT publication n. CSR-89-3, Austin, Texas.

*Ciufolini, I., et al.,* 1989: ASI-NASA Study on LAGEOS III, CNR, Rome, Italy.

*Ciufolini, I., Paolozzi, A. et al.,* 1998: LARES, Laser Relativity Satellite, for the study of the Earth gravitational field and general relativity measurement, Phase A Report for ASI.

*Peterson, G. E.,* 1997: Estimation of the Lense-Thirring Precession Using Laser-Ranged Satellites, Ph. Dissertation, Univ. of Texas, Austin.

*Iorio, L.,* 2005: The impact of the new Earth gravity models on the measurement of the Lense-Thirring effect with a new satellite, New Astronomy, 616-635.

*Ciufolini, I.,* 2006: On the Orbit of the LARES Satellite. arXiv:gr-qc/0609081.

*Ciufolini I., Paolozzi A., Pavlis E. C., Ries J. C., Koenig R. and Matzner R.,* 2010: The LARES Relativity Experiment, in: General Relativity and John Archibald Wheeler, I. Ciufolini and R. Matzner eds. (Springer) 467-492.

Paolozzi A., Ciufolini I., Vendittozzi C., 2011*: Engineering and scientific aspects of LARES satellite. Acta Astronautica,* 127-134, 2011.

*Paolozzi A., I. Ciufolini, C. Vendittozzi, F. Passeggio, L. Caputo, G. Caputo,* 2009: Technological challenges for manufacturing LARES Satellite. In: IAC Proceedings. Daejeon, Republic of Korea, 12-16 October 2009, p. 1-6.

*Paolozzi A., I. Ciufolini, I. Peroni, C. Paris, M. Ramiconi, F. M. Onorati, L. Acquaroli,* 2009: Testing the LARES separation system breadboards. In: IAC Proceedings. Daejeon, Republic of Korea, 12-16 October 2009, p. 1-6.

*I. Ciufolini, A. Paolozzi, G. Sindoni, E. Pavlis, A. Gabrielli, S. Pirrotta, D. Barbagallo, E. Mangraviti,* 2009: Objectives of LARES Satellite. Proceeedings of XX AIDAA Congress, Milano, Italy, June 29–July 3, 2009.

*Paolozzi A., I. Ciufolini, C. Paris,* 2011: Contribution of strain measurements to the LARES satellite mission. International Conference on Structural Engineering Dynamics (ICEDyn), Tavira, Portugal, 20-22 June 2011, pp. 1-7.

## Correspondence

Antonio Paolozzi
DIAEE – Sapienza Università di Roma
Via Salaria 851 – Palazzina Plasma
00138 Rome – Italy

antonio.paolozzi@uniroma1.it

# Benefits of SLR in epoch reference frames

*Mathis Bloßfeld, Horst Müller, Manuela Seitz, Detlef Angermann*

ABSTRACT

In the actual terrestrial reference frame realizations the station motions are approximated by linear velocities (multi-year reference frames). But this parameterization is not adequate, since we know that the station movements include not modeled non-linear parts due to various geophysical effects. One possibility to overcome this deficiency in the modeling is to estimate the station positions more frequently by computing epoch reference frames in addition to the conventional multi-year reference frames. SLR is the primary technique to determine the origin of the reference frame (i.e., center of mass) together with station coordinates, EOP and gravity field parameters. To combine the station coordinates of the different techniques (SLR, GPS, VLBI), stations with at least two techniques available (colocation sites) are used. The coordinates of the different techniques at the colocation sites are tied together using terrestrial difference vectors (local ties). The quality of the transfer of the origin information from SLR to the other techniques depends strongly on the connection of the different station networks within the combination. Therefore and because of the different accuracies of the local ties, the selection of the local ties, which should be used, is one crucial part of the combination process.

In this study we analyze the quality of the datum realization by comparing the obtained epoch reference frames with a multi-year solution. Furthermore we discuss the impact of the temporal resolution on the datum realization. The coordinates of the terrestrial pole are validated w.r.t. the International Earth Rotation and Reference Systems Service (IERS) 08 C04 time series.

# 1. Introduction

The station coordinates in global terrestrial reference frames are changing with time. In the latest realization of the International Terrestrial Reference System (ITRS), the ITRF2008, the station coordinates are parameterized as a coordinate triple (X, Y, Z) at a reference epoch $t_0$ and a constant velocity per station coordinate component [Altamimi et al., 2011]. The DGFI realization of the ITRS is called DTRF2008 [Seitz et al., 2011]. Due to this parameterization multi-year reference frames do not consider high-frequency time variations like seasonal signals caused by inter alia atmospheric loading. These discrepancies between a regularized position and the instantaneous position should be considered with conventional corrections [Petit et al., 2010]. Since recent geophysical models are not accurate enough, possibilities to overcome this deficiency in the parameterization are to consider not modeled non-linear station motions by mathematical functions. Another possibility is to estimate epoch reference frames which are valid only for a certain time interval assuming that the movement of the station is negligible within that time period. Abrupt changes in the station coordinates, which are caused for example by an earthquake, could be considered in multi-year reference frames by introducing discontinuities whereas epoch reference frames consider them automatically. Epoch reference frames allow the estimation of station coordinates in an inter-technique combination (GPS, VLBI, and SLR) with a high temporal resolution (Fig. 1). The temporal resolution of the obtained solutions depends on the arc length (7-day/28-day) in the SLR only solution. Fig. 1 shows the different parameterizations of the station coordinates (x-component) of the GPS station Arequipa in Peru (Domes number 42202M005). In the multi-year solution, five jumps were introduced to approximate the abrupt change and the non-linear post seismic behavior of the coordinates with a piecewise linear polygon (solution numbers A01 to A06). The station coordinates are not included within the multi-year solution during the year right after the earthquake (24.6.2001 until 25.8.2002) because to the short time spans.

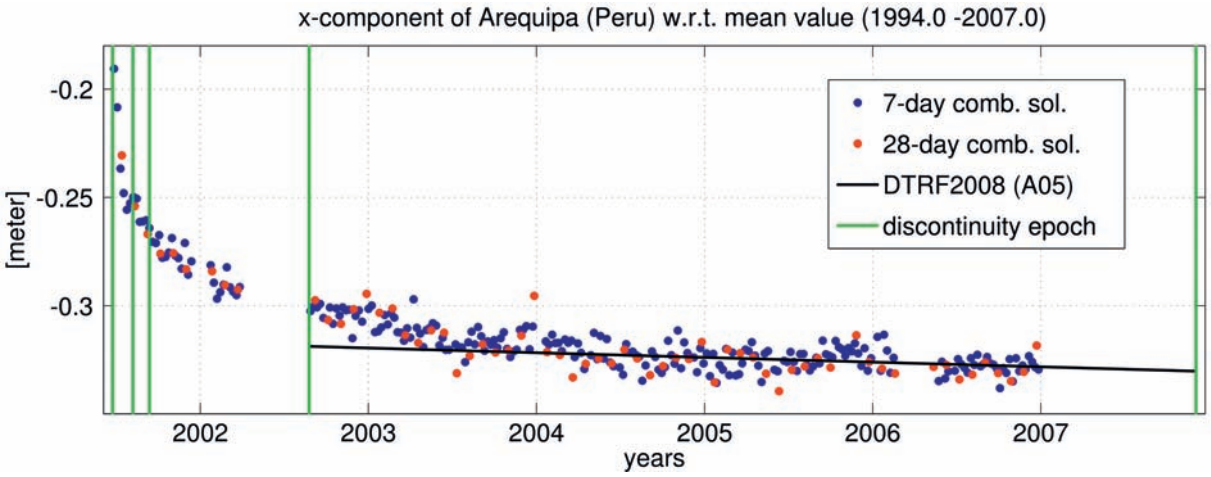


**Fig. 1: Different parameterizations of the station position of the GPS station Arequipa (Peru).**

# 2. Epoch reference frames

## 2.1 Data and processing scheme

The calculation of epoch reference frames at DGFI is based on the combination at the normal equation level (see Fig. 2). For SLR normal equations (NEQs) with an arc length of seven days or 28 days are used. The GPS NEQs have a daily resolution starting from midnight whereas the VLBI NEQs contain the observations of a 24-hour observation session which start at various epochs different from midnight. If the different techniques are combined, the EOPs are the only common parameters and are stacked whereas the station coordinates are handled as different parameters. To combine the station coordinates, the terrestrial difference vectors (local ties) between the techniques at the colocation sites (station, where at least two techniques are available) are used. The calculation of epoch reference frames could be distinguished into two main steps. In the first step, the intra-technique treatment, the technique-specific NEQs are prepared for combination which means that different parameterizations for example of the EOPs have to be equalized. This is necessary because the VLBI EOPs are parameterized as an offset and a rate at the reference epoch of the observation session. This parameterization has to be adapted to the piecewise linear polygon parameterization of the SLR and GPS EOP. In the second step of the calculation the different space geodetic techniques are combined. Therefore, the local ties at the colocation sites are introduced in the combination. Variance factors are estimated in order to obtain relative weights of the different techniques.

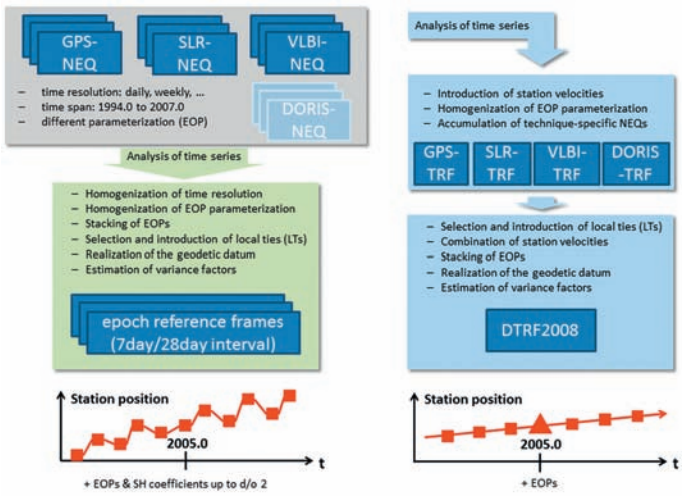


**Fig. 2: Processing scheme for epoch and multi-year reference frames.**

## 2.2 Geodetic datum

The geodetic datum is defined by assessing the origin, the orientation and the scale of the estimated reference frame. One way to define this is described in the IERS Conventions 2010 [Petit et al., 2010]: the origin of the ITRF2008 should not show any translations at a reference epoch $t_0$ or any translation rates w.r.t. the SLR technique-only solution. The scale of the ITRF2008 should be realized as a weighted mean scale of SLR and VLBI. Hence, there should be no scale factor at a reference epoch t0 and no scale rates w.r.t. the weighted mean scale of SLR and VLBI. The orientation of the ITRF2008 should be defined by a No-Net-Rotation (NNR) condition for a subset of GPS stations w.r.t. the previous realization of the ITRS, the ITRF2005. Therefore, the rotation angles between the epoch solution and the multi-year solution should be zero at a reference epoch $t_0$. The rotation rates should also be zero over time. In contrast to the multi-year reference frames (datum definition by the IERS Conventions), for epoch reference frames only the time-independent part of the datum definitions has to be realized which means that no conditions for the rates of the datum parameters have to be introduced in the combination (Fig. 3).

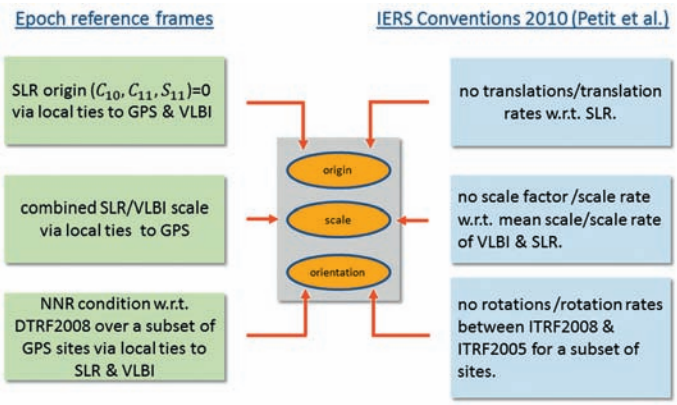


**Fig. 3: Different realizations of the geodetic datum.**

In the combination process the local ties play a very crucial role. The quality of the geodetic datum of the estimated epoch reference frames depends strongly on the accuracy of the local ties and the global distribution of the colocation sites. The local ties are used for connecting the station coordinates of the different techniques in order to get a most stable and homogeneous global station network within the combination. Because of this the local tie handling in the combination directly affects the quality of the datum realization in the different network parts. For the orientation in x- and y-direction, the coordinates of the terrestrial pole play an important role in the combination, too.

## 2.3 Results and Comparisons

Additionally to the station coordinates, the epoch solutions contain consistently estimated ERPs and gravity field parameters of degree two (parameters of degree zero are fixed to one, parameters of degree one are fixed to zero). To validate the quality of the realized datum parameters, the transformation parameter time series of a seven parameter Helmert-Transformation are derived w.r.t. a multi-year solution like the DTRF2008 which has a much more stable geodetic datum than the obtained epoch reference frames. The coordinates of the terrestrial pole are compared to the official reference time series IERS 08 C04. The estimated UT1-UTC values and the gravity field parameters of degree two are analyzed in Bloßfeld et al., 2011.

### 2.3.1 Quality of the realized geodetic datum

The left side of Fig. 3 shows which techniques are used for realizing the datum parameters. To validate the quality of the realized origin, the mean offsets of the SLR technique-only solution w.r.t. the DTRF2008 and the mean offsets of the GPS and the VLBI stations of the combined terrestrial reference frame (TRF) could be compared. Tab. 1 shows that the GPS stations of the combined TRF of the 7-day solution are in a good agreement with the DTRF2008, whereas the SLR only solution shows an offset of about -3 mm in the x-direction. Furthermore, the VLBI stations of the combined TRF show an offset of -4 mm in the y-component of the origin. The weighted RMS (WRMS) values for all techniques are between 4 and 6 mm for the x- and y-translation parameters and around 1 cm for the z-translation parameters, respectively. These accuracies also hold for the 28-day solution.

The orientation of the combined TRF is realized by a NNR condition for a subset of GPS stations w.r.t. the DTRF2008. Tab. 1 shows the rotational offsets of the GPS only solution and the SLR/VLBI part of the combined TRF. The NNR condition ensures that the rotation angles of the GPS only solution are equal to zero. Nevertheless Tab. 1 shows that small rotations are estimated. This is an effect of the transformation, where the GPS stations are not weighted equally and therefore

small rotations are estimated. The agreement of the datum information within the combination is below 2 mm for the SLR station network and 3.5 mm for the VLBI station network, respectively. The WRMS values of the rotation parameters for the GPS only solution are less than 1 mm whereas the WRMS values for the SLR/VLBI station network in the combination are between 3 and 4 mm for the 7-day and the 28-day solution. This increased scatter of the gained parameters is caused by the inhomogeneous distribution of colocation sites and stations used for transformation and the accuracy of the used local ties.

The scale is realized as the mean scale of SLR and VLBI, which is emphasized by the values given in Tab. 1. The GPS network scale in the combined solution is a good approximation of the mean scale of SLR and VLBI.

| [cm] | Tx | Ty | Tz | Rx | Ry | Rz | Sc |
|---|---|---|---|---|---|---|---|
| **SLR** | -0.293 | -0.173 | 0.093 | | | | 0.138 |
| **GPS** | | | | 0.083 | 0.066 | -0.008 | |
| **VLBI** | | | | | | | -0.274 |
| **comb. (SLR)** | | | | -0.090 | 0.174 | -0.032 | |
| **comb. (GPS)** | -0.055 | -0.142 | 0.095 | | | | -0.081 |
| **comb. (VLBI)** | -0.023 | -0.428 | -0.085 | -0.312 | -0.002 | 0.243 | |

**Tab. 1: Mean offsets of the transformation parameters between the epoch reference frames and DTRF2008. Only values which are relevant for the validation of the geodetic datum are displayed.**

### 2.3.2 Quality of the pole coordinates (x, y)

The ERPs are compared with the IERS 08 C04 time series. The left side of Fig. 4 shows the differences of the coordinates in x-direction of the terrestrial pole w.r.t. to the IERS reference time series. It is clearly visible, that SLR shows the highest scatter. The corresponding WRMS values are displayed on the right side of Fig. 4. All solutions use a piecewise linear polygon representation of the pole coordinates with estimated offsets at midnight. The WRMS of the GPS and VLBI only solutions and both combined solutions (7-day/28-day) is below 1 cm. The GPS only solution shows the smallest WRMS value (cca. 3 mm). The scatter of the combined solutions is higher than the scatter of the GPS only solution. This could be due to the fact that the WRMS of the SLR only solution is about 1.2 cm. The high scatter results from the not well estimated coordinates of the terrestrial pole at the borders of the satellite arc. Also the VLBI only pole coordinates could be affected by some systematic effects and therefore could cause the increased scatter within the combination. If the two combined solutions are compared, the 28-day solution has a higher scatter than the 7-day solution which needs to be further investigated.

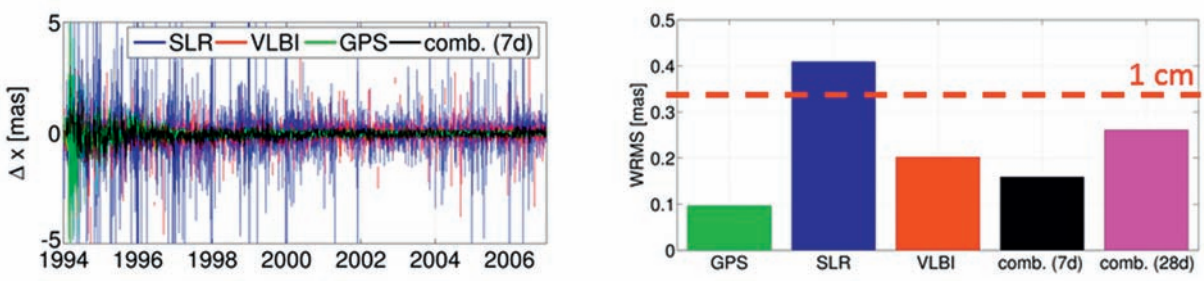


**Fig. 4: Left: X-component differences of the terrestrial pole w.r.t. the IERS 08 C04 time series. There are displayed the technique-only solutions SLR, GPS and VLBI and the combined solution with a seven day arc length; Right: WRMS values of the differences of the technique-only solutions and both combined solutions (7-day/28-day).**

# 3. Conclusions

The DGFI SLR solution contains consistently estimated station coordinates, ERPs and gravity field parameters. In the combination with GPS and VLBI, SLR plays a fundamental role for realizing the geodetic datum. SLR is the unique technique to provide the most stable information about the origin and together with VLBI it is used to realize the scale. The results in subsection 2.3.1 show that the geodetic datum in epoch reference frames could be realized with a mean accuracy of 3 mm and WRMS values of about 5 mm for the orientation and the scale w.r.t. the multi-year solution DTRF2008. The origin shows offsets below 4.5 mm with WRMS values up to 1 cm. Therefore, the accuracy of the geodetic datum of the more stable multi-year solution DTRF2008 could not be reached with the epoch solutions at present. However, the epoch reference frames could be a reasonable additional product to the multi-year solutions in order to represent the non-linear station motions in a better way. The validity of the station coordinates after big earthquakes could also be improved with epoch reference frames. The results discussed in subsection 2.3.2 show that the most accurate estimation of the coordinates of the terrestrial pole in the combined solution could be estimated if a temporal resolution of seven days is used. The 28-day solution has a higher scatter. The pole coordinates of the GPS only solution show the smallest scatter of the analyzed solutions. The SLR only and VLBI only pole coordinates might be falsified by systematic effects within the solutions.

## Acknowledgements

The presented results are worked out in a project within the research group “Earth rotation and global dynamic processes”. This research group is funded by the German Research Foundation DFG. The authors want to thank the DFG for making the work in this project possible.

## References

*Altamimi, Z., Collilieux, X., Métivier, L.*: ITRF2008: an improved solution of the international terrestrial reference frame, Journal of Geodesy, doi: 10.1007/s00190-011-0444-4, 2011

*Bloßfeld, M., Müller, H., Angermann, D.*: Adjustment of EOP and gravity field parameter from SLR observations, Proceedings of the 17th International Workshop on Laser Ranging, Bad Kötzting, Germany, May 16-20, 2011

*Petit, G., Luzum, B.*: IERS Conventions (2010), Verlag des Bundesamts für Kartographie und Geodäsie, Frankfurt a.M., 2010

*Seitz, M., Angermann, D., Bloßfeld, M., Drewes, H., Gerstl, M.*: The 2008 DGFI realization of ITRS: DTRF2008, submitted to Journal of Geodesy, 2011

## Correspondence

Mathis Bloßfeld
Deutsches Geodätisches Forschungsinstitut
Alfons-Goppel-Straße 11
80539 München

blossfeld@dgfi.badw.de
http://www.badw.dgfi.de

# The SLR monitoring crustal movement in South America

*Yin Zhiqiang, Han Yanben, Liu Weidong*
*(National Astronomical Observatories, Chinese Academy of Sciences, and Beijing, China);*
*R.Podesta, A. Pacheco, A.Ester*
*(Observatorio Astronomico Felix Aguilar, San Juan Uni., Argentina)*

ABSTRACT
The M8.8 Chilean earthquake of February 27, 2010 caused a large surface displacement near its epicenter. Satellite Laser Ranging (SLR) station 7405, cooperatively operated by Germany and Chile about 130 km from the epicenter was affected by the earthquake. Another SLR station, No. 7406, operated jointly by the National Astronomical Observatories of the Chinese Academy of Sciences and San Juan University of Argentina, was about 600 km from the epicenter. Combining the observations of these two SLR stations with global SLR station observations, we calculate the geocentric coordinates of the two stations based on ITRF2000. The results show that the coordinates of the two stations have changed by varying degrees. SLR-7405 moved substantially towards the southwest with displacements of about 3.11, 0.52 and 0.49 m in X, Y, Z directions; the corresponding displacements for SLR-7406 are about 0.02, 0.03 and 0.02 m. The follow-up analysis showed that SLR-7405 station is still influenced by the subsequent medium earthquakes close to it during 2010-2011.

## 1. Introduction

In South America, there are several SLR stations. One of them is SLR station co-operated between German and Chile in Concepción City, and the equipment number is 7405 in the ILRS network. Northeast of the 7405 about 700 km, where is the Observatory of San Juan University of Argentina, there is another joint establishment of the SLR stations by National Astronomical Observatories of China and San Juan University, and its number is 7406 in the ILRS network.

The magnitude 8.8 quake struck near Maule of Chile on Feb. 27, 2010. It caused the movement of the entire city of Concepción by ~3-meter to the west, major damage and a tsunami near the epicenter at the same time. SLR-7405 ($\varphi = -36°.843, \lambda = -73°.025$) is about 80km from epicenter ($\varphi = -36°.122, \lambda = -72°.898$) of Chile M8.8 earthquake, it was struck by the major earthquake and was fully operational again near May 2010. SLR-7406 ($\varphi = -31°.509, \lambda = -68°.623$) is about 650km from the epicenter, its observation was not interrupted by the earthquake. The distance between SLR-7405 and SLR-7406 is about 716 km. Utilizing the observations of these two SLR stations with global SLR observations, we calculate the geocentric coordinates of the two stations.

## 2. Data Analysis

The Lageos-1 laser-ranging satellite was designed especially for geodynamic research and is also one of the preferred satellites for the global SLR network. Therefore, observations from of Lageos-1 are abundant as well as highly precise. We selected Lageos-1 data supported by all the SLR stations (http://ilrs.gsfc.nasa.gov/). Methods of accurately determining the orbit of Lageos-1 are undertaken based on similar sets of input parameters (Yin Z.Q., et al, 2011). The reference frame, measurement and force models basically follow the IERS conventions. After analysis of the observations after the M8.8 Chilean earthquake of 2010, station SLR-7405 was determined to have moved 3.11, 0.52 and 0.49 m in X/Y/Z directions, while station SLR-7406 moved about 0.02, 0.03 and 0.02 m. After that, there still are many subsequent earthquakes during the last year. Taking concepcion as a center, we select the earthquakes M>6 in 1000 km radius, some of them are listed in Table 1. The station coordinates of SLR-7405 are also calculated, and the result is showed in Figure 1.

| Year Mon Day | TIME | LAT | LONG | DEP | MAG | DIST |
|---|---|---|---|---|---|---|
| 2010 07 14 | 08 32 21.49 | -38.07 | -73.31 | 22 | 6.6 | 138 |
| 2010 09 09 | 07 28 01.72 | -37.03 | -73.41 | 16 | 6.2 | 40 |
| 2011 01 02 | 20 20 17.69 | -38.37 | -73.35 | 24 | 7.1 | 171 |
| 2011 02 11 | 20 05 30.79 | -36.47 | -73.12 | 27 | 6.8 | 41 |
| 2011 02 11 | 23 39 21.31 | -37.20 | -73.20 | 15 | 6.0 | 42 |
| 2011 02 12 | 01 17 01.41 | -37.02 | -72.95 | 16 | 6.1 | 21 |
| 2011 02 13 | 10 35 06.74 | -36.65 | -73.18 | 17 | 6.0 | 25 |
| 2011 02 14 | 03 40 09.92 | -35.38 | -72.83 | 21 | 6.6 | 163 |

**Table 1: Subsequent earthquake near Concepción after Chile 2010 earthquake**

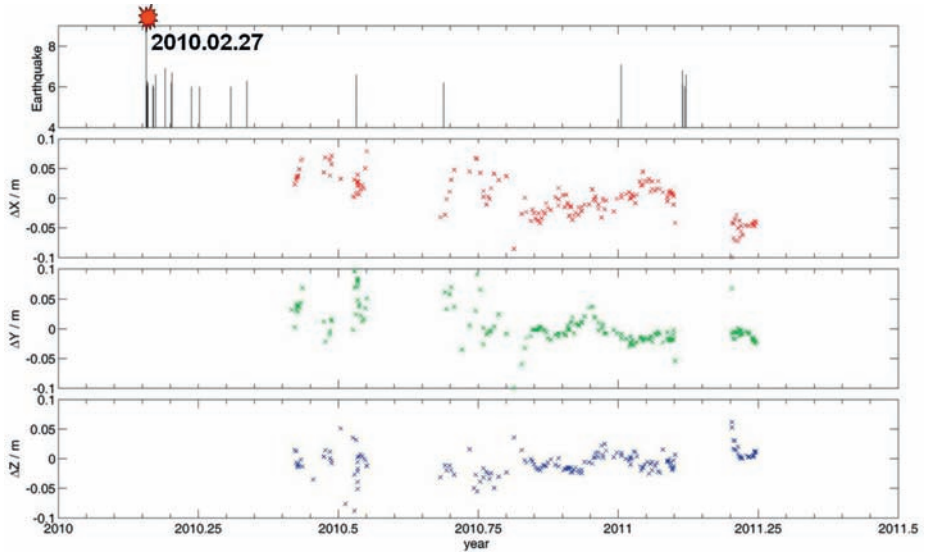


**Figure 1: the earthquake sequence and coordinate of Concepción (7405) after the Chilean 2010 earthquake**

# 3. Conclusions

Combining the observations of these two SLR stations with global SLR observations, we calculate the geocentric coordinates of the two stations based on ITRF2000. The results show that the coordinates of the two stations have changed by varying degrees. SLR-7405 moved substantially towards the southwest with displacements of about 3.11, 0.52 and 0.49 m in X, Y, Z directions; the corresponding displacements for SLR-7406 are about 0.02, 0.03 and 0.02 m, respectively. The continual analysis about the two stations showed that concepcion station is still affected by the subsequent earthquakes close to it. For example, the measurable movement of concepcion station might cause by the frequent earthquakes about 20-40 km away during February 11-13, 2011 (see Figure 1), the systematic displacement is about 2 cm on SLR-7405 station. San Juan station 7406, separated from station 7405 by about 700 km, did not show the obvious movement during these bunch of earthquakes periods. This solution, as an independent result derived from SLR observations, could provide an essential external check for other positioning techniques such as GPS.

## Acknowledgements

This work was supported by the Foundation of International Science and Technology Cooperation (2009DFB00130, 2010DFB53100), the External Cooperation Program of the Chinese Academy of Sciences (GJHZ200813).

## References

*Yin Z Q, Han Y B, Podestá R, et al, 2011*: South American SLR stations monitoring ground displacement caused by the M8.8 Chilean earthquake of 2010. Chinese Sci Bull, 56: 738–742, doi: 10.1007/s11434-010-4324-8

## Correspondence

Zhiqiang Yin
National Astronomical Observatories, Chinese Academy of Sciences
20A Datun Road, Chaoyang District,
Beijing, China

yinzhq@nao.cas.cn

# Assessment of the non gravitational forces acting on the Lageos satellites, and impacts on gravitational parameters

*Florent Deleflie, Jean-Michel Lemoine, Franck Reinquin, Gilles Métris, François Barlier, Pierre Exertier*

ABSTRACT

The Lageos-1 and Lageos-2 satellite motions have been at the origin of a relevant literature, developing various models accounting for non-gravitational forces. In this paper, some past results are recalled, and then extended toward recent observations to show which changes can now be observed, in relation with the time evolution of the satellite spin. We then analyze the long-term evolution of the Lageos satellite orbits, tracked by the Satellite Laser Ranging network over more than 20 years. The level of residuals enables to show very small perturbations in the orbit, that can be reasonably attributed to non- gravitational effects. These perturbations are displayed through time series of empirical residual accelerations, linked to the non- gravitational effects. We then discuss the impact on the determination of the gravity field coefficients of degree 2.

## 1. Introduction

In the mid-seventies, a new generation of geodetic satellite were launched to make available ideal geodetic targets in space. These satellite were spherical, very dense (to minimize the effects of non gravitational perturbations), and covered by retro-reflectors for the laser tracking. Two first satellites were launched, Starlette launched by CNES in 1975 and Lageos launched by NASA in 1976. Other satellites of this type were launched, in particular Lageos-2 satellite built by Alenia-Spazio in Italy and launched by NASA in 1992. In the mid 90'th, UT CSR group (J. Ries, R. Eanes) pointed out unexplained residual excitations on the Lageos eccentricity vector.

Non gravitational phenomena perturbing the artificial satellite motion has attracted considerable attention in past years, mainly because the precision of the satellite orbit determination has continually increased since the launch of the SLR satellites. Over long periods of time, more and more dynamical effects become apparent, especially those inducing small but cumulative effects on the orbits.

As mentioned in (Métris and Vokrouhlicky, 1997), a main difficulty to study non gravitational effects acting on Lageos-1 orbit is a "lack of firm knowledge of the satellite spin axis evolution. Several important effects, notably the thermal phenomena and the optical anisotropy effect, depend criticaly on the spin axis orientation. A lack of the theoretical understanding of this evolution has posed (and still poses) an important obstacle in the non gravitational force modeling process." This difficulty to model the spin axis orientation has been increased since the middle of the 90's, because the rotation Lageos-1 rotation period has been considerably decreased by the action of the eddy current dissipation.

In addition to the well-known radiation pressure, and to the discover in 1981 by Smith and Dunn of an unexplained decreasing of the semi-major axis of about 1.1mm/day, (corresponding to a constant along track acceleration of $-3.3\ 10^{-12} m/s^2$), different non gravitational effects have been enlightened in the LAGEOS-1 orbit, and produce very specific perturbations on the orbital motion, and mainly: (i) the Yarkovsky-Shah thermal effect which requires a model for the satellite spin axis, (ii) effets induced by the asymmetric reflectivity of the satellite surface, (iii) effects induced by the asymmetric thermal emissivity of the Earth (albedo).

Metris demonstrated that a modified (empirically) thermal model using Farinella et al spin axis model, allowed to reconstruct the observed residual excitation both for a, $e^*\cos\omega$ and $e^*\sin\omega$. This was the case up to 1996...

In this paper, we have recomputed empirical accelerations for the two Lageos satellites using the GRGS GINS s / w. We provide an analysis of the time series over the period 1990-2011, and we estimate the impact of the non gravitational modelling on the gravity field time series estimation.

# 2. Lageos-1 & -2 long orbital arcs

## 2.1 Parameterization

We have recomputed long orbital arcs of the two Lageos satellites over the period 1990-2011 for Lageos-1, and over the period 1993-2011 for Lageos-2. The modelling follows the guidelines provided by the Analysis working Group of the ILRS, except for the following points:

- Best known dynamical model but without thermal effects neither optical asymmetry
- 65 days arc, to avoid absorbing a large part of non gravitational effects through the initial state vector. It was checked that suchg a long period of time was suitable with the purposes of the study.
- Adjusted parameters:
  - 6 initial conditions
  - 1 set of bias (BT,BTC, BTS, BNC, BNS) every 5 days (13 sets / arc)
  - 1 Solar radiation pressure coefficient.
- No range bias related to the station measurements.

The estimated biases are supposed absorb the long period part of unmodeled accelerations, and the main unmodeled accelerations are due to non-gravitational effects such as thermal effects. The estimated biases can be interpreted as follows:

- BT, BTC, BTS are related to the so called along-track direction (T) and eccentricity vector excitations : $\Delta T(t) = BT + BTC \cos(\omega + M) + BTS \sin(\omega + M)$, and are related to the eccentricity vector excitations,

$$\frac{\Delta \dot{a}}{a} \approx \frac{2}{na} BT$$

$$\Delta \frac{d}{dt}(e\cos\omega) \approx \frac{1}{na} BTC$$

$$\Delta \frac{d}{dt}(e\sin\omega) \approx \frac{1}{na} BTS$$

- BNC and BNS are related to the across-track (N) direction : $\Delta N(t) = BNC \cos(\omega + M) + BNS \sin(\omega + M)$

## 2.2 Post-fit residuals level

The levels of magnitude of the 65-day orbital arc residuals are very similar for the two satellites, and have the same typical values as the weekly operational orbital arcs provided by the GRGS ILRS Analysis Center : 1.37cm for Lageos-1 (Figure1), 1.40cm for Lageos-2 (Figure2).

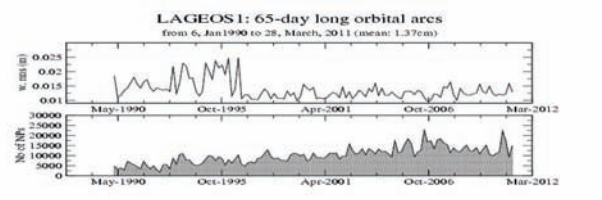


**Figure 1: Lageos1 orbital arc residuals.**

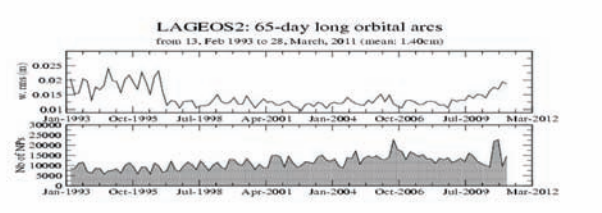


**Figure 2: Lageos2 orbital arc residuals.**

It is rather difficult to understand properly the dramatic improvement of the residual level after 1995, but it is likely to be due to a terrestrial reference frame effect, and a further study should be carried out to point out to what extent this fall is related (or not) to the lack of range bias... But, since no effect is induced on the empirical coefficient and gravity field time series, it is not discussed in that paper.

Another issue has to be kept in mind: the level of Lageos-2 residuals is growing slowly but regularly since a couple of years, and the correlation between a possible change of the spin axis rotation regime could be an explanation (it could be confirmed by studies of the same kind as in (Kuchardski, 2007) or (Bianco 2001)), as we will see hereafter.

## 2.3 Modelling the SRP coefficient

The case of the Solar Radiation Pressure coefficient can be interpreted separatly from the others, since there is no physical reason why it should vary: it can be interpreted, mainly, as a variation of the optical properties of the satellite surface from the nominal values provided by the builders. It appears (Figure 3) that no clear modelling can be adjusted for Lageos-1 (mean value: 1), and that an exponential model can be adjusted for Lageos-2:

$$\begin{aligned} FS(LA_1) &= 1 \\ FS(LA_2) &= (7.04651\ \ 10^{-4}(t-1990)^2 \\ &\quad +0.0166(t-1990)+1.01985) \\ &\quad \times exp(-0.0254067(t-1990)) \end{aligned}$$

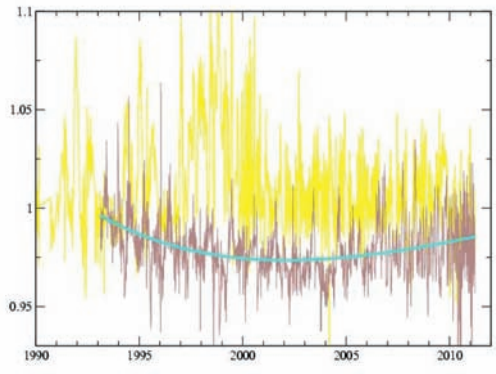


**Figure 3: Solar Radiation Pressure coefficient, for the Lageos1 (time series in yellow), and Lageos 2 satellites (time series in brown, modelling in brown).**

# 3. Time series of empirical parameters

The results of empirical accelerations (towards the tangential direction) obtained between 1990 and 2011 are now presented (Figures 4 & 5). A significant change can be seen on the 3 coefficients.

For Lageos-1 (Figure 4), the decrease of the semi-major axis corresponding to a mean value of BT of about $-3\,10^{-12}$ m/s$^2$ is to some extent predicted by Farinella and Vokroulhicky in 1996, or (Scharroo, 1991) but the precise behaviour is poorly observed. The behaviors of BTC and BTS are very different after 2000. This fact could be probably linked to the motion of the spin axis and precession rate of the spin axis which tends to be large. Indeed short periodic excitations yield small amplitudes compared to long periodic excitations.The problem is open and new modeling of the spin axis would be suitable for the present period.

Concerning Lageos-2 (Figure 5), the correlation between the Solar Radiation Pressure coefficients is much more visible. The change of behavior in 2009-2010 could be an indicator as a spin axis starting to be chaotic.

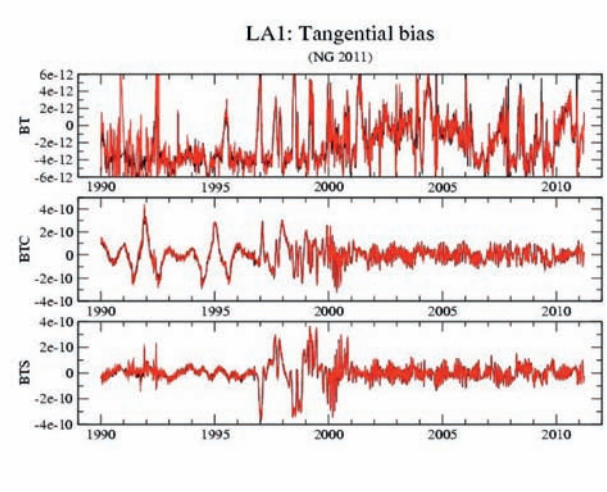


**Figure 4: Empirical Tangential time series coefficient for Lageos-1: without constraining the SRP coefficients (black), or by constraining to 1 the SRP coefficients (red).**

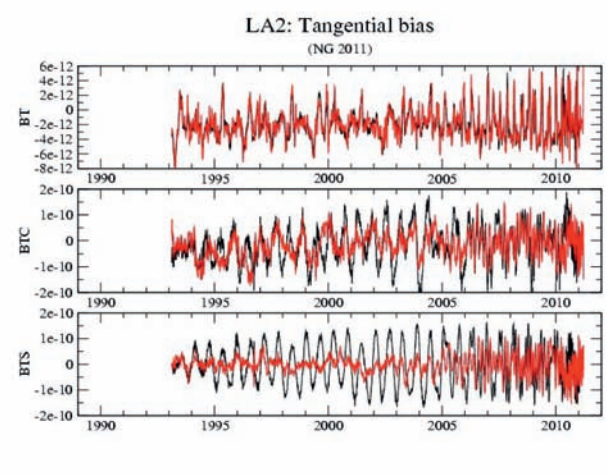


**Figure 5: Empirical Tangential time series coefficient for Lageos-2: without constraining the SRP coefficients (black), or by constraining the SRP coefficients described in the previous section (red).**

# 4. Consequences on Gravity Field parameters time series

## 4.1 Degree1: geocenter motion

Figure 6 shows the time series of the degree 1 of the gravity field, namely the geocenter motion. It contains a "dynamical" approach, based on the variations of the C(1,0), C(1,1), S(1,1) coefficents, as well as a "geometrical" approach, based on a global motion of the station network. Both approaches are fully compatible.

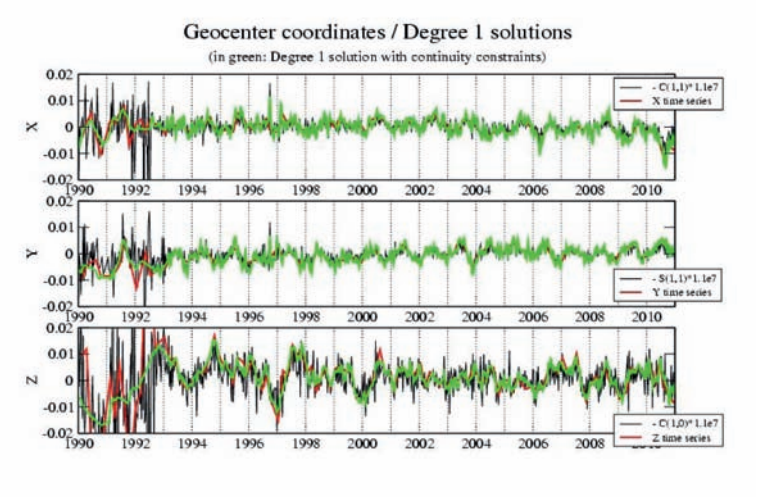


**Figure 6: Geocenter motion deduced from Lageos-1 and Lageos-2 trajectory analysis**

## 4.2 Degree2, including dynamical flattening of the Earth

We show here the impact of two different strategies concerning the empirical coefficient: constraining or not the SRP coefficient variations, and resolving simultaneously the degree 2 of the gravity field and the coefficients towards the normal direction.

Figure 7 shows the time series (in red) of the degree 2 of the gravity field, for the coefficients C(2,0), C(2,1), S(2,1), deduced from an inversion of a normal system containing as well the empirical coefficients through the normal direction. It appears that the time series are much more noisy than the reference models using, as well, data from the GRACE mission.

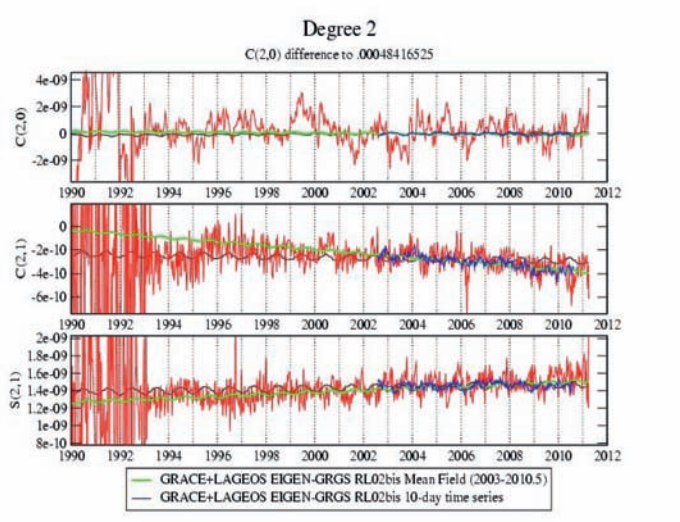


**Figure 7: Gravity Field coefficient time series (degree2).**

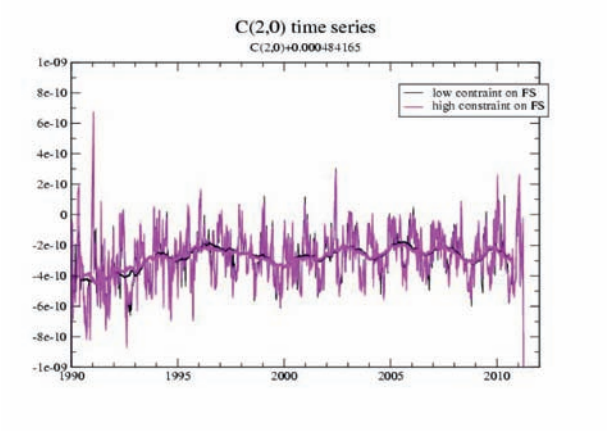


**Figure 8: C(2,0) time series, the Solar Radiation Pressure coefficients being constrained or not**

Figure 8 shows only the variations of the dynamical flattening of the earth (C(2,0)), as well as a windowed averaging: the main values as well as the secular variation as not the same whether the Solar Raditation Pressure coefficient if modelled or not. This is confirmed in the following table, as well as for the other coefficients of degree 2:

```
C(2,0)
FSfree: y = -1.1767e-08 + 5.7414e-12 * x
FSmod.:y = -3.6696e-09 + 1.7037e-12 * x

C(2,1)
FSfree: y = 9.1414e-09 - 4.7157e-12 * x
FSmod.:y = 4.8405e-09 - 2.5765e-12 * x


S(2,1)
FSfree: y = -1.8107e-08 + 9.7533e-12 * x
FSmod.:y = -9.866e-09 + 5.647e-12 * x

C(2,2)
FSfree: y = 2.4251e-06 + 7.0939e-12 * x
FSmod.: y = 2.4154e-06 + 1.1951e-11 * x

S(2,2)
FSfree: y = -1.3879e-06 - 6.1596e-12 * x
FSmod.: y = -1.3848e-06 - 7.7051e-12 * x
```

A new error budget, as the one provided in (Deleflie, 2003) should be performed again, to quantify the amplitudes of the various components of the signal, as J2dot and the 18.6 year tide.

# 5. Conclusion

We investigated the consequences of the non gravitational forces parameterization of the Lageos-1 & -2 satelite trajectories over the period 1990-2011. We built long orbital arcs suitable to describe the correlations between the various coefficients adjusted in the orbital computation process : initial state vector, time series of empirical parameters, gravity field coefficient time series.

The Lageos-1 spin axis chaotic behavior seems to be confirmed through the time series of empirical coefficients. Concerning Lageos-2, a change of regime on the tangential direction has been detected.

We showed that the strategy used for the empirical coefficients supposed to compensate for a lack of non gravitational forces modelling has a non negligible impact on the gravity field time series deduced from the orbital motion. A forthcoming paper will analyse each of them very carefuly, but the preliminary conclusions are the following : (i) the gravity field time series have not the same characteristics whether the Solar Radiation Pressure coefficints are modelled or are free ; (ii) the gravity field coefficients time series are highly correlated with the empirical coefficients towards the normal direction. The impacts of the C(2,0) time series are at the level of a few $10^{-10}$, and an impact on the secular variation can also be quantified.

## References

*Deleflie, F., P., Exertier, G,. Métris, P., Berio, O., Laurain, J.-M. Lemoine, R., Biancale*, 2003: Why the 18.6 year tide cannot explain the change of sign observed in J2dot?, Adv. Geosci., 1, 103-108

*Métris, G., D. Vokrouhlicky, J.C., Ries, R.J., Eanes,* 1997: Non gravitational effects and the LAGEOS eccentricity excitations, J. Geophys. Res., 102(B2), 2711-2729

*Scharroo, R., K.F., Wakker, B.A.C., Ambrosius, R., Noomen*, 1991: On the Along-Track Acceleration of the LAGEOS Satellite, Journ. Geophys. Res., 96(B1), 729-740

*Kuchardski, D., G., Kirchner, S., Schillak , E., Cristea*, 2007: Spin determination of Lageos from kHz laser observations, Adv in Space Res.

*Bianco, G., M., Chersich, R., Devoti. et al.*, 2001 : Measurement of Lageos-2 rotation by SLR observations, GRL

## Correspondence

Florent Deleflie
Institut de Mécanique Céleste et de Calcul des Ephémérides, Observatoire de Paris, GRGS

77 Avenue Denfert Rochereau F-75014 Paris
Florent.Deleflie@imcce.fr, Florent.Deleflie@obs-azur.fr

Jean-Michel Lemoine, Franck Reinquin
Observatoire Midi-Pyrénées, CNES, GRGS, 14 Avenue Edouard Belin, F-31000 Toulouse
Jean-Michel.Lemoine@cnes.fr

Gilles Métris, François Barlier, Pierre Exertier
Observatoire de la Côte d'Azur, GRGS, Avenue Nicolas Copernic, F-06130 Grasse

# On the Calibration of TanDEM-X Precise Baselines via SLR

*R. Koenig, Y. Moon, L. Grunwaldt*

ABSTRACT

The TanDEM-X mission strives for the generation of a digital elevation model of the Earth from SAR measurements taken by the TerraSAR-X and TanDEM-X satellites. As a requirement to achieve height accuracies of a few meters, the baseline between the two satellites needs to be known with millimeter accuracy. The baseline is operationally derived solely from the GPS measurements of the geodetic grade IGOR receivers onboard both satellites. Quality assessment is possible via comparison of results by independent solutions within GFZ and from outside institutions. It was foreseen from the beginning of the mission to also validate the GPS based baselines via SLR. As SLR data are sparse in time and space, they may not be used in operational baseline generation. However as the SLR technique may provide range measurements with millimeter accuracy, they may advantageously be used for validation of the GPS based baseline. With the newly developed interleaving technique at Herstmonceux, a method to range to both satellites by switching from one to the next without loss of time, and in use also at Potsdam, a means of measuring the differential motion of the two satellites is available. The data of the two stations are analyzed and results and conclusions with view on baseline validation are given.

## 1. Introduction

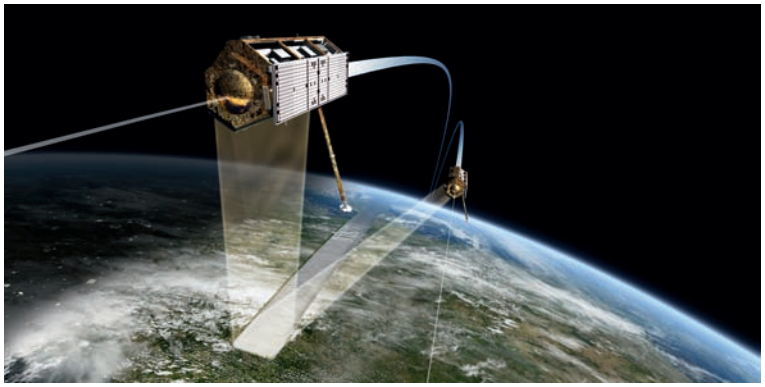

**Figure 1: TanDEM-X artist's view (courtesy DLR)**

The TanDEM-X (**T**erraSAR-X **a**dd-o**n** for **D**igital **E**levation **M**easurement) mission (Fig. 1, Krieger et al., 2007) is based on two nearly identical satellites, TerraSAR-X (TSX) and TanDEM-X (TDX). TSX was launched on June 15, 2007, TDX on June 21, 2010. Since then both satellites are flying in a close formation forming a Synthetic Aperture Radar (SAR) interferometer in space in order to generate a global digital elevation model (DEM). Mission goal is to reach meter level DEM accuracies in height, for this the relative position between the two spacecrafts, the "baseline", has to be known with millimeter accuracy. The GFZ German Research Centre for Geosciences has supplied the geodetic grad, two-frequency Integrated GPS and Occultation receiver (IGOR, Rothacher et al., 2007) to both satellites. By these data, the baseline can be inferred with millimeter accuracy as was demonstrated for the GRACE mission firstly by Kroes et al., 2005 and independently by Jaeggi et al., 2007.

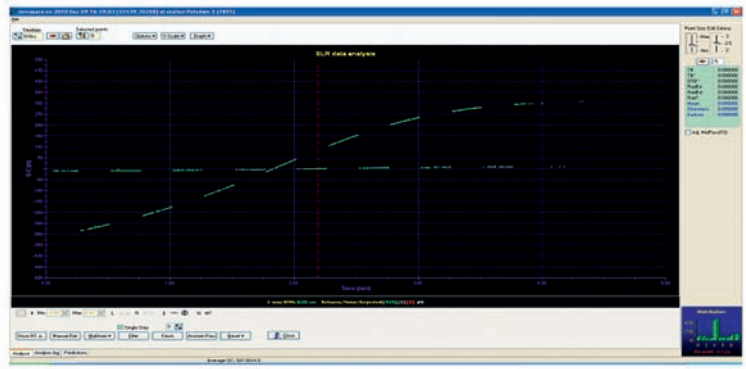

**Figure 2: Screen shot of ranging residuals in the inter-leaving mode**

Within the TanDEM-X mission ground segment the baseline is operationally generated from the IGOR data only. Also in this case the baselines are determined with millimeter accuracies as can be concluded from comparing independent solutions and from calibrating the baselines via SAR data takes over well known test sites.

Satellite Laser Ranging (SLR) data would be too sparse in time and space for the operational generation of baselines. However as the SLR data potentially can

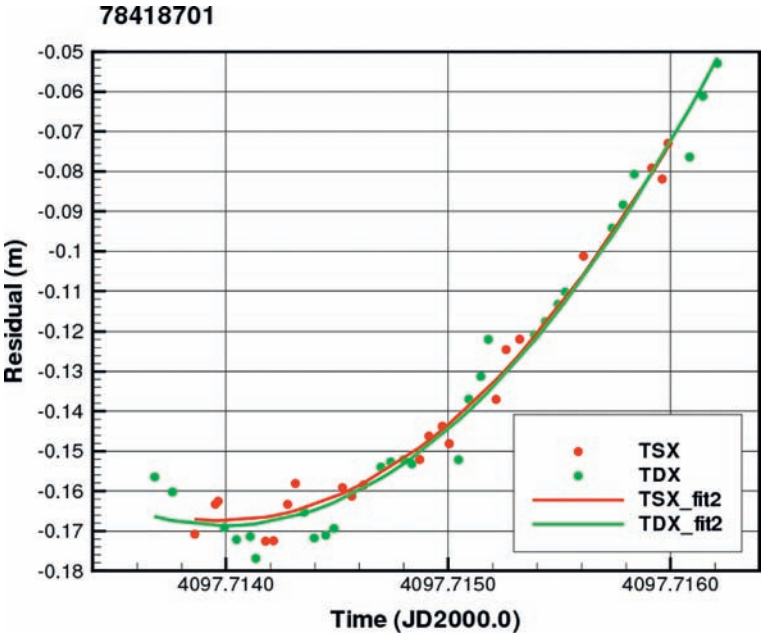


**Figure 3: Degree 2 polynomials for one pass over Potsdam**

provide millimeter level ranging accuracy, they could be adopted to validate the GPS only based baseline. In particular the interleaving tracking technique invented recently in Herstmonceux by Gibbs, 2010, supports this idea. The interleaving technique allows to track both satellites with seamless switching between TSX and TDX within one pass (see Fig. 2).

In the following we analyze SLR interleaving data gathered at Herstmonceux and Potsdam, where this technique was implemented as well, over a recent four months period. From the results we can draw some first conclusions.

# 2. Analysis

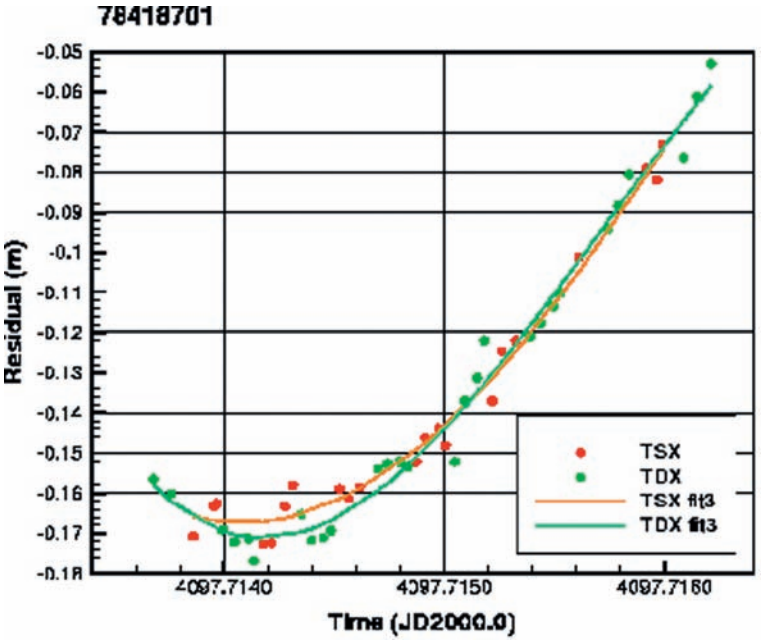


**Figure 4: Degree 3 polynomials for one pass over Potsdam**

In order to check the potential accuracy of recent Herstmonceux and Potsdam ranging data to TSX and TDX, residuals from Precise Orbit Determinations (POD) with GFZ's Earth Parameter and Orbit System – Orbit Computation (EPOS-OC) software (for features of the software see Zhu et al. 2004) are analyzed. POD methods and achievable orbit accuracies for Low Earth Orbiters (LEO) are discussed e.g. in Michalak and Koenig, 2010. For TSX and TDX EPOS-OC delivers orbits with accuracies of a few centimeters. From these PODs, the residuals are taken for all interleaving passes observed by Herstmonceux and Potsdam in the period January to April 2011. Due to imperfect modeling in the dynamic POD approach used, some systematics remain in the residuals that behave smooth to a large extent and can be modeled pass-wise by simple polynomials of low degree. In order to assess the impact of the degree of the polygon, Fig. 3 depicts a degree two polynomial fit to the residuals of either TSX or either TDX for one pass over Potsdam. For TSX the fit is 4.4 mm for TDX the fit is 6.2 mm. Fig. 4 shows the degree three polynomial fits for the same constellation, for TSX the fit is 4.4 mm, for TDX the fit is 4.9 mm, a slightly better performance for TDX. This behavior is observed in few more numbers of cases, so for the further analyzes the degree of the polynomial fit is restricted to three. Fig. 5 completes the resume thus far by a view on a degree three polynamial fit for one pass of range residuals by Herstmonceux. For TSX the fit is 2.8 mm, for TDX 3.1 mm.

A graphics displaying all degree three polynomial fits of all interleaving passes tracked by Herstmonceux and Potsdam in the analysis period is given in Fig. 6. The overall fit for Herstmonceux amounts to 3.3 mm inferred from 81 passes, for Potsdam the fit results little worse with 5.6 mm inferred from 66 passes.

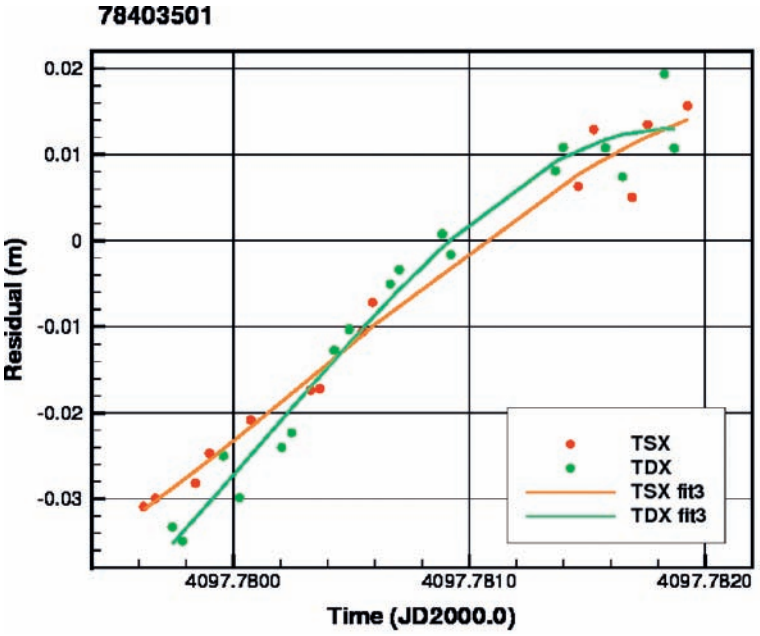


**Figure 5: Degree 3 polynomials for one pass over Herstmonceux**

# 3. Conclusions

Within the TanDEM-X ground segment precise baselines are generated from the onboard IGOR data with millimeter accuracies. This is validated by comparisons of independent solutions and via SAR calibration over known test areas. The SLR interleaving technique implemented at Herstmonceux and Potsdam offers differential ranging to both satellites. If millimeter accuracies of the ranges would be available, SLR could validate the GPS based baselines. As however the accuracies of the analyzed SLR data is still at the few millimeter range as shown, the SLR system need to enhance their accuracy to the sub-millimeter region which is probably achievable once they migrate to kHz or few-kHz systems. The impact of the geometry has not been considered here and is going to be analyzed next.

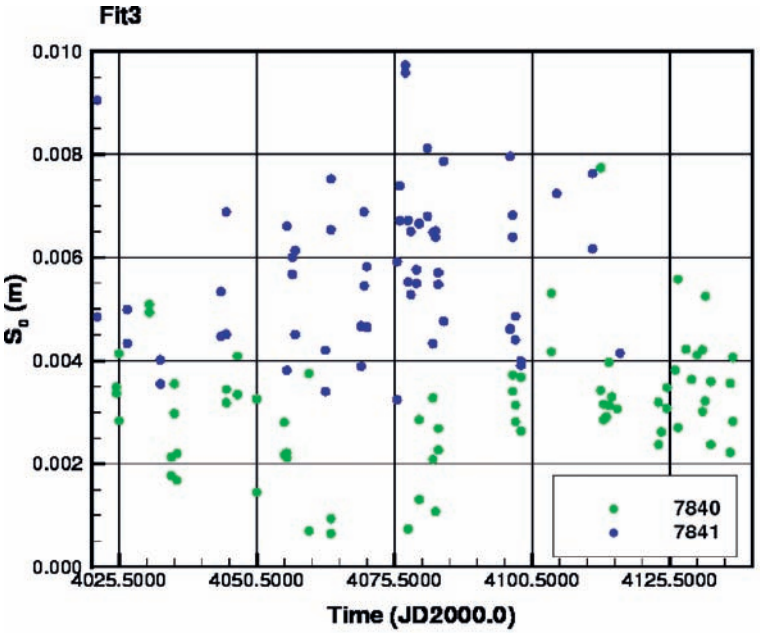


**Figure 6: Degree 3 polynomial fits for all passes over Herstmonceux and Potsdam**

## References

*Gibbs*, P. 2010: Tracking TerrasarX and TandemX, SLR Electronic Mail, No. 1927, ftp://cddis.gsfc.nasa.gov

*Kroes, R., Montenbruck, O., Bertiger,W., Visser, P.N.A.M.* 2005: Precise GRACE baseline determination using GPS, GPS Solutions, 9(1), 21-31, doi:10.1007/s10291-004-0123-5

*Jaeggi, A., Hugentobler, U., Bock, H., et al.* 2007: Precise orbit determination for GRACE using undifferenced or doubly differenced GPS data. Adv. Space Res., 39(10), 1612-1619, doi: 10.1016/j.asr.2007.03.012

*Michalak, G., Koenig, R.* 2010: Improvements for the CHAMP and GRACE Observation Model, in: Flechtner, F., Gruber, T., Guentner, A., Mandea, M., Rothacher, M., Schoene, T., Wickert, J. (Eds.), System Earth via Geodetic-Geophysical Space Techniques, Springer, 29-39, doi: 10.1007/978-3-642-10228-8

*Krieger, G., Moreira, A., Fiedler, H., et al.* 2007: TanDEM-X: a satellite formation for high-resolution SAR interferometry, IEEE Transactions on Geoscience and Remote Sensing, 45(11), 3317-3341, doi: 10.1109/TGRS.2007.900693

*Rothacher, M., Tapley, B.D., Reigber, C., et al.* 2007: The Tracking, Occultation and Ranging (TOR) Instrument onboard TerraSAR-X and on TanDEM-X, IEEE International Geoscience and Remote Sensing Symposium (IGARSS), 4983-4986, doi: 10.1109/IGARSS.2007.4423980

*Zhu, S., Reigber, C., Koenig, R.* 2004: Integrated adjustment of CHAMP, GRACE, and GPS data, Journal of Geodesy, 78(1-2), 103-108, doi: 10.1007/s00190-004-0379-0

## Correspondence

Dr. Rolf Koenig
GFZ German Research Centre for Geosciences
c/o DLR Oberpfaffenhofen
82234 Wessling
GERMAN

koenigr@gfz-potsdam.de

# The Global Geodetic Observing System: Space Geodesy Networks for the Future

*Michael Pearlman (Harvard-Smithsonian Center for Astrophysics, Cambridge MA, USA)*
*Erricos Pavlis (University of Maryland, Baltimore MD, USA)*
*Chopo Ma (NASA GSFC, Greenbelt MD, USA)*
*Zuheir Altamini (Institut Geographique National, Champs-sur-Marne, France)*
*Carey Noll (NASA GSFC, Greenbelt MD, USA)*
*David Stowers (Jet Propulsion Laboratory, Pasadena CA, USA)*

ABSTRACT
Ground-based networks of co-located space geodetic techniques (VLBI, SLR, GNSS, and DORIS) are the basis for the development and maintenance of the International Terrestrial Reference Frame (ITRF), which is our metric of reference for measurements of global change. The Global Geodetic Observing System (GGOS) of the International Association of Geodesy (IAG) has established a task to develop a strategy to design, integrate and maintain the fundamental geodetic network and supporting infrastructure in a sustainable way to satisfy the long-term requirements for the reference frame. The GGOS goal is an origin definition at 1 mm or better and a temporal stability on the order of 0.1 mm/y, with similar numbers for the scale and orientation components. These goals are based on scientific requirements to address sea level rise with confidence, but other applications are not far behind. Recent studies including one by the US National Research Council has strongly stated the need and the urgency for the fundamental space geodesy network. Simulations are underway to examining accuracies for origin, scale and orientation of the resulting ITRF based on various network designs and system performance to determine the optimal global network to achieve this goal. To date these simulations indicate that 24 – 32 co-located stations are adequate to define the reference frame and a more dense GNSS and DORIS network will be required to distribute the reference frame to users anywhere on Earth. Stations in the new global network will require geologically stable sites with good weather, established infrastructure, and local support and personnel. GGOS will seek groups that are interested in participation. GGOS intends to issues a Call for Participation of groups that would like to contribute in the network implementation and operation. Some examples of integrated stations currently in operation or under development will be presented. We will examine necessary conditions and challenges in designing a co-location station.

## 1. Introduction

Ground-based networks of co-located space geodetic techniques (VLBI, SLR, GNSS, and DORIS) are the basis for the development and maintenance of the International Terrestrial Reference Frame (ITRF), which is our metric of reference for measurements of global change. These networks provide measurements of static and time-varying components of the Earth's gravity field; precision orbit determination, calibration, and validation for active satellites systems for altimetry; and time transfer and determination of fundamental constants. Data from these networks provide Earth Orientation Parameters, time history of ground station positions and baseline length, strain models, mean sea level and ocean surface topography, marine tide models, atmospheric and ionospheric parameters.

## 2. GGOS and the Geodetic Reference Frame

The Global Geodetic Observing System (GGOS) of the International Association of Geodesy (IAG) has established a task to develop a strategy to design, integrate and maintain the fundamental geodetic network and supporting infrastructure in a sustainable way to satisfy the long-term requirements for the reference frame. The GGOS goal is an origin definition at 1 mm or better and a temporal stability on the order of 0.1 mm/y, with similar numbers for the scale and orientation components. These goals are based on scientific requirements to address sea level rise with confidence, but other applications are not far behind. Recent studies including one by the U.S. National Research Council (see Figure 1) have strongly stated the need and the urgency for the fundamental space geodesy network. The needs are articulated

in more detail on *The Global Geodetic Observing System: Meeting the requirements of a global society on a changing planet in 2020 (Plag, H-P and Pearlman, M.R., 2009)*. These levels of accuracy and precision are about a factor of 15 - 20 better than the current reference frame models and represent significant challenge in both measurement and modeling techniques.

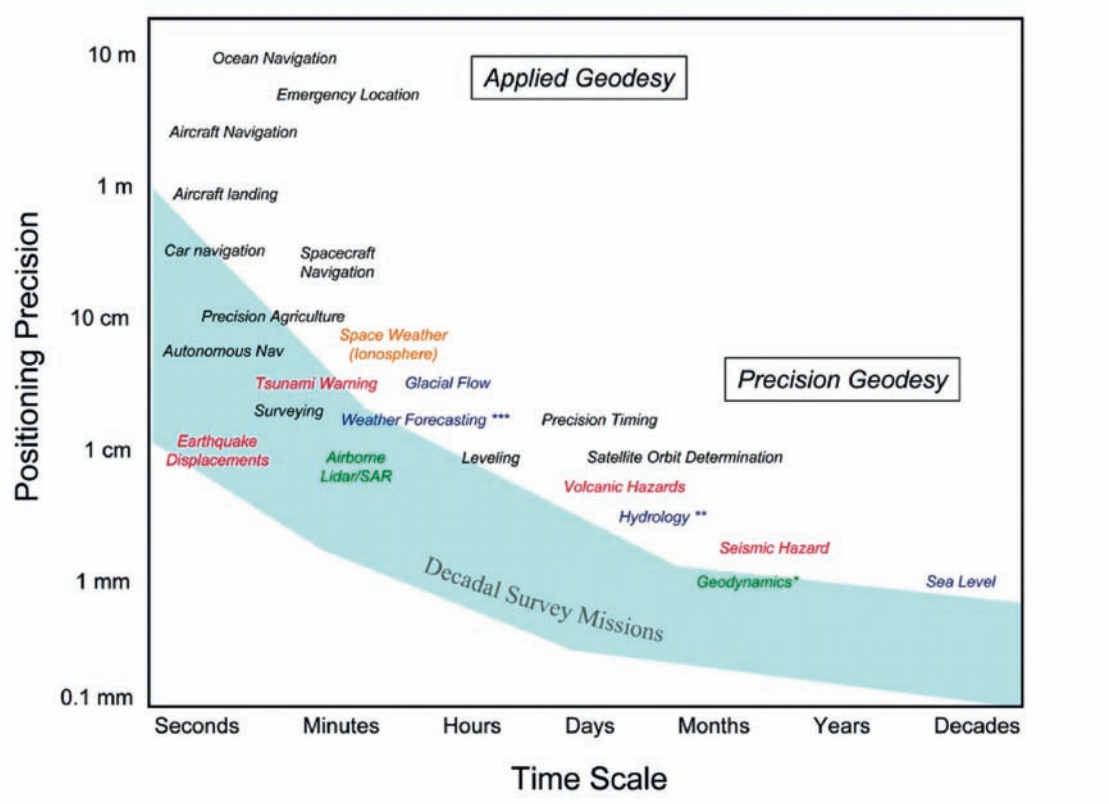


**Figure 1: Positioning precision requirements**

# 3. The Fundamental Station

The reference frame is defined through a global network of co-located VLBI, SLR, GNSS and DORIS Fundamental Stations and a more dense network of GNSS and DORIS ground stations will be required distribute the reference frame globally to the users so that geophysical measurements anywhere in the world can be positioned in the frame any time of day. The four techniques measure different quantities in different ways and each has a different set of systematic errors. Proper combination allows us to take advantage of the strengths and mitigate the weaknesses of each. The techniques are co-located so that the measurements among them can be related to sub-mm accuracy. These sites will also have ancillary measurement including absolute and cryogenic gravimeters, tide gauges, seismometers, etc, to connect other geophysical measurements to the reference frame (see Figure 2).

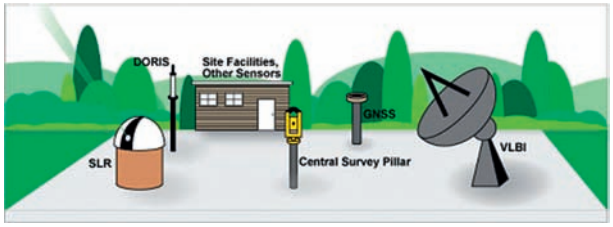


**Figure 2: Schematic of a fundamental station**

The first version of a Site Requirements for a GGOS Fundamental Station has been written, and is available at *http://cddis.gsfc.nasa.gov/docs/GGOSSiteRequirements_v1.pdf*. The document includes the justification for a Fundamental Site and desirable site conditions. It is recognized that not all sites will meet all conditions, so some trade-offs will be necessary.

# 4. Network Simulations

Simulations have been conducted by E. Pavlis to examine accuracies for origin, scale and orientation of the resulting ITRF based on various network designs and system performance to determine the optimal global network to achieve this goal. These simulations show that about 30 co-located stations, with modern technology, will be adequate to define the reference frame. Stations in the new global network will require geologically stable sites with good weather, established infrastructure, and local support and personnel.

Today nearly all SLR and VLBI stations have GNSS and some have DORIS. SLR and VLBI are the most costly systems at Fundamental Stations, so co-location of these techniques is the largest undertaking. There are presently eight stations with co-located SLR and VLBI and several more are in the process of being built or are planned, as shown in Figure 3. The co-location network is building, but there will still be significant shortfalls on numbers and geographic coverage.

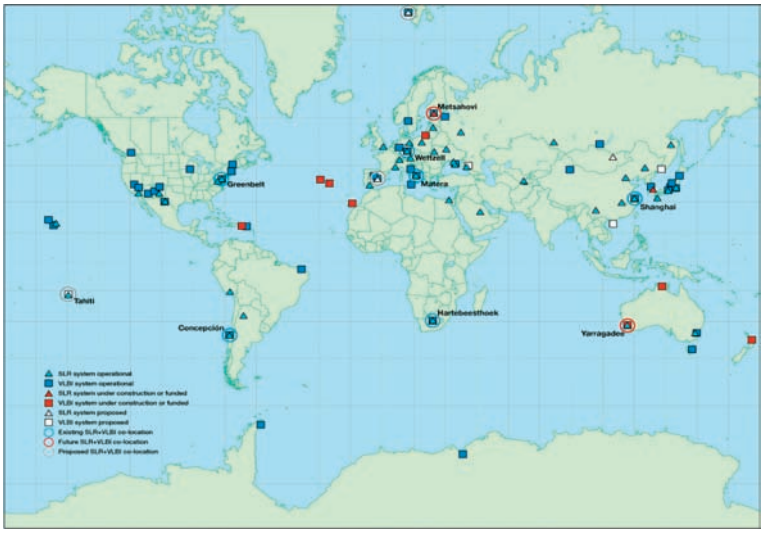


**Figure 3: Map of SLR and VLBI stations with Co-Locations highlighted**

An essential aspect to co-location are the intersystem vectors that must be determined to sub-mm accuracy in order to place the measurements from the separate systems in the same reference frame. Baselines between closely located, accessible geodetic markers can be measured to sub-mm accuracy with modern instruments, but the necessary extrapolation to system reference points (intersection of the axes, antenna phase centers, etc) which are not readily accessible is the real challenge. This requires fairly elaborate measurement and extrapolation procedures to estimate the reference points, which limits the overall accuracy and in many cases, is a limiting factor in the overall reference frame itself. Approaches continue to be refined and one recent proposed methodology is to use a multi-technique, well-calibrated satellite to determine the co-located intersystem vectors from space.

# 5. System Upgrades

All of the space geodetic techniques are in the process of upgrading their technologies. SLR has several systems working at higher repetition rates (100Hz – kHz), new fast detection, and automated control systems with the resulting increased data yield, data quality and daylight ranging. Considerable progress is being made on the placement of retroreflector arrays on GNSS satellites. The VLBI2010 prototype with its new front and back ends providing substantially increased observation and recording bandwidth is deployed at several stations, including the new stations at in Tasmania, Katherine, and Yarragadee.

GNSS performance is improving with additional frequencies and new constellations. The DORIS network is already nearly at its planned global distribution and will benefit from additional satellites schedule for launch and from new beacons now being deployed.

# 6. NASA's Space Geodesy Project

As a part of the GGOS Network, NASA has undertaken a program to provide its contribution to a worldwide network of modern space geodesy fundamental stations. The first phase of a proposal has been funded for a 2-year activity to:

- Complete network simulations to scope the network and examine geographic, operational and technical tradeoffs based on LAGEOS and GNSS tracking with SLR;
- Complete the prototype SLR (NGSLR) and VLBI (VLBI2010) instruments;
- Co-locate these instruments with the newest generation GNSS and DORIS ground stations at GSFC;
- Implement a modern survey system to measure inter-technique vectors for co-location;
- Develop generalized station layout considering RFI and operations constraints;
- Undertake supporting data analysis;
- Begin site evaluation for network station deployment;
- Develop a full network implementation plan for a follow-on phase for deployment for up to 10 stations

## Correspondence

Michael Pearlman
Harvard-Smithsonian Center for Astrophysics
60 Garden Street
Cambridge MA 02138
USA

mpearlman@cfa.harvard.edu

# Session 2:
# Operations: Spatial and Temporal Coverage

# Statistical Analysis in 20xx

*Horst Müller*

ABSTRACT
This paper deals with the statistic of SLR tracking since 2000, trying to see if there are changes in data quantity and quality which can influence the results for station coordinates and velocities and the definition of the origin and scale of the ITRF. We also had a look into the distribution of tracking data between northern and southern hemisphere, day and night, and identified a weekend effect. An other aspect were the quality of the new Khz systems. For our analysis we used the statistical information available at the ILRS Web-pages and results from the processing of SLR tracking data to the Lageos and Etalon satellites at DGFI.

## 1. Introduction

In the last years the quality of SLR tracking has slightly improved. Since 2001 the mean orbit adjustment of the weekly arcs in the DGFI SLR solutions is below 5 mm for the core sites and for all stations around 1 cm, see figure 1. The slight degradation since 2007 comes from new sites with still no good coordinates. But the station network has changed with time as well as the data quantity is not constant over this period.

This paper shows the development of SLR tracking since 2000 and some aspects of data distribution and balance which may influence the SLR results for station velocities and the definition of the origin of the network. The graphics are copied from the ILRS Web-pages (ilrs.gsfc.nasa.gov) or generated from analysis results at DGFI.

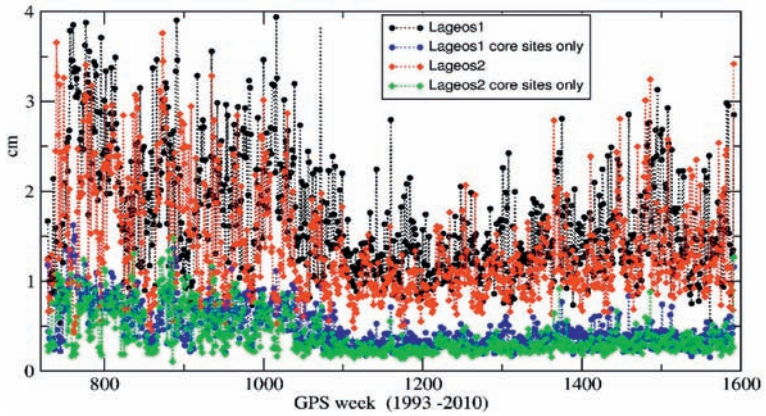


**Figure 1: Mean weekly orbital fit of the DGFI SLR solutions in cm for Lageos1 and Lageos2 in cm from 1993 to 2010, for all stations and the core stations only.**

## 2. Spatial and Temporal Distribution

Presently SLR stations have a good tracking record to all satellites equipped with retro reflectors. An overview on the recently tracked passes can be found on http://ilrs.gsfc.nasa.gov/stations/recent_groundtrack.html. The spatial distribution is very good with the known gaps over the oceans, Africa and parts of Asia. But most passes are from Ajisai, an easy target, whereas the Etalon passes are sparse. The statistic on the last years tracking to all satellites can also be found on the ILRS Web-pages, in section: stations/site info/global_report_cards. Figure 1 shows the temporal distribution for

the Lageos and Etalon satellites, with some distortions since the individual points shown in the graphic are too large. It can be seen that the coverage of the Lageos arcs are quite good whereas the Etalon arcs are sparsely covered. For a single day this can only be 3 4 normal points for one of the Etalon satellites. For the last two years the mean number of observations for a weekly arc are 1540 for Lageos1, 1420 for Lageos2, 180 for Etalon1 and 160 for Etalon2 which is in the case of the Etalons not enough to compute a stable orbit and solving for parameters.

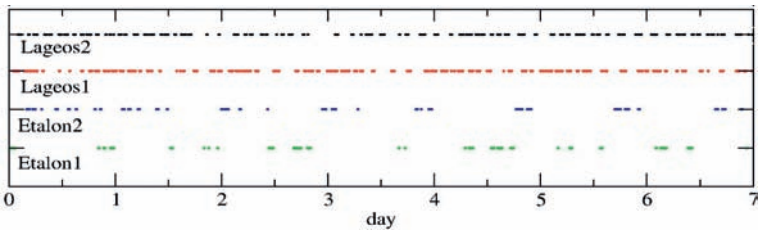


**Figure 2: temporal distribution for a weekly arc, for presently used satellites**

# 3. History and Balance of SLR tracking since 2000

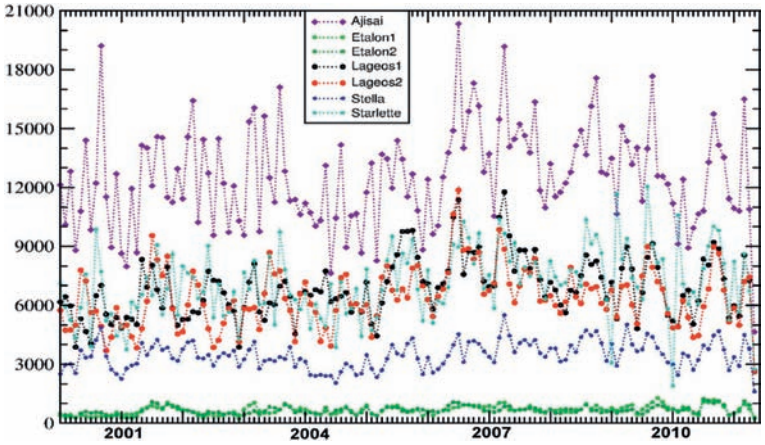


**Figure 3: Number of SLR observations per month, sorted by satellite**

Since 2001 the number of observing stations is nearly constant though there were some changes of stations. Most stations track all geodetic satellites, but some have problems tracking the Etalons. The highest number of normal points are from Ajisai, an easy target, whereas Stella and especially Etalon1/2 are sparsely tracked, see figure 3. For the number of tracked passes the figure is similar only the dominance of Ajisai is not as visible, because of the shorter bin width. The total number of tracking sites per month show only small variations, though some new stations had been installed but older stations were shut down.

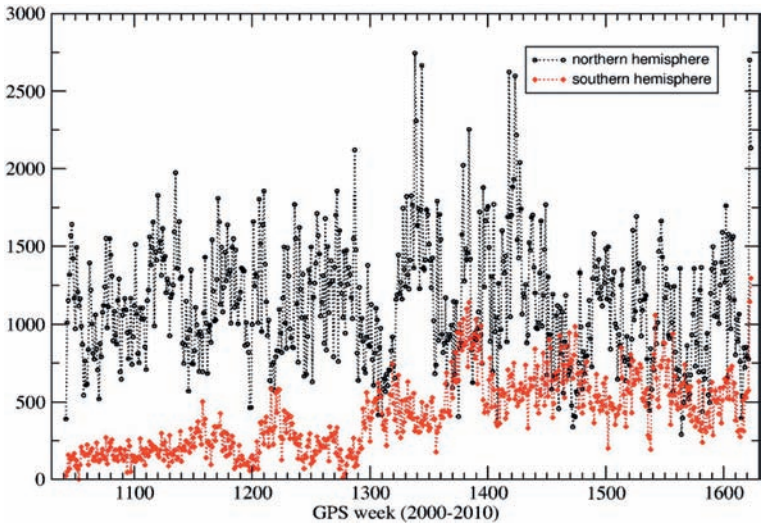


**Figure 4: Number of observations from nothern and southern hemisphere for weekly Lageos1 arcs**

To examine the balance of tracking data between northern and southern hemisphere we computed for both hemispheres the number of observations per week, see figure 4. The number of observations for the nothern hemisphere is nearly constant over the whereas the southern hemisphere contributes more in the last years with only 6 tracking stations compared to up to 24 from the northern part.

The distribution along the x- and y-axes of the pole has more stations along the x-direction but the number of observations are nearly the same.

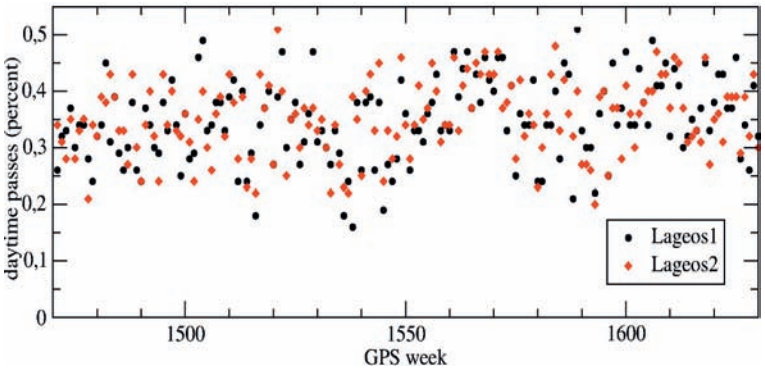


**Figure 5: Percentage of day time passes**

The distribution between day and night is another aspect of good orbit coverage and with a good value of around 40 % daytime passes it is constant for the last years, see figure 5. The situation is different for Etalon1/2 with only a few day time passes but similar for Lageos2, Starlette, Stella and Ajisai.

A clear weekend effect can be seen in the data records. Table1 shows the observations sorted by day of the week from mid 2008 to mid 2011 for the Lageos and Etalon satellites. There are significantly less observations on Saturdays and Sundays. For Etalon is a peak of the observations on Tuesday and very few on Sunday, which we cannot yet explain. From the aspect of orbit computation this situation is not optimal because the standard SLR orbits which were used for the ITRF computations were calculated from Sunday to Saturday, a full GPS week, so that the borders of the arcs have fewer observations then the other days.

| | Lageos1/2 | Etalon1/2 |
|---|---|---|
| Sunday | 57970 | 14662 |
| Monday | 71540 | 16541 |
| Tuesday | 78560 | 27326 |
| Wednesday | 77867 | 16055 |
| Thursday | 74395 | 18977 |
| Friday | 72067 | 11453 |
| Saturday | 60195 | 5058 |

**Table 1: Observation sorted by weekday (June 2008 to May 2011)**

# 4. Quality Aspects of Khz systems

To see the effect of the new Khz systems we examined the system at Graz (7839) which was the first tracking station with a Khz laser in October 2003. Although the number of observations per normal point and hence the accuracy has increased, see figure 6, we could not find an improvement in the orbital fit for that station. This is an indication that the system was always a good tracking site and that remaining systematic errors are dom-inant. The history of the r.m.s. Orbit fit for the Graz station is given in figure 7. It shows small variations and some outliers up to 1.5 cm. But in general the accuracy is around 5 mm and is similar for Lageos1 and Lageos2.

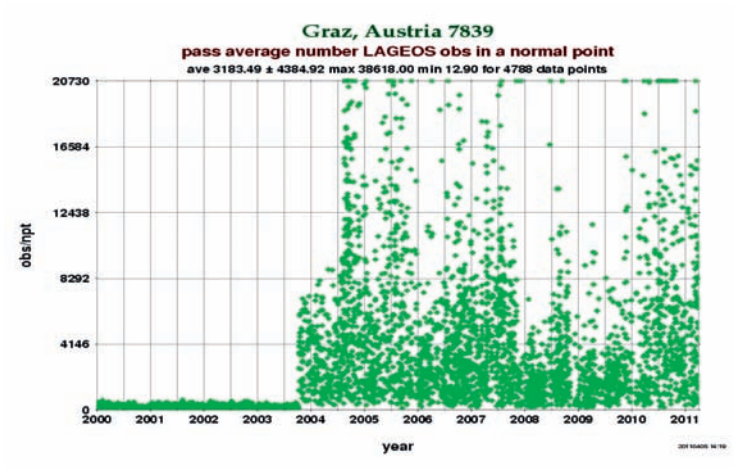


**Figure 6: Pass avarage Lageos obs per normal point, Graz (7839). (from http://ilrs.gsfc.nasa.gov)**

The same situation applies to all other new Khz systems. We did not see differnces between the 10 Hz and the Khz tracking for these sites and the system of Yarragadee (7090) has the same quality as the new Khz systems. But with the recently developed better center of mass correction models this can change.

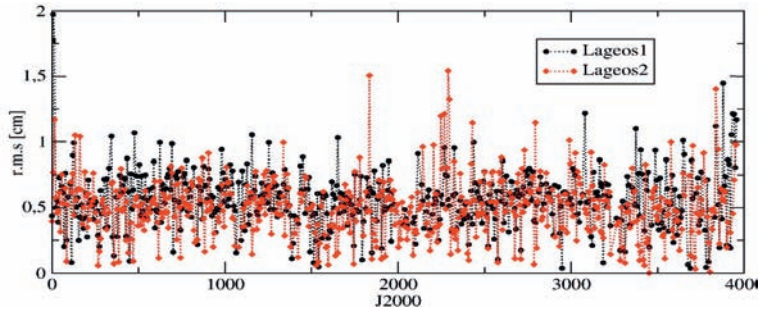


**Figure 7: Graz (7839) r.m.s. orbital fit for weekly Lageos1 and Lageos2 arcs in cm (2000-2011)**

# 5. Conclusion

The quality of SLR tracking has reached the sub-centimeter level, with a clear improvement since 2001. To verify these results we looked into the data and results since 2000 to see if there are improvements in the data quality or distribution. Since 2000 the number of tracking stations and normal points are constant with seasonal variations. The ratio of day vs. night time passes is constant over the time, which gives a good coverage of the Lageos arcs in contrast to the Etalon arcs, which need more tracking. A clear weekend effect can be seen in the tracking records. Since 2006 the 6 southern hemisphere stations contribute nearly as much as the northern hemisphere stations.

The present situation of SLR is quite good, concerning Lageos1/2, Starlette and especially Ajisai, but the tracking of Etalon could be improved. Since Lageos1/2 and Etalon1/2 are the only satellites used for the present official ILRS product, earth ori-entation parameters and weekly station coordinates, an intensified Etalon1/2 tracking could help to improve the product.

## Acknowledgements

I thank CDDIS and the ILRS Central Bureau for maintaining the ILRS Web-pages, Mark Torrence for the good graphics design and the SLR community for the excellent tracking.

## References

*Pearlman, M.R., Degnan, J.J., and Bosworth, J.M* , **"The International Laser Ranging Service"**, Advances in Space Research, Vol. 30, No. 2, pp. 135-143, July 2002.

## Correspondence

Horst Müller
Deutsches Geodätisches Forschungsinstitut,
Alfons-Goppel-Str. 11
D-80539 München, Germany

mueller@dgfi,badw.de

# Current situation and future of cooperative San Juan SLR station between China-Argentina

*Liu Weidong, Wang Hongqi, Han Yanben,Yin Zhiqiang, Tian Lili, Wang Zheng, Zhao You, Li Jinzeng, Huang Dongping, Wang Rui*
*(National Astronomical Observatories Chinese Academy of Sciences, Beijing, China);*
*R.Podesta, A. Pacheco, A.Ester, E. Actis*
*(Astronomical Observatory Felix Aguilar National University of San Juan, Argentina)*

ABSTRACT
San Juan 7406 SLR station is operated by the National Astronomical Observatories of Chinese Academy of Sciences (NAOC) and the Observatorio Astronomico Felix Aguilar (OAFA) of National University of San Juan of Argentina. Now, San Juan SLR station has obtained excellent results and become an important station in ILRS network, especially in the southern hemisphere. Our SLR team is carrying out the upgrade project on the SLR system. We hope that the SLR system can implement daylight tracking and kHz operating, also improve the precision of observations. A new project of ~ 40-meter radio telescope started to be performed in the beginning of this year, the station will fulfill collocated measurements with multiple techniques in the future.

## 1. Introduction

San Juan 7406 SLR station is operated by the National Astronomical Observatories of Chinese Academy of Sciences (NAOC) and the Observatorio Astronomico Felix Aguilar (OAFA) of National University of San Juan (UNSJ) of Argentina. The SLR station began to operate in the end of February of 2006. Due to the colleagues of the SLR team hard works and the lot of clear nights in San Juan region, San Juan SLR station obtained excellent results in the past years. At present, we are updating the SLR system on daytime tracking and kHz laser. In this year, a new collaboration project about ~ 40-meter radio telescope between NAOC and UNSJ just begin to carry out both astrometric and astrophysics works in the future. San Juan station will become a comprehensive station include multiple techniques such as SLR, GPS and VLBI.

## 2. Progress of Upgrading works

KHz repetition Satellite Laser Ranging with the advantages of fast target acquisition, large amount of returns, high measuring accuracy and high normal point data density, has become the trend of international laser ranging technology. In the end of 2009, we started upgrading work of kHz and daylight tracking in order to improve the precision of observations and obtain more high-quality data for the ILRS. The scheme design of the system upgrading was completed in early 2010. In the year, a company in China started to make a new kHz laser for the SLR system. We emphasize maintainability of the laser, set up multiple test points in the laser, and request easy replacement of devices. The main peremeters of the new Laser are exhibited in Table 1. Now, the design of photoelectric conversion receiver has finished. The upgrades of control and operating system are developed by the cooperation between NAOC and Changchun Station in 2011. An A033-ET event timer will be used for kHz operations, the Start and C-SPAD Stop Pulse adopt a set of the Pulse Distribution Module (design by Graz Station) and their output NIM logic Pulse is for A033-ET, to utilize a set of pco.1600 camera for night and daylight tracking, a set of steel grating encoders instead of old AZ-EL inductosyns. The system integration and test is being done via the cooperation with Changchun and Beijing stations. First trial observation of the laser was carried out during March, 2011. Observations of LARETS satellite showed the r.m.s is 25.8mm, the r.m.s of target is about 7mm (see figure 1). But serious multi-pulse phenomena appeared in the first time laser testing.

**Table 1: Specification of the new laser**

| | | | |
|---|---|---|---|
| wavelength | 532 nm | divergency | 1 mrad |
| frequency | 500Hz-1KHz | diameter of beam | 2 mm |
| pulse energy | 2.5 mJ at 1kHz | polarization | horizontal |
| pulse to pulse instability | 2% RMS (8 hours) | beam point instability | <50 urad |
| pulse width | <15 PS | operating temperature | 15-30 $^{o}$C |

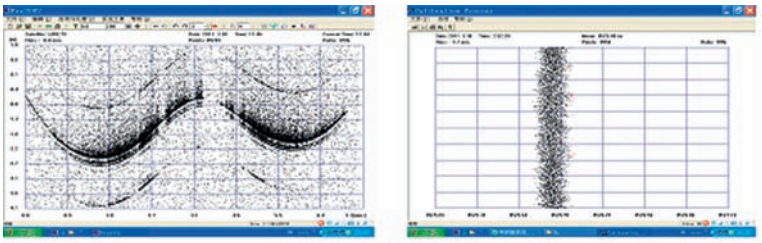

**Figure 1: Laser testing (first time, at Changchun SLR Station)**

The second time laser testing was carried out at Beijing SLR Station. We adjusted electro-optic switch to filter multi-pulse, replaced KTP with LBO (frequency doubling crystal), reduced the divergence angle to about 0.5mrad. The r.m.s is about 10-20 mm on the LEO satellites observations and target accuracy (r.m.s) is about 5-6 mm with diffuse surface target (see figure 2). The subsequent laser testing is carried out at Changchun SLR Station still. After completion of the preparation, the equipments will be delivered to San Juan Station and the upgrading will be completed in 2012.

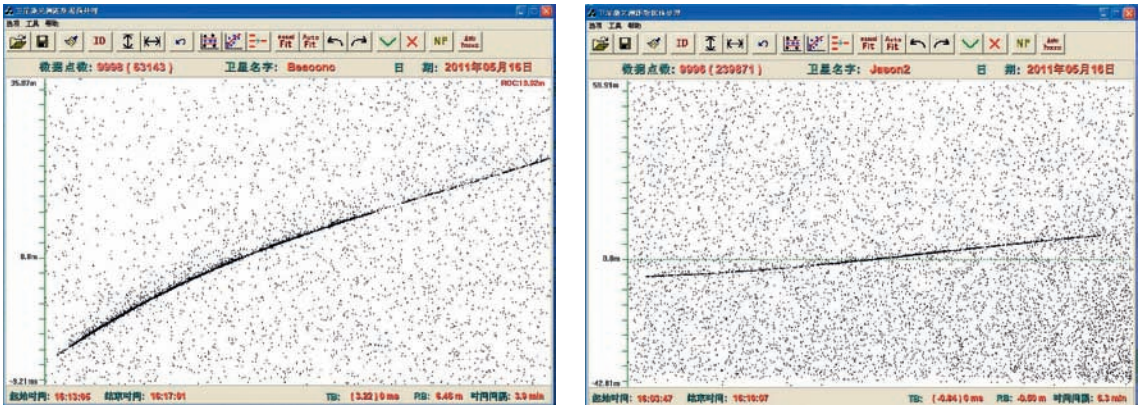

**Figure 2: Laser testing (second time, at Beijing SLR Station)**

# 3. Observation status in 2009-2010

Observations of Sun Juan SLR system were kept the good status in 2009. However the SLR station met some problems in 2010. Examine and maintenance of the power supply of the observatory led to a halt of observation in one month and more, a variety of equipment failure began to appear, the supply of dichloroethane encountered a serious problem. We also met bad weather in San Juan in the whole 2010. All of these caused significant reduction of observational days. The equipment failures of the SLR have been solved in 2011 and its operation is normal now.

# 4. Future Development of San Juan Station

The SLR system in San Juan will realize routine observation of kHz and daylight tracking in 2012. In the end of 2010, the 40-meter radio telescope cooperative project (VLBI) between NAOC and UNSJ has been approved by the both sides. We hope that the station will have GPS and VLBI collocated with the SLR system in coming years.

## Acknowledgements

This work was supported by the Foundation of International Science and Technology Cooperation (2009DFB00130, 2010DFB53100), the External Cooperation Program of the Chinese Academy of Sciences (GJHZ200813).

## Correspondence

Liu Weidong
National Astronomical Observatories, Chinese Academy of Sciences
20A Datun Road, Chaoyang District,
Beijing, 100012
China

wdliu@nao.cas.cn

# Hazards and Risk@SLR Network
# A Preliminary Overview

*Jorge R. del Pino* *

ABSTRACT
Risk/emergency management has become a useful tool for complex, globally distributed organizations as the ILRS. The basic concepts are introduced, and a set of case examples of the most common hazards and vulnerabilities, in particular the seismic hazard, that could affect the SLR Network is presented. Several general recommendations are proposed.
Keywords: SLR, hazard, vulnerability, risk, disaster, mitigation, seismic microzoning.

## 1. Introduction

Risk/emergency management has become a useful management tool for any complex economical/scientific system. The ILRS, with a globally distributed system, comprising four basic components (SLR stations, Analysis Centers, Communication Network and the human component -SLR community-) can benefit from its application. This will result not only in the reduction of long term costs, by minimizing the losses due to natural/manmade disasters, but also by guaranteeing the operation of stations during critical situations of high scientific values affecting them, e.g. in case of very strong earthquakes.

The basic concepts of

**Hazard:** a situation that poses a level of threat to life, health, property or environment
**Vulnerability:** the extent to which changes could harm a system or be affected by the impact of a hazard
**Risk:** the potential that an action or activity will lead to a loss or negative outcome
**Disaster:** when the risk is realized

are used to identify the hazards affecting the system, the vulnerabilities present and the possible disaster outcomes in order to create a **mitigation** program to reduce the possible risks. This is an important part of the standard **emergency management** procedure.

## 2. Hazards

The hazards have been classified into five principal categories: geological, hydrological, climatic & atmospheric, wildfire and anthropogenic. Not all hazards are of interest to the SLR Network either globally or to individual stations in particular. This preliminary overview was focused on several of the most typical hazards affecting some components of the ILRS system: human factor (SLR community), lifelines and SLR stations (buildings, equipment and operation).

### 2.1. Hazards, Vulnerabilities & Risks, Case Studies

The **human factor** (SLR community): the risk of losing part of the SLR community historical memory and/or a reduced amount of knowledge transfer to the next SLR generation is a possibility, due to retirement or death of the community first generation.

**Lifelines:** Defined as the essential infrastructures and supplies for the functioning of the society or a system, as: utilities, communication/transport and human organization factors (sheltering, security, law & order). The lifelines' vulnerability reduction at the SLR stations is of capital importance if the SLR stations are to be kept operational during and immediately after a disaster. This was demonstrated with the 2010 earthquake effects at 7405 Concepcion.

**SLR stations:** several hazards that could affect the buildings, equipment or the SLR operations are presented, with real examples when relevant:

## 2.2. Hurricanes/Typhoons.

The hurricane/typhoon hazard is a seasonally permanent one which is geographically localized. Based on the paths for all hurricanes/typhoons during the period 1945-2006, the highest at risk stations are in Japan, coastal China and the U.S. Eastern seacoast with a quite low impact on the Pacific basin stations. Because of the advanced hurricane path prognosis and by managing the vulnerabilities associated with strong wind/rain, this hazard impact can be minimized.

## 2.3. Fires

Two cases are presented: the Australian 2003 Mt. Stromlo fire, which partially destroyed the observatory including the SLR system, and the Texas's April 2011 Rockhouse Fire in which the McDonald Observatory survived intact, in a good part due to the excellent mitigation program "Firewise Community" started in 2004.

## 2.4. Lightning

This is a very common hazard which many SLR stations had already experienced, the typical station vulnerabilities related to this hazard are defective grounding and long antenna cables.

## 2.5. Computers/Internet.

The computer/internet is a key part of the SLR station operation and it is probably one in which its vulnerabilities are underestimated.

There are three basic vulnerabilities types:

**Hardware related** (old PC models lacking spares, component catastrophic failures)
**Software related failures** (as the lack/loss of software code know-how, viruses) and **the lack of secured copies** of the program codes and directory/data structure
**Loss of the internet connection** due to local/global problems, This latter vulnerability is an important one due to the short CPF lifetimes and the current lack of any emergency point-to-point backup communication procedures.

## 2.6. Earthquakes.

Up to early 2011, five SLR stations have reportedly been affected by earthquakes, and one of them (7405 Concepcion) was damaged by the 8.8 Maule Earthquake on February 27, 2010. Given the global SLR distribution, this is a permanent hazard that could affect a good part of the SLR network.

Because the local **seismic microzoning** - which is the standard seismic hazard evaluation method - was not available for all the stations and even if it was available to all SLR stations, it could use different methodologies. It was decided to use a **by proxy** homogeneous analysis by extracting from the USGS global catalogue all the potentially damaging strong earthquakes with magnitudes >6.5 occurring since January 1910. This proxy analysis gives an underestimation of the hazard situation as the data sampling is only 100 years, and the local geophysical parameters are not taken into consideration.

The two basic seismic microzoning parameters, the **maximum earthquake intensity** expected at the place (the "shake") and the **recurrence period** for the strongest earthquake expected (the "when"), were approximated by the closest/strongest earthquake and the number of earthquakes within a given radius for each SLR station.

According to the minimum distance to a strong earthquake, all SLR stations were classified into four hazard level categories:

| | | |
|---|---|---|
| Very low hazard | >1000 km. | (8 stations) |
| Low hazard | 1000~500 km. | (10 stations) |
| Medium hazard | 500~250 km. | (10 stations) |
| High (at risk) hazard | <250 km. | (15 stations) |

The relevant seismic parameters for the 15 “at risk” SLR stations are presented in Table 1.

| Station | Closest Earthquake | | | Strongest | | | # Radius | | | % time 2005-2010 |
|---|---|---|---|---|---|---|---|---|---|---|
| | m | Date | d Km. | m | Date | d Km. | 0-250 | 250-500 | 0-500 | |
| Arequipa | 7.3 | 1/15/1958 | 4 | 8.5 | 10/11/1939 | 150 | 13 | 21 | 34 | 1.21% |
| Tanegashima | 6.6 | 10/18/1996 | 7 | 8.0 | 2/1/1916 | 126 | 12 | 5 | 17 | 0.52% |
| Simosato | 8.3 | 12/7/1944 | 15 | 8.3 | 12/7/1944 | 15 | 16 | 37 | 53 | 1.13% |
| San Juan | 7.8 | 1/15/1944 | 16 | 7.8 | 1/15/1944 | 16 | 4 | 33 | 37 | 6.49% |
| Simeiz | 6.8 | 9/11/1927 | 27 | 6.8 | 9/11/1927 | 27 | 1 | 11 | 12 | 0.98% |
| Katzively | 6.8 | 9/11/1927 | 27 | 6.8 | 9/11/1927 | 27 | 1 | 11 | 12 | 1.59% |
| Concepcion | 6.6 | 3/5/2010 | 36 | 8.8 | 2/27/2010 | 81 | 18 | 18 | 36 | 3.27% |
| Koganei | 8.3 | 9/1/1923 | 46 | 8.3 | 9/1/1923 | 46 | 19 | 56 | 75 | 1.10% |
| Monument Peak | 6.7 | 11/24/1987 | 56 | 7.3 | 6/28/1992 | 145 | 10 | 2 | 12 | 3.29% |
| Kunming | 7.7 | 1/4/1970 | 93 | 7.7 | 1/4/1970 | 93 | 2 | 13 | 15 | 0.18% |
| Haleakala Maui | 6.7 | 10/15/2006 | 98 | 7.2 | 11/29/1975 | 200 | 4 | 0 | 4 | 1.65% |
| Matera | 6.5 | 11/23/1980 | 116 | 6.5 | 7/23/1930 | 121 | 2 | 15 | 17 | 4.01% |
| Beijing | 7.5 | 7/27/1976 | 179 | 7.6 | 3/22/1966 | 244 | 3 | 3 | 6 | 1.38% |
| Graz | 6.5 | 5/6/1976 | 187 | 6.5 | 5/6/1976 | 187 | 4 | 0 | 4 | 5.98% |
| San Fernando | 7.0 | 3/29/1954 | 248 | 7.0 | 3/29/1954 | 248 | 1 | 1 | 2 | 3.03% |

**Table 1: The relevant seismic parameters of the “at risk” SLR stations.**

The stations outlined had already reported in their log files a strong felt earthquake.
This group of stations generated 35.8% of the tracking time data during the 2005-2010 period.

It is possible to rank the hazard level of the “at risk” stations using a semiquantitative analysis. The 7 stations with highest hazard level are in descending order: Arequipa, Simosato, Koganei, Concepcion, San Juan, Tanegashima and Monument Peak. Even if this proxy analysis is done ending in December 2009 (so the recent earthquakes in Chile and Japan are not used), the station list remains the same.

The importance of the concurrent operation of an IGS GNSS station at the SLR station premises during a disaster should not be underestimated due to the much shorter station coordinates’ time resolution in comparison with the SLR systems and its reduced vulnerabilities with regard to power and communication needs. A good example for the high time resolution of the GPS during the latest strong earthquakes in Concepcion and Mizusawa is shown in the analysis carried out by Simon Banville at the University of New Brunswick (cf. Fig. 1).

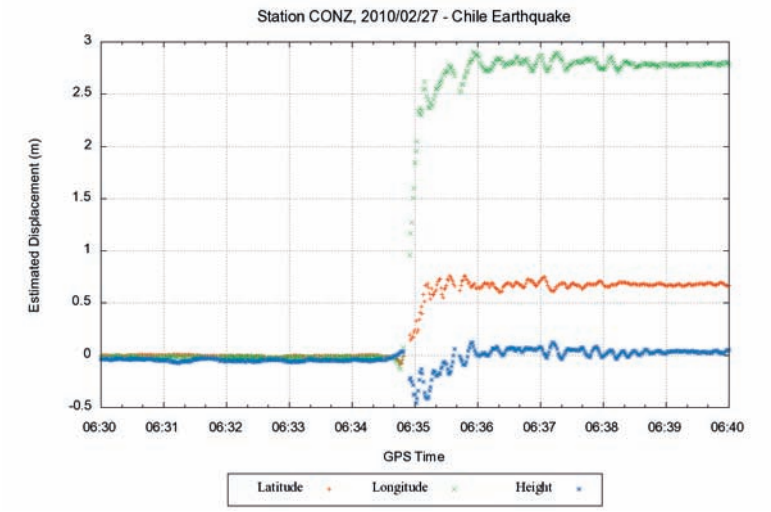


**Figure 1: Displacement at station Concepcion during the earthquake of 2010**

# 3. Recommendations

**It is recommended for the stations/agencies**

- to carry out a full hazard analysis for the SLR stations.
- to identify the vulnerabilities and rank them by impact importance.
- to implement and execute a cost-effective risk management program.
- To perform regular crew training in mitigation procedures.

  In particular at the Seismical At-Risk Stations:

  - to support the local microzoning updating.
  - to create and implement a full seismic mitigation program.
  - to guarantee the stations' IGS GNSS receivers should be operational during a disaster.
  - to facilitate at/near the premises the operation of seismical instrumentation.

**The ILRS should encourage**

- the inclusion of hazard/risk analyses into the design of new stations.
- the regular hazard/risk analysis updating for the current stations.
- the sharing of experience on mitigation procedures.
- the conservation of the ILRS historical memory.
- all SLR stations should to have an IGS station operating on the premises which should be operational during a disaster
- to upgrade the IGS stations to the maximum sampling rate possible, in particular at the At-Risk stations.

**The ILRS should discuss the possibility of**

- the creation of a “hot line” phone(s) number(s) for:
  - centralized emergency communication
  - point-to-point two-way emergency data transfer.
- the creation of a centralized software/HDD image security bank (off-line and password-protected.)
- a two-way approach to In-Sky laser safety by
  - promoting the generalization of cost-effective technologies and solutions.
  - the creation of a reporting mechanism for incidents.

## Acknowledgements

The author wants to thank the colleagues at the CENAIS’s Seismic Engineering Department, in particular Dr. Fernando Guasch, for the in-depth discussions during the preparation of the work.

## Correspondence

Dr. Jorge R, del Pino
Donato Mármol 472
Santiago de Cuba, 90100
Cuba

pino@cenais.cu
pino@gfz-potsdam.de

***formerly at the National Center for Seismological Research (CENAIS), Cuba**

# Session 3
# Atmospheric Refraction Correction: Hardware and Modeling

# The Photoconductive Antenna - A new device for Spacegeodetic Applications

*S.Riepl, C.Plötz Bundesamt für Kartographie und Geodäsie*
*R.Zeitlhöfler, Technische Universiät München*
*A.Nothnagel, Universität Bonn*

ABSTRACT
Emerging from Terahertz technology, photoconductive antennae (PCAs) are usually applied to generate terahertz radiation out of short optical laser pulses in a rather instantaneous way. As PCAs can be constructed for custom applications, this paper outlines the application of a PCA for generating microwave pulses out of picosecond laserpulses capable of being detected by VLBI systems. This could serve as an independent calibration signal for the internal VLBI signal path from feed horn to data registration. Further customization of PCAs for the relatively low VLBI frequency domain can lead to very interesting applications starting from verification of local ties up to intersystem timetransfer between SLR and VLBI systems, giving way to an experimental approach of combination of space geodetic measurements in the GGOS sense.

## 1. Introduction

Photoconductive antennae (PCA) are devices emerging from terahertz technology. Being a bidirectrional device, as the name antenna suggests, it is capable of transmitting an electromagnetic pulse preferable in the terahertz frequency domain, on excitation with short optical laser pulses and, vice versa, detecting a terahertz pulse in temporal coincidence with an optical laser pulse. The customized design of a PCA leads to lower frequency output in order to access the microwave region, the frequency domain where VLBI observations are carried out. Thus PCAs constructed for the operation in the microwave region can be used as a link device between microwave and optical space geodetic techniques in a variety of ways, e.g. the verification of local ties between SLR and VLBI systems, the optical to microwave time transfer and even the replacement of the existing phase calibration device.

## 2. Experimental setup

A first experiment was set up in order to do a phase noise measurement of a laser pulse induced microwave pulse train using the existing Ti:Sa laser system of the Satellite Observing System Wettzell (SOS-W). The laser consists of an oscillator which can be synchronized to a frequency standard by means of an external frequency synthesizer providing the nominal pulse repetitive frequency of 73MHz. This frequency synthesizer can in turn be synchronized as well to a stable reference frequency provided by a maser for time transfer experiments. For nominal SLR operation, the oscillator output is amplified at a repetition rate of 1kHz. This option hasn't been used throughout this experiment due to the fact that the phase noise analysis of 73MHz is much more comfortable with the equipment in use. Figure 1 illustrates the setup with the laser head on the right side. The output is guided by two steering mirrors onto the PCA where the optical pulses are converted to microwave pulses. These are detected by a comercial satellite TV receiver (LNB) at a bandwidth of 11GHz. Next to a schematic setup of the experiment the inlet of figure 1 shows the signals displayed with a 50GHz sampling oscilloscope. The upper pink trace corresponds to two adjacent optical laser pulses.

# 3. Phase noise analysis

For the phase noise analysis, the laser oscillator is operated synchronously with the 73MHz output of a frequency synthesizer, which is also used to provide a 10MHz reference signal for the phase noise analyzer. The phase noise analyzer (Rhode&Schwarz) is connected to the output of the LNB mentioned in the experimental setup section. To give an overview on the frequency bandwidth of the obtained LNB output an electrical spectrum was recorded from 10MHz up to more than 13GHz. The obtained frequency comb with equidistant spacings of the 73MHz pulse repetition frequency is displayed in figure2. The slope of the spectral power corresponds to a gaussian pulse shape of 40ps width.

The phase noise measurement shown in firgure 3 is performed on the signals first harmonic. The signal starts at a carrier normalized level of -40dBc for 1Hz offset frequency and reaches the noise floor at -130dBc and an offset frequency of 300kHz. The slope shows some volatile peaks of spurious signals as well as some residual phase noise arising from the laser oscillator length stabilization.

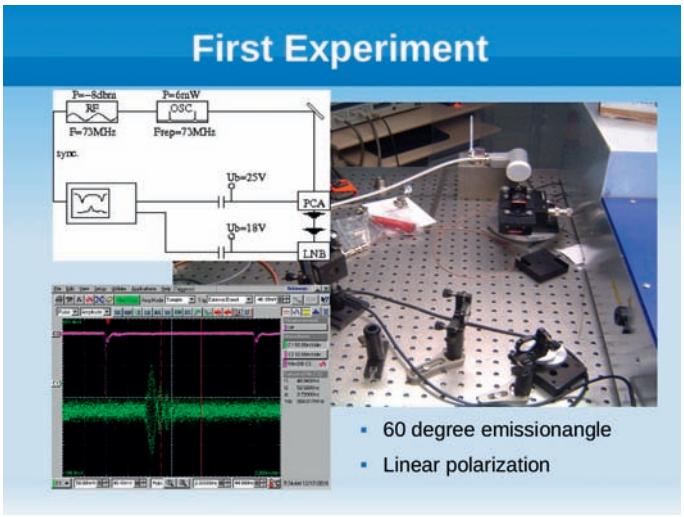


**Figure 1: Basic schematic setup, illustration and oscilloscope traces of the first photoconductive antenna experiment.**

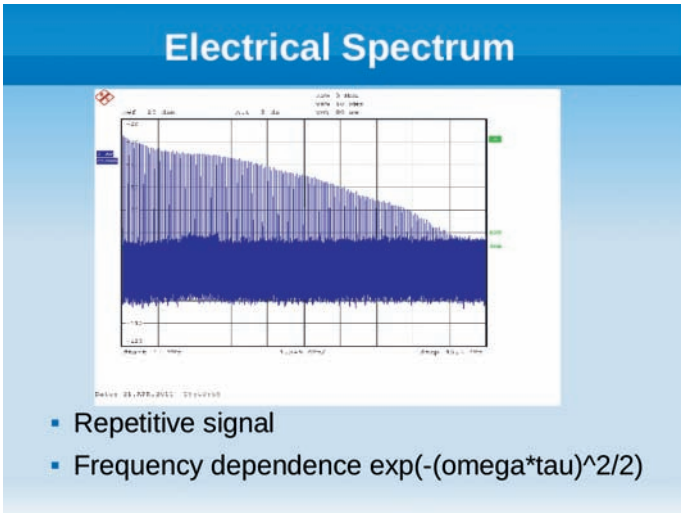


**Figure 2: Frequency comb obtained from electromagnetical signal of a photoconductive antenna detected by an LNB and recorded by an electtrical spectrum analyzer**

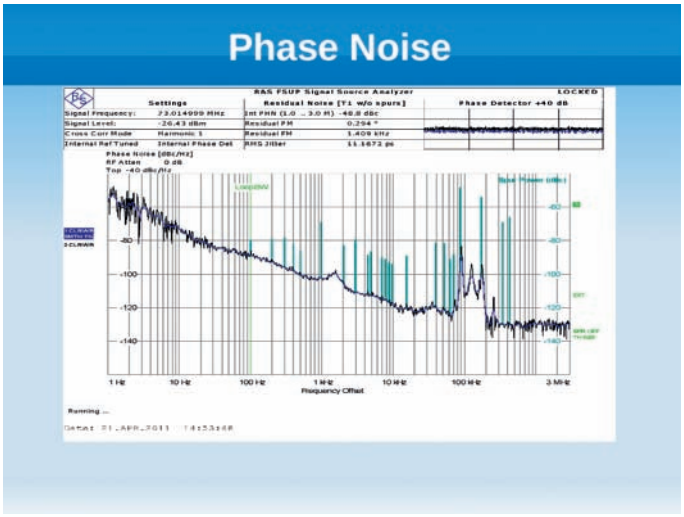


**Figure 3: Frequency comb obtained from electromagnetical signal of a photoconductive antenna detected by an LNB and recorded by an electtrical spectrum analyzer**

## Correspondence

S. Riepl
Bundesamt für Kartographie und Geodäsie
Sackenriederstr. 25
93444 Bad Kötzting

stefan.riepl@bkg.bund.de

# Session 4
# SLR Techniques

# Co-optical Path kHz SLR at Kunming Station

*Li Zhulian, Fu Honglin, He Shaohui, Zheng Xiangming,*
*Li Rongwang, Li Yuqiang, Zhai Dongsheng, Xiong Yaoheng*

ABSTRACT
Kunming station (7820) laser ranging system is co-optical path means, and low repeat frequency (<10Hz) laser ranging was routinely done in it ago. With the development of sciences and techniques, high repeat frequency laser ranging method, which would get more data per second and higher precision, appeared and would play an important role in this field. The paper will introduce our co-optical path kHz SLR system and give some observed data.

## 1. Introduction

### 1.1 Low Repeat Frequency System

Kunming station has begun to do Satellite Laser Ranging (SLR) work since 1998, and produced a series of valuable data for users, who utilize it to do some science research. Before 2009, this system had 1 ~ 10Hz ranging frequency with 3cm ranging precision. To low repeat frequency system, co-optical path laser ranging is relative easy to realized by using rotating mirror to change emit and receive optical path. With the development of the electronic technique and other relative sciences, high repeat frequency SLR technique appeared and quickly developed.

### 1.2 High Repeat Frequency System

Co-optical high repeat frequency Satellite Laser Ranging technique is very difficult, so we planed to carry out 20Hz SLR before 2009, and ordered the laser from Continus Company. Unfortunately, the order was denied by U.S government, so our work to update Kunming station's system to 20Hz ranging system has been delayed several years. Finally we tried to develop our Kilo-hertz (kHz) co-optical laser ranging system with kHz laser.

Here, we would introduce it carried out principle and technique, and indicate some observed data.

## 2. Co-optical path kHz system

### 2.1 Co-optical path

Kunming station's SLR system uses co-optical path ways, i.e. our 1.2m telescope is used as both transmit and receive instrument [1]. The laser trace during ranging is showed in picture 1, the outgoing laser coming from kHz laser will go through the 1.2m telescope to the target (satellite), and it will be reflected to observation station by retro-reflectors, the incoming laser. It will also fly through the same telescope to receiving detectors.

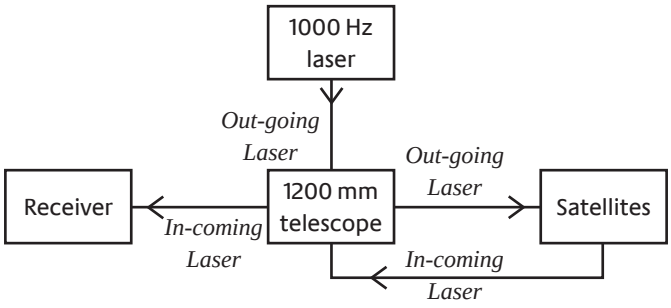


**Figure 1: Laser Trace in Co-optical SLR**

## 2.2 Ranging Control

### 2.2.1 Hardware

Ranging control system consists of Rotation Shutter (RS), Industrial Personal Computer (IPC), Laser, Event Timer (ET), and C-SPAD etc. Its block diagram is showed in Figure 2.

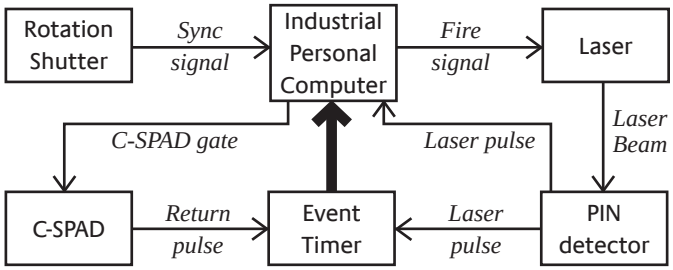


**Figure 2: Ranging Control Block Diagram**

Laser ranging procedure: RS continuously generates synchronization signal to IPC, when IPC detects these signals, it will give fire instructions to Laser and begin to detect the laser pulse from Pin detector. Once detects the laser pulse, it will generate a C-SPAD gate signal to C-SPAD return detector. Laser transmit epoch and its return epoch was recorded by ET.

### 2.2.2 Software

The software consists of Run Ranging Software, Orbit Prediction, Telescope tracking, Data collecting and Data processed functions. Because all functions don't work in a same time, so we developed our user application software with Single Document Multi-Interview (SDMI) of visual C++, Ranging Operational Process is showed in Figure 3.

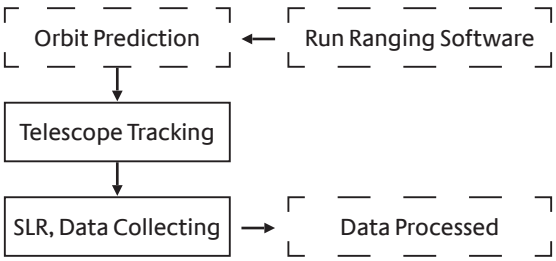


**Figure 3: Ranging Operational Process**

# 3. Observed Data

This co-optical path ranging system calibrates the system delay by measuring a ground target, which is put at 200m from observing station. During observation, we do range it every one hour or after each satellite observed. The average of system delay is about 2358.9cm with 0.5cm precision. [2]

## 3.1 Night Ranging Data

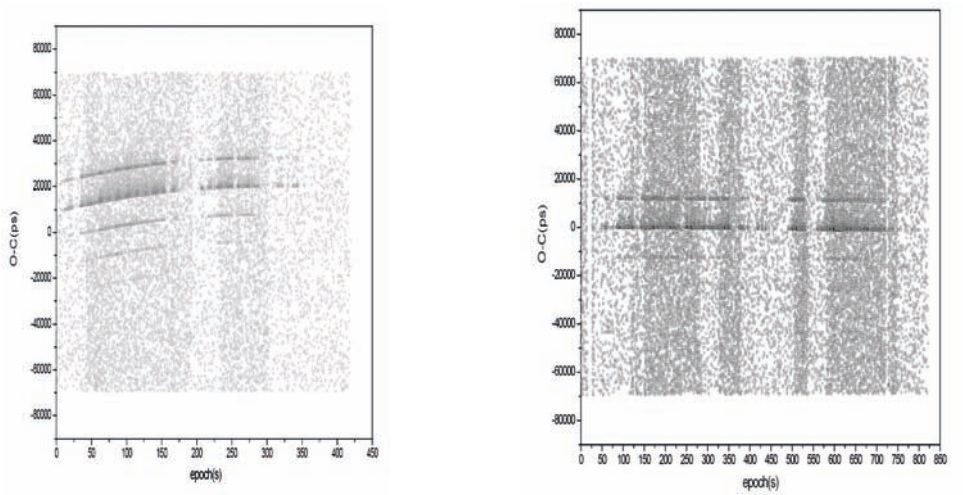


**Figure 4: Jason2 and Lageos2 Night Ranging Data**

Kunming station's SLR system successfully got night ranging data in April, 2010. Figure 4 shows the night ranging data from Jason2 and Lageos2 satellite. They have separately 1.17cm and 1.46cm accuracy.[2]

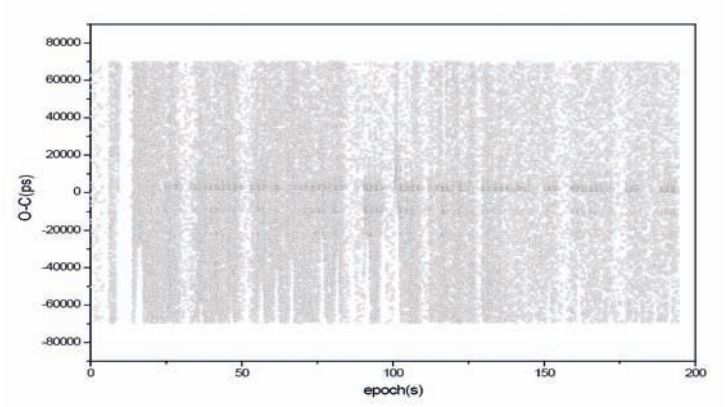


**Figure 5: Ajisai Daylight Ranging Data**

## 3.2 Daylight Ranging Data

Kunming station SLR system successfully got daylight ranging data in lately October, 2010. Figure 5 shows the daylight ranging data from Ajisai satellite. It has 1.41cm accuracy. [2]

# 4. Conclusion

It is not easy to carry out high repeat frequency co-optical path SLR, and our experiment of realizing kHz co-optical path SLR at Kunming station has completely proved this. However, at the same time, our experiment said that co-optical path kHz satellite laser ranging technique could be fulfilled.


## Acknowledgements

Thanks to CRUSTAL MOVEMENT OBSERVATION NETWORK OF CHINA!


## References


*[1] Xiong Yaoheng, Fu Honglin. Opto-Electronic Engineering,* 1998: Optical System of the Yunnan Observatory 1.2m Telescope.

*[2] Zheng Xiangming,Li Zhulian, Fu Honglin et al. ACTC OPTICAL SINICA.,* 2011: 1.2m Telescope Satellite Co-optical Path kHz Laser Ranging System.


## Correspondence


Li Zhulian

Yunnan Astronomical Observatory Chinese Academy of Sciences Kunming
China

lzhl@ynao.ac.cn

# Experimental Laser System for Monitoring of GLONASS Time/Frequency Synchronization

*Sadovnikov M.A., Fedotov A.A., Shargorodskiy V.D.*

*A laser-based system is presented for high-accuracy in-flight calibration of regular RF means used for comparison of GLONASS on-board and on-ground clocks, as well as for mutual synchro-nization of on-ground clocks at different far-away points of territory. The system operation principle is based on comparison of two-way time-of-flight attained by satellite laser ranging (SLR) of the GLONASS spacecraft, equipped with optical retroreflector arrays, and data of one-way laser mea-surements using on-board photo receivers. Parameters and methods of on-board and on-ground equipment calibration are presented, as well as a measurement data processing algorithm providing simultaneous operation of multiple laser stations observing the GLONASS spacecraft. The ex-pected measurement accuracy is also evaluated.*

At all stages of the Russian GLONASS navigation system development, laser systems have been widely used in the regular ground control structure. All navigation spacecraft (SC) are equipped with retroreflector arrays providing high-accuracy ranging by means of SLR stations. Range measurements are used for calibration of regular RF monitor stations providing orbit parameter deter-mination, refinement of SC orbit disturbing force models, determination of precise station coordinates in the geocentric reference frame, as well as for verification of ephemerides translated to the navigation SC by control stations.

The high accuracy of navigation is provided primarily by high-accuracy ephemerides calculation as well as by high-accuracy synchronization between the SC on-board clock and the GLONASS system time scale.

In the GLONASS system (Fig. 1), the system time scale is formed by the main synchronizer using an hydrogen maser en-semble, while the time/frequency correction values (relative to the system time scale) for the SC clocks are calculated in the system control center. The calculation is based on comparison of range values measured by two-way RF ranging station with pseudo-range values measured by one-way RF station [1]. Currently, the accuracy of such RF clock comparison measurements is not better than 2...3 ns (at the moment of measurement).

The experimental GLONASS time/frequency synchronization laser-based control system is developed for comparison of on-board and on-ground clocks with random and systematic errors less then 100 ps. The system purpose is:

- verification of GLONASS RF synchronization system measurement results;
- mutual synchronization of on-ground etalon clocks located at distant points.

The laser-based control system includes satellite laser ranging (SLR) stations located near to the corresponding on-ground etalon clocks, on-ground laser equipment units (GLEU) connected to the SLR stations and to the etalon clocks by optical fiber links for translation of synchronizing time marks from the clocks and laser pulses from the SLR stations to the GLEU, as well as an on-board laser equipment unit (BLEU) connected to the SC clock.

The laser-based control system operation principle is as follows. The SLR station measures the laser pulse time-of-flight (TOF) to the retroreflector array (RRA) on the SC and back. The on-ground unit receives the laser pulse translated from the SLR station via the optical fiber link and determines its radiation moment in the on-ground clock time scale. The on-board unit detect the laser pulses coming to the SC and measures their arrival time in the SC clock time scale.

The SC arrival time moments and calibration corrections for the SC measurements are translated via the RF telemetry link to the system control center where they are converted into an SC measurement data file. Also the center becomes from the GLEU a ground measurement data file comprising laser pulse radiation moments, TOF values and calibration corrections for on-ground measurements. During the data processing, the time difference between on-board and on-ground time scales is determined.

For the experiment SLR station are used which are located near Moscow, near Komsomolsk-na-Amur, and within the Altay Optical and laser tracking center, all of them being part of the Russian Laser Tracking Network. The stations are in regular operation mode for a long time, and are equipped with laser transmitters with a pulse repetition rate of 300

Hz; currently they are also being equipped with single photon receivers SPAD K14 developed by the Czech Technical University. The SLR station near the Moscow is located near the GLONASS main synchronizer, while the Komsomolsk and Altay stations are equipped with hydrogen masers.

The on-board unit (Fig. 2) is located in the upper part of the Glonass-M space craft; its mass is 6.5 kg and power consumption is 35 W (including the thermo-regulation system). The main parts of the on-board unit are the multiaperture photoreceiver and the timer measuring the arrival time of laser pulses detected by the photoreceiver (in the SC time scale).

The multiaperture photoreceiver has 7 channels with separate receive lenses (8 mm in diameter with a 9° field of view) and avalanche photodiodes placed in the focal planes of the lenses. The single channel threshold discriminator outputs are combined in an OR circuit and thus operating as a whole. The multiaperture design provides full covering of the visible Earth disk and reducing of the back ground noises caused by the solar radiation. The photoreceiver operating wavelength is 532 nm; the background power is reduced by narrow-band interference filter having a bandwidth of 3 nm. The input pulse energy range in which the required accuracy of arrival time moment determination is provided, is 0.02 to 2 fJ/mm$^2$. The on-board memory provides up to 2 million pulses during an observation session, and allows volume-limited selections from the data array due to the SC measurement delivering time.

The single-shot pulse arrival time random error is defined by the laser pulse duration as well as by the receiver noise and timing jitter (phase noise of timer and on-board synchronizer). With the total timing resolution of the 200 ps and laser pulse duration less then 300 ps, the single-shot arrival time measurement error may be evaluated as no more than 300 ps.

The on-board arrival time measurement systematic error is defined by the calibration accuracy of time delays in cable connection to the on-board synchronizer, in the timer, and in the photoreceiver, as well as by the accuracy of the time difference determination between the moments of the pulse arrivals at the RRA reflection center and at the on-board unit optical center. This difference depends on the navigation SC attitude angles; thus the calibration should be performed at zero incidence angle of the laser beam, while the angle-dependent correction value is calculated in the system control center during the on-ground measurement data processing. To avoid the effects of variable delays caused by signal strength dependent arrival time measurement variations, the photoreceiver channels are provided with amplitude measurement devices, and the amplitude measurement data are translated to the system control center (within the total measurement data array). Before and immediately after the measurement session, the total measurement path is calibrated by an active calibration system including a laser diode placed in the on-board unit optical center, thus allowing to take into account the variable delays caused by the environment temperature variations.

The on-ground laser equipment unit (Fig. 3) is placed directly on the SLR station and is in fact an additional SLR module. Its main parts are an optical-to-electronic converter (OE converter) placed near the on-ground etalon clock, a measuring photoreceiver, and a timer measuring the SLR station laser pulse radiation time moment in the on-ground time scale. The etalon clock may be at a considerable distance from the SLR station (up to 1 km), so for its connection with the GLEU a wideband fiber-optical link is used.

For the on-ground etalon clock precise time mark forming (high-accuracy time scale), the zero transition moments of its sine signal are used. The OE converter transforms the electrical signals of the high-accuracy time scale into optical signals to be translated via the fiber-optical link. The optical time mark pulse duration is 35 ps, at the 1.3 μm wavelength. The optical time mark pulses from the on-ground etalon clock are delivered to the on-ground unit photoreceiver input, where also attenuated pulses from the SLR station are delivered via a short optical link.

A germanium photodiode with a response time of 70 ps is used as a measuring photodetector. The pulse time difference is measured by an event timer with a measurement accuracy of 40 ps. The measurement data processing is performed by a computer forming an on-ground measurement data file with an account for the SLR measurement data and for the calibration data.

The return optical pulse arrival time single-shot error with an account for the on-ground etalon clock time scale tie-up errors is defined by the laser pulse duration, the SLR station return signal receiver resolution, the SLR station and GLEU timers random errors, as well as the on-ground etalon clock optical mark pulse jitter. With the SLR station receiver resolution of 30 ps and laser transmit pulse duration of 300 ps, the GLEU single-shot error may be evaluated as less then 220 ps.

The on-ground measurement systematic error is defined by calibration accuracy of the time delays in the fiber-optic connections of the measuring photoreceiver with the on-ground etalon clock and the SLR station laser transmitter, as well as by the accuracy of the SLR station system correction value determination.

To check the optical time mark delay in the fiber-optic link, an additional optical fiber loop is used. The loop is laid together with the main fiber-optic link and has a double length as compared with the main link. As a result, the time delay in the loop is twice the optical time mark pulse time delay in the path from the on-ground etalon clock to the GLEU. The optical signal from the loop output is fed to the GLEU measuring photoreceiver; at its output electrical pulses from the main link and from the loop are formed, with the time interval between them corresponding to the current delay in the fiber-optic connection.

To increase the SLR station system correction value determination accuracy, a calibration procedure is anticipated directly during the laser ranging session, with a following averaging of multiple system correction value measurement results.

The mutual processing of on-board and on-ground measurements is performed in the system control center using the following algorithm:

1. Calibration correction values are introduced in the on-board and on-ground measurement results, reducing the results to the RRA reflection center of the navigation SC and to the SLR station mount axes crossing point.

2. Using a priori data, on-board measurement results are selected corresponding to each SLR station laser pulse radiation moment.

3. For the on-board and on-ground measurement results, separately using the least-square method, one-way laser pulse TOF values $\tau_b$ and $\tau_g$ are determined.

4. Using the $X = \tau_b - \tau_g$ relationship, the difference between on-board and on-ground time scales is calculated.

Thus, the difference between the on-board and on-ground time scales is determined as the difference between the one-way laser pulse TOF value derived from on-board measurements, and the one-way TOF value derived from the on-ground measurements.

The expected total error of multiple time difference measurements (synchronization accuracy) is $\sigma_x / \sqrt{N}$, where $\sigma_x$ is the single-shot RMS measurement error, and $N$ is the total number of measurements during the observation time interval $T$. With the observation time interval $T = 1000s$ and the average return signal arrival frequency 2 Hz, the expected error is about 5 ps. The expected error of relative stability of the SC clock estimation $\sigma_y$ is $\sqrt{3} \cdot \sigma_x / T \cdot \sqrt{N}$, which in the same observation condition is about $8 \cdot 10^{-15}$.

Thus, the expected parameters of the GLONASS synchronization monitoring laser system offer an increase of the time scale difference determination accuracy by more then an order of magnitude relative to the regular RF synchronization means. Currently, the equipment developed with an account for the higher reliability and lifetime requirements is in the final testing phase, and will be soon delivered for ground testing within the spacecraft. The first flight of the Glonass-M spacecraft with the laser synchronization monitoring system is scheduled for the end of 2011 year.

## References

*1. Edited by Perov A. and Harisov V.*, 2005 GLONASS. Principles of construction and operation, Moscow, Radiotechnika.

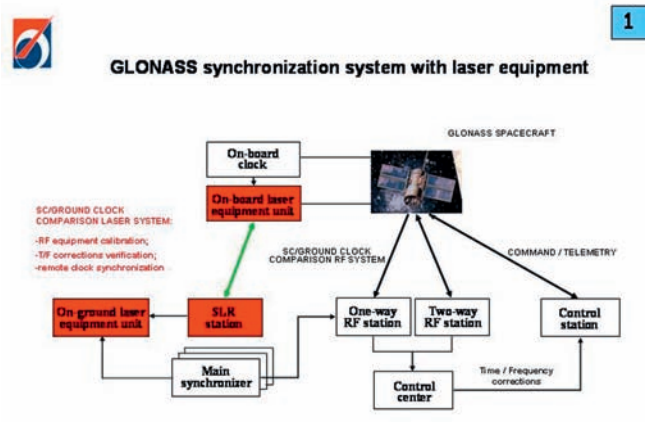


**Figure 1: GLONASS synchronization system with laser equipment**

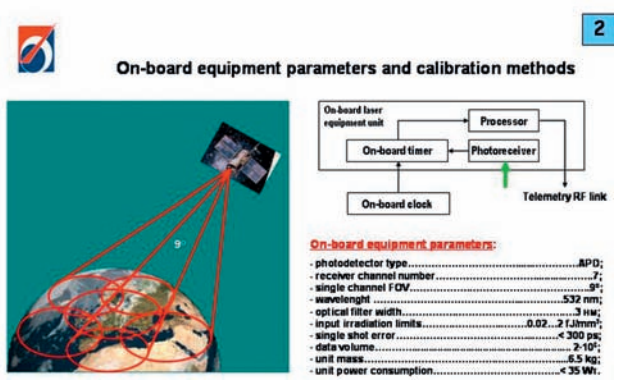


**Figure 2: On-board equipment parameters and calibration methods**

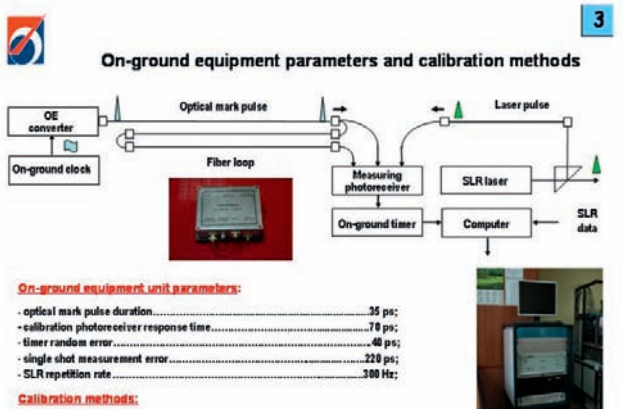


**Figure 3: On-ground equipment parameters and calibration methods**

Mikhail Sadovnikov
53 Aviamotornaya st. Moscow 111024 Russia OJC “RPC “PSI”

msadovnikov@gmail.com

# New 2kHz capable software in Metsähovi

*Kirco Arsov*

ABSTRACT
Metsähovi SLR system is currently going through a major renovation. A new 2KHz laser has been bought together with the timing devices, C-SPAD and other necessary electronics. This change from old 1Hz system to our new 2KHz SLR requires improvement in all the hardware and software in Metsähovi accordingly. Since in 2KHz scenario many operations are time critical, our old 1Hz SLR software was not capable of many tasks, and together with the hardware a decision has been made to write a new operational SLR software. The software is written in C++ by the use of MFC libraries and is fully capable of handling 2kHz scenario. Main objective of this paper is to give an overview of performance/development, as well to identify all the critical items and their solution. Some test performances will be also outlined, presented and documented.

## 1. Introduction

The Metsähovi fundamental station was founded in the mid-1970s, and over the years it has become an essential part of the activities of the Finnish Geodetic Institute. The instrumentation of the station serves both the Institute's own research and the international scientific community. The following instruments are currently installed at the Metsähovi fundamental station: satellite laser ranging (SLR), geodetic VLBI (Very Long Baseline Interferometry) in a co-operation with the Helsinki University of Technology, GPS and GLONASS receivers, a DORIS beacon and a superconducting gravimeter. Absolute gravity is regularly measured in the gravimetric laboratory where the National reference point of gravity exists. There is also a seismometer of the University of Helsinki. Metsähovi is one of the few fundamental stations in the world where all major geodetic observing instruments are installed in the same site.

SLR is one very important segment of our station. It has been operational with 1Hz from 1994-2005. In 2007 we decided to completely replace the old 1 Hz system with the new 2 KHz SLR. Therefore, a new 2kHz capable laser was purchased from the HighQ companyt in 2006, and it was delivered in the station in the first half of 2007.

Due to the new laser, the necessary improvement and modernization of the old equipment was necessary too. A new C-SPAD replaced our old PMT, new GPS receiver together with the new meteo station was also purchased, and for the time critical tasks we ordered the well known Graz ISA fpga board. This board was planned initialy to operate separately in DOS. We left this concept later by development of our own PCI fpga board who perform all the time critical tasks in the main program. It is slightly improved version of the old ISA Graz board. Our old 1 Hz SLR software was not able to manipulate, control and operate all this new equipment. Therefore, we decided to write a new, modern and powerful 2kHz software from scratch. In the following context of the paper we give an overview of thus developed software package.

## 2. Software description

As we already mentioned, the quantum leap from 1 Hz to 2 kHz implied writing from scratch the whole operational SLR software. Our old SLR software used old Linux installation together with some obsolete libraries, the person who developed the software over many years was not present in the station anymore and it was impossible to get any documentation on the current software situation. Even (re)compiling of the software was very difficult, due to obsolete or missing libraries, different hardware etc. So, to summarize, our old SLR software was far of being able to handle the new 2 kHz system. Taking all of the above mentioned into account, a decision has been made to develop a new modern 2 kHz capable SLR software from scratch in Metsähovi. It has been started in the second half of 2007 and in the following we give a short description of its capabilities so far:

- Platform: Windows 7 operating system with intel i9 -> 8 threads. Operator knowledge is limited only to using the mouse; no scripting or other out-of-software actions needed.
- Implemented as option DOS communication, but later dropped off by the use of our own PCI fpga SLR controller. Old DOS communication interfaces are left if needed for something in the future.

- C++ as programming language, and GUI was programmed by MFC libraries.
- No real time operating system needed because:
  - All tasks are performed in hardware PCI fpga board.
  - Tests show that Windows system is never later thren 1msec. This is especially true if one uses loops or threads.
  - Timer used is A032-ET and it has around 12000 FIFO points for reading the measurements, so no need of direct response.
  - In the fpga board most of the tasks are performed by using FIFOS so also this does not imply real time system.
  - Only important thing is to get the data from timers and fpga within the time-of-flight of the satellite which in case for example of GOCE satellite is about 1.4-2 *msec*.
  - Graphics is done by usage of DirectX10 inside PCIe graphics board. All rendering plotting etc is done inside the graphics board. For graphics manipulation, we used DXSDK (DirectX Software Development Kit) . No additional burden on the CPU.
  - All writings to disk are done binary in threads by writing big amount of data at once, ex after 5 min observing.
- Implemented GUI modules for session downloading, CPF treatment, session planning, observation etc.
- Full 2 kHz scenario uses only 20 % of the CPU.

Metsähovi SLR OS software is developed based on object-oriented programming. It consists of different classes tailored to different tasks to be performed. In Fig. 1 we give the basic objects of which Metsähovi SLR OS software consists. Dashed squares represent objects that are programmed but not used anymore. In the DOS option for example, we used as data trans-fer our own developed protocol with the parallel PCI-DIO96 board because of almost no latency time in handshaking (8255 chip) and together with that very fast data transfer compared to GBit LAN after handshaking. In this DOS scenario, for upload of orbits, time and meteorological data, we used from the DOS side TCP/IP or UDP protocols. But for the real time software status control, time/range biases upload and residuals upload to windows we used the parallel DIO96 board because of its very fast response. It is also interesting maybe to mention that on the DOS side we used the DJGPP C++ compiler who made it possible for us to use 32 bit addresses as well as whole 3Gbyte RAM in pure DOS environment. The old Graz ISA fpga board was mounted in the DOS computer and its main task was range gate computation/setting, event timing with 5ns resolution, laser and CCD control, calibration etc. Now these tasks are performed in the main computer via our own PCI fpga board. We used at the beginning also one NI-PCI6601 counter for time synchronization, very rough event timing, time counting etc, and the dashed box is one class we developed for manipulating this counter. It is now obsolete and not used, since we do also these operations with the fpga board, but is present anyway in the software, so if someone wants to do something in the future to be available as option.

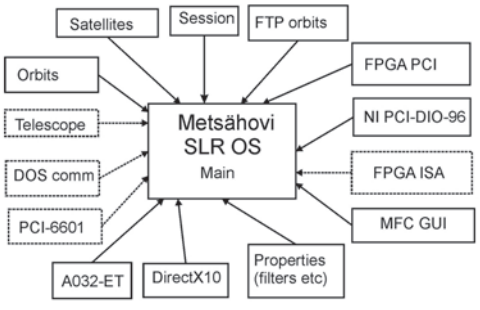


**Figure 1: Main objects of Metsähovi SLR OS program**

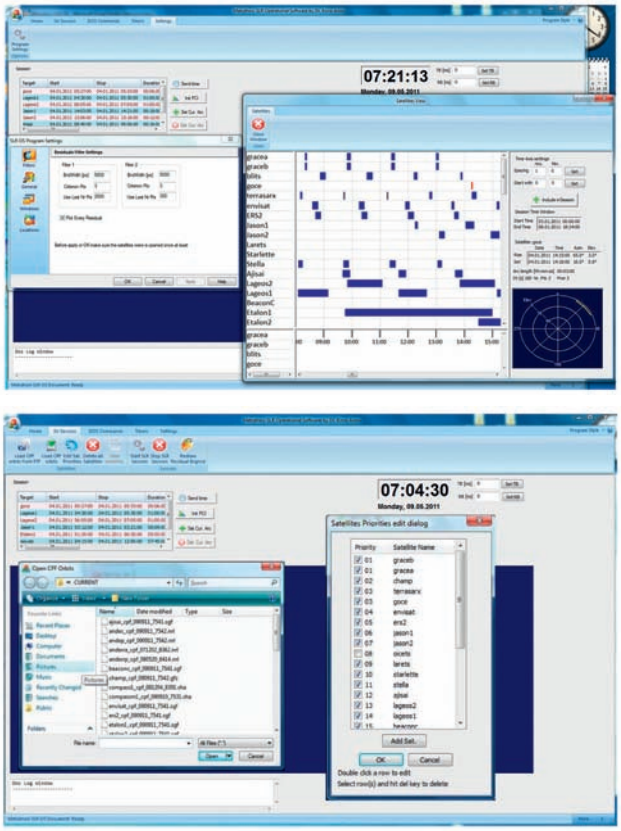


**Figure 2: Some screenshots of the Metsähovi SLR OS**

In Fig.2 we give some screenshots of the software. As it is seen in Fig.1 the program has some parts dealing with satellites, satellite orbits, download of the orbits via ftp, their manipulation, loading in the program etc. It is also possible to manipulate satellites used, to add new satellites, to set priorities, delete satellites etc. For loading the cpf orbits we used as starting point the EOS submitted class in the ILRS pages with some modifications regarding additional test of cpf orbits and programming some wrappers to better fit to our software general interface. We also as may be seen from Fig. 1 and 2 programmed window for session planning, satellites management and including certain passes in the session. Also setting of range and time bias is possible on-the-fly. There is also TCP/IP interface to the timing and meteorological station so it has been updated and checked from threads every predefined certain amount of time. There is also an option of setting the filters for the residuals,as explained in Kirchner 2004 and it offers a great flexibility in the filtering and screening of the residuals. It is capable of finding 0.1 % returns present in the measurements. For real time plotting, the requirement is to process 4000 points per second. It is managed by using DirectX10 SDK and is uploading the plot 30 times per second. All rendering of these points etc is done in the external graphics board and is not using the CPU. The only CPU usage in the graphics is to react from a thread to timer trigger 30 times per second and to instruct the graphics board to do the refreshing of the residuals plot. The program also controls our own developed PCI fpga board for range gate setting, event timing, laser control, CCD control etc. The overlapping avoidance is done in the fpga board automatically, so no CPU time is needed for that at all. There is also object for reading the A032-ET event timer from Riga and it is red in real time from our software to get the start and stop epochs. For this purpose, we redesigned the RIGA's C program for reading the timer, and wrote one wrapper for our program so it directly reads the timer, checks for available measurements, performs calibration, scaling, absolute orientation to UTC etc. At this point it should be mentioned that it is foreseen to make our software **freely available to the SLR community** for non-profit usage. For this purpose a necessary modifications are done in terms of allowing usage of MAXII cheap cpld for time critical tasks for example (since our PCI fpga board is now obsolete and can not be bought from Altera), writing excessive documentation of the software to make it more easy to install and use etc. No present code will be removed from the current version affecting these modifications. Also all obsolete code will be left (such as the DOS case for example) so in the future if someone interested may use it. We do hope that in few months the Metsähovi SLR OS software will be available for download from our ftp site and/or from the ILRS homepage.

# 3. Software future work

Software writing is always long process and one is actually never finished and has one “final” version of the program. Same holds also for our Metsähovi SLR OS program. In the current version, main focus was put to be able to perform one full 2 kHz closed loop simulation and be able to perform all time critical tasks without any problem. Well we succeed to meet this goal so far. We are able to perform one full 2 kHz measurement scenario with the current version. Our Plans for future are to manage a bit more elegant the setting of the program parameters, to include more automation in the computation, to perform automatic setting of the range gate as well as automatic control of the satellite search, time bias, range bias management of the program etc. What is also not done is performing the calibration. We assume in the current version that the calibration is perfectly known what in praxis of course is not true. Our PCI fpga board is capable of automatic control of the range gate pulses needed for calibration, so what we need to implement in the future is just the software part into our operational software together with some statistics. For now we assume also that the telescope is perfect what is also not true. For this reason one interface with the telescope should be programmed and implemented in the future as well. And last but not least, one post processing object should be developed in the future with functions to post process the raw measurements, send auto e-mail to ILRS data centers, archive the sessions etc. We also plan in the future to make the program more flexible to the hardware used, since there are certain options following our hardware development, so if someone is testing or using the software, for him should be possible to select hardware from within the options dialog window. Currently, this is hard-coded in the program according to current hardware used and one has to uncomment/comment these lines in the program and recompile it for specific hardware. For example, we developed 2 fpga boards, one with cyclone II fpga, but since this development board is now obsolete, we also have one lightweight MAXII PCI cpld version capable of handling 2 kHz scenario, and dependant on what board someone wants to use the code has to be changed. The reason for MAX II project is the free code option, so if someone wants to test it and this cyclone board is not anymore available, the alternative is MAXII. This board is not as capable as cyclone, but we still programmed the most basic functionality for kHz SLR. Hard coding also holds for cable delay, meteorological and time server IP address, address of the parallel port for A032-ET, other boards addresses, directory name for measurements, naming conventions of output files etc. Anyway, at the end we conclude that 2kHz is a powerful SLR method, we were able to produce one piece of software being able to deal with this high rate without any problems by putting all time critical tasks to be executed in hardware, and finally we would like to mention that for stations having lower rates, the upgrade to kHz might need writing new software from scratch. We believe that this is the right way to do instead of modifying the old one as our experience showed.

## Acknowledgements

Author would like to acknowledge all the great help he got from Graz Observatory in general and from Georg Kirchner in particular. All the fruitful discussions, free lessons on kHz SLR and all the great help Georg and his team offered during my few visits in Graz are herewith greatly acknowledged.

## References

*Kirchner, G., Koidl, F.*, 2004 Graz KHz SLR System: Design, Experiences and Results, 14th ILRS Workshop
*G. Kirchner*, 2004, Range Gate Generator at Graz, Proceedings of KHz SLR Meeting, Graz, Austria

## Correspondence

Dr. Kirco Arsov,
Finnish Geodetic Institute
Geodeetinrinne 2,
02431 Masala, Finland

Kirco.arsov@fgi.fi

# Session 6:
# Modeling and Bias issues

# Modeling and Bias Issues: Keynote Paper

*Toshimichi Otsubo (Hitotsubashi Univ, Japan), Daniela Thaller (AIUB, Switzerland), and Vincenza Luceri (e-GEOS, ASI/CGS, Italy)*

## 1. Introduction

The global satellite laser ranging stations have strived to increase the measurement precision since the early days in 1960's, and it currently reached, in the best cases, 3 mm in single-shot RMS and, theoretically, around 0.1 mm in a normal-point basis of kHz laser ranging. On the other hand, the repeatability and the accuracy of the analysis products have not achieved the same level as the normal-point precision (Thaller, et al., 2011; Luceri, et al., 2011). Systematic error sources are considered to stem from various components and procedures such as timer, detector, laser, optics, meteorological sensor, calibration, local survey, operational software and also on-board reflector array. Systematic error also arises from the analysis procedures such as the physical models and parameter estimation configurations (Appleby, et al., 2011).

As an introductory paper in the session "Modeling and Bias Issues," this paper presents the measurement accuracy with respect to detection intensity. It is important to look into how such error behaves in the real observation data through precise orbit determination, and to convey the information back to the stations.

## 2. Intensity-dependent Range Bias

In this section, the precise behavior of satellite laser ranging data is studied with respect to intensity. Otsubo and Obara (2006) demonstrated that the number of returns per normal-point bin can be used as a parameter that represents intensity, and that an intensity-dependent trend is found in a number of stations using 2005-2006 data. We apply this procedure using our analysis software package 'concerto v4.10' to the laser ranging data of LAGEOS and AJISAI in 2010.

A series of 6-day arc orbit determination of LAGEOS-1 and -2 reduces the normal-point residuals at 1.5 to 2 cm RMS. A series of 2-day arc orbit determination of AJISAI reduces them at about 3 cm RMS. One set of station coordinate and range bias are also solved for together with orbital parameters. The residuals are sorted by the number of single-shot returns per bin. This parameter should be strongly related with the signal intensity into a detector. If the detection signal intensity varies, and if the detection timing is dependent on it, there will be an intensity dependent bias. It is also related to the so-called target signature effect, which can cause a station-dependent and intensity-dependent bias, at maximum, by 4 to 5 cm for AJISAI and ETALON, and 1 cm for LAGEOS (Otsubo and Appleby, 2003).

Figure 1 shows a part of the results for the most productive three stations in 2010: Yarragadee, Zimmerwald and Mt Stromlo. The full contents for the most productive 20 stations are available at the website of Geoscience Laboratory of Hitotsubashi University:

**http://geo.science.hit-u.ac.jp/research-en/memo-en/koetzting-update**

The negative trend is intuitively expected and is actually found in a number of stations, as seen in the case of Mt Stromlo in Figure 1. It should be noted here that a C-SPAD detector which tuned by a simple (single reflector; zero-signature) ground target ranging does not compensate the satellite signature effects, and it results in a negative trend. On the other hand, there are also a few cases in which the trend is positive, opposite to what we expect. Photomultipliers are, in general, more robust, but there is sometimes still a trend remaining. In this way, the intensity-dependent error is also dependent on the target and also on the station.

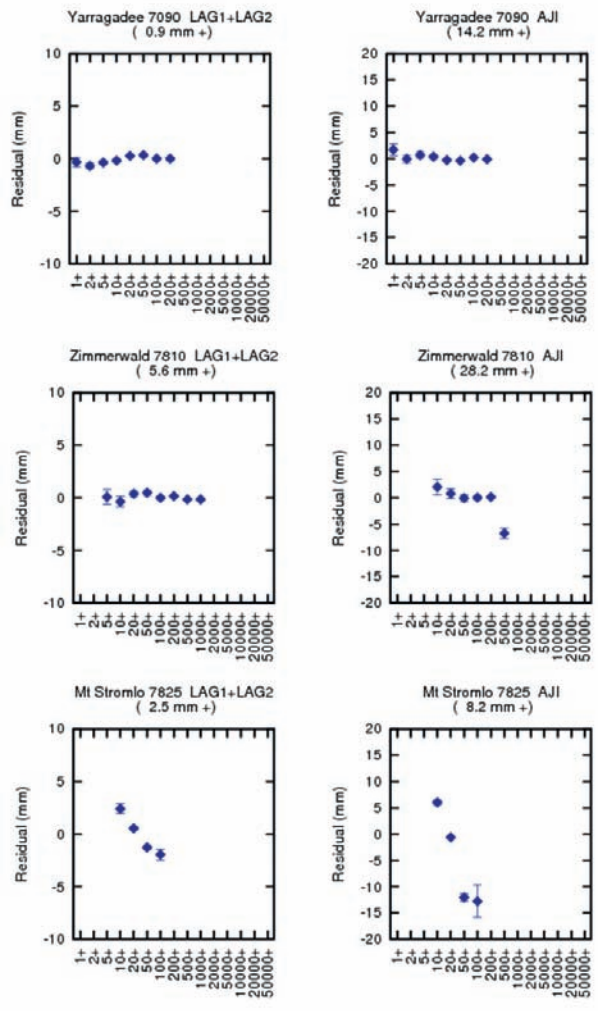


**Figure 1: Intensity dependence of laser ranging data.**

A few stations show different characteristics from the 2005-2006 period in the previous study. For instance, Graz data that had a negative trend in the past does not have any intensity dependence probably due to their recent policy change in the data reduction to use the first trace (closest reflector) only for these satellites.

The signal intensity is closely related to the elevation angle, and as a result the height component of station coordinates can be affected constantly. Therefore this method is likely to underestimate the true intensity dependence, i.e., the intensity-dependent error is likely to be more than the one presented in the graphs. It is essential to check and remove such a systematic effect by the stations themselves.

# 3. Conclusions

A quality assessment method is demonstrated using the global satellite laser ranging data obtained in 2010, to quantify the intensity-dependent systematic error. Despite the sub-mm measurement precision achieved in a normal-point basis, the range observations for a number of stations are statistically found to have strong intensity dependence up to 1 cm for the two LAGEOS satellites, and up to 2 to 3 cm for the AJISAI satellite. It is desirable to eliminate such systematic error sources to make full use of the high measurement precision of the modern laser ranging techniques.

## References

*Appleby, G. M., V. Luceri, and T. Otsubo*: Improvements in understanding systematic effects in laser ranging observations, in these proceedings, 2011.

*Luceri, V., G. Bianco, C. Sciarretta*: Improving ILRS products after in-depth characterization of station biases, in these proceedings, 2011.

*Otsubo, T., and N. Obara*: Systematic range bias 2005-06, Proc. 15th International Workshop on Laser Ranging, 2006.

*Otsubo, T. and G. M. Appleby*: System-dependent Centre-of-mass Correction for Spherical Geodetic Satellites, Journal of Geophysical Research, Vol. 108, No. B4, 2201, doi:10.1029/2002JB002209, 2003.

*Thaller D., K. Sosnica, R. Dach, A. Jaeggi, G. Beutler, M. Mareyen, B. Richter*: GNSS satellites as co-locations for a combined GNSS and SLR analysis, in these proceedings, 2011.

## Correspondence

Toshimichi Otsubo
Hitotsubashi University
2-1 Naka
Kunitachi, 186-8601 Japan

t.otsubo@r.hit-u.ac.jp

# Improving ILRS products after an in-depth characterization of station biases

*V. Luceri[1], G. Bianco[2], C. Sciarretta[1]*

ABSTRACT

The correction of station systematic errors is a non-trivial aspect of the SLR data analysis mostly due to the fact that many biases are not known nor reported by the stations. The ILRS Analysis Working Group has devoted a big effort in modelling the biases during the definition of the ILRS contribution to ITRF2008 with the establishment of guidelines to be followed by each analysis center for the individual solutions.

The in-depth characterization of the station biases has improved the quality of the latest ILRSA combined solution for ITRF2008 and some indicators will be presented.

The bias monitoring is an ongoing work to keep the ILRS routine product at a high quality standard. A few analysis centers are involved in this activity, in close contact with the site engineers, to estimate the biases whenever a field measured correction doesn't exist and keep the bias list updated.

## 1. SLR systematic errors

SLR is a clean, absolute ranging technique with the two possible kinds of systematic errors due to problems at the stations (e.g. calibration and/or synchronization issues, hardware malfunctioning): time biases and range biases. The range bias is the most critical, being highly correlated with height over short periods; the presence of intermittent biases can introduce jumps in the coordinate time series and a non homogeneous treatment of biases through the different Analysis Centers affects the combined product.

The ILRS Analysis Working Group (AWG) paid attention to the bias correction from the very beginning of its activities. Its main product is the weekly estimate of site coordinates and Earth Orientation parameters, using LAGEOS and ETALON tracking data, obtained from the combination of individual Analysis Centers (AC) solutions; the time series of weekly solutions is its fundamental contribution for the International Terrestrial Reference Frame (ITRF). The delivery of ITRF2005, the first reference frame obtained from the time series of solutions submitted by the various geodetic Services (ILRS, IVS, IGS and IDS), pointed out the problem of the jumps in the coordinates time series of some sites due to unmodelled errors and evidenced the necessity to make a deeper investigation on the systematic errors in the SLR data.

### 1.1 Error handling

The aim of the AWG was the establishment of guidelines to be followed by each analysis center for the individual solutions and the first important step was the recovery of information, above all for the historical data. Main sources of information were the engineering bias reports collected at the CDDIS database (technical report, station communication, ecc.) and the rapid, daily bias analysis report from the ILRS Analysis Centers. This information were not sufficient and, in order to compile a more complete list of biases in the data, a dedicated multi-year solution was made following the old fashioned way of doing global multi-year solutions: a wide data span back to 1983 was analysed to recover a single set of station coordinates and velocities, daily EOP and LOD, orbit parameters and time series of biases for all the stations of the worldwide network. This type of solution was chosen above all to obtain estimated biases de-correlated from the station height. The bias time series was a precious source of information to detect changes in the station configuration or unreported issues and was used, together with the information in the site logs, to define a mean correction to be applied whenever the presence of bias is clear and its value is not known. It is worthwhile to underline that this work was done in strict collaboration with the stations engineers and the resulting mean corrections followed the timeline of real changes made at the stations.

[1] e-GEOS S.p.A., ASI/CGS, Matera, Italy

[2] Agenzia Spaziale Italiana, ASI/CGS, Matera, Italy

The result was the definition of the ILRS AWG data handling file containing: the corrections to be applied in the SLR data analysis, the biases to be estimated, the unrecoverable data to be deleted. The file is available on the ILRS website and is maintained by the ILRS AWG.

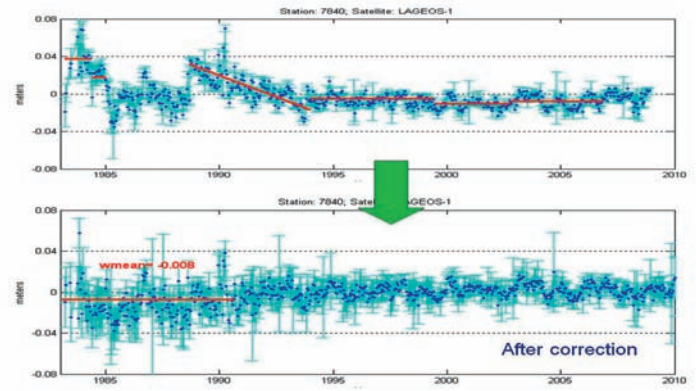


**Figure 1: Herstmonceux systematic errors, before and after corrections**

Figure 1 is an example of the LAGEOS range bias time series for Herstmonceux derived from the multi-year solution without any corrections (graph in the top) and after the application of the mean error correction shown as red segments in the graph at the top of the figure. Each single jump in the time series corresponds to a change in the station configuration: the last one is the replacement of the Stanford time interval counter. As easily seen, a refinement is needed for the data taken before 1991 because a small systematic error is still present.

The monitoring of the systematic correction is a continuous work. The AWG is providing feedback to the station whenever an error is visible in the data and is setting up an integrated alert system in order to support the stations 24 hours per day. One of the last cases is the range bias affecting Wettzell from the beginning of 2009 (see Figure 2), due to a calibration problem; the problem is now solved but the corrections are unrecoverable and the AWG will take care of that.

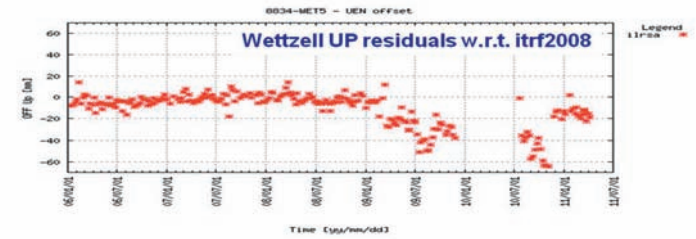


**Figure 2: Wettzell systematic height time series**

# 2. The ILRS contribution to ITRF2008

The realization of the last International Terrestrial Reference System, ITRF2008, follows the same strategy of ITRF2005 and is based on an inter-technique combination of geodetic solutions. The ILRS contribution to ITRF2008 is a time series of loose solutions containing SSC and EOP, from 1983.0 to 2009.0. Each weekly solution is obtained through the combination of weekly solutions submitted by the official ILRS Analysis Centers (ASI, DGFI, GA, GFZ, GRGS, JCET and NSGF) and the AC solutions have strictly followed the ILRS/AWG guidelines, bias policy included.

The major upgrades, with respect to the previous submission for ITRF2005, are the larger time span (starting from 1983 instead of 1993) and the application of the error corrections as defined in the data handling file.

An immediate evidence of the benefit coming from the proper data error correction is the elimination of artifacts in the coordinate time series. As stated before, a range bias is correlated with the site height over short periods and the change of the bias value can introduce jumps in the coordinate time series not corresponding to a real site movement. The problem is obviously bigger when affecting stations with a valuable and extended data set as, for example, in the mentioned case of Herstmonceux. Figure 3 shows the plot of the Herstmonceux UP component, as computed in

ITRF2005, and a discontinuity is clearly visible at the beginning of 2001 while there is no physical reason that can justify its presence; the artifact is not present anymore in ITRF2008.

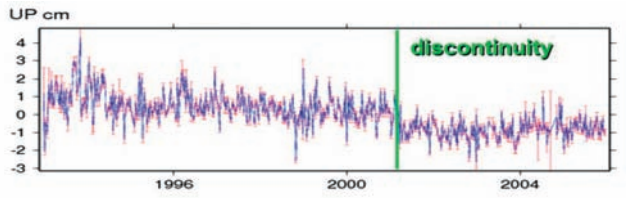


**Figure 3: Herstmonceux height time series in ITRF2005 (plot from itrf.ensg.ign.fr)**

The improvement in the estimate of the individual site coordinates has a direct impact in the reference frame datum. The ILRS SLR time series plays a fundamental role in the definition of the ITRF2008 origin (null translation parameters at epoch 2005.0 and null translation rates with respect to the ILRSA SLR time series) and a major role in the definition of the ITRF2008 scale (null scale and scale rate between ITRF2008 and the average of VLBI and SLR scales/rates).

## 2.1 Origin and scale

The time behavior of the ITRF origin and scale defines the stability of the reference frame: any non linearity or discontinuity is directly mapped into the geophysical results.

The translation and scale factors at epoch 2005.0 and their rates from the ILRS SLR solution to ITRF2008 are reported in the following table. The values have been estimated on the time span 1983-2009 according to the following formula

$$\mathbf{ITRF2008} = \mathbf{T} + \mathbf{SF} \cdot \mathbf{R} \cdot \mathbf{AC}$$

where T is the translation vector, SF the scale factor, R the rotation matrix and AC the SLR solution

| **AC** | | **Offset @ 2005.0**<br>**mm** – *ppb* | **Slope**<br>**mm/y** – *ppb/y* |
|---|---|---|---|
| ILRSA (core sites) | TX | 0.09 ± 0.14 | 0.10 ± 0.02 |
| | TY | -0.01 ± 0.12 | 0.05 ± 0.02 |
| | TZ | -0.66 ± 0.25 | -0.08 ± 0.05 |
| | SF | 0.58 ± 0.02 | 0.04 ± 0.00 |

The translations and their rates should be in principle equal to zero because the ITRF2008 origin is based on SLR and, generally, they are within the 3-sigma. A slope is present in the X translation and it can be explained by a 1 centimeter offset in the period 1982-1988 that will be investigated. All the parameters estimated considering the time range 1993-2009 are within 1-sigma.

Figure 4 shows a graphical representation of the linear fit of the scale estimated in the two time ranges.

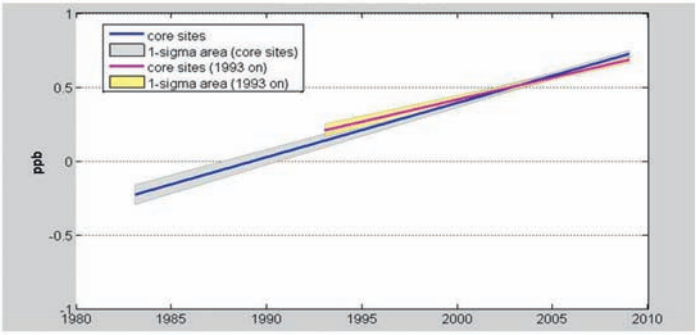


**Figure 4: ILRSA scale offset and rate to ITRF2008**

The realization of ITRF2005 showed a discontinuity in the SLR scale and a low level of agreement between the SLR and VLBI scales (Altamimi et al., 2009), 1.4 (±0.11) ppb at epoch 2005.0 and 0.08 (±0.01) ppb/yr for the scale and scale rate respectively. The effort spent in the improvement of the technique solutions for ITRF2008 brought an increase in the agreement level to 1.05 (±0.13) ppb at epoch 2005.0 for the scale and 0.049 (±0.010) ppb/yr for the scale rate. The SLR scale discontinuity is reduced within the error of the parameter.

# 3. Conclusion

The latest ILRS official product for ITRF2008 has adopted a common bias strategy for the single AC solutions (data handling SINEX file available). The effort devoted by the ILRS AWG has improved the quality of the SLR contribution to ITRF.

The bias monitoring is an ongoing work to keep the ILRS routine product to a high quality standard, in close contact with the site engineers.

## References

*Altamimi,Z., Collilieux,X., Métivier,L.*, 2011 (ITRF2008:an improved solution of the international terrestrial reference frame, J.Geod., doi:10.1007/s00190-011-0444-4)

## Correspondence

Vincenza Luceri
e-GEOS S.p.A.
Contrada Terlecchia SN
75100 Matera

cinzia.luceri@e-geos.it

Giuseppe Bianco
Agenzia Spaziale Italiana
Contrada Terlecchia SN
75100 Matera

giuseppe.bianco@asi.it

Cecilia Sciarretta
e-GEOS S.p.A.
via Cannizzaro 71
00156 Roma

cecilia.sciarretta@e-geos.it

# GNSS satellites as co-locations for a combined GNSS and SLR analysis

*D. Thaller, K. Sośnica, R. Dach, A. Jäggi, M. Mareyen, B. Richter, G. Beutler*

ABSTRACT
GNSS microwave data were analyzed together with SLR observations to GPS, GLONASS, LAGEOS and ETALON satellites for a time span of five years. The GNSS satellites are used for connecting GNSS microwave and SLR range data. Consistently estimated SLR-GNSS range biases, offsets for the satellite microwave antenna as well as for the laser reflector array are derived. Corrections to the official values of about 3.3 cm are obtained for the laser reflector array. The corrections for the microwave antenna differ between the GPS and GLONASS satellites and are in average about 2.5 cm and –14 cm, respectively.

## 1. Introduction

SLR range observations to satellites of Global Navigation Satellite Systems (GNSS) are taken for a long time, especially satellites of the Global Positioning System (GPS) or the Russian GLONASS. The ILRS stations are tracking both GPS satellites equipped with a Laser Reflector Array (LRA), i.e., GPS-05 and GPS-06, as well as a sub-set of the active GLONASS satellites, i.e., for most of the time three satellites in parallel, and since August 2010 the number was increased to six GLONASS satellites. Additionally, Herstmonceux is tracking the full GLONASS constellation since December 2009.

It is well known from the daily Quicklook reports sent out by AIUB (see ftp://ftp.unibe.ch/aiub/slr/gnss_report.txt for the latest report), that the biases seen in the pure SLR range residuals to given GNSS orbits (based on microwave data only) are at the level of a few centimeters. The possible reasons for the biases present in the pure SLR range residuals are manifold:

- bad SLR station coordinates (fixed to SLRF2005),
- discrepancies in the underlying terrestrial reference frames of GNSS (used for the satellite orbits) and SLR (used for the station coordinates), mainly regarding scale and geocenter,
- deficiencies in the modeling of the orbits of the GNSS satellites (problematic issues are, e.g., solar radiation pressure and Earth albedo),
- errors in the phase center model of the GNSS microwave antenna (offsets and variations),
- errors in the offsets of the LRA,
- unknown SLR range biases for GNSS satellites.

## 2. Combined analysis of microwave and range data

In order to overcome the deficiencies with the pure SLR range residuals mentioned above, we performed a combined analysis of SLR range data to the GPS and GLONASS satellites together with the microwave data of a global GNSS network of about 240 stations. The time span 2006 – 2011 (beginning) has been considered, i.e., five years in total. The analysis of the microwave data as well as the SLR data has been done using the Bernese Software (Dach et al., 2007). This guarantees that identical models and parameterizations are used for the analysis of all data.

The analysis of the GNSS microwave data was done in the framework of a combined GPS-GLONASS reprocessing performed by Dach et al. (2011). The phase center model igs05.atx (Schmid et al., 2007) has been used for modeling the a priori antenna phase center offsets and variations. Daily normal equations (NEQs) including GNSS station coordinates, Earth rotation parameters (ERPs), geocenter coordinates, GNSS orbit parameters and satellite antenna offsets (SAOs) were generated.

The SLR data to GNSS satellites have been analyzed using the same orbit modeling for the GNSS satellites as in the analysis of the microwave data. For the time span considered, SLR observations from all stations are available for two GPS satellites and altogether ten GLONASS satellites. SLR data to all GLONASS satellites collected by the station Herstmonceux since December 2009 have been considered additionally. Daily NEQs were generated containing SLR station coordinates, ERPs, geocenter coordinates, GNSS orbit parameters, LRA offsets, and range biases for all stations.

As a result from both steps, combined daily NEQs have been generated with the GNSS orbits determined by both, i.e., microwave and SLR data.

As a third step, SLR data to LAGEOS and ETALON have been analyzed and weekly NEQs were generated. The inclusion of these data should mainly stabilize the estimation of the SLR station coordinates as the amount of SLR data to the GNSS satellites is comparably small (i.e., in average only 10-20 observations per day and satellite).

All NEQs described above have been accumulated for the entire time span of five years. Finally, a combined multi-year solution has been generated with station coordinates and velocities estimated (amongst the other parameters). The station network is aligned to the official TRF by applying no-net-rotation conditions with respect to IGS05 using a subset of GNSS stations. Local ties have not been applied. This implies, that the two space-geodetic techniques GNSS and SLR are connected only at the GNSS satellites tracked by SLR.

The focus of this contribution is on three different parameter types: SLR-GNSS biases (parameterized as a range bias), SAOs for the GNSS microwave antennas, and offsets for the LRA. In order to study these parameters and their correlations, four different solutions have been generated. The characteristics of the solutions are summarized in Table 1. GNSS-SLR bias parameters are estimated as one range bias per station in all solution types. In the case of fixing the SAO parameters to the official values given by igs05.atx (Schmid et al., 2007) it is clear that any errors in the microwave phase center model might show up in the SLR-related parameters, e.g., in the SLR-GNSS biases. The same holds for the solutions with LRA offsets fixed to their official values. These considerations lead to the conclusion that the GNSS-SLR bias parameters resulting from solution types 1-3 cannot be considered to represent real SLR range biases. Only the bias parameters resulting from solution type 4 represent real SLR range biases. The question arises, however, whether the three parameter types estimated in solution type 4 can be de-correlated.

| | Solution 1 | Solution 2 | Solution 3 | Solution 4 |
|---|---|---|---|---|
| GNSS-SLR “range” bias parameter | 1 bias per station estimated | 1 bias per station estimated | 1 bias per station estimated | 1 bias per station estimated |
| LRA offset | Fixed to official values | Fixed to official values | Correction for the z-component estimated | Correction for the z-component estimated |
| Microwave SAO | Fixed to values of igs05.atx | Correction for the z-component estimated | Fixed to values of igs05.atx | Correction for the z-component estimated |

**Table 1: Types of combined GNSS-SLR solutions.**

# 3. Results

## 3.1 SLR-GNSS bias parameters

The estimated SLR-GNSS bias parameters per station are shown in Figure 1 for the different solution types listed in Table 1.

In the first solution, i.e., assuming the LRA as well as the SAO to be correct, the estimated bias parameters are at the centimeter level and quite systematic (almost all negative). This leads to the conclusion that several effects are absorbed by these parameters such that they cannot be considered to be actual SLR "range biases".

When estimating corrections for the SAO (solution 2, not shown in Figure 1), the bias parameters do not change significantly: the median of the differences compared to the first solution is 0.4 mm. Therefore, we conclude that errors in

the SAO values do not map into the SLR-GNSS range bias parameters. On the other hand, the resulting bias parameters still cannot be considered to be an SLR "range bias", as already stated for solution 1.

In the case of the third solution (i.e., estimating corrections to the LRA offsets), the resulting bias parameters clearly change (see Figure 1). In general the values are smaller than in the solutions discussed before, and they are less systematic with positive as well as negative values. The differences compared to solution 1, however, are rather systematic, i.e., about 25 mm for almost all stations. From this behavior we may conclude that the biases we see in the pure SLR range residuals might be due to an error in the LRA offset.

Compared to the third solution, the estimated bias parameters do not change significantly for the fourth solution (median difference compared to solution 3 is 0.0). This is a good indication that all parameter types can be estimated together.

The resulting SLR-GNSS bias parameters may represent real SLR range biases only in the case of solution types 3 and 4.

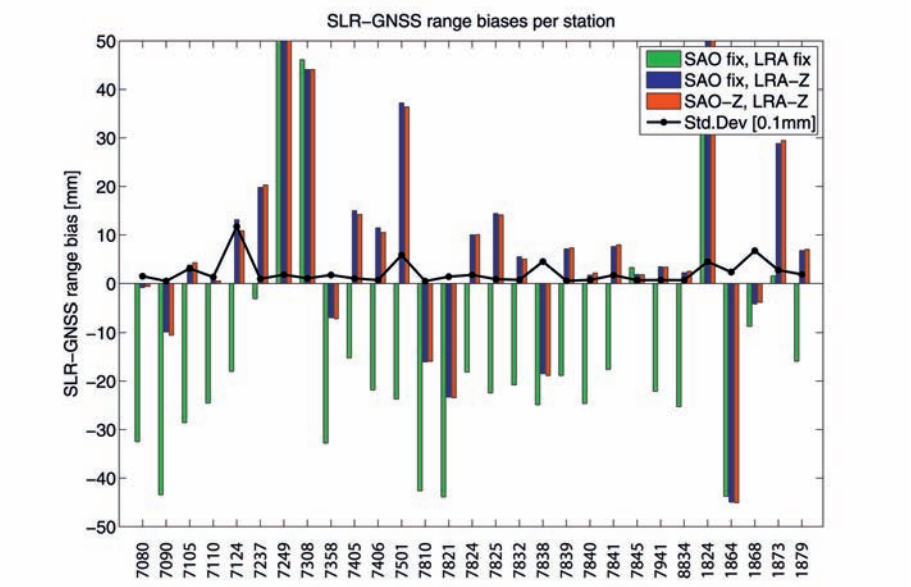


**Figure 1: Station-specific SLR-GNSS range bias parameters including their formal errors.**

## 3.2 Z-Offsets for Laser Reflector Array

Independently of estimating corrections for the microwave SAO or fixing them to igs05.atx values, the corrections to the LRA z-offset are in the order of about 3 cm. The estimates are shown in Fig. 2a for the two GPS satellites tracked by the ILRS sites and all GLONASS satellites. The mean corrections for the GPS and GLONASS constellation for solution types 3 and 4 are given in Table 2. We can see that the impact of additionally estimating corrections for the microwave SAO is negligible for GPS and only at the level of a few millimeters for GLONASS. This can be explained by the fact that the SAO for GLONASS given in igs05.atx are obviously not correct (see e.g. Dach et al., 2011).

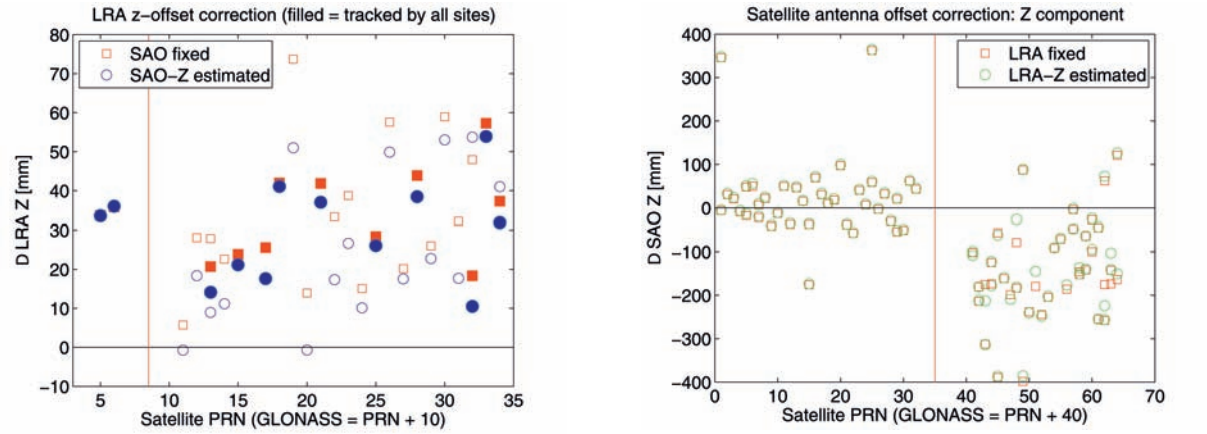


**Figure 2: a) Corrections to the LRA offsets in z-direction (filled signatures: satellites tracked by all SLR stations; open signatures: satellites tracked only by Herstmonceux since Dec. 2009); b) Corrections to the microwave SAO in z-direction.**

## 3.3 Z-Offsets for GNSS microwave antenna

The estimated corrections to the SAO in z-direction are shown in Figure 2b for the full GPS and GLONASS constellations. The corrections are quite different for both constellations: only about 25 mm in average for GPS (see Table 2), whereas about 140 mm for GLONASS and even with opposite sign. This confirms the assumption made already in Sec. 3.2 that the igs05.atx values for GLONASS are wrong, and it confirms earlier studies by Dach et al. (2011) and Thaller et al. (2011). The differences between solution types 2 and 4 (i.e., additionally estimating LRA corrections or not) are about 3 mm, thus, they are negligible. This behavior confirms that the three parameter types SLR-GNSS range bias, LRA offset and SAO can be estimated together.

| | **Mean correction for LRA z-offset [mm]** | | **Mean correction for SAO in z [mm]** | |
|---|---|---|---|---|
| | GPS | GLONASS | GPS | GLONASS |
| **Solution 2** | - | - | 23.3 | -142.4 |
| **Solution 3** | 34.8 | 33.6 | - | - |
| **Solution 4** | 34.8 | 26.5 | 25.9 | -138.8 |

**Table 2: Estimated corrections to the offsets of the LRA and the microwave antenna: Mean corrections for the GPS and GLONASS constellations.**

# 4. Conclusions

Combined solutions based on GNSS microwave data, SLR observations to GNSS satellites, LAGEOS and ETALON allow to estimate the relevant geodetic parameters consistently, i.e., station coordinates, satellite orbits, ERPs, SLR range biases as well as offsets at the GNSS satellites to the microwave antenna and the LRA. The accurate knowledge of the latter two parameter types is essential for combining both observation types, i.e., microwave and range data. Our studies revealed that the offsets provided by igs05.atx as well as the official LRA offsets do not fit together and do not fit to the observations. Corrections to both offsets are estimated at the centimeter level. Improvements may arise if the newly provided ITRF2008 and the corresponding SAO values of igs08.atx are used. Furthermore, the studies revealed that the three parameter types range bias, offsets for the LRA and microwave SAO can be estimated together. When estimating only range bias parameters, the resulting values do not represent a real SLR “range bias”, but absorbs as well errors in the two offsets.

## Acknowledgements

The IGS and ILRS are acknowledged for providing microwave and SLR tracking data.

## References

*Dach, R., Hugentobler U, Fridez P, Meindl M (2007)*: Bernese GPS Software Version 5.0. Astronomical Institute, University of Bern.

*Dach, R., Schmid R, Schmitz M, Thaller D, Schaer S, Lutz S, Steigenberger P, Wübbena G, Beutler G (2011)*: Improved antenna phase center models for GLONASS. GPS Solutions, Vol. 15(1), pp. 49-65, DOI 10.1007/s10291-010-0169-5.

*Schmid, R, Steigenberger P, Gendt G, Ge M, Rothacher M (2007)*: Generation of a consistent absolute phase center correction model for GPS receiver and satellite antennas. J Geod, Vol. 81(12), pp. 781–798. DOI 10.1007/s00190-007-0148-y.

*Thaller, D, Dach R, Seitz M, Beutler G, Mareyen M, Richter B (2011)*: Combination of GNSS and SLR observations using satellite co-locations. J Geod, Vol. 85(5), pp. 257-272, DOI 10.1007/s00190-010-0433-z.

## Correspondence

Thaller Daniela
Astronomical Institute, University of Bern, AIUB
Sidlerstrasse 5
CH-3012 Bern
Switzerland

thaller@aiub.unibe.ch

# Spin of Ajisai: influence of Solar Irradiation on the spin period and precession of the spin axis measured by the Graz 2 kHz SLR system

*D. Kucharski[1], G. Kirchner[2], T. Otsubo[3], F. Koidl[4], M. Kobayashi[5]*

ABSTRACT

Using Graz 2 kHz SLR data of more than 5 years we calculated spin period of Ajisai with an accuracy of 84 µs (0.0042% of the spin period value). The spin period is increasing with an exponential trend: T = 1.9028 • Exp(0.014859 • (Year - 2003.0)) [s]. This slow down is mainly caused by gravitational and magnetic fields of the Earth. The high accuracy of the spin period determination allows detection of small perturbations of the spin period caused by non-gravitational effects related to the solar energy flux to which the satellite is exposed.

The high repetition rate of the laser makes it possible to determine the epoch time when the laser is pointing directly between two corner cube reflector rings of the satellite. Identification of many such events during a few (up to 3) consecutive passes allows to calculate the satellite orientation in the inertial frame. Analysis of 6 years of 2 kHz SLR data delivered 331 orientation values which clearly show precession of the spin axis with a period of 117 days. Accurate measurements of Ajisai's spin parameters are necessary for the envisaged laser time transfer via Ajisai mirrors.

## 1. Introduction

The Japanese Experimental Geodetic Satellite Ajisai is a fully passive object equipped with 1440 corner cube reflectors (CCRs) for SLR and 318 mirrors. Spin parameters of Ajisai have been investigated scientifically (Kirchner et al., 2007; Kucharski et al., 2009, 2010; Otsubo et al., 1998; 2000). The knowledge of spin period and spin axis orientation of such passive satellite allows for investigation and improvement of physical models of the perturbing forces which are of magnetic, gravitational and non-gravitational nature.

## 2. Spin period determination

Ajisai, like the other Low Earth Orbit (LEO) satellites, reflects strong laser pulses to a receiving telescope of the SLR station. The detection system at Graz SLR allows to measure the distance to the nearest CCRs of Ajisai. Fig. 1 – left shows the range residuals (measured minus predicted range) for a two second part of a Graz kHz SLR pass from September 9, 2008.

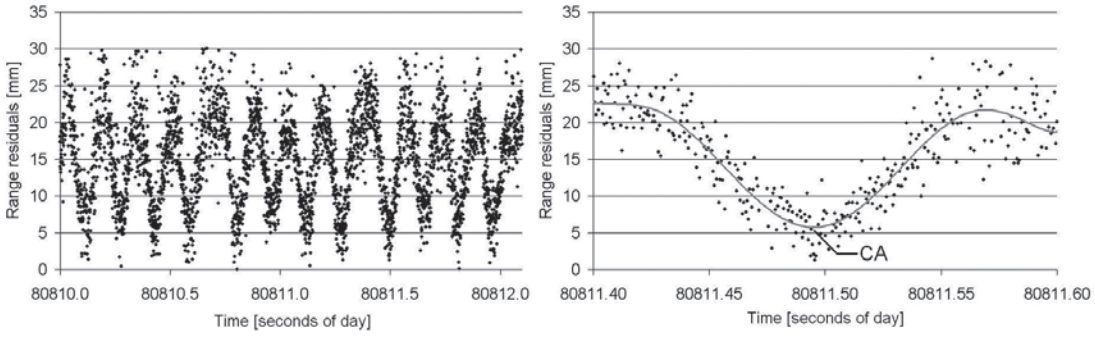


**Fig. 1: Left: Ajisai range residuals of Graz 2 kHz SLR observation taken on September 9, 2008 (~2 seconds part only); the 0 level is the mean level. Right: closer look to a single peak, the gray curve is a 6th degree polynomial function – the minimum value of the function indicates the closest approach (CA) between the CCR panel and the SLR station.**

Fig. 1 – right gives a closer look to a single peak. In order to calculate the epoch time of the closest approach (CA) between a given CCR panel and the SLR station we approximate the range residuals of a single peak with a polynomial function. The minimum value of this curve defines the epoch time of the CA; it is determined with an accuracy of 5 - 7 ms.

The epoch times of the peaks are used for calculation of Ajisai spin period. The method is based on a model of Ajisai spin (fig. 2), where two coordinate systems are introduced: the Construction Coordinate System (CCS – c index) which is satellite body fixed (and is spinning with the satellite), and the inertial Spin Coordinate System (SCS – s index) which is centered at the satellite. Ajisai spins around its symmetry axis of the body $Z_C$ which coincides with $Z_S$. Since the Ajisai spin axis is almost parallel (± 1-2 °) to the Earth spin axis and is stabilized by a passive nutation damper, the SCS is set to be parallel to the Inertial Coordinate System (J2000). This model neglects polar motion of the Earth. As Ajisai is spinning clockwise the phase angle φ between $X_S$ and $X_C$ is decreasing with time.

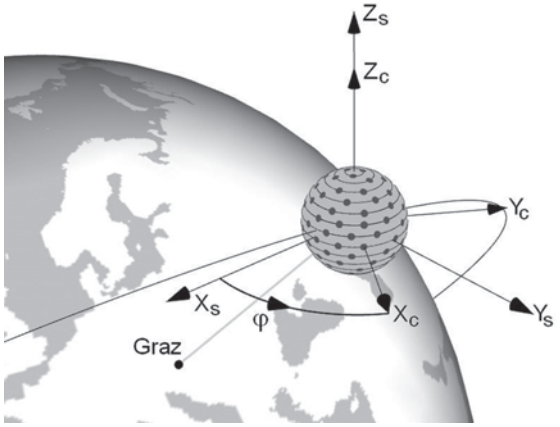


**Fig. 2: Ajisai spin model. The Construction Coordinate System (c index) is fixed with the body of the satellite, and spins within the Spin Coordinate System (s index). The phase angle φ between the two coordinate systems decreases with time.**

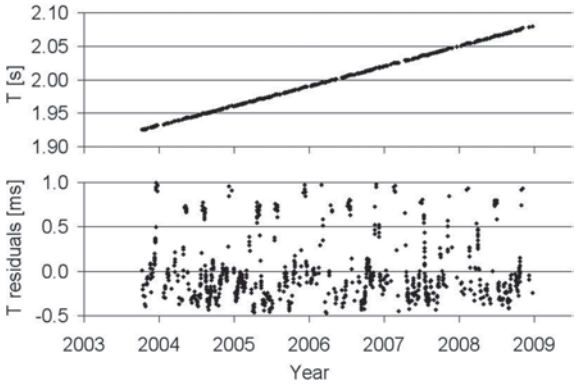


**Fig. 3: Top: Ajisai spin period values calculated from 877 Graz 2 kHz SLR passes from October 9, 2003 to December 22, 2008. Bottom: spin period residuals calculated to the exponential trend function of the spin period values.**

In order to calculate Ajisai spin period for a given pass the epoch times of the peaks are calculated (Fig. 1-right). Because Ajisai spin axis orientation is almost parallel to the Earth's spin axis, it is possible to define which CCR ring Graz station is ranging to at a given epoch. For an epoch time of a given peak the spin model allows identification of the phase angle φ at which the corresponding CCR panel has the nearest distance to the SLR station. Usually it is possible to identify around 300 peaks during a single pass, which indicate a linear decrease of the body's phase φ. This methodology was applied to 877 Ajisai kHz SLR passes measured at Graz kHz SLR station between October 9, 2003 and December 22, 2008. The spin period results are presented on fig. 3 – top and show an exponential trend: T = 1.9028818 • Exp (0.0148591 • (Year - 2003.0)) [s]. Fig. 3 – bottom presents spin period residuals calculated to this exponential trend function. The distribution of the spin period residuals indicates that the slowing down rate of Ajisai is not constant, what is caused by the solar energy flux received by the satellite and known as Yarkovsky and Yarkovsky – Schach effects. We used Total Solar Irradiance (TSI; at the Earth's distance) parameter to build a model for Ajisai spin period residuals. The model of the spin period residuals is calculated as a mean value of the TSI acting on Ajisai during one orbital cycle (116 minutes).

Fig. 4 – top presents the model function and Ajisai spin period residuals for the year 2004. The value of the model function is low when Ajisai orbit is partially (up to 30%) in the shadow of the Earth (fig. 4 – bottom). When the orbit is completely out of shadow, the satellite constantly receives solar energy, and the value of the model is high. The RMS of the T residuals around the model function calculated for the full set of data (877 Ajisai passes, more than 5 years) is 84 μs – about 0.0042 % of the spin period value.

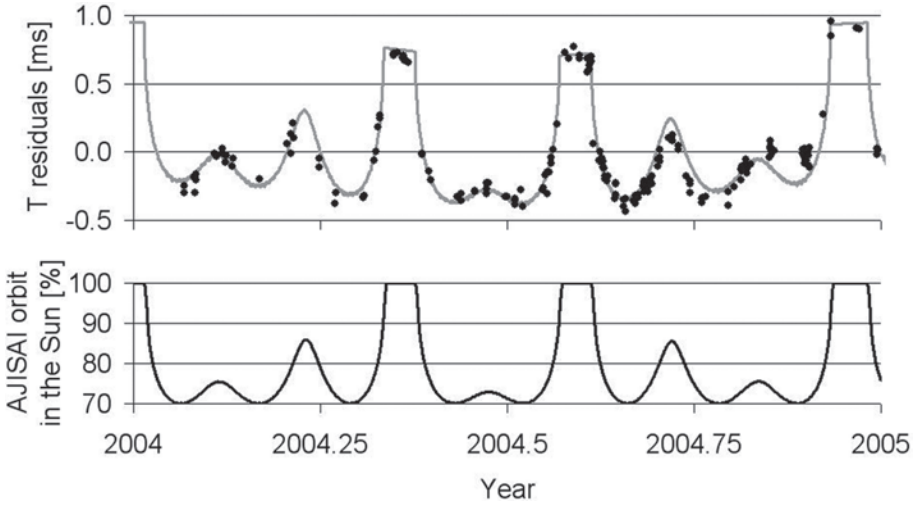


**Fig. 4: Top: Ajsiai spin period residuals (black points) and the model function (grey line); year 2004. Bottom: Percent of Ajsiai orbit being in the Sun (penumbra zone included).**

# 3. Spin axis orientation determination

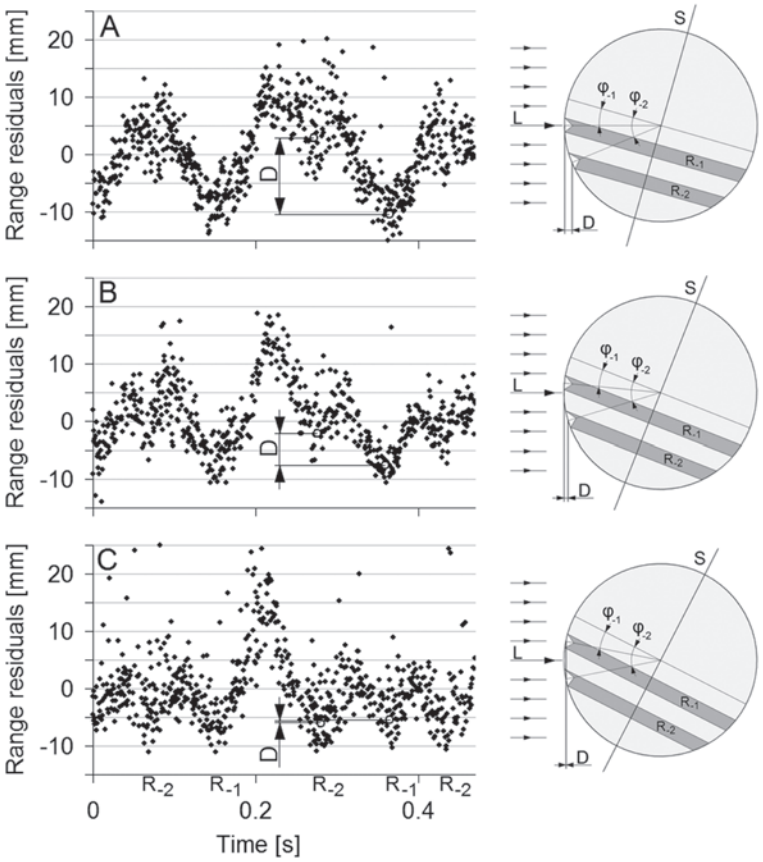


During a single pass the satellite is changing its attitude to the SLR station, thus the laser is pointing to different latitudes of the satellites body. Because the Ajisai spin axis orientation is roughly known, it is possible to predict the body's latitude that the Graz station is ranging to at a given epoch time. During the ranging the SLR system detects photons reflected by the CCRs of the neighboring rings. Fig. 5, case A: the $R_{-2}$ ring is more distant for the incident laser beam than $R_{-1}$ thus the SLR residuals show the distance D between the CA of the corresponding peaks. As the station – satellite mutual attitude is changing during the pass, the distance D is decreasing (situation B). Case C occurs when the laser is pointing directly between the $R_{-1}$ and $R_{-2}$ rings, thus the distance D is close to zero.

In order to determine the spin axis orientation we search in the data for the epoch time $t_0$ when D = 0. The linear change of the D value within a short time slot of the pass allows estimating $t_0$ with precision of 2 – 3 s.

**Fig. 5: Left: Ajisai range residuals. Right: laser axis L is pointing to the CCRs of the rings. S is the satellite's spin axis; $R_{-1}$ and $R_{-2}$ are the CCR rings which are placed on different latitudes of the body ($\varphi_{-1}$, $\varphi_{-2}$). L is pointing: A) directly to the $R_{-1}$, B) between $R_{-1}$ and $R_{-2}$, C) exactly to the middle between $R_{-1}$ and $R_{-2}$. D is the distance between peaks given by CCR panels from the two neighboring rings.**

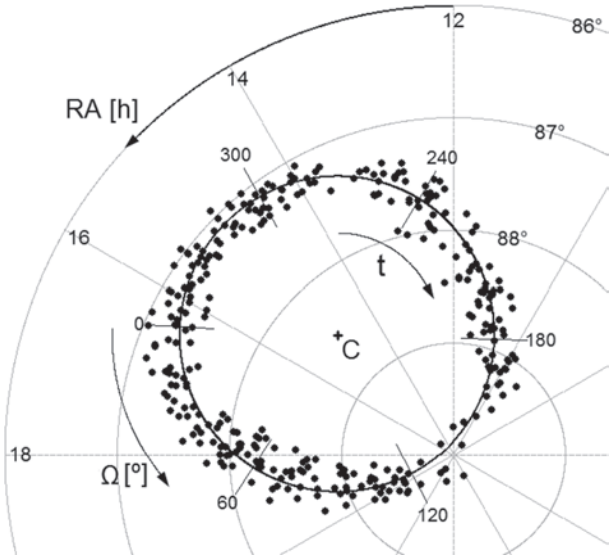


**Fig. 6: Spin axis evolution in J2000.0 celestial reference frame: measurements (dots), precession cone (circle with center C) is scaled with values for the right ascension of the ascending node of the orbit (Ω). Time follows t arrow.**

Determination of $t_0$ and identification of the observed rings gives the body's latitude where the laser beam is pointing to. This information is sufficient to find possible spin axis orientations that Ajisai can have at a given epoch time. Investigating at least two $t_0$ events allows calculation of a single solution for the spin axis orientation. We used 749 passes and calculated 331 spin axis orientation values. In order to determine single orientation value we have processed SLR data from passes measured within 6 hours, assuming that the change of the spin axis is negligible within this time.

Fig. 6 presents the spin axis orientations (black points) plotted in the J2000.0 celestial reference frame. The spin axis vector is precessing along a cone centered (C) at $14^h56^m2.8^s$ in right ascension and at 88.512° in declination with the half aperture angle θ of 1.405°; the residual RMS of the orientation measurements is 0.128°. The orientation of the central vector C is estimated by applying a least squares method to the spin axis orientation measurements. The period of the spin axis precession is close to 117 days and is equal to the period of the right ascension of the ascending node (Ω) of Ajisai's orbit.

# 4. Conclusions

Graz 2 kHz SLR system is able to measure the spin period and spin axis orientation of the passive, geodetic satellite Ajisai during day and night. The spin period is measured with the best accuracy ever reached: 84 μs RMS, corresponding to 0.0042% of ~2 s spin period. Analyzing the range measurements to single CCR panels of Ajisai enables determination of the actual attitude of the satellite, thus accurately deriving its spin. The spin period is slowing down with an exponential trend under influence of the gravitational and magnetic fields of the Earth. KHz SLR also enables identification of the small spin perturbations caused by the solar energy as it is acting on the satellite. Knowledge of this phenomenon is essential to investigate the small forces and torques caused by non-gravitational effects (Yarkovsky, Yarkovsky – Schach) which perturb the satellite motion.

Analysis of six years of 2 kHz SLR ranging delivered 331 orientation values determined with RMS of 0.124° in declination and 7' – 40' in right ascension. The accuracy of the spin axis orientation determination can be improved by measuring distance to Ajisai from a few different ground locations (kHz SLR systems). The spin axis is precessing along a cone centered at $14^h56^m2.8^s$ in right ascension and 88.512° in declination with the half aperture angle θ of 1.405°. The axis is precessing with a 117 days period which is equal to the period of right ascension of the ascending node of Ajisai's orbit. This coincident can be a result of the orbital plane orientation to the Sun radiation vector.

Spin determination of Ajisai is essential for the next generation time transfer (Kunimori et al., 1992) – transmission of laser pulses between SLR stations via Ajisai mirrors to compare time scales at the picosecond level. The achieved accuracy of the spin period and spin phase determination allows precise predictions of epochs at which a single mirror of Ajisai is orientated properly to reflect laser pulses between the participating SLR stations.

## Acknowledgments

The study of Ajisai spin period was sponsored by the Space Research Institute of the Austrian Academy of Sciences. The study of Ajisai spin axis orientation was sponsored by the Hitotsubashi University (under grant of National Institute of Information and Communications Technology; NICT, Japan).

## References

*Kirchner, G., Hausleitner, W., Cristea, E.*, 2007. Ajisai Spin Parameter Determination Using Graz Kilohertz Satellite Laser Ranging Data. IEEE Trans. Geosci. Remote Sens., 45 (1), 201-205.

*Kucharski, D., Kirchner, G., Otsubo, T., et al.*, 2009. 22 years of Ajisai spin period determination from standard SLR and kHz SLR data. Adv. Space Res., 44 (5), 621-626, doi: 10.1016/j.asr.2009.05.007.

*Kucharski, D., Kirchner, G., Otsubo, T., et al.*, 2010. The impact of solar irradiance on Ajisai's spin period measured by the Graz 2 kHz SLR system. IEEE Trans. Geosci. Remote Sens., 48 (3), 1629-1633, doi:10.1109/TGRS.2009.2031229.

*Kunimori, H., Takahashi, F., Itabe, T., et al.*, 1992. Laser ranging application to time transfer using geodetic satellite and to other Japanese space programs. In Proc. 8th Int. Workshop on Laser Ranging Instrumentation, Annapolis, NASA Conf. Pub. 3214, 1-38-1-42.

*Otsubo, T., Amagai, J., Kunimori, H.*, 1998. Measuring Ajisai's spin motion. In Proc. 11th Int. Workshop on Laser Ranging, Deggendorf, Germany, 674–677.

*Otsubo, T., Amagai, J., Kunimori, H., et al.*, 2000. Spin Motion of the Ajisai Satellite Derived from Spectral Analysis of Laser Ranging Data. IEEE Trans. Geosci. Remote Sens., 38 (3), 1417-1424.

## Correspondence

1) Daniel Kucharski; Space Science Division, Korea Astronomy and Space Science Institute; 776, Daedeok-Daero, Yuseong-Gu, Daejeon, 305-348, South Korea; e-mail: daniel@drdk.org , daniel@kasi.re.kr

2) Georg Kirchner; Space Research Institute of the Austrian Academy of Sciences; Lustbuehelstrasse 46, A-8042 Graz, Austria; e-mail: georg.kirchner@oeaw.ac.at

3) Toshimichi Otsubo; Hitotsubashi University; 2-1 Naka, Kunitachi, 186-8601 Tokyo, Japan;
e-mail: t.otsubo@r.hit-u.ac.jp

4) Franz Koidl; Space Research Institute of the Austrian Academy of Sciences; Lustbuehelstrasse 46, A-8042 Graz, Austria; e-mail: franz.koidl@oeaw.ac.at

5) Mihoko Kobayashi; Hitotsubashi University; 2-1 Naka, Kunitachi 186-8601 Tokyo, Japan;
e-mail: mihoko.kobayashi@r.hit-u.ac.jp

# BLITS: spin parameters and its optical response measured by the Graz 2kHz SLR system

*D. Kucharski[1], G. Kirchner[2], H.-C. Lim[3], F. Koidl[4]*

ABSTRACT

The nanosatellite BLITS (Ball Lens In The Space) is the first object designed as a passive, spherical retroreflector of the Luneburg type, dedicated for Satellite Laser Ranging. The 2 kHz SLR station Graz measures spin parameters and the optical response of this satellite, providing information about the rotational dynamics and the optical properties of the body. The measurements obtained during the period from September 26, 2009 to November 24, 2010 show a significant change of the spin configuration. The spin axis was dynamically precessing since the launch and currently is sinus-like behaving between coordinates RA 120°...150°, Dec 30°...60° (J2000 inertial reference frame). The angle between the symmetry axis and the spin axis of BLITS is not constant, but is decreasing since the launch, while its spin period is rather stable with a mean value of 5.613 s (clockwise rotation). The satellite was dynamically changing its attitude during the first three months after deployment; after this time the spin parameters are relatively stable.

The optical response of BLITS has been also measured and compared with the response of the classical retroreflector arrays (RRA) of the Low Earth Orbiting satellites such as ERS-2 and Stella. The optical response of BLITS is flat and featureless, comparable with the signature of a point-source or a flat target, and suggests that this innovative design will deliver a higher Normal Point (NP) accuracy (2.55 mm) than any other SLR target currently in orbit. The high reflectivity of the glassy BLITS (about 60% of the return rate from the multi-reflector Stella) is found to be decreasing by about 30% per year, probably due to the solar irradiation. The high return rate of SLR measurements proves that the spherical lens can be a perfect successor of the classical RRA panels mounted on active satellites such as CHAMP, GOCE and GRACE.

## 1. Introduction

The BLITS (Vasiliev et al., 2007) satellite has been designed and manufactured by the FSUE-IPIE (Federal State Unitary Enterprise - Institute for Precision Instrument Engineering, Moscow, Russia). The purpose of this passive, spherical nanosatellite (radius 85.16 mm, mass 7.53 kg) is an experimental verification of the spherical glass retroreflector satellite concept (Luneburg lens), as well as obtaining SLR data for the solution of scientific problems in geophysics, geodynamics, and relativity by millimeter and sub-millimeter accuracy range measurements.

The satellite consists of an inner glass sphere (radius 53.52 mm) covered by concentric glass half-shells. The inner sphere and the outer half-shells have different refraction indices (inner: 1.76, TF105 type; outer: 1.47, LK6 type). The external surface of one of the half-shells is aluminum coated and protected by a varnish layer. In this way, the nanosatellite BLITS demonstrates a new concept of the geodetic satellites which is an alternative for the conservative structure of a spherical body equipped with glass Corner Cube Reflectors (CCR). BLITS was launched on September 17, 2009 into a sun-synchronous, near-circular orbit with a mean altitude of 832 km (orbital period 101.3 minutes), and an inclination of 98.85°.

## 2. Spin determination

The geodetic SLR satellites are typically designed as fully passive spheres equipped with CCRs, BLITS is the first satellite which is a single, passive retroreflector by itself what reduces available spin measurement techniques to kHz SLR only (Kucharski et al., 2011a, 2011b). As the satellite is spinning, the laser beam of the SLR system is alternately pointing to the transparent or coated hemisphere, thus series of measurements / no measurements intervals during a pass are visible. Fig. 1 presents range residuals (O-C, observed minus predicted range) calculated for a pass measured on November 14, 2010. The range residuals presented show that the duration of the intervals is changing during a pass. It is a consequence of a specific configuration of the satellite's body in reference to its spin coordinate system (Fig. 2). Fig. 2 presents the configuration of the satellite centered coordinate systems. The Body (B) spins within the Spin (S) coordinate system around the spin axis $Z_S$. The symmetry axis $X_B$ of the body is crossing the tops of the half-shells and is orientated towards the reflective one. The $Z_B$ axis crosses the border between the half-shells. The orientation of the B system

within the S frame is expressed by two angles: spin phase α and latitude φ of the symmetry axis. The non-equal intervals visible in Fig. 1 indicate that φ is different from 0°. At begin of the pass (Fig. 1, top) shorter intervals of measurements are visible. If the spin period during a pass is constant, the incident angle between the laser beam and the spin axis $Z_S$ defines the duration of the observed intervals.

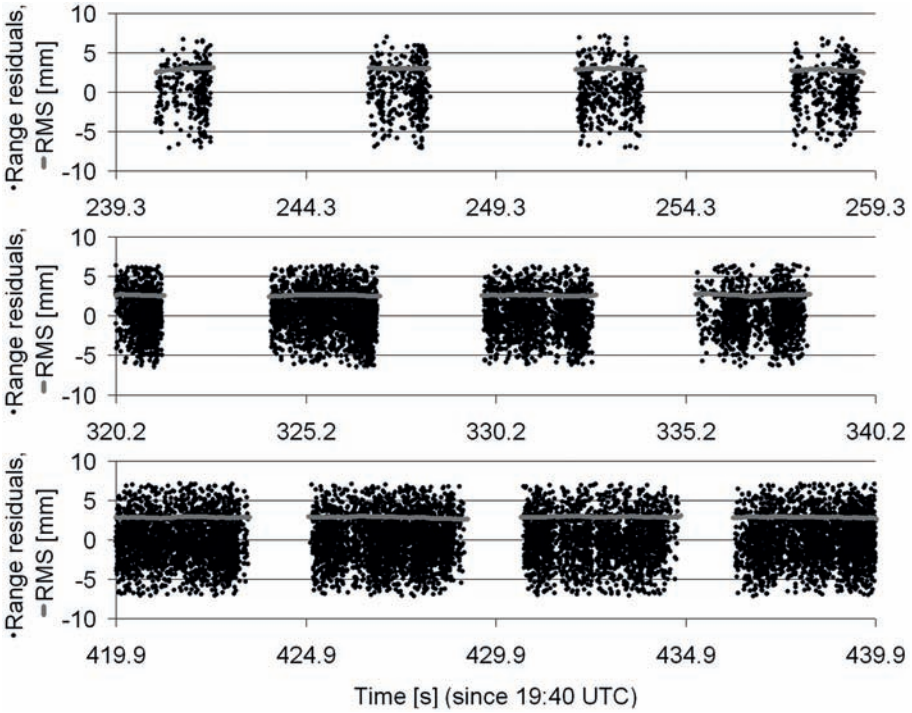


**Fig. 1: Range residuals of BLITS; pass on November 14, 2010 (423 days after launch). Three slots (20 seconds each) from different parts of the pass show change of interval durations. The 0 level is the mean value.**

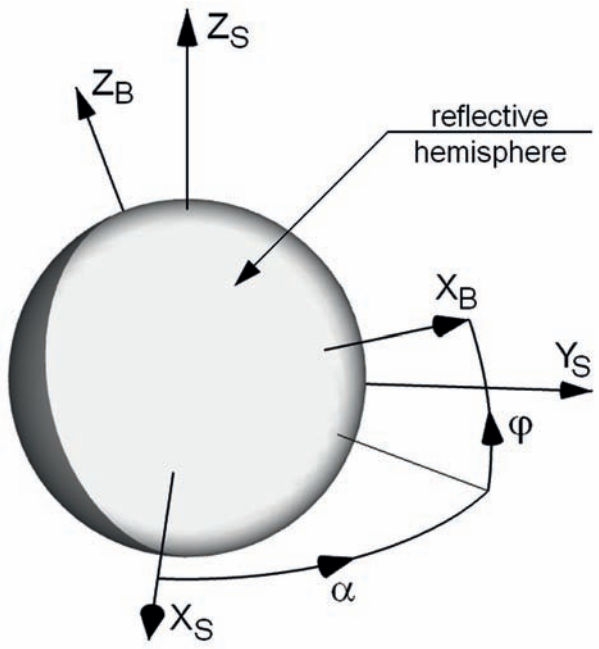


**Fig. 2: Sat. centered coordinate systems (right-handed, Cartesian): Body (B) and Spin (S). The spin phase is expressed by angle α and the latitude of the symmetry axis within the spin coordinate system by angle φ.**

During the middle of the pass (Fig. 1, middle) the laser beam is approximately perpendicular to the spin axis, thus the duration of intervals with returns and intervals without returns are similar. At the end of the pass (Fig. 1, bottom) the incident angle causes longer illumination periods of the reflective hemisphere. Simulating the SLR measurements to BLITS allows investigation of its spin parameters. 41 passes measured from September 26, 2009 to November 24, 2010 by the Graz 2 kHz SLR station were used for the calculation of the latitude angle φ – the result is presented in Fig. 3. The obtained φ values show a sinusoidal change of the latitude angle φ: increase for CCW and decrease for CW direction of the spin. The trends indicate that the symmetry axis is sinusoidally approaching the spin axis since the deployment. This may be caused by the gravity field which is forcing the body to spin around its symmetry axis. Coincidence of the symmetry axis and the spin axis will eliminate the periodical appearance of return / no-return intervals during a single pass, and will introduce long, full-pass phases where the inertial orientation of the satellite determines possibility of the laser ranging. The solutions of the angle φ (CW and CCW) were applied to all (70) good passes measured by Graz

from September 26, 2009 to November 24, 2010. For each single pass the latitude angle φ was predicted and examined by simulations with the full range of possibilities for the spin axis orientation. The best fit criterion of the duration of the return intervals between simulations and observations was used in order to find the actual spin axis orientation and spin period. The RMS of the obtained spin period values around a trend function is 4.77 ms for CW and 5.49 ms for CCW spin direction. The difference in the RMS is caused by the apparent spin effect, which is related to the station – satellite mutual attitude change during a pass. This effect is correctly removed by simulations for the CW case, what indicates the rotation direction of BLITS. The solutions for RA, Dec and spin period obtained for CW rotation are depicted in Fig. 4. The obtained trends indicate that the spin axis orientation was very unstable after launch, but after about 100 days since deployment it is tumbling around the same area. The spin period of the satellite remains almost constant ($T_{mean}$ = 5.613 s), however two trends are visible. The first stage (up to day 72 after launch) shows a slight increase of the spin period, while the second stage (from day 187 after launch) shows the opposite trend. This behavior can be forced by the initial, very dynamic change of the spin axis orientation.

# 3. Optical response of BLITS

During a single pass of a satellite laser range measurements are performed. The obtained raw range values are converted into range residuals (O-C, measured minus predicted range). Fig. 5 presents range residuals calculated for three example passes measured by the Graz 2 kHz SLR station: top) BLITS, pass measured on March 29, 2010; epoch time of the first data point on the plot: 19:12:58 (UTC); RMS of the normal points $RMS_{NP}$=0.047 mm; middle) ERS-2, August 31, 2009; 20:39:42, $RMS_{NP}$=2.208 mm; bottom) Stella, August 26, 2009; 0:29:12, $RMS_{NP}$=0.088 mm. The plots present the response of the three different reflector types. The spherical lens BLITS allows to obtain a symmetrical, Gaussian distribution of the range residuals (Fig. 5-top). During the pass the distribution of the residuals around the mean remains symmetrical (flat) allowing for sub-millimeter accuracy of the range determination between the SLR station and the center-of-mass (COM) of this spherical satellite. The RRA of ERS-2 (Fig. 5-middle) presents the response of a CCR panel. Due to the construction of the panel only one CCR will be observed at a given attitude of the satellite. As the satellite is passing the station, the pointing of the laser beam around the CCR panel is changing and different prisms are observed. Therefore the mm-scale range variations can be distinguished.

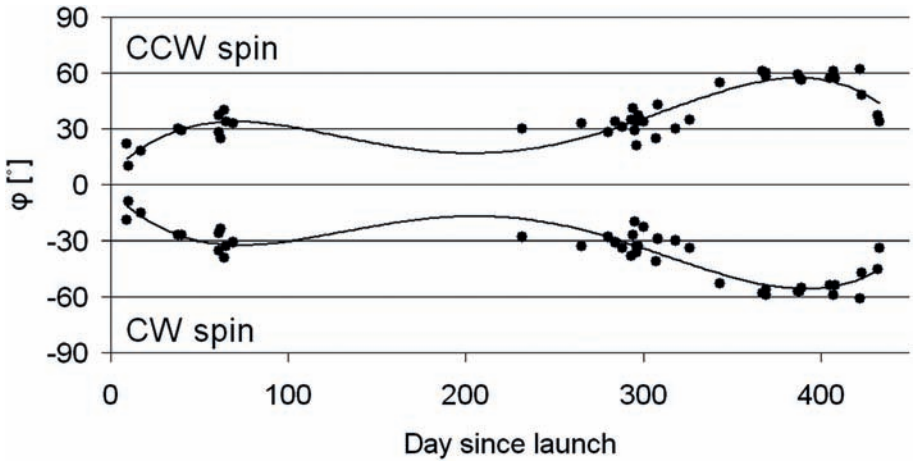


**Fig. 3: Values of the latitude angle φ, obtained from 41 passes for clockwise (negative φ) and counter-clockwise (positive φ) spin direction. The results are approximated by 4th degree polynomial functions. RMS calculated to the trend function: $RMS_{CCW}$=6.25°, $RMS_{CW}$=5.85°.**

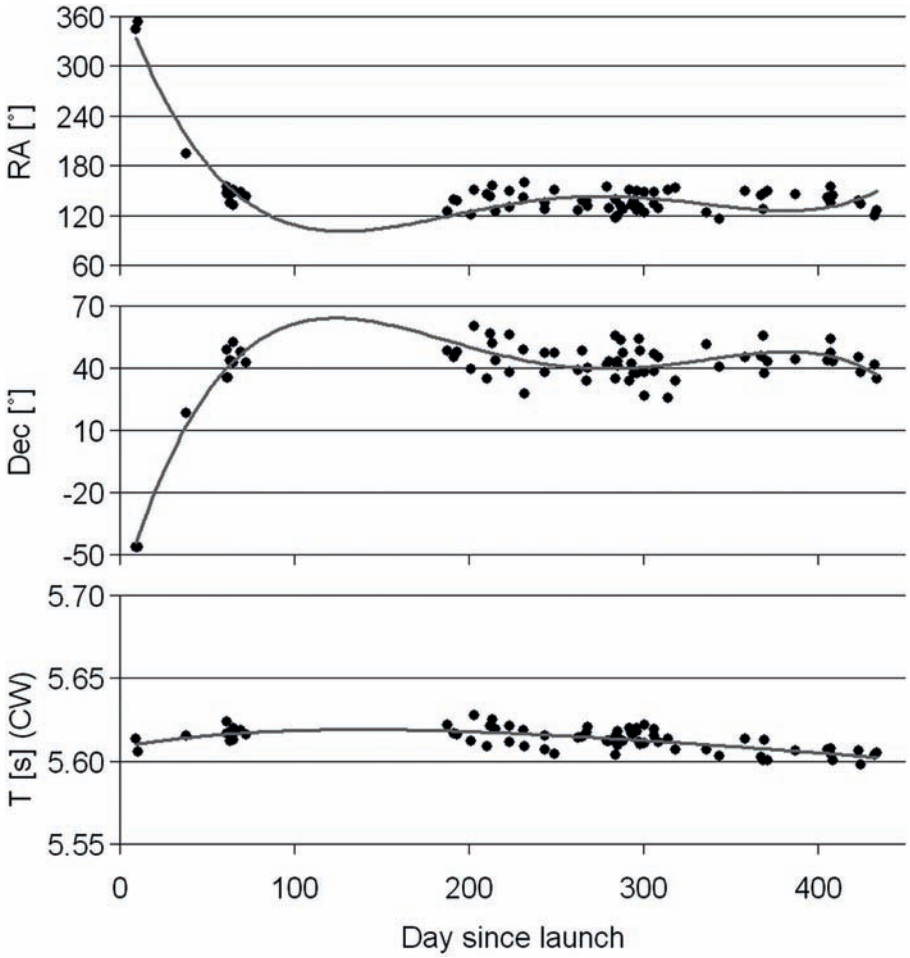


**Fig. 4: Spin axis orientation and spin period obtained for CW spin direction. The values are expressed in the J2000 inertial reference frame. Mean value of the spin period $T_{mean}$ = 5.613 s. RMS calculated to the trend functions: $RMS_{RA}$=14.7°, $RMS_{Dec}$=7.02°, $RMS_{T}$=4.77 ms.**

The spherical RRA of Stella (Fig. 5-bottom) is not free from the transition effect between the single CCRs. In this case, however, the large number of CCRs (60) uniformly distributed over the body ensures that during the pass there will always be at least one CCR pointing (almost) directly to the SLR station thus representing the face front of the satellite. The dense distribution of the CCRs allows the measurement of reflections from multiple CCRs at any given attitude of the satellite – this effect is represented by the up/down slope traces above the leading edge. Such a property causes a nonsymmetrical distribution of the range residuals thus decreasing the accuracy of the station – COM distance determination.

In order to determine a systematic deviation of an SLR system the SLR station regularly performs range measurements to a flat ground target. The range residuals calculated for such a calibration have a symmetrical, Gaussian distribution (not influenced by the satellite signature) and indicate the accuracy of the SLR system.

RMS of the range residuals used for NP formation during the period September 17, 2009 – February 10, 2011 (Graz SLR station only) is for BLITS: *2.55 mm*, ERS-2: 2.87 mm, Larets: 3.11 mm, Stella: 4.34 mm and LAGEOS-1: 5.09 mm. The RMS of the system calibrations to the flat, ground target is *2.25 mm*. The unique construction of BLITS allows achieving very stable and more accurate NPs compared to the classical RRA.

In order to investigate the stability of the BLITS return rate, satellite Stella was selected as a reference. Stella was launched on September 26, 1993 into a circular orbit at 800 km altitude and an inclination of 98.6° (BLITS: 832 km, 98.77°). The coincidence of these parameters between Stella and BLITS helps to compare the two different RRAs. Similar orbits

of those objects assure that the Graz SLR station measures similar ranges to the satellites at given elevation. The relative response expressed by a return rate ratio BLITS/Stella allows, to some extent, to eliminate the SLR system dependent factors, which may change over time.

The relative return rate BLITS/Stella calculated for the elevations of 50° - 80° is decreasing by about 30% per year.

# 4. Conclusions

BLITS is the first satellite designed as a spherical retroreflector for SLR. The body has a clear symmetry axis around which the mass of the transparent and coated hemispheres is distributed. During the deployment the separation system made the satellite spin around an axis almost perpendicular to the symmetry axis of the body. Graz 2 kHz SLR measurements indicate that the spin parameters of the satellite were not stable after the launch. The initial, very dynamic, change of the spin axis orientation could be caused by a direct action of the deployment mechanism or by the influence of Earth's gravity field, due to an offset between the geometrical center and the center-of-mass of the satellite. The large scatter of the spin axis orientation ($RMS_{RA}$=14.7°, $RMS_{Dec}$=7.02°) and the angle φ (RMS=5.85°) around the trend functions might be a result of irregular mass distribution over the body: non-uniform density of the lenses and the glue layer between the inner core and the outer shells; non-uniform thickness of the aluminum coating and the varnish layer.

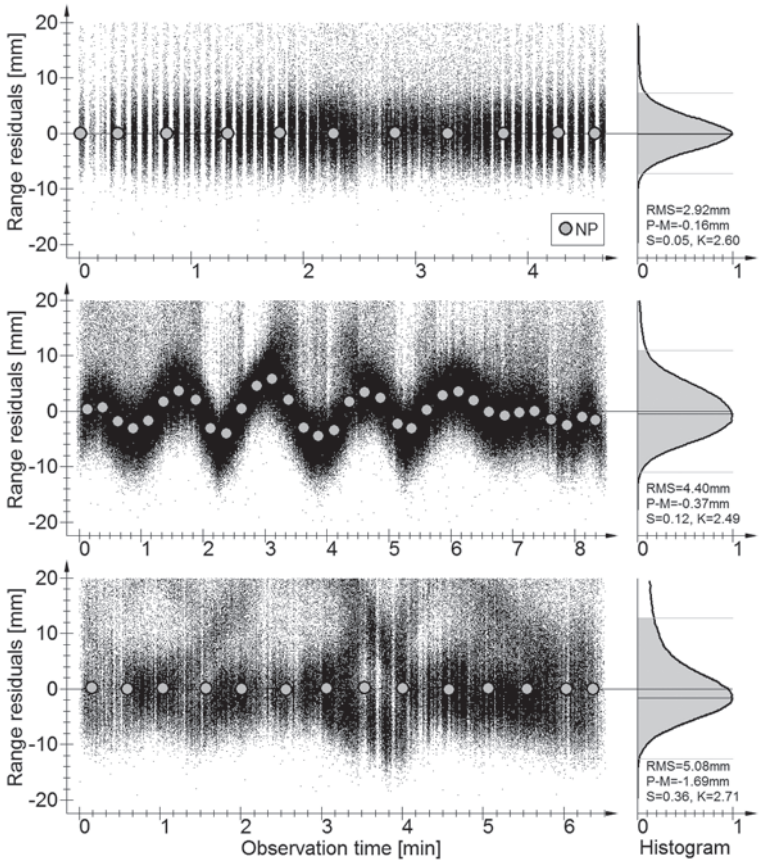


**Fig. 5: Range residuals obtained from Graz 2 kHz SLR measurements to: BLITS (top), ERS-2 (middle), Stella (bottom). Zero level is a mean value after 2.5 σ filtering. The NPs (grey circles) are calculated with steps of 30 s (BLITS, Stella) and 15 s (ERS-2). Normalized histograms on the right side show the distribution of the range residuals (grey area - after σ filtering); statistical parameters of the distributions are RMS, peak minus mean (P-M), skewness (S) and kurtosis (K).**

Due to construction of BLITS, the optical range correction (the distance from the apparent reflection point to the center-of-mass of the satellite) is constant down to sub-mm scale, and is independent of the attitude of the satellite. The flat response of BLITS allows for the most precise range measurements among the SLR satellites on the precision

level of measurements to the ground target. Information about spin parameters and spin evolution of the fully passive satellites helps to understand, describe and model the forces and torques caused by the gravity field, the magnetic field and the non-gravitational effects which influence the orbital motion of satellites. The successful application of the spherical retroreflector satellite concept allows recommending this solution for future active satellites such as the LEO missions CHAMP, GOCE or GRACE. Using a spherical reflector, instead of a classical RRA, would provide more accurate and stable determination of the COM – at sub-mm level, instead of > 5 mm variations for classical RRA – and a wider incident angle between the laser beam and the nadir direction over which SLR measurements can be obtained for the stabilized satellites.

## Acknowledgments

The study of BLITS spin parameters was sponsored by the Space Research Institute of the Austrian Academy of Sciences, and the study of BLITS optical response was sponsored by the Korea Astronomy and Space Science Institute.

## References

*Kucharski, D., Kirchner, G., Koidl, F.*, 2011a. Spin parameters of nanosatellite BLITS determined from Graz 2 kHz SLR data. Adv. Space Res. 48 (2), 343-348, doi: 10.1016/j.asr.2011.03.027.

*Kucharski, D., Kirchner, G., Hyung-Chul Lim, Koidl, F.*, 2011b. Optical response of nanosatellite BLITS measured by the Graz 2 kHz SLR system. Adv. Space Res., doi: 10.1016/j.asr.2011.06.016, in presss

*Vasiliev, V. P., Shargorodsky, V. D., Novikov, S. B., et al.*, 2007. Progress in laser systems for precision ranging, angle measurements, photometry, and data transfer. ILRS Fall 2007 Workshop, Grasse, France, 25-28 September 2007.

## Correspondence

1) Daniel Kucharski, Space Science Division, Korea Astronomy and Space Science Institute, 776, Daedeok-Daero, Yuseong-Gu, Daejeon, 305-348, South Korea, e-mail: daniel@drdk.org , daniel@kasi.re.kr

2) Georg Kirchner, Space Research Institute of the Austrian Academy of Sciences, Lustbuehelstrasse 46, A-8042 Graz, Austria, e-mail: georg.kirchner@oeaw.ac.at

3) Hyung-Chul Lim, Space Science Division, Korea Astronomy and Space Science Institute, 776, Daedeok-Daero, Yuseong-Gu, Daejeon, 305-348, South Korea, e-mail: hclim@kasi.re.kr

4) Franz Koidl, Space Research Institute of the Austrian Academy of Sciences, Lustbuehelstrasse 46, A-8042 Graz, Austria, e-mail: franz.koidl@oeaw.ac.at

# Session 7: Improving Ranging Accuracy, Calibration and Local Ties I.

# Alternative approach to the SLR data precision

*Ivan Prochazka*

ABSTRACT
We are presenting an alternative approach to assess the SLR data precision limit. The precision estimate calculated as a time deviation using the Allan algorithm is common in time and frequency community. Its application in SLR data processing might provide an independent check of data quality and reveal some effects and biases. Several recommendations for the future SLR development are listed.

## 1. General

Satellite Laser Ranging (SLR) is a space measuring technique which provides unique feature of direct range measurement. Its role is inevitable in ITRF definition and calibration of numerous other techniques [1]. The constantly increasing requirements on SLR product precision and accuracy represent a permanent challenge for stations themselves and data analysts as well. High precision limit is prerequisite for high accuracy. The precision s of the mean value should increase

$$s \sim 1/SQR(N), \qquad (1)$$

where N is a number of averaged values as a consequence of a data normal distribution. The question is - how long (up to what N) one can average to increase the precision? Or in another words, what is the precision limit when averaging over a longer period of time? This precision is limited by the system stability and biases involved. An alternative tool to investigate the precision limit is the computation of the precision in terms of time deviation. This technique is used as a standard in a time and frequency scientific community, the software package applied is a commercial one [2].

## 2. Precision limit of Graz SLR data

The time variance algorithm STABLE32 [2] was applied to Graz SLR data acquired in 2011. The Graz station is operating at 2 kHz rate, the laser pulse length is 10 ps, the echo pulses were detected by the time walk compensated C-SPAD detector, the timing was maintained by the Graz ET device based on Thales-Dassault Event Timing Modules.

The example of pure single photon SLR is in Figure 1, where ranging data of the CompassM1 pass are plotted. The modest single shot precision was 7 mm is corresponding quite well to the system performance and target characteristics. One can note that the precision is increasing with increasing averaging time following exactly the equation (1) up to the averaging time of about 100 seconds. For these averaging times the precision limit is 0.2 mm.

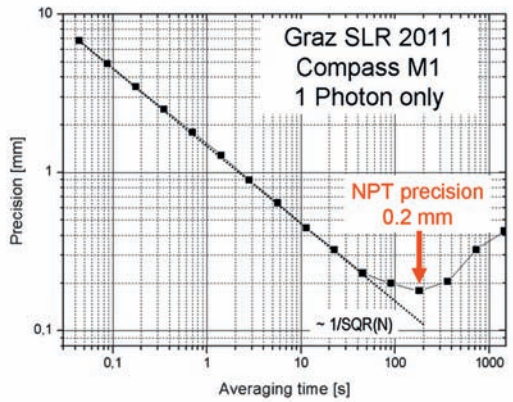


**Figure 1: Precision in terms of time deviation evaluated for SLR data to Compass M1 satellite at Graz. Note the precision limit of 0.2 mm and precision increase following the theoretical curve up to ~ 100 s.**

For comparison, look at the precision evaluated in terms of time deviation for the same SLR system ranging to ERS-2 satellite in Figure 2.

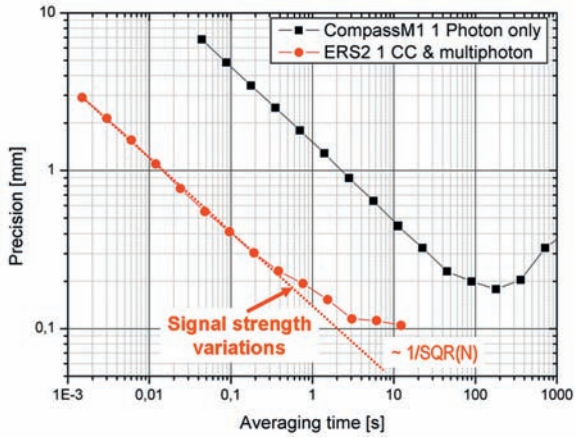


**Figure 2: Precision in terms of time deviation evaluated for SLR data to ERS-2 satellite at Graz.**

Note the precision limit of 0.1 mm achieved for 10 s averaging time and precision increase not following the theoretical curve due to additional biases – induced by signal strength variation in this case. Only a short part of the entire pass was selected for the situation, when single retro-reflector was involved, thus the target depth was negligible. The echo signal strength corresponded to multi-photons. The single shot precision was 2.9 mm RMS.

The additional satellite laser ranging data were added in Figure 3. The Lageos data were edited for the "first retro" [3].

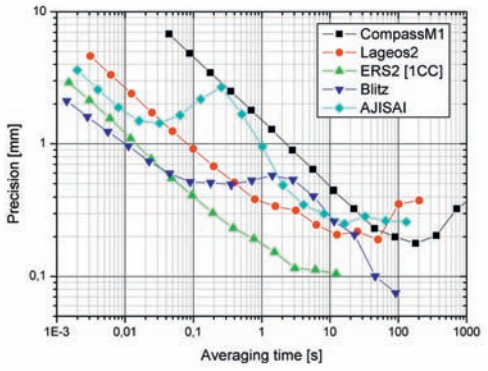


**Figure 3: the precision in terms of time deviation evaluated for Compass M1, Lageos2, ERS2, Blitz and Ajisai satellites, SLR Graz.**

The influence of the complex structure of the satellite retro reflector array together with the signal strength variations influence on the detection delay may be seen for Lageos, Blitz and Ajisai satellites.

# 3. Conclusions made on the basis of Tdev data

Numerous important conclusions may be done on the basis of interpretation Time deviation data:

- precision limit for all the satellites is below 0.3 mm
- the normal points of 5 seconds will provide sub-mm precision normal points with sufficient margin for all targets,
- data editing procedure applied (in Graz) for Lageos data [3] is increasing the resulting precision, however the appropriate CoM correction must be applied in this case.
- the behavior of Blitz data needs further investigations. Surprisingly, the deviation from the ideal curve of precision versus averaging time is large. Probably the echo signal strength variations are responsible for the effect.

The most important conclusion, although not unexpected, is:

**The ultimate precision and accuracy SLR may be obtained by high repetition rate system operating on purely photon counting level.**

## References

*[1] Z. Altamini et al,* "ITRF2008: an improved solution of the international terrestrial reference frame", J Geod, DOI 10.1007/s00190-011-0444-4.

*[2] Hamilton J.*, Hamilton Technical Services 650 Distant Island Drive Beaufort, SC 29907 USA, 2010

*[3]G. Kirchner et al,* "Millimeter Ranging to Centimeter Targets", proc.of the 16th WLRI, Poznan, Poland, 2008, p 338-340

## Correspondence

Ivan Prochazka
Czech Technical University in Prague
Brehova 7
115 19 Prague
Czech Republic
e-mail prochazk@cesnet.cz

# ILRS Standardization of Hardware, Software, and Procedures

*Randall Ricklefs*
*The University of Texas at Austin*
*Center for Space Research*

ABSTRACT
Over the years, the ILRS has established and refined standards for station performance. However, standardization of hardware, software, and procedures appropriate for ILRS stations and operations, analysis, and data centers has been spotty. Advantages and disadvantages of standardization are explored. Finally, a proposal is made to augment the current performance-based standards with a standard station reference design and additional software as a way to facilitate new station construction.

## 1. Introduction

Whenever a technology advances beyond it primitive stage, there is an urge to establish standards to pass the collective wisdom on to other potential users and to keep acceptable options at a manageable level. The technology used in the International Laser Ranging Service is no exception. The organization has standards for many activities from data distribution procedures to data formats. The overarching standard for the entire group is the stations' level of performance. The issue of standards is examined here in terms of the level of standardization that best promotes the goals of the ILRS. In discussing this topic, one must consider what is already standardized, what can be standardized, and how standards can be enforced. As an outcome of these discussions a proposal is presented to codify the ILRS best practices into a laser ranging station reference design.

## 2. Standardizing on Performance

The ILRS currently focuses on levels of performance of each of its stations, publishing a quarters “report card” for all the world to see. [1] The guidelines that separate the high performance stations from those aspiring to perform well were presented at the Shanghai laser workshop in 1996 and published on the ILRS web site [1]. They are as follows.

**Yearly Data Quantity Guidelines**

- 1000 Low Earth Satellite (LEO) passes
- 400 LAGEOS 1,2 passes
- 100 High Satellites passes

**Data Quality Guidelines**

- 1 cm LAGEOS normal point precision
- 2 cm short term bias stability
- 1 cm long term bias stability

**Operational Compliance Guidelines**

- Data delivery with 12 hours (latency)
- Specified ILRS normal point format
- Current site and system information form (i.e., site log)

In addition to the performance standards, the ILRS web site provides many standards for data formats, sample software, and various procedures.

# 3. What do we want from standardization?

There must be a point to having standards. For instance, they need to encourage reliable, accurate performance, which is especially true as the stations push their accuracy to the 1 mm level. To reach this and related goals, the standards must incorporate the best mature hardware, software, and procedures available. Some of the results should be a reduction in cost of design, operations, and maintenance of laser stations and their sub-systems. While there will always be a need for research on new or refined techniques, good standards will reduce unproductive duplication of effort. However, standards should not stifle creativity and progress, but channel it, and encourage innovation and flexibility. Standardization should be a resource, not a "ball and chain."

# 4. Who and what is involved?

It is important to identify the stakeholders in the standardization discussion. The stations will receive most of the attention, since they are the critical point where data is taken and processed. Stations are complicated systems, encompassing hardware, software, and procedures which must be considered for standardization. Standards for the operations, data, and analysis centers deal mainly with procedures, as will be explained below. Also below, the current status and potential expansion of standardization is examined for hardware, procedures, and software/algorithms by stakeholder.

## 4.1 Hardware (Stations)

Listed below are some of the hardware subsystems found on nearly all laser ranging stations. These are all candidates for some type of standardization.

Time standards (GPS, cesium, etc.)

Range gate generator

Detectors (APD, SPAD, MCP)

Radar

Other infrastructure

Laser (10Hz, 100Hz, 2kHz, 10kHz)

Timers (event and interval; some to avoid)

Calibration piers

Telescope/dome

Delving into standards for each of these items is beyond the scope of this paper. However, it should be mentioned that one difficulty in creating a set of stations with identical hardware is that the market changes quite rapidly. Today's best detector may not be on the market in 6 months or may have been produced in limited quantities, and 2 copies of the same timer model may not contain the same components. While the ILRS workshop papers show a certain undercurrent of commonality in many of these subsystems, the bottom line is that each station is its own standard.

## 4.2 Procedures

### 4.2.1 Stations

Some of the key areas of the ranging stations with important procedures are listed below. Many of these overlap with underlying hardware and software that implement them.

Surveys (how often; what gets surveyed)

Prediction and restriction (Go/No-go) downloads

Status messages (NASA LORs; EUROLAS status)

Site log/system configuration file maintenance

Station change notice (for data quarantine)

Range calibrations (how often, etc.)

Ranging satellites

Ranging data uploads

Adding new targets

Telescope mount modeling

Where these procedures interface with the rest of the network, such as prediction download and data uploads, standardization already exists to prevent chaos. Creating the required procedures is only the first step. The stations must then actually use the procedures to conduct surveys, maintain site log and configuration files, and send station change notices to the ILRS!

### 4.2.2 Centers

Operations centers need to ingest and distribute new data at a certain time and from/to specific locations. They also need to screen the data for format compliance and perform quality checks. They also must handle quarantined data from new and updated stations and make it available only to analysts for validation. Data centers also need to ingest and distribute new data at a certain time and from/to a specific location. They also report data statistics.

Analysis centers have the same need to ingest data, along with screening and fitting data to solve for a host of parameters. They also create and distribute data products for the ILRS. Another part of their effort is to validate new or upgraded stations to insure that data quality is acceptable. They also tell stations when they find problems with data.

Many of the procedures above are already standardized to allow for consistent handling of ranging data and products. Some procedures such as handling quarantined data are works in progress. Quarantining data also requires the stations to make it known when significant changes have been made to their equipment. There are differences in the content and philosophy of creating daily normal point files, and the data screening done by the EDC and NASA OCs is somewhat different. The file and directory naming conventions are generally compatible between the centers for data in the CRD format, for which consistency has been a priority. The naming disparities with the old data format are considerably more serious.

## 4.3 Software/Algorithms

While it is quite important to have fully documented algorithms, having the algorithms implemented in ready-to-use source code can make life much easier for station developers and maintainers. Each station has a common set of software needs, often expressed and implemented in very different ways. It is important to examine which of these needs can be filled with a standard piece of software. As an alternative to standard code, sample code has been made available for certain projects like Consolidated Prediction Format (CPF) and Consolidated Ranging Data format (CRD). The distinction is that sample code consists of programs or subroutines that can be tailored to the needs of each station, or can just be a starting point for writing custom code. Standard code would be used as written.

### 4.3.1 Station Data Acquisition

There are several areas in which the data acquisition system, to the extent that is a separate from the data reduction system, presents several opportunities for standardized, or at least sample, code. Some of these are discussed below.

Telescope mount model fitting: Software that takes stars' observed-calculated (o-c) point angle residuals and fits them to a particular mount model is something each station needs. The mount model itself may be different at each station due to mount peculiarities. However there is a common set of 5-10 terms most telescopes will need, so including at least a basic model would be helpful. Other mount-specific terms can be added by the stations as needed. The software to point and track the stars to take the o-c residuals will contain more station dependencies, although the NASA network is able to run 5 different telescope designs with one carefully "ifdef-ed" program. There is also a need for other mount model software to handle very telescope-dependent needs, such as Fourier transform modeling of optical encoders.

Star and planet prediction and refraction: There are at least 2 sets of well-tested free star and planet prediction software packages available to developers, the US Naval Observatory's NOVAS code and the Rutherford-Appleton Labs Starlink (now maintained by the University of Hawaii). [2][3] JPL provides FORTRAN and c code to manipulate its DE series of lunar and planetary ephemerides. [4] There are also several refraction routines available, one developed by Mendes and Pavlis, who are involved in ILRS analysis. [5]

Sun avoidance: Whenever laser stations are engaged in daytime ranging, it is very important to keep the telescope from pointing at the sun. Many stations have developed algorithms and code to accomplish sun avoidance, so it is also a good candidate for standardization.

Tracking restrictions: In the last few years, it has become increasingly important for stations to implement methods of getting and using go/no-go files, pass segment files, and the like. [6] While much of the code for this task remains station-dependent, the ILRS could gain from having publicly available code capable of interacting with the standard restriction file formats.

Prediction sample routines: FORTRAN and c routines to read, write, check, interpolate, and convert CPF files already exist on the ILRS website. [7]

Range data sample routines: Similar to the CPF code, FORTRAN and c routines to read, write, check, and convert CRD format files are also available. [8]

There are undoubtedly more data acquisition system software packages that could become candidates for standardization, depending on the level of hardware abstraction used. At some point in the SLR data acquisition system, ranging and computer system hardware and operating system dependencies make further standardization difficult if not impossible..

### 4.3.2 Station Data Processing

There are some clear candidates for standardization on the station data analysis system. Prediction download/preparation and data upload software can be shared among stations with similar operating systems. The data pre-filtering software (e.g., Poisson filtering) and normal point generation are modular enough to be common between systems, although there are one yet available from the ILRS. In fact, there is already a set of routines called *distrib* on the ILRS web site that calculates data averages, moments, and the like, and can be used as the heart of data calibration programs. [9] Of course, the CPF and CRD sample code mentioned above also has application on the data processing systems. Some years ago, Herstmonceaux made available the *npcheck* program. It checks normal points for obvious errors including out-of-bound rms-es and calibration values. Another example is the *eurostat* software, developed at Zimmerwald, which has made sharing current station status simple. [10] There is a clear need for additional “standard” programs to be made generally available to ILRS stations.

### 4.3.3 Centers

The Operations, Data, and Analysis Centers have less code that has historically been shared. Clearly, it is important than algorithms be similar. CRD/CPF sample code can be used in each of these types of centers. The IERS Conventions (2003 is currently used) offer algorithms and code that the ILRS analysts all use. [11] However, the precision orbit determination (POD) software is decidedly not standardized, with the following programs being used at the operations and analysis centers shown in parentheses. [12]

| | | |
|---|---|---|
| GEODYN (JCET, ASI, GA) | EPOS (GFZ) | DOGS (DGFI) |
| GINS (GRGS) | SATAN (NSGF) | NAPEOS (ESA) |
| Bernese (BKG) | | |

This is perhaps the area most suited for separate software packages, since using diverse software sets that produce similar results with the same data strengthens ones convictions that the results can be believed. Similar to the overall ILRS standardization philosophy, here the performance is the standard.

# 5. Standards Enforcement

Standards have no effect unless used. Since the ILRS is a volunteer organization in which each station is funded and operated by different entities, each with its own goals, the ILRS must appeal to common needs to achieve its common goals. Since ILRS members have united to gain benefits from cooperating, educating each ILRS component about the needs and benefits of maintaining standards is the only effective enforcement mechanism. Part of this mechanism has been the agreement that the quarterly report cards with its cut lines can be used to commend good performance or encourage better performance. Those below the line need to improve their hardware, software, and procedures (or funding!) to bring performance up to par and to ensure that their data can be used in a meaningful way.

# 6. SLR Reference Design

Another approach for using standardization to convey best practices is to maintain an SLR station reference design, probably on the ILRS website. This design would incorporate the best, proven, and available hardware and software, and "best practices" procedures. It would also provide viable alternative standards and their compatibility with other sub-systems. This "station" need not be built, but its design can be a starting point for any group wanting to build or update an SLR station.

The components of such a design would be at least block diagrams of hardware, software, and procedures, a list of manufacturers, a list of deprecated components, reference articles by subsystem, and a list of "experts" for each component or sub-system. Some of these items already exist on the ILRS website, and such a project could unify and fill in the gaps in the existing work. [13]

# 7. Conclusion

For many reasons, absolute standardization of ILRS satellite laser ranging stations is not possible, even were every station to be replaced. The current standardization on performance, not on hardware and software, has functioned well, but can be augmented by a further online resources, including more "standard" and "sample" software and a station reference design. Standards need to be enforced, but here again, the existing system of quarterly report card provides a good motivator, while education and additional resources provide a good reward for the ILRS's efforts.

## Acknowledgments

We would like to thank NASA for support through NASA contract NNG06DA07C.

## References

[1] http://ilrs.gsfc.nasa.gov/stations/site_info/global_report_cards/index.html

[2] http://aa.usno.navy.mil/software/novas/novas_info.php

[3] http://starlink.jach.hawaii.edu/starlink

[4] http://www.projectpluto.com/jpl_eph.htm

[5] http://ilrs.gsfc.nasa.gov/engineering_technology/index.html

[6] http://ilrs.gsfc.nasa.gov/satellite_missions/restricted.html

[7] http://ilrs.gsfc.nasa.gov/products_formats_procedures/predictions/cpf.html

[8] http://ilrs.gsfc.nasa.gov/products_formats_procedures/crd.html

[9] http://ilrs.gsfc.nasa.gov/products_formats_procedures/normal_point/np_algo.html

[10] W. Gurtner, "Near Real Time Status Exchange", Proceedings of the 14th International Laser Ranging Workshop, San Fernando, Spain, June 2004 (543-547).

[11] http://tai.bipm.org/iers/conv2003/conv2003.html

[12] E. Pavlis, private correspondence, 13 April, 2011.

[13] http://ilrs.gsfc.nasa.gov/engineering_technology/timing/index.html

# Event Timer A033-ET: Current State and Typical Performance Characteristics

*Artyukh Yu., Bespal'ko V., Boole E., Vedin V.*

ABSTRACT

The main results of experimental evaluation of precision characteristics (conventionally considered as well as new ones) for the Event Timer A033-ET are presented in this report. These results allow to suppose that the A033-ET really provides the measurement precision and rate that altogether seem sufficient for both routine and advanced KHz SLR.

## 1. Introduction

The Event Timer A033-ET represents the latest model of Riga event timers intended for SLR. It has been developed as an advanced version of the previous model A032-ET [*Bespal'ko V., et al.*, 2008] that is well known in SLR community. As it was announced at the 16th ILRS Workshop [*Artyukh Yu., et al.*, 2009], the A033-ET became commercially available from 2010, and up to now 10 units of this device have been manufactured and carefully tested. Consequently, significant statistics have been accumulated to reliably specify the A033-ET typical performance characteristics

Generally the A033-ET and A032-ET are closely related instruments in terms of general architecture and functionality. The main difference concerns the A033-ET precision which has been considerably improved, making the A033-ET one of the highest precision event timers commercially available. In this paper we'll focus on specification of the actually obtained precision characteristics.

## 2. A033-ET precision characteristics

### 2.1 Single-shot RMS resolution

We consider the single-shot RMS resolution as the main parameter specifying the practicable A033-ET precision and define that as the standard deviation of instrumental error in asynchronous measurement of time intervals between events. The commonly used way to specify the actual value of the single-shot RMS resolution for particular instrument is direct repetitive measurement of time intervals between events defined by a periodic test pulse sequence. For that we used low-jitter (RMS<1 ps) crystal clock oscillators with period of test pulses which is virtually incommensurable with internal clock period of the timer. The evaluated in this way single-shot RMS resolution typically is in the range 2.5-3.0 ps (Fig.1).

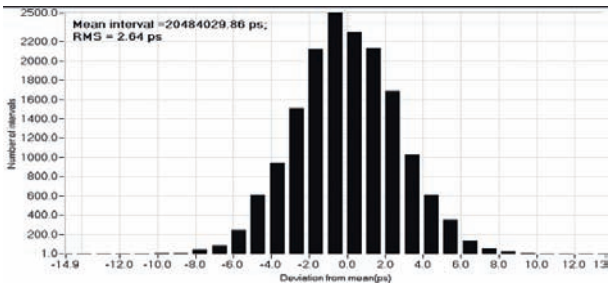


**Figure 1: Histogram of time intervals measured by the A033-ET**

It should be noted that the A033-ET offers the best resolution under stable measurement conditions. In particular, natural fluctuations of the ambient temperature result in a slight long-term instability of the practicable resolution (Fig.2).

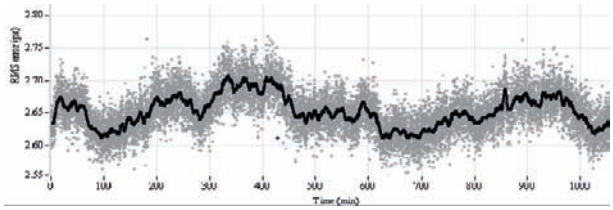

**Figure 2: RMS resolution vs. time under ambient temperature variation in the range ±2.5 °C**

As can be seen, such instability is quite acceptable to support the measurement for long without recalibration.

The A033-ET supports the above resolution at relatively high (for such high resolution) measurement rate: up to 20 MSPS for bursts of up to 2 600 events, and up to 12.5 MSPS for bursts of up to 16 000 events. As for the maximum average rate of continuous measurement, it is limited mainly by the hardware interfacing with PC. For PC under MS Windows it is not less than 12 KSPS but can be increased by using the operating systems better adapted to real-time applications.

## 2.2 Non-inearity errors

There are two kinds of non-linearity errors in event timing. The integral non-linearity error represents a systematic error in event measurement that depends on the position of measured event over interpolation interval. Stand-alone specification of the integral non-linearity errors can be important mainly for the case of synchronous measurements when the measured events are located in some fixed areas of interpolation interval. In this case results of their measurements can be biased by these errors. For asynchronous measurements the integral non-linearity errors are not of particular interest since they get in the total instrumental error as its random-like component, limiting the single-shot resolution. Statistical method for such error evaluation is offered in [*Artyukh Yu., et al.*, 2008]; in our case applying this method allows to define the A033-ET integral non-linearity with sub-picisecond precision (Fig.3).

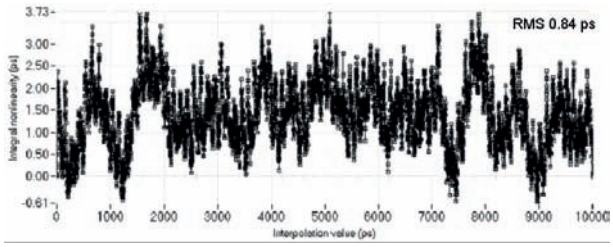


**Figure 3: Integral non-linearity error over 10 ns interpolation interval**

On average these errors are specified by the value of their standard deviation, representing significant component of single-shot RMS resolution. Typically the A033-ET integral non-linearity RMS error is less than 1 ps directly after device calibration. In this case the actual integral non-linearity decreases the the timer's RMS resolution by 25-30% approx. Note that for Riga event timers the integral non-linearity considerably depends on the calibration quality that has been significantly improved as compared to the previous instrument.

Unlike the integral non-linearity error, the interval non-linearity error is a systematic error in measurement of time interval between adjacent events, depending on the value of this interval. Mostly specification of the interval non-linearity error may be important for the case of measurements of time-intervals varied in a wide range. However, the A033-ET provides negligible interval non-linearity errors (peak-to-peak value less than ±0.2 ps approx) in a wide range of time intervals. Exceptions represent very small time intervals (close to the timer's dead time) where the errors can be a little greater.

## 2.3 Single-input offset drift

The A033-ET has a single-channel configuration. This means that all events provided by either input of the timer's hardware are measured sequentially in the same manner and by the same means. Owing to this there is no any noticeable error in time intervals between measured events when these events come at only one input. However there is some offset drift in measurement of a single event coming at this input (so called Single-input offset drift). Outwardly, it is seen as long-term instability (phase deviation) of the internal time-base relative to the external 10 MHz reference frequency, depending mainly on the ambient temperature variation. Typically the A033-ET single-input offset drift does not exceed 2 ps/$^0$C (Fig.4).

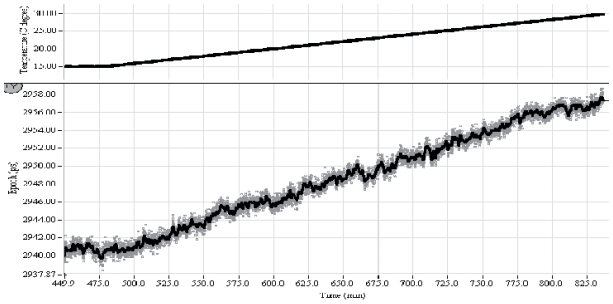

**Figure 4: Single-input offset drift in line with slow linear changing of ambient temperature from 15 to 30 $^0$C**

Generally such offset drift is not too important for the applications related to the time interval measurement, except for very long time intervals during which the ambient temperature can be significantly changed.

## 2.4 Input-to-input offset drift

When the events come at the different inputs some offset in time interval measurement appears. It is caused by a difference between internal propagation delays of input signals before coming to the common measurement unit. These delays slightly vary with the ambient-temperature change, causing certain offset drift (so called Input-to-input offset drift) and corresponding long-term instability in time interval measurements. Outwardly, it is seen as long-term deviation of systematic error in time interval measurement between Start and Stop events coming at the different inputs A and B of the event timer respectively.

The A033-ET input-to-input offset drift typically is about of 0.1 ps/$^0$C (Fig.5), i.e. it is much less than the single-input offset drift due to partial compensation of two similar offsets.

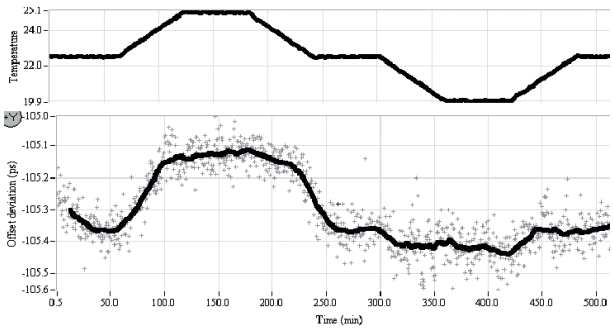


**Figure 5: Input-to-input offset drift in line with slow linear changing of ambient temperature from 20 to 25 $^0$C**

Actually this offset is tangible only during warming-up the timer's hardware after power-up.

# 3. Summary

As the Table 1 below suggest, the model A033-ET, in comparison with the previous model A032-ET, is distinguished by considerably advanced precision concerning different essential aspects of its specification.

**Table 1: Precision comparison**

| Model | Resolution | Integral error | Interval error | Single-input offset drift | Input-to-input offset drift |
|---|---|---|---|---|---|
| **A032-ET** | 7 – 8 ps | < 2 ps | < 1 ps | N/A | < 0.4 ps/$^0$C |
| **A033-ET** | 2.5 – 3 ps | < 1 ps | < 0.2 ps | < 2 ps/$^0$C | < 0.1 ps/$^0$C |

In principle even better measurement precision is possible but its achievement leads to much higher production cost. However the Riga event timers have been always conceived as commercially available instruments which have an attractive price/ performance ratio. In this case currently we have come to the conclusion that single-shot RMS resolution of them should be limited by 3 ps approx. to achieve relatively simple and inexpensive technical solution.

Newertheless, it seems that the A033-ET currently offers resolution and measurement speed that are quite sufficient for the most of ground-based SLR stations that provide both routine and KHz SLR. Taking that into account, currently we focus our research activity on advancing of other important performance characteristics of Riga event timers, such as their reliability, friendliness and hardware simplicity [*Artyukh Yu., et al.*, 2011].

## Acknowledgements

This paper reflects the research results that were obtained in frameworks of the R&D project No. 2DP/2.1.1.1.0/10/ APIA/ VIAA/084 co-sponsored by the European Union.

## References

*Bespal'ko V., Boole E., Vedin V., 2008*. The Model A032-ET of Riga Event Timers// Proceedings of the 15th International Workshop on Laser Ranging, Canberra, Australia, 2008, Vol.2, pp. 321-326.

*Artyukh Yu., Bespal'ko V., Boole E., 2008*. Non-linearity errors of High-precision Event Timing.– Automatic Control and Computer Sciences, Vol. 42, Nr. 4(68), pp. 191-196.

*Artyukh Yu., Bespal'ko V., Boole E., Vedin V., 2009*. Advances of High-precision Riga Event Timers// Proceedings of the 16th International Workshop on Laser Ranging, Poznan, Poland, 2009, Vol.2, pp. 398-403.

*Artyukh Yu., Bespal'ko V., Boole E., Stepin V., Stepin D., Vedin V., 2011*. Main Directions of Riga Event Timer Development and Current Results (these Proceedings).

## Correspondence

Yuri Artyukh
Institute of Electronics and Computer Science
14 Dzerbenes Str.
Riga LV-1006
LATVIA

e-mail: artyukh@edi.lv

# Session 8: Improving Ranging Accuracy, Calibration and Local Ties II.

# Main Directions of Riga Event Timer Development and Current Results

*Artyukh Yu., Bespal'ko V., Boole E., Stepin V., Stepin D., Vedin V.*

ABSTRACT

The present-day high-performance event timers (including Riga event timers) already offer the resolution and measurement speed that are quite enough for Satellite Laser Ranging applications. Taking that into account, currently we focus our research activity on the compact design and advancing of other important performance characteristics of Riga Event Timers, such as their reliability, friendliness, hardware simplicity, affordable price, etc. In this report we present current results of such activity and suppose that a next model of Riga event timer could be offered already in the nearest future to cover a wider range of applications (including airborne ones).

## Introduction

The Riga event timers represent computer-based instruments that measure time instants when input events (represented by NIM logic pulses) occur. Distinguishing feature of these instruments is a high precision combined with a high measurement rate due to the innovative DSP-based technology for event timing [*Artyukh Yu*, 2001]. In particular, the latest model A033-ET of the Riga event timers offers single-shot RMS resolution better than 5 ps and measurement rate up to 20 MHz, making this instrument one of a few best event timers currently available [*Artyukh Yu.*, et al., 2011]. Combining the A033-ET with application-specific software, a number of top-quality and reasonably priced event timer systems can be created. But there are some essential characteristics, which can be improved to provide the SLR users with more reliable, simplified and friendly device retaining the precision and performance of the A033-ET.

We are working on three main directions of Riga Event Timer (ET) project advancing:

1. Supporting of stable repeatability of the precision at the level 3 ps RMS in a wide temperature range by means that include:
   - temperature stabilization of the main measurement node,
   - temperature compensation schematic,
   - more robust and timekeeping calibration procedure;.
2. More compact design and faster operating by the means that include:
   - integration of all digital functions in single FPGA of the timer's hardware,
   - higher clock frequency (considerably more that the previously used 100 MHz),
   - higher-speed PC interfaces, such as USB3, PCIe, Ethernet 1G, etc;
3. User interface friendliness including integration and simplification of user-initiated function on PC.

The state of these directions and their evolution will be considered below in more detail.

# 1. The best and stable precision

The main factor impacting on Riga ET measurement precision is a temperature variation. Due to the environment temperature variation all electronic components of the timer's hardware change their characteristics. As a result, the transfer function, describing the event-to-time conversion, slightly changes, too. At the beginning of the A033-ET development the single-shot RMS resolution degradation by more than 10 percent occurred beyond the range of calibration temperature ± 3 °C. We thought it would be enough for effectively employing a thermostat. For this reason firstly we have made some experiments with a placement of the measurement node into a self-made small thermostat. Our experiments showed that neither thermostat with heating elements nor thermostat with cooling on the base of Peltier elements could not provide a sufficient precision stability and were not the best solution in terms of the hardware simplicity, compactness and power consuming.

Therefore other solutions of the problem were investigated. Unlike the temperature stabilization, right temperature compensation, where it is possible, leads to a sufficiently effective solution. In the latest versions of the A033-ET such temperature compensation is applied for both precision stabilization and decreasing the single-input offset drift [*Artyukh Yu., et al.*, 2011]. The last parameter seems most essential in the tasks related with one-way laser ranging and time transfer experiments. Temperature dependences typical for the A033-ET precision and epoch offset are presented in Figure 1.

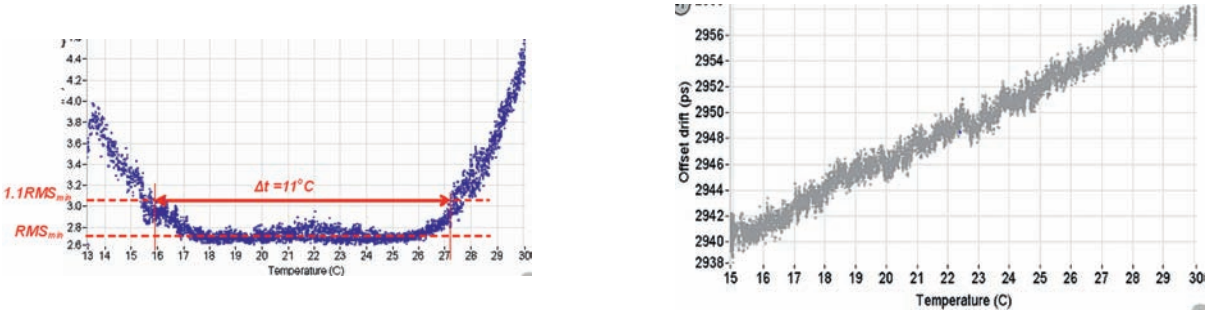


a) b)

**Figure 1: Temperature impact on A033-ET performance: a) precision degradation; b) single-input offset drift**

One can see in Figure 1a, that, as the result of temperature compensation, temperature range is considerably expanded around the temperature when the device calibration has been performed. In this case the single-shot RMS resolution degradation by more than 10 percent occurs beyond the range of 11 °C. Such compensation also decreases the single-input offset drift and, as can be seen from Figure 1b, this drift is only a little greater than 1 ps/ °C.

In the case of essential temperature change there is no possibility to compensate electronic component parameters drift without traditional calibration procedure. The calibration procedure includes calculating a new, more adequate, transfer function in accordance with the current ambient environment. In Riga ET the calibration procedure is executed using a dedicated signal, which is produced by a generator embedded into Riga ET hardware. The problem occurs when this generator frequency is out of the range of frequencies, which are the best for calibration. For example, as a result of frequency deviation in full working temperature range 0 – 50 °C, there can appear the frequencies, which give very bad calibration results (increasing the single-shot RMS resolution up to 100 ps!). In other words, such "bad frequencies" are unacceptable for calibration procedure.

Currently this problem is solved by means of switching the embedded generator between two adjacent frequencies, differing by only about 0.3 ppm. A choice between these frequencies is done on the base of specially developed estimate of the frequency "badness". From two adjacent frequencies the frequency with the lower estimate is chosen. This approach allows providing the required resolution "almost always".

Another approach to solve this problem lies in stabilizing the selected frequency and keeping it in a narrow range of the best frequencies for calibration. The first experiments with Frequency-Locked Loop (FLL) and Phase-Locked Loop (PLL) solutions for optimal frequency synthesis showed the effectiveness of such approach. In this case every new calibration always allows to get the RMS resolution for the single-shot interval measurement at the lowest limit in a wide temperature range (figure 2).

Both FLL and PLL synthesizers give the good results independent on a temperature variation. Theoretical basis and practice for PLL generator implementations is well developed, and there are some specialized chips which are ready to use. PLL synthesizer is more suitable for very stable frequency retention, but in off-the-shelf devices there are restrictions in an output frequency choice. FLL synthesizer can be oriented to the slight frequency adjusting but has more complicated retention mechanism, but in case of large FPGA using this is not a problem.

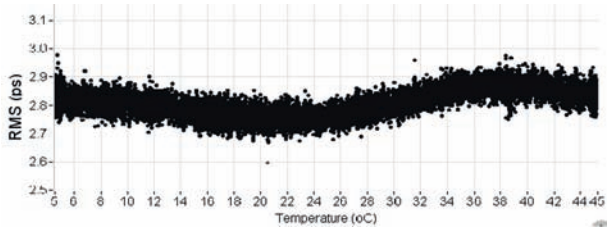


**Figure 2: RMS error after re-calibrations with use of PLL synthesizer**

As an alternative solution, it is possible to create preliminary calibration tables for different temperature ranges of the Riga ET operation, and automatically select one of the tables, taking into account the current internal temperature. Evident advantage of this approach is actual exclusion of the calibration as a complicated online operation. Practicability of this approach has been experimentally confirmed in Event Timer Module realization [*Artyukh Yu., et al.*, 2008]. It seems that, in combination with the right temperature compensation, this approach will allow to considerably improve precision characteristics of the Riga Event Timers.

# 2. More compact design and faster operating

Taking into account a performance of the modern super-high integration chips that have more and more integrated functions and provide higher operation speeds, it is possible to make the Riga ET design more compact, operating at higher frequencies, and having a faster interface with user tasks in PC.

In the A033-ET device the functions, associated with the control of measurement process in accordance with commands from PC, and the timing data recording into a buffer memory chip, are implemented in FPGA from Altera Corp. Now there are more complicated FPGAs containing a few millions of logic gates and a few millions bits of memory. This will allow to implement in FPGA all digital functions of the Riga ET, including:

- creating and supporting a large buffer memory,
- executing the calibration procedure and storing the interpolation tables,
- a clock pulses counting for time of event coarse fraction,
- providing the timer arming with a time of stop event prediction,
- managing the input signal conditioning and normalizing,
- a digital processing of ADC samples and event time-tag formation,
- processing the commands from and delivering timing data to user tasks in PC.

Implementation of timing related digital functions on single FPGA will allow to make the timer hardware more reliable and compact, with lower power consumption.

It seems attractive to increase the device internal clock frequency. Higher clock will allow to get better RMS resolution and shorter “dead time”, which are considered as the main performance characteristics of the event timers. But with higher clock the problem of logic competitions in ADC and FPGA can appear, so the alternative choice between speed and safety should be done.

PC interfaces with peripherals include a wide variety of types and performances. The most popular for measurement devices connection are: new USB3, providing data transfer at 400 Mbyte/s; PCI Express, having exchange speed from 250 Mbyte/s up to 1 Gbyte/s; and Gigabit Ethernet – from 12 Mbyte/s up to 3 Gbyte/s. Application of such high-speed interfaces will allow considerable increasing the average rate of continuous event timing and extending the control

functionality from the user tasks. First attempt of function integration and performance increasing is realized in our Event Timer Module [*Artyukh Yu., et al.,* 2008]. This module, having the same RMS resolution 3-5 ps, is distinguished by compact size (130x110x20 mm), and faster USB2 interface.

# 3. User interface friendliness

The A033-ET operation is fully controlled by the ET-client via TCP/IP network or directly by a user program, which is built on the base of the sample program delivered with the A033-ET. To prepare the A033-ET for measurements the user executes the next procedures: calibration procedure to get an interpolation table; time synchronization with external GPS to get an offset of the ET time scale; and arming command sequence for certain measurement mode. After that the events coming at the inputs of the ET device are logged in the internal buffer memory and this timing information can be read into PC. To get the epoch time-tag in seconds for logged events the user reads from the ET device 8 bytes containing the number of hardware internal clock counts and ADC samples for each event, and converts these bytes to epoch in seconds, using the interpolation table and offset. If the ET gating mechanism is used it is necessary, on a base of the time of the Start event marked by a special flag, to calculate the time until Stop event and write this time back to the ET device.

To make the user interface with the Riga event timer friendlier, it is necessary minimize the volume of processing and the number of executed command. We plan to transfer some procedures, currently executed in PC, into hardware device, leaving to user only the main functions: start measurement in desired mode, and get directly the epoch time-tags expressed in seconds for all registered events.

## Summary

Thus we have defined three main directions of further Riga Event Timer development, based on our view of SLR problems:

- the best and stable precision
- more compact and faster realization
- user interface friendliness

Some results are already achieved such as single-shot RMS resolution less than 3 ps, weakened dependence on temperature, robust calibration independents on temperature variation, and modular design with USB2 interface. All other tasks are planned for realization in the near future.

## Acknowledgements

This paper reflects the research results that were obtained mainly in frameworks of the State Research Program sponsored by the Latvian Ministry od Education and Science, and partly - in framework of the R&D project No. 2DP/2.1.1.1.0/10/APIA/ VIAA/084 co-sponsored by the European Union.The last concern results of experimental investigation.

## References

*Artyukh Yu.*, 2001: Method of continuous extreme-precision time-interval measurement// Automatic Control and Computer Sciences, vol.35, No.5, pp.11-18, 2001

*Artyukh Yu., Bespal'ko V., Boole E., Vedin V.*, 2008: Advances of High-precision Riga Event Timers. Proceedings of the 16th International Workshop on Laser Ranging, October, 2008, Poznan, Poland, pp.398 – 403.

*Artyukh Yu., Bespal'ko V., Boole E., Vedin V.*, 2011 Event Timer A033-ET: Curent State and Typical Performance Characteristics (these Proceedings).

## Correspondence

Eugene Boole
Institute of Electronics and Computer Science
Dzerbenes str.14
Riga LV-1006
LATVIA.

e-mail: buls@edi.lv

# New technologies for sub – millimeter laser ranging

*Ivan Prochazka, Jan Kodet, Josef Blazej, Petr Panek,*

ABSTRACT
We are presenting the work progress and recent results in a development and construction of new technologies for sub–millimeter laser ranging and picosecond accuracy laser time transfer. The key hardware components: the Start detector and discriminator, the echo signal detector, the timing device and signal cablings were studied in detail. The new devices have been designed, built and tested in our lab. The new hardware was tested in an indoor calibration experiments. We have achieved the single shot resolution of 4 mm rms. The temperature and temporal stability of the individual components is excellent. The drift is typically below 200fs / K for each contributor. The overall temperature drift of the entire laser ranging chain is below 300 fs/ K. The long term stability of the ground target calibration is better than +/- 800 fs within 3 days. During this period the environment temperature changed by more than 4 degrees Celsius. In the sense of time deviation Tdev the stability of 300 fs was achieved. The presented components will enable to carry out laser ranging with sub-millimeter normal points stability and reproducibility. The accuracy of the "ranging machine" based on these devices will reach sub-mm values, as well.

## 1. Concept

To minimize the systematic errors of the entire laser ranging chain the photon counting approach has been selected. The ranging chain components have been designed and optimized with a goal of single shot resolution of several millimeters and sub-millimeter normal points and overall system stability. The Start detector & discriminator are constructed as a single device to optimize their matching and maintain stability. The NPET timing system based on surface acoustic wave interpolator has a resolution of 800 fs and 4 fs long term stability. The echo detector is based on innovated SPAD detector optimized for high repetition Gate rate and minimal dark count rate. Both the detectors output signals have ultrafast slew rates $<$200 ps / 1V. In connection to the 6 GHz bandwidth of the timing system inputs these fast slew rates improves the timing and temperature stability along with the RF interference immunity.

## 2. Start detector

The Start detector & discriminator is constructed as a single device to optimize their matching and maintain stability. The detector consists of an ultrafast avalanche photodiode, both silicon and germanium types may be used, they will cover the wavelength range of 350 to 1550 nm. The analog signal of this photodiode is sensed by the ultrafast comparator with 6 GHz bandwidth. The ps clock driver is used to generate the fast rise / fall time output pulses, with the amplitude of 0.8 Volt and $<$ 100 ps edges. Two complementary outputs are available. Additionally the positive TTL levels pulse and the LED optical indication are available, see Figure 1.

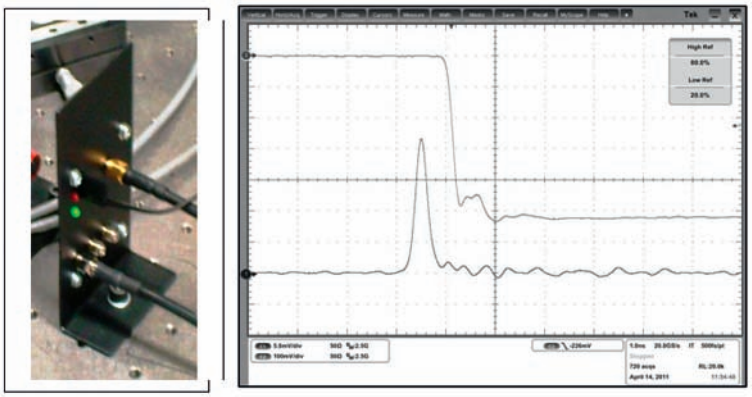

**Figure 1: The Start detector + discriminator + output circuits installed on a laser table (left). The linear signal monitor and the output pulse fall time (right), the scope setting is 1ns/div.**

The jitter contribution of the Start detector itself is on units of picoseconds level, detection delay temperature dependence is well below 300 fs /K. The device uses a standard +5 V, 200 mA power supply.

# 3. Timing system

A novel time interval measurement method which provides sub-picosecond timing, linearity and stability was developed. It makes use of a transversal surface acoustic wave (SAW) filter as a time interpolator. A two-channel New Picosecond Event Timer (NPET) device based on this new technique has been designed and realized [1,2,3].The timing jitter is typically 800 fs per channel, the timing non-linearity lower than 200 fs over an entire range and the long term stability of the order of ~10 fs / hour is achieved. The temperature dependence of the measured time intervals is typically as low as ~200 fs/K. The new version of the timing electronic board has been developed and installed in a shielding box maintaining the passive heat removal and temperature stabilization, see Figure 2.

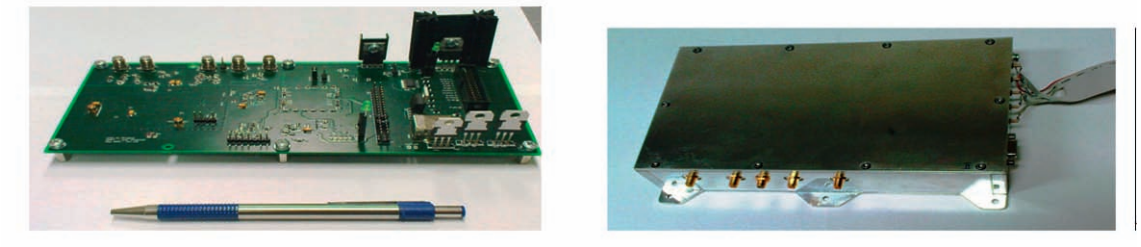

a/ b/

**Figure 2: The single channel sub-ps timing system board (a) and the board enclosed in a shielding and heat radiation enclosure (b)**

The single shop timing jitter is plotted in Figure 3 a).

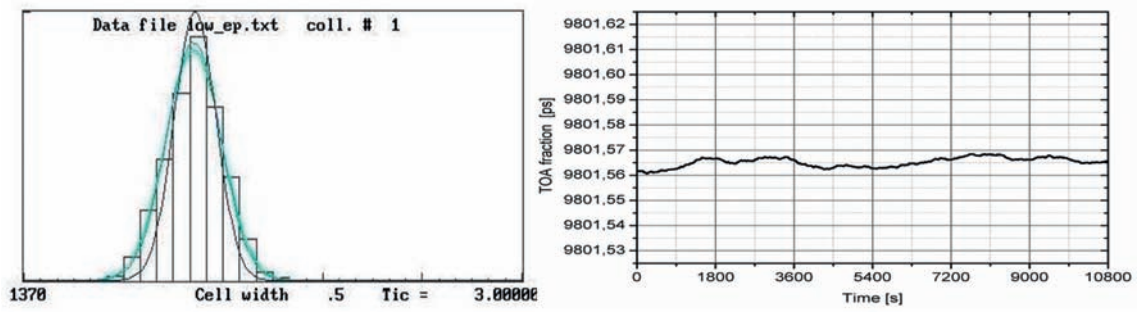


**Figure 3 a): Timing jitter of NPET, synchronous time markers, timing jitter ~ 800 fs. b) Epoch reading stability, moving average, note the long term timing stability +/- 4 fs over 3 hours (!).**

The long term stability of the epoch reading is plotted in Figure 4. The synchronous time marker Time of arrival (TOA) was recorded with 763 Hz repetition rate. The moving average over 256 seconds is plotted in Figure 3 b).

The new version of NPET has independent interfaces for each timing channel, thus the timing system is suitable for kHz rate SLR applications. Maximum repetition rate using the USB interface is > 1 kHz, the Ethernet version, which is expected to be available in 2012, will provide rates > 10 kHz.

The important feature of the NPET timing system is the fact, that thanks to its design and operating principle it is completely self-calibrating. No field calibration and adjustment of the device is needed ever. All the timing accuracy is maintained by providing high spectral purity clock signal of 100 or 200 MHz only. The two channel version is housed in a standard 19" 2U unit, see Figure 4.


**Figure 4: The two channel sub-ps timing system NPET.**

To summarize – the newly designed timing device provides sub-picosecond timing resolution, long term stability and non-linearity. The device is completely self-calibrating, it needs no field adjustment and/or calibration ever.

# 4. Echo signal detector SPAD

For high repetition rate SLR the existing SPAD detector package has been upgraded for higher stability and lower dark count rate. The package is designed for single photon signal, only. The time walk compensation is not implemented. The SPAD detection chip is thermoelectrically cooled K14 chip 200 um in diameter in a vacuum housing. The mechanical and optical design of the package remained unchanged, the device should be 1:1 replaceable with the previous versions.

**Figure 5: The SPAD detector package optimized for kHz single photon only ranging purposes.**

The new detector electronics is based exclusively on high (>= 6GHz) bandwidth electronic components having extremely low thermal drifts. No active board temperature control is used. The output pulse has NIM specs, however, the fall edges are < 100 ps. The active quenching loop delay was reduced down to < 3 ns, what resulted in reducing the effective dark count rate at kHz gates rates typically 3.5 times. The optimum electronic board and grounding design resulted in lower internal cross-talks. This enables to Gate ON the detector quite close to the expected arrival of photon of interest. This enables the use of tight range gating for high background daylight operation.

# 5. Low thermal drift signal cables

The dependence of signal propagation delay versus temperature is a serious issue in sub-mm laser ranging. The thermal coefficient of a standard coaxial cable is of the order of ~ 1 ps/K/ meter of cable length. Considering the signal cables length at a typical SLR site, one can expect millimeter changes in system delay (and hence in the calibration constant) for temperature changes of the order of one degree.

The new types of coaxial cables having thermal coefficients lower by one to two orders of magnitude are available, now. The PhaseTrack 210 cable is a ¼"cable, it has a thermal coefficient typ. 50 fs/K/m and is reasonably flexible for field use. The LDF50 cable has a similar temperature coefficient and ½" diam. it is suitable for fixed installation of long signal path, where the losses are an issue.

# 6. Laser ranging performance

The laser ranging performance of the individual components listed above was tested in a series of indoor experiments. The laser pulse length of 42 ps at 778 nm was used. The laser frequency was 400 Hz, the mean echo rate was 8 % thus maintaining pure single photon echoes. The experiment was carried out over weekend, the ambient temperature dropped from 28.5°C to + 24.0°C within this period. The results are plotted in Figure 5 a).

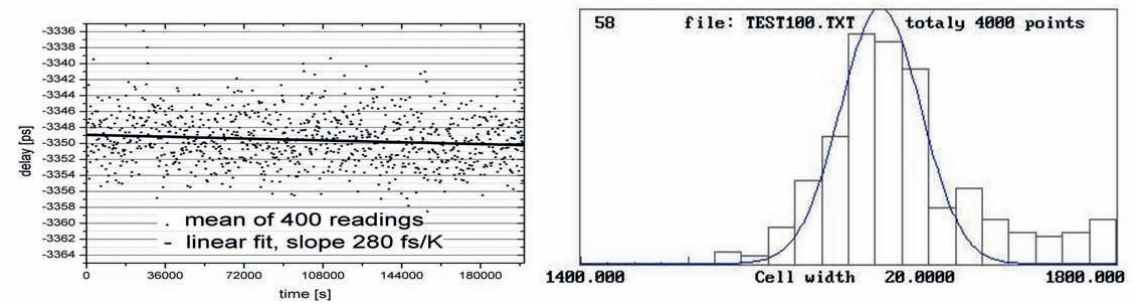


**Figure 5 a): Indoor laser ranging, Start detector+NPET+SPAD, single photons, 8 %, 400 Hz. b) Photon counting results of indoor laser ranging data histogram, the normal distribution curve is added, RMS = 28ps.**

Note the excellent overall system stability, the long term (thermal) drift was 1.25 ps peak to peak, what results in a overall system delay temperature drift of 280 fs/K.

The single shot resolution was 4 mm RMS, see Figure 5 b), where the data distribution histogram is plotted. The fitting curve is added. The asymmetrical distribution (distribution tail) is a consequence of the laser wavelength used 778nm. At 532 nm and shorter wavelength the distribution will be close to symmetrical one. The same experimental data have been processed in terms of a time deviation graph, the result is plotted in Figure 6.

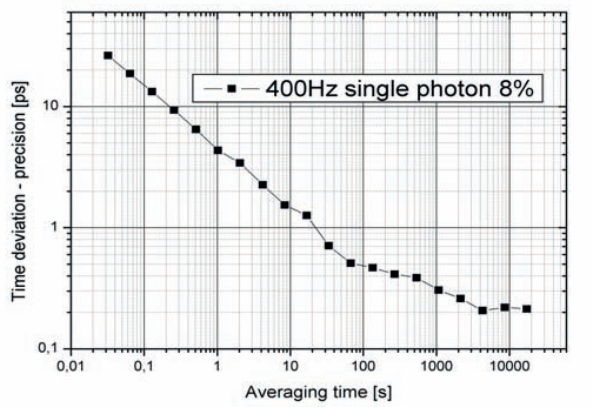


**Figure 6: Indoor laser ranging tests, 2.5 days, 400 hz, 8% rate**

Note the effect of averaging following exactly 1/SQR(N) rule down to sub-ps level corresponding to 0.1 mm precision ranging. The overall system stability in the sense of Tdev is ~ 200 fs over several hours.

# 7. Conclusion

The new components of the laser ranging chain have been developed and tested. The indoor calibration tests indicate that 4 mm precision single shot and better than 0.1 mm precision normal points are achievable together with better than 0.1 mm system overall stability over the period of several hours. These extreme precision and stabilities will contribute to the achievements of sub-mm system accuracy.

## References


[1] *Pánek P.*, "Time Interval Measurement Based on SAW Filter Excitation," IEEE Trans. Instr. Meas, , vol. 57, no. 11, pp. 2582 - 2588, Nov 2008

[2] *Prochazka I, Panek P.*, Rev. Sci.Instr. 80,(7), 076102, 2009

[3] *Panek P, Prochazka I.*, Rev.Sci.Instr.78, (1), pp 78-81, 2007

[4] *Pánek, P. - Procházka, I. - Kodet, J.*: "Time measurement device with four fs stability". Metrologia. 2010,Vol.47/ 5, L13-L16


## Correspondence


Ivan Prochazka

Czech Technical University in Prague
Brehova 7
115 19 Prague
Czech Republic
e-mail prochazk@cesnet.cz

# Studies on system stability and calibrations of H-SLR station

*Makram Ibrahim*

ABSTRACT

The paper concerns on the calibration and the system stability of the Satellite Laser Ranging station (SLR) at Helwan. The geometrical setup of the calibration method, applied at the H-SLR station, is explained. The calibration constant produced from the calibration of the system is computed and the results are summarized for two periods using two kinds of Photo multipliers (PMT). The average root mean square values of the calibrations carried out during the period from the year 1991 to the year 2008 are computed. The stability of the H-SLR station are studied for two different years before and after the upgrading. To clarify the precision of the Helwan-SLR station, the results of its calibration are compared with the results of the calibrations of the other SLR-Stations.

## 1. Introduction and System Configuration

The satellite laser ranging (SLR) is a space geodetic technology, which can measure the distance between a ground station and a satellite most precisely in current methods. The absolute time of flight of photons so that the geometry of satellite and laser station can be determined precisely as long as the system calibration error is controlled in a negligible level, equivalent to the accuracy of 1 cm or less. For this end, brief information about the Helwan SLR station is given. The mount configuration is Azimuth/Elevation with a coude system of mirrors for the transmitted beams as shown in fig. 1. The guiding of the mount is a computer controlled. The receiving system of the mount is a spherical mirror lens of diameter 40 cm, and optical filter of 6 nm with 80 % transmission. The type of the used detector is a Photomultiplier (PMT) manufactured by Hamamatsu model H6533. The quantum efficiency of this PMT is 10 % at 532 nm and of normal gain equal 5.6 million. The mode of the PMT is single photoelectron detection (Cech, M., et.al, 1998).

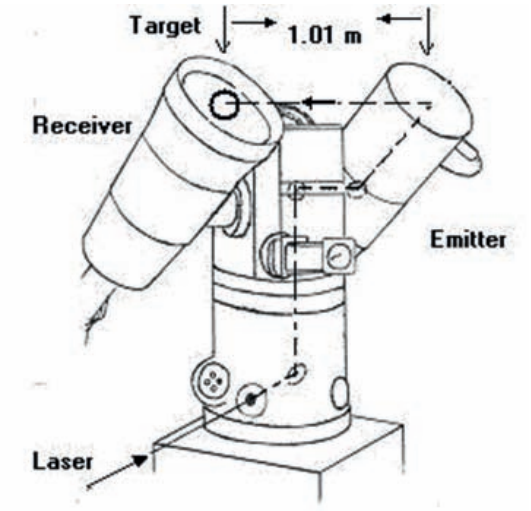


**Fig 1: Three coude mirrors inside the mount to guide the laser beam and the fourth mirror is outside the mount for calibration.**

The used laser is composed of Nd: YAG oscillator, pulse selector, three amplifiers system and a Second Harmonic Generator (SHG); it produces a semi train of pulses (Jelinkova, J., 1984, Prochazka, I., 1989). The wavelength of the laser pulses is 0.53 μm with pulse width of 20 psec and of repetition rate of nearly 5 Hz with 80 mj in energy. The divergence of the laser beam is adjustable and can reach to 0.1 mill radians. The laser transmitter is placed outside the mount and then the laser beam is directed to the satellite through the mount via a four coude mirrors. The ranging electronics of the system consists of a time interval counter of type a Stanford SR620 of resolution equal 4 psec. The start channel is

a special optoswitch and the stop channel discriminator Ortec is a constant fraction (Cech, M., et.al, 1998). The time and frequency system is GPS Time/Frequency standard, manufactured by Helwlett-Packard of model 58503B, which is providing the 1pps epoch signals with accuracy better than 110 ns. The meteorological station (MET-3) is installed to improve temperature, humidity and atmospheric pressure s' measurements. The pressure sensor model is a Digiquartz MET3 and it measures with accuracy of 0.1 mbar. The temperature sensor model is Platinum resistance temperature probe and it measures with accuracy ~ 0.5 deg C. As for the model of the humidity sensor, it is a capacitance probe and its accuracy is 2 % at 25°c. To study the system stability we will carry out calibrations of the station and from the studies we will concern on the measurements of the resulted calibration delays.

# 2. The calibration method

The Helwan - SLR station is calibrated using internal calibration method. It is accomplished by ranging on a fixed target placed at a distance of 1.01 meter from the laser. A detailed description of the calibration method is shown in Fig 1. For the purpose of the calibration, both the emitter and the receiver are covered. The cover of the emitter has a hole followed by mirror to reflect the beam to the direction of the target. The computation of the calibration constant is the average of nearly 100 returns (echoes) by using the counter SR620, but it was the average of 150 echoes by using the time interval counter of type HP5370B. The first channel is used for processing the signal from the start detector; the second channel is used for discriminating pulses from the PMT. The time delays of both, i.e. the start and stop channel were adjusted to the lowest time jitter. The first results show the mean value of the system calibration is about 85 nsec and time jitter is about 50 psec where the counter HP5370B is used for ranging (Cech, M., et.al, 1998). There are some parameters are affecting the calibration results. By fixing all except the PMT in some cases and the time interval counter in others, it will easy to describe the result. For the purpose of this study, we concerned on the results of the calibration, which is applied to the Helwan SLR-station in two periods. The first period is from Aug. 1991 to Sept. 1997. During that time the photomultiplier (PMT) of type RCA 31034A has been used. Due to the long operating time of that PMT, its sensitivity had been decreased by approximately 3 times (Cech, M., et.al, 1998) .In May, 1998 the receiver package was completely upgraded and the PMT RCA 31034 was replaced by the PMT Hamamatsu H6533 box with PMT tube 4998. It consists of a PMT tube and high voltage (HV) with precise divider. The Tennelec TC 952A high voltage power supply with stable 2500 volts was used as a source for the PMT, to obtain standard parameters. On the other hand, the old preamplifiers HP8447A (400 MHz) and HP8447D (1.3 MHz) have been replaced by EG & G Ortec1 GHz pre-amplifier Model 9306. It is a four-stage preamplifier based on Hewlett Packard MMIC chips. Hence, the second period is from May 1998 till December 2008, in which this new PMT are in use.

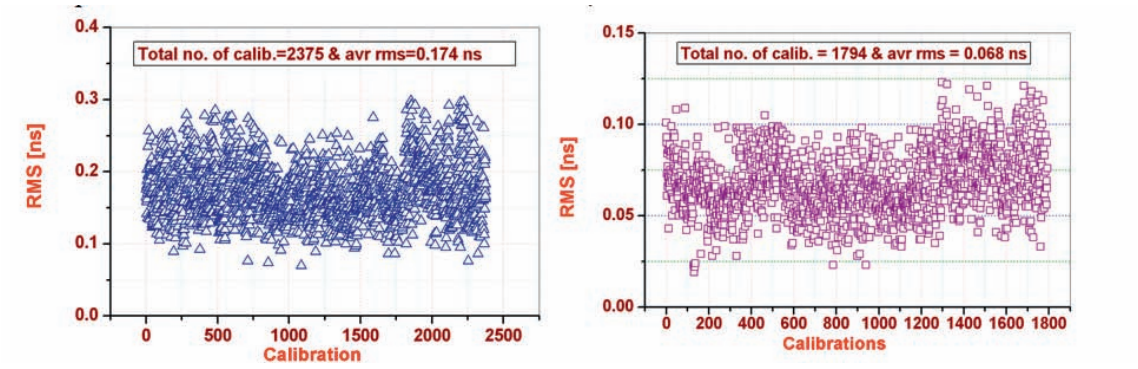


(a) (b)

**Fig. 2: The calibrations vs. the RMS values for all the calibrations carried out using the old PMT in (a) and the new PMT in (b) .**

For all the calibrations, the RMS value are computed in which the root mean square value is selected corresponding to rejection criteria of 2 Sigma (Hamal, K., 1978). The calibrations applied to the station within the whole period from 1991 to 2008 are computed and the results are shown in Fig. 2. During the first period, there are 2375 calibrations, have been applied. The RMS values of these calibrations are computed and the results are shown in Fig.2 (a). The average RMS value of the calibrations is found to be 0.174 nsec. Similarly, the results of the calibrations of the system applied during the second period, in which the new PMT package is used, are shown in Fig.2 (b). The total number of calibrations occurred

in that period are 1794 and the average precision is found to be 0.068 nsec, which is nearly 2.6 times better than the precision of the calibrations produced by the old PMT. It is also agree with the results produced by reference (Cech, M., et.al, 1998). For comparison purposes, the numbers of calibrations as well as the average root mean square value are computed for each year individually and the results are given in Tab.1.

**Tab. 1: The calibrations applied to the station in the period from 1991 to 2008, the average RMS value of the calibration per year is given as well.**

| Year | Nr. of calibrations | Average RMS |
|---|---|---|
| 1991 | 307 | 0.177 |
| 1992 | 401 | 0.181 |
| 1993 | 453 | 0.168 |
| 1994 | 389 | 0.160 |
| 1995 | 282 | 0.171 |
| 1996 | 214 | 0.198 |
| 1997 | 329 | 0.175 |
| 1998 | 428 | 0.064 |
| 1999 | 418 | 0.066 |
| 2000 | 320 | 0.061 |
| 2001 | 119 | 0.068 |
| 2002 | - | - |
| 2003 | - | - |
| 2004 | 120 | 0.075 |
| 2005 | 226 | 0.077 |
| 2006 | 55 | 0.079 |
| 2007 | 77 | 0.077 |
| 2008 | 31 | 0.074 |

In the first period of the Tab.1, it is clear that the worst precision of the calibrations occurred at the year 1996 with RMS value of 0.198 nsec and the best one is during the year 1994 with RMS value of 0.160 nsec. However in the case of the second period, using the new PMT, the worst precision of the calibrations occurred at the year 2006 with RMS value of 0.079 nsec and the best one is at the year 2000 with RMS value of 0.061 nsec. Actually, this reason is not only refer to the PMT but also to other parameters such as the method of measurements of metrological conditions. As it is mentioned in section 2, there is a new instrument for measuring the temperature, humidity and pressure with a high precision, which has not been available in the year 1996. It is also clear from the table that the average RMS value of the years from 1998 to the year 2002 is below 0.07 nsec while from the year 2004 till 2008 the average RMS values are higher than 0.07 nsec.

The precision of the measurements of the Helwan SLR station is compared with the precision of the other SLR stations, and the results are given in Fig. 3(a) for the satellite Starlette in the period from October 1, 2007 through December 31, 2007 (http://ilrs.gsfc.nasa.gov/images/2007_12_cal_rms.html) . It shows that the root mean square value of the calibration measurements is 6 mm as measured for the H-SLR station. As for Fig.3 (b), it shows the results as measured for the satellite Starlette in the same period of 2008 (http://ilrs.gsfc.nasa.gov/images/2008_12_cal_rms.html). It shows that the root mean square value of the calibration of H-SLR station is also 6 mm as for the other SLR-Stations the results are given as shown in Fig. 3.

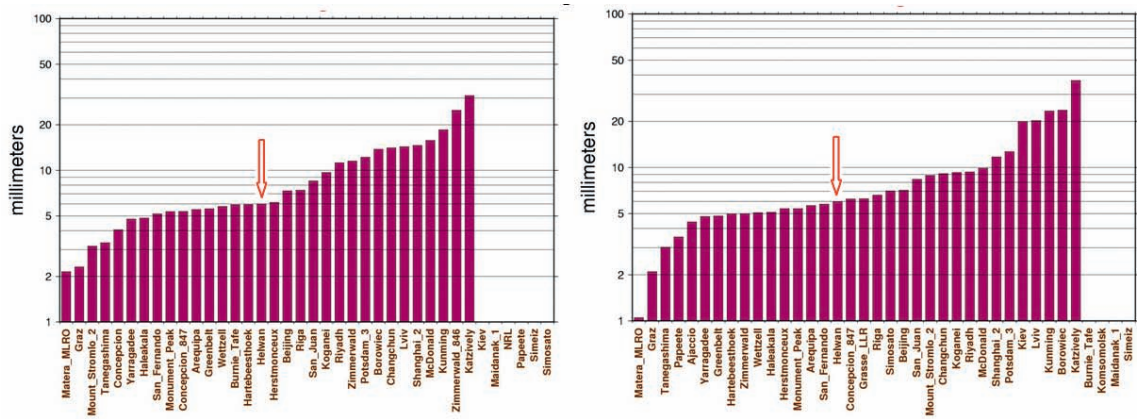


(a) (b)

**Fig. 3: The deduced precision of the average single-shot calibration RMS, in millimeters, during the last quarter of 2007 in (a) and during the last quarter of 2008 in (b) .**

# 3. Calibration constant and system stability

The calibration constant of the system or the system delay is one of the important parameters, has been carried out before satellites ranging. Changes in calibration value indicate that something has happened and may be bias the range data. The calibration constant has been computed for two different periods (as of the availability of the data), one of them after using the new PMT at the year 2000 and the other by using the old PMT during the year 1996. The results show that, the system delay is much more stable at the year 2000 than that at the year 1996, as shown in fig. 4. However in fig. 4 (a) the data symbol by circles are produced using the old time interval counter of type HP5370B, since the new time interval counter SR620 has not been yet installed at the station. The data obtained by the new the interval counter is shown in fig.5 (b). This also proves that the stability of measurements of the system delay obtained using the new time interval counter is better than the measurements of the system delay obtained using the old counter as shown in Fig 5.

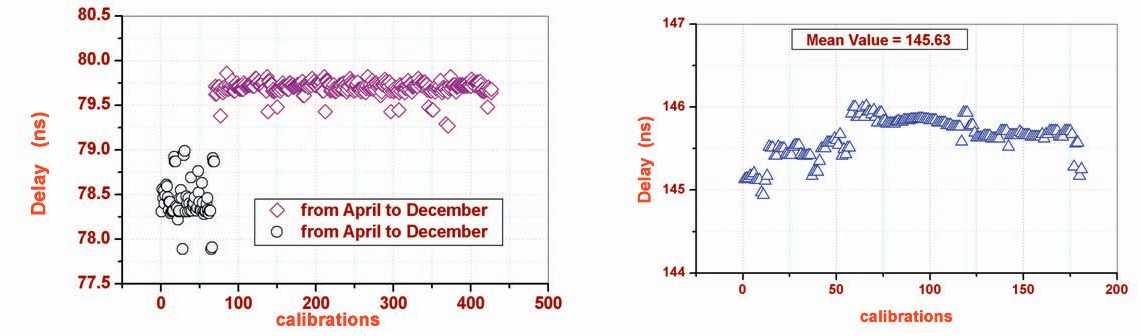


(a) (b)

**Fig. 4: The calibration constant obtained by calibrating the system during the year 2000 in (a) and 1996 in (b)**

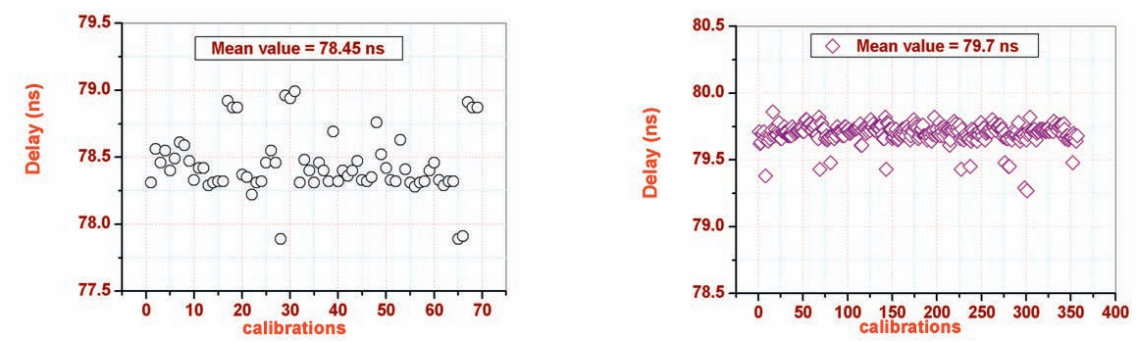


(a) (b)

**Fig. 5: The system delay produced by using the time interval HP5370B in (a) and SR620 in (b) during the year 2000.**

# 4. Conclusion

The calibrations which have been carried out at the Helwan-SLR station during the period from 1991 to 2008 are studied. There are 4196 calibrations carried out with two kinds of photomultipliers. In the first period from 1991 to 1997, there are 2375 calibrations are carried out using the old PMT. The second period which carried out from May 1998 till 2008 in which the new PMT is in use there are 1794 calibrations are carried out. The average RMS value of the calibration for using the old PMT is found to be 0.174 nsec, while for the new PMT is 0.068 nsec. It means that the calibrations produced using the new PMT package are nearly 2.6 times better than that of the calibrations produced using the old PMT.

It is also clear that the average RMS value of the calibration data obtained through the years from 1998 to the year 2002 is below 0.07 while from the year 2005 till 2008 the average RMS values are higher than 0.07 ns. From the measurements of the system delay, it is found a much more stability at the data obtained after upgrading the system than that of the stability of the data obtained before the upgrading. By the way, the system stability of using the new time interval counter SR620 is better than that of using the old counter HP5370B.

## References

*Cech, M., Hamal, K., Jelinkova, H., Novotny, A., Prochazka, I., Helali, Y.E. and Tawadros, M. Y.*, 1998 : Upgrading of the Helwan Laser Station (1997-98), Proc. of the 11th International Workshop on Laser Ranging, Deggendorf, Germany, September 21-25,(1998), pp. 197.

*Hamal, K. , 1978* : Calibration of the Interkosmos Laser Radar No 12, Proc. of the 3rd International Workshop on Laser Ranging Instrumentation, Lagonissi, Greece, May 23-27, (1978), pp. 198 .

*Jelinkova, H., 1984*: Mode Locked Train Laser Transmitter, Proc. of the 5th International Workshop on Laser ranging Instrumentation, Herstmonceux, U.K., published by Geodetic Institute, Univ. Bonn,(1984), pp. 224 .

*Prochazka, I, 1989* : Mode locked semitrain laser ranging data processing software, Proc. of the 7th International Workshop on Laser Ranging Instrumentation, Matera, Italy October 2-8, published by OCA/CERGA, Grasse, France,(1989), pp. 405 .

**"This research has been partially supported by the grant of the Czech Scientific Foundation GA205/05/0110 and by the research framework MSM6840770022 of Ministry of Education of Czech Republic."**

## Correspondence

Makram Ibrahim

National Research Institute of Astronomy and Geophysics (NRIAG),
Helwan, Cairo, Egypt.

makikh@yahoo.com

# Ground Survey and Local Ties at the Geodetic Observatory Wettzell

*Thomas Klügel, Swetlana Mähler and Christian Schade (BKG, Wettzell, Germany)*

ABSTRACT

The geodetic space techniques VLBI, SLR and GNSS are realized at the Geodetic Observatory Wettzell since several decades. The space observations are accompanied by an extensive local survey at more or less regular intervals. Beside local tie vectors, which are required for the combination of the different space geodetic techniques, the local survey provides evidence of the long term stability of the geodetic reference points defining the ITRF. The analysis of the different survey campaigns covering a time span of 24 years and the big number of geodetic markers allow a reliable identification of instable pillars and ground markers, while the reference points of the space geodetic techniques are considered as stable.

In addition this paper presents different techniques of determining the invariant reference points of the VLBI and SLR telescopes, which are usually not directly accessible.

## 1. Relevance of ground survey

Each measurement is affected by errors, either statistic or systematic. In the case of the geodetic space techniques these errors enter into global solutions degrading products like the international terrestrial reference frame (ITRF) or Earth orientation parameters (EOP). Measuring errors may arise from:

- local displacements of the antenna reference point
- unsufficient knowledge or variations of the phase center with respect to the reference point
- delays in cables and electronic components
- multipath effects

While statistic errors are reduced with the number of observations, the systematic errors can be identified only by comparison between different techniques. In order to compare station coordinates resulting from different measuring systems, the exact knowledge of the tie vectors connecting the reference points is essential. This is realized by a local network of geodetic markers, pillars or ground marks, using classical survey instruments like theodolites, tachymeter, or levels.

The second purpose of the local network, usually covering less than a few hundred meters, is the proof of the local stability of the reference points of the space technique systems, and the identification of unstable monuments.

A regional network usually spanning several or a few tens of kilometers could be established in order to demonstrate the stability of the surrounding area and to show whether the station is representative for the entire region. Such a network is mostly realised by GNSS stations.

## 2. The local network in Wettzell

### 2.1 Network description

The local network at the Geodetic Observatory Wettzell recently consists of 25 survey pillars and 22 ground marks, tying together a number of 12 space technique reference points (3 VLBI, 2 SLR and 7 GNSS monuments) (fig. 1). The network is measured in regular intervals, usually each 2-3 years, and the coordinates are determined in a free least square adjustment. Between 1985 (7 pillars, 8 ground marks) and 2009 (16 pillars, 20 ground marks) 11 measuring campaigns were performed. This allows the creation of time series showing the long term behaviour of the geodetic markers and the reference points.

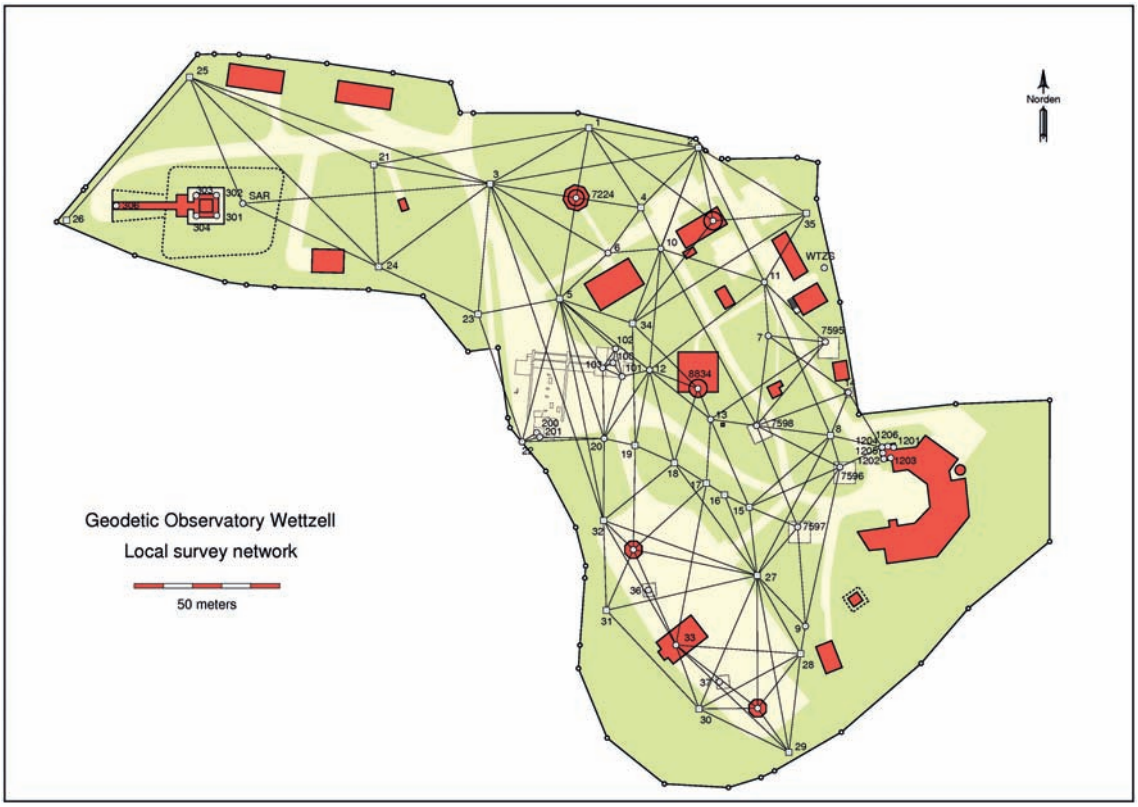


**Figure 1: Local survey network at the Geodetic Observatory Wettzell.**

## 2.2 Height variations

The height uncertainties (1 sigma) of the adjusted solutions are less than 0.1 mm in most cases. They may reach up to 0.5 mm for the reference points of the radio telescope (RTW) and the laser ranging telescope (WLRS) due to the difficulty in the point determination. This high precision allows the identification of very tiny displacements of individual markers. As an example the pillars 1-5 being distributed around the radio telescope show height variations of less than 0.5 mm over 13 years with the exception of the year 2004, when a subsidence of up to 1 mm is detectable at each pillar (fig. 2 left). This is obviously a consequence of the very dry summers in 2003 and 2004, having lead to a shrinking of the soil. One ground mark (11) being located directly beside an access road shows a continuous subsidence of 2.4 mm over 16 years, pointing to a soil compaction by traffic. Sudden changes in height are related to close construction work in most cases, e.g. 1.4 mm at ground mark 10 between 2004 and 2006.

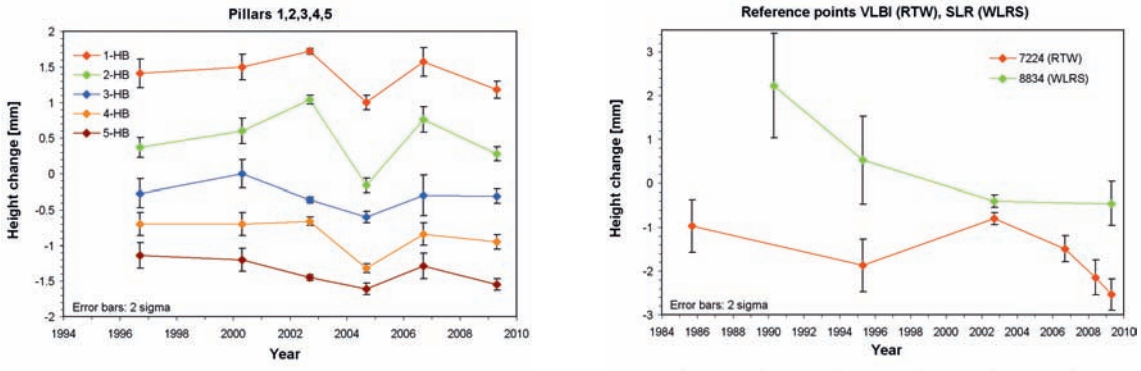


**Figure 2: Height variations of survey pillars (left) and reference points of the VLBI and SLR system (right).**

As can be expected the vertical displacements of the big telescopes are somewhat bigger. The WLRS monument subsided by 2.5 mm during the first 10 years and is stable since then (fig. 2 right). The RTW shows vertical variations of less than 1 mm up to the year 2002. Then it starts to subside by 1.5-2 mm until 2009. This points to a beginning abrasion of the elevation bearing, which had to be changed in 2010 due to destruction.

One survey in January 2009 has been rejected due to extreme deviations of up to 20 mm for some ground marks. Vertical expansion by frozen water is obviously a severe problem for some kind of markers.

## 2.3 Horizontal displacements

The 1 sigma uncertainties for the horizontal position is mostly below 0.2 mm. Poorly constrained points at the network rim reach up to 0.6 mm. Most of the pillars and ground marks show an irregular variation in position of 1-3 mm over 2 decades (fig. 3 top). One pillar (4) moved by 18 mm over 24 years and is clearly identified as unstable. Another pillar (2) being close to the entrance gate shows a sudden displacement of 3 mm, which can be clearly related to construction work.

The horizontal displacements of space technique reference points are similar small. After a horizontal motion of 2 mm between 1985 and 1995, the RTW remained stable within 1 mm since then (fig. 3 bottom). The displacement of the WLRS reference point is less than 1 mm since 1995. The position of the GNSS points at the roof of the GNSS tower varied by up to 1.5 mm.

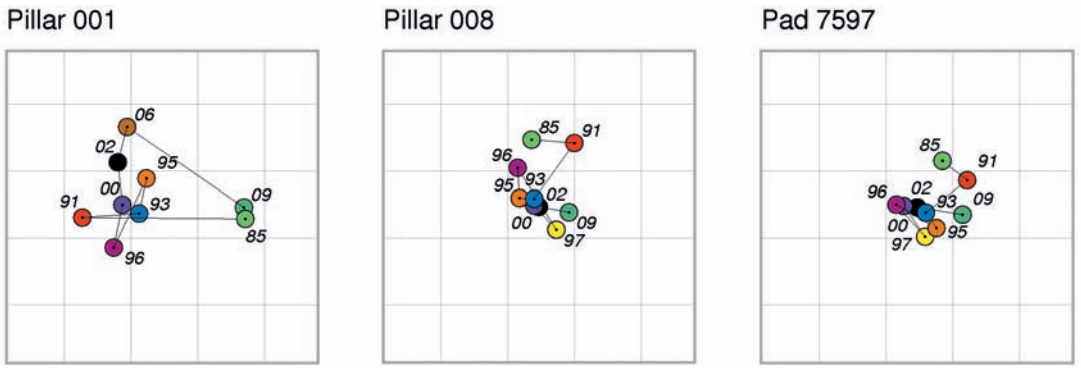

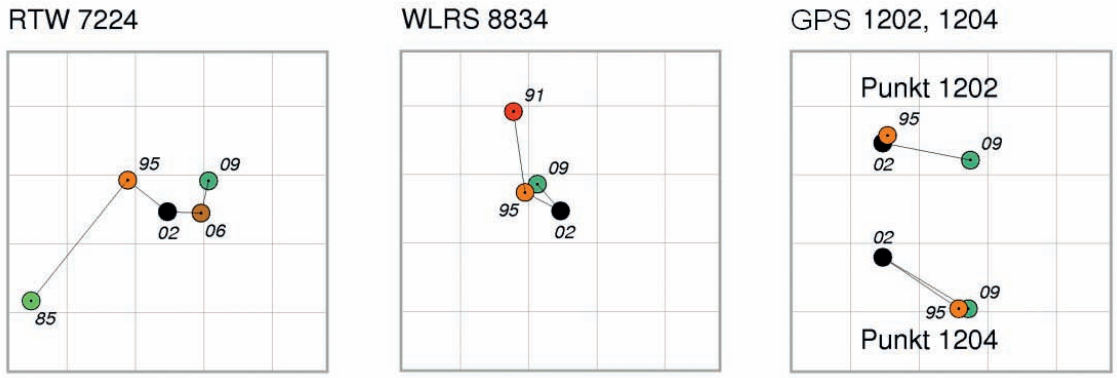


**Figure 3: Horizontal motion of selected survey marks (top) and reference points (bottom). Line spacing is 1 mm, years are indicated by numbers.**

## 2.4 Transformation

In order to compare the locally measured coordinates with the solutions of the geodetic space techniques, they have to be transformed into the global geocentric system. For this purpose the data from two GPS campaigns performed in 2000 and 2003 were used. The 2000 campaign lasted 4 days and 4 points of the station network were occupied by GPS antennas. During the 2003 campaign 6 station network points were occupied measuring continuously over 9 days. Data from the 4 permanently runnings GNSS stations were also included in the analysis.

For the combination the GPS solutions were downweighted in such a way that they only provide the orientation of the network, while the scale is dominated by the high precision of the ground survey.

# 3. Determination of invariant points

The geodetic reference point at a moving telescope is defined as the intersection of the azimuth and the elevation axis, which is the invariant point (IVP). It is usually not directly accessible and has to be constructed through observations of markers being attached to the telescope at different telescope positions. There are 3 different ways to construct the IVP:

- determine azimuth and elevation axis independently, intersect both axes
- determine center of elevation arcs at different azimuths, construct center of azimuth circle
- 3D least square adjustment of sphere surface

Table 2 shows the results of 2 different IVP determinations. While the different adjustment techniques yield nearly the same results, the use of different instruments or the analysis of different campaigns yield differences of up to 0.5 mm or 1 mm, respectively.

| Method | East | North | Up |
|---|---|---|---|
| | Tachymeter data: | | |
| 2D adjustment + height (NetzCG) | 269.71713 | 187.69011 | 622.46484 |
| 3D adjust. (JAG3D) | 269.71715 | 187.69011 | 622.46482 |
| circle adjustment | 269.71720 | 187.69008 | 622.46502 |
| max. difference | 0.07 mm | 0.03 mm | 0.2 mm |
| | Laser tracker data: | | |
| 3D adjust. (JAG3D) | 269.71739 | 187.69056 | 622.46506 |
| Difference to above | 0.24 mm | 0.45 mm | 0.24 mm |

| Method | East | North | Up |
|---|---|---|---|
| | Campaign 09-23-2009: | | |
| sphere adjustment (MatLab LSGE-bib) | 316.92438 | 180.04237 | 616.51454 |
| 3D adjust. (PANDA) | 316.92439 | 180.04240 | 616.51425 |
| circle adjustment | 316.92438 | 180.04250 | 616.51454 |
| max. difference | 0.01 mm | 0.13 mm | 0.29 mm |
| | Campaign 09-01-2009: | | |
| 3D adjust. (PANDA) | 316.9253 | 180.0426 | 616.5134 |
| Difference to above | 0.9 mm | 0.1 mm | 0.85 mm |

**Table 2: Results from IVP determination of the Radio Telescope Wettzell (Lösler 2008, left) and the Satellite Observing System Wettzell (right) using different adjustment techniques, instruments, and measuring campaigns.**

# 4. Conclusions

Repeated ground surveys at the Geodetic Observatory Wettzell show that the reference points of the space technique systems are stable with respect to the local network. The good repeatability, also when using different instruments, indicate small systematic errors. Stable markers show displacements not exceeding 2-3 mm in 24 years. A few unstable markers were clearly identified since the network is made up by a sufficient number of markers forming a stable geometry. Construction work is a major source of marker displacements.

The determination of invariant points yield the same results within ± 0.15 mm when using different adjustment techniques. Difference between tachymeter and laser tracker results do not exceed 0.5 mm. However, different survey campaigns yielded differences up to 1 mm, which is a consequence of different network geometry, environmental conditions, and deformations.

It is concluded that the accuracy of the local ties in Wettzell are in the order of 1-2 mm.

## References

*Lösler, M.*, 2008: Reference point determination with a new mathematical model at the 20 m VLBI radio telescope in Wettzell. J App Geod, 2, S. 233-238, doi: 10.1515/JAG.2008.026.

## Correspondence

Thomas Klügel
Geodetic Observatory Wettzell

Sackenrieder Str. 25
D-93444 Bad Kötzting

thomas.kluegel@bkg.bund.de

# Can Continuous Cartesian Connections realize local ties at 0.1 mm level?

*Sten Bergstrand*

ABSTRACT
We present an approach to achieve continuous Cartesian connections at geodetic co-location stations. The concept builds on the classical idea of traditional local tie surveys and extends it to the needs of the 21st century. The objective is to provide the most accurate achievable continuous connection of the reference points of the various geodetic equipment in a local truly Cartesian coordinate system. This task appears to be a necessary pre-requisite for reach the objectives of the Global Geodetic Observing System (GGOS).

## 1. Introduction

The primary project of the International Association of Geodesy (IAG) in the coming years is to realize a Global Geodetic Observing System (GGOS) which will support the monitoring of the earth system and global change research (Rummel et al., 2005). The GGOS aims at a combination and integration of various geodetic techniques in order to benefit from all their advantages and to work around intrinsic shortcomings. An important ingredient of the GGOS are the geodetic co-location stations that host equipment for different geodetic space techniques (e.g. Satellite Laser Ranging (SLR) and/or Very Long Baseline Interferometry (VLBI) combined with Global Navigation Satellite Systems (GNSS)), geophysical sensors (gravimeters, seismometers, tide gauges, etc.), and atmospheric sensing devices (e.g. ground based microwave radiometers). A necessary pre-requisite for a meaningful combination and integration of the different observations and the derived results can only be achieved if the local geodetic relations at the geodetic co-location stations are accurately known. These relations or local ties are the coordinate differences between the reference points of the different techniques, including their temporal variations. To achieve the objectives of the GGOS it is required that the reference points are known with an accuracy better than 1 mm in a global reference frame (Niell et al., 2006) and that the full covariance information is available in both the temporal and spatial domains. This is also of major importance for the International Terrestrial Reference Frame (ITRF) (Altamimi et al., 2007) that combines the various techniques to derive a stable reference frame for the observations. Both GGOS and ITRF desire local tie information that is accurate on a level of 0.1 mm (Rothacher et al., 2009, Ray and Altamimi, 2005). In this article we briefly describe a possible way to establish a continuous Cartesian connection (3C) system that will facilitate full integration of separate techniques' observations at a co-location station to the currently highest achievable standard. Furthermore, we propose that a coherent 3C system is established at all co-location stations in order to reduce the uncertainties of future geodetic observations.

## 2. Local ties at geodetic co-location stations

Traditionally, the coordinate differences between the reference points of the different techniques at geodetic co-location stations are determined by so-called local tie surveys. These surveys are usually performed on a more or less regular basis every couple of years. This low repeat frequency is to a large extent due to the fact that local tie surveying is an engineering task that lies beside normal operations. In the local tie, the reference points of the various geodetic techniques are connected to a local survey network that is usually materialized by survey pillars that can be equipped with geodetic survey instrumentation to measure distance, angles, and height differences between them. An overview of available local tie techniques has been compiled by Pearlman (2008).

### 2.1 Local tie difficulties

In many cases the actual observation reference points cannot be observed directly, e.g. the axis intersections of radio telescopes used for geodetic VLBI, or the phase centers of antennas used for GNSS observations. In these cases indirect survey methods are usually applied. For radio telescopes the indirect methods make use of the instrument's symmetry

properties, see e.g. Sarti et al. (2004). To perform the necessary measurements the radio telescopes then have to be positioned according to a predefined scheme. This is maintenance task that usually involves external expertise and means considerable and undesirable downtime from normal operation. Only recently has a new approach been proposed that shall allow reference point determination of a radio telescope while the instrument is in normal operation (Lösler, 2009). Traditionally, local tie surveys are often a combination of direction and distance measurements with tachymeters and height differences from spirit leveling. These survey instruments are oriented with respect to the local plumb line. The coordinates in the local coordinate system of the survey work thus dependent on the local gravity field and are not given in a local truly Cartesian (LTC) system, and hence add unnecessary uncertainties to the observations. Furthermore is the local tie information often incomplete, i.e. the covariance information is not available (Thaller et al., 2005). A transformation between results derived from space geodetic techniques that refer to global Cartesian systems (e.g. GNSS, SLR, VLBI) and such traditional local not-truly-Cartesian systems impose an increased loss of accuracy due to the uncertainties added in the transformation.

## 2.2 Desired properties of local ties

The accuracy of today's space geodetic techniques is on the order of 1 ppb and better on a global scale, and it is expected that 0.1 ppb will be approached in the near future. For example, the next generation geodetic VLBI system, VLBI2010, aims at an accuracy of 1 mm on a global scale (Niell et al., 2006, Petrachenko et al., 2009). To preserve this high accuracy and meet the requirements of the GGOS, it appears necessary to know the local coordinate differences between the reference points of the co-located techniques with even higher accuracy. Space geodetic techniques deliver coordinate results that refer to global Cartesian coordinate systems. Therefore, also the local coordinate differences need to be expressed in truly Cartesian local coordinate systems in order to avoid any accuracy losses in the transformation, and of course the complete covariance information must also be provided. It is desirable to monitor the local coordinate differences more often than in the past, and continuous monitoring will help to detect disturbances on the instruments and will aid to identify the reasons behind perturbations. Such disturbances could be of periodic or episodic character, e.g. air temperature, ground water column, or ground settling.

# 3. Continuous Cartesian connections

In the following we outline the 3C concept for geodetic co-location stations. These ideas could be realized at already existing geodetic co-location stations, and they are highly relevant for new stations to be established, e.g. in connection with the ongoing VLBI2010 efforts (Behrend et al., 2008). The initial step of the 3C concept is to establish an LTC coordinate system at the station. Subsequently, the reference points of the various different geodetic techniques and sensors are to be determined in this coordinate system. Since not all reference points can be observed directly, indirect methods usually need to be applied. Additionally, a number of targets with a stable geometric relation with respect to the reference points can be deployed; these targets can be used to represent the specific space geodetic equipment in a monitoring situation. In the following, the whole network shall be monitored in an automated fashion without disturbing the normal operations at the co-location station. Statistical analysis can be used in real-time or close to real-time to check the stability of the network. Post-processing data analysis will be used to derive the necessary transformation information for combination and integration purposes. Furthermore, any disturbances of the reference point locations can be investigated in detail in post-processing, too.

## 3.1 Local truly Cartesian coordinate systems

As mentioned earlier are local tie surveys traditionally often a combination of direction and distance measurements by e.g. tachymeters and height differences from spirit leveling. This implies that the local coordinate system is not truly Cartesian since the instruments are oriented with respect to the local plumb line. This effect is on the order of 3 mm for the z-component in survey networks with an extension of 200 m and need to be accounted for by local geoid and ellipsoid models. However, an LTC coordinate system that facilitates a direct transformation between different coordinate systems can be established e.g. by a laser tracker instrument. This type of instruments allows accurate distance mea-

surements in interferometric and absolute mode as well as direction measurements. These instruments have many applications in e.g. industrial measurements (Juretzko and Hennes, 2008) and do not require any particular orientation with respect to the local gravity field.

An example for the application of a laser tracker is described in (Lösler and Haas, 2009) where such an instrument was used to determine the reference point of the 20 m radio telescope at the Onsala Space Observatory and the local tie between this reference point and the reference point of the GNSS monument. By using a laser tracker, an LTC coordinate system can be established and the reference points of the individual techniques and all survey pillars can be surveyed and expressed in this system. Additional retro-reflecting targets that are eccentrically mounted at some of the sensors can be included in the network. This is particularly important for sensors that have not-easily accessible reference points. These eccentric targets should be mounted in a way that the geometrical relation with respect to the sensor's reference point is known, and a continuous monitoring of these eccentrically mounted targets can be used to indirectly monitor the sensor's reference point. For example can GNSS antennas be mounted coaxially on top of 360° retro-reflecting prisms that allow surveying and monitoring from all horizontal directions within about ±30° elevation angle. At VLBI or SLR telescopes, such retro-reflecting prisms could be mounted at representative positions of the telescope structure.

## 3.2 Continuous monitoring

Once the LTC coordinate system has been established and all reference points as well as additional reference targets have been determined directly or indirectly in this system, the continuous monitoring may commence. The complete local survey network has to be equipped with suitable targets. A motorized total station is needed that can be computer controlled to perform angular and distance measurements following a predefined monitoring cycle. Near-real-time checks can be done already on the level of raw observations with simple statistical tools, e.g. histograms. Post-processing analysis needs to take into account the meteorological situation in order to do the corresponding corrections of the distance measurements. Time series of target coordinates and their uncertainties is one of the post-processing products, and the post-processing should include the determination of coordinates of all targets with their complete covariance information. Another product is the complete information needed for the transformation between the different geocentric Cartesian systems.

## 3.3 Experience from monitoring projects

The ideas of the 3C concept have emerged from the experience gained in a set of local tie monitoring campaigns where the temporal behavior of reference points have exceeded the GGOS specifications by more than an order of magnitude (Haas and Bergstrand 2010, Lösler et al. 2010, Haas et al. 2011). An example of movement patterns for four differently designed GNSS antenna monuments is displayed in Figure 1.

# 4. Conclusions and outlook

We presented a proposal to achieve continuous Cartesian connections between the reference points of different space geodetic techniques at geodetic co-location stations. Results from initial studies at different co-location stations indicate that there might be differential deformations on diurnal time scales with signatures on the order of 1 mm or larger. We are convinced that the information from the 3C is necessary to achieve the objectives of the GGOS and that co-location stations to be established e.g. in connection with the GGOS efforts should utilize the 3C-concept from the beginning. Furthermore can the 3C-concept be established on existing co-location stations in order to reduce uncertainties in coordinate transformation between different techniques, and if made in a standardized manner also included in the analysis.

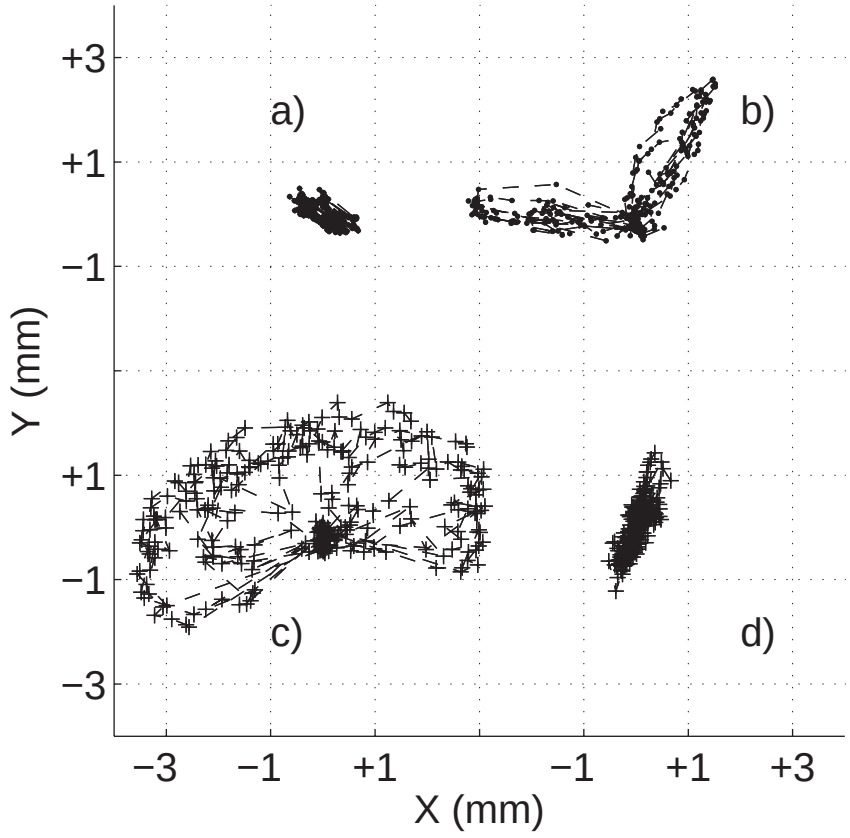


**Figure 1: Variability of the horizontal position of four different GNSS monuments. The movement patterns reflect the interaction of solar radiation on monuments with different cross sections and are considerably larger than 0.1 mm for all the evaluated monuments.**
**(From Haas et al., 2011)**

## Acknowledgements

Expenses for Dr Bergstrand's visit to the workshop were covered by the Smithsonian Institution with funds from NASA contract NNG07DA00C.

## References

*Altamimi Z., Collilieux X., Legrand J., Garayt B., Boucher C.*, 2007: ITRF2005: A new release of the International Terrestrial Reference Frame based on time series of station positions and Earth Orientation Parameters. J. Geophys. Res., 112, B09401, doi:10.1029/2007JB004949

*Behrend D., Böhm J., Charlot P., Clark T., Corey B., Gipson J., Haas R., Koyama Y., MacMillan D., Malkin Z., Niell A., Nilsson T., Petrachenko B., Rogers A.E.E., Tuccari G., Wresnik J.*, 2008: Recent Progress in the VLBI2010 Development. In: Proceedings of the 2007 IAG General Assembly, Perugia, Italy, July 2-13, 2007, ed. M. Sideris, Springer, 133(5), 833–840, ISBN/ISSN:9783540854258

*Haas R., Bergstrand S.,* 2010: COLD MAGICS – Continuous Local Deformation Monitoring of an Arctic Geodetic Fundamental Station, IVS 2010 General Meeting Proceedings, http://ivscc.gsfc.nasa.gov/publications/gm2010/haas.pdf

*Haas R., Bergstrand S., Lehner W.,* 2011: Evaluation of GNSS monument stability, REFAG2010 proceedings, IAG proceedings series (in press).

*Haas R., Eschelbach C.,* 2005: The 2002 Local Tie at the Onsala Space Observatory. In: Proc. IERS Workshop on site co-location, edited by B. Richter, W. Schwegmann and W.R. Dick, IERS Technical Note, 33, Verlag des Bundesamts für Kartographie und Geodäsie.

*Juretzko M., and Hennes M.,* 2008: Monitoring of the spatiotemporal movement of an industrial robot using a laser tracker. Proc. 1st Intern. Conf. Machine Guidance & Control, June 24-26, 2008, Zurich, CH.

*Lösler M.,* 2009: A new mathematical model for reference point determination of an azimuth-elevation type radio telescope. Journal of Surveying Engineering, Vol. 135, No. 4, November 2009, 131-135, doi http://dx.doi.org/10.1061/(ASCE)SU.1943-5428.0000010

*Lösler M., Eschelbach C., Schenk A., Neidhardt, A.,* 2010: Permanentüberwachung des 20 m VLBI-Radioteleskops an der Fundamentalstation in Wettzell; zfv - Zeitschrift für Geodäsie, Geoinformation und Landmanagement, Vol. 135, Nr. 1, pp 40-48, Wißner-Verlag, ISSN 1618-8950.

*Lösler M., Haas R.,* 2009: The 2008 Local-tie Survey at the Onsala Space Observatory, In: Proceedings of the 19th European VLBI for Geodesy and Astrometry Working Meeting, 24-25 March 2009, Bordeaux, pp. 97-101.

*Niell A., Whitney A., Petrachenko B., Schlüter W., Vandenberg N., Hase H., Koyama Y., Ma C., Schuh H., Tuccari G.,* 2006*: VLBI2010*: Current and Future Requirements for Geodetic VLBI Systems. in: IVS Annual Report 2005, edited by D. Behrend and K. Baver, NASA/TP-2006-214136, 13–40

*Pearlman M.R. (ed.),* 2008: Report of TLS (Terrestrial Laser Scanner) Workshop, http://ilrs.gsfc.nasa.gov/docs/TLS_2008Workshop_Report.pdf

*Petrachenko B., Niell A., Behrend D., Corey B., Böhm J., Charlot P., Collioud A., Gipson J., Haas R., Hobiger T., Koyama Y., MacMillan D., Malkin Z., Nilsson T., Pany A., Tuccari G., Whitney A., Wresnik J.,* 2009: Design Aspects of the VLBI2010 System. Washington, DC, USA, 52 pp., NASA/TM-2009-214180

*Ray J., Altamimi Z.,* 2005: Evaluation of co-location ties relating the VLBI and GPS reference frames, J Geod, 79: 189–195, doi:10.1007/s00190-005-0456-z

*Rothacher M., Beutler G., Bosch W., Donnellan A., Gross R., Hinderer J., Ma C., Pearlman M., Plag H.-P., Richter B., Ries J., Schuh H., Seitz F., Shum C.K., Smith D., Thomas M., Velacognia E., Wahr J., Willis P., Woodworth P.,* 2009: The future Global Geodetic Observing System. in: Global Geodetic Observing System, edited by H.-P. Plag and M. Pearlman, Springer-Verlag, Heidelberg/Berlin, 237–72, doi:10.1007/978-3-642-02687-49

*Rummel R., Rothacher M., Beutler G.,* 2005: Integrated Global Geodetic Observing System (IGGOS) – science rationale. J Geodyn, 40, 357–362

*Sarti P., Sillard P., Vittuari L.,* 2004: Surveying co-located space-geodetic instruments for ITRF computation. J Geod, 78: 210–222, doi:10.1007/s00190-004-0387-0

*Thaller D., Schmid R., Rothacher M., Tesmer V., and Angermann D.,* 2005: Towards a rigorous combination of VLBI and GPS using the CONT02 campaign. International Association of Geodesy Symposia, 128, Springer Verlag, 576–581, doi:10.1007/3-540-27432-4_98

## Correspondence

Sten Bergstrand
SP Technical Research Institute of Sweden
Box 857
SE -501 15 Borås

sten.bergstrand@sp.se

# Session 10: Improving support for GNSS and other challenging missions

# Tracking Many GNSS: Introduction

*Matthew Wilkinson*

ABSTRACT

The Global Navigation Satellite Systems (GNSS) technique has evolved to become the most widely available positioning tool used by both civilians and scientists. The Global Positioning System (GPS) has been fully operational since 1994 and the Global Navigation Satellite System (GLONASS) continues to take shape and is on track to having a full constellation in the coming year. SLR has supported both GPS and GLONASS since 1993. However a significant change is about to take place with a large increase in the number of retro-reflector target carrying GNSS satellites orbiting the Earth, potentially placing an increased demand on SLR tracking. This paper provides an overview of SLR tracking of GNSS as an introduction to the session "Improving support for GNSS and other challenging missions". It also draws upon the experience and describes the GNSS tracking activities of the Space Geodesy Facility (SGF), Herstmonceux SLR station in the UK.

## 1. ILRS support of GNSS constellations

SLR provides useful tracking support to GNSS missions and acts as a valuable, independent check on microwave orbits through a technique that is insensitive to the ionosphere and has only a small refraction delay due to tropospheric water vapour (Pavlis et al, 2009). SLR aids the modelling of on-board clocks, the alignment of the GNSS reference frames to the ITRF and helps to improve and validate spacecraft dynamics.

In 2009 the ILRS held a workshop in Metsovo, Greece, entitled "SLR tracking of GNSS Constellations" during which position papers from each of the GNSS projects described SLR as a valuable tool for verification of orbital parameters and models. SLR was described as particularly useful in the initial phases of satellite deployment and also provides a common, independent measurement technique for each GNSS constellation.

Combination of GNSS observations and SLR measurements with accurate space ties could strengthen the determination of the ITRF (Thaller, *et al.*, 2011) and daytime SLR observation are desirable for the modelling of solar and terrestrial radiation forces acting on satellites (Flohrer, 2008).

At present, the ILRS supports one GPS satellite (GPS-36, PRN-06) that carries a retro-reflector target, two GIOVE satellites for validation of the upcoming Galileo mission, one COMPASS satellite at GNSS height and six GLONASS satellites. In addition the first Quasi-Zenith Satellite System (QZSS) satellite is tracked by those stations under its geo-synchronous orbit footprint. Each of these missions will launch additional retro-reflector target carrying satellites in the coming years with each GNSS mission evenually reaching full constellations, with QZSS having a total of three satellites.

This increases significantly the number of satellites available for SLR tracking at GNSS heights and, since a SLR station can only track one satellite at a time, will place increased demands on the ILRS network. Best practice support from the ILRS and tracking priority at individual stations should be driven by the scientific benefit of tracking multiple GNSS satellites in a given constelation.

# 2. GNSS tracking at Herstmonceux

Herstmonceux, like many ILRS stations, has over many years gained a significant amount of experience of tracking high orbiting satellites, at altitudes of 20 000km. These remain the most challenging targets that need high quality telescope pointing, minimal beam divergence and clear and cloud-free skies. At night the targets are easily tracked using a camera to display the telescope iris, which allows the beam and possibly the sunlight satellite to be positioned at the centre of the field of view. Searching for the best relative alignment between the satellite image and the laser beam or for invisible satellites in shadow may also require small azimuth and elevation offset searches. In the clearest skies, GNSS satellites can also be tracked at Herstmonceux during daylight hours. This requires a small iris, a very narrow daylight spectral filter (~0.2nm, centred on 532nm), close gating of the SPAD detector and a daytime camera system to see and align the laser beam to the centre of the iris. Daylight tracking of GNSS satellites is not always successful at Herstmonceux as the sunlit telescope is open to non-uniform heating which introduces error into the telescope pointing model. The most difficult GNSS satellites, GPS and GIOVE, are not attempted during the day because of the low return rates, respectively due to the small on-board retro-reflector array and greater radial distance.

The Herstmonceux SLR station tracks all ILRS GNSS and Etalon satellites and in addition now tracks all of the remaining operational GLONASS satellites. As there are 24 operational GLONASS this increases the number of GNSS altitude satellites being tracked by 2.5 times. This scenario could be similar to that requested of the ILRS from GNSS missions in the future. Taking on this additional burden should be fully considered in terms of any impact on other SLR tracking priorities. Figure 1 contains the results from an investigation that used the predicted SGF schedule for 2011. Firstly the left hand plot was for all satellites at LAGEOS altitudes and below, finding the total time each day that the telescope is required for SLR. This is then repeated including the Etalon, GIOVE, COMPASS-M1 and GPS satellites, which gave the right hand plot. On an average day the SLR facility is only required for approximately 35% of the time for LAGEOS or lower altitude satellites. Considering only those satellites appearing in night-time hours shows greater variation in the demand for SLR with the system requirement varying from less than 20% to more than 50% of the night over the course of a year. The right hand plot shows this demand increase to 80% of the day with the addition of the high altitude satellites.

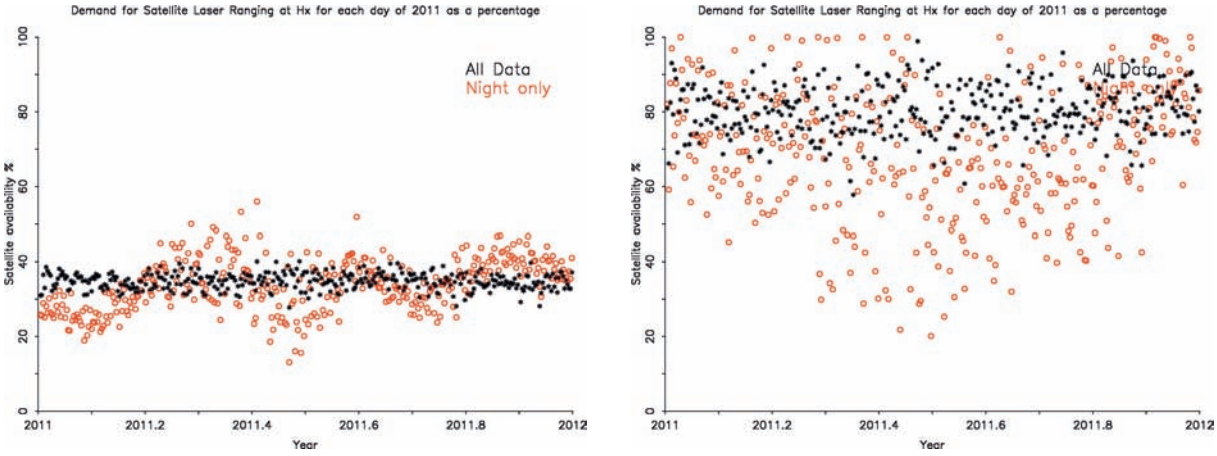


**Figure 1: The left had plot shows the percentage during which LAGEOS or LEO satellites can be tracked for the whole day (in black) and for night hours only (in red). The right plot shows the percentages for the LAGEOS, LEO, Etalon, GIOVE, COMPASS-M1 and GPS. This work was in collaboration with P. Gibbs.**

Figure 1 shows that there is a large amount of spare capacity in the LAGEOS and LEO schedule. Adding the high orbiting satellites significantly reduces the spare capacity, but this is only the case because it includes the entire high altitude satellite passes. A GNSS satellite takes about 5-6 hours to pass from horizon to horizon and does not need to be tracked for the whole duration. Reducing the tracking of a high altitude satellite to 5-10 minutes when it is ascending, overhead and descending reduces this demand considerably.

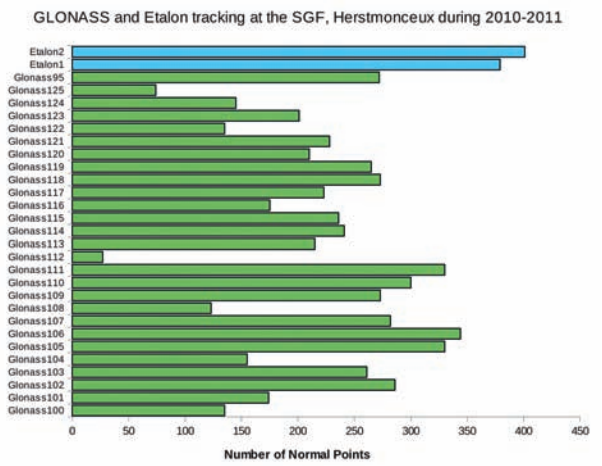


**Figure 2: The number of normal points collected at the Herstmonceux station for all the GLONASS and Etalon satellites tracked from the beginning of 2010 to mid-2011.**

Figure 2 shows the total number of GNSS and Etalon normal points acquired by the SGF from the beginning of 2010 to mid-2011. At the top of the plot are the higher priority Etalon targets with subsequently higher yield. The next satellite normal point total is Compass-M1 and then follows the GIOVE and GPS totals, which are comparatively fewer due to these being more difficult targets. Then in green are the GLONASS satellites which show a reasonably even distribution of normal point for each satellites, with fewer normal points recoded if a satellite is newly launched or has reached the end of its operational lifetime. This plot shows the successful tracking of all GLONASS by SGF, Herstmonceux, over this period.

## 2.1. Real time precision

If the SLR observer has multiple satellite passes at one time he or she will decide what is the best use of the SLR system taking satellite priority into account but to also aiming to support each satellite for at least a proportion of its pass. This means that the observer needs to be able to decide when the data collection on one pass is sufficient and it is time to move from one pass to another. For the high altitude satellites which use longer normal point bin intervals this maybe before the end of a normal point, particularly at stations such as Herstmonceux with the high-rate 2kHz system. The SGF has implemented a real-time estimation of normal point precision for display and when the precision reaches 1mm the observer is advised to move to another satellite. This is particularly useful when the observer has, for example, 5 or 6 GNSS satellites to be tracked and only a short gap between observing higher priority satellites.

The real time normal point precision estimation relies on the satellite residuals having near to zero along track time bias and so being flat in the range window. This is regularly the case for LAGEOS and GNSS altitude satellites. In addition, reliable track detection software is also required.

## 2.2. Efficient satellite switching

Using a high repetition rate laser allows 1mm normal point precision to be reached in a short time within the time duration of the normal point. After reaching this precision the observer is then free to consider the other satellites in the schedule and switch, with the option of returning to the previous satellite later in its pass. This leads to a novel approach to SLR observing where only minimal time is spent on one satellite before switching to the next. Figure 3 shows an attempt to track a high number of coinciding satellite passes and to minimise the time spent on one satellite with efficient satellite switching. Working in this manner requires the observer to be closely aware of which satellites have recently been tracked and which satellites should be the next priority for SLR.

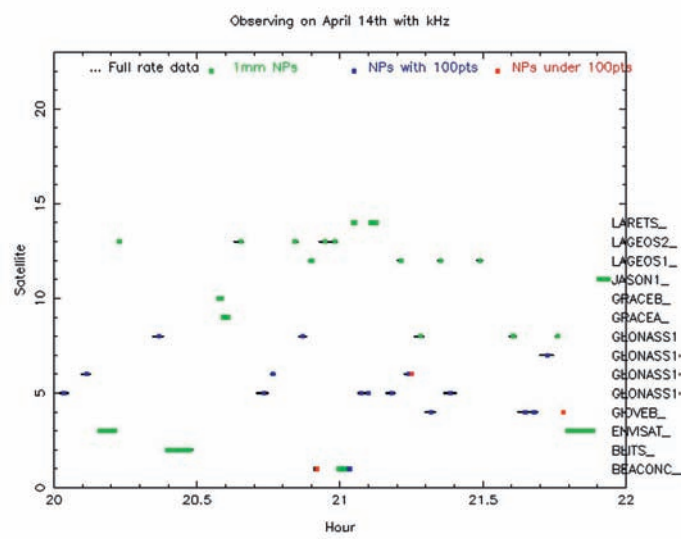


**Figure 3: Supporting many satellites with efficient satellite switching using the 2kHz system. This work was carried out by P Gibbs.**

# 3. Conclusion

Should the ILRS decide to support all future GNSS satellites this will mean a significant jump in the number of satellites tracked. The experience of the Herstmonceux station shows that there is sufficient capacity in the SLR station schedule to observe many GNSS, and at present all GNSS, without impacting on the priority LAGEOS and LEO tracking. It should be demonstrated whether SLR support for full GNSS constellations is beneficial or support limited to only certain selected satellites is sufficient.

## References

*Flohrer, C.*, Mutual validation of satellite-geodetic techniques and its impact on GNSS orbit modelling, Geodatischgeophysikalische Arbeiten in der Schweiz, Schweizerische Geodatische Kommision, Institut fur Geodasie und Photogrammetrie, Eidg. Technische Hochschule Zurich, Zurich, Switzerland. ISBN: 978-3-908440-19-2, 2008.

*Pavlis, E., LaBrecque, J., Ries, J., Gross, R.*, Impact of SLR tracking of GNSS constellations on science, SLR Tracking of GNSS Constellations, Metsovo, Greece, 2009.

*Thaller, D., Dach, R., Seitz, M., et al.* Combination of GNSS and SLR observations using satellite co-locations. Journal of Geodesy 85 (5), 257–272, doi:10.1007/s00190-010-0433-z, 2011.

## Correspondence

Matthew Wilkinson
NERC Space Geodesy Facility
Herstmonceux Castle
Hailsham
East Sussex
BN27 1RN
United Kingdom

matwi@nerc.ac.uk

# The achievements of the dedicated Compass SLR system with 1m aperture telescope: GEO satellite daylight tracking and Laser Time Transfer (LTT)

*Zhang Zhongping[1], Yang Fumin[1], Zhang Haifeng[1], Meng Wendong[1], Wu Zhibo[1], Chen Wenzhen[1], Chen Juping[1], Ivan Prochazka[2]*

ABSTRACT

Since 2008, Shanghai Observatory began to construct the dedicated SLR system with 1 meter aperture telescope for tracking Chinese Compass satellite from 20,000 to 40,000km with the precision of 2~3cm. Now the dedicated SLR system has the ability to routinely track Compass satellites at the night and daytime. This paper presents the achievements and measuring results of the SLR system: daylight tracking Compass GEO/IGSO satellites and the LTT experiments with improved LTT payload onboard IGSO satellite.

## 1. Introduction

Shanghai observatory has been building the 1 meter laser ranging system for the Chinese regional satellite navigation system (COMPASS) in Beijing since 2008 and the main performances of this laser system is following: 1) Receiving telescope: 1000 mm; 2) Transmitting telescope: 300 mm; 3) Nd:YAG laser: 150mJ@532nm, 250ps pulse width, 20 Hz; 4) Targets: GEO/IGSO/MEO, 20,000~40,000km; 5) Ranging precision: 2~3cm; 6) Daylight tracking ability; 7) Laser Time Transfer (LTT).

In Jan. 2009, the 1m aperture telescope was installed and Figure1 shows the 1 meter aperture telescope in the assembly shop. After finishing servo-tracking control system, the laser system, coude path system and electronical control system, the dedicated Compass laser ranging system successfully got the returns from Lageos, GPS36, Glonass, Giove at night-time in March 2009. On 21 April 2009, returns are obtained firstly from COMPASS GEO2 satellite at night-time and the range is about 3, 8800Km at the precision of about 2cm.


**Figure 1: The view of the 1 meter aperture telescope**

This paper will introduce the following two achievements of the Compass SLR system, GEO/IGSO satellite daylight tracking and Laser Time Transfer for IGSO satellite.

[1] Shanghai Observatory, Chinese Academy of Sciences, Shanghai, China
[2] Czech technical University, Czech

# 2. GEO/IGSO satellites daylight tracking

Technologies are solved for daylight tracking: 1) Good performances of tracking and pointing of telescope mount; 2) Space filter: receiving field of view of 24~45 arc second; 3) Spectrum filter: Narrower filter with 0.15nm band width, Transparency of central wavelength of over 50%; 4) Parallelism of transmitting and receiving path with better than 5 arc second; 5) Daylight Laser beam monitor.

## 2.1. Two computer controlling mode

For increasing the stability of tracking and pointing of 1 meter telescope mount, one computer is used for the telescope control to track satellites and stars and another computer is used for laser ranging operation and both software interfaces can be seen from the Figure 2. According to the above operating mode, the tracking accuracy is less than 1 arc second for tracking High Earth Orbit satellites, especially in daylight and pointing accuracy is better than 3 arc second after star calibration. Figure 3 shows the tracking error of 1 meter telescope mount.

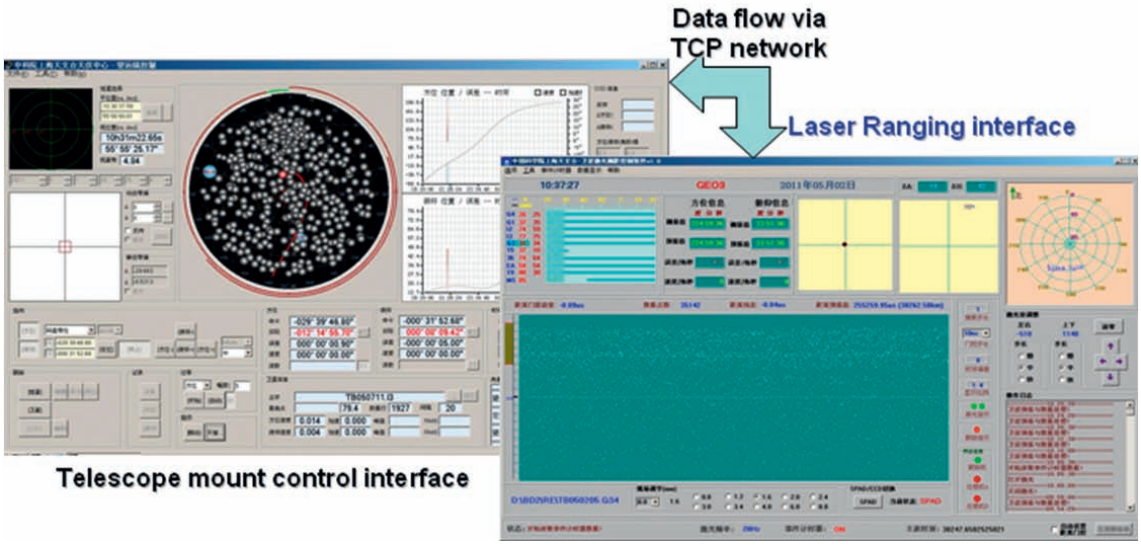


**Figure 2: The software interface of laser ranging and telescope mount controlling**

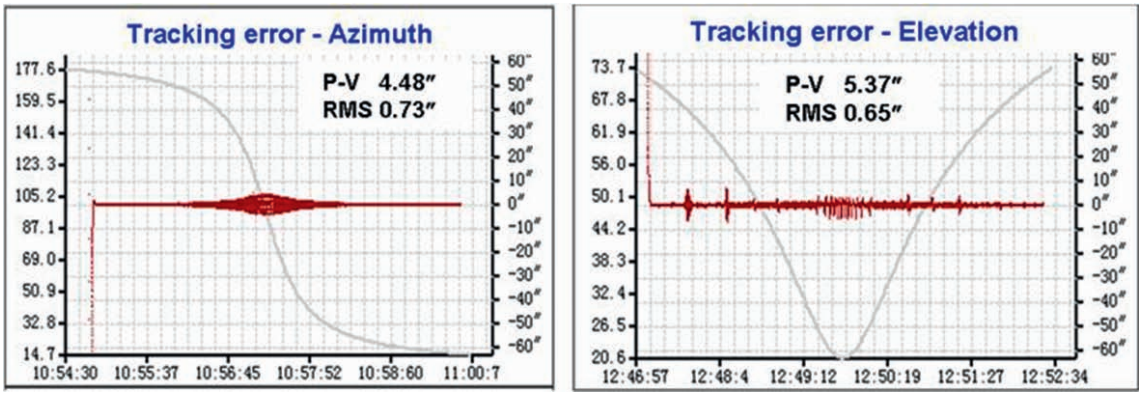


**Figure 3: Tracking error of 1 meter aperture telescope, RMS<1 arc second**

## 2.2. Other methods tested for daylight tracking

Before daylight tracking experiments, we successively tested the methods of space filter, spectrum filter, range gate and laser beam monitor during laser ranging at nighttime and then daylight laser ranging experiments were implemented for Lageos, Etalon, Glonass, Compass M1.

## 2.3. Laser ranging results from GEO/IGSO in daylight

On 1 April 2010, laser returns from Compass GEO satellite at daylight are firstly obtained and the measuring range is about 38,000km. Through further improving the laser ranging system, many passes of Compass GEO and IGSO satellite are measured successfully. Figure 4 shows the results of daylight tracking to Compass GEO1 and IGSO2 satellites and the local time is 12h am and 4h pm respectively.

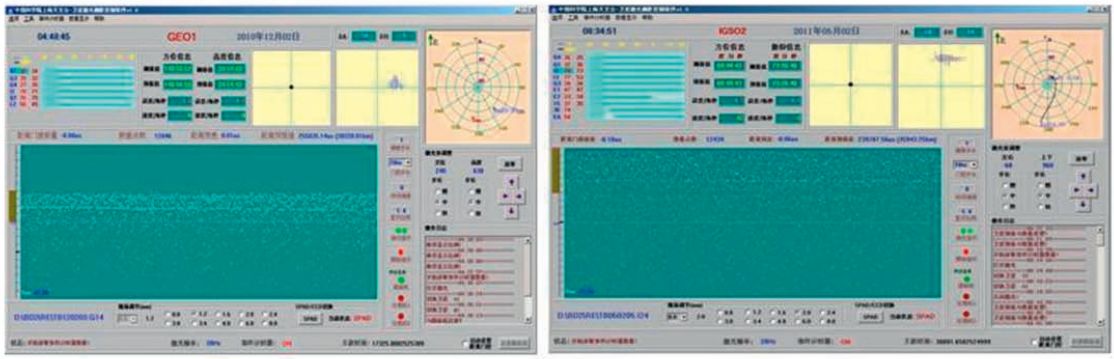


**Figure 4: Daylight tracking real-time ranging interfaces for GEO and IGSO satellite**

# 3. Laser Time Transfer for IGSO satellites

In Dec. 2007, Shanghai Observatory have successfully actualized Laser Time Transfer (LTT) experiment at Changchun SLR station (60cm aperture telescope) for Compass-M1 satellite (altitude 21,500km)[1][2].

## 3.1. New LTT payload

Based on the above experiment, some improved technologies are applied for the new LTT payloads, such as one gate mode adopted, two different FOV used, narrower filter etc. After the Compass IGSO1 satellite (altitude 36,000km) with improved LTT payloads was launched, the first measuring experiment was implemented successfully by using the 1 meter laser ranging system at the end of August in 2010 and the clock difference between satellite and ground was obtained. Compared to LTT experiment of Compass-M1 satellite, the performances of the new LTT payload on Compass IGSO1 and Laser Ranging system on ground are more advanced. And LTT measurement is also performed easily. Figure 5 is the view of photo-detector on the new LTT payload and its main performances.

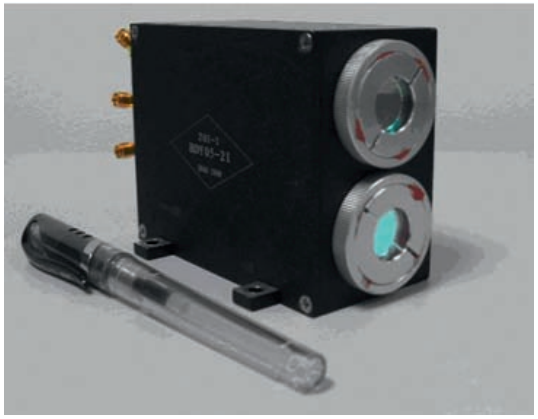

Main performances of new photo-detector

- Dual-SPAD detector
- 500g, < 2W, 105 × 70 × 80 mm
- Two Field of View: 15°/11°,
- for different background noise
- 40A bandwidth filter

**Figure 5: The photo-detector of the new LTT payload**

## 3.2. Laser Fire Control

For simplifying the design of LTT payload on satellite, the gate mode for detector is different from the one in routinely SLR, adopting a fixed range gate (about 70ns after start pulse). To reduce the effect of noises, the laser fire time on ground must be accurately calculated according to laser pulse flight time, predicted clock difference between space and ground, system delays, etc. Let the laser pulse arrive at the detector on onboard, just after the gate pulse of detector.

For strictly controlling laser fire time, the laser on ground should be actively switched, and laser with passive or pass-active switched cannot be used. The firing jitter of the new laser in this system is about 10ns and meets the requirement of LTT measurement.

## 3.3. Measuring Results

Table1 lists the some results of LTT measurement for Compass IGSO satellite and Fig.6 shows the clock difference. The measuring precision of the LTT experiment is more or less 300ps.

**Table 1 Some results from new LTT**

| Date | Points | Pass(min) | Precision(ps) | Slope of Clock Difference |
|---|---|---|---|---|
| 2010.08.30 | 315 | 10.1 | 283.1 | 2.322E-10 |
| 2010.09.21 | 2672 | 156.2 | 311.5 | -3.636E-10 |
| 2010.09.22 | 4830 | 251.0 | 315.1 | -3.567 E-10 |
| 2010.11.01 | 4345 | 47.6 | 296.6 | -3.572E-10 |
| 2010.11.02 | 7396 | 59.2 | 299.82 | -3.571E-10 |

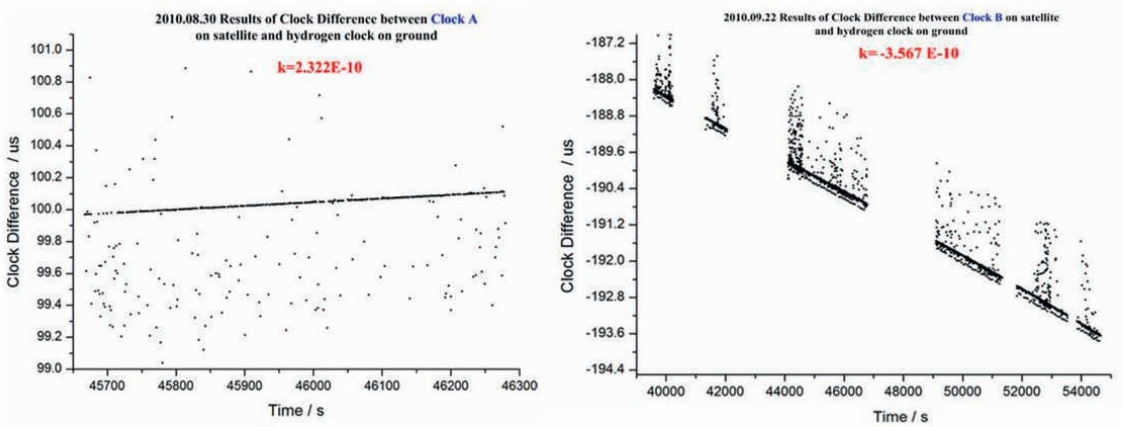


**Figure 6: Results of Clock Difference between satellite and ground**

# 4. Summary

The dedicated Compass SLR system in Beijing has being playing an important role in tracking Compass satellites (nighttime and daylight) for calibrating the microwave or radio ranging technique and the precise orbit determination of satellites. It is the first time to implement LTT experiment on IGOS1 satellite (altitude 36,000km) at the precision of more or less 300ps. The drift and stability of frequency onboard are about 10E-10 and 10E-13 respectively. Compass IGSO3 with the same LTT payload was launched and the LTT experiment was implemented successfully with the precision of 280ps in May 2011. Through LTT between satellite and ground, time synchronization for different stations on ground in the Chinese regions or beyond China will be carried out in the future.

## References

*Yang Fumin,* 2008: The preliminary results of Laser Time Transfer (LTT) Experiment, Proceedings of the 16th International Workshop on Laser Ranging

*Yang Fumin,* 2008: Laser Retro-reflector Arrays on the Compass Satellites, Proceedings of the 16th International Workshop on Laser Ranging

## Correspondence

Zhang Zhongping
No.80, Nandan Road
Shanghai
China

zzp@shao.ac.cn

# Comparative verification of return rate on GNSS LRA

*Shinichi Nakamura, Ryo Nakamura, Takahiro Inoue, Hiroyuki Noda, and Motohisa Kishimoto*

ABSTRACT

Recently, GNSS mounted LRA for precise orbit determination, precise clock estimation, and precise orbit validation. As regional navigation satellite, JAXA has launched QZS-1 on September 2010. JAXA confirmed a return rate of LRA on QZS-1 as initial check out. As a result, LRA on QZS-1 works well as expected.

Moreover, we are interested in other GNSS LRA since there are some kind of GNSS LRA, for example, non coated or coated CCR. We focused on the return rate for each CCR. At this workshop, we have reported performance of each GNSS LRA, which based on actual tracking through ILRS network. As a result, there is no merit on coated CCR, since all return signal come from low incident angle, which mea\ns total inertial reflection.

# 1. QZSS LRA and Its Performance

## 1.1. About QZSS

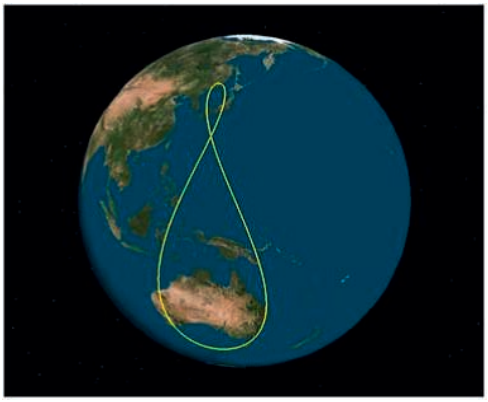

The Quasi-Zenith Satellite System (QZSS) is a regional space-based positioning system. Typical orbital elements are shown in Table 1.1. Three satellites are in elliptical and inclined orbits in different orbital planes to pass over the same ground track. The QZSS is designed so that at least one satellite out of three satellites exists near zenith over Japan [Fig. 1.1].

The first satellite, which is called QZS-1, has launched in 11 September 2010. At preset, checkout for navigation service including ground system and tuning for QZS-1 orbit and clock synchronization are performed.

**Fig.1.1: Image of Ground Track of QZS**

**Table 1.1: Orbit during QZS operation**

| Semimajor Axis | Eccentricity | Inclination | RAAN | Argument of Perigee | Center Longitude |
|---|---|---|---|---|---|
| 42164.17km (ave) | 0.075+/- 0.015 | 43 deg+/-4 deg | NA | 270 deg+/-2 deg | 135 degE+/- 5 deg |

## 1.2. LRA on QZS-1

### 1.2.1 Reference LRA at GEO

Tanegashima (GMSL), Koganei (KOGC), Yaragadee (YARL), Changchun, and Mt. Stromlo (STL2) were success tracking for ETS-8. [Note that ETS-8 located 146 deg East longitude]. Tracking result is shown in Table 2.1.

**Table 2.1: Summary of ETS-8 Tracking**

| Station Name | Return Rate | Note |
|---|---|---|
| Tanegashima | 5% to 15 % | 250mJ laser, 10Hz fire |
| Koganei | typically 1 % | 50mJ laser, 20Hz fire |
| Yaragadee | 1% to 3 % | 100mJ laser, 5Hz fire |
| Changchun | 0.1% to 1 % | 150mJ laser, 20Hz |
| Mt. Stromlo | 0.1 % to 1% | 21mJ laser, 60Hz |

### 1.2.2. Design for QZS-1 LRA

Though range for QZS-1 is farther than one for ETS-8, JAXA expects that QZS-1 LRA has same performance as ETS-8 even though farthest range of QZS-1. Here, we pay attention to the return rate from QZS-1. At tracking QZS-1, compared to ETS-8, the range between SLR station and QZS-1 is longer than ETS-8 case by 10%. According to the inverse four law, number of cube is calculated by

$$N = 36 \times \left(\frac{11}{10}\right)^4 = 52.7$$

Therefore, JAXA has designed LRA which has 56 (=7*8) CCRs, shape is shown in Fig1.2.2.

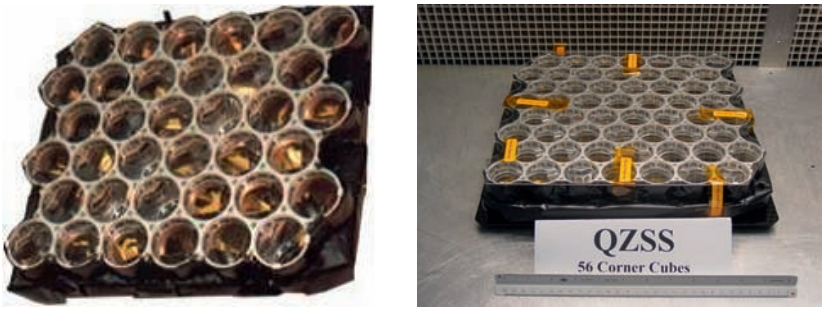


**Fig.1.2.2: Shape of LRA for ETS-8 (up) and QZS-1 (down).**

## 1.3. Performance of LRA on QZS-1

Obtained return rate, only typical case, is shown in Fig.1.2.3a. At Yarragadee, higher return rate corresponds to higher elevation angle, since higher elevation angle correspond to shorter range between SLR station and QZS-1. However, at Tanegashima, higher return rate is obtained at middle elevation angle.

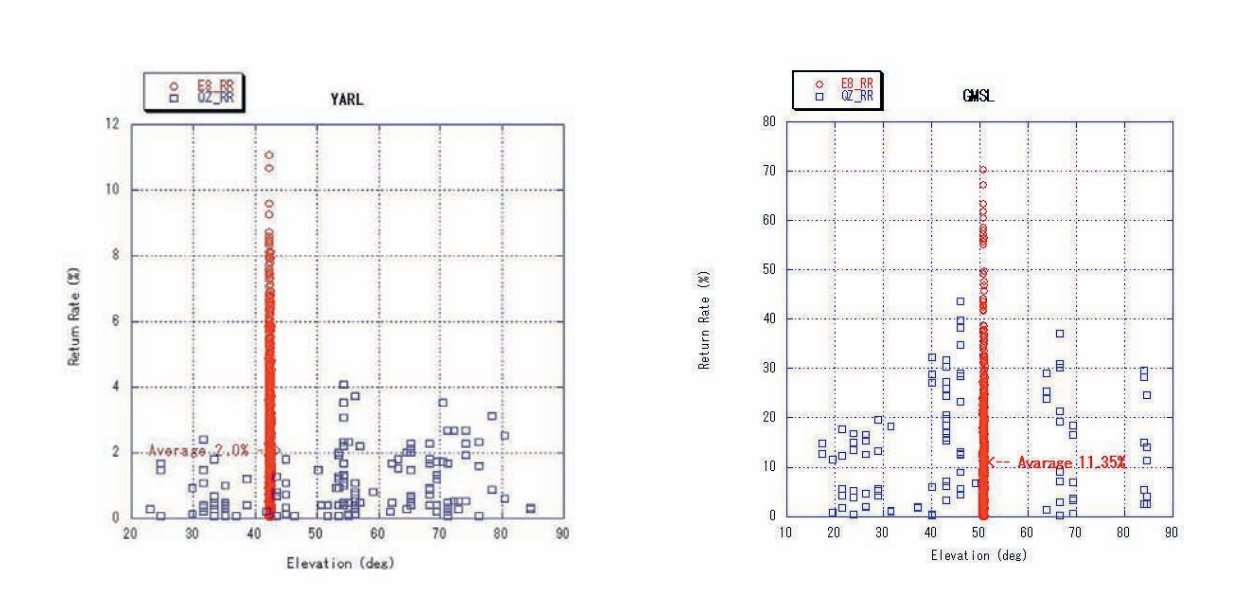


**Fig.1.3-1: The return rate at Yarragadee (left) and Tanegashima (right). Horizontal axis and vertical axis denote elevation angle and the return rate, respectively.**

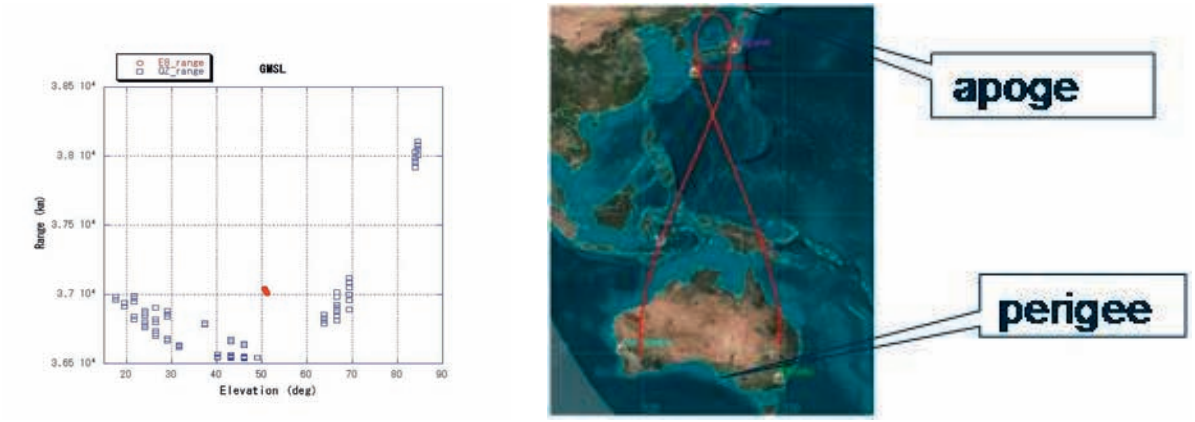


From Fig.1.2.3b, minimum range is given at middle elevation angle, due to characteristic orbit of QZS-1, where apogee located north hemisphere. Therefore, generally speaking, SLR station at north hemisphere, higher return rate is observed at middle elevation angle. Since the elevation dependence of the return rate is interpreted from relation between range and elevation angle, as a result, LRA for QZS-1 is working well as we expected.

# 2. Comparative verification among GNSS LRA – coated & uncoated

## 2.1. LRA spec at high orbit

LRA at high orbit falls into two categories, Uncoating or Coating. Typical Satellites are listed in Table 2-1. In this section, by evaluating the return rate, we forcus on the difference between coated and uncoated CCR.

| | Sat Name | Altitude(Km) | LRA | Note |
|---|---|---|---|---|
| Un-Coat | ETS-8 | 36,000 | 36 CCRs diameter 40.6 mm | GEO JAXA |
| | QZS-1 | 32,000-40,000 | 56 CCRs diameter 40.6 mm | RNSS JAXA |
| | Compass-M1 | 21,500 | 42 CCRs diameter 33 mm | GNSS Chinese Defense Ministry |
| Coat | GPS36 | 20,030 | 32 CCRs diameter 28.6 mm | GNSS United States DOD |
| | GLONASS-102 | 19,140 | 396 CCRs hexagonal 28.3mm | GNSS Russian Federation |
| | GIOVE-B | 23,916 | 67 CCRs diameter 27 mm | GNSS EU/ESA |

**Table. 2- 1: List of LRA at high orbit.**

## 2.2. Difference between coated and uncoated CCR

### 2.2.1. Range and Return Rate

The return rate from GNSS is shown in Fig.2-2. In Fig.2-2, green, red, blue and black dot correspond to GIOVE, Compass-M1, GPS and GLONASS, respectively. Horizontal axis and vertical axis denote range and the return rate, respectively. As well known, the return rate is decrease according to increase altitude. From Fig.2.2, there is no difference between coated and uncoated CCR.

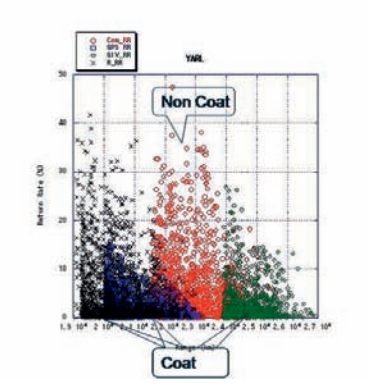


**Fig. 2-2: The return rate from GNSS at Yarragadee.**

### 2.2.2. Incident Angle and Return Rate

Uncoated CCR reflect laser pulse by a total internal reflection. This total internal reflection is arisen for small incident angle, the threshold angle is called the critical angle which determined by refractive index of CCR. In order to overcome this restriction, uncoated CCR was adopted, we supposed. We made a assumption, that is, coated CCR had a advantage for high incident angle. In fact, through analysis for LAGIOS and AJISAI which installed uncoated CCR, there is no return signal over 18 degree, that is, cut off angle of uncoated CCR is about 18 degree (Otsubo and Graham 2003).

Obtained return rate with regard to incident angle at Yarragadee is shown in Fig.2.2.2. Horizontal axis and vertical axis denotes incident angle and the return rate, respectively. Left and right hand side express the return rate from uncoated CCR and coated CCR, respectively. On the left hand side, blue and red dot correspond to the return rate from Compass-M1 and QZS-1, respectively. On the right hand side, red, blue and green dot correspond to the return rate from GPS, GIOVE, and Glonass, respectively. What is important is all return signal come form less than 14 degree in incident angle for both graph in Fig. 2.2.2. It is impossible to find the merit of coated CCR, at least, for high orbit satellite.

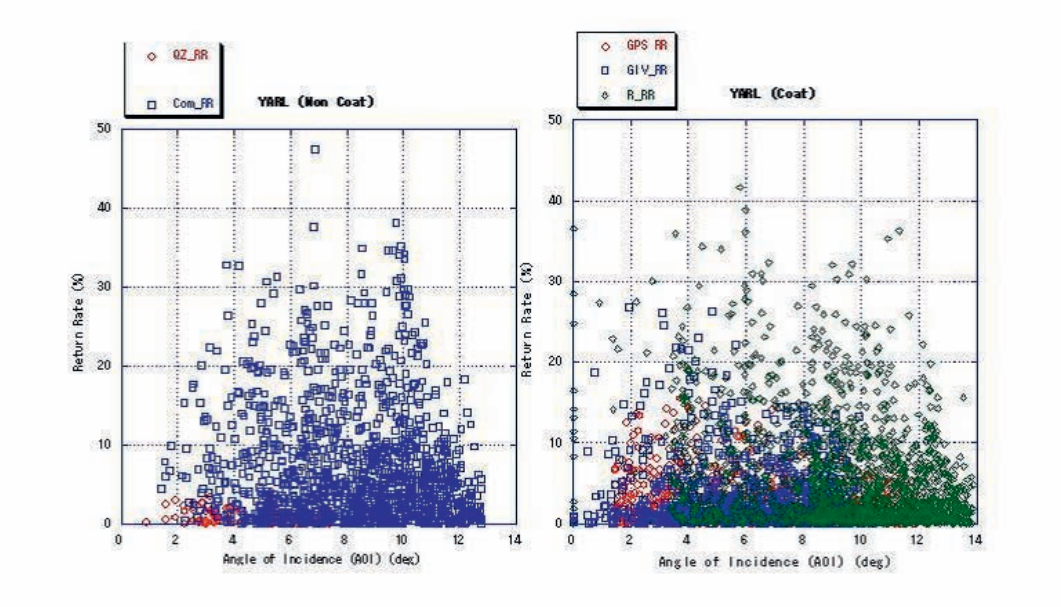


**Fig.2.2-3 The return rate relation with regard to incident angle at Yarragadee.**

## 2.3. Summary ~ from comparison return rate from coated with uncoated~

At least, when we evaluate LRA performance for GNSS (high orbit), there are no difference between coat and uncoat CCRs. At the view point of thermal control, coated CCR has more complexity than uncoated CCR. Through our study, focusing on the return rate and incident angle, there is no merit of coated CCR

## Acknowledgements

My special thanks are due to Yarragadee, Mt. Stromlo, and Koganei SLR stations for providing us with the ranging data through ILRS network. I gratefully acknowledge helpful discussion with Dr. Matthew Wilkinson on several points in this paper.

## References

*Toshimichi Otsubo and Graham M. Appleby,* System-dependent center-of-mass correction for spherical geodesic satellites, Journal of Geophysical Research, Vol. 108, 2003

*Matthew Wilkinson and Graham Appleby,* In-orbit assessment of laser retro-reflector efficiency onboard high orbiting satellites, http://dx.doi.org/10.1016/j.asr.2011.04.008

## Correspondence

Shinichi Nakamura
2-1-1 Sengen, Tsukuba, Ibaraki, 305-8505
Japan

nakamura.shinichi@jaxa.jp

# Improvements at NASA's NGSLR in Support of GNSS Ranging

*Jan F. McGarry,*
*Thomas Varghese, Thomas W. Zagwodzki,*
*John J. Degnan, John W. Cheek*
*Howard Donovan, Donald Patterson, Christopher Clark*
*Donald B. Coyle*
*Demetrios Poulios*

ABSTRACT
The NASA Space Geodesy Program (SGP) requires day-night ranging to Global Navigational Satellite System (GNSS) satellites. To meet this new requirement, the NGSLR eye safe laser was replaced with a NASA GSFC-built 1 milliJoule (mJ) 200 picosecond (ps) laser and the ~10% Quantum Efficiency (QE) quadrant anode Photek MCP-PMT was replaced with a high QE (40%) single anode GaAsP MCP-PMT from Hamamatsu. This improved transmitter-receiver combination is estimated to yield a link augmentation of 30X over the previous configuration. NGSLR tracks with fine pointing using a tight laser beam divergence of ~4 arcseconds (FWHM) and a narrow receiver field of view (FOV) of ~11 arcseconds enabled by a Risley Prism pair for laser point-ahead. Further reduction in day time optical noise and laser backscatter is planned by adding a telescope sun shield, narrowband spectral filter, and a gated optical shutter. The improvements in the signal to noise ratio (SNR) as well as the link margin should significantly enhance the NGSLR GNSS tracking and operations automation efforts. System configuration and early operational results are discussed.

## 1. Introduction

NASA's Next Generation Satellite Laser Ranging (NGSLR) system was originally designed for eyesafe day-night satellite laser ranging to Low Earth Orbiting (LEO) satellites and LAGEOS [1] [2]. The maximum laser energy exiting the 40cm telescope system was limited to ~60 microJoule at 532 nm for a pulsewidth of 300 picoseconds. This laser configuration met the stringent radiation safety requirements of the US Federal Aviation Administration (FAA) for autonomous operations by being eyesafe at all times and operated without the need for any safety monitoring mechanism. During the last few years, many technical challenges unique to the eyesafe laser were solved and system issues pertaining to the eye-safe laser configuration and operations automation were addressed.

## 2. Eyesafe Laser Configuration and Performance

The laser was developed by Q-Peak under a NASA Small Business Innovative Research (SBIR) program and was used for many years in NGSLR. The beam divergence control, as low as 4 arcsec, was accomplished via computer control of a Special Optics Beam Expander which changed the spacing among a lens triplet to maintain the beam size while changing the beam divergence. A passive polarization T/R switch, interfaced to two orthogonally polarized receive optical paths, combined the return signal efficiently in space and time at the receiver. Two configurations employing quadrant anode MCP-PMT detectors were used for single photoelectron detection: the first involved a Photek MCP-PMT with a Quantum Efficiency (QE) of ~ 12% and the second used a Hamamatsu Quadrant anode MCP-PMT with a QE of ~35%, almost a 3-fold improvement in QE. The latter device was damaged after several years of operations and was replaced by the Photek MCP-PMT. The four outputs of the detectors, when combined with the four separate channels of the Constant Fraction Discriminator (CFD) and the Event Timer (ET), can provide an equal number of precise simultaneous range measurements. This approach was in the works for near real-time tuning of the telescope pointing via spatial discrimination of the received photon, but was not fully implemented.

To reduce the solar background for daylight ranging, the receiver field of view (FOV) is kept at ~ 11 arcseconds enabled by laser point-ahead using a pair of Risley Prisms. External day time background optical noise is further suppressed via a narrow band (0.3nm) spectral filter. Since NGSLR uses a common transmit-receive telescope optics, the backscatter is an issue. This is attenuated over the initial 70 microsecond period of the atmospheric propagation by a blanking circuit for the receive detector, which proved to be adequate under eyesafe laser transmission. The pulse repetition frequency (PRF) of the laser was dynamically modulated under software control from 2 kHz to 1.96 kHz to avoid collisions of transmit and receive pulses [2]. Precise telescope pointing and tracking were enabled by an effective mount model that often provides a global RMS fit as low as 1.5 arcseconds using star calibration (nominally 50 stars).

In this configuration, NGSLR has successfully tracked LEO satellites and LAGEOS during day and night. Tracking to 20 degrees elevation was consistently achieved for LAGEOS, while lower elevation (down to 10 degree) tracking was routinely performed on LEO satellites. There was also success with GLONASS and ETALON ranging. In this case, tracking was successful only above 60 degrees elevation, where the link is better due to the shorter range and reduced atmospheric losses.

# 3. NGSLR Augmentation for Daylight Ranging to GNSS

NASA formulated an integrated multi-technique Space Geodesy Program (SGP) to set the directions for the global space geodesy efforts. A key SLR requirement that emerged from this new program was the need for day-night ranging to Global Navigational Satellite System (GNSS) satellites. The link to 20,000 km GNSS satellites is weak for daylight ranging using the eye-safe laser and the previous detector configuration. A stronger (an order of magnitude greater) link margin configuration was required at the station to meet this new requirement. It was recognized that the best way to accomplish this was by boosting the laser energy and increasing the QE of the receive detector.

## 3.1. Laser upgrade

A new laser was built by a NASA GSFC laser group [Coyle and Poulios] that has built many lasers for NASA airborne and spaceborne applications. The original NGSLR eyesafe laser was a 1064nm passively Q-switched microchip laser (Northrop Grumman Synoptics) with 15 microJoule energy per pulse. A proprietary diode pumped multi-pass Q-Peak amplifier scaled the output energy producing ~250 microJoule/pulse at 532nm. The table below summarizes the characteristics of the two lasers.

| | **Q-Peak** | **GSFC mJ** |
|---|---|---|
| Energy | ~ 0.1mJ | ~ 1mJ |
| Pulsewidth | 350 ps | < 200 ps |
| Wavelength | 532nm | 532nm |
| PRF | 2 KHz | 2 KHz |
| Divergence | 5-8 arcsec | 4 arcsec |

The new laser utilizes a regenerative amplifier seeded by a 200 ps gain-switched diode laser. The regenerative amplifier cavity is 1.5 m long and utilizes a pair of Nd:YAG zigzag slabs in a crossed-head configuration as the gain medium. The regenerative amplifier system is designed to run at a repetition rate of 2 kHz with ~1 mJ/pulse at 532 nm and a ~200ps pulse width. A pulse from the diode seeder is trapped in the regenerative amplifier cavity using a Pockels cell, where it can make many passes through the gain medium. When the pulse reaches its maximum energy, it is then switched out and directed through a KTP frequency doubler. The folded 1.5m long stable resonator cavity design enabled a package size small enough to fit within the Q-Peak footprint and avoid a NGSLR system redesign. This laser has the PRF flexibility from 1–2000 Hz. The upgraded laser needed further technical work to improve the pulse amplitude stability and is currently removed the station. It is expected back at the station by the end of August 2011.

## 3.2. Detector upgrade

The quadrant Photek detector (gain ~ 3.0 E+5, rise time ~180 ps, transit time spread ~45 psec) will be replaced with a higher QE Hamamatsu single anode GaAsP detector. This single element Hamamatsu model R5916U has a 40% QE, rise time of 178 ps, gain of 3.0E+5, and a transit time spread of ~136psec. The improvements to the laser transmitter and receiver configuration should provide a significant enhancement (factor of 30) to the link budget.

## 3.3. Noise reduction

NGSLR uses common transmit-receive optics and consequently backscatter from the optical surfaces as well as the atmosphere is a serious problem. To eliminate as much backscatter as possible, all optical surfaces in the transmit path (after the harmonic generator) are AR coated for 532nm and are kept optically clean. Backscatter into the MCP detector is also minimized by a very small angular tilt of all transmitting optics. Efficient beam dumps (>99% absorption) are used, where needed, and beam paths are baffled to improve optical isolation. Further reduction in back scatter should be possible by the use of a liquid crystal optical gate developed for NASA by Sigma Space [3]. Additional optical noise reduction is expected through the use of a narrower range gate, a solar shield on telescope, a narrow (0.1nm) spectral filter bandwidth, and a spatial filter operating at $\leq$ 11 arcsec.

## 3.4. Laser Hazard Reduction System (LHRS)

The new NGSLR configuration needs a Laser Hazard Reduction System (LHRS) for aircraft avoidance. A LHRS, which uses a 9.4GHz X-band radar transceiver and discriminating electronics to inhibit the laser from radiating the aircraft, is in place. This system, co-aligned with the laser beam, works automatically for aircraft detection, target discrimination, and laser beam inhibit.

## 3.5. Preliminary Results

Very preliminary tracks of GLONASS-102 and GLONASS-120 show the system now has the ability to track GNSS to below 40 degrees elevation at night. Initial LAGEOS passes show a higher return rate than previously achievable.

# 4. Conclusions

A systematic engineering upgrade effort is in progress to transition NGSLR station from its eyesafe configuration to a higher power laser configuration for increased link margin on high earth orbiting satellites. This link margin is further augmented by a high quantum efficiency high gain receive detector and a receive electronics system with a single photoelectron threshold. Significant SNR enhancement is also sought using a variety of optical noise filtering and isolation techniques. This new system configuration should provide a strong link budget to consistently track GNSS (using the ILRS standard array lidar cross section of 1E+8 $m^2$) during night or day. The suite of engineering developments, now underway, will offer full compliance with SGP needs for GNSS tracking and operational automation while meeting the ILRS performance standards for SLR.

## Acknowledgements

NGSLR SLR development is funded by the NASA/HQ Science Mission Directorate. The authors would like to thank John LaBrecque of NASA/HQ for his continued support of the NGSLR SLR work.

## References

*1- McGarry, J., T. Zagwodzki, T. Varghese, J. Degnan, J. Cheek, C. Clarke, P. Dunn, A. Mallama, A. Mann, D. Patterson, R. Ricklefs,* 2008: NGSLR: Sharing Eye-safe Kilohertz SLR with Transponder Ranging, Proceedings of the 16th International Workshop on Laser Ranging, Poznan, Poland.

*2- McGarry, J., T. Zagwodzki,* 2006: SLR2000: The Path toward Completion, Proceedings of the 15th International Workshop on Laser Ranging, Canberra, Australia.

*3- Degnan, J. J., and D. Caplan,* 2006: Performance of a Liquid Crystal Optical Gate for Suppressing Laser Backscatter in Monostatic Kilohertz SLR Systems, Proceedings of the 15th International Workshop on Laser Ranging, Canberra, Australia.

## Correspondence

Jan McGarry
NASA Goddard Space Flight Center
Code 694
Greenbelt, Maryland 20771
USA

Jan.McGarry@nasa.gov

# Direction of the light displacement vector in laser ranging of the artificial Earth satellites

*Yu.V. Ignatenko[1], I.Yu. Ignatenko[2], A.A. Makeev[1] and V.N. Tryapitsyn[1]*

ABSTRACT

In this article the method of construction of the three-dimensional laser beam deviation vector using satellite laser ranging observations is described. The scheme of deduction of the equation of this vector by its two projections onto the focal plane of a telescope at different instants of time during a satellite pass is stated. Influence of the Earth orbital velocity on the direction of the light deviation 3D-vector is estimated. Solutions are given in the inertial frame with an origin in the solar system mass center. Earth rotation and orbital motion irregularities are taken into account. Observed deviation of light from preset direction is a result of composition of the satellite relative-to-observer velocity, the Earth orbital velocity, and velocity of the luminiferous medium.

## 1. Introduction

The laser ranging of the artificial earth satellites with a laser beam of a small angular spread allows to measure a value and direction of anomalous light beam deflection (for details see [1, 2]). In the course of these measurements one registers the magnitude of projection of the beam displacement onto the picture plane of the telescope. During one fly-over of the satellite, it is observed as a rule over an arc larger than 100 degrees. Within such angular interval one can distinguish a few pairs of points which can be associated with a projection of the beam displacement onto the picture plane. For each of distinguished pairs of projections we constructed a spatial (three-dimensional) vector of beam displacement.

## 2. Data processing procedure

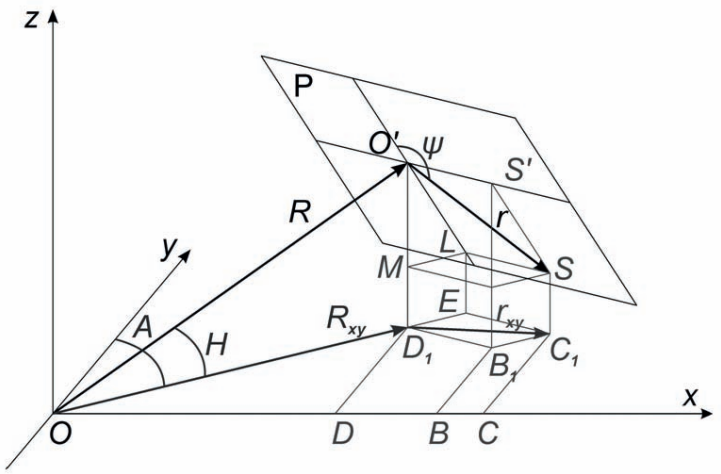


**Figure 1: Schematic sketch of the picture plane for derivation of equation for a three-dimensional vector of beam displacement.**
$P$ **– picture plane,** $R$ **– radius-vector of the target point,** $r$ **– vector of beam displacement,** $A$ **– azimuth,** $H$ **– height.**

[1] Crimean Laser Observatory of the Main Astronomical Observatory of the National Academy of Sciences of Ukraine, 98635 Katzively, Yalta, Crimea, Ukraine

[2] Federal State Unitary Enterprise "National Research Institute for Physical-Technical and Radio Engineering Measurements" (VNIIFTRI), 141570 Mendeleevo, Moscow region, Russia

The schematic reconstruction of the three-dimensional vector from its two known projections can be performed as de-scribed below. First we construct a plane passing through the projection of the displacement vector at the moment $t_1$ erpendicular to the picture plane. The same procedure is then made for the moment $t_2$. The angle between the resulting planes corresponds to the arc of the satellite orbit between the moments $t_1$ and $t_2$. A sought-for vector is situated on the line of intersection of these two planes. In order to derive the equations of these planes we take three points on them. For two time moments $t_1$ and $t_2$ these are the coordinates of the initial and terminal points of the radius-vector $R$ (the coordinates of the points $O$ and $O'$) and the coordinates of the point $S$ (Figure 1). Using the absolute value of the displacement vector $r$ and the angle $\psi$ in the coordinate system of the picture plane as well as the topocentric coordinates of the satellite, distance $R$ and calculated azimuth $A$ and height $H$, we can compute the coordinates of two points: the target point $O'$ and a point $S$, from which the reflected laser beam is coming. The target point is determined by the direction of outgoing laser pulse, while point $S$ is the satellite image. According to Figure1 we can write the coordinates of the target point $O'(x, y, z)$ in the form:

$$(1) \quad \begin{cases} x = R\cos H \sin A \\ y = R\cos H \cos A \\ z = R\sin H \end{cases}$$

Respectively, one gets the following expressions for the coordinates of the reflection point :

$$(2) \quad \begin{cases} x' = R\cos H \sin A + r \cdot (\cos A \sin\psi - \sin A \sin H \cos\psi) \\ y' = R\cos H \cos A - r \cdot (\sin A \sin\psi + \cos A \sin H \cos\psi) \\ z' = R\sin H + r\cos H \cos\psi \end{cases}$$

Here $R$ is the radius-vector of the target point, $r$ is a laser beam deflection from a given direction or angular distance between a target point and a signal point. As in paper [2], we consider $r$ as a vector. Coordinates of both these points and the observing laser station (locator) are transferred into the inertial system JD2000, and then are reduced to the center of mass of the Solar system. Observations of one satellite result in two sets of such points corresponding to two different time moments $t_1$and $t_2$. The coordinates $(x_1, y_1, z_1)$ correspond to the time moment $t_1$, while the coordinates $(x_2, y_2, z_2)$ correspond to the time moment $t_2$. For each set of three points one constructs the equation of plane to which they belong: $Ax + By + Cz + D = 0$.

The coefficients A, B, C, D can be calculated according to a well-known equation of plane through three points.

For two sets of three points each we get a system of equations:

$$(3) \quad \begin{cases} A_1 x + B_1 y + C_1 z + D_1 = 0 \\ A_2 x + B_2 y + C_2 z + D_2 = 0 \end{cases}$$

This system sets an equation of a straight line which is a line of intersection of these two planes:

$$(4) \quad \frac{x - x_1}{x - x_2} = \frac{y - y_1}{y - y_2} = \frac{z - z_1}{z - z_2}$$

The coordinates $(x_1, y_1, z_1)$ and $(x_2, y_2, z_2)$ set two points belonging to this straight line.

Setting a value of $x_1$, one can determine $y_1$ and $z_1$ from the system (3). Similarly, for a given value of $x_2$one can determine $y_2$ and $z_2$. The values of $x_1$ and $x_2$ are taken far enough from the solar system so that the annular parallax of corresponding points is less than 1". Using the coordinates $(x_1, y_1, z_1)$ and $(x_2, y_2, z_2)$ transferred from the inertial coordinate system with the reference point in the center of mass of the Solar system into the second equatorial system, we get the coordinates of points in this system $(\alpha_1, \delta_1)$ and $(\alpha_2, \delta_2)$.

# 3. Results

Figure 2 shows the points (in the second equatorial system) corresponding to the directions of the displacement vector calculated on the basis of observational data (laser ranging) on the satellites LAGEOS-1 and LAGEOS-2 in 2007-2008 in the frame of proposed scheme. It should be mentioned that the displacement vectors were computed with the use of vectors marked by a digit 3 in figures from [1]. These vectors were made free from the influence of the relative velocity of the satellite movement by means of a scheme presented in the same paper.

From papers [1, 2] one can conclude that for unknown reasons a described phenomenon is of universal character. It ma-nifests itself not only in the near-Earth space in the process of laser ranging of artificial earth satellites but in the immediate vicinity of the Earth surface as well [2]. This conclusion is qualitatively confirmed by the studies of Miller [3]. This leads to a necessity to consider a picture of the phenomenon after exclusion of all possible factors which can affect a value and direction of light de-flection.

In order to investigate a pure phenomenon it is necessary to exclude the influence of the Earth orbital velocity equal to 30 km/s or expressed in angular units according to a well-known formula $\varphi = 2v / c$ as 41". In order to solve this problem, the vector of the Earth orbital velocity at the moment of observations should be added to the vector, the coordinates of which are shown in Figure2. It should be just added because the light is deflected in the direction opposite to the direction of movement. Let us note that the magnitudes of vectors shown in Figure 2 to which the corresponding vectors of the orbital velocity should be added range from 5" through 11".

The addition of these vectors is easier to perform graphically with acceptable accuracy. Angular coordinates of both a three-dimensional displacement vector (Figure 2), and the orbital velocity vector for a corresponding date were used to calculate the angle between the vectors in the orthodromic plane according to a well-known formula:

$$\cos AB = \sin\delta_1 \sin\delta_2 + \cos\delta_1 \cos\delta_2 \cos(\alpha_2 - \alpha_1), \qquad (5)$$

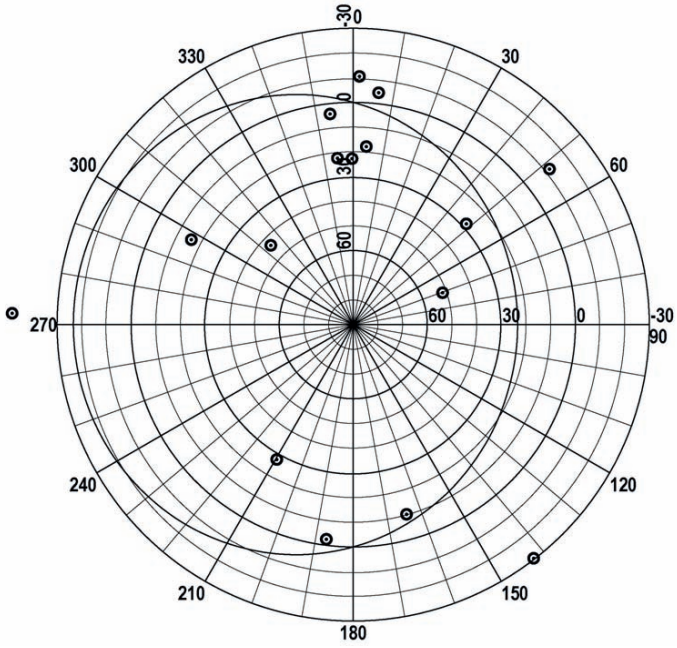


**Figure 2: Distribution of directions of the light displacement vector with account for velocity aberration depending on the satellite velocity**

where $AB$ – is an arc of a great circle in the angular units, ($\alpha_2$, $\delta_2$) – the coordinates of the point $A$ (the direction of computed vector, see Figure2), ($\alpha_2$, $\delta_2$) – the coordinates of the point $B$ (direction of the vector of the Earth orbital velocity at the moment of observation). The coordinates of the Earth orbital velocity vector for a given date was found as a point of intersection of the ecliptic line with a beam pointing from the coordinates centre to the direction of orbital velocity. Using the magnitudes of the vectors and the angle between them, one can obtain the magnitude and direction of the resultant vector of beam displacement with excluded orbital velocity of the Earth. The coordinates of the constructed resultant vector lie on the orthodromic line connecting a point with coordinates of the Earth velocity vector and a point with coordinates of the light displacement vector at a given time moment (Figure2).

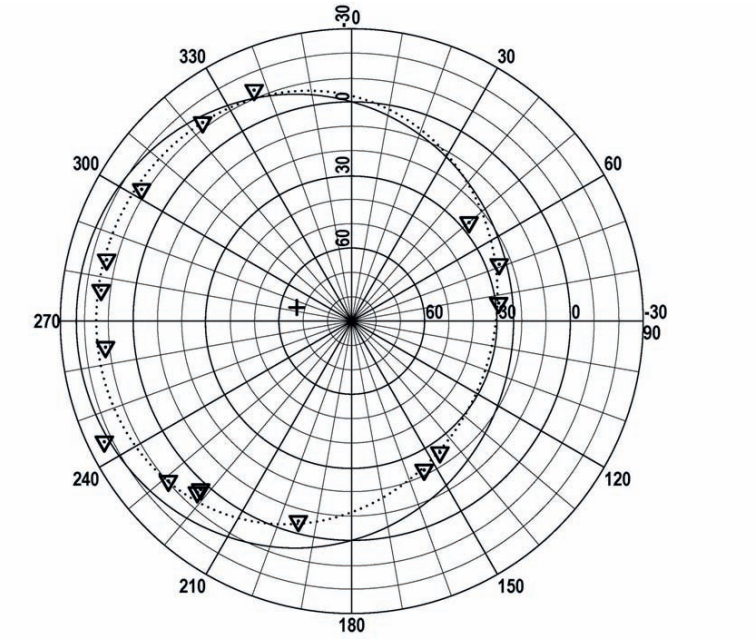


**Figure 3: Distribution of directions of the light displacement vector with account for both the satellite and Earth orbital velocity (The directions of movement of the luminous media in the Solar system depending on the season in the vicinity of the Earth orbit)**

Figure 3 shows results of calculations described above. Points denote the directions of beam displacement in the absence of orbital motion. This direction of the space displacement vector is determined by the Earth position on the orbit at a given time moment under condition that there is no orbital motion at this moment. Such a picture of the phenomenon can be explained on the grounds of adopted conception about the presence of luminous media in the ambient space. [1]. From this figure one can conclude that the Earth together with the Solar system is moving in the galaxy with the velocity close to that of the luminous media. Such movement is often referred to as a motion in the wake flaw. Closed regression line is drawn through the experimental data points. Its centre has the following coordinates: $\alpha = 284°$, $\delta = 67°$. Double point means that observations were performed twice during a night 28.07.2007 for the satellites Lageos-1 and Lageos-2 with a time lag of one hour. The orbits of these satellites lie in different planes. The angle between them is 42°. Such coincidence can confirm the correctness of both the reduction methods and interpre-tation of the results obtained.

The most similar results have been obtained by Miller [3]. Small discrepancy is caused by essential difference in expe-rimental methods. Miller performed observations on the earth surface and used interferometric technique. In addition, his work is dated back more than 70 years.

## References

1. *Yuriy V. Ignatenko, Vladimir M. Tryapitsyn, Igor Yu. Ignatenko*. Determination of Speed Aberration While Laser Loca-tion of Earth Artificial Satellites. Journal of Automation and Information Sciences 2004, Volume 36 / Issue 4, p. 26 - 28.

2. *Igor Yu. Ignatenko, Yuriy V. Ignatenko, Vladimir M. Tryapitsyn, Andriy A. Makeyev*. Measurment of Anomalous Angle of Deviation of Light During Satellite Laser Ranging, Proceedings of the 16th International Workshop on Laser Ranging. October 2008, Poznań, Poland, Volume 1, p. 92-96.

3. *Dayton C. Miller*. The Ether-Drift Experiment and the Determination of the Absolute Motion of the Earth. Reviews of Modern Physics, Volume. 5, p. 203–242, 1933.

## Correspondence

Igor Yu. Ignatenko
IgIg@bk.ru

Yuriy V. Ignatenko
YuIg@bk.ru

Vladimir M. Tryapitsyn
Clogao@rambler.ru

# Polarisation at the SGF, Herstmonceux

*Matthew Wilkinson, Toby Shoobridge, Vicki Smith*

ABSTRACT

A property of a light wave is the orientation of the electric field vector, or its polarisation. Laser light, used in Satellite Laser Ranging (SLR), is highly polarised in comparison to other light sources which emit light randomly at all polarisations and are termed to be unpolarised. The performance of optical elements used in SLR, such as mirrors, can depend on the incident polarisation and this is particularly the case if the element is old and has degraded. To understand fully the impact of polarisation on the SLR system at the Space Geodesy Facility (SGF), Herstmonceux, a series of experiments were devised and carried out to first explain some observed phenomena, then to identify and specify an upgrade to a poorly performing optic and finally to consider the control and application of polarisation to the advantage of SLR.

## 1. Assessment of the impact of polarisation on SLR

It was the suspicion at the SGF that two unexplained observations were caused by a variation of the laser polarisation. The first of these was during calibrations of the two lasers in operation, the original Nd:YAG 12Hz laser and the newly installed Nd:VAN 2kHz laser. The primary SLR calibration target is due west on a nearby water tower and there is also a secondary target due south at a greater distance. Strong return rates from calibrations with the 12Hz laser on the primary target were not replicated when it calibrated on the southern target. However, on calibrating the kHz laser it was quickly apparent that the southern target gave by far the stronger return signal, in opposition to the experience with the 12Hz system. An experiment was devised, fitting an 'analyser' polarising sheet in the emitter telescope, see figure 1. This analyser was rotated 360°, in steps of 10°, during calibrations at each target for each laser and the return rates were recorded.

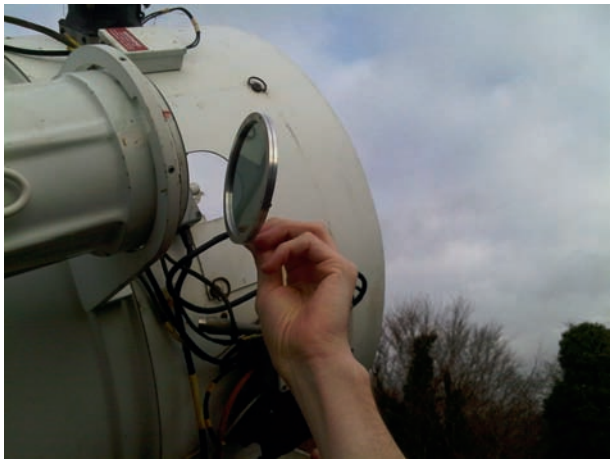

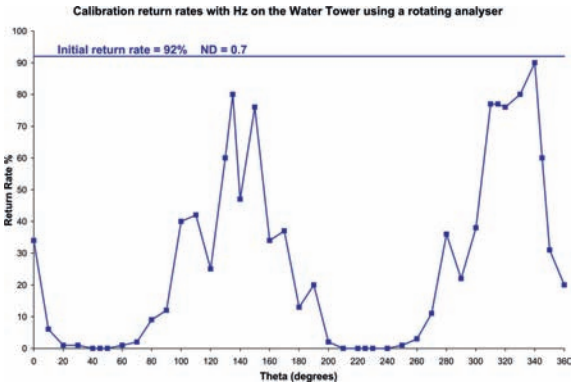


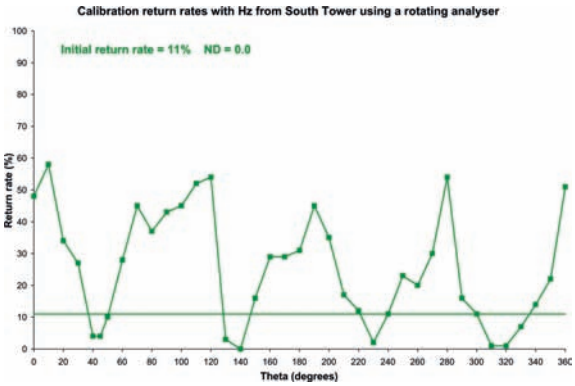


**Figure 1: A photograph of the analyser being placed into the emitter and plots of the recorded return rates for calibrations using the 12Hz laser at the western target, left, and the southern target, right.**

Figure 1 contains two plots of return rates as the analyser was rotated 360°. The left plot contains results using the 12Hz laser on the primary target in the west and shows two peaks where the emitted laser pulse polarisation is aligned with the transmission axis of the polarising sheet and two extinctions where the light is blocked by the analyser. The right plot is for the 12Hz laser during calibration on the southern tower. In contrast to the previous plot there are now 4 peaks and more surprisingly the low return rate increases with the insertion of the analyser from its initial rate of 11% up to nearly 50%. The analyser rotates the emitted polarisation to a more favourable orientation for the receive optical path. The kHz laser plots were similar but in reverse for the targets. The two lasers were later found to emit orthogonally opposite linear polarisations.

The second observation was made using the daytime camera by viewing the laser beam in the telescope iris, which would disappear in certain parts of the sky. To record this, two photomultipliers were used simultaneously to measure the backscattered laser light at the primary port where the SPAD detector is installed and at the secondary port, which receives light reflected by a dichroic mirror. Backscattered light largely retains its polarisation if scattered by small particles such as air molecules or water vapour, but this is not necessarily the case for larger scatterers such as pollutants, aerosols or ice crystals. Figure 2 shows the results recorded by these two devices as the telescope was pointed to the zenith and rotated steadily in azimuth, which causes the emitted polarisation to rotate. Both plots show variability with azimuth, but the peaks are in opposite phase. This suggests that the dichroic mirror, internal to the telescope, reflects more at certain polarisations and so transmits less and for other polarisations reflects less and transmits more.

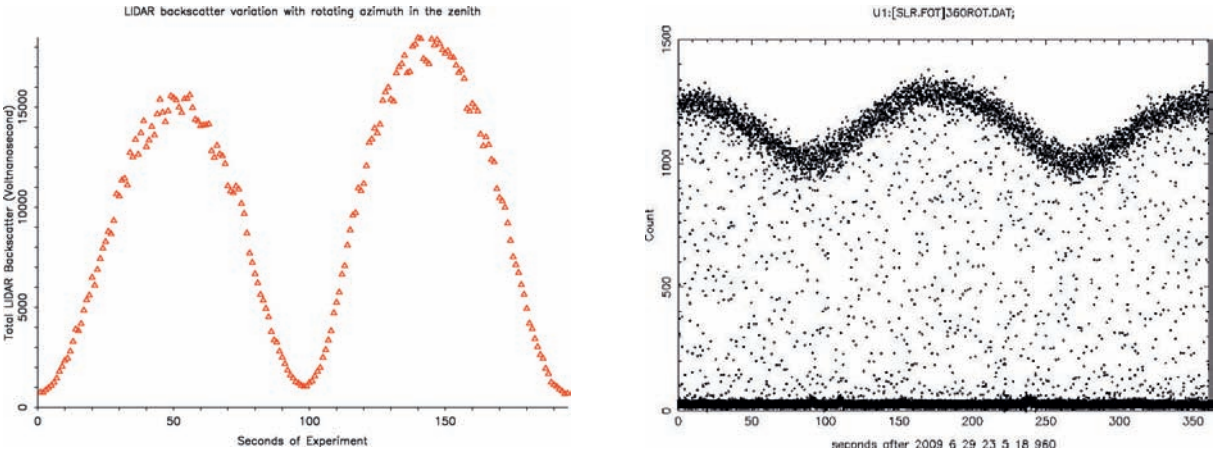


**Figure 2: The light detected at the primary port, transmitted through the dichroic, on the left and reflected by the dichroic to the secondary port on the right.**

# 2. Specifying a replacement dichroic mirror

The dichroic was removed from the telescope and an experimental set-up was designed to test the polarisation variability of the mirror. This consisted of an adjustable half-wave plate in the laser path, a 45° mount for the mirror and an energy monitor. The energy monitor was first placed to record the transmitted laser light and then the reflected laser light as the half-wave plate rotated the polarisation incident on the dichroic mirror. A large variation was seen in both measurements as shown in the left plot in figure 3.

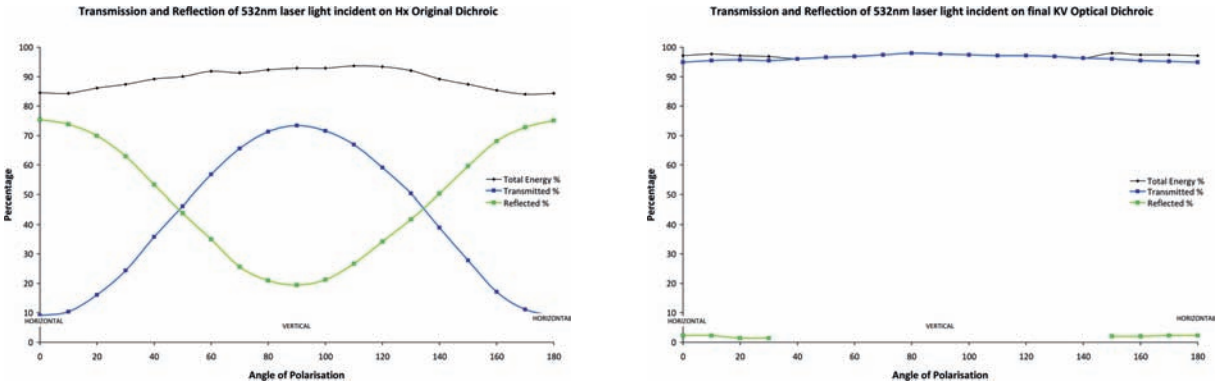


**Figure 3: The transmission and reflection recorded from the old dichroic (left) and new dichroic (right)**

A replacement for the dichroic was specified and manufactured after testing a number of samples using this standardised laser bed test. On receiving the new dichroic it was tested for transmission and reflection at 532nm and gave the results present in the right hand plot in figure 3. This dichroic replacement improved SLR return rates from satellites by more than 100%. A duplicate dichroic was later sourced by the Graz SLR station and similar improvement was seen.

Further tests were made using the standard laser bed setup on mirrors in the coudé chain and a range of behaviour was discovered. The newer mirrors performed well with near 100% reflectance for all states of incident polarisation. The older mirrors showed reduced reflections for polarisations parallel to the plane of reflection. For most this was to approximately 95% but for an old mirror, previously at the end of the coudé chain which experienced prolonged exposure to sunlight, this reduced to around 65% reflection. In addition to this, the second mirror in the coudé was found to convert linear polarised light to circularly polarised light at certain positions; this mirror was replaced with an old spare.

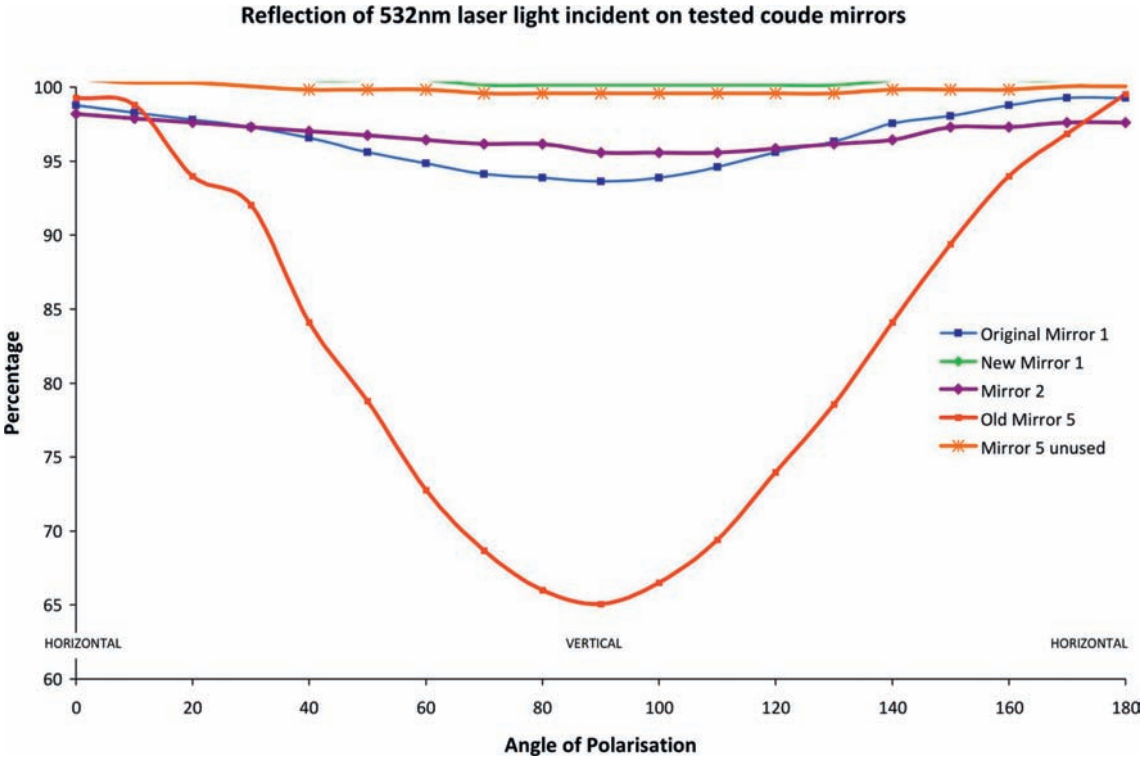


**Figure 4: The reflectances of mirrors tested for polarisation variability.**

# 3. Modelling and controlling the emitted polarisation

During SLR the telescope tracks the satellite in azimuth and elevation as it passes overhead. This rotates the optical path of the laser light as it travels to a smaller side telescope attached to the large, 60cm, receiving telescope. This rotation results in a varying emitted polarisation orientation, which depends on both azimuth and elevation.

In order to model this variation the laser beam polarisation was considered as two components, perpendicular to each other and to the direction of the laser light. Polarisation parallel to the plane of reflection, figure 5a), is preserved after a 45° reflection when considered in the frame of the direction of the light. Polarisation perpendicular to the plane of reflection undergoes a 180° phase shift, as shown in figure 5b).

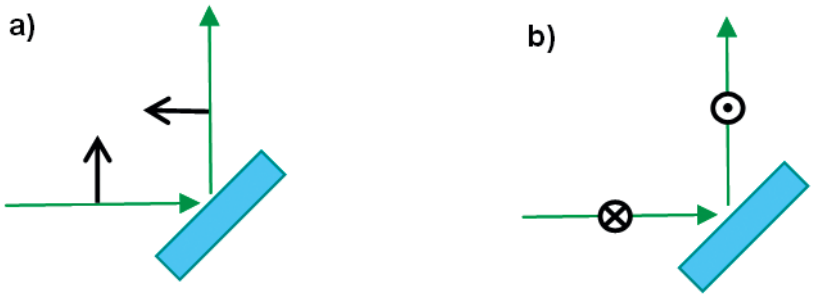


**Figure 5: Polarisation parallel a) and perpendicular b) to the plane of reflection**

If the polarisation is represented by a two-component vector [**S P**] where S is the perpendicular component and P is the parallel component then a mirror reflection can be represented by the following matrix $\begin{bmatrix} -1 & 0 \\ 0 & 1 \end{bmatrix}$. At the SGF, and considering the 2kHz laser which emits linearly polarised light, orientated parallel to the laser bed, the first coudé mirror is similar to that in figure 5b) where the polarisation is perpendicular to the plane of reflection and is shifted 180° in phase. The second mirror is not as straight forward as the first. The second mirror moves with the azimuth of the telescope so that the reflection is always 45° but not always so that the polarisation is parallel or perpendicular to the plane of reflection. The method used for mirror 2 was to consider the new plane of reflection at a particular azimuth and calculate the magnitude of the parallel and the perpendicular components. Then the reflection could be treated with the same simple matrix operator as the first mirror. The translation matrix in this case was calculated to be $\begin{bmatrix} \cos(\theta) & -\sin(\theta) \\ \sin(\theta) & \cos(\theta) \end{bmatrix}$, where θ is the telescope azimuth. The third and fourth mirrors are in the same reflection plane as the second mirror and so no translation matrix was needed, only the reflection matrix. The fifth mirror moves with telescope elevation and again a translation was used to calculate the polarisation parallel and perpendicular components in the new plane of reflection. This translation was $\begin{bmatrix} \sin(\varphi) & \cos(\varphi) \\ -\cos(\varphi) & \sin(\varphi) \end{bmatrix}$, where φ is the telescope elevation.

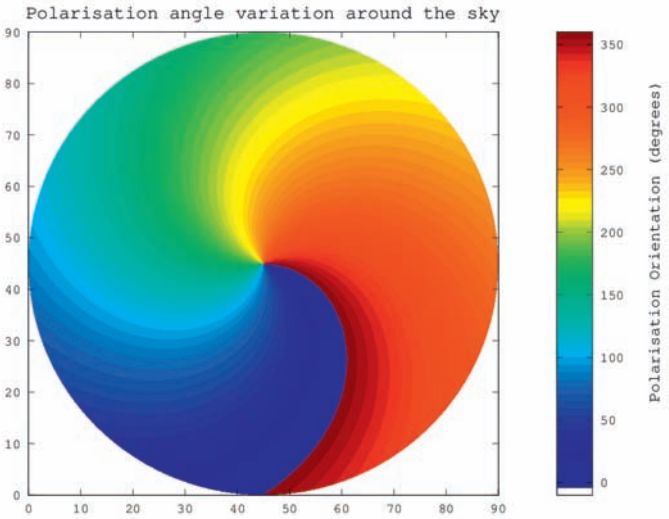


**Figure 6: The polarisation of the kHz laser beam leaving the emitter at different telescope azimuth and elevations.**

Simulating the change of the laser polarisation as it travels through the coudé and as the telescope moves in azimuth and elevation was straight forward once this model was complete and this is presented in figure 6. The model was tested using the analyser in the telescope emitter and by driving the telescope to an arbitrary position. The model predicted the laser polarisation leaving the emitter and the analyser was positioned to screen the laser. The prediction was then confirmed by firing the laser on low power and with protective eyewear, this was repeated for a series of different telescope positions.

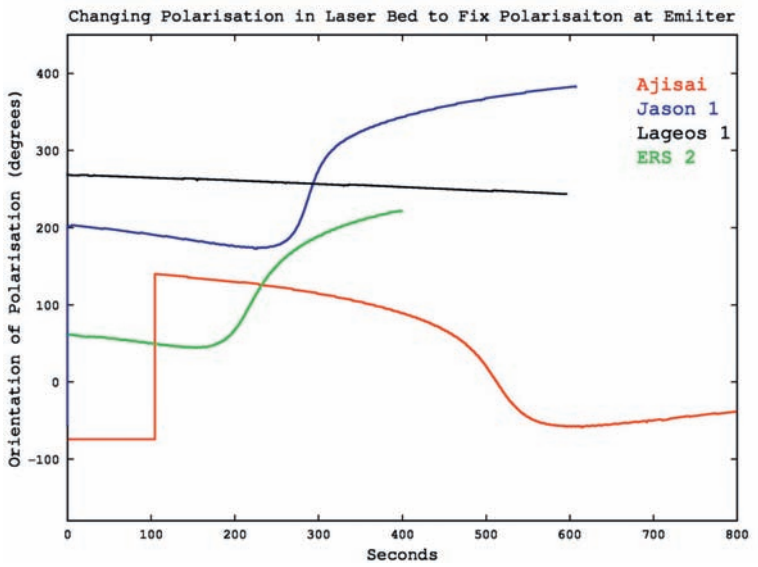


**Figure 7: The rotational change of the half-wave plate for satellite passes to fix the emitted polarisation.**

The model was then reconstructed to run backwards through the mirrors using a fixed end polarisation, parallel to the telescope elevation axis. This gave the polarisation parallel and perpendicular components required from the laser to produce the fixed polarisation at the emitter. To test this the analyser was reinserted into the emitter in a position to screen the fixed polarisation, the telescope was driven to arbitrary points and the input polarisations were predicted and provided using a half-wave plate. The effective screening of the output laser was observed, projected on the closed dome and through a camera mounted on the telescope and was confirmed with small movements of the half-wave plate.

An application to control the emitted laser polarisation is a future possibility. This could be done either to fix the polarisation at a particular orientation, which could then be used to screen the returning laser light, or, with knowledge of each satellite retro-reflector target, to optimise the outgoing polarisation to give increased return rates. Figure 7 shows the calculated position of the half-wave plate for a number of satellite passes to fix the outgoing polarisation. The movement of the half-wave plate is steady and continuous.

# 4. Conclusion

The Herstmonceux SLR station now has a far better understanding of the impact of polarisation in the system. This work lead to identifying the dichroic mirror to be not performing as required and replacing this mirror gave an improvement in SLR return signal of more that 100%. The polarisation orientation of the emitted laser beam varies across the sky and this has been modelled. Fixing the polarisation emitted would be possible by controlling a 1/2-wave plate in real-time. This could benefit the SLR of more difficult targets such as GNSS either by noise filtering or by optimising polarisation for return rate.

## References

*Luck J, Smith V, Moore C*, Circular Polarization Experiment & Herstmonceux Energy Tests. Proceedings of Fall ILRS Workshop, Grasse, France, 2007.

*Hecht E.*, Optics, Fourth Edition, Addison Wesley.

## Correspondence

Matthew Wilkinson

NERC Space Geodesy Facility
Herstmonceux Castle
Hailsham
East Sussex
BN271RN
United Kingdom

matwi@nerc.ac.uk

# Session 11:
# Satellite Subsystems: Retroreflector Arrays

# Retroreflector and Retroreflector Array: Keynote Paper

*Toshimichi Otsubo, Reinhart Neubert,*
*Scott Wetzel*

ABSTRACT
Key issues and key parameters are reviewed for the up-to-date technological development in retroreflectors and retroreflector arrays for satellite laser ranging and lunar laser ranging. Both numerical optical simulations and real observations play important roles both in the pre-launch design phase and in the post-launch data handling.

## 1. Introduction

The ranging precision of satellite laser ranging (SLR) and lunar laser ranging (LLR) is improving toward 1 mm or even better in a normal-point basis, and there are increasing number of earth-orbiting satellites that carries retroreflectors for the SLR technique and also a few lunar exploration projects for the LLR technique as well. SLR retroreflector panels are usually composed of multiple retroreflectors and they are often required to be compact from the viewpoint of target signature effects (Otsubo and Appleby, 2003) and also of limited onboard weight. It is, therefore, important to make the retroreflectors efficiently designed.

From low-earth-orbit satellites to the Moon, a large variety of retrorefelctors have been widely used for laser ranging. This is because there are a various range of geometrical parameters, such as a station-reflector distance, an angle of incidence, attitude control, and velocity aberration. The onboard retroreflectors have to be chosen or optimized to satisfy these conditions.

This paper is introductory to the Session 11 "Satellite Subsystems: Retroreflector Arrays," and therefore the key issues and the key parameters are reviewed in the field of retroreflectors and retroreflector arrays.

## 2. Key issues

### 2.1 Maximizing the intensity

Generally speaking, laser ranging operation will become easier if a satellite carry a large size of retroreflectors and/or a large number of retroreflectors. In the real world, we have to maximize the intensity of return signals in order to cope with the limited weight for onboard instrument.

Given a certain type of a retroreflector (or a retroreflector array) and a certain station-satellite distance, the optical response in SLR and LLR is described as a four-dimensional function, i.e., two dimensions for angle of incidence including azimuthal angle, and two dimensions for velocity aberration that is a two-dimensional relative velocity vector perpendicular to the line of sight. The range of angle of incidence and the range of velocity aberration are dependent on the orbits and attitude control policy of a satellite.

Key parameters in this category are: the retroreflector size, the number of retroreflectors, the shape of a front face, the coating of back faces, the dihedral angle offset, the curvature of front/back faces, and so on. For instance, a metallic coat on back faces produces a wide angle of incidence whereas an uncoated retroreflector causes a strong azimuthal dependence. The dihedral angle offset is commonly adopted in Earth-orbiting satellites and essential especially for low orbiters, to compensate the velocity aberration. It should be noted here that the actual optical behavior of a ret-

roreflector is heavily influenced by the thermal environment in space and such laboratory simulation is also playing an important role (Dell'Agnello, et al., 2011).

## 2.2 Minimizing the target signature effects

Optical intensity and measurement precision are often incompatible. Carrying a large number of retroreflectors causes a pulse spread due to the combined contribution from multiple reflection points. As a result, the interval between the leading edge and the centroid of the pulse becomes longer than a simple single reflector typically used as a ground target for calibration, and it causes ambiguity in the center-of-mass correction of such satellites.

Initially such pulse broadening had been found in large-size retroreflector arrays such as Topex/Poseidon, Ajisai, Etalon, GLONASS, etc. However, sub-centimeter wobbles are today detected in small-size arrays like LAGEOS and ERS-2, by highly precise laser ranging systems. In order to fully utilize the currently achievable laser-ranging precision, the center-of-mass correction should be applied in a more complicated way in the future, for instance, by considering the satellite orientation and the geometry of a retroreflector array.

A "zero-signature" retroreflector array is being proposed and realized. Japanese ADEOS satellite was the first example of a corner-cube reflector (Sugimoto and Minato, 1996) and Russian BLITS satellite is an innovative Luneberg-sphere lens (Vasiliev, et al., 2011). A single corner-cube reflector system is also envisaged for the future GNSS satellites and also for the future LLR targets.

The key parameters to be considered in this category are: the arrangement of reflectors (especially in depth), the coating of back faces, the data reduction (i.e. normal-point generation and noise clipping) procedure, the observation policy, etc.

# 3. Conclusions

A number of aspects should be taken into account for designing a future laser ranging target as well as for understanding the optical behavior of active onboard retroreflectors. The balance between the "observability", i.e., the intensity of retro-reflected signal, and the "precision," i.e., the time spread of retro-reflected signal, has to be carefully reviewed for existing and future missions.

## References

*Dell'Agnello, et al.*: Creation of the new industry-standard space test of laser retroreflectors for the GNSS and LAGEOS, Adv. Space Res., 47, 5, 822-842, 2011.

*Otsubo, T. and G. M. Appleby*: System-dependent Centre-of-mass Correction for Spherical Geodetic Satellites, Journal of Geophysical Research, 108, B4, 2201, doi:10.1029/2002JB002209, 2003.

*Sugimoto, N., A. Minato*: Optical characteristic of the retroreflector in space (RIS) for the ADEOS satellite, Optical Review, 3, 62-64, 1996.

*Vasiliev,V. P., V. D. Shargorodsky, N. N. Parkhomenko*: BLITS: The first autonomous zero-signature satellite in orbit, in these proceedings, 2011.

## Correspondence

Toshimichi Otsubo
Hitotsubashi University
2-1 Naka
Kunitachi
186-8601 Japan

t.otsubo@r.hit-u.ac.jp

# Design of LRA for Compass GEO and IGSO Satellites and Observations

*Chen Wanzhen, Yang Fumin, Zhang Zhongping, Wang Yuanming, Zhang Haifeng, ,Li Pu*

ABSTRACT

Geostationary orbit (GEO) and Inclined Geostationary orbit (IGSO) satellites are important parts in the Chinese regional satellite navigation system (COMPASS). All of those satellites will be equipped with LRA designed and manufactured by Shanghai Astronomical Observatory for calibrating the microwave, radio measuring techniques and precision orbital determination. This paper introduces the characteristics of LRA of Compass GEO and IGSO satellites and the method of inclined installing LRA for GEO satellites. The observation to GEO and IGSO satellites by the dedicated Compass SLR system with 1 meter aperture telescope are also presented.

## 1. Introduction

COMPASS is the Chinese regional satellite navigation system and the constellation will consist of 5 GEO, 3 IGSO and 4 MEO satellites. At last workshop, Yang Fumin reported the LRA on Compass MEO orbital satellites and the observations by using the 60 cm aperture SLR system in Changchun. This paper will introduce the characteristics of LRA on Compass GEO and IGSO satellites and the observations by the dedicated Compass SLR system with 1 meter aperture telescope. Considering Compass GEO satellites mainly serving for Chinese region, a method of inclined installing LRA was adopted for increasing LRA reflective area for Chinese SLR stations, with the normal direction of LRA pointing to the Chinese continent rather than the geocenter. The theoretical calculation and measuring results show that the method of inclined installing LRA is very effective.

## 2. Design and Performance of the LRA for Compass GEO and IGSO satellite

The orbital altitude of the Compass GEO and IGSO satellites is 36,000Km and compensation of the velocity aberration: 0.6 arc-seconds dihedral offsets with uncertainty of about 0.5 arc-seconds. Due to farther than Compass MEO, the design of LRA on GEO and IGSO satellites should be more efficient in order to get enough laser returns. For High Earth Orbital satellites, the critical angle of incoming laser beam to the corner cubes almost does not appear during the observation, so the all the surfaces of the corner cubes are without coating and each corner cube was in an independent chamber, fixed into the planar base made of aluminum alloy material. Figure 1 shows the view of LRA on the Compass GEO and IGSO satellites and its main parameters. The LRA of Compass GEO and IGSO satellites is the hexagon array to reduce the returned pulse spread and to achieve better ranging precision and the effective reflective area is about 770 cm2 that is two times than the one of Compass MEO.

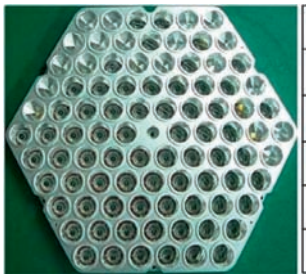

| | |
|---|---|
| Size | 49×43×3.0cm |
| Diameter of corner cube | 33mm |
| Number of corner cube | 90 |
| Reflective area | 770cm$^2$ |
| Dihedral offset | 0.6″ |
| Weight | 5.0 kg |

**Figure 1: The view of LRA of Compass GEO and IGSO and its main parameters**

For testing the optical performances of LRA, Shanghai Observatory imported the ZYGO interferometer and established special laboratory. Each corner cube of LRA must be carefully measured to insure the high quality before installed. Figure 2 shows the ZYGO interferometer and one of the measurements.

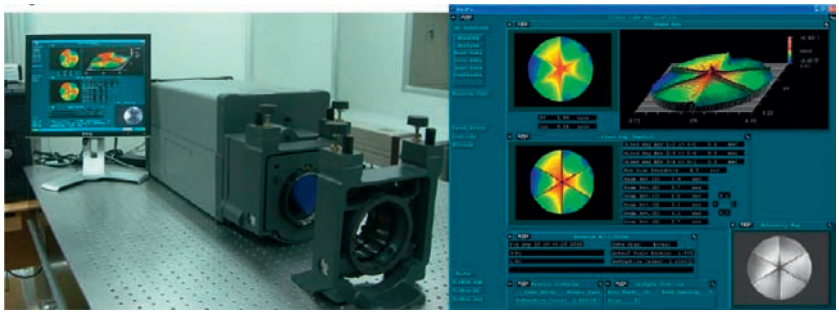

**Figure 2: Optical performance testing of LRA with ZYGO interferometer**

# 3. Calculation of the incidence angle of LRA inclined installed

In order to increase the effective reflective areas for Chinese region, the method of LRA inclined installed is adopted to make the normal direction of LRA pointing to the Chinese continent rather than the earth's center. Figure 3 shows the relative place of satellite (S), ground station (O) and the intersection of the normal of LRA and ground (C) in the geocentric coordinate system (E-XYZ) and the coordinates are ( $\alpha_S$,$\beta_S$), ($\alpha_O$,$\beta_O$ ), ($\alpha_C$,$\beta_C$ ) respectively.

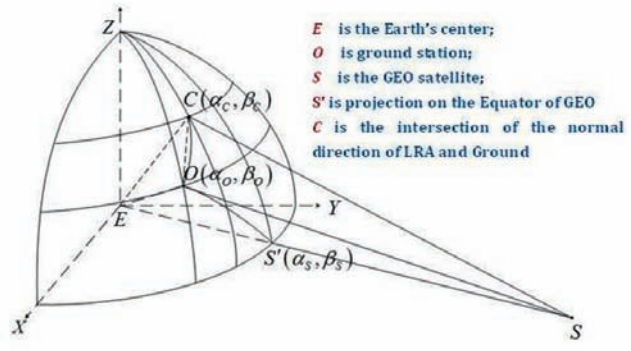


**Figure 3: Diagram of the relative place of satellite, ground station and the intersection of the normal of LRA and ground**

For the normal of LRA oriented to the Earth's center, the incidence angle (i) can be calculated by the following formula:

$$i = \arcsin\left(\frac{R_E}{R_{SO}}\sin\left(\arccos\left(\cos\beta_0\cos\left(\alpha_S-\alpha_O\right)\right)\right)\right)$$

$$R_{SO} = \sqrt{R_E^2+\left(R_E^2+h_S\right)^2-2R_E\left(R_E+h_S\right)\cos\left(\angle OES\right)}$$

Where, $R_E$ is the radius of the Earth, $R_{SO}$ is the slant distance from ground station to satellite, $h_S$ is the satellite height above sea level, ( $\alpha_O$,$\beta_O$ ) is the coordinates of ground station, ( $\alpha_S$,$\beta_S$ ) (for GEO satellite, $\beta_O = 0$ ) is the coordinates of the satellite.

If the normal of LRA of Compass GEO satellites points to the intersection C ($\alpha_C$, $\beta_C$), the incidence angle can be calculated by using formulas of spherical triangle:

$$i_C = \arccos\left(\left(R_{SC}^2 + R_{SO}^2 - l_{CO}^2\right)/2R_{SC}R_{SO}\right)$$

Where

$$R_{SC} = \sqrt{R_E^2 + \left(R_E^2 + h_S\right)^2 - 2R_E\left(R_E + h_S\right)\cos\left(\beta_C\right)\cos\left(\alpha_S - \alpha_C\right)}$$

$$R_{SO} = \sqrt{R_E^2 + \left(R_E^2 + h_S\right)^2 - 2R_E\left(R_E + h_S\right)\cos\left(\angle OES\right)}, \quad l_{CO} = 2R_E \sin\left(OC/2\right)$$

$\cos(OC) = \cos(90° - \beta_O)\cos(90° - \beta_C) + \sin(90° - \beta_O)\sin(90° - \beta_C)\cos(\alpha_C - \alpha_O)$

$= \sin\beta_O \sin\beta_C + \cos\beta_O \cos\beta_C \cos(\alpha_C - \alpha_O)$

Where, $i_C$ is the incidence angle between ground station (O) and the satellite (S), $R_{SC}$ is the slant distance from the intersection (C) to the satellite, $I_{CO}$ is the curve distance from station to the intersection (C).

Considering the Compass tracking network consisting of several independent SLR system on ground, so the geometrical center of several SLR stations on ground is chose as the normal of LRA directing to point (C). Based on the coordinates of the intersection and Compass GEO satellites, the inclined angle of LRA of all GEO satellites is less than 7 degree. Table 1 shows the increasing rate of effective area for different position GEO satellites and ground stations after the LRA of GEO satellites inclined installed. The effective areas are increased up to 20.56% at the maximum. Although the increasing rate is not very much for every satellite, it is considerable significant for ground stations.

**Table 1: The increasing rate of effective areas for different GEO satellites and stations**

| | GEO Satellite A | GEO Satellite B | GEO Satellite C |
|---|---|---|---|
| Ground Station 1 | 20.56% | 15.73% | 10.36% |
| Ground Station 2 | 13.37% | 7.07% | 1.50% |
| Ground Station 3 | 8.66% | 7.08% | 12.34% |

# 4. Observations

Up to now, there are several Compass GEO and IGSO satellites launched into different positions over the equator in last year and this year. The laser tracking for these satellites has been done at a new dedicated Compass SLR station located in Beijing since April 2009 and a great amount of laser tracking data were obtained. The parameters of the dedicated SLR system can be seen from another report in this workshop. Figure 4 shows two passes of measuring results (Compass GEO2 and IGSO3) by the dedicated SLR system. For GEO2 satellite, the average returns per minute are about 38.

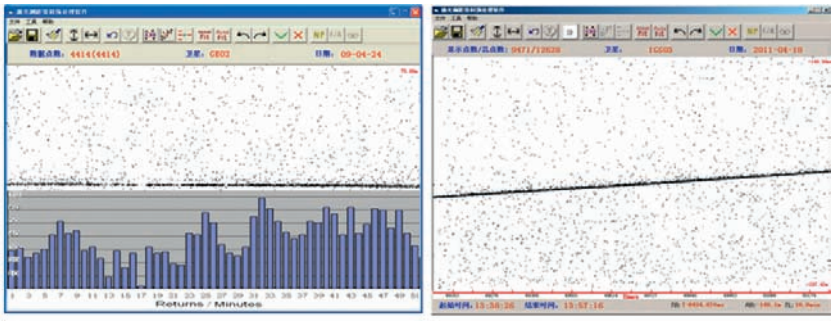


**Figure 4: Measuring results from GEO and IGSO satellites by dedicated SLR system**

Shanghai SLR station also tracked some passes of these satellites with the new kHz laser ranging system (1.5 mJ energy in 532nm, 15 ps pulse width, 1 kHz repetition). Figure 5 shows the measuring results of Compass GEO1 and IGSO1 by using Shanghai kHz SLR system. For GEO1 satellite, the average returns per minute are about 580.

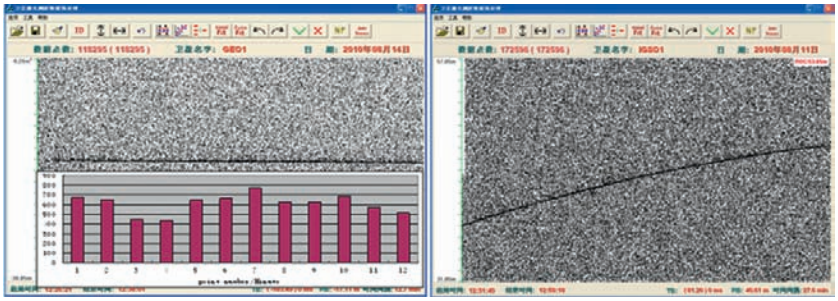

**Figure 5: Measuring results of GEO and IGSO1 satellites by Shanghai kHz SLR system**

# 5. Conclusion

Shanghai Observatory has accomplished 14 sets of LRA for Compass satellites and 8 satellites have been launched into the different orbit. A great amount of laser tracking data was obtained by using the Compass SLR system and the significant role was played in calibrating the microwave, radio measuring techniques and Compass satellite precise orbit determination. During the design of LRA for GEO satellites, the method of inclined installing LRA is adopted to make its normal direction point to the stations on ground, not to the Earth's center. This original way of installation makes the reflective area and returns increased effectively. Measuring results show that the performances of LRA on COMPASS satellites are well. The methods of design and manufacture of LRA on COMPASS satellites have successfully applied to other satellites.

## Reference

*Yang Fumin*, 2008: Laser Retro-reflector Arrays on the Compass Satellites, Proceedings of the 16th International Workshop on Laser Ranging

*Yang Fumin*, 2006: Design of Laser Retr-reflector Array and Laser ranging experiment for Shenzhou-4 satellite, Proceedings of the 15th International Workshop on Laser Ranging

## Correspondence

Zhang Zhongping
No.80, Nandan Road
Shanghai
China

zzp@shao.ac.cn

# ETRUSCO-2: an ASI-INFN Project of Development and SCF-Test of GNSS Retroreflector Arrays (GRA) for Galileo and GPS-3

*S. Dell'Agnello [1], G. O. Delle Monache [1], C. Cantone [1], R. Vittori[2], D. G. Currie[3], A. Boni [1], G. Patrizi [1], S. Berardi [1], M. Tibuzzi [1], C. Lops [1], M. Maiello [1], M. Garattini [1], N. Intaglietta [1], M. Martini [1], R. Tauraso [4], F. Vivio [4], D. A. Arnold [5], M. R. Pearlman [5], G. Bianco [6], S. Zerbini [7], J. F. McGarry [8], C. Sciarretta [6], V. Luceri [6], T. W. Zagwodzki [8]*

ABSTRACT

The SCF-Test [1] is a new test procedure to characterize and model the detailed thermal behavior and optical performance of cube corner laser retroreflectors for the GNSS in laboratory-simulated space conditions, developed by INFN-LNF and in use by NASA, ESA and ASI. Under ASI-INFN Contract n. I/077/09/0 ETRUSCO-2 (Extra Terrestrial Ranging to Unified Satellite COnstellations-2) we are building a new experimental apparatus (our second), the "Satellite laser ranging (SLR) Characterization Facility optimized for Galileo and the GPS-3" (SCF-G) to characterize and model the detailed thermal behaviour and the optical performance of cube corner GNSS Retroreflector Arrays (GRAs). Galileo is Europe's flagship programme for GNSS (Global Navigation Satellite System). For the GPS-3, a collaborative effort with the US GNSS community is in preparation. ETRUSCO-2 goals will be achieved using the innovative test procedure described in [1], the SCF-Test, and its evolution and refinement outlined here, the SCF-Test/Revision-ETRUSCO-2. We are also developing an innovative prototype GRA of Hollow retroreflectors (GRA-H). Depending on the outcome of the GRA-H SCF-Test, a full-size GRA will be built using either the hollow or the solid fused silica technology.

Preliminary results of an integrated thermal and optical modelling of an uncoated retroreflector on a GNSS orbit, tuned to SCF-Test data of a selection of specific uncoated reflectors (LAGEOS and Galileo In-Orbit Validation, IOV), will be presented. Structural modelling of a specific hollow retroreflector provided by GSFC, tuned to its SCF-Test data, will also be reported. SCF-Testing, under a non-disclosure agreement (NDA) between INFN-LNF and ESA, of a prototype uncoated cube deployed on the 4 Galileo IOV satellites, is a major step forward and a successful application of the SCF. In fact, the IOVs are the first 4 of the 30 satellites of the Full Orbit Capability (FOC) Galileo constellation. Late breaking news: on August 30, 2011, ESA has authorized INFN-LNF to publish the results of the IOV prototype SCF-Test carried out in 2010.

## 1. The ETRUSCO-2 project

This project is the continuation of an INFN R&D experiment, ETRUSCO (Terrestrial Ranging to Unified Satellite COnstellations) carried out in 2006-2010, which concluded with a comprehensive, refereed publication [1], where the SCF-Test is fully described and the main experimental results are reported. The ILRS reference payload standard, LAGEOS, has also been SCF-Tested for the first time ever [2], using the LAGEOS "Sector" engineering model provided by NASA. While ETRUSCO-2 is a co-funded ASI-INFN project, the SCF-Test is background intellectual property of INFN.

INFN-LNF has built a new clean room, class ISO 7 or better, of 85 $m^2$, now operational, for the existing SCF (Satellite/lunar laser ranging Characterization Facility). Based on the experience made with the SCF, the SCF-G is being developed and will be operated in 2012 in the same clean room infrastructure. Additional, separate laboratory space is also in use. The SCF is being further optimized for Lunar Laser Ranging (LLR) [3] and for (inter)planetary applications with another dedicated INFN R&D experiment, MoonLIGHT-ILN (Moon Laser Instrumentation for General relativity High-accuracy

[1] Laboratori Nazionali di Frascati (LNF) dell'INFN, Frascati (Rome), Italy
[2] Aeronautica Militare Italiana (AMI) and Agenzia Spaziale Italiana (ASI), Rome, Italy
[3] University of Maryland (UMD), College Park, MD, USA,
[4] University of Rome "Tor Vergata" and INFN-LNF, Rome, Italy
[5] Harvard-Smithsonian Center for Astrophysics (CfA), Cambridge, MA, USA
[6] ASI, Centro di Geodesia Spaziale "G. Colombo" (ASI-CGS), Matera, Italy
[7] University of Bologna, Bologna, Italy
[8] NASA, Goddard Space Flight Center (GSCF), Greenbelt, MD, USA

Tests for the 'International Lunar Network' concept developed for a lunar geophysical network; see also http://iln.arc.nasa.gov/). The primary goal of these doubled and extended retroreflector metrology capabilities is to provide critical diagnostic, optimization and validation tools for SLR to all flagship GNSS programmes (not only Galileo and GPS-3) and for LLR. The capability will allow us to optimize GRA designs to maximize ranging efficiency, to improve signal-to-noise conditions in daylight, to provide pre-launch validation of retroreflector performance under accurately laboratory-simulated space conditions and/or characterize 'as-built' payloads. Implementation of optimized GRA designs will help to improve GNSS orbits, which will then increase the accuracy, stability, and distribution of the International Terrestrial Reference Frame (ITRF), to provide better definition of the geocenter (ITRF origin) and the scale (ITRF unit of length).

## 1.1 SCF-Test/Revision-ETRUSCO-2 and thermal-optical modelling

This test evolution inherits from the old one the SLR/LLR Key Performance Indicators (KPIs): (1) the thermal relaxation time of reflectors ($\tau_{CCR}$) and array mounting elements; (2) the reflector optical the Far Field Diffraction Pattern (FFDP), with Orthogonal Laser Polarizations (OLP) important for single, uncoated solid CCRs. The novel KPIs are: (3) the thermal-optical conditions experienced by reflectors during a GNSS Critical half-Orbit (GCO, see Fig. 1); (4) the reflector Wavefront Interferogram (WI) in space conditions. Optionally, we provide software modelling of the test data for KPIs 1) to 4), as shown below. The GCO test has been developed with ETRUSCO, WI for GNSS with ETRUSCO-2. The GCO is the orbit with the nodal line parallel to the Sun-Earth joining line. Orbit conditions are reproduced in laboratory rotating the GRA inside the cryostat, in quasi-real time, for the proper GCO duration: 7 hrs for Galileo, 6 hrs for GPS. Initially, the GRA and its reflectors are parallel to the solar simulator (SS) beam; then the GRA is gradually rotated experiencing sunrise, eclipse (simulated by obscuring temporarily the SS) and sunset. At the end of the GCO the GRA is reversed by 180 degrees. During the GCO, the GRA is periodically rotated towards the optical and infrared windows of the cryostat to take temperature and optical measurements of the reflectors, and rotated back to its progressing GCO orientation, all in a few seconds. This quick measurement rotation has a negligible influence on the thermal and optical behaviour of the GRA along the GCO. The GCO test has been successfully applied to a prototype Galileo IOV reflector, which INFN-LNF was provided with by ESA. These preliminary results can be published soon, since ESA has given INFN-LNF the necessary authorization on August 30, 2011.

Here we report a preliminary thermal and optical modelling of an uncoated retroreflector on a GCO tuned to SCF-Test data of a selection of specific uncoated reflectors types (LAGEOS and IOV protyotypes). The reflector has 33 mm diameter, Dihedral Angle Offsets (DAOs) = 0.0 arcsec, mounting scheme taken from LAGEOS (which is different from Galileo IOV). The simulated temperature field inside the reflector and its time evolution (carried out with in-house and Thermal Desktop software by C&R Technologies) are the input to the optical simulation (CodeV by ORA Inc.), where the dependency of the refractive index from the temperature inside the fused silica is taken into account. The laser polarization is in the GCO plane, which in the IOV SCF-Test is horizontal. One physical edge of the cube corner is also oriented along the GCO plane (horizontal in the IOV SCF-Test) so that during sunrise in Fig. 1 and 2 there is no loss of total internal reflection (optical breakthrough), which occurs during sunset instead. Figure 2 shows the variation of FFDP average intensity at 24 μrad. During sunrise, sunrays heat up the reflector and the temperature difference between reflector tip inside the cavity (which is warmer) and the outer face increases thus reducing the FFDP intensity. When the reflector goes in the Earth shadow there is a sudden cooling of the outer face, which again involves FFDP intensity reduction (apparent discontinuities at entrance/exit of the shadow are an artifact due to lack of modelling of earth penumbra). Later on the temperature difference decreases and intensity goes up. At sunset, due to optical breakthrough, sunrays heat directly the cavity and consequently the retroreflector tip, thus reducing the FFDP intensity. Heating and cooling is convoluted with the (relatively) long LAGEOS-like $\tau_{CCR}$(modelled after the SCF-Test of the LAGEOS Sector), which damps and delays in time thermal degradations.

# 2 Modelling the world-first SCF-Test of a Hollow reflector

The new GRA-H, made of 7 hollow cubes, one in the center and six in circle around it, has been built in 2011 and is now under test at the SCF. Depending on the behaviour of the GRA-H, a full-size GRA will be built with hollow or solid reflector technology. This GRA will be characterized with the SCF-G using the SCF-Test/Revision-ETRUSCO-2 described in the previous section. A major hollow reflector development that could benefit from an SCF-Test is reported in [4].

With ETRUSCO a hollow reflector prototype by NASA-GSFC has been tested in 2010 and result reported in [2]. Comparisons between these test measurements and thermo-structural simulations are reported in [5] and here. The GSFC hollow reflector is made by three Al-coated mirrors on pyrex substrates glued together; one of which is also glued to a holding structure (foot).

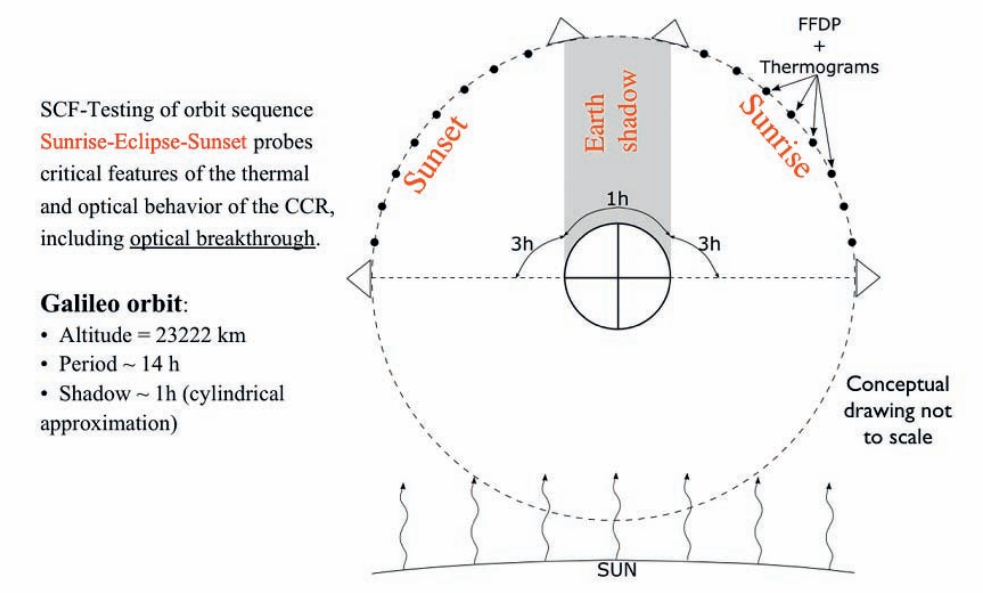


**Figure 1: Conceptual drawing of the SCF-Test/Revision-ETRUSCO-2 and the GNSS Critical half-Orbit (GCO).**

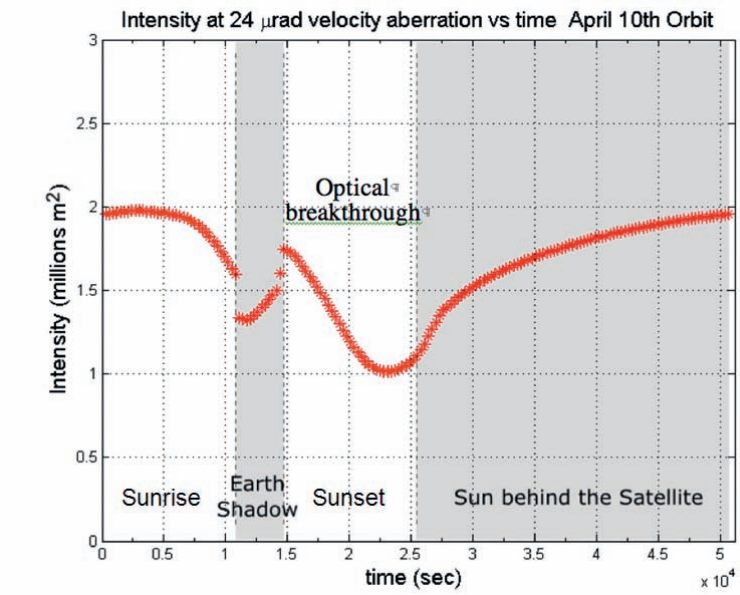


**Figure 2: Thermal-optical modelling for the SCF-Test/Revision-ET-2 (preliminary): variation of the CCR average FFDP intensity at 24 μrad (velocity aberration for GNSS like satellites) along the GNSS Critical half-Orbit (GCO).**

The reflector has been screwed inside an Al cavity, which is thermally controlled. One thermal probe was fixed in the center of every mirror substrate: the two substrates not connected to the foot showed almost coincident thermal behaviour. In the part of measurements reported here the reflector was irradiated by the SS for > 1.5 hr with a short sun-off interval of 2 min. Thermal simulations aim to find the best suitable values for thermal conduction among the mirrors through the glue and between the reflector and the cavity through the holding structure. When simulation

results match satisfactorily measured temperatures, the temperature field (time dependent) becomes the input for structural simulation. Structural deformation data are post-processed to evaluate the parameters affecting the optical performance i.e. deviation from nominal mirror flatness, and nominal DAOs = (0.0 ± 0.5)". At the beginning of Fig. 3, our simulation indicates that DAOs are beyond these limits and the measured FFDP, inset on the left, looks different from nominal; at the end DAOs are inside limits and measured FFDP, inset on the right, can be considered satisfactory, since it is close to the expected shape (an Airy pattern).

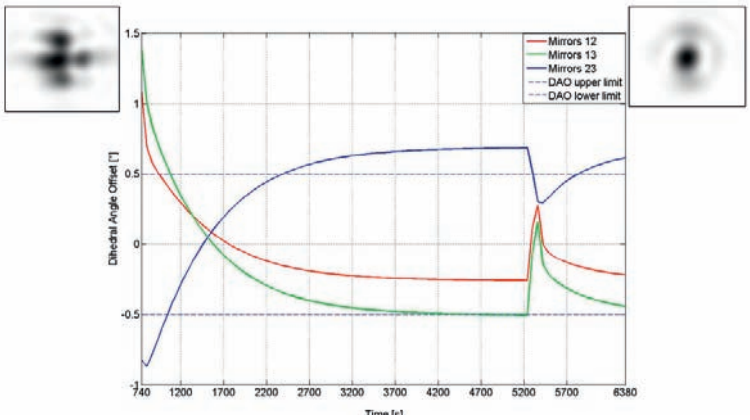


**Figure 3: Modelling of the variation of DAOs between the mirrors. Dashed lines define specification limits. The plots at the top left and right of the main graph are the two FFDPs at the beginning and at the end of time span.**

## References


[1] *Dell'Agnello, S., et al,* 2011: Creation of the new industry-standard space test of laser retroreflectors for the GNSS and LAGEOS, Adv. in Space Res. 47 (2011), 822-842.

[2] *Boni, A., et al,* 2011: World-first SCF-Test of the NASA-GSFC LAGEOS Sector and Hollow Retroreflector, 17th International Workshop on Laser Ranging, Bad Kötzting, Germany, May 16 - 20, 2011.

[3] *D. Currie, S. Dell'Agnello, G. Delle Monache*, A Lunar Laser Ranging Retroreflector Array for the 21st Century, Acta Astron. 68 (2011) 667–680.

[4] *Neubert et al,* 2011: Single Open Reflector for MEO/GNSS Type Satellites. A Status Report, 17th International Workshop on Laser Ranging, Bad Kötzting, Germany, May 16 - 20, 2011.

[5] *Cantone, C., et al*, 2010: Structural analysis and preliminary space characterization of a prototype hollow laser retroreflector,. 61st International Astronautical Congress, Prague, Czech Republic, 27 September - 1 October, 2010.


## Correspondence


Claudio Cantone
INFN-LNF
claudio.cantone@lnf.infn.it,

# World first SCF-Test of the NASA-GSFC LAGEOS Sector and Hollow Retroreflector

*A. Boni[5], S. Berardi[1], M. Maiello[1], M. Garattini[1], S. Dell'Agnello[1], G. O. Delle Monache[1], C. Lops[1], C. Cantone[1], N. Intaglietta[1],G. Patrizi[1], J. F. McGarry[2], M. R. Pearlman[3],G. Bianco[4], D. A. Arnold[3], T. W. Zagwodzki[2], M. Ruggieri[6]*

ABSTRACT

With the INFN experiment "ETRUSCO (Extra Terrestrial Ranging to Unified Satellite COnstellations)" we used the "Satellite/lunar laser ranging Characterization Facility" (SCF) [3] located at INFN-LNF in Frascati, Italy, to characterise and model the detailed thermal behavior and the optical performance ("SCF-Test")of LAGEOS [1] and of a prototype hollow cube corner retroreflector. Our key experimental innovation is the concurrent measurement and modeling of the optical far field diffraction pattern (FFDP) and the temperature distribution of the retroreflector payload under thermal conditions produced with a close-match solar simulator. These unique capabilities provide experimental validation of the space segment for Satellite and lunar laser ranging (SLR/LLR). Uncoated retroreflector with properly insulated mounting can minimize thermal degradation and significantly increase the optical performance, and as such, are emerging as the recommended design for modern GNSS[2] satellites. We report some results of an extensive, first-ever SCF-Test program performed on a LAGEOS engineering model retroreflector array provided by NASA (the "LAGEOS Sector"), which showed a good performance. The LAGEOS sector measurements demonstrated the effectiveness of the SCF-Test as an SLR/LLR diagnostic, optimization and validation tool in use by NASA, ESA and ASI. We also report the first-ever SCF-Test of a prototype hollow retroreflector provided by NASA, which showed an acceptable performance in the limited tested temperature range. These unprecedented results are the starting point for the development and validation of compact and (potentially) lightweight arrays of hollow laser retroreflectors with the size and the optical specifications to be selectively chosen depending on the specific space mission (that is satellite velocity aberration).

## 1. Introduction

An improvement of positioning accuracy, stability and precision with respect to the ITRF[3] of modern GNSS constellations is highly recommended by ILRS in order to strengthen determination and stability of the ITRF [1].Space and ground colocation of SLR and MW techniques would make possible to align a GNSS reference frame to the ITRF, whose origin and scale are mostly determined with the SLR technique. In order to achieve these results, Laser Retroreflector Arrays (LRAs) deployed on these satellites, should guarantee an adequate level of effective cross section coming back at the stations, as defined by ILRS [1,2].Hence LRAs performance must be improved. The INFN, with experiment ETRUSCO (Extra Terrestrial Ranging to Unified Satellite COnstellation), started to build, in 2005 a facility (SCF) and developed a standard test (SCF-Test) in order to characterize and validate the optical performance of GNSS LRAs, with particular attention on Galileo [3]. During the years we tested prototypes and flight models of first generation retroreflectors (coated) and LRAs for GNSS [3]. Those types of retroreflectors, both from actual SLR measurements and our SCF tests, proved to have problems that cause a low return rate to SLR stations and signal strength drop in certain parts of the orbit. New generation GNSS constellations are moving to uncoated retroreflectors, which with a proper mounting design can minimize thermal degradation of optical performance. Uncoated reflectors are deployed on one of the standard SLR target: the LAGEOS satellite. So in order to show a calibration of our SCF-Test, we tested in 2009 an engineering model of the LAGEOS satellite, lent by NASA-GSFC. In section 2 we report the results of these tests. Looking further in the future, new retroreflector designs are under study for SLR or LLR application, which consider the use of hollow re-

[1] Laboratori Nazionali di Frascati (LNF) dell'INFN, Frascati (Rome), Italy
[2] NASA, Goddard Space Flight Center (GSFC), Greenbelt, MD, USA
[3] Harvard-Smithsonian Center for Astrophysics (CfA), Cambridge, MA, USA
[4] ASI Centro di Geodesia Spaziale (CGS), Matera, Italy
[5] University of Rome "Tor Vergata" and INFN-LNF, Rome, Italy
[6] University of Rome "Tor Vergata", Italy

[1] Laser Geodynamic Satellite
[2] Global Navigation Satellite System
[3] International Terrestrial Reference Frame

troreflectors. Again in collaboration with NASA-GSFC, in 2010, we received a prototype of an hollow retroreflector to be tested in a realistic space environment. In section 3 we report tests performed on this prototype. This last test was part of a research activity of the Work Package 5200 of the 3 year study (June 2007, May 2010) of ASI on "Cosmology and Fundamental Physics" (COFIS).

# 2. SCF-Test of the LAGEOS engineering model

The LAGEOS engineering model, LAGEOS Sector, is an aluminum spherical sector of the whole satellite which includes the CCR [4] on the pole and three successive rings, 37 CCRs in total (as in Fig. 1).

**Figure 1: LAGEOS Sector inside the SCF on the positioning system**

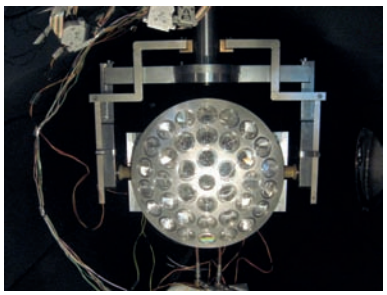

Prior to the beginning of the SCF-Test we deeply optically tested all of the CCRs in air and at room temperature. FFDP were taken in three different orientations of the CCRs (each physical edge vertical). A first analysis is presented in [4]. After this analysis, we implemented a refined one in order to overcome some of the weaknesses of the former one. The attempt to find characteristic structures from the FFDP, made the analysis subject to the particular settings of the measurements (orientations of CCRs with respect to polarization vector). We'll show some of the results obtained with such an analysis on FFDP tests performed in air, at $\lambda = 532$nm on the Sector. What we did was,first, derive average intensity plots from both measured and simulated FFDPs. Measurements plotted came from each CCR orientation; simulations plotted were those with on spec DAOs (1.25" on the three edges) and the extremes of the ±0.5" error band. Fig. 2 shows the results.

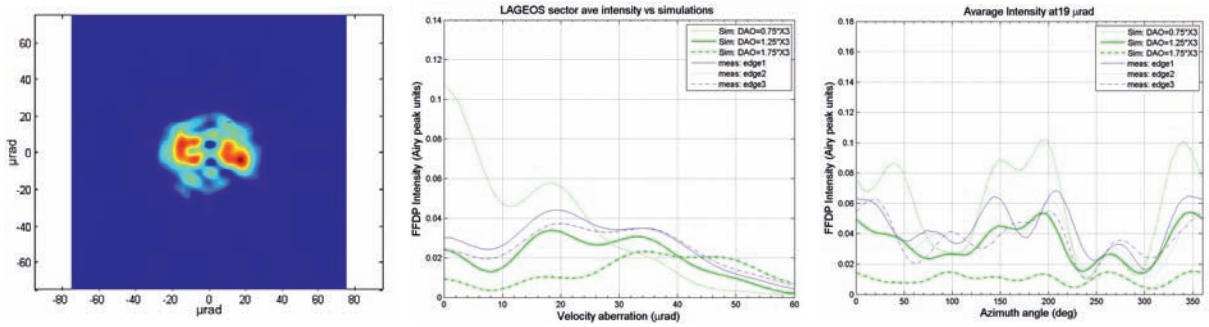


**Figure 2: Left: edge 1 FFDPs . Center: average intensity vs distance from FFDP center. Right: Intensity along a circle at 19 μrad. Comparison between simulated patterns (CODEV) and measured patterns. Measured intensity has ±25% relative error not shown**

The one above is a CCR with DAOs close to its specifications, as the measured average intensity is close to the bold green line. The average intensity gives however just part of the information we can extract from these measurements. After we analyzed the intensity fluctuations at a certain velocity aberration, to see how the intensity level changes along that ring (one never knows were the station will be in the FFDP domain). For now we identified positions of peaks in simulated average intensity plots and checked the intensity fluctuations there. Again, we compared measurements with simulations. Fig. 2 is the result at 19 μrad. Measurements, as expected, cannot respect exactly the symmetry of the simulations, so do their peaks, but, within errors, we can arrive at the same conclusions given for the average intensity.

[4] Corner Cube Retroreflector

For the SCF-Test we installed the Sector inside the SCF on the rotation+tilt positioning system, controlled in temperature by an interface copper plate. Temperature sensors recorded its temperature, while an IR (InfraRed) camera measured CCRs' front face temperatures. Measurements were performed in several conditions:

- With the Sector held at 300K we placed the polar CCR inside its housing with two different torque screws of the aluminum retainer rings: 0.135 Nm (LAGEOS nominal value) and 0.2 Nm.
- With a screw torque of the polar CCR, as defined above, set at 0.2 Nm we maintained the Sector at three different temperatures: 280K, 300K and 320K.

Concurrent optical and thermal measurements were performed only on the polar CCR, while full thermal analysis has been performed also on the first and second CCR rings of the Sector.

As described in [3] the SCF-Test consists of a first phase in which prototypes, reached a stationary state, are heated under the Sun Simulator beam and then cooled down. From the thermal analysis point of view, the output is the thermal relaxation time, $\tau_{CCR}$, of the CCR, based on IR measurements of the variation of the CCR's front face temperature. $\tau_{CCR}$ is taken from the following formula:

$$T_1 = T_0 \pm \Delta T \, (1 - \exp(t / \tau))$$

In Fig. 3 is shown a typical plot of the front face temperature variation and the results of the analysis for the case in which we changed the Sector's temperature. Actual values of the relaxation times will be subject of a future publication, but at this stage we can observe few outcomes from these measurements. The right plot in Fig. 3 shows the average relaxation times, between heating and cooling phases, of each of the thermally analyzed CCRs. The first important outcome of the measurements is that $\tau_{CCR}$ decreases as the temperature of the aluminum increases. The ratio between the average values of all the relaxation times, at each temperature, is close to the following: $\tau_{T1}/\tau_{T2} \approx (T_2/T_2)^3$.

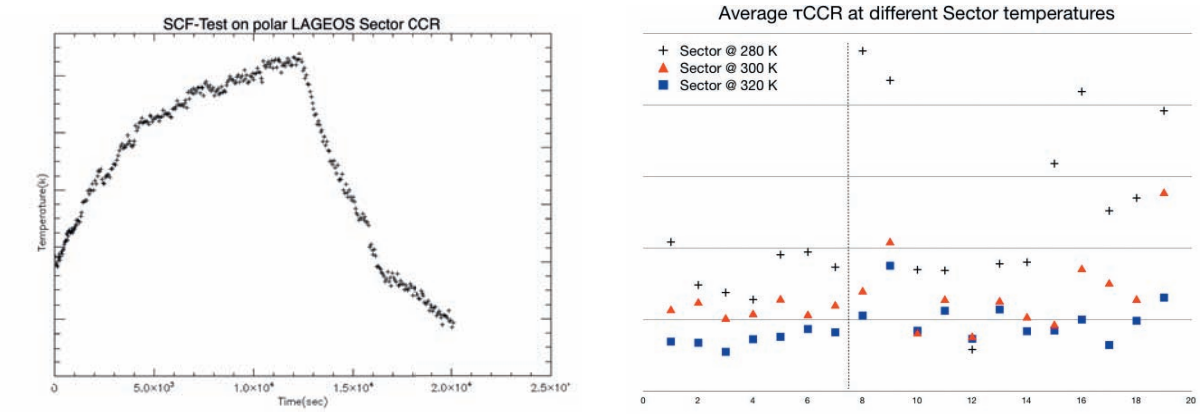


This behaviour is clearer for the first seven CCR in the plot (the polar one and the first ring) than for the rest; this could be due to two reasons: effect of the breakthrough on CCRs or difficulty of the IR camera to focus properly the CCRs of the second ring.

**Figure 3: Left: SCF-Test performed on polar CCR with Sector held at 300K. Right: average $\tau_{CCR}$ for all of the CCR at various Sector temperatures.**

Concurrent FFDP measurements were performed during the test, in order to check the variation of the intensity at a defined velocity aberration. We analyzed the variation of the intensity at 35 μrad (~ the velocity aberration of LAGEOS). Fig. 4 shows the outcome of the measurements for case 1 and 2. An increase in the screw torque from the nominal value decreases the intensity of the FFDP, after the CCR is illuminated by the Solar Simulator (SUN OFF phase). An increase in the temperature of the aluminum decreases the intensity of the FFDP in the SUN OFF phase.

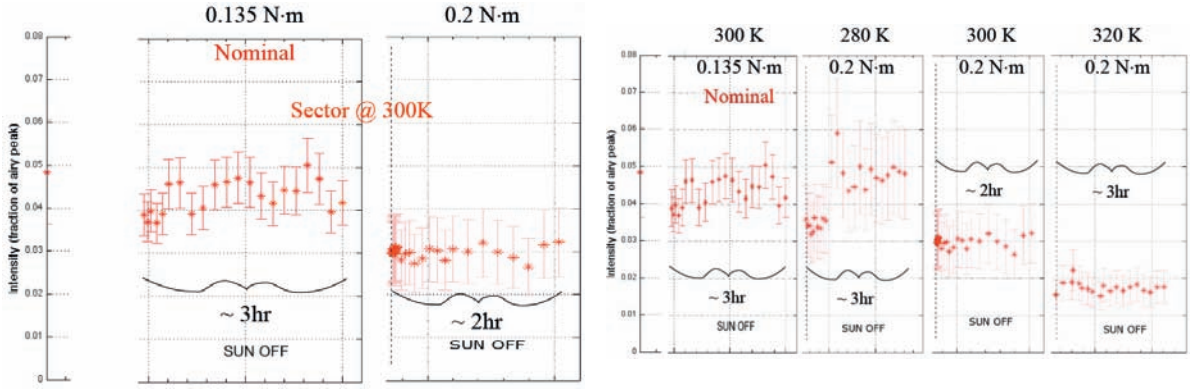


**Figure 4: Effect of polar CCR screw torque (left) and on Aluminum temperature (right) on FFDP intensity after SUN ON phase. Relative error is ±10%**

# 3. SCF-Test of the Hollow retroreflector prototype

The Hollow corner cube we tested at the SCF is a prototype made by three pyrex faces, with a metallic reflecting surface coating of optical quality. Joints between the surfaces are made with stycast glue for space applications. The whole unit is supported, at the bottom, by an Invar foot, screwed to just one of the faces. Fig. 5 shows the CCR.

**Figure 5: NASA-GSFC Hollow retroreflector tested at INFN-LNF**

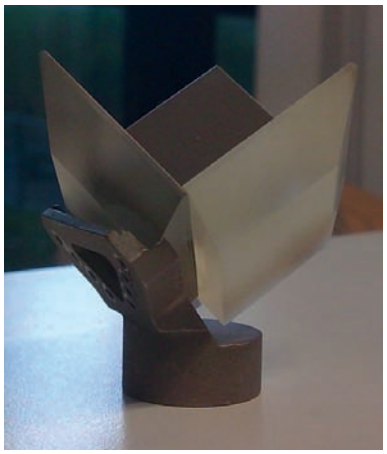

The CCR was held inside the SCF with an aluminum housing, with the Invar foot in thermal contact with the aluminum. The housing was built in order to simulate the presence of other CCRs around the one under test. With respect to the cryostat the CCR was positioned with one physical edge (the one opposite to the face linked with the Invar foot) horizontal. Three Platinum RTD probes measured the temperature of each of the three reflecting surface, giving us only the information of the overall temperature of the reflecting surfaces, not gradients throughout them. The housing was controlled in temperature at 300K with a Peltier cell on the back of aluminum base. The Solar Simulator illuminated the CCR orthogonally.

The procedure used for its test was the same, described earlier in this paper, for the LAGEOS Sector test, and the variation of faces' temperatures is the one in Fig. 6. As we can see from this figure the SCF-Test started in a condition in which the three reflecting faces were not at the same temperature, as at the beginning in air; the one in contact with the Invar foot ("left face") was at an higher temperature. This face also experienced, during the whole test, a temperature variation smaller than the other two.

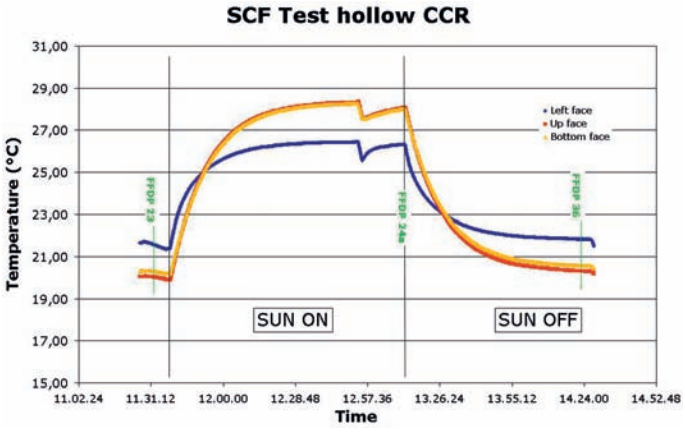


| | $\tau_{heating}$ (sec) | $\tau_{cooling}$ (sec) |
|---|---|---|
| left face | 617 | 671 |
| up face | 871 | 879 |
| bottom face | 889 | 897 |

**Figure 6: Left: SCF-Test of the hollow CCR. Right: Table 1: Thermal relaxation times of the three hollow retroreflector's faces for heating (SUN ON) and cooling (SUN OFF) phases. $\sigma(\tau)$= 80s**

This behaviour is caused by the thermal contact we induced between the Invar foot and the aluminum housing. Analyzing these data we came out with the thermal relaxation times of Tab. 1. The effect of the thermal link is clear also looking at $\tau_{CCR}$ values. The "left face" has a smaller relaxation time than the other two. The other two faces have the same relaxation time. Between the heating and cooling phase we can say that, considering the quoted errors on $\tau$, relaxation times are equal.

To analyze the optical performance we took first an FFDP in air at room temperature, which was our reference, then another FFDP prior to the beginning of the SCF-Test; passed the SUN ON phase with no measurements, we took a series of patterns during the SUN OFF phase at increasing time intervals. Results are in Fig. 7. The temperature difference between the faces of the CCR, at the beginning of the SCF-Test, influenced the intensity of the FFDP. The FFDP in air had a peak intensity of 1.00 which dropped to 0.31 at the beginning of the SCF-Test. During the SUN ON phase the FFDP almost recovered its "in air" shape, hence the intensity of the peak increased almost twice. The relaxation during the SUN OFF made the intensity come back to its first value (beginning of SCF-Test).

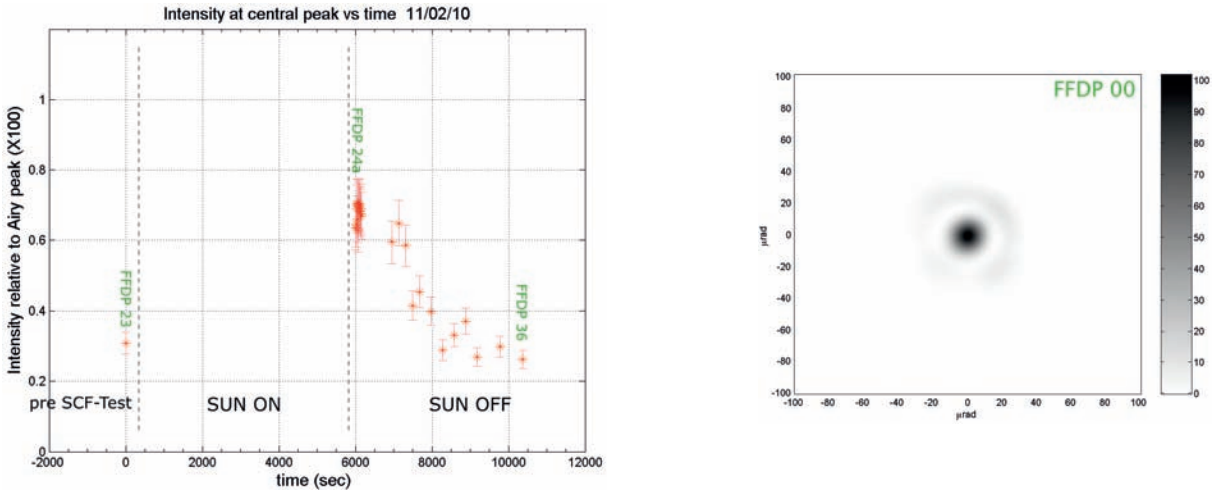


**Figure 7: Intensity variation of FFDP at the central peak during the SCF-Test(left). FFDP in air-room temp (right)**

# 4. Conclusions

The SCF has proven to be the right facility for the first-ever test of LAGEOS and hollow CCRs in an accurate laboratory-simulated space environment. The fruitful collaboration with NASA-GSFC, CfA and ASI-CGS is one of our best achievements. LAGEOS SCF-Test has shown the good space performance of what is now the reference ILRS payload standard. This paper extends the LAGEOS results reported in [3]. In particular the SCF-Test showed that:1) increasing the retroreflector mount conductance, by increasing the screw torque, with respect to nominal, degrades the FFDP intensity , 2) increasing temperature of the satellite degrades the FFDP intensity affecting the retroreflector thermal behaviour. A future publication will report the full FFDP analysis of the whole dataset of the LAGEOS measurement campaign. We demonstrated the hollow CCR prototype performance in our laboratory-simulated space conditions in a limited temperature range near 300K. We found an effect of the mounting foot arrangement on the performance of the CCR. Moreover we measured a significantly shorter hating/cooling retroreflector relaxation time, compared to LAGEOS.

## References

1. http://lrs.gsfc.nasa.gov/docs/retroreflector_specification_070416.pdf

2. *Pearlman, M.R.*, International Technical Laser Workshop on SLR Tracking of GNSS Constellations, Metsovo, Greece, 2009: Technological challenges of SLR tracking of GNSS constellations

3. *Dell'Agnello S., et al.*, Creation of the new industry-standard space test of laser retroreflectors for the GNSS and LAGEOS, Adv. in Space Res., 47 (2011), 822-842

4. *Boni A., et al.*, Optical Far Field Diffraction Pattern test of laser retroreflectors for space applications in air and isothermal conditions at INFN-LNF, INFN-LNF Report LNF-08/26(IR), 2008.

## Correspondance

Alessandro Boni
alessandro.boni@lnf.infn.it

# Single Open Reflector for MEO/GNSS type Satellites. A Status Report

*Reinhart Neubert[1], Ludwig Grunwaldt[1], Christian Schopf[2], Engelbert Hofbauer[2], Jost Munder[3], Mark Herding[3]*

ABSTRACT

The status of a project to design, manufacture and test a single open reflector breadboard model is reported. The main advantage of this concept is the absence of any spreading of the return pulses. The practical realization places high challenges on mechanical/thermal design, material selection and manufacturing accuracy. A critical analysis based on numerical calculations and performance simulations is presented.

## 1. Requirements for a GNSS Reflector

The laser reflectors of existing navigation satellites are of the flat array type equipped with a large number of solid cube corner prisms. This design is possible because the angle of incidence in the case of high satellites is always small. It is obvious that a single cube corner would be advantageous in this situation because it avoids the pulse spreading of the large array. To achieve a sufficient return signal, the reflector should have an active area of at least 15 cm in diameter as we show in the following. Unfortunately, existing optical materials like fused quartz are not suitable because of too large thermal distortions under sun illumination. This is the main reason for the present use of small cube corners (4 cm diam. or less). For an open reflector, materials of higher thermal stability are available. Therefore, we proposed its use for a GALILEO-reflector [1]. Another important design requirement is due to the velocity aberration. The laser station is not in the center of the far field of the returned beam, but shifted by 21...25 µrad. The most efficient solution would be a two-spot far field as used in the case of the CHAMP reflector for instance. In the case of satellites like GALILEO with no fixed orientation relative to the velocity vector this would require to mount the reflector self-orienting. If we want a completely passive device, the only solution is an annular far field.

## 2. Optical Design

The aberration angle depends on the relative velocity between the station and the satellite. Following an idea of Otsubo[2], we got the distribution of aberration angles by a simulation process assuming a circular orbit for the GALILEO satellite and the station fixed on the rotating Earth. The distribution depends on the latitude of the station. Fig. 1 shows examples for an equatorial station and a station with 45° latitude as well as a cumulating distribution for stations between 0° and 60°. As can be seen, the aberration varies between 21 µrad and 25 µrad with a maximum probability at 23 µrad. In an alternative representation, Fig. 2 shows the components of the aberration vector in a coordinate system compliant with far field diffraction patterns (cf. legend of Fig. 2).

[1] GFZ Potsdam

[2] Fachhochschule Deggendorf

[3] SpaceTech GmbH Immenstaad

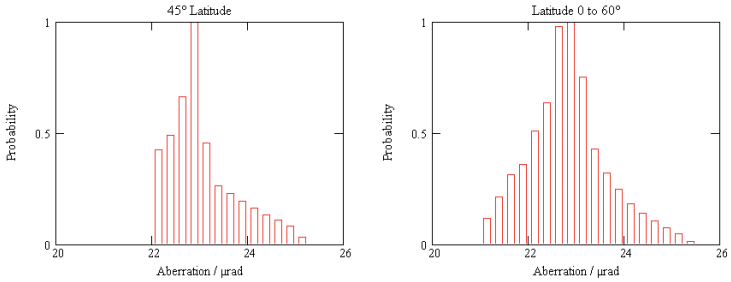


**Fig. 1: Distribution of the velocity aberration for a station at 45° latitude (left) and the cumulative distribution for stations between 0° and 60° latitude.**

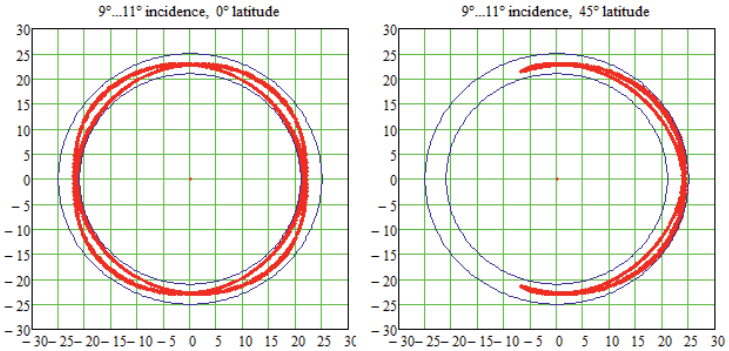


**Fig. 2: Representation of the aberration vector in asystem compliant with far field diffraction patterns.Horizontal axis orthogonal and vertical axis parallel to the plane of incidence (formed by the Nadir direction and the light beam direction)**

The proposed reflector has an active aperture of about 20 cm (ref. [1] and Fig. 3). The required annular far field pattern is produced by 3 equal dihedral offset angles (2", smaller than 90°) and an additional conical shape of the 3 mirrors according to the equation:

$$h(x,y) = \frac{\delta}{2} \cdot \left( \sqrt{x^2 + y^2} - x - y \right) \qquad , \qquad \delta = 0.97 \cdot 10^{-5} \cong 2''$$

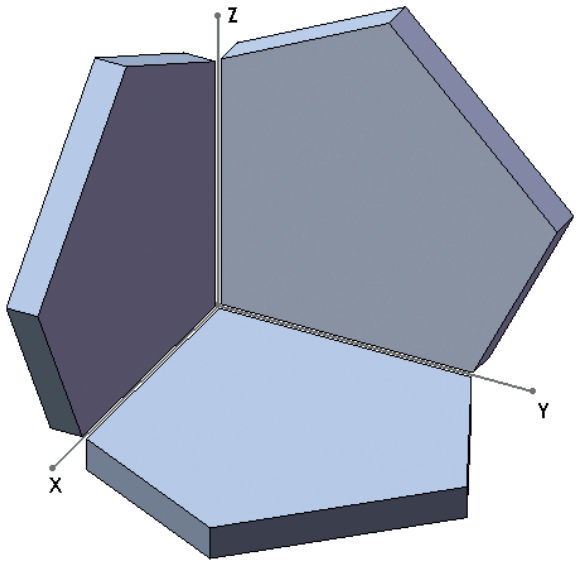


**Fig.3: Schematic drawing of the reflector**

The wave front of such a configuration has the shape of a circular crater producing an annular far field. To calculate the wave front matrix we are using a ray tracing model regarding first the reflector as orthogonal and then adding the optical path differences caused by the offset angles on surface shape. From this wave front matrix the far field is obtained by a discrete Fourier transform. This model agrees well with the results of a CODE-V as well as an earlier ASAP model [1]. In Fig. 4, the far fields for two special orientations are shown. It can be seen that the far field has 6 maxima in the case of normal incidence. In Ref. [1] it has been shown that a uniform annulus can be obtained using a circular active aperture and slightly elliptic mirror surfaces. This could not be achieved using the full hexagonal active aperture. However, for non-zero incli-

nation the far field intensity always depends on the azimuth. The diagrams right to the far fields in Fig. 4 give an idea of the achievable effective cross section of the reflector. It varies between about 200 and 500 million square meters. This is about 2 times higher than the cross section of a standard prism array with 60 cube corners.

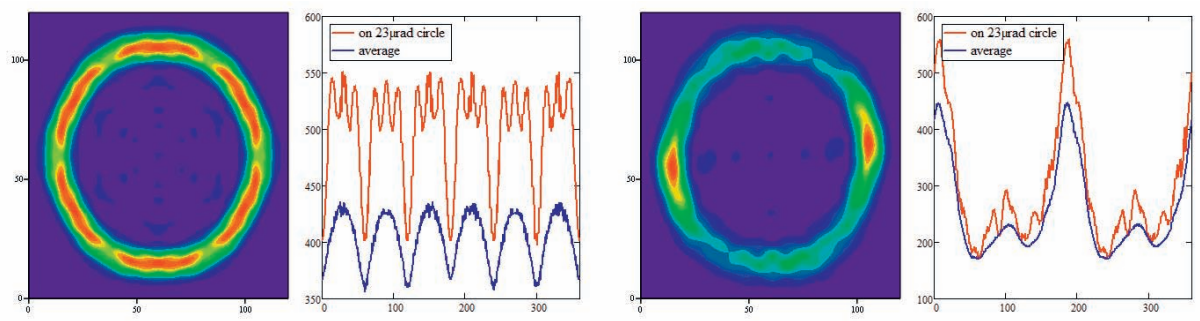


**Fig. 4: Far fields of the open reflector for incidence angles of 0° (left two diagrams) and 10° (right two diagrams). The full scale of the far field patterns is 60 µrad. The diagrams right to the far field patterns are showing the cross section on a circle with 23 µrad radius (red curve) and the average over the full width of 4 µrad (blue curve)**

The cross sections given in Fig. 4 are due to an ideal reflector. Any deviation from the given parameters will decrease the effective cross section. These are mainly errors of the dihedral angle offset and surface deformations. Simulations have shown that the decrease of the cross section may be kept below 20% if the individual angle errors are below 0.3" and the sum of the three angle errors is below 0.2". Surface deformations tend to broaden the far field annulus thereby decreasing the cross section but making it less sensitive to angular errors. The surface deformations should be smaller than about 50 nm. Main reasons of surface deformations are stress by the coatings and the mount as well as thermal effects (next chapter).

# 3. Thermal Design

Starting point of the thermal layout was the design of a fully passive device thermally isolated from the body of the satellite. In addition, the operating temperature shall be lower than the ambient temperature at assembly. Simulations show that this can be achieved by a properly MLI-isolated cavity and radiating surfaces (Fig.5). The main aim is to minimize the deformations caused by thermal gradients. The transient thermal behavior depends on the thermal properties of the substrate material and on the coefficients of absorption and emission of the coatings. As promising materials, SiC ceramics as a highly stiff material and enhanced silver coatings have been selected. Simulations have shown that with this combination the thermal deformations can be kept below 50 nm.

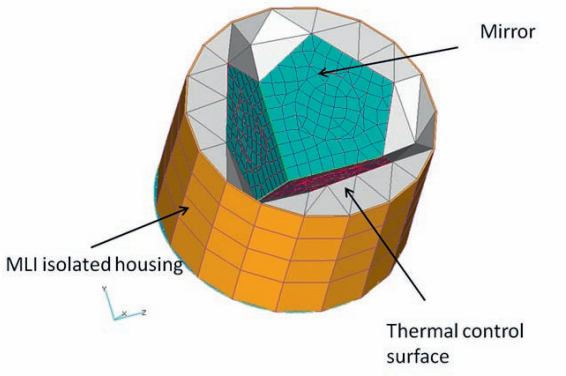


**Fig.5: General design of the thermal shield**

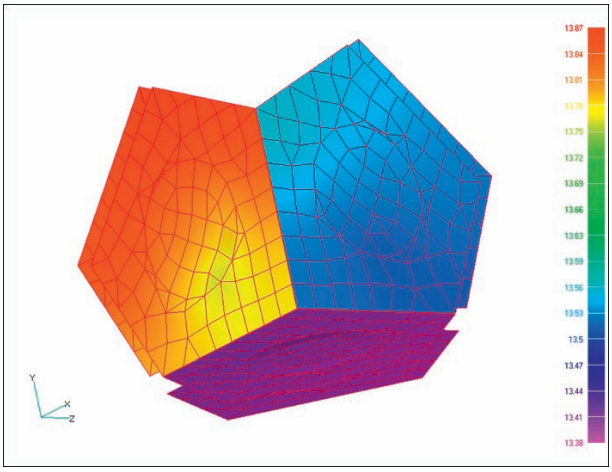

**Fig.6: Example of the temperature distribution if only one mirror is heated by the sun. The maximum thermal gradient is about 1°C**

# 4. Status of Realization

It soon became clear that a new assembly technology has to be developed to achieve the high angular accuracy needed. The present way is to cement the three mirrors in a rigid frame under continuous interferometry control. As a first step, experiments have been started to cement a small glass plate on a larger one as parallel as possible. The influence of the temperature and the long-term stability can then be studied easily. Fig. 7 shows the surface plot of a good example. The tests have shown that an angular accuracy of 0.2" can be attained, but there are still problems with the thermal and long-term stability.

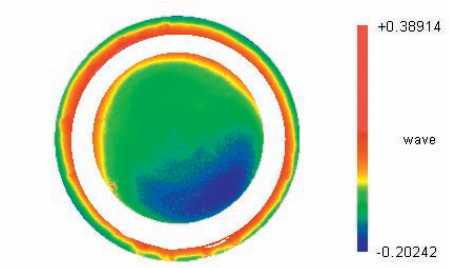


**Fig. 7: Surface diagram of a test doublet obtained by a ZYGO interferometer. The centraldisc corresponds to the small plate (78 mm diam.), the outerannulus to the periphery of the large plate. The white area is eliminated by software because it contains excess cement. (the scale is in parts of the He-Ne laser wavelength). The angle is 0.3" in this case.**

## Acknowledgements

The partial funding of the project by BMWi (BundesministeriumfürWirtschaft und Technologie) is greatly acknowledged.

## References

[1] *Neubert,R., Neubert,J., Munder,J, Grunwaldt,L,* 2009: Proposed Single Open Reflector for the GALILEO Mission, International Technical Laser Workshop on SLR Tracking of GNSS Constellations, http://147.102.106.44/ILRS_W2009/docs/Neubert_reflector_engl.pdf

[2] *Otsubo,T.,* 2009: Simulation of Optical Response of Retroreflectors for Future Lunar Laser Ranging , Advances in Space Research 45 (2010) 733–740

## Correspondence

Ludwig Grunwaldt
GFZ Potsdam
Telegrafenberg
D-14473 Potsdam
grun@gfz-potsdam.de

# BLITS: The first autonomous zero-signature satellite in orbit

*V.D. Shargorodskiy, V.P. Vasiliev, N.N. Parkhomenko*

ABSTRACT

The blits satellite has been designed as an experimental zero-signature slr target, providing a target error value of less than 0.1 Mm. It is a 17-cm-diameter glass ball lens made of two different types of glass and partly covered by a metal coating, so that it is in fact a retroreflector with a cross-section of about $10^5$ sq m at a wavelength of 532 nm, and access solid angle of about $2\pi$.

The satellite was launched into a circular 835-km-high orbit september 21, 2009, and since then most of the global slr network stations provide regular ranging data confirming the basic design parameters. The satellite spin period is about 5.6 Sec, and remains constant during the ~ 20 months of operation.

A modified version of this satellite is under design, to be launched into a higher orbit where the atmosphere drag is much less than at the present orbit height.

Last-generation SLR stations (at least, some of them) are itself able to provide measurement accuracy better than ±1mm. However, to achieve this level of ranging accuracy, corresponding zero-signature or low-signature targets should be used, and the atmosphere refraction should be taken into account with a correspondingly low error.

To make progress in solving of one of the above problems, late September 2009 an SLR target satellite of a new type was launched: the BLITS (Ball Lens In The Space). It is in fact a spherical retro-reflector (slide 1) providing a very low target error (less than 0.1 mm, and caused primarily by some uncertainty of the actual temperature and hence the refraction index of the glass which constitutes the ball lens body). The satellite is in a sun-synchronous circular orbit 832 km high, and most of the global SLR network stations are providing its regular observation data (as far, 35 stations have provided about 30,000 data points). Due to the large amount of accumulated data, some conclusions can be made.

During nearly 20 months of observations, the BLITS target parameters - cross-section and spin period - remain stable (50...100 thousands of square meters and ~5.6 seconds, correspondingly).

The temporal distribution of return signals demonstrates that the spin axis does not lie exactly in the plane dividing the transparent and reflecting surface parts of the ball lens; this is probably caused by a misfunction of the separation system (during the BLITS separation from the carries spacecraft METEOR-M). This does not directly affect the SLR data quality, but may cause some difficulties in observation at certain station locations during some time periods.

At the same time, the return pattern stability for a given station location during more than a year demonstrates the spin axis orientation stability.

The long-term spin parameter stability of BLITS is an advantage in comparison with SLR target satellites having an metal body (LAGEOS, LARETS, WESTPAC, etc.) that suffer from spin slowdown and spin axis orientation instability. Concerning the cross-section value, it is important to continue the BLITS observations for prediction of its possible degradation which may be caused by radiation effects.

One more important result obtained during the BLITS observation campaign is the possibility of observation at longer wavelengths than the 532 nm wavelength typical for most of the SLR stations. Namely, the Concepcion station data (49 data points in 12 passes) obtained at the 847 nm wavelength show the possibility of BLITS observations in the near infrared region, in spite of the large chromaticity of the ball lens. The effective input aperture is in this case not a circular spot on the optical axis, but a narrow ring around this axis (see slide 2). The calculated radius of the ring depends on the wavelength and is about 28 mm for the 847 nm wavelength. The calculated cross-section value at 847 nm is about an order of magnitude less than at 532 nm, and the range correction value is also different (193,31 mm instead of 196.94 mm at 532 nm) due to the wavelength dependence of the glass refraction index. Calculation shows that, if necessary, the BLITS may be observed even in the 1.06 μm wavelength region where the laser transmitter efficiency may be much higher then at 532 nm, and the atmosphere transparency is also higher. The possibility of simultaneous observation of a zero-signature target at widely separated wavelengths may be important for minimization of the atmosphere refraction error, using the well-known two-wavelength refroctometer approach.

For future applications we are currently developing a modified ball lens retro-reflector satellite. The development goal is to increase the cross-section while retaining the low target error. This will provide accurate and efficient SLR observations in a higher orbit (1.5 ... 2 thousand kilometers) with more stable orbit parameters. The modified design will also provide an increase of the expected lifetime in orbit (less degradation caused by radiation effects).

Nevertheless, even now we have an SLR target applicable for high-accuracy ranging, which may be used for specific research in geodynamics and possibly for solving some other problems where extremely high accuracy of range measurements is required. We also hope it may stimulate further improvements in precision measurement hardware and methods.

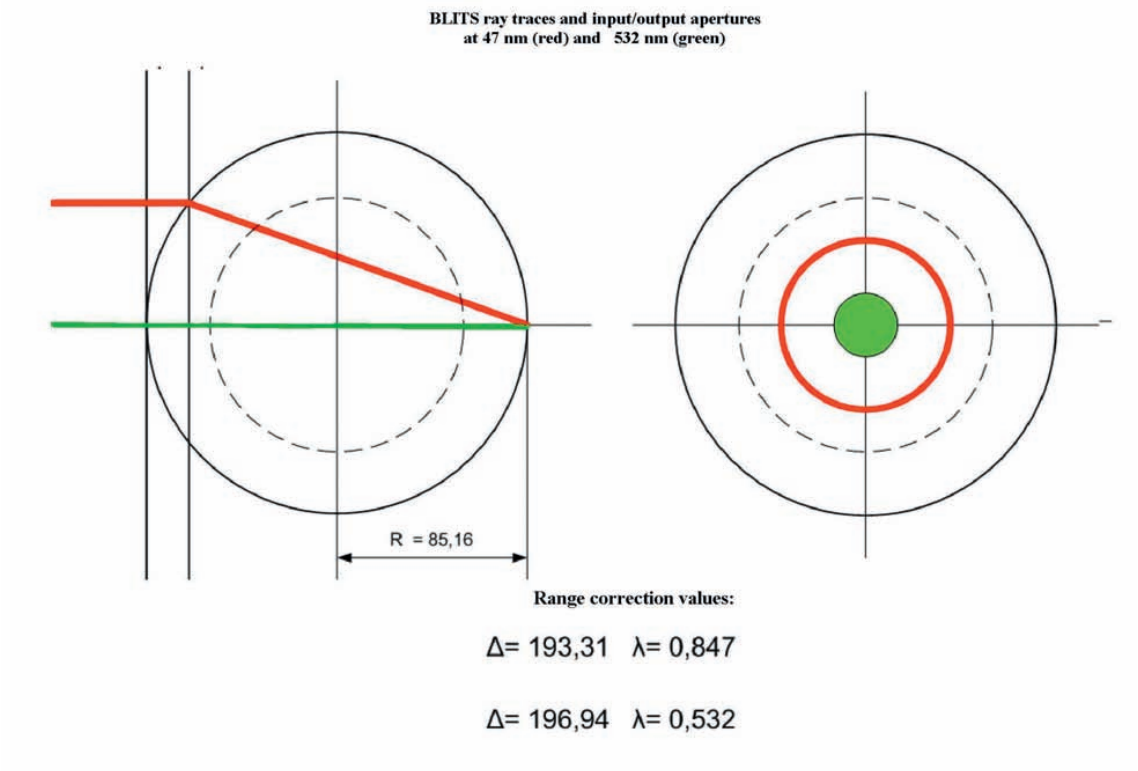


**Figure 1: BLITS ray traces and input/output apertures at 47 nm (red) and 532 nm (green)**

## Correspondence

Natalia Parkhomenko

53 Aviamotornaya st.
Moscow 111024 Russia OJC “RPC “PSI”

parknataliya@yandex.ru

# Session 12:
# Interaction between Data-User and Stations

# The estimation of the SLR data

*Stanisław Schillak*

ABSTRACT
The paper presents the list of parameters which can be used to estimation of the accuracy of the SLR data for each station. The results of the determination of the station coordinates stability in the long term period (from 1994 up to 2008) for the select few stations are presented in the five years blocks. Some examples of time series are added. The results show a deterioration in the accuracy of the several important stations in the last five years. This effect can be explain by smaller number of normal points for some stations in the last period and jumps in the vertical component. The author propose current control of N, E, U components in the one month periods for all stations. GPS coordinates transferred to the SLR reference point for the same epochs should be added. This method enable not only control of each station but also permits to find very quickly the source of biases and estimation of the effect of the new equipment and methods on site, also new analysis models and parameters.

## 1. Introduction

One of the most important task of the satellite laser ranging (SLR) data analysis is estimation of the accuracy of the SLR measurements. The analysis centers use several parameters which give information about accuracy based on the differences between observed and computed values (O-C). The orbits are determined from the all or the best SLR stations. We can to maintain that the mean value of the orbital satellite position is the nearest to true value. The list of the parameters which can to estimate accuracy of the SLR measurements are as follows:

- Long term bias stability – variation of the one month range biases
- Short term bias stability – variation of the one satellite pass range biases
- RMS of fit per station
- NP residuals per one arc – graphic presentation
- Station position stability (3D)
- N, E, U deviations of the station position - graphic presentation

From the list of these parameters the best seems to be station position stability in 3D form. Generally the most stations have the fixed position which is confirmed also by GPS results with exception of the stations in the earthquake regions or in the areas of the vertical postglacial movements. The answers for the several important questions are very important for future activity of the SLR: Where we are, how far to 1 mm? What we can to do for accuracy improvement of the best stations? What limits are from observations side and computations side? The excellent job of the ILRS Analysis Working Group (AWG) gives answers for some parts of these questions. But very important is also view on the long time process of the SLR accuracy. Have we really the better results with time? How quality of results change? What is the reason of these changes? This work try to answer for these questions.

## 2. Data analysis

The computations of the station positions were performed by NASA Goddard's GEODYN-II orbital program. The station positions were determined only for the sites which had continuous work in the last 15 years and high quality of measurements. These stations are presented in table 1. The several stations had excellent activity, only one or two months in 15 years without results! The stations Potsdam and Orroral-Mount Stromlo had two and three different SLR systems in the time of study.

The final results of the computations contain station geocentric coordinates for the first day of each month transformed to the common epoch 2005.0, standard deviation of the coordinates determination, stability of each component and 3D for three five years periods: 1994-1998, 1999-2003, 2004-2008.

| STATION | Station No | First – Last Points | Number of points |
|---|---|---|---|
| McDonald | 7080 | 94-01–08-12 | 179 |
| Yarragadee | 7090 | 94-01–08-12 | 178 |
| Greenbelt | 7105 | 94-01–08-12 | 170 |
| Monument Peak | 7110 | 94-01–08-12 | 175 |
| Graz | 7839 | 94-01–08-12 | 179 |
| Herstmonceux | 7840 | 94-01–08-12 | 179 |
| Wettzell | 8834 | 94-01–08-12 | 171 |
| Potsdam | 7836–7841 | 94-01–08-12 | 172 |
| Orroral-Mt.Stromlo | 7843-7849-7825 | 94-01–08-12 | 154 |

**Table 1: Stations 1994-2008**

# 3. Results

The station positions stability for the all nine stations is presented in Fig. 1.

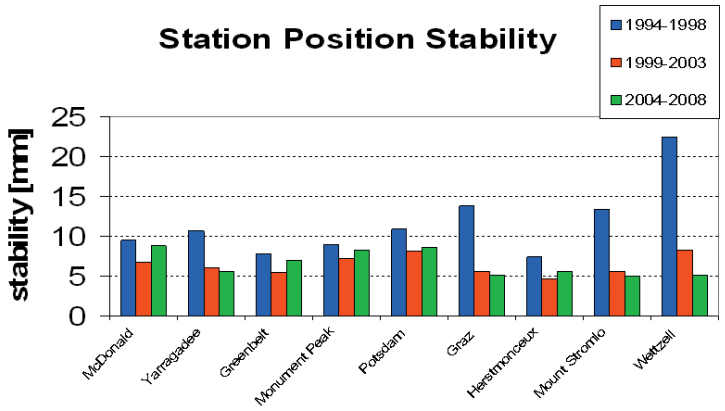


**Figure 1: Station positions stability**

All stations had significant improvement of stability between first (1994-1998) and second (1999-2003) periods. In the comparison to the next period (2004-2008) only four stations had better results, the most significant improvement is observe for Wettzell, five stations had worse stability. The explanation of the worse stability of the stations McDonald, Greenbelt and Monument Peak is visible in table 2 as the effect of significant decrease of the number of normal points in the last period. In the case of Herstmonceux the worse stability in the last period is results of jump in vertical component in February 2007 (Fig. 2) probably due to exchange of the Time Interval Counter to the Event Timer. Potsdam in the last period used different SLR system.

| | 1994-1998 | | | 1999-2003 | | | 2004-2008 | | |
|---|---|---|---|---|---|---|---|---|---|
| STATION | No | Stability [mm] | Number NP | No | Stability [mm] | Number NP | No | Stability [mm] | Number NP |
| McDonald | 7080 | 9.5 | 19812 | 7080 | 6.7 | 26927 | 7080 | 8.8 | 17293 |
| Yarragadee | 7090 | 10.7 | 61852 | 7090 | 6.1 | 72511 | 7090 | 5.6 | 112322 |
| Greenbelt | 7105 | 7.8 | 35330 | 7105 | 5.5 | 40325 | 7105 | 7.0 | 17492 |
| Monument Peak | 7110 | 9.0 | 59045 | 7110 | 7.2 | 58348 | 7110 | 8.3 | 30596 |
| Graz | 7839 | 13.8 | 37947 | 7839 | 5.6 | 50716 | 7839 | 5.1 | 44958 |
| Herstmonceux | 7840 | 7.4 | 45896 | 7840 | 4.7 | 57709 | 7840 | 5.6 | 55778 |
| Wettzell | 8834 | 22.5 | 31101 | 8834 | 8.3 | 28068 | 8834 | 5.1 | 37006 |
| Potsdam | 7836 | 10.9 | 17506 | 7836 | 8.1 | 10354 | 7841 | 8.6 | 18099 |
| Orroral-Mt.Stromlo | 7843 | 13.4 | 26272 | 7849 | 5.6 | 40136 | 7825 | 5.0 | 68217 |

**Table 2: Station position stability vs number of normal points**

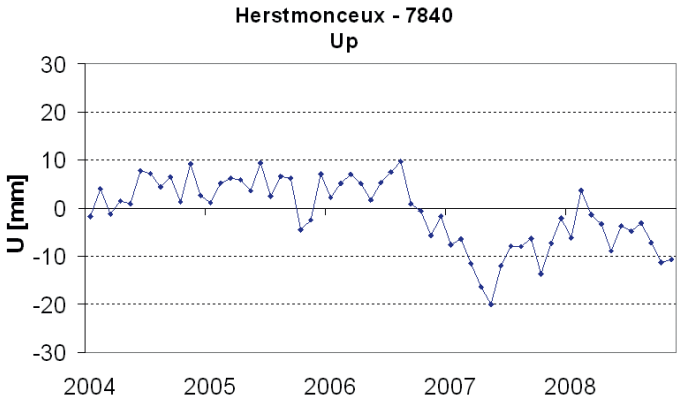


**Figure 2: Station Herstmonceux - vertical component 2004-2008 in comparison to ITRF2008**

The results presented in Fig. 1 and table 2 show also limit of the station positions stability on the level of 5 mm which any station can not to exceed from 1999 despite the fact that in the last ten years precision of the SLR measurements was significantly improved and many systematical biases were eliminated. It means that it is some unknown effect which blocked further improvement of the SLR accuracy. It is probably the atmospheric correction which uncertainty in the opinion of many analysts is estimated on the level of 5 mm. In this case without two-color ranging the improvement of the quality of the SLR results will be rather impossible.

On the other hand it is observable improvement step by step of the station positions stabilities as result the introduction of the new models in orbital programs. The difference between the same data computed in 2000 and presented here in table 2 is 2 mm. This is the effect of the better models of the Earth gravity field (most important), ocean tides, or terrestrial reference frame. Important problem is what part of our uncertainty of the station positions comes from observation errors or from computations?

The lack of significant improvement of the station positions in the last 15 years is presented on Fig. 3 as residuals of the vertical component of the nine stations. The significant data improvement is observed in 1996/1997, later the residuals are on the near same level with little bit improvement with time.

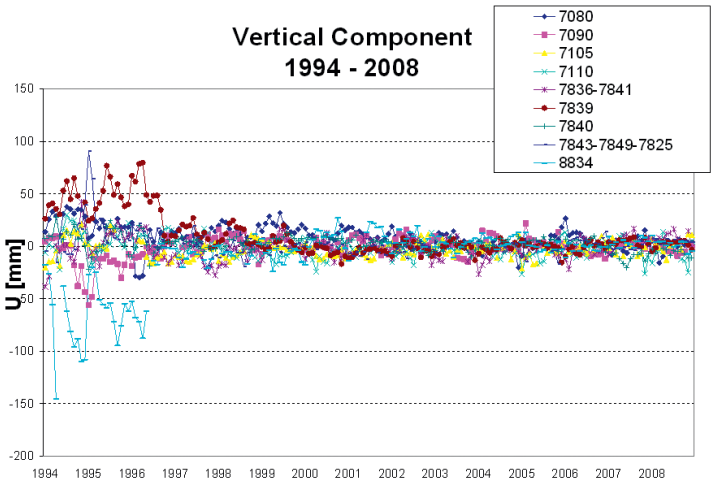


**Figure 3: Residuals of the vertical component in 1994-2008 for the nine stations.**

# 4. Control of the data

The several analysis centers present current results for each station. These results are in different forms: range bias, precision, single shot RMS per each pass, long term bias stability, short term bias stability, N, E, U deviations of the station positions in the graphic presentation. The author suggest to complement the graphic presentation of the station position N, E, U by GNSS results, then will be better control of the significant deviations as for example is presented on Fig. 4. This figure shows 25 mm jump in the SLR results after exchange time interval counter to event timer in February 2006. After jump the SLR results are in good agreement with GPS.

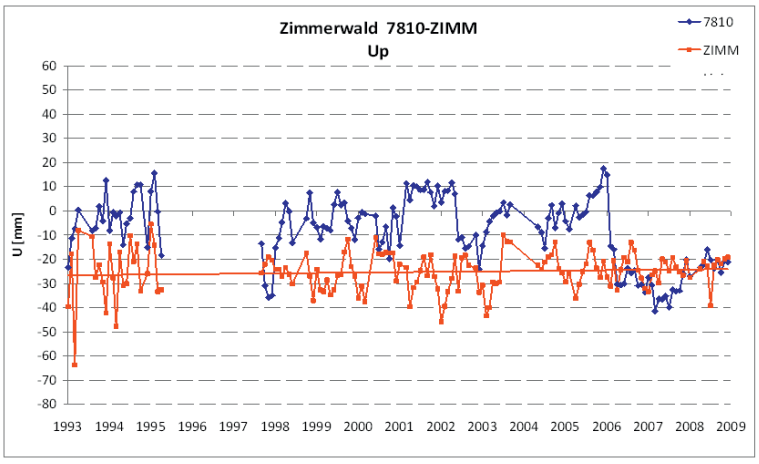


**Figure 4: Vertical component residuals for SLR reference point (ITRF2005), Zimmerwald station, blue – SLR, red - GPS**

The next proposition is the normal points residuals for one site in the form of graphic presentation. The erroneous points and passes will be clearly visible and the stations could be very quickly to correct systematic errors. Also some trends in residuals could be detect. These graphs should be send immediately to each station in one months periods.

# 5. Conclusions

The paper gives several answers for the questions presented in Introduction. The best estimation of the SLR accuracy seems to be 3D stability of the station coordinates. Analysis of the data of the best stations from 15 years shows the accuracy limit on the level of 5 mm, which can to be results of atmospheric correction model. The new two-color SLR system in Wettzell can to answer for this question. Very important for SLR accuracy improvement is the number of normal points per site. We have to observe as many points of LAGEOS satellites as possible. The idea of observations at the beginning, in the middle and in the end of the pass seems to be for LAGEOS satellites not acceptable. Also detection of the all significant jumps in results and their quick elimination by current control of the common SLR and GNSS results is very important. The problem of the estimation of the errors sources from the observation side and the computation side is not too clear. The new models and new effects including in the orbital process should little bit to explain the role of orbital computations in the global SLR errors budget. A deterioration in the SLR accuracy in the last years for the several the best stations is alarming. Come back to the quality of results from beginning of 2000 years is very important. The control of data form the next five years 2009-2013 gives answer if the further significant improvement of the SLR accuracy up to 1 mm in the next few years will be possible.

## Acknowledgements

NASA GSFC for consent to use GEODYN-II program, ILRS stations for their continuous efforts to provide high-quality SLR data, Borowiec SLR team: Piotr Michałek, Danuta Schillak and Stanisław Zapaśnik for their help in data analysis. This work has been supported by financial resources for science in 2010-2013 as a research project No. N N526 231839

## Correspondence

Stanisław Schillak
Borowiec, ul. Drapałka 4
62-035 Kórnik
Poland

sch@cbk.poznan.pl

# New Performance Assessment "Hit Rate" for Laser Ranging Stations

*Toshimichi Otsubo and Mihoko Kobayashi*

ABSTRACT
The performance of the world laser ranging stations is assessed using a new concept "hit rate" which is the ratio of the actual data acquisition out of all the possible opportunity. A number of station-by-station "hit rate" statistics are generated from a number of different aspects, such as day/night, sunlit/umbra, elevation angle, etc. They clearly show strong and weak points of each station and hint what they should do to improve their productivity.

## 1. Introduction

Observability of laser ranging technique is restricted primarily due to the weather, and also due to the availability of facility, the limited human resources and so on. This is in contrast to microwave-based, fully automated techniques like GNSS. It is therefore of interest to know how efficient the laser ranging stations are observing satellites.

It is useful for the ILRS (International Laser Ranging Service) and each laser ranging station to know how the stations track their targets. Detailed tracking policy and actual pattern in each station are typically unknown to the public.

The overall productivity report on the tracking amount has been issued every three months as "SLR Global Performance Report Card" in the ILRS website (Torrence and Noll, 2011), which has been useful to see the overall productivity of each station. Hitotsubashi University also examines quantitative analysis as well as the daily quality control analysis (Otsubo, et al., 2008). In this paper, we introduce a new statistical concept "hit rate" and, based on the results, we try to assess more detailed productivity of laser ranging stations.

## 2. "Hit Rate"

### 2.1 Definition

Let us first define the new parameter "hit rate" here. This is simply the ratio of successful tracking out of all possible opportunity regardless of weather. When we count the number of passes, it is expressed as:

$$[\text{pass-based hit rate}]\,(\%) = [\text{number of observed passes}] / [\text{number of fly-over passes}] \times 100 \quad (1)$$

where the elevation cutoff of 'fly-over' is set at 20 degrees. It can be also defined for the number of normal-point (NP) observations as:

$$[\text{NP-based hit rate}]\,(\%) = [\text{number of observed NPs}] / [\text{number of fly-over NPs}] \times 100 \quad (2)$$

where the elevation cutoff is set as the same as above.

The number of fly-over passes and NPs are calculated based on the CPF orbit prediction and the SLRF2005 station coordinates.

Since the laser ranging tracking does not always cover the whole pass, for instance, a pass can be made of just one NP, the pass-based hit rate should be always higher than the NP-based hit rate.

## 2.2 Overall statistics

We simply apply the equations (1) and (2) to the two-year (2009 and 2010) laser ranging data. The statistics are taken for each of the most productive 20 stations according to the "SLR Global Performance Report Card", and also for three satellite groups, "STARLETTE and STELLA", "LAGEOS-1 and -2", and "ETALON-1, and -2", from low to high orbital altitude. The pass-based and NP-based hit rates are plotted in Figure 1.

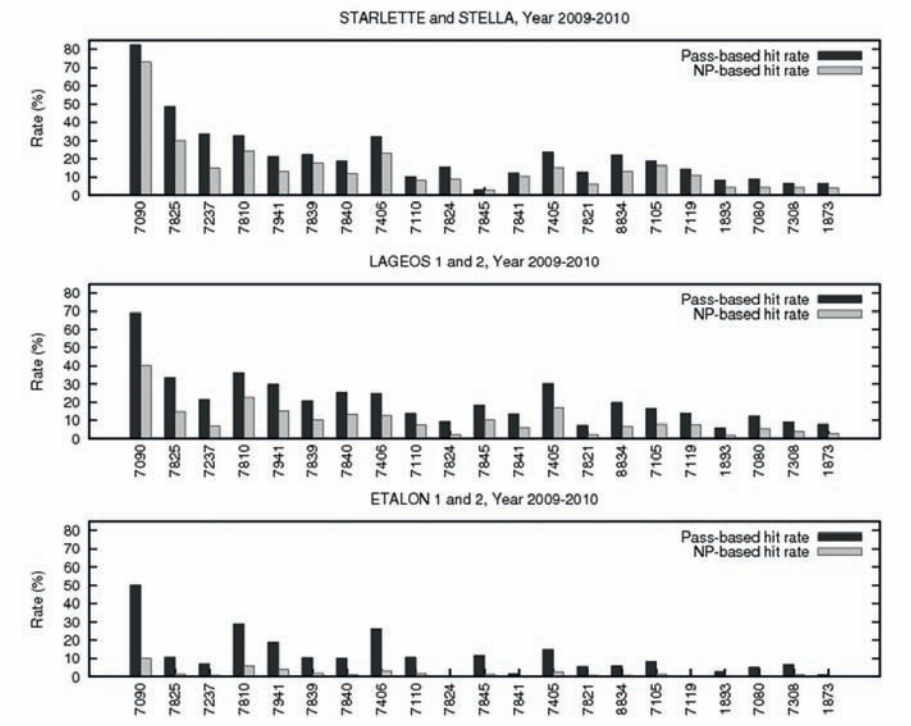


**Figure 1: Overall hit rate. Pass-based and NP-based. The 4 digit numbers are the CDP station IDs.**

Obviously the performance of Yarragadee station (station ID 7090) is dominating; 82%, 69% and 50% pass-based rates for the three satellite groups. It can also be read that the high satellites, especially shown in the NP-based hit rate, are sparsely tracked than the low satellites. We should be aware the fact that the majority of fly-over passes are being missed from the ILRS tracking network — this is in contrast to microwave-based, weather-independent techniques in which the "hit rate" is almost always 100%.

## 2.3 Categorical statistics

We are able to look into further details on the observation policy and pattern of each station. Due to the limit of pages, the graphs of the categorical statistics cannot be shown here, and are placed at the website of Geoscience Laboratory of Hitotsubashi University:

**http://geo.science.hit-u.ac.jp/research-en/memo-en/koetzting-update**

that contains the following plots and we can read the following issues:

- **Day/Night**: It is clearly seen that some stations are operating only at nighttime. The daytime hit rates for high satellites (ETALON-1 and -2) are significantly reduced for the majority of stations, but there are a couple of stations, Zimmerwald and Matera, whose daytime hit rate for high satellites nearly matches its nighttime one.
- **Sunlit/Umbra**: Satellites are sometimes illuminated by the sun, and sometimes in umbra (shadowed region). The nighttime observations are categorized into these two groups. There is typically no preference on sun light illumination for low satellites, but there are a few stations whose nighttime tracking requires illumi-

nation. On the other hand, most of the stations obtained significantly more amount of high satellite data when illuminated than shadowed. The exceptions are Yarragadee, Monument Peak, Greenbelt and Koganei, who more or less equally observes regardless of the sunlight illumination.

- **Elevation**: Laser ranging to high satellites flying at a low elevation angle seems a hard task for the vast majority. However, this does not seem so difficult for Yarragadee, Zimmerwald, Matera and San Juan.
- **Number of pass segments, and pass duration**: Zimmerwald and Graz are likely to switch the tracking target frequently, and the average duration of a pass is longer for these stations. The "interleaving" observation is found to be effective to cover the whole pass.

# 3. Conclusions

A new quantitative assessment of "hit rate" is proposed and tested at Hitotsubashi University. The "hit rate" categorical statistics, such as day/night, sunlit/umbra, elevation angle, are found to be useful to know how a laser station is being operated. These statistics can clearly point out what they are good at and also what they should do to improve their productivity.

## References

*Torrence, M., and C. Noll*: SLR Global Performance Report Card, http://ilrs.gsfc.nasa.gov/stations/site_info/global_report_cards/index.html, 2011.

*Otsubo, T., M. Kobayashi, T. Gotoh, T. Kubo-oka*: Daily quality control system of satellite laser ranging data for the ILRS network, Journal of Geodetic Society of Japan, 54, 2, 69-79, 2008 (in Japanese, with English abstract).

## Correspondence

Toshimichi Otsubo

Hitotsubashi University
2-1 Naka, Kunitachi
186-8601 Japan

t.otsubo@r.hit-u.ac.jp

# Session 13:
# New Laser Ranging Technologies and Capabilities that must be developed to support future missions

# Introduction to laser transponders for precise interplanetary ranging and time transfer

*John J. Degnan*

## 1. Introduction

Our decades of experience with Lunar Laser Ranging (LLR) have demonstrated the extreme difficulty of single-ended ranging to retroreflector arrays, even over relatively short lunar distances (R = 385,000 km). In LLR, the $R^{-4}$ dependence of the received signal strength drives us to large meter-class telescopes and moderately powerful lasers. However, since double-ended (two-way) laser transponders have active transmitters on both ends of the link, the signal strength falls off only as $R^{-2}$, and this makes interplanetary ranging and time transfer possible. Figure 1 illustrates three transponder types –*echo, asynchronous, and one-way.*

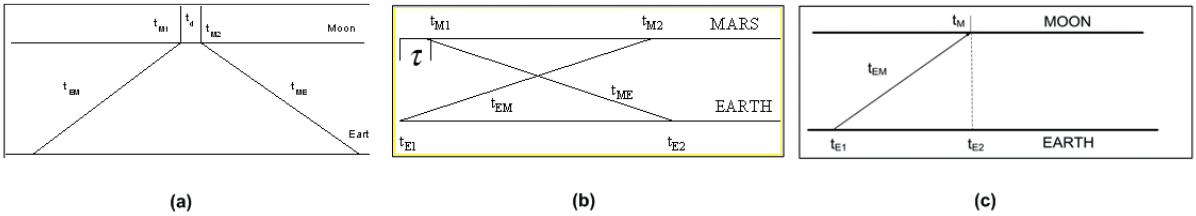


**Figure 1: Types of transponders: (a) Echo; (b) Asynchronous; and (c) One-Way.**

The more familiar *echo* transponder works well on "short" links (e.g. to the Moon) where the single shot detection probability at both terminals can be high. The spacecraft transponder detects pulses from Earth and fires a reply pulse back to the Earth station. To determine range, the time delay between the detected and reply pulses, $t_d$, must be known a priori or measured onboard and communicated back to Earth. The delay is then subtracted from the measured start-stop interval at the Earth station to obtain the actual pulse time of flight[Degnan, 2002].

With an *asynchronous* transponder, the transmitters at opposite terminals fire asynchronously (independently). The signal from the opposite terminal must be acquired autonomously via a search in both space and time. The spacecraft transponder measures both the local transmitter time of fire and any received "photon events" (signal plus noise) on its own time scale and transmits the information back to the Earth terminal via the spacecraft communications link. The spacecraft range and spacecraft/Earth clock offsets are then computed from the combined data set. The *asynchronous* approach works well on "long" links (e.g., interplanetary) even when the single shot probability of detection is relatively small [Degnan, 2002].

The *one-way* transponder assumes excellent synchronization between the ground-based and spaceborne clocks [Christophe et al, 2009]. To do one cm accuracy ranging, clock synchronization ($t_M$-$t_{E2}$) must be within 33 psec.

An early demonstration of the accuracy with which time transfer could be accomplished via laser was an airborne experiment conducted by Professor Carroll Alley and his students at the University of Maryland. Two sets of synchronized atomic clocks were placed in a ground-based trailer and an aircraft. The trailer contained a 100 psec laser transmitter firing at 30 pps which continuously tracked the aircraft for 16 hours as it followed an oval "racetrack" pattern. A retroreflector on the side of the aircraft provided a stop pulse to the ground receiver while an onboard detector measured the time of arrival in the time frame of the airborne clocks. In the absence of relativistic effects associated with the lower

gravity field and the aircraft velocity on the airborne clock rate, the two sets of clocks would remain synchronized, but the clocks were observed to drift at a rate of roughly 3 nsec per hour of flight in good agreement with Einstein's predictions (see Figure 2).

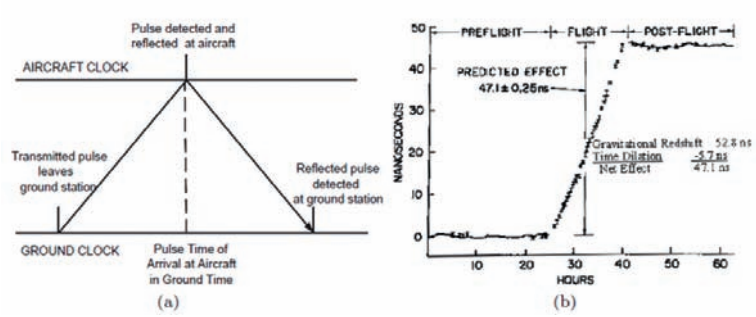


**Figure 2: University of Maryland Atomic Clock Experiment (a) Minkowski Space-Time diagram is similar to that of an echo transponder with zero delay; (b) Cumulative time offset between the airborne and ground-based clocks was roughly 3 nsec per hour of flight.**

# 2. Transponder experiments to date

All of the early attempts to establish two-way laser transponder links were made by the 1.2 meter telescope facility at NASA Goddard Space Flight Center (GSFC) to interplanetary satellites carrying onboard laser altimeters, consisting of both laser transmitter and a ranging receiver. Since the altimeters all used the fundamental Nd:YAG wavelength of 1064 nm rather than the 532 nm second harmonic wavelength favored by the SLR community, the experiments were necessarily carried out in the Near InfraRed (NIR).

The first attempt, conducted in December 1997 to the Mars Orbiter Laser Altimeter (MOLA-2) on the NASA Mars Global Surveyor (MGS) spacecraft at a distance of 10 million km, was unsuccessful due to exceptionally cloudy skies at GSFC. A second attempt, made one month later in January 1998 to the Johns Hopkins University Applied Physics Lab (JHU/APL) Near Earth Asteroid Rendezvous (NEAR) spacecraft at a distance of 5 million km, was also foiled by heavy cloud cover during the period allocated to the experiment. Later that year, Mission Managers at the Jet Propulsion Laboratory agreed to a second MOLA transponder experiment while MGS was still enroute to Mars. However, the distance to the spacecraft during the experiment period would be roughly 100 million km, and, while the Earth transmitter divergence was narrow enough to establish the uplink to MOLA, the GSFC 1.2 meter telescope was deemed to have insufficient aperture for a successful downlink given the wider divergence of the MOLA transmitter. Therefore, the GSFC team arranged to use the 3.5 m telescope at the US Air Force (USAF) Starfire Facility for the experiment. After integrating their SLR hardware into Starfire and successfully tracking a variety of artificial satellites, the team was ready to make its second MOLA attempt. Unfortunately, on the weekend prior to the official start of the second transponder experiment, the MGS spacecraft experienced technical difficulties and was placed in "Safe Mode" for several months just prior to its arrival at Mars to begin its primary mapping mission.

Finally, in late May-early June of 2005, successful two-way experiments, between GSFC and the Mercury Laser Altimeter (MLA) on the NASA Messenger spacecraft, were carried out over a distance of 24 million km [Sun et al, 2005; Smith et al, 2006]. GSFC analysts were able to use the data to compute the actual spacecraft distance to within about 20 cm, or about one part in 100 billion. Three months later, in September 2005, approximately 500 GSFC laser pulses were successfully detected by MOLA-2 at a distance of 80 million km. Although MOLA-2 was still in Mars orbit, its laser was no longer operational and is topographic mapping mission was terminated. For a more detailed history of these early attempts, the reader is referred to the following articles [Zuber, 2006; Degnan, 2007].

Messenger and MOLA were experiments of opportunity rather than design. Since the available spacecraft had no ability to lock onto the opposite terminal or even the Earth image, the spaceborne lasers and receiver FOV's were scanned across the Earth terminal, providing only a few seconds of mutual observation and data. Detection thresholds were also relatively high due to the choice of wavelength (1064 nm) and analog detectors, and range precision was limited

to decimeters by the long altimeter laser pulsewidths (~6 nsec) and comparable receiver bandwidths. Nevertheless, these early experiments clearly demonstrated the near term feasibility of precise interplanetary laser ranging and time transfer using transponders.

The first truly operational use of the one-way transponder technique has been carried out by a subset of ILRS stations to the Lunar Orbiter Laser Altimeter (LOLA) on the NASA Lunar Reconnaissance Orbiter (LRO) spacecraft, orbiting the Moon since 2009 at a distance of 385,000 km [McGarry et al, 2011].

# 3. Some transponder applications

Potential transponder applications include [Degnan, 2007]:

- Solar System Science
  - Solar and Planetary Physics: gravity field, internal mass distribution and rotation
  - Few mm accuracy lunar ephemerides and librations
    - Improves ranging accuracy and temporal sampling over current lunar laser ranging (LLR) operations to Apollo retroreflectors on the Moon with small, low energy, ground stations
  - Decimeter or better accuracy planetary ephemerides
  - Mass distribution within the asteroid belt
- General Relativity
  - Provides more accurate (2 to 3 orders of magnitude) tests of relativity and constraints on its metrics than LLR or microwave radar ranging to the planets, e.g.
    - Precession of Mercury's perihelion
    - Constraints on the magnitude of G-dot ($1x10^{-12}$ from LLR)
    - Gravitational and velocity effects on spacecraft clocks
    - Shapiro Time Delay
- Lunar and Planetary Mission Operations
  - Decimeter or better accuracy spacecraft ranging
  - Calibration/validation/backup for DSN microwave tracking
  - Subnanosecond transfer of GPS time to interplanetary spacecraft for improved synchronization of Earth/spacecraft operations
  - Transponder can serve as independent self-locking beacon for collocated laser communications systems

In recent years, there have been a number of fundamental physics flight mission studies submitted NASA [Turyshev et al, 2010] , ESA (GETEMMEE and SAGAS), and the Chinese Academy of Science [Ni, 2007].

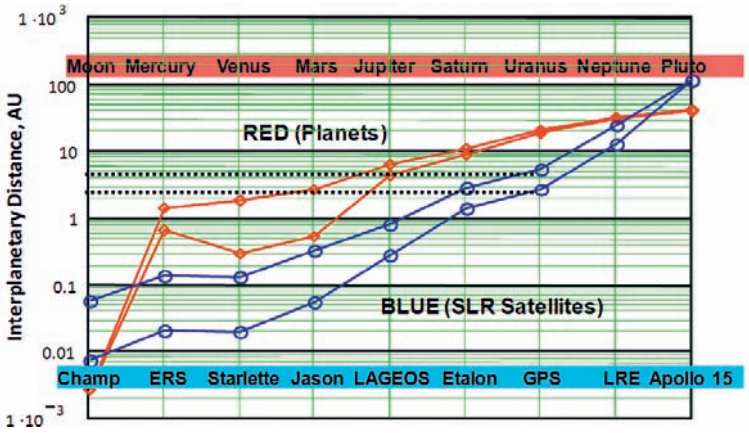


**Figure 3: The upper and lower red curves bound the Earth-planetary distance (1AU ~150 million km) while the upper and lower blue curves bound the equivalent transponder range at satellite elevations of 20 and 90 degrees respectively. From [Degnan, 2007].**

# 4. Summary

The ability of laser transponders to simultaneously measure range, transfer time between distant clocks, and indirectly monitor the local gravity field at the spacecraft via the relativistic gravity effect on atomic clock rates make it a useful tool for fundamental physics studies within the Solar System [Degnan, 2007; Christoph et al, 2009, Turyshev et al, 2010]. The successful experiments to the Messenger and MGS spacecraft clearly demonstrate that the space-qualified technology for decimeter accuracy interplanetary laser transponders is already available. The physical size, weight, and ranging/timing accuracy of future interplanetary transponder terminals will clearly benefit from current SLR photon-counting technologies, including:

– Multi-kHz, low energy, ultrashort pulse lasers (10 to 300 psec)

– Single photon sensitivity, picosecond resolution, photon-counting detectors and receivers

– Automated transmitter point ahead and receiver pointing correction s as currently being demonstrated in NASA's NGSLR system.

Furthermore, it has been shown that interplanetary transponder and laser communications links up to 100AU (through the Earth's atmosphere) can be inexpensively simulated and tested, prior to actual initiation of a flight mission, using existing retroreflector arrays on Earth-orbiting satellites and the Moon [Degnan, 2007]. From the horizontal dashed lines in Figure 3, for example, we see that tracking GPS at 90° elevation is equivalent to a worst case Mars experiment on the far side of the Sun (2.5 AU) while tracking GPS at 20° elevation is equivalent to a best case Jupiter experiment at PCA (4.5 AU). The Apollo 15 reflector on the lunar surface can be used to simulate transponder/lasercom experiments at 100 AU, i.e., beyond Pluto (40 AU) and the outer limits of the Kuiper Belt (~55 AU).

## References

*J.F. Chandler, M.R. Pearlman, R.D. Reasenberg, and J. J. Degnan*, "Solar-System Dynamics and Tests of General Relativity with Planetary Laser Ranging", Proc. 14th International Workshop on Laser Ranging, San Fernando, Spain, June 6-10, 2004.

*B. Christophe et al,* "Odyssey: A Solar System Mission", Experimental Astronomy, pp. 23:529-547, 2009.

*J. J. Degnan*, "Asynchronous Laser Transponders for Precise Interplanetary Ranging and Time Transfer", Journal of Geodynamics, Vol. 4, pp. 551-594, November, 2002.

*J. J. Degnan*, "Asynchronous Laser Transponders: A New Tool for Improved Fundamental Physics Experiments", Int. J. Modern Physics D, 16, pp. 2137-2150, 2007.

*J. McGarry et al*, "The First ILRS Laser Transponder Mission: Laser Ranging to NASA's Lunar Reconnaissance Orbiter (LRO)", these proceedings, 2011.

*W.T. Ni*, "ASTROD (Astrodynamical Space Test of Relativity using Optical Devices) and ASTROD I" , Nuclear Physics B- Proceedings Supplements, Vol. 166, pp. 153-158, April 2007.

*D. E. Smith, M. T. Zuber, X. Sun, G. A. Neumann, J. F. Cavanaugh, J. F. McGarry, and T. W. Zagwodzki*, "Two-way Laser Link over Interplanetary Distance", Science, 311, p. 53, 2006.

*X. Sun, G. A. Neumann, J. F. McGarry, T. W. Zagwodzki, J. F. Cavanaugh, J. J. Degnan, D. B. Coyle, D. R. Skillman, M. T. Zuber, and D. E. Smith*, "Laser Ranging between the Mercury Laser Altimeter and an Earth-based Laser Satellite Tracking Station over a 24 Million Kilometer Distance", OSA Annual Meeting, Tucson, AZ, October 16-20, 2005.

*S. G. Turyshev, W. Farr, W. M. Folkner, A. R. Girerd, H. Hemmati, T. W. Murphy Jr., J. G. Williams, and J. J. Degnan*, "Advancing Tests of Relativistic Gravity via Laser Ranging to Phobos", Experimental Astronomy, pp. 28:209-249, 2010.

*M. T. Zuber*, "Seconds of Data, Years of Trying", Photonics Spectra, Vol.40, Issue 5, pp. 56-63, 2006.

## Correspondence

John J. Degnan
Sigma Space Corporation
Lanham, MD
20706, USA

Email: John.Degnan@sigmaspace.com

# The First ILRS Laser Transponder Mission: Laser Ranging to NASA's Lunar Reconnaissance Orbiter

*Jan McGarry[1], Christopher Clarke[2], Julie Horvath[2], Dandan Mao[3], Mark Torrence[4]*

ABSTRACT

Since the launch in June 2009 of LRO, Laser Ranging (LR) to LRO has been a huge success, accumulating over 1000 hours of one-way laser ranging data. The participation of the global community of stations has been a very large part of that success. Ten stations around the world contribute to the ranging data, including NASA's Next Generation Satellite Laser Ranging (NGSLR) system, McDonald Laser Ranging System, many of the NASA MOBLAS systems, and four European stations. A brief overview of the LRO-LR technique will be followed by a summary of the results to date.

## 1. Background

LRO-LR is the first mission for the ILRS whose primary laser tracking method is transponder ranging. LRO-LR is a one-way (uplink only) ranging technique where the Earth laser station measures the fire times of its outgoing laser pulses and the Lunar Orbiter Laser Altimeter (LOLA), one of the instruments onboard LRO, measures the receive times [1] [2]. The range gate for the Earth received pulses in LOLA's detector #1 is called the Earth Window. During this window the detector is gated on to receive Earth events. LOLA performs signal processing on the received Earth events and provides the signal processing results to the ground via its housekeeping packets.

These housekeeping packets are routed through the LRO Mission Operations Center (MOC) to the LOLA Science Operations Center (SOC) where the relevant data is extracted and put into a real-time website which is displayed from the Crustal Dynamics Data Information System (CDDIS) server. This real-time LRO-LR website provides feedback to all participating stations while they are ranging to LRO. Unlike two-way ranging where the laser light returns to the station and provides the feedback, this website is the only feedback that the stations have while they are ranging to LRO. The latency of the website is nominally 10 to 20 seconds, but has been observed to be as long as several minutes.

## 2. Participating Stations

There are ten stations supporting laser ranging to LRO. These stations are shown in Table 1 along with their first successful ranges and their system characteristics.

An initial Call for Participation to ILRS stations was issued in 2008. The requirements on the ground stations includes laser energy density at the spacecraft (1 to 10 femtoJoules per sq.cm), wavelength (532.2 +/- 0.15 nm), number of pulses per second (no more than 28 Hz fire rate), fire timing resolution (100 picosecond), and the ability of the station software to use the ILRS Go/NoGo flag. The Call for Participation can be found on the LRO-LR website [3].

Written agreements were made with each of the stations. Included in the Agreements were the above system requirements, the need to maintain the security of the predictions, and the requirement to range to LRO only when scheduled.

Fire data is sent in from all stations in the Consolidated Ranging Data (CRD) format [4]. The files sent in from the stations have the file extension FRF for fire only data. NASA systems (NGSLR and MOBLAS) also send in their data in a NASA Internal Transponder Data Format (iTDF).

[1] NASA Goddard Space Flight Center
[2] Honeywell Technology Systems Incorporated
[3] Sigma Space Corporation
[4] Stinger Ghaffarian Technologies

| Station | Location | Synch to LOLA? | Firerate (Hz) | Max # / sec in LOLA window | Expected energy at LRO (fJ / sqcm) | Station Frequency Source | Date of first successful ranging to LRO | LR Status |
|---|---|---|---|---|---|---|---|---|
| NGSLR | Maryland, US | Yes | 28 | 28 | 1 to 5 | Maser (18-Oct-2010) | 30-Jun-2009 | Operational |
| MLRS, McDonald | Texas, US | No | 10 | 2 to 4 | 1 to 10 | Cesium | 02-Jul-2009 | Operational |
| MOBLAS-7, Greenbelt | Maryland, US | No | 10 | 2 to 4 | 1 to 3 | Maser (18-Oct-2010) | 02-Jul-2009 | Operational |
| Herstmonceux | Great Britain | Yes | 14 | 14 | 1 to 3 | Maser (13-May-2010) | 13-Jul-2009 | Operational |
| Zimmerwald | Switzerland | Yes | 14 | 14 | 1 to 3 | Ovenized crystal oscillator | 20-Jul-2009 | Operational |
| Wettzell | Germany | No | 7 | 7 | 1 to 10 | Cesium | 30-Oct-2009 | Operational |
| MOBLAS-6, Hartebeesthoek | South Africa | No | 10 | 2 to 4 | 1 to 3 | Maser | 05-Dec-2009 | Operational |
| MOBLAS-5, Yarragadee | Australia | No | 10 | 2 to 4 | 1 to 3 | Maser (14-May-2010) | 25-Jan-2010 | Operational |
| MOBLAS-4, Monument Peak | California, US | No | 10 | 2 to 4 | 1 to 3 | GPS steered Rubidum | 03-Feb-2010 | Operational |
| Grasse/MEO | France | No | 10 | 2 to 4 | 1 to 10 | Cesium | 18-May-2010 | Operational |

**Table 1: Participating ILRS stations and their characteristics**

Four of the participating stations are NASA MOBLAS systems. These systems were modified to permit ranging to LRO. A new Windows computer with a Guidetech timing card (model GT658) was added to each system to provide the precision needed for the fires, and the systems were all modified to fire their laser at 10 Hz.

Some of the participating ground stations control their laser fires to ensure the pulses arrive when the LOLA Earth Window is open. These systems are referred to as synchronous ranging stations. NGSLR, Herstmonceux and Zimmerwald are all synchronous stations. All other systems are asynchronous. The MOBLAS systems and Grasse all fire at 10 Hz. MLRS fires at approximately 10 Hz. Systems that fire at 10 Hz get two pulses per second into the LOLA Earth Window most of the time, and occasionally they will get four pulses per second into the Window. Wettzell fires at 7 Hz and they tune their fire frequency to match the range-rate.

# 3. Laser Ranging Results

As of this Workshop there were over 1000 hours of Laser Ranging data collected from all of the stations. NGSLR has over 45% of the global data collected since launch, with Yarragadee at 18%, Monument Peak at 15%, and MLRS at 13%. The global data rate appears to be increasing as shown in the plot of Figure 1.

In the early months after launch only a single station was scheduled to range to LRO at any time. This was to give the stations some experience in using the real-time LRO-LR website for feedback. Simultaneous ranging to LRO by two or more stations allows comparison of station ranging and biases. Three-way simultaneous ranging can potentially provide a geometric solution of the spacecraft location. Simultaneous ranging opportunities are now scheduled for all NGSLR, MLRS, MOBLAS-7 (Greenbelt), and MOBLAS-4 (Monument Peak) passes. In addition Grasse and Zimmerwald are also always scheduled for simultaneous ranging opportunities. More stations will be simultaneously scheduled in the near future.

The first successful ranging to LRO was done by NGSLR on June 30, 2009. The first successful three-way simultaneous ranging was performed on November 1, 2010 by NGSLR, MLRS and Monument Peak. There have been many two and three-way simultaneous passes to LRO over the last 2 years and one successful four-way simultaneous pass as of this Workshop (NGSLR, MOBLAS-7, MLRS and Monument Peak).

Analysis of the LR data is reported in D. Mao's paper in this Proceedings[5].

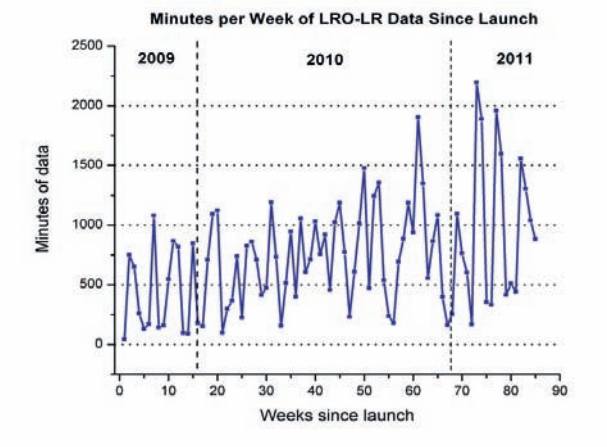


**Figure 1: Plot of LR data from launch (June 2009) to present**

# 4. Summary

With LRO-LR entering year 3 of successful operations, one-way (uplink only) laser transponders have now been proven to work operationally. Thanks to the support of the ILRS and the participating stations, over 1000 hours of LR data has been collected and used to determine spacecraft time to UTC, and will be used to provide more precise orbits. In addition time transfer between ground stations using LRO will be attempted later in 2011, initially between Wettzell and NGSLR.

LRO will move from its current Mission Mapping circular orbit of 50 km to an elliptical 30 km x 200 km orbit late in 2011. LRO-LR is expected to continue through 2012.

For details, pictures, and the latest information please see: http://lrolr.gsfc.nasa.gov

## Acknowledgments

The authors would like to express their thanks to the LOLA and LRO-LR Principle Investigators, David E. Smith and Maria T. Zuber (Massachusetts Institute of Technology), as well as to Instrument Scientist, Xiaoli Sun (NASA Goddard), and to Co-Investigator Gregory Neumann (NASA Goddard).

## References

*1- Zuber, M.T., D.E. Smith, R.S. Zellar, G.A. Neumann, X. Sun, J. Connelly, A. Matuszeski, J.F. McGarry, et al*, 2009: The Lunar Reconnaissance Orbiter Laser Ranging Investigation, Volume 150, Numbers 1-4, January.

*2- McGarry, J., R. Zellar, G. Neumann, C Noll, M. Torrence, J. Horvath, C. Clarke, R. Ricklefs, M. Pearlman, A. Mallama,* 2008: Laser Ranging to the Lunar Reconnaissance Orbiter: a Global Network Effort, "Proceedings of the 16th International Workshop on Laser Ranging," October 13-17, Poznan, Poland.

3- http://lrolr.gsfc.nasa.gov/docs/Call_for_Participation.pdf

4- http://ilrs.gsfc.nasa.gov/products_formats_procedures/crd.html

*5- Mao, Dandan, David D. Rowlands, Jan F. McGarry, Maria T. Zuber, David E. Smith, Mark H. Torrence, Gregory A. Neumann, Erwan M. Mazarico,James Golder, Xiaoli Sun, Thomas W. Zagwodzki, John F. Cavanaugh*, 2011: Laser Ranging Experiment on Lunar Reconnaissance Orbiter: Timing Determination and Orbit Constraints, This Proceedings.

## Correspondence

Jan McGarry
NASA Goddard Space Flight Center
Code 694
Greenbelt, Maryland 20771
USA

Jan.McGarry@nasa.gov

# Laser Ranging Experiment on Lunar Reconnaissance Orbiter: Timing Determination and Orbit Constraints

*Dandan Mao, Jan McGarry, Mark Torrence, Gregory Neumann, Erwan Mazarico, Michael Barker, Xiaoli Sun, David Rowlands, James Golder, Thomas Zagwodzki, John Cavanaugh, Maria Zuber, David Smith*

ABSTRACT

Accurate ranges from Earth to the Lunar Reconnaissance Orbiter (LRO) spacecraft Laser Ranging (LR) system supplement the precision orbit determination (POD) of LRO. LRO is tracked by ten LR stations from the International Laser Ranging Service (ILRS), using H-maser, GPS-steered Rb, and Cs oscillators as reference clocks. The LR system routinely makes one-way range measurements via laser time-of-flight from Earth to LRO. Uplink laser pulses are received by a telescope mounted on the high-gain antenna of LRO, transferred through a fiber optic cable to a Lunar Orbiter Laser Altimeter (LOLA) detector, and time-tagged with respect to the spacecraft clock. The range from the LR Earth stations to LRO is derived from paired outgoing and receive times. Accurate ranges can only be obtained after solving for both the spacecraft and ground station clock errors and removing temperature effects. The drift rate and aging rate of the LRO clock are calculated from data provided by the primary LR station, NASA's Next-Generation Satellite Laser Ranging System (NGSLR) in Greenbelt, Maryland. The results confirm the LRO clock oscillator mid- to long- term stability measured during ground testing. These rates also agree well with those determined through POD. Ten-cm level LR observations are used in the POD procedure to form strong orbit constraints. We have processed the entire LRO mission with the radiometric and LR data, and estimated the impact of the LR data on the orbit reconstruction and accuracy. The orbit residual fits of the LR data over 14 days are less than 10 meters, nominally smaller than the 15-meter residuals of the S-band data. The difference between the orbit results determined with and without LR contribution is up to 10 meters.

## 1. Introduction

The laser ranging (LR) system has been set up to track the Lunar Reconnaissance Orbiter (LRO) (*Chin, G., et al., 2007*) in order to supplement the precision orbit determination (*Zuber, M., et al., 2010*) since June, 2009. The system includes two primary components: a flight system and ground system. The ground system consists of 10 participating Earth-based satellite laser ranging (SLR) stations, which regularly transmit laser pulses to LRO. These laser pulses give one-way time-of-flight measurements of the range between the ground station and LRO in orbit around the Moon. The flight system includes a telescope attached to the LRO high-gain antenna (HGA), which receives the laser pulses and sends them to the detector on the Lunar Orbiter Laser Altimeter (LOLA) instrument (*Smith, D.E., et al., 2009*) through a fiber optic cable bundle. The LOLA timing electronics then time-tag the pulse for later processing. These time-tags are synchronized with the LRO Mission Elapsed Time (MET), based on an oven-controlled quartz ultra-stable oscillator (USO) which is stable to several nano-seconds per hour. The USO and the accurate ground station clocks collectively enable the LR to achieve sub-meter level measurements. The precision of LOLA time stamps is about 0.5 ns in standard deviation depending on receive pulse width and energy, which is equivalent to 15 cm precision of one-way ranging measurement. To obtain the one-way range, ground station laser transmitted times are paired with corresponding LOLA receive times using predicted one-way time-of-flight in the consolidated prediction format (CPF) if the predicted receive time and the LOLA time stamp differ by less than 200 ns.

Detailed laser properties of all ten participating SLR stations are listed in *McGarry, J., et al.* (2011). The nominal precision of received pulses from the primary ground station, NASA's Next-Generation Satellite Laser Ranging System (NGSLR), is about 15 cm root mean square (RMS), and 10 cm to 30 cm for other stations. Analysis figures for all SLR stations can be found in *McGarry, J., et al.* (2011b). In the current precision analysis, a range walk correction based on the NGSLR pulse shape has been applied to the LOLA receive times for all ground stations. The laser properties, such as the energy, the wavelength, and the pulse shape, are station-dependent. Hence the range walk correction, which minimizes NGSLR's RMS, is not necessarily optimal for data from other stations. New range walk corrections will be derived in the future for each ground station and applied to the analysis in order to improve the ranging precision from non-NGSLR stations.

# 2. Timing Determination

The LRO MET time can be related to Coordinated Universal Time (UTC) through space clock kernel corrections, provided weekly by NASA flight dynamics facility (FDF) to an accuracy of better than 3 ms. Using Hydrogen-maser or Cesium/Rubidium oscillators as reference at the ground stations, LR has the ability to more accurately cross reference LOLA MET time tags to UTC time within a couple milliseconds over several months by pairing up outgoing laser time and LOLA receive time, given the precise locations of the ground stations and preliminary knowledge of the LRO satellite. The long- term stability of the LRO clock was characterized using 10 months of NGSLR ranging data from February 2010 to December 2010. A time drift rate of 71.05 ns/s and a frequency aging rate of 2.044e-8 ns/s$^2$ were derived by fitting the outgoing and receive time pair differences with a quadratic polynomial without correcting for relativistic effects. The Newtonian residuals after removing the fitting polynomial remain less than ±0.25 milliseconds over 10 months with an obvious monthly behavior as expected (shown in Fig. 1). The drift and aging rates are in agreement with the pre-launch test in 2009, which found a drift of 76.59 ns/s and aging rate of 2.89e-9 ns/s$^2$. The LRO clock has also been characterized bi-weekly by the GEODYN software (*Pavlis, D.E., et al.*, 2001) which applies relativistic corrections to the ground station clock and the satellite clock, accounting for gravitational potential and motion with respect to a solar system barycentric reference frame. The results are plotted in Fig. 2. Both the drift and aging rates estimated by GEODYN agree with those from LR analysis. The largest difference between the drift rates is about 0.066 ns/s due to relativistic effects.

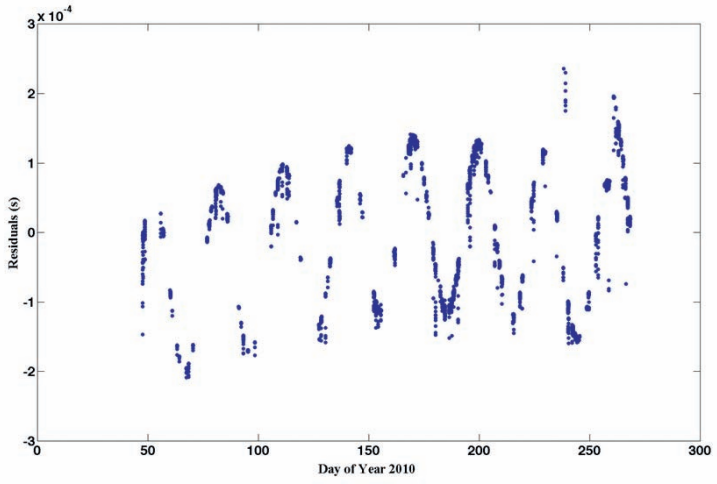


**Figure 1: Newtonian light time residuals with LRO clock drift and aging removed.**

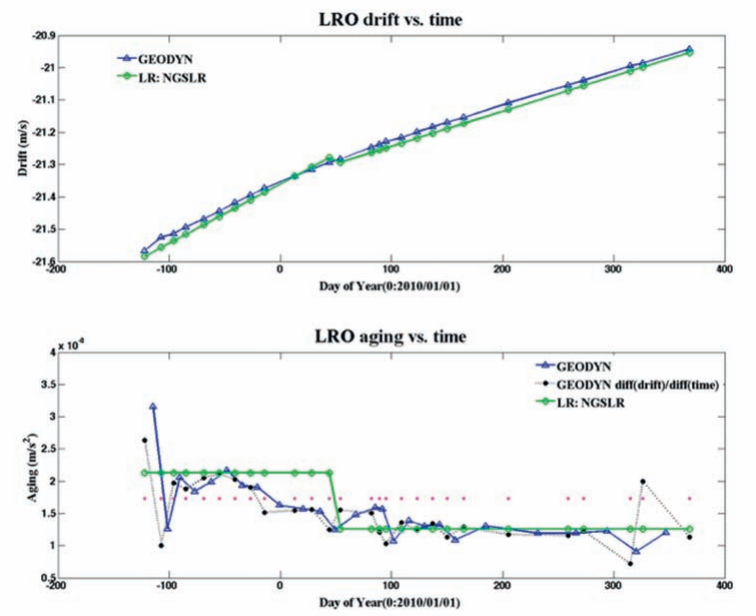


**Figure 2: Long-term LRO clock stability derived from LR data (green) and GEODYN estimation (blue), and the aging rate from pre-launch testing (magenta) plotted as a constant.**

The long-term behavior of the LRO clock can be monitored not only by the data from NGSLR, but also by the data from other participating ground stations. Using the spacecraft clock as the common reference, the difference among clocks at Earth-based stations can be obtained. The LRO clock drift rates derived from the LR data collected by NGSLR and six other stations are presented in Fig. 3 with respect to the NGSLR estimation. The slope of each station in Fig. 3 shows that the clocks at different ground stations have slightly different frequencies. Although this analysis provides information about the difference in long-term behavior among the ground station clocks, it doesn't give the relative time difference in a short time period. This short-term relative timing can be obtained by having more than one station range to LRO at the same time. Simultaneous ranging experiments have been performed successfully among two, three, and four participating stations from the same continent many times in the past two years, and simultaneous ranging shows the possibility to perform time transfer among ground stations.

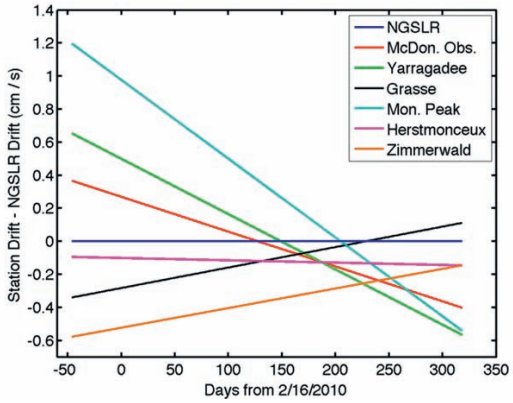


**Figure 3: LRO clock drift rate for different LR stations relative to NGSLR.**

# 3. Orbit Constraints

LR data were used in GEODYN to provide additional constraints to POD. *Mazarico, E., et al.*, 2011 relied on another tracking data type, the S-band radiometric tracking, which is supported by NASA's White Sand station and stations from the Universal Space Network (USN) for the LRO mission. The line-of-sight measurements taken with S-band tracking yielded a precision of 0.5 – 1 meter in the range observations, and two-way Doppler observations better than of 1 mm/s. Using GEODYN, we fit the tracking observations by integrating the LRO trajectory over 2-week time intervals. To achieve the

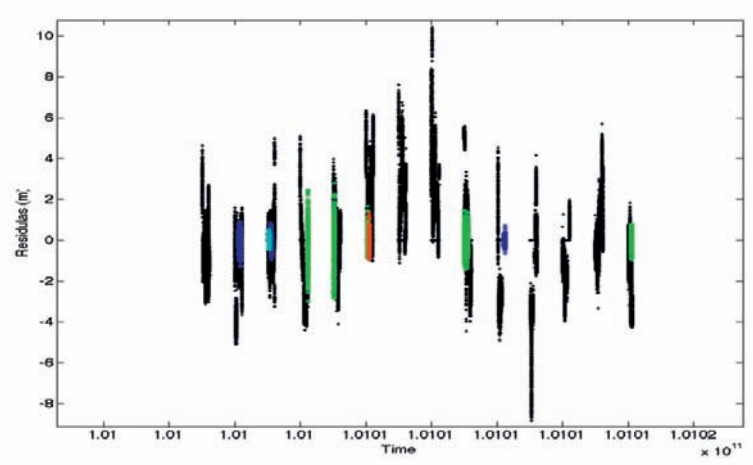


**Figure 4: Orbit residuals of S-band data (black) and LR data from Yarragadee (green), McDonald (blue), Hartebeesthoek (red), and Zimmerwald (cyan).**

best possible fit to the tracking observations, we adopted the latest lunar gravity field from LRO data, LLGM-1 (*Mazarico, E., et al.*, 2011), and iteratively adjusted several input parameters, such as timing and ranging biases. Weekly empirical constant along-track and once per revolution cross-track accelerations were also adjusted in the calculations. For comparison, the calculations were carried out, first, using radio-tracking data only and, second, with radio-tracking and LR data.

The orbit residuals resulting from a well-converged two-week arc, with S-band and LR data from 09/30/2010 to 10/13/2010, are shown in Fig. 4. The residuals of the LR passes are nominally less than 10 meters, while those of the S-band ranging passes are generally less than 15 meters. The RMS values of the arc by arc LRO orbit differences from the calculations are plotted in Fig. 5, covering the time period from the start of the LRO mission, 07/02/2009, to 01/31/2011. The along-track direction shows the largest orbit difference of up to 7 meters, while the difference along the radial direction is the smallest, no larger than 2 meters. The total orbit difference is less than 10 meters. In addition, only 10% to 15% of the data used in the orbit determination process is contributed by LR. Such a low percentage might weaken the constraints of the LR constraints on the orbit, but optimal data weighting could mitigate this issue. The POD results with LR data is are expected to be further improved by better calibrating the ground and LRO clock using other telemetry data, such as temperature.

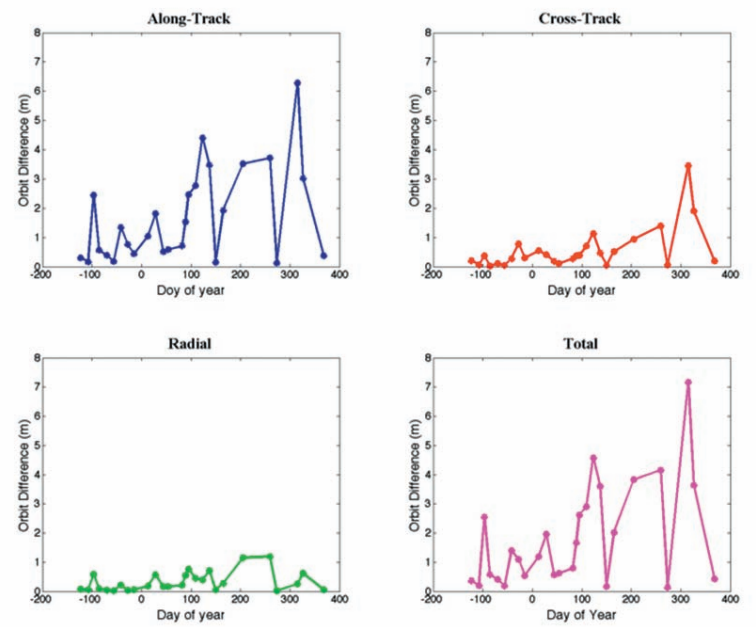


**Figure 5: Orbit difference between GEODYN calculations with and without LR data in three directions, along track (blue), cross track (red), radial (green), as well as the total orbit difference (magenta).**

# 4. Summary

The one-way LR experiment has been performing daily from July, 2009 to the present with contributions from NGSLR and nine other participating ground stations from the ILRS network. LR proved its ability to obtain time information from the LRO clock oscillator accurate to 0.25 ms over ten months, and showed the possibility for future time transfer between a ground station and a satellite as well as among different ground stations. In addition to timing determination, LR data were also used to form constraints on the LRO orbit determination calculations. Meter-level changes were observed in orbit solutions after adding LR data to S-band tracking data in the GEODYN analysis. Further calculations will be carried out to examine the quality of the new orbits due to the contribution of LR observations.

## References

*Chin, G., et al.,* 2007: (Lunar Reconnaissance Orbiter overview: The instrument suite and mission) Space Sci. Rev. 129, 209-241.

*Zuber, M., et al.,* 2010: (The Lunar Reconnaissance Orbiter Laser Ranging Investigation) Space Sci. Rev. 150, 63-80.

*Smith, D. E., et al.,* 2009: (The Lunar Orbiter Laser Altimeter (LOLA) investigation on the Lunar Reconnaissance Orbiter (LRO) mission) Space Sci. Rev. 129, 391-419.

*Pavlis, D.E., et al.,* 2001: (GEODYN Operations Manuals) Raytheon ITTS Contractor Report, Lanham, MD.

*McGarry, J., et al.,* 2011: (The First ILRS Transponder Laser Ranging Mission) this volume.

*McGarry, J., et al.,* 2011b: (Laser Ranging to NASA's Lunar Reconnaissance Orbiter (LRO): Ranging Data Results) this volumn.

*Mazarico, E., et al.,* 2011: (Orbit determination of the Lunar Reconnaissance Orbiter) Journal of Geodesy, in press, doi: 10.1007/s00190-011-0509-4.

## Correspondence

Dandan Mao
dmao@sigmaspace.com
NASA Goddard Space Flight Center, Building 33, Room F321B
8800 Greenbelt Rd., Greenbelt, MD, 20771 USA

# Simulation of Two-Way Laser Transponder Links: The Wettzell Experience

*K. U.Schreiber[1,2], P. Lauber[2], A. Schlicht[2], I. Prochazka[3], J. Eckl[1], G. Herold[1], H. Michaelis[4]*

ABSTRACT

Satellite Laser Ranging (SLR) is a two-way measurement technique where the space segment is made from passive cube corners. The advantage is a simple to handle, straightforward failsafe payload design. All the complexity of the measurement process remains on the ground, where the hardware is accessible. The disadvantage is the comparatively large weight the reflector array adds to the spacecraft and the high overall signal loss in the measurement process. In addition to this many satellites do not provide the required space on the surface to fit an array of retro reflectors in. For ranges much in excess of the Earth – Moon distance only active transponders provide a reasonable link margin. Simulating the performance of active transponders and investigating the properties of such devices under real world scenarios is difficult in the laboratory, because of the unpredictable nature of all the involved processes among them the signal attenuation in the atmosphere. By operating two independent ranging systems side by side on the ground a full test of all aspects of the one-way ranging application becomes feasible.

## 1. Introduction

Transponders offer the opportunity to extend the maximum observable distance for laser ranging applications from the Earth orbit to interplanetary distances [1,2]. This enormous increase in the covered range requires higher complexity of the space segment. While SLR provides the great advantage, that all the instrumentation with the exception of an array of cube corners is concentrated on the ground within reach for upgrades and maintenance, the disadvantage is the rapidly decreasing link margin, which falls off with $1/r^4$. This limits the application of SLR to distances up to the lunar orbit and the latter already requires well-equipped stations in preferred locations at high altitudes and low latitudes. Instead of a two-way distance coverage transponders have to traverse the 1-way range only. As a result of this fact the signal loss scales with $1/r^2$ only. Another important drawback of 1-way ranging is the requirement for tight clock synchronization between the two timescales on each end of the range vector [1].

Because of the inherent complexity of the space segment, 1-way ranging system had little relevance in space exploration so far. Ranging to the Lunar Reconnaissance Orbiter (LRO) is the only example. Since LRO carried a laser altimeter anyway, the payload was already available to serve two purposes at the same time. In fact SLR is used on LRO to provide improvements for orbit determination of the satellite. Future space missions to the outer planets with high-resolution cameras, will require a much higher data transmission bandwidth than current missions can provide and this will make rf-transmitters too inefficient. It is foreseeable that optical data links will become more and more necessary so that a combination of laser communication and reciprocal 1-way ranging may develop into a viable future technology.

It is difficult in general to do the first steps of exploiting this technology, because it is expensive to place such transponder devices as a payload to space exploration programs and to evaluate their properties in real world experiments. However, if two independent ranging systems are available in close proximity, many aspects for interplanetary 1-way ranging are accessible for a realistic proof of concept as enough satellites with cube corners are available to bend the ranging path back to the observatory on Earth.

[1] Bundesamt für Kartographie und Geodäsie, GO- Wettzell, 93444 Bad Kötzting, Germany

[2] Forschungseinrichtung Satellitengeodaesie, Technische Universitaet Muenchen, 80333 München, Germany

[3] Czech Technical University in Prague, 16627 Prague, Czech Republic

[4] Deutsches Zentrum für Luft- und Raumfahrt, Institut für Planetenforschung, Berlin, Germany

# 2. Transponder Concept Study

We have built an independent ranging system by using a small frequency doubled Nd:YAG laser of 20 mJ energy on the second harmonic, a pulse-width of ≈ 5 ns and 20 Hz repetition rate, manufactured by Quantel. The beam was expanded to 3 cm in diameter and collimated with the help of an external target at 200 m distance. A small Maksutov type 10 cm diameter aperture astronomical telescope was used as a receiver unit. The telescope was equipped with a variable field of view, a 10 nm wide spectral filter and a SPAD avalanche photo diode for signal detection. All components were mounted on a breadboard, which in turn was placed on top of the SLR telescope of the Wettzell Laser Ranging System (WLRS). Figure 1 shows the experimental setup, after both systems were aligned to point into the same direction, with the help of a landmark about 5 km away. Apart from laser and detector, the auxiliary system was also using a dedicated event timing system.

**Figure 1: The auxiliary ranging system on top of the telescope of the WLRS.**

A realistic simulation of the entire ranging system is possible, when both systems range independently to a satellite target, using the retro reflectors of the satellite as a mirror folding the signal path of the "ground terminal" (WLRS) back to the transponder module. The relationship for the equivalent "deep space distance" from such a two-system folded beampath approach was investigated in [3] and resulted in the transponder simulation equation:

$$r_t = r_s \sqrt{\frac{4p}{s} \frac{1}{T^{\sec\Theta}}} \quad ,$$

where $r_t$ is the equivalent transponder distance, $r_s$ the distance to the satellite used for the experiment, $\sigma$ the effective laser cross-section of the satellite and T the transmission of the atmosphere, depending on the zenith distance $\theta$.

**Table 1: Link budget for different system configurations and targets**

| Configuration | $n_{ph}$ AJISAI | $n_{ph}$ ERS | $n_{ph}$ LAGEOS |
|---|---|---|---|
| WLRS – Transp. | 4.5k | 1.5k | 10 |
| Transp. – WLRS | 36.8k | 12.3k | 85 |
| WLRS – WLRS | 830k | 275k | 1.9k |
| Transp. – Transp. | 816 | 272 | 1.9 |

Solving the laser link equation for some prominent satellites provides a good estimate for the laser link from one system to the other and vice versa as well as the ranging link for each ranging system. Table 1 gives an overview.

For several satellites with different laser cross-section and different orbit heights ranging in transponder mode has been carried out successfully. Figure 2 shows an example of simultaneous transponder daylight ranging to Beacon C. Both systems were working asynchronously on a different repetition rate. A fuller account of this experiment is given in [4].

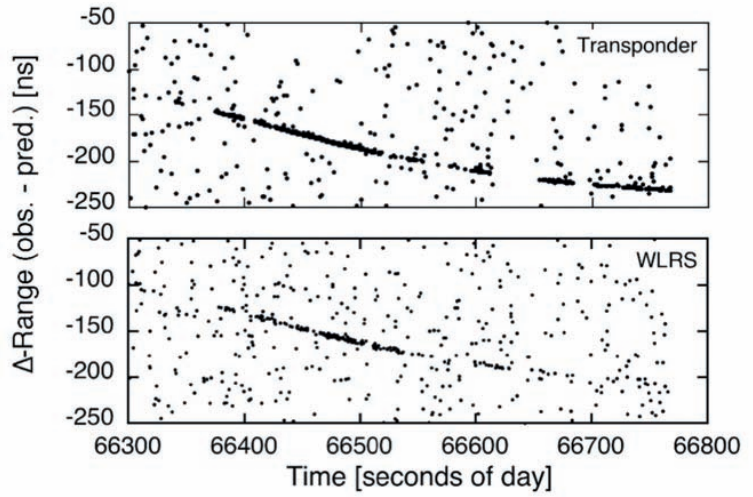


**Figure 2: Simultaneous observation of a Beacon C passage**

# 3. Laser Time Transfer Study

The feasibility of optical time transfer by laser link has been shown with the T2L2 experiment on Jason 2 [5]. For the Atomic Clock Ensemble in Space (ACES) a higher accuracy of the time transfer can be expected because of the better timing reference on the International Space Station. Since the ACES clocks will be compared with various ground stations via a two-way microwave link, the optical laser link uses the same timing hardware, which simplifies the space segment. Therefore it was desirable to study the behavior of the complete one-way laser link, including the timing device of the space segment [6]. The laser path was folded back to the SLR station as in the transponder case. Then the receive signal path was split up in two branches. The major signal path recorded the satellite echo with the WLRS timing device and a MCP photomultiplier. The other much weaker signal was used to detect laser return signal on the microwave link timer with a SPAD diode. Figure 3 shows the sketch of the experimental set up.

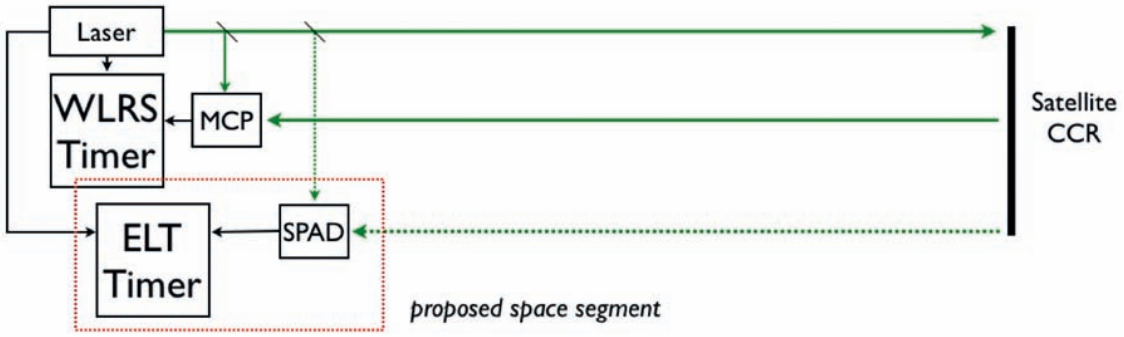


**Figure 3: Sketch of the timer comparison at the WLRS. The hardware components inside the dashed red box belong to the space segment of the ELT experiment.**

The beamsplitter was chosen such, that 90% of all the return signal was delivered to the MCP. Only 10% of the receive signal was available for the SPAD in order to limit the operation to the single photon mode. An Ajisai path with good signal coverage was chosen to evaluate the characteristics of the two independent timing devices in a time deviation plot. Figure 4 shows the corresponding TDEV. A fuller discussion of the ELT experiment can be found in [6]. Both detectors (MCP – gray and SPAD – black line in fig. 4) and the respective timing devices provide comparable data quality.

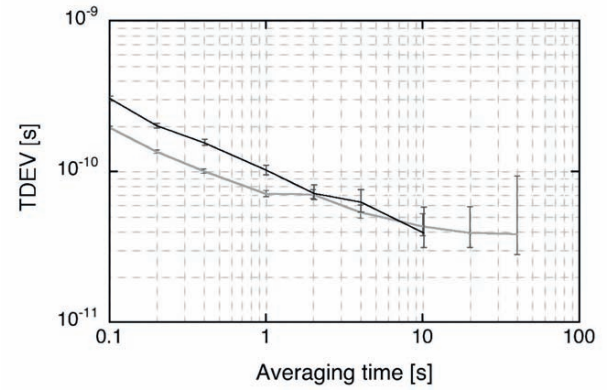


**Figure 4: TDEV measurements of the WLRS ranging stability obtained from measurements of a satellite pass of Ajisai using simultaneously recorded observations from the MCP and SPAD detector.**

# 4. Conclusion

Transponder and special missions like ELT require active hardware (detection, timing and transmission) as a payload on the spacecraft instead of passive cube corner arrays. In order to investigate specific experimental properties of active satellite terminals it is possible for most of the functions to do a thorough simulation, which is testing the entire ranging chain, including the contribution of the atmosphere. By folding back the ranging path to the observatory, both end terminals of the ranging experiment under test are accessible. The modular design of the WLRS is supporting such efforts additionally.

## Acknowledgements

The authors acknowledge the support of ASTRIUM and the assistance of the WLRS crew.

## References

[1] *Degnan, J. J.*, Asynchronous laser transponders for precise interplanetary ranging and time transfer, 2002: Journal of Geodynamics, 34, 551–594

[2] *Yoshino, T., Kunimori, H., Amagai, J., Schreiber, U., Kawano, N., Kondo, T., Schlüter, W., Degnan, J.*, 1999: Lunar Laser Ranging By Optical Transponder Collocated VLBI Radio Sources On The Moon; Proceedings of the SPIE, Vol. 3865, 20 – 26, doi:10.1117/12.373027

[3] *Degnan, J. J.*, 2007: Simulating Interplanetary Transponder and Laser Communications Experiments Via Dual Station Ranging To SLR Satellites; Proceedings of the 16th International Workshop on Laser Ranging ...

[4] *Schreiber, K. U., Hiener, M., Holzapfel, B., Michaelis, H., Brandl, N., Haufe, K.-H., Lauber, P., Neidhardt, A.*, 2009, "Altimetry and transponder ground simulation experiment," Planetary and Space Science, 57, pp. 1485–1490, doi:10.1016/j.pss.2009.07.016

[5] *Samain, E., Exertier, P., Guillemot, P., Pierron, F., Albanese, D., Paris, J., Torre, J-M., Petitbon,I. and Leon, S.*, 2009 "Time transfer by laser link T2L2 first results," Frequency Control Symposium, 2009 Joint with the 22nd European Frequency and Time forum. IEEE International, pp. 194–198, doi: 10.1109/FREQ.2009.5168168

[6] *Schreiber, K. U., Prochazka, I., Lauber, P., Hugentobler, U., Schäfer, W., Cacciapuoti, L. and Nasca, R.*, 2010, "Ground-based demonstration of the European Laser Timing (ELT) experiment," Ultrasonics, Ferroelectrics and Frequency Control, IEEE Transactions on, vol. 57, no. 3, pp. 728–737, doi: 10.1109/TUFFC.2010.1471

## Correspondence

K. Ulrich Schreiber

Bundesamt für Kartographie und Geodäsie
GO- Wettzell
93444 Bad Kötzting
Germany

Schreiber@fs.wettzell.de

# The European Laser Timing Experiment and Data Center

*Anja Schlicht, Ulrich Schreiber, Ivan Prochazka, Luigi Cacciapuoti*

ABSTRACT
Atomic Clock Ensemble in Space (ACES) is an ESA fundamental physics mission, which will operate atomic clocks in the microgravity environment of the International Space Station. The on-board timescale will be distributed to Earth via a microwave link (MWL) and via a pulsed optical link, the European Laser Timing (ELT) Experiment. These two time and frequency comparison methods complement each other. The optical link is a combination of one-way and two-way laser ranging and will be carried out by the SLR stations of the ILRS.

## 1. Introduction

Atomic Clock Ensemble in Space (ACES) will be ready for launch in 2014. ACES is an ESA mission in fundamental physics, which will establish a very precise time scale in space [Cacciapuoti 2009]. The basis of this time scale is an active hydrogen maser for short and medium-term stability and a laser-cooled caesium clock for long-term stability and accuracy. A frequency comparison and distribution package (FCDP) ensures the on-board comparison of the two clocks and distributes the clock signal to a microwave link (MWL), which finally transfers the ACES time scale to Earth.

Connected to this mission is a secondary way for time transfer, the European Laser Timing experiment (ELT). It uses a combination of one-way and two-way laser ranging to compare the ACES clocks with ground clocks at SLR stations. The ACES payload will carry a retroreflector array, a SPAD detector and an event timer to time tag laser pulses in the ACES time scale. The ELT experiment will show its capabilities in the accuracy of the time transfer between space and ground and in synchronising ground clocks to better than with the MWL. Optical ranging can therefore be used to calibrate the MWL. On a ground-based experiment the capability of an ELT like time transfer method was demonstrated [Schreiber et al. 2010]. Laser ranging will be performed by the satellite laser ranging (SLR) community. So the support of the International Laser Ranging Service (ILRS) is needed.

The ELT-data centre (ELT-DC) has the responsibility to provide the information needed by the SLR stations to track the ACES module, collect the two-way ranging events from the stations and the one-way ranging data from ACES, to combine these data to defined products, and to send raw data and products to the ACES USOC for archiving. As sole interface between ESA and the ILRS the ELT-DC will organize common view campaigns, build up a communication platform, and provide special ranging software or even organise hardware for the SLR stations.

## 2. ACES objectives

ACES will operate a new generation of atomic clocks in the microgravity environment of the International Space Station. Two clocks, a primary frequency standard based on laser cooled Cs atoms, called PHARAO and an active hydrogen maser SHM, will be coupled to generate the precise ACES time scale (see figure 1).

The ACES mission objectives are both technological and scientific [Cacciapuoti 2009]. ACES will perform laser cooling experiments in a microgravity environment, characterizing the PHARAO clock using cold atoms to a stability better than $10^{-13}\ t^{-1/2}$ for up to 10 days and to an accuracy better than $3{\cdot}10^{-16}$. The Allan deviation of SHM exceeds the one of PHARAO over short and medium term time intervals (see figure 1). The MWL will allow a comparison of frequencies in space and on ground up to 0.4 ps over an ISS pass (300 s) and 8 ps to 25 ps depending on integration time from 1 to 10 days. Common view comparison of ground clocks should be better than 1 ps and non-common view with $10^{-13} \cdot t^{-1/2}$. The MWL will allow ground clocks synchronisation with an uncertainty of 100 ps. In addition,, ACES will contribute to International Atomic Time Scale (TAI) .

In the fundamental physics domain, ACES will test general relativity to high accuracy. In particular, it will perform a precision measurement of the gravitational red-shift, it will search for time variations of fundamental physical constants, and test the Local Lorentz Invariance principle by verifying isotropy and constancy of the light velocity.

# 3. ELT principle

The principle of time transfer via a pulsed optical link is shown in figure 2. Short laser pulses fired towards ACES by a laser ranging station will be time tagged with respect to the ground time scale ($t_{start}$). Once detected in space they are time tagged in the ACES time scale ($t_{stop1}$). The returned signal from the retroreflector to the SLR station will although be registered in the ground time scale ($t_{stop2}$). So the ELT experiment is a coupled one-way and two-way laser ranging method.

For each laser pulse the offset between the ground and the space clock is the difference between the time a ground observer expects the laser pulse to be at the ISS in ground time scale and the time $t_{stop1}$ as it was registered at the ACES module. The correction, that have to be taken into account are due to short term fluctuations in the atmosphere, geometry (the laser reflecting point does not coincide with the detection point) and relativistic effects.

$$\tau_{offset} = \frac{t_{stop2} - t_{start}}{2} - t_{stop1} + t_{relativity} + t_{atmosphere} + t_{geometry}$$

The ELT payload consists of a retroreflector array, a SPAD detector [Procházka 2010] and an event timer. The coupling to ACES time scale is via the microwave link, in the way that the MWL and ELT share the same timing information. The gating of the SPAD detector is locked to the 10 pps signal (100 pps in discussion) on ACES time scale and is expected to work in single photon mode.

# 4. ELT objectives

Space to ground comparison of clocks via ELT has similar long term stability as the MWL, about 7 ps at 10 days delay time. The short term stabioity is with 4 ps at one pass (300 s) about 10 times worse than MWL. On the contrary, ELT accuracy for time transfer experiments is better than 50 ps. The same accuracy is expected for the synchronisation of ground clocks.

The advantages of the MWL are a high availability due to the fact that it can be operated easily and at all weather conditions. ELT on the other hand is a single shot method and allows accurate time tagging, therefore it can be used to calibrate the MWL. The advantage of an optical wavelength is the low dispersion in the atmosphere.

In the ACES project three time and frequency transfer methods can be compared: MWL, ELT and via GNSS network. Due to the different wavelength that are used the signals are affected in different ways by the atmosphere. By direct comparison of microwave and optical ranges the effect of the troposphere can be investigated. Differences in mapping functions and asymmetries can be determined. The influence of the ionosphere on the propagation delay of the microwave signal is eliminated by the use of two different microwave frequencies.

# 5. ELT data centre

The data streams of the ACES ground segment all end up at the ACES USOC. There the telemetry data from the payload is collocated via the ISS NASA and the Columbus control centre. The MWL ground terminals will be remotely controlled and the data will be collected by the ACES USOC. The data from the SLR stations will be sent to the EUROLAS data centre and further transmitted to ACES USOC. The ELT data centre (ELT-DC) as sole interface to ACES USOC is integrated in EDC. So the predictions, fullrate, and normal point data can take the routine way except safety issues.

The ELT-DC has two different functions: it is a communication centre and a scientific mission centre. As a mission centre it has the responsibilities to provide the SLR stations with predictions, collect SLR data, define and generate products, support the SLR stations with software and if possible organize hardware, monitor the space instruments and make a calibration campaign. A quicklook tool will be established to warn the SLR stations not working in single photon mode. As a communication centre it is a network interface between ESA, ILRS, data user, and the fundamental physics community. It will establish a web site and publish a bulletin.

# 6. SLR station participation prerequisites

Stations participating in the ELT experiment should have an ability to control the laser firing time to within 100 ns to the proposed opening of the detector gate and the ability to maintain desired signal photon flux density at the ISS orbit to ensure the single photon mode of the onboard detector. Simultaneously, the ground station must be capable to get SLR data of the ISS.

The other key hardware needed, is a precise local oscillator with frequency stability comparable to the ACES time scale – Hydrogen maser..

If the participating station is interested in a quick response the fullrate data with picosecond resolution of the start event should be sent as soon as possible, latest one hour after the pass, to the SLR data centres. The ISS accommodating the ACES module is a cantilevered structure orbiting in 350 km height, so the station participating to ELT should be able to track low orbiting satellites and handle orbit predictions every 90 min. For safety reasons a proper handling of the go/no-go flag must be demonstrated.

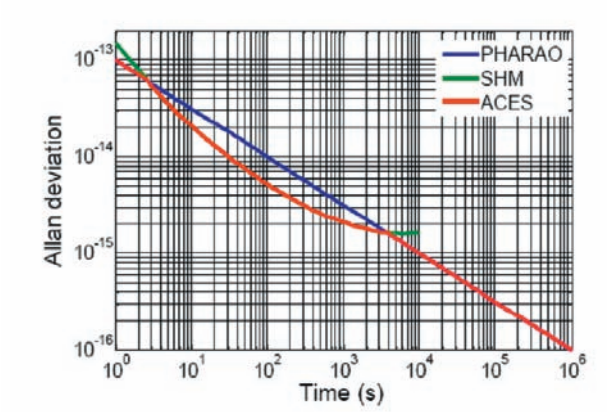


**Figure 1: (Allan deviation of PHARAO clock, blue, SHM, green, and in red the best combination for the ACES time scale realized with two feedback loops)**

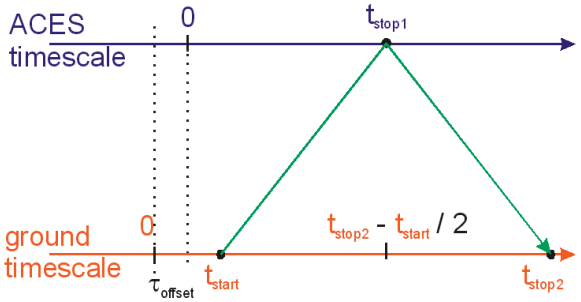


**Figure 2: (Principle of combined one-way and two-way laser ranging.)**

## References

*Cacciapuoti, L., Salomon, Ch.,* 2009: (Space clocks and fundamental tests: The ACES experiment) Eur. Phys. J. special Topics 172, 57-68, DOI 10.1140/epjst/e2009-01041-7.

*Procházka, I., Kodet,J., Blazej, J., Schreiber, U., Cacciapuoti, L.,* 2010: (Development of the European Laser Timing instrumentation for the ACES time transfer using laser pulses) Proceeding of the EFTF, Noordwijk, The Netherlands.

*Schreiber, U., Procházka, I., Lauber, P., Hugentobler, U., Schäfer, W., Cacciapouti, L., Nasca, R.,* 2010: (Ground-based Demonstration of the European Laser Timing (ELT) Experiment) IEEE Transactions on Ultrasonics Ferroelectrics and Frequency Control, 57 (3), 728-737.

## Correspondence

Anja Schlicht
FESG
Technische Universität München
Arcisstr. 21
80333 München

schlicht@bv.tum.de

# Session 14:
# Lunar Laser Ranging

# Simulation of optical response for next-generation single-reflector LLR targets

*Toshimichi Otsubo[1], Hiroo Kunimori[2], Hirotomo Noda, Hideo Hanada, and Hiroshi Araki[3]*

ABSTRACT
Optical response is numerically simulated for lunar laser ranging (LLR) targets in the future. The optical response of large-size, single-reflector arrays can be maximized by the proper choice of dihedral angle offsets. Since the velocity aberration in LLR does not spread symmetrically in the two-dimensional velocity field, we have found that an asymmetric combination of dihedral angle offsets should efficiently illuminate the terrestrial station where the laser pulse is transmitted.

## 1. Introduction

There are several research groups who envisage the first LLR target in 40 years since the Apollo-Lunakhod era. A 10-cm-diameter uncoated prism retroreflector has been designed and tested by Currie et al. (2011). A preliminary optical simulation has been demonstrated by Otsubo et al. (2010) demonstrated that suggested the velocity aberration should be taken into account for a large-size retroreflector. The primary advantage of the concept of the single, large-size retroreflector system is to ultimately minimize the so-called target signature effect which makes measurement less precise due to the multiple reflection points and the resultant pulse spreading.

In this paper, we focus on large-size, hollow-type corner cube reflectors. Assuming that the manufacturing precision and the environmental stability are satisfied, a hollow-type reflector is, in general, more efficient choice than a prism reflector in terms of weight.

## 2. Velocity aberration in LLR

Velocity aberration should be taken into account when we design a corner cube reflector for satellite/lunar laser ranging. Because of the fast motion of an artificial satellite (up to $>$ 7 km/sec), the velocity aberration reaches 50 microradians for low-earth-orbit satellites. On the other hands, it amounts merely to 3.5 to 7 microradians for lunar laser ranging (Otsubo et al., 2010), which is resulted from the orbital revolution speed of the Moon ($\sim$ 1 km/sec) and also from the Earth rotation speed ($<$ 0.5 km/sec).

From a viewpoint of a reflector placed on the Moon, its two-dimensional distribution is not uniform because the Earth is always moving more or less toward a fixed direction (opposite to the relative velocity of the Moon observed from the Earth). Let us define the target-fixed coordinate system as the +X direction pointing toward the Mean Earth, and the +Z direction pointing the rotational axis of the Moon, and the Y axis composing a right-hand system. The two-dimensional statistical distribution is calculated in this system as shown in Fig. 1.

[1] Hitotsubashi Univ, Japan
[2] NICT, Japan
[3] NAOJ, Japan

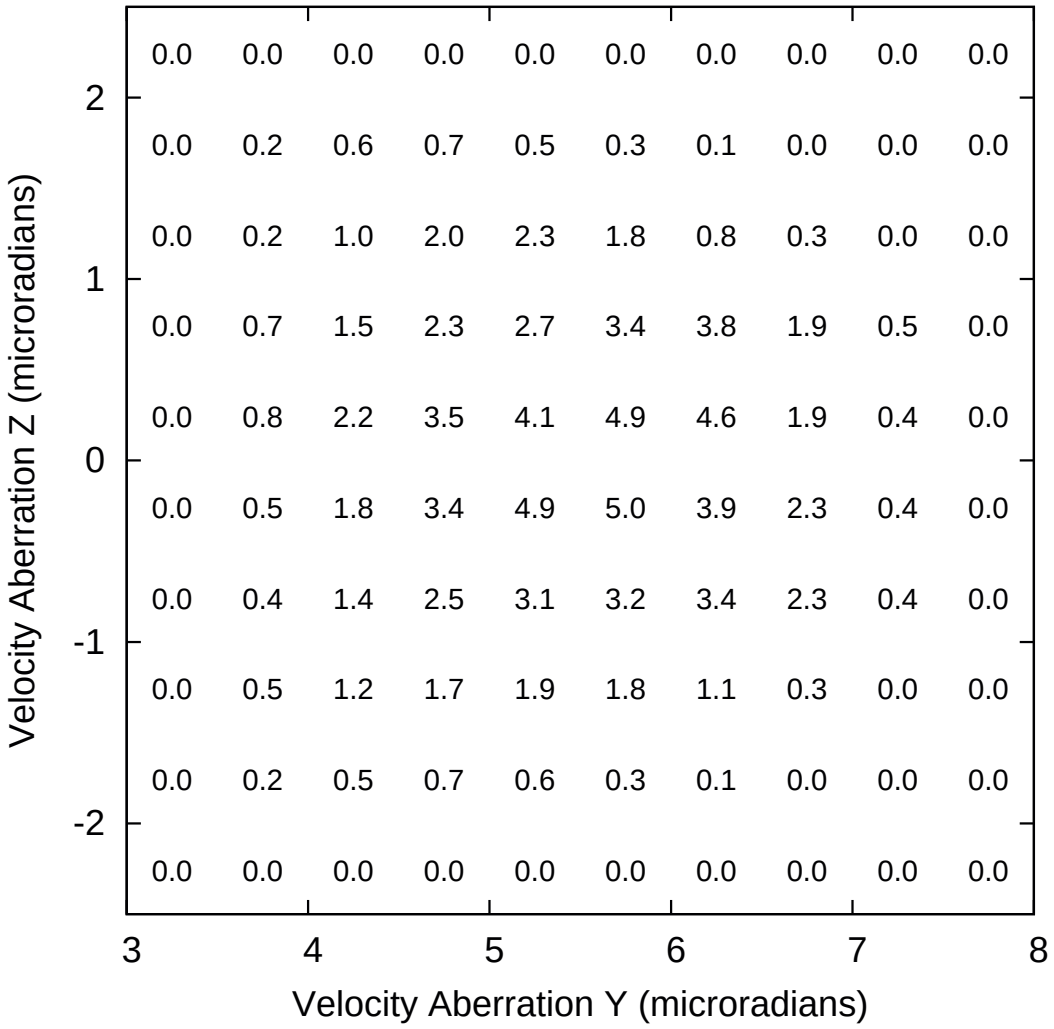


**Figure 1: Probability distribution of the velocity aberration vector in the simulated 18.6 years span of lunar laser ranging. The probability to fall in a 0.5 microrad x 0.5 microrad bin is given in percent.**

The distribution is obviously deflected to +Y direction by 5 to 6 microradians, and in other words, it has a very strong azimuthal convergence. The distribution in Z components is limited within -2 to +2 microradians. A lunar target is required to efficiently illuminate this region.

# 3. Simulated far-field diffraction pattern

A hollow-type corner cube reflector with zero dihedral angle offsets will produce a far-field diffraction pattern similar to the Airy disk. The size of the disk is inversely proportional to the diameter of the reflector. If the reflector size is small enough like Apollo's 38 mm, the diffraction pattern sufficiently cover the velocity aberration computed in the previous section. However, if we assume a reflector with 200 mm diameter, the optical energy is too concentrated around the origin of the Y-Z frame and it does not fall in the wanted velocity aberration region (Fig. 2 (a)).

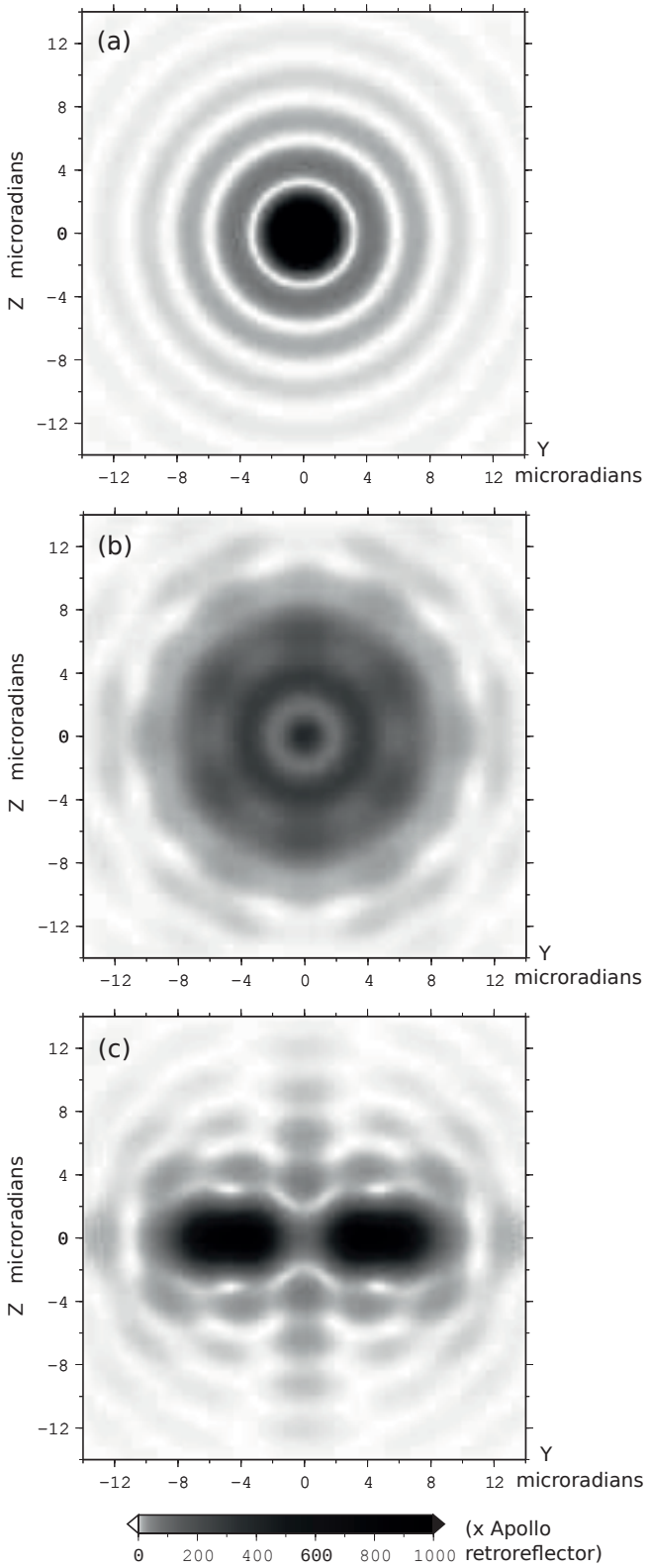


**Figure 2: Far-field diffraction patterns simulated for a 200-mm diameter, circular aperture, hollow-type retroreflector when a green 532 nm laser is assumed for the incident beam. The dihedral angles are set to all zero in the case (a), and all 0.35 arcseconds in the case (b). One dihedral angle is set to 0.65 arcseconds and the other two angles are set to zero in the case (c).**

Dihedral angle offsets are therefore required in such a case. Otsubo et al. (2010) found the best dihedral angle offsets at 0.35 arcseconds under the condition that the all the three dihedral angles are equal. The far-field diffration pattern is plotted in Fig. 2 (b). It indeed largely improves the optical energy, but it does not seem very efficient because the energy scatters toward any azimuthal directions.

We therefore attempt to increase the degree of freedom, by freeing three dihedral angle offsets. Through a number of numerical experiments, we find that the best combination is around at 0.65 arcseconds for one angle and 0.00 arcseconds for the other two angles. The far-field diffraction pattern in this case is given in Fig. 2 (c) where the azimuthal distribution is restricted toward the wanted region and the opposite region. The optical energy is further improved as clearly seen in the graph: 3 or 4 times of the case (b). Note that this result is preliminary since more numerical experiment is required for the precise determination of the best dihedral angle combination.

# 4. Conclusions and future studies

The velocity aberration in lunar laser ranging is deflected to +Y direction by 5 to 6 microradians. A numerical simulation study reveals that the asymmetric dihedral angle offset improves the optical budget by a factor of 3 or 4, compared to the previous study where the symmetric dihedral angle is assumed.

More detailed numerical simulation is required to aim at the precise optical design: for instance, the weight averaging procedure using incident angle and velocity aberration, the precise determination of the best dihedral angle offsets, the reflector size dependence, and so on.

## References

*Currie, D.G., S. Dell'Agnello, and G.O. Delle Monache*: Lunar Laser Ranging Retroreflector for the 21st Century, in these proceedings, 2011.

*Otsubo, T., H. Kunimori, H. Noda and H. Hanada*: Simulation of optical response of retroreflectors for future lunar laser ranging, Advances in Space Research, 45, 733-740, 2010.

## Correspondence

Toshimichi Otsubo
Hitotsubashi University
2-1 Naka, Kunitachi
186-8601 Japan

t.otsubo@r.hit-u.ac.jp

# Lunar Laser Ranging – recent activities at Institut für Erdmessung (IfE)

*Jürgen Müller[1,2], Franz Hofmann [1,2], Xing Fang [1], Liliane Biskupek [1]*

ABSTRACT

Lunar Laser Ranging (LLR) is carried out for 41 years to measure the distance between Earth and Moon with ever increasing precision. This paper gives an overview about the observation statistics and the recent developments in the LLR analysis at the Institut für Erdmessung (IfE), where the benefit from refined gravity field modelling and a more sophisticated weighting scheme were investigated. For mm accurate analysis, the complete gravity field up to degree and order 5 for the Moon and up to degree and order 4 for the Earth should be considered. A better combination of all LLR data was reached by applying a variance component estimation. The new determination of two relativistic parameters (equivalence principle parameter and time-variation of the gravitational constant) extended the upper limit for a possible violation of general relativity.

## 1. Introduction

The first retroreflector for LLR was deployed on the Moon by the Apollo 11 astronauts on July 21, 1969. Until 1973, four more reflectors were deployed by the Apollo 14 and 15 missions as well as by the soviet missions Luna 17 and 21 with their lunar rovers Lunokhod 1 and 2 (see Fig. 1 for the distribution of the reflectors on the lunar surface). For nearly 40 years, the Lunokhod 1 reflector could not be used for measurements due to the missing knowledge of its exact position on the Moon. It was re-discovered by the Lunar Reconnaissance Orbiter in April 2010 and was successfully tracked by the APOLLO observatory (Murphy et al., 2011). The Lunokhod 1 reflector is close to the lunar limb and therefore well suited for a better determination of lunar librations. The positions of the recent active LLR observatories as well as possible future stations are shown in Fig. 2. The Hawaiian LURE observatory performed LLR data from 1984 to 1990 and is not shown in Fig. 2.


**Fig. 1: Position of lunar retroreflectors**


**Fig. 2: Active (green arrows) and possible future (green/grey arrows) LLR observatories**

From 1970 to 2011, about 17000 normal points were collected. The percentage of measurements to each reflector is shown in Fig. 3, the statistics for the observatories in Fig. 4. The APOLLO observatory helps to obtain more data from the smaller reflectors (others than Apollo 15), due to its high signal to noise ratio for all observed reflectors. This leads to a more balanced measurement statistics as before. In addition, there are also few measurements from the observatories at Orroral, Wettzell and Matera, which are not displayed here.

[1] Institut für Erdmessung (IfE), Leibniz Universität Hannover, Schneiderberg 50, 30167 Hannover, Germany
[2] QUEST – Centre for Quantum Engineering and Space-Time Research, Leibniz Universität Hannover, Welfengarten 1, 30167 Hannover, Germany

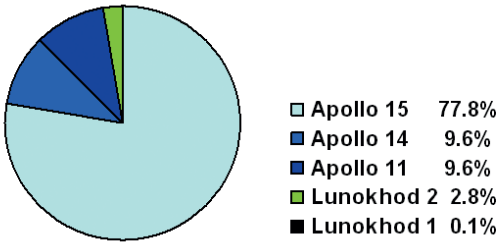


**Fig. 3: Measurement statistics of the reflectors**

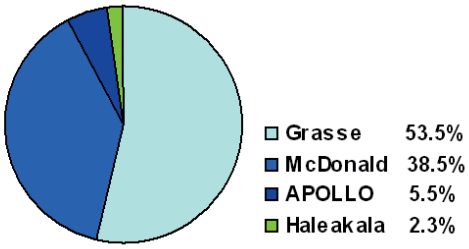


**Fig. 4: Measurement statistics of the observatories**

# 2. Improvement of IfE LLR analysis

## 2.1 Improvement of functional modelling

After implementing a new algorithm for atmospheric corrections of the light travel time (Mendes et al., 2002 and Mendes & Pavlis, 2004) and for the lunar interior (Williams et al., 2001), we turned the focus to the gravity field modelling of the Earth and the Moon, with the goal to determine the required spherical harmonic expansion for achieving mm accuracy in these model parts. The idea is to compare an ephemeris with different expansions of the gravity field with a highly accurate reference ephemeris. Goal was to identify when the difference between the two ephemerides falls below 1 mm.

Table 1 gives an overview about the already implemented gravity field modelling of Earth and Moon and their interactions, indicated by arrows. Possible extensions for the gravity field model are:

a) increase Earth's expansion interacting with the point mass Moon,
b) increase Moon's expansion interacting with point mass Earth,
c) increase both Earth's and Moon's expansion interacting with corresponding point masses of Moon and Earth,
d) add figure-figure coupling between Earth's degree 2 (complete) and Moon's degree 2 and 3 (complete) in the equations of translational motion,
e) add figure-figure coupling effects between Earth's degree 2 (complete) and Moon's degree 3 (complete) in the equations of rotational motion of the Moon.

In the following, the cases a) to c) are investigated in detail. The couplings to the sun are not discussed in this paper.

**Tab. 1: Implemented gravity field model for Earth and Moon**

| Equations of translational motion | Equations of rotational motion of the Moon |
|---|---|
| Earth, degree 2-4 zonal ←→ Moon, point mass | Earth, point mass → Moon, complete |
| Moon, complete up to degree 4 ←→ Earth, point mass | Earth, degree 2 complete → Moon, degree 2 complete |

The first step was the generation of a reference ephemeris for every case a) to c). Therefore the complete gravity field up to degree and order 10 for Earth (case a) and c)) and Moon (case b) and c)) was considered. For the Earth, we used the EGM2008 and for the Moon the LP165P gravity field models. The computation of the reference ephemeris is an iterative process (including the parameter estimation). The result of this iteration is a set of initial parameters (station and reflector coordinates, initial values for lunar orbit and rotation, some lunar potential coefficients, time travel biases for the observatories, lunar elasticity parameters and the product of the gravitational constant with the Earth and Moon mass) for following studies. In the last iteration, only the initial lunar orbit (position and velocity) and rotation are estimated and the final ephemeris computed.

The second step comprises the computation of the comparison ephemeris for the cases a) to c) with different gravity field expansions. In the iteration procedure, only the initial lunar orbit and rotation is estimated, all other parameters are fixed to the values of the corresponding reference ephemeris.

For the comparison of both ephemeris (from first and second step), computed over 80 years from 1979 to 2050, the distance between the geocenter and the Lunokhod 1 reflector $\Delta dL_{uno1}$ is used:

$$\Delta d_{\mathrm{Luno1}} = d_{\mathrm{Luno1\_comp}} - d_{\mathrm{Luno1\_ref}} \quad .$$

Figs. 5-8 illustrate the results for case a). Fig. 5 shows $\Delta d_{Luno1}$ using our old model. The differences are at the mm level and can be reduced by taking into account the complete degree 4 gravity field of Earth, see Fig. 6. The corresponding power spectra, Fig. 7 and Fig. 8, show the strong reduction of a daily part (Earth rotation) in the new result. The disadvantage of using Earth's non-zonal gravity field in the ephemeris computation is the increased computation time for the ephemeris integration, because it is now determined by the rotating Earth.

The result for the extended gravity field modelling of the Moon, case b), is shown in the Fig. 9 and Fig. 10. The difference $\Delta d_{Luno1}$ for our old model clearly exceeds the mm level, see Fig. 9. The remaining offset does not show a radial effect between the center of mass of Earth and Moon, but a rotational offset of the Moon. This behaviour is not clearly understood so far and needs further investigation. When taking into account the complete gravity field up to degree and order 5, $\Delta d_{Luno1}$ is below the mm limit, Fig. 10.

For the combined consideration of the extended Earth's and Moon's gravity field, case c), the results show nearly the same behavior as for case b), it is not shown here. The improved modelling of the lunar gravity field shows the biggest difference to the previous computation. The improved Earth's field reduces a daily effect at the 1 mm level only.

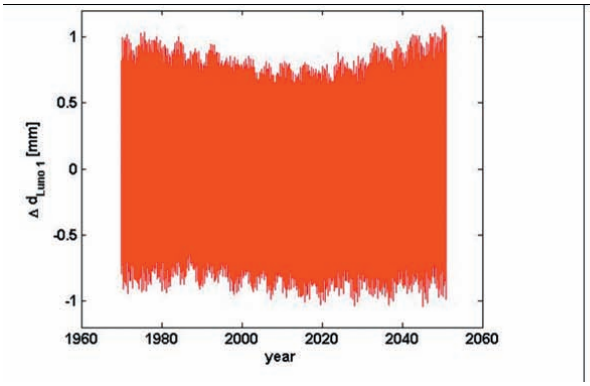


**Fig. 5: Case a) Lunokhod 1 distance from geocenter with zonal Earth field up to degree 4**

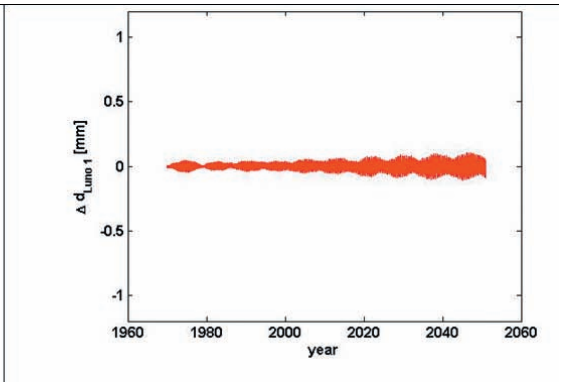


**Fig. 6: Case a) Lunokhod 1 distance from geocenter with complete Earth field up to degree 4**

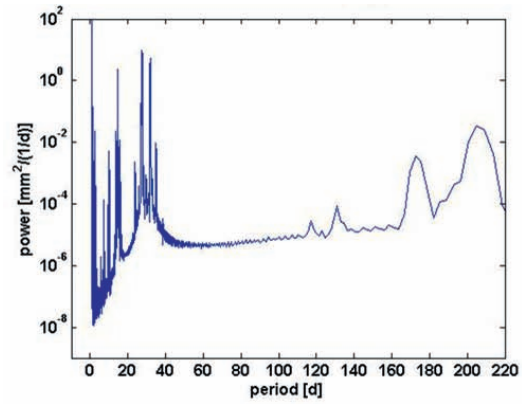


**Fig. 7: Case a) power spectrum to Fig. 5**

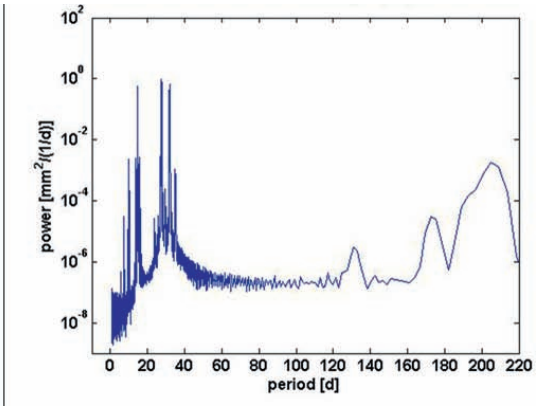


**Fig. 8: Case a) power spectrum to Fig. 6**

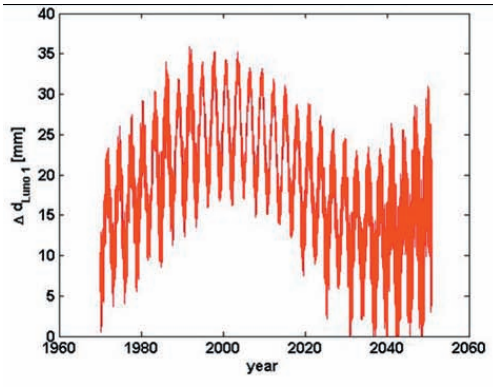


**Fig. 9: Case b) Lunokhod 1 distance from geocenter with complete lunar field up to degree 4**

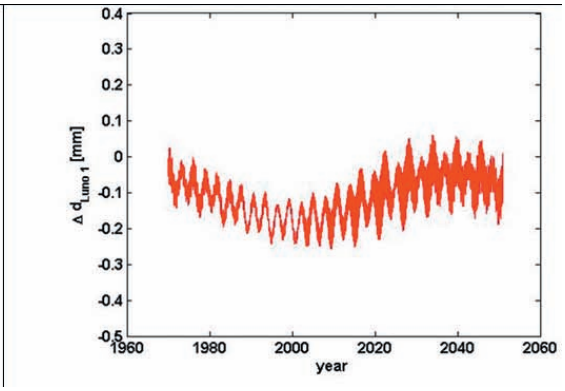


**Fig. 10: Case b) Lunokhod 1 distance from geocenter with complete lunar field up to degree 5**

## 2.2 Improvement of stochastic modelling

On the stochastic side of the analysis, a variance component estimation was implemented for fine tuning the weighting of the observation data. The effect on the annual averaged residuals is shown in Fig. 11. The standard solution (blue curve) denotes the result with the previous IfE weighting scheme which is based on modified error estimates of the normal points including station and time dependent corrections. The red curve shows the annual residuals with the data weighting computed from the given normal point accuracies (original error estimates) for the APOLLO (APO) station. The highly accurate APOLLO data of the past few years also affect the result in the previous years, they "deform" the solution. The red dotted curve shows the result with a variance component estimation (VCE) for APO station applied. It is close to the result with our standard weighting scheme. The best stochastic modelling is subject to further investigation.

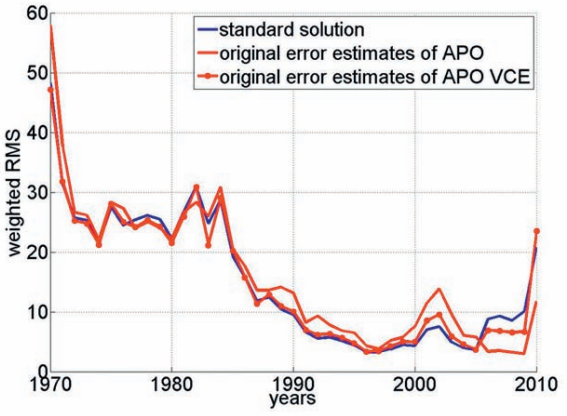


**Fig. 11: Effect of different weighting schemes for the APOLLO station represented as WRMS annual residuals**

# 3. Results - relativistic parameters

The long time series of highly accurate LLR measurements for lunar orbit determination, the large (compared to Earth based) dimension of the Earth-Moon "laboratory" and the astronomical size of Earth and Moon as test bodies make LLR an excellent tool for testing general relativity. Here, we present the results for two relativistic parameters (see also Hofmann et al., 2010). A possible variation of the gravitational constant $G$ was tested by implementing a time-variability of $G$. This gives

$$\dot{G} / G = (1 \pm 4) \times 10^{-13}\,\mathrm{yr}^{-1} \quad .$$

The Earth-Moon system can also be used for testing a violation of the Strong Equivalence Principle. A violation would lead to a polarization $\Delta r_{EM}$ of the lunar orbit towards the sun with the synodic angle $D$ and an amplitude of 12.8 m (Nordtvedt, 1995)

$$\Delta r_{EM} = 12.8\,\mathrm{m}\ \eta \cos D \ .$$

The Nordtvedt parameter η was determined in our parameter fit as

$$\eta = (1 \pm 5) \times 10^{-4} .$$

Both values do not show any significant deviation from their Einsteinian values ($\dot{G}/G = 0$, $\eta = 0$) and extend the upper limit for a possible violation of general relativity.

# 4. Conclusions

The ongoing LLR activities at IfE include work on an improved functional and stochastic modelling. We refined the modelling of the Earth's and Moon's gravity field and showed that the complete field up to degree and order 5 for the Moon is necessary for an accuracy below 1 mm. For the Earth, the old IfE model is very close to the mm level when the zonal field up to degree 4 is used. For sub-mm accuracy, the complete field up to degree and order 4 is needed. An improvement in the combination of the other LLR data with the new APOLLO data was reached by refined weighting based on variance component estimation. The estimation of two relativistic parameters, temporal variation of the gravitational constant and the Nordtvedt parameter for testing the equivalence principle, improve the upper limits for a possible violation of general relativity relative to previous IfE results by a factor of two. Future steps will include enhanced studies on lunar interior, Earth rotation and relativity.

## Acknowledgements

Current LLR data are collected, archived and distributed under the auspices of the International Laser Ranging Service (ILRS) (Pearlman et al., 2002). We acknowledge with thanks, that the more than 41 years of used LLR data has been obtained under the efforts of the personnel at the Observatiore de la Côte d'Azur in France, the LURE Observatory in Maui, Hawaii, the McDonald Observatory in Texas as well as the Apache Point Observatory in New Mexico. We would also like to thank the International Space Science Institute (ISSI) in Bern for supporting this research. This research was funded by the Centre for Quantum Engineering and Space-Time Research QUEST and the DFG, the German Research Foundation, within the research unit FOR584 "Earth rotation and global dynamic processes".

## References

*Hofmann, F., Müller, J., Biskupek, L.,* 2010: Lunar laser ranging test of the Nordtvedt parameter and a possible variation in the gravitational constant. A&A, 522, L5
*Mendes, V.B., Pavlis, E.C.,* 2004: High-accuracy zenith delay prediction at optical wavelengths. GRL, 31, L14602
*Mendes, V.B. et al.,* 2002: Improved mapping functions for atmospheric refraction correction in SLR. GRL, 29(10), 1414
*Murphy, T.W. et al.,* 2011: Laser Ranging to the Lost Lunokhod 1 Reflector. Icarus, 211, 1103-1108
*Nordtvedt, K.,* 1995: The relativistic orbit observables in lunar laser ranging. Icarus, 114, 51-62
*Pearlman, M.R., Degnan, J.J., Bosworth, J.M.,* 2002: The International Laser Ranging Service. Advances in Space Research, 30, 135-143, doi: 10.1016/S0273-1177(02)00277-6
*Williams, J.G. et al.,* 2001 : Lunar rotational dissipation in solid body and molten core. JGR, 106, 27933-27968

## Correspondence

Jürgen Müller
mueller@ife.uni-hannover.de

# Development of Pulse Detection IC for LIDAR on Planetary Lander

*Takahide MIZUNO, Hirokazu IKEDA, Kousuke KAWAHARA*

ABSTRACT

In recent years, LIDAR has been used in remote sensing systems, obstacle avoidance systems on planetary landers, rendezvous docking systems, and formation flight control systems. A wide dynamic range is necessary for LIDAR systems on planetary landers and in rendezvous docking systems. For example, a dynamic range of 60 dB was required for the receiving system used in the Hayabusa mission in order to measure distances between 50 m and 50 km. In addition, an obstacle detection and avoidance system of a planetary lander requires a ranging resolution of better than 10 cm. For planetary landers, ISAS/JAXA is developing a customized integrated circuit (IC) for LIDAR reception. This report introduces the design of the customized IC and reports the results of preliminary experiments evaluating the prototype, LIDARX03.

## 1. Introduction

In recent years, planetary exploration missions aiming to elucidate the origin of the solar system have been conducted, such as Hayabusa (Japan) [1], NEAR (USA), and Rosetta (Europe). Many of the explorers currently in operation or planned for observation of the moon and planets, such as SELENE, the Lunar Reconnaissance Orbiter, Messenger, Bepi-Colombo, and the Mars Global Surveyor, incorporate LIDAR as a critical navigation sensor for long-range measurements. The LIDAR system enables planetary explorers to measure distance from the target planet.

The receiving circuit of Hayabusa's LIDAR consists of discrete electric devices. In the present study, we aim to reduce the circuit area and shorten the development period, by using techniques for fabricating sub-micron analog integrated circuits (ICs) that were developed in the field of high-energy physics.[2] The proposed device also incorporates a circuit for timing detection and an interpolator. In addition, the proposed device must cover the wide signal dynamic range that is particular to planetary explorers. In the case of Hayabusa mission, the required ranging coverage of LIDAR was 50 m to 50 km. The distance from 50 m to 50 km corresponds to a dynamic range of 60 dB for the power of the incoming optical signal. The wide dynamic range is required not only an asteroid lander, but also required in the lunar lander SELENE2 mission.

In this paper, we discuss the required performance and functionality for LIDAR receiving circuits of planetary explorers. After this introduction, we present the design of a customized IC and report the current state of its development.

## 2. Required Specifications

We assume that the transmitting power (Pt) is 5 mJ, the wavelength of the laser is 1.064 um, the transmitted pulse width is 10 ns, the target reflectivity is 5%, the diameter of the receiving antenna is 100 mm, the system efficiency is 70%, and the distance from the target is 50 m. In this case, the incoming signal power is $6.87 \times 10^{-11}$ J[3]). The corresponding number of photons is $1.5 \times 10^{10}$. Under the conditions described above, the efficiency and the multiplication of the APD are 40% and 100, respectively. In the case of R=50 km, the incoming signal power becomes $6.87 \times 10^{-17}$ J ($1.5 \times 10^{4}$ photons). When the target distance changes from 50 m to 50 km, the incoming electrical charge changes from 2400 pC to 0.0024 pC. We are developing a customized IC that has a dynamic range of 60 dB for planetary explorers.

Since Hayabusa's LIDAR does not have a clock interpolator, the resolution of the ranging is decided by the clock of the 75-MHz digital counter. For this reason, its resolution was ±1 m. Scientific observations and navigation systems require improved resolution; however, improvements in the time resolution by adopting a higher frequency digital clock are not possible considering chip fabrication, screening tests, and the power consumption of the digital device. Then, in order to obtain higher resolutions a new device that employs a moderate-frequency clock, e.g. 20 MHz, together with a clock interpolator is raised as a candidate.

# 3. Design of Proposed Device

These procedures are fully conducted as a part of the in-house activity except for the third and fifth items. A photograph of the prototype bare IC chip referred to as LIDARX03 is shown in Figure 1. The procedure for fabrication is the Taiwan Semiconductor Manufacturing Company (TSMC) complementary metal-oxide semiconductor (CMOS) 0.35-um process that allows dependable manufacturing, with which we have considerable experience. The size of the bare chip is 3 x 3 $mm^2$. The package is a ceramic quad flat package (QFP) with a size of 14 x 14 $mm^2$ (80 pins). The following list is the development procedure:

Figure 2 shows the circuit structure of LIDARX03. LIDARX03 consists of a divider module, an integrator module, a timing detector module and a time-to-analog converter (TAC). The APD is located on an external test board and converts light signals to electrical charge. As mentioned above, there is a difference of about 60 dB between the signal levels of short-range and long-rang measurements.

The divider consists of a T-shaped circuit with a capacitor that is mounted on the outside of the device and divides a large quantity of electrical charge at short range into a suitable amount of charge. The dividing ratio of charge can be decided based on the ratio of internal and external capacitors. The combinations of external and internal capacitors are selectable with mechanical switches. Consequently, the device has five input channels through the various combinations of the dividers and the integrator. Therefore, the device has five steps of coarse adjustment for the gain. Each channel (CH0-CH4) has a gain range with a factor of 16, and the total dynamic range of the device reaches 60 dB ($16^5 \doteq 10^6$).

The integrator consists of a filter and amplifiers that can change the gain by changing the value of the feedback capacity. The feedback capacity can be changed with a 4-bit command. Using this function, the gain of the integrator can undergo fine adjustment. The compensation circuit of the pole/zero, PZC, is installed on the stage next to the integrator. The PZC circuit is to stablilize the DC level of the following leading/differential waves, and , hence, the influence of the input signal level on the detection timing is significantly mitigated.

The timing detector transforms the leading wave to a bipolar wave, which is referred to as a differential wave, and detects its zero-cross timing as the pulse detection timing. In order to prevent false detections caused by noise overlap on the differential wave, a threshold is set up for the leading wave; thus, only when the pulse height of the leading wave exceeds the threshold level that is set by external voltage, the HIT signal is generated at the zero-cross timing. The main functions of this device are its 60-dB dynamic range with the divider and the integrator and timing detection using the timing detector.

The TAC is activated by the HIT signal generated in the timing detector. A saw wave (about 4 mV/ns) begins to rise upon detection of the leading edge of the HIT signal. Then, the analog voltage of the saw wave is held at the timing of STOP signals synchronized with the digital clock and output the held voltage. The zero-cross point is estimated from the analog voltage of the TAC. In order to estimate the zero-cross timing, the inclination of the saw wave is highly important. However, the inclination has a non-negligible depencence on temperature, power-supply voltages and possibly drifts as a function of time. Therefore, the TAC produces an analog voltage twice. As a result of this function, the change in the inclination of the saw wave does not influence the estimation.

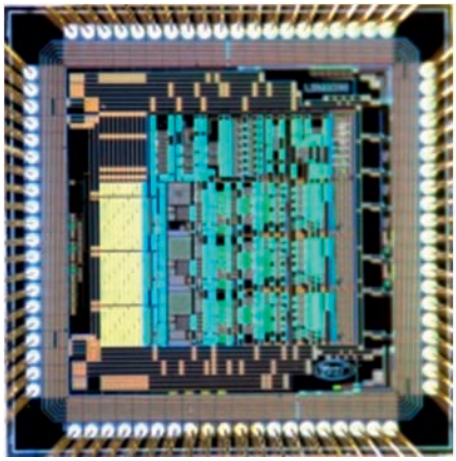

**Fig. 1: Bare chip of prototype IC (LIDARX03)**

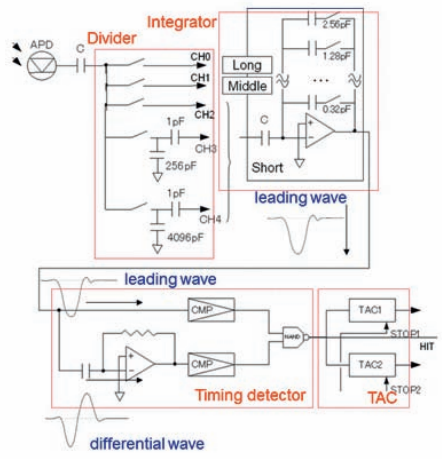


**Fig. 2: Circuit outline (LIDARX03)**

In the evaluation system, the clock of the digital controller is 15.625 MHz, and thus the interval time of STOP signals is 64 ns. Since the timing estimation uses analog voltage, the resolution of interpolation depends on the resolution and the accuracy of analog-to-digital converter (ADC) mounted on the test board.

This device has a test port (TP) in order to evaluate the internal circuit without an APD. The TP is directly connected to the integrator by an internally mounted capacitor. Thus, a voltage step can be substituted for the signal from the APD.

# 4. Results of Evaluation

Figure 3 shows typical output waveforms from LIDARX03. The top waveform is a bipolar wave that is transformed from a leading wave. The timing detector detects the zero-cross timing of this waveform and generates a HIT signal (second waveform). The saw wave from the TAC starts rising upon being triggered by the leading edge of the HIT signal. The amplitude of the saw wave is generated twice according to the timing of the digital clock following the HIT signal. These two analog values are output as TAC1 (third waveform) and TAC2 (forth waveform). The HIT timing is estimated with TAC1 and TAC2. Therefore, stability and repeatability are important for measuring TOF. The zero-cross timing of bipolar waves must be stable, because this is the origin of the HIT signal.

The main function of the proposed device is timing detection of light pulses in a 60-dB dynamic range at the input level. In order to evaluate this function, we measured the behavior of this device by changing the input electrical charge. The amount of input charge changed from 0.001 pC to 3000 pC. Figure 4 shows the input charge dependence of the detected pulse (HIT) timing and the signal amplitude. In this figure, marks show coarse adjustment of CH and line styles show fine adjustments of gains. CH0 is designed for a long-distance measurement, and CH4 is designed for a short-distance measurement. The gain setting of "0000" means maximum gain of the integrator and "1111" means minimum gain of it. The vertical axis of Fig.4(a) shows the time from the system trigger of the digital counter, thus, only the relative timings of each channels and gain settings are important.

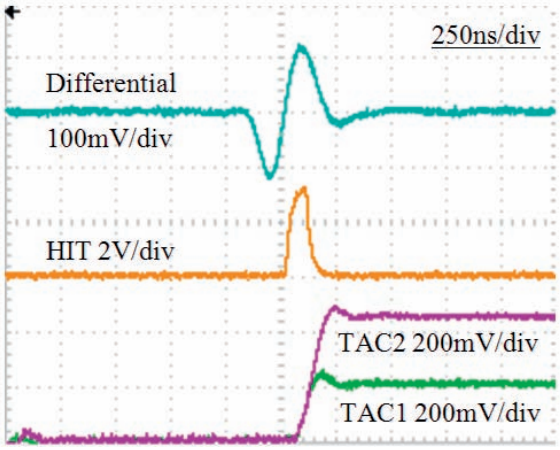


**Fig. 3: Typical output waveforms from LIDARX03**

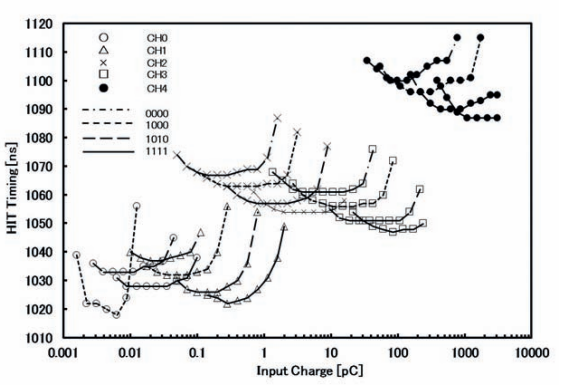


**(a) Detected pulse timing**

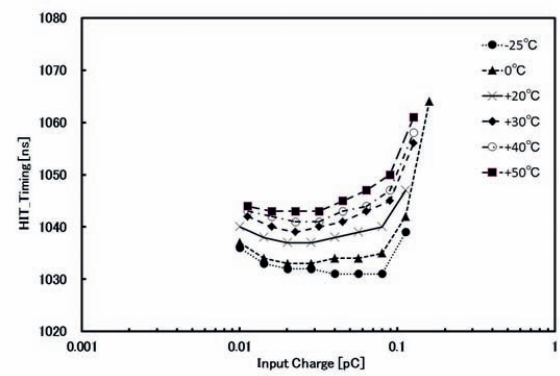


**Fig. 5: Temperature dependence of detection timing (b)**

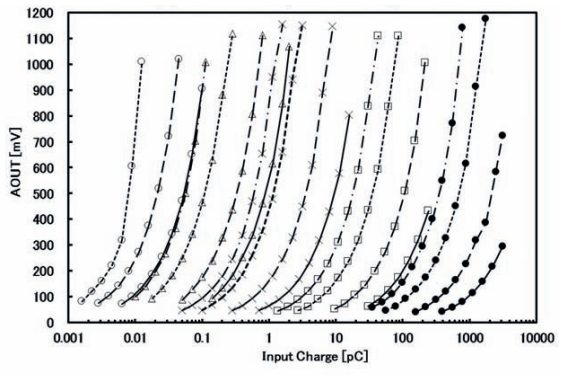


**(b) Signal amplitude**

**Fig. 4: Input charge dependence of the device outputs**

Since the result has high repeatability, the measurement can reach sub-nanosecond-level accuracy if we construct a suitable calibration curve. After constructing a calibration curve, it will be necessary to further improve the resolution of the measurement system and further evaluate the system. In addition, we consider it likely that we can achieve an accuracy level of several nanoseconds in a range of greater than 0.02 pC by constructing a calibration curve.

Figure 4 shows that the dynamic range of this device is about 60 dB; in fact, the minimum input charge level is 0.001 pC and the maximum level is 3000 pC. Furthermore, each channel has a dynamic range of over 10 dB and the channels overlap. Therefore, the device can conduct measurements over the entire 60-dB dynamic range. From Fig.4 (b), the amplitude of the signal is between 80 mV to 1000 mV. In this range, the HIT signal is output normally. The timing dispersion $\sigma$ of the HIT signal is smaller than 3ns. When the signal amplitude is larger than 200mV, $\sigma$is smaller than 1ns. When the signal amplitude is between 80 mV to 800 mV, we can find that the HIT timing is comparatively uniform and independent from the input charge level. Therefore, in order to obtain a good quality timing signal, the gain settings must be adjusted to limit the signal amplitude within this range. If the amplitude of the leading wave is limited to the range of 80 mV to 800 mV, the coverage of each channel is overlapping and the device still obtains a 60-dB dynamic range.

The temperature dependency of HIT between -25 and +50 degree C is shown on Fig.5 for the case of CH1-0000. Other cases have more or less similar characteristics. The timing delay increases about 10 ns as the temperature increases from -25 to +50 degree C. We can find that low temperature brings good flatness of the timing curve. Because there is no thermal hysteresis, and reproducibility is good, the temperature dependency can be compensated by a table of correction-for-temperature.For this purpose, LIDARX03 has a bipolar transistor whose base-to-emitter voltage has a temperature dependency of -1.63 mV/degree.

# 5. Conclusion

The background, design and evaluation of a prototype IC for LIDAR pulse detection are reported in this paper. According to the evaluation results, all the main functions of the IC for pulse detection in a 60-dB dynamic range, the pulse timing generation, and the interpolation of the digital clock were confirmed to operate effectively. In the future, we plan to evaluate this device using light pulses.

## References

1) *Mizuno, T., Tsuno, K., Okumura, E. and Nakayama, M.*: LIDAR for Asteroid Explorer Hayabusa: Development and On-board Evaluation, JJSASS, Vol. 54 No. 634 (2006), pp. 514-521.

2) *Manobu, T., Hirokazu, I., Mitsuo, I. and Susumu, I.*: Performance of a Monolithic Time-to-Amplitude Converter for High Precision TOF Measurements, Nuclear Instruments and Methods in Physics Research A312 (1992), pp. 585-590.

3) *T.Mizuno, H.Ikeda, K.Kawahara*: Pulse Detection IC for a Laser Altimeter Using CMOS Technology, The 28th International Symposium on Space Technology and Science (2011), 2011-d-77

## Correspondence

Takahide Mizuno
3-1-1 Yoshinodai Chuo-ku Sagamihara Japan

tmizuno@isas.jaxa.jp

# Lunar Laser Ranging: Support Tools for observers *(http://polac.obspm.fr/PaV/)*

*S. Bouquillon[1], G. Francou[1], J-M. Torre[2], T. Carlucci[1], C. Barache[1], F. Deleflie[2,3], D. Feraudy[2], H. Manche[3]*

ABSTRACT

We developed two web-tools to assist LLR observers. The first tool allows us to compute predictions of topocentric and geocentric coordinates of lunar targets (as retro-reflectors or craters) and predictions of round-trip times of laser-pulses between terrestrial stations and lunar retro-reflectors. The second tool allows observers to compute differences between their LLR observations and POLAC reduction model for LLR data. The residuals obtained in this way allow observers to have a validation of their observations. These tools can be used in already operational observatories for the laser lunar ranging but they are more particularly aimed at the new teams who begin to carry out LLR observations.

## 1. Introduction

These tools have been developed by the POLAC team of Paris Observatory (SyRTE) in collaboration with some colleagues from Me0 station (GeoAzur/Observatoire de la Côte d'Azur) and from IMCCE (Observatoire de Paris). These two tools are usable on-line on the web. The access is available by a single web site: http://polac.obspm.fr/PaV/ (where “PaV” means “Predictions and Validations”). Each tool has its own main page divided into two frames: the left frame is dedicated to the user request while the right frame is used to display the results of the user request (see tools screen shots below). The next section explains in detail how to use "Prediction" web page and "Validation" web page. In the last section, we briefly describe some planed improvements and report a recent change which allows an alternative access to these tools by electronic mail.

## 2. Tools quick overview

These two tools are based on the computer code of POLAC reduction model for LLR data developed since 1997 and based on an improved version of the semi-analytical solution of the Moon ELP2000-82B (Chapront-Touzé M. & Chapront J., 1988, 1996) (a numerical ephemeris is also used for the motion of the Earth-Moon barycenter and for numerical complements to the lunar libration and orbital motion). Initially, the lunar coordinates given by this solution are referred to the dynamical mean ecliptic of the date. The change to the equatorial frame of the Celestial Ephemeris Pole (J2000) is carried out by analytical expressions of the precession-nutation. This solution is fitted to the Lunar Laser Ranging observations made from 1972 until 2010 (for more details about this model see: Chapront J. & Francou G. (2002)).

As LLR observations are measurements of round-trip times of laser-pulses between terrestrial stations and lunar retro reflectors, it is necessary to know the accurate coordinates of LLR stations and lunar targets to be able to right compute predictions and validations.

With these tools, the usable LLR stations are the following ones (the list is not exhaustive and any station could be added by a request to polac administrator: polac.contact[at]obspm.fr).

- MLRS2 McDonald Laser Ranging Station (McDonald Observatory,Texas, USA)
- GRASSE Station MeO, Plateau de Calern (Observatoire de Côte d'Azur, France)
- APOLLO Apache Point Observatory (New Mexico, USA)
- MATERA Agenzia Spaziale Italiana (Matera, Basilicata, Italy)
- WETTZELL Bundesamt für Kartographie und Geodäsie (Bad Kötzting, Germany)
- KOGANEI Communications Research Laboratory (Koganei, Japan)

[1] SYRTE/Observatoire de Paris, 61 Av. de l’Observatoire, Paris, France

[2] GeoAzur/Observatoire de la Côte d’Azur, 2130 Route de l’Observatoire, Saint-Vallier-de-Thiey, France

[3] IMCCE/Observatoire de Paris, 61 Av. de l’Observatoire, Paris, France

The lunar targets usable with these tools are given below (the lunar targets can be one of the 5 reflectors put on the Moon since 1969 or a lunar site close to these reflectors). The available reflectors are the following ones:

- APOLLO 11, July 1969 (Mare Tranquillitatis)
- LUNAKHOD 1, November 1970 (Mare Imbrium)
- APOLLO 14, February 1971 (Fra Mauro Highlands)
- APOLLO 15, July 1971 (Mons Hadley)
- LUNAKHOD 2, January 1973 (Le Monnier crater)

The available lunar craters are the following ones: Bancroft, Mosting, Diophantus, Adams, Reiner-a, Messier-a, Bessel (Sarabhai), Posidonius and Gambart.

Both of these tools need the most recent values for the "Earth Orientation Parameters" (EOP) to compute accurate LLR predictions or residuals. To do that, a daily automatic update has been implemented to download the latest EOP combined C04 series and the latest EOP predictions file computed by the Earth Orientation Center of IERS.

The next two sub-sections explain respectively how to use the tool for LLR predictions and the tool for LLR validation.

## 2.1 Tools for “reaching” Moon's retro-reflectors (Prediction-tool).

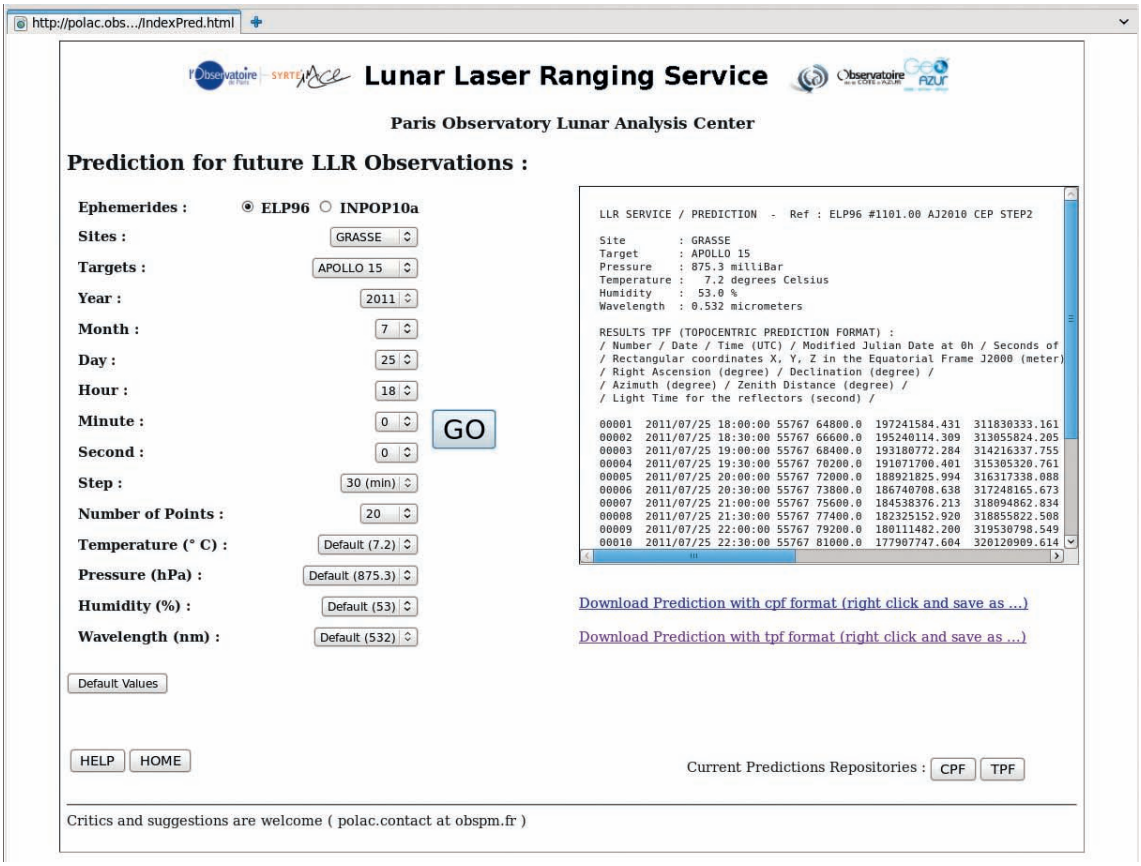


**Screen shot of Prediction-tool**: The left part of the screen is the request area (with selected options in drop-down menus). On the right part of the screen, the results are displayed (predictions file with cpf or tpf format).

Request: When using the Prediction-tool, besides the selected LLR station and lunar target, the user must also specify in his request the initial date and time of the first prediction, the step size between two successive predictions, the number of steps, the weather conditions and the wavelength of the laser used.

Results: By default, the display format of this prediction is a format we developed and that we named TPF (Topocentric Prediction Format). This format gives for each instant chosen by the user: the topocentric apparent equatorial coordinates of the selected lunar target seen from the selected site, the corresponding right ascension and declination in degrees, the corresponding azimuth and zenith distance in degrees and the corresponding round-trip light time in seconds.

The prediction could also be computed with the format CPF (Consolidated Laser Ranging Prediction Format) which has been created by the ILRS Predictions Formats Study Group for satellite laser ranging and lunar laser ranging. An explanation of this format can be found in: http://ilrs.gsfc.nasa.gov/products_formats_procedures/predictions/.

TPF & CPF Repositories: Everyday, predictions are automatically computed for 3 days: 150 points since the current date 0h with an interval of 30 minutes with some default values for pressure, temperature, humidity and laser wavelength. The user has access to them by the web site with the link: “Current Predictions Repositories XXX” or by ftp anonymous on “polac.obspm.fr” server in the folder “/pub/llr_repository/XXX_REPOSITORY” and the generic name for these predictions is: "llr_serv_TargetName-Day-Month-Year.XXX (where “XXX” is TPF or CPF).

## 2.2 Tools for computing LLR residuals (Validation-tool).

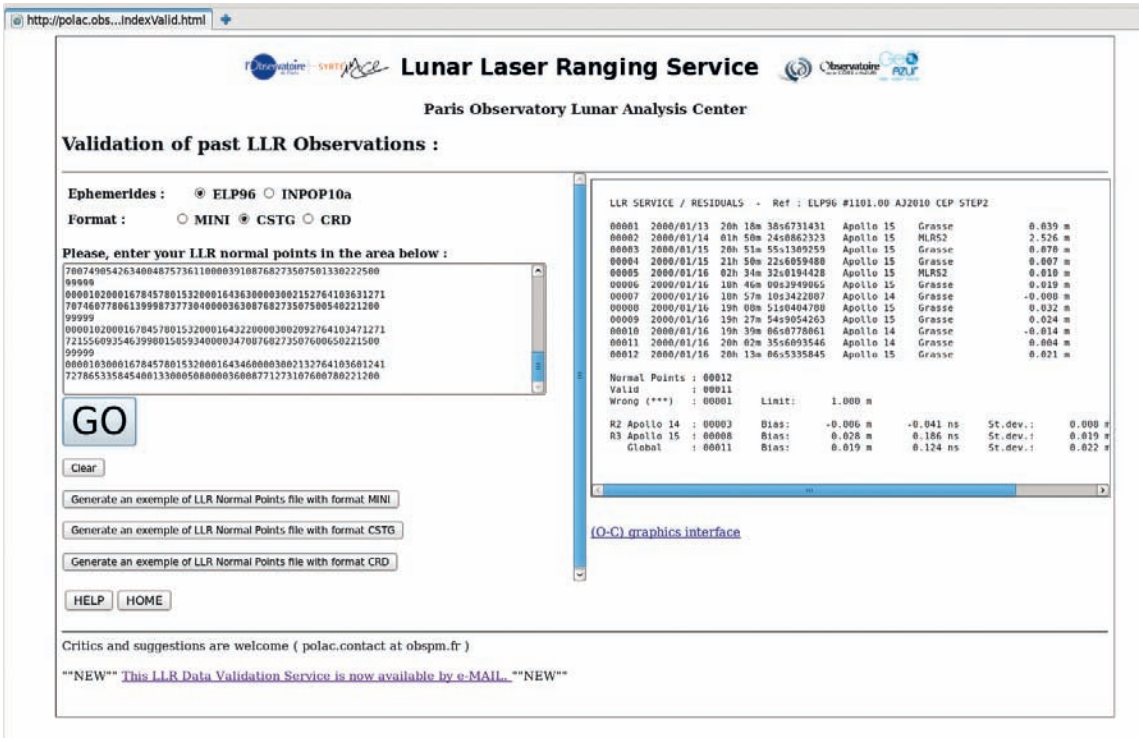


**Screen shot of Validation-tool**: As in the Prediction-tool, the left part of the screen is the request area (with a capture area where the user pastes his LLR data). The right part of the screen is used to display the results (residuals, statistics, graphics).

Request: When using the Validation-tool, for uploading LLR observations, the user selects and copies his own LLR data (normal points) from a file and then pastes them into the “user’s data capture area” in the left part of the screen (for time processing reasons the number of LLR observations is limited to 1000). The available formats for user data uploading are:

- the format MINI (explanation at: http://www.physics.ucsd.edu/~tmurphy/apollo/norm_pts.html ),
- the format CSTG (explanation at: http://ilrs.gsfc.nasa.gov/products_formats_procedures/ ),
- the format CRD (explanation at: http://ilrs.gsfc.nasa.gov/docs/crd_v1.01.pdf ).

Results: For each LLR observations, a line of results is given. This line contains: the number of processed observation according to submission order, the date and time of the observation, the name of the station, the name of the reflector and the difference between observed light time and computed light time in nanoseconds and its equivalent in meters for the station reflector distance.

The bias and the standard deviation of residuals are given (individually by reflector or globally) and graphs of residuals are also available according to the stations, the reflectors, the time units and the residuals units.

In the table below, we give the statistical results of this validation processing for the 942 LLR Normal Points from Apache Point Observatory (2006-2010). We see that the global standard deviation for all the reflector is 5 cm.

| REFLECTORS | Nb. NP | Bias (cm) | St. dev. (cm) |
|---|---|---|---|
| R0 Apollo 11 | 00176 | 1.4 | 5.1 |
| R1 Lunokhod 1 | 00029 | 0.0 | 2.3 |
| R2 Apollo 14 | 00180 | 2.7 | 4.8 |
| R3 Apollo 15 | 00506 | -0.8 | 4.8 |
| R4 Lunokhod 2 | 00051 | 0.6 | 5.4 |
| Global | 00942 | 0.4 | 5.0 |

**Example of statistical results of the Validation-tool for Apache Point LLR Observations (2006-2010).**

# 3. Recent and planed improvements

Further to a request of Randall L. Ricklefs (McDonald Observatory), we recently added an alternative access by e-mail to the tool for computing the residuals of LLR observations. To use this option, LLR observations are sent to the following address: polac.processing[at]obspm.fr in accordance with a specific format (which is described in the following document: http://polac.obspm.fr/PaV/MailService.html). The comparison between this observations and POLAC reduction model will be computed on POLAC server and a reply with the results of the comparison will be automatically send back.

After some discussions with Mark H. Torrence (NASA/GSFC), we plan to also incorporate into the Prediction-tool some orbital data of LRO spacecraft to avoid LLR ranging when LRO is between the LLR station and one of the LLR reflector arrays.

We also plan to add some alternative to POLAC reduction model. First, we plan to add INPOP reduction model for LLR data developed by H. Manche at Paris Observatory (IMCCE) (Manche et al, 2010) but also any other available model being able to reduce LLR data.

## Acknowledgements

We would like to thank Randall L. Ricklefs who helps us a lot to understand specificities of CPF format for LLR data and Pierre Tessandier who helps us to neatly compute the relativistic aberration for LLR observations.

## References

*Chapront-Touze M., Chapront J.*, 1988, "ELP 2000-85 - A semi-analytical lunar ephemeris adequate for historical times", A&A, 190, 342.

*Chapront J., Chapront-Touze M.,* 1996, "Lunar Motion: Theory and Observations",Celest. Mech., 66, 31.

*Chapront J., Chapront-Touze M., Francou G.*, 2002, "A new determination of lunar orbital parameters, precession constant and tidal acceleration from LLR measurements", A&A, 387, 700.

*Manche H. et al,* 2010, "LLR residuals of the latest INPOP solution and constraints on post-Newtonian parameters", Proceedings of the "Journées Systèmes de Référence Spatio-temporels 2007". Observatoire de Paris, N. Capitaine (eds.)

## Correspondence

POLAC
Observatoire de Paris (SyRTE)
77, avenue Denfert-Rochereau
75014 Paris

polac.contact[at]obspm.fr
Web: http://polac.obspm.fr/

# Session 15:
# In-Sky-Laser-safety

# Implementation of the LASER Traffic Control System at Haleakala Observatories

*D.O'Gara, E.Kiernan-Olson, C.Giebink,* D.Summers,

ABSTRACT

The University of Hawai'i Institute for Astronomy Haleakala Observatories (HO) was for many years occupied only by Mees Observatory and the LURE Laser Ranging Observatory. The LASER system at LURE could operate at night without disturbing other science operations because Mees is a solar observatory.

Since 2000, several astronomical observatories have been built at HO, and more are being planned. In order to prevent scattered laser light from interfering with the science operations of the optical observatories, HO is implementing a version of the Laser Traffic Control System (LTCS). W.M. Keck Observatory primarily developed the LTCS, with additional support provided by several other Mauna Kea observatories. The LTCS can predict when telescopes and laser beams will enter each other's field of view, allowing the observatories to take preventative action.

The LTCS currently supports laser guide star adaptive optics (AO) operations at Mauna Kea Observatories (MKO) Hawaii, the Canary Islands (Spain), and in Chile.

This paper will discuss the features of the LTCS, the limitations when SLR observatories are included in the current system, and the implementation of a test system at the Haleakala Observatories. This is just a brief explanation of the system as it is being implemented at HO. For an in-depth explanation of the LTCS, please access the original papers written by the designers of the system [1,2,3].

## 1. System Description

The LTCS as implemented at the Mauna Kea Observatories was designed to solve the problem of how to keep the light from an AO laser (via Rayleigh scattering or from the fluorescence of the guide star) from entering into the Field Of View of other telescopes on the mountain

The LTCS is web based, and is implemented as a client/server system. Each participating observatory is a client to the

| | |
|---|---|
| **TIMESTAMP1=1304228999** | **# Time of URL update in Unix Seconds** |
| **TELESCOPE=TLRS4** | **# Telescope Name** |
| **RA= 4.60881** | **# Telescope Right Ascension in Hours** |
| **DEC= 61.87089** | **# Telescope Declination in Degrees** |
| **EQUINOX=2011.32943300** | **# Equinox and Epoch of coordinates** |
| **FOV=1.667** | **# Diameter of telescope Field Of View (FOV)** |
| **LASER_IMPACTED=NO** | **# Telescope is (or is not) LASER sensitive** |
| **LASER_STATE=ON** | **# Telescope is (or is not) projecting LASER light** |
| **LOG_DATA=ON** | **# Flag to enable/disable logging of pointing data** |
| **TIMESTAMP2=1304228999** | **# Time of URL update in Unix Seconds** |

LTCS, and must provide access to a URL (Universal Resource Locator) file that describes that particular system for the LTCS.

Following is a sample URL file generated by the TLRS-4 system. This file is stored once per second in the WWW file structure of a Linux system at TLRS-4 running an Apache Web Server. The LTCS reads the file via HTTP.

The LTCS uses the configured positions of the participating telescopes, along with the information contained in the URL files, to calculate the FOV cones of telescopes and laser beams. From this the intersection of the cones can be calculated and appropriate action taken.

The LTCS has a sophisticated priority scheme. For the HO implementation, the TLRS-4 laser was given lowest priority and will shutter the laser when any collision situation arises.

# 2. LTCS at Haleakala

The LTCS was not designed to include SLR into the mix of observatories. It was obvious that some of the features of the Mauna Kea system would not work at HO as intended without modification. The foremost difference in requirements for SLR is that the SLR systems are not tracking in sidereal mode. The AO systems are (generally) only tracking in sidereal mode.

The LTCS system is currently operating at HO in a simulation mode only. Full implementation is still several months away. The simulation has shown that a useful LTCS system that incorporates SLR is possible with only modifications to the configuration files.

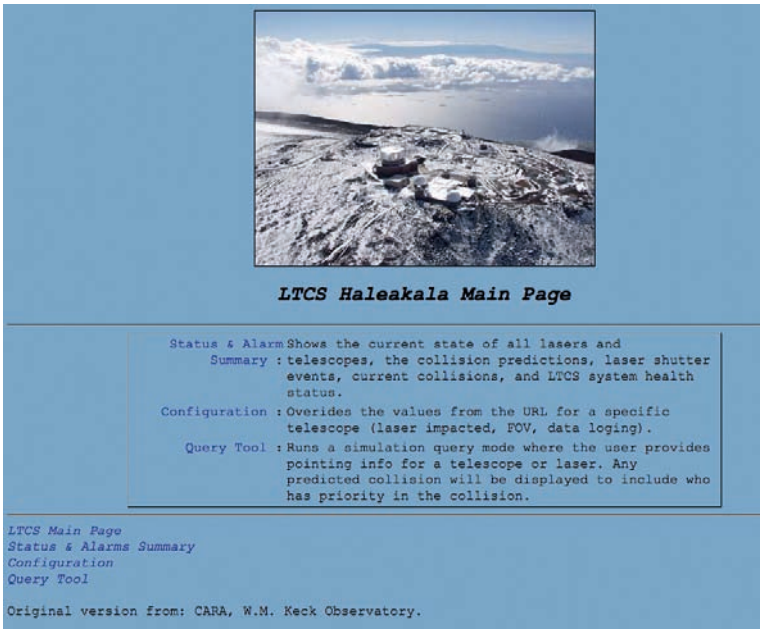


The main LTCS screen is shown in figure 1. From here each observatory is able to view the status of the system and to make changes to their own system configurations.

The "Query Tool" provides sidereal tracking telescopes with the ability to determine if a collision will occur now, or in the future. This tool was not designed to provide accurate information to SLR observatories.

A second major difference is the tracking speed of an SLR system when compared to a telescope tracking in sidereal mode.

In order to overcome the differences noted above, the update rate for reading the TLRS-4 URL was set to the system minimum of one second and the declared FOV of the laser system was set to the maximum 1.667 degrees. The actual divergence of the laser beam at TLRS-4 is about 0.02 degrees. This added spatial and temporal buffer compensates for the fast tracking speed of the laser, and the fact that the Pan-STARRS telescopes have an extraordinary 3.0 degree field of view (full angle).

Also, the configurable altitudes that locate the sodium layer (minimum and maximum altitude) for the LTCS were changed so that satellites being tracked from a 300 Kilometer orbital altitude up to 20,000 Kilometers orbital altitude would mimic a Laser Guide Star and cause a collision alert if the satellite is tracked through the FOV of another telescope. The maximum altitude for Rayleigh Scattering was left unchanged at 50Km.

A method to integrate the LTCS into the TLRS-4 Laser Interlock system has been devised. Currently, if a collision occurs, a "SHUTTERED" event is entered into the LTCS log and the *Status & Alarm Summary* GUI is updated. Once this integration is completed, a laser/telescope collision will be handled as a laser interlock violation which will automatically shutter the laser until the collision condition no longer exists, and the operator has manually cleared the alarm.

# 3. Simulated Collision. PS1 and TLRS-4

The following figures are screen shots of a simulated collision between TLRS-4 laser and Pan_STARRS.

The screen capture below (Figure 2) shows the LTCS *"Status and Alarms Summary"* web GUI on the left, and a real-time 3-D plot of the simulation on the right. The 3-D plot is not part of the LTCS but runs independently on the host system.

It was added as part of the simulation tests done at HO. It can be manipulated in real time (i.e. grabbed with the mouse and rotated about the origin, which is configured to be TLRS-4) and provided real time visualization during the installation tests.

The LTCS *"Observatories"* panel shows that there are 4 active observatories with one (TLRS-4) being an active laser system. The *"On-Sky"* message indicates that the laser currently is being propagated.On the right of the LTCS panel is the *"Predictions"* indicator that warns of future collisions. The prediction algorithms are assuming all telescopes are tracking in sidereal mode. The TLRS-4 is not tracking in sidereal mode so any prediction involving TLRS-4 is not reliable. In this example, the impending collision was predicted by coincedence. The second screen capture (Figure 3) shows the system indicating a collision has occurred. At the time of collision, a "SHUTTER" alert is sent to the LTCS log file. Because the LTCS was configured with the TLRS-4 laser being lowest priority, the TLRS-4 will receive the alert and block transmission of the laser.

As mentioned before, the *"Shutter Event Duration"* calculation will not be accurate when an SLR system is involved. The calculated duration shown is 3,599 seconds. The actual duration of this simulated event was about 60 seconds.

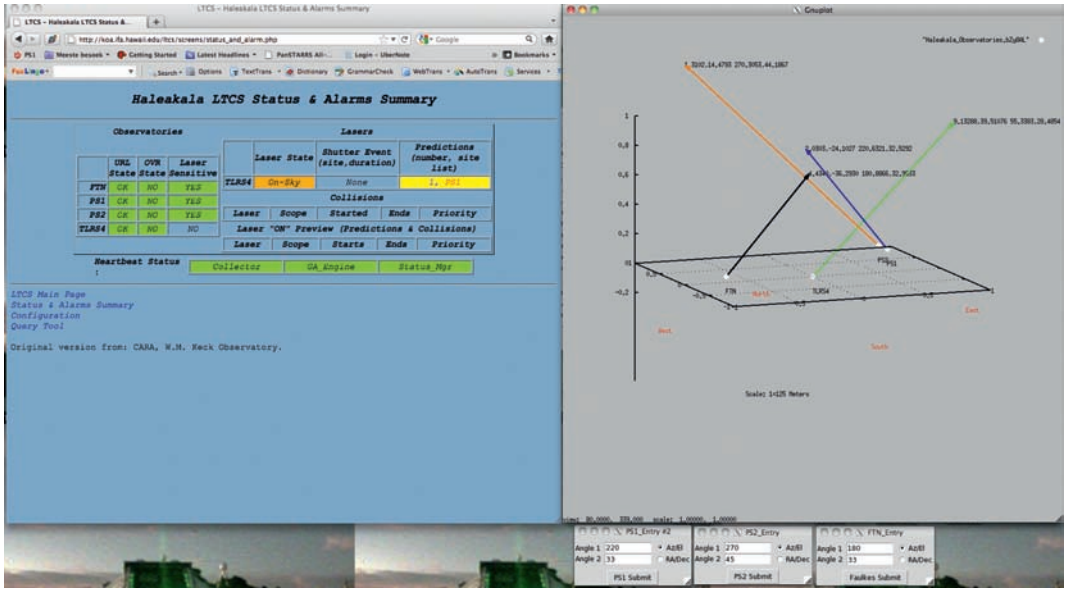


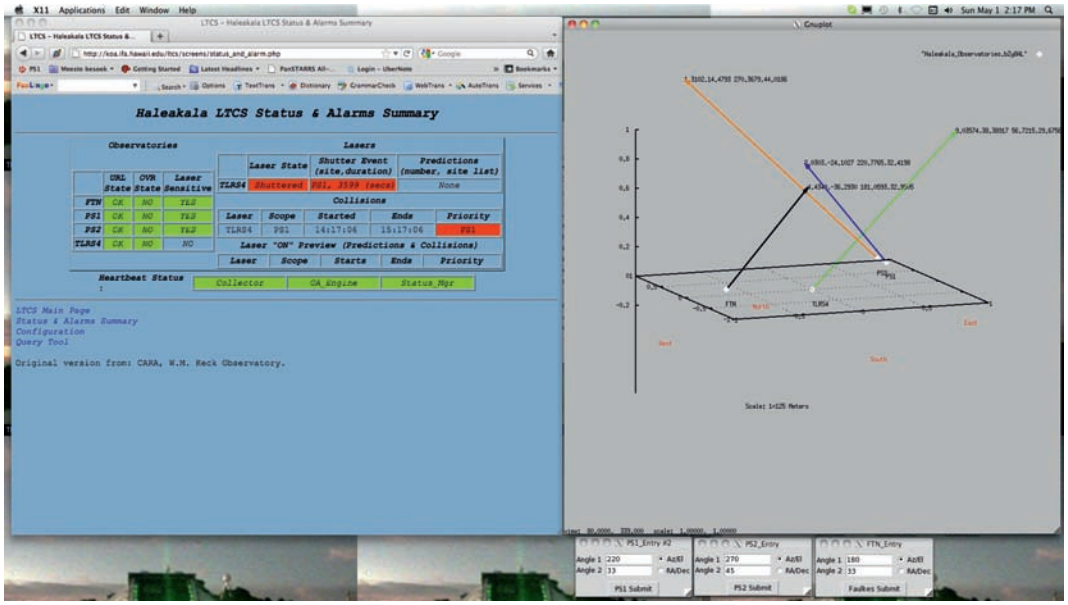

# Conclusions

- The LTCS is a mature software system that has been installed at three astronomical sites that are operating laser guide stars in support of adaptive optics systems.
- The basic design of the system has shown that it can be used by SLR sites that are also home to optical telescopes.
- In order to be used at sites that operate SLR and AO lasers along with optical telescopes, methods to handle combined Laser Guide Star and SLR targets will need to be developed. Interface changes to support non-sidereal target modeling would prove beneficial for astronomical and SLR use. This feature enhancement has been discussed and may be added to LTCS in a future update.

## References

1. *Summers. et al.*. 2003. Proceedings of the SPIE (2003) Vol. 4839: Implementation of a Laser Traffic Control System supporting Laser Guide Star Star adaptive Optics on Mauna Kea.

2. *Douglas Summers, WM Keck Observatory. Nikolaos Apostolakos, Rene Rutten, Gordon Talbot, Isaac Newton Group,* 2005: Second Generation Laser Traffic Control; Algorithm Changes Supporting Mauna Kea, La Palma, and Future Multi-Telescope Laser sites.

3. *Y.Hayano and M.Iye, NAO of Japan. H.Takami and N.Takato, Subaru Telescope, NAO of Japan. W.Gaessler. Max-Planck-Institute for Astronomy. Y.Minawo. University of Tokyo. P.Wizinowich and D.Summers. W.M.Keck Observatory. Publications of the Astronomical Society of the Pacific,* 2003: Observational Impact of Scattered Light from the Laser Beam of a Laser Guide Star Adaptive Optics System.

## Correspondence

Daniel O'Gara
University of Hawaii Institute for Astronomy Haleakala Observatories
34 Ohia Ku, Pukalani, HI. 96768

ogara@ifa.hawaii.edu

# Skyguide and Flarm - Two In-Sky-Laser-Safety Systems used at Zimmerwald Observatory

*M. Ploner, A. Jaeggi, J. Utzinger*

ABSTRACT

At the Observatory in Zimmerwald SLR measurements can be performed automatically without any interaction of an operator. Because of its close distance to the airport of Bern sometimes it may happen that aeroplanes are flying in very low altitude over the observatory. During the flyover the SLR measurements have to be interrupted automatically due to safety reasons. For this task two independent systems are installed, Skyguide and FLARM. Both systems will be introduced and their implementation in our SLR software will be presented.

## 1. Zimmerwald Observatory

The Observatory in Zimmerwald is located about 5km south-west of the airport Bern/Belp (Figure 1). Although the airport is very small in comparison to other ones like Zürich-Kloten, it is frequently used by gliders and helicopters of the REGA (air-rescue organisation). This is why aeroplanes sometimes are flying in very low altitudes over the station. In-sky-laser-safety is thus an important issue during SLR measurements which are performed 24 hours per day, depending on the weather conditions. Due to the fact that the system sometimes is running for a few hours per day in an automatic mode and supervised only by an operator's remote interactions, it is obvious that the SLR measurements have to be automatically suspended during the flyover of aeroplanes in this case as well. Two systems are used: SKYGUIDE and FLARM.


**Figure 1: Topographic map of the Zimmerwald Observatory surroundings**

## 2. Skyguide

Skyguide is commissioned by the Swiss government to manage and monitor all air traffic in the country's airspace. Since 2001, Skyguide's mandate has covered both civil and military air traffic. The radar data (time, position relative to Zürich Airport, velocities and aircraft identification codes for all aircrafts) is provided through a VPN connection to a Skyguide server in a continuous data stream. A software module provided by Skyguide receives and decodes the binary data, extracts and reformats the track data needed by the SLR system and makes it available as ASCII records.

- Syntax: Cat030,<TIME>,<Record_Number>,<Position>,<Velocity>,<Aircraft_Identification_Code>
- Example: Cat030 id=3658 Time=13:48:14.92 X=-78.42NM Y=-63.66NM Z=30000ft VX=-290.258789knot VY=323.657227knot VZ=0ft/min SSR=5725

This example means that here is an aircraft with ID 5725 -78 miles west and -63 miles south of the Airport Zürich, the actual aircraft altitude is 30000 feet. The aircraft is flying with a speed of 290/324 knots in northwest direction The climbing rate is 0 feets/min.

However, gliders and other light aircrafts are often not recorded. This is why a second in-sky-laser-safety system, called FLARM, was installed for the safety of that aircraft types.

# 3. Flarm

FLARM® is a low-cost collision-warning unit for gliders and light aircrafts. More than 12'000 own devices manufactured by FLARM® plus over 5'000 devices manufactured by licensed 3rd parties are in use in many countries and continents.

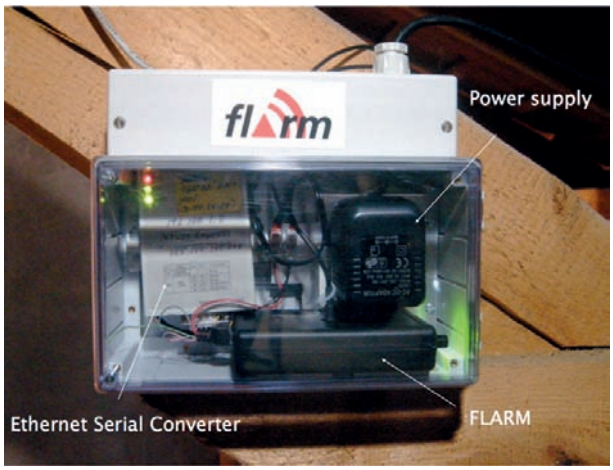


**Figure 2: Image of FLARM**

FLARM is the only prevalent alternative to the commercial airliners' expensive ACAS/TCAS system. Especially in Switzerland almost all light aircrafts are equipped with FLARM. Compatible systems, which use the same hardware architecture and licensed core software are available from the following companies:

- LXNAV, LX Navigation, Tiadis, Ediatec, Swift Avionics, Artronic

FLARM receives position and velocity information from an internal 16 channel GPS receiver with an external antenna. A pressure sensor further enhances the accuracy of position measurements. The predicted flight path is calculated by FLARM, and the information - including a unique identifier – is transmitted by radio signals at one-second intervals. If these aircrafts are within receiving range, the signals are almost at the same time received by further aircrafts also equipped with FLARM. The incoming signal is compared with the flight path predicted by calculation for the second aircraft. FLARM determines the risk of dangerous proximity to one or more aircrafts or obstacles, thus warning the pilots against the most serious danger at that moment. The GPS and collision information received from other aircrafts can be made available for third party equipment via a serial data output. The data streams will be sent continuously without any request. One data stream with identifier PFLAA contains position, velocity and identification code of an aircraft. In additional, information is provided about the aircraft type and the alarm level.

- Syntax: PFLAA,<AlarmLevel>,<RelativeNorth>,<RelativeEast>,<RelativeVertical>,<IDType>,<ID>,<Track>,<TurnRate>,<GroundSpeed>,<ClimbRate>,<AcftType>
- Example: PFLAA,0,2662,53,149,2,DDAE90,247,,45,12.2,3

There is a helicopter with static ID „DDAE90" 2.6km north and 53m east of the station Zimmerwald, the actual aircraft altitude is 149m higher than the station height. The helicopter is flying with a ground speed of 45m/s and a climbing rate of 12.2m/s. There is no danger.

Further data streams (PFLAU, PGRMZ) contain data about the operation status (power, GPS and transmission status) and the barometric pressure. The operating range crucially depends on the antenna installation in the aircraft. The typical range is 3 -5km.

- Syntax: PFLAU,<RX>,<TX>,<GPS>,<Power>,<AlarmLevel>,<RelativeBearing>,<AlarmType>
- Example: $PFLAU,1,1,1,1,0,,0,,

FLARM is working properly (Transmission, GPS and Power are ok) and receives one other aircraft.

- Syntax: PGRMZ,<Value>,F,2
- Example: $PGRMZ,3100,F,2

The barometric altitude of the station Zimmerwald is 3100ft (939m)

# 4. Air Traffic Control Server

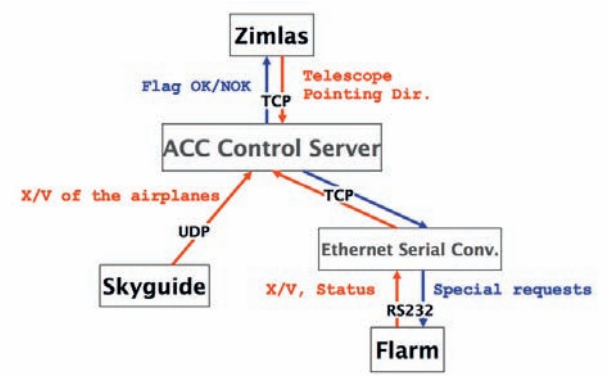


**Figure 3: Data Stream**

The ACC control server receives the data from Skyguide via an UDP connection, and the data from FLARM via a TCP connection. In contrast to the unidirectional connection between Skyguide and ACC control server there is a bidirectional connection between FLARM and the ACC control server. Special requests can be sent to FLARM. For example, you can set maximum horizontal distance of aircrafts to be processed. The server builds/maintains a table of all aircraft positions. A client (ZIMLAS) can send the pointing direction of the telescope to the ACC server. The server checks the pointing vector against all aircraft positions for a given instant of time. Aircraft positions will be extrapolated if necessary and an OK or NOT-OK message together with the number of the checked aircrafts will be replied. The minimum allowed horizontal and vertical distance between aircraft and laser beam can be adjusted independently for Skyguide and FLARM data (depending on update rate):

## References

*FLARM, Technology GmbH..*, 2011: Operating Manual Flarm Collision Warning Unit

*FLARM, Technology GmbH..*, 2011:Data Port Specifications

## Correspondence

Dr. Martin Ploner
Universität Bern
Astronomisches Institut
Sidlerstrasse 5
CH-3012 Bern

martin.ploner@aiub.unibe.ch

# WLRS: In-Sky Laser Safety

*Johann Eckl, Martin Ettl, Alexander Neidhardt, Andreas Leidig, Uwe Hessels, Günter Herold*

ABSTRACT

This article gives an overview about the in-sky laser safety situation of satellite laser ranging (SLR) station in general and especially reveals the current situation at the Wettzell Laser Ranging System (WLRS). After a clarification of the sky circumstances, general in-sky laser safety strategies for SLR systems are introduced, followed by the advantages and disadvantages of the applied in-sky laser safety methods at the WLRS. The final part deals with the principle of an ADS-B receiver and shows some features of the new SLR 2.0 software package, currently developed for our SLR systems.

## 1. Introduction

A GGOS station is equipped with a collection of sensitive microwave and high power optical measurement systems. The dangerous thing with high optical powers is that exposure to the human eye leads to irreversible injury. Therefore, measurements have to be taken to avoid the damage of humans with our equipment. At the WLRS site, there is a flight restriction zone with a horizontal radius of 10 km and a vertical distance of 1.6 km. Within this area, powerless aircrafts like gliders, hang-gliders, paragliders and balloons are not allowed. As a result, the main problem is to detect engine driven aircrafts at a distance from 1.6 to about 40 km, which is the border of the outer atmosphere. The strategies for detecting objects can be categorized into passive and active systems.

In general, passive systems are capable of visualize an aircraft by scattered electromagnetic waves on its surface. Therefore, a detection system for a dedicated wavelength is required. In the optical region, this can be done by a camera system with pattern recognition software or an human observer. In addition, there are existing passive radar systems on the market using reflections and information gathered by the Doppler shift, which come from well known microwave emitters scattered on the aircrafts surface. A further passive detection system is realized by the ADS-B detector, which receives an aircrafts position by signals sent from the aircraft itself.

Active systems also detect scattered electromagnetic waves on aircraft surfaces, but they also transmit the detected radiation. This optical and microwave approaches are available with their specific advantages and disadvantages.

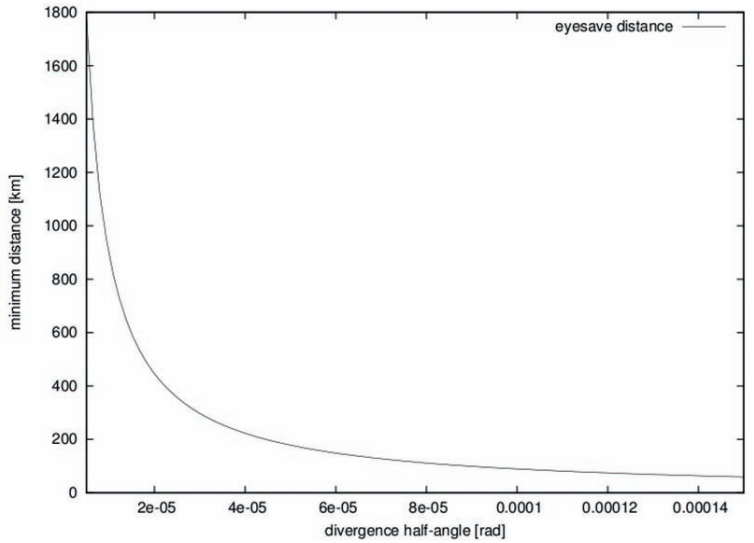


**Figure 1: The minimum distance for eye safe SLR from the WLRS**

# 2. The in-sky safety concept

The WLRS works with a four stage in-sky laser safety system, where one stage is currently under development. Thereby increasing the divergence can not full fill inner atmosphere safety restrictions calculated by following formula:

$$d(\varphi) = \sqrt{\frac{E_T}{\pi \cdot E_{MPE}}} \cdot \frac{1}{\varphi}$$

Especially, if there are no atmospheric and system transmission efficiencies considered (worst case scenario). In the formula above, the variable $d$, is the minimum distance for eye safety, $E_T$ is the transmitted energy, $E_{MPE}$ is the maximum permissible energy and $\rho$ is the divergence of half angle, which is up to 30 arcsec (15E-5 rad). At least, this method seems suitable for time transfer experiments to the outer atmosphere (see figure 1).

The currently camera system consists of a camcorder, which is mounted outside of the telescope tube. The captured images are shown on screen at the observation room. This allows to permanently observing that parts of the sky, where the laser is pointing during ranging. On the top of this setup, a hardware switch allows us to immediately interrupting the laser signal, when an aircraft is detected by the observer. This concept strongly depends on the constitution of the observer and can therefore not be accepted as an eye safe concept. The Honeywell Laser Hazzard Reduction System (LHRS), which is an officially approved system, is the main safety component at the WLRS site. It seems to satisfy the requirements of an in-sky safety device, being operable within the required measuring range of 1.6 to 40 km. The acquisition costs for a LHRS, are much more expensive, compared to a camera system. Since we are operating with our LHRS, we were faced with more clutter, which reduced the data density during the observation. As a result, this leaded to less number of normal points and lowered accuracy. In addition, for future GGOS station requirements, the LHRS cannot be recommended, because of its transmitting frequency, which collides with the VLBI receiving spectrum. As a fact, this leads to massive disturbance of the VLBI receiving device. In order to evaluate the technological requirements for a GGOS station, we installed an ADS-B receiver recently.

# 3. ADS-B receiver

The Automatic Dependent Surveillance - Broadcast (ADS-B) is a European Aviation Safety Agency (EASA) approved sole working aviation surveillance system. The global implementation is planned by 2015 in Europe [1]. ADS-B works as follows: the aircraft computes its position from the Global Navigation Satellite System (GNSS) and continuously transmits its position undirected. Therefore, anyone with this receiver equipment is able to get the position of aircrafts within a maximum distance of approximately 200 miles.

For the WLRS an AirNav® RadarBox PRO[1], which costs about 500€ was bought. In addition, an antenna and an amplifier, which cost together about 200 €, were installed. To ensure good receiving conditions, the antenna was mounted on top of a mast next to the WLRS. The AirNav-Box provides support for MS Windows software, which can be used via USB port. In order to be able to use the Windows PC together with the SLR 2.0 Linux system, an adapter had to be written. This adapter was realized with idl2rpc, a middleware generator [2]. It creates, according to give a set of interface functions, a client and server source code template. In this case, the server receives the data, coming from the AirNav-Box, via serial interface, makes the necessary coordinate transformations and provides the data for the client. According to the given client/server-architecture, the client asks the server for the current aircrafts positions and displays it on the graphical user interface (GUI). A screenshot of our skyplot-window, displaying aircrafts and satellite passages, is depicted in figure 2. This system is still under evaluation, because not all aircrafts are detected by the system at the moment. Another open issue is the implementation of avoidance zones, around the detected aircrafts. They can be similarly treated like the well-known sun-avoidance area, which is also shown in figure 2 (yellow, circular area).

[1] http://www.airnavsystems.com/

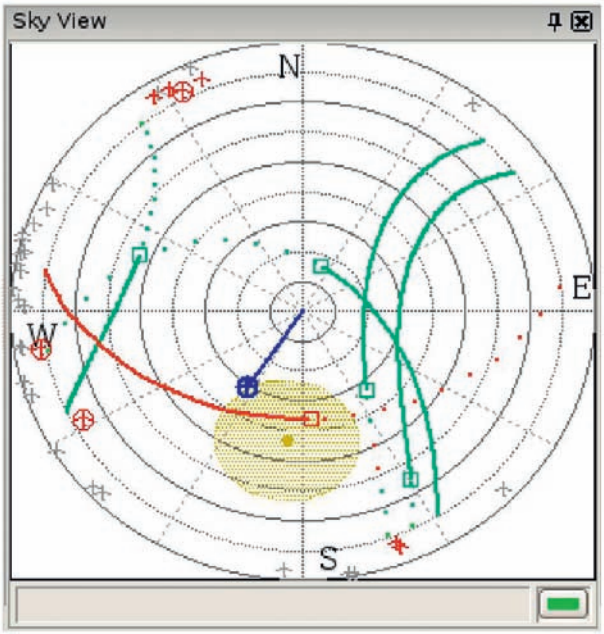


**Figure 2: WLRS SLR 2.0 Sky View, grey and red: aircrafts, blue: telescope position, green and red: satellite traces, yellow: telescope sun avoidance zone**

# 4. Conclusion and future work

The collocation of different techniques in future GGOS stations has a set of open problems, which have to be solved. One of them is the in-sky laser safety issue. Applied techniques for eye protection could not convince, so far. Either the safety is not ensured or there is no compatibility with other space geodetic techniques. The ADS-B receiver can not solve this problem entirely, because there is no law for using it in aircrafts. At the other side, it seems to fit well as a redundant system because of its low costs, simple implementation and its sufficient range. For the future ADS-B may get a more important safety device. A further solution may exist in developing LIDAR-systems for aircraft detection. Another way could also be, to switch to the *more* eye safe wavelengths. In future, we will further extend our system monitoring concept about such techniques [3].

## References

[1] *R. Weibel, M. Jenkins, R. J. Hansman*: Automatic Dependent Surveillance Broadcast (ADS-B) Costs, Benefits, Applications, and Implementation Challenges, Airline Advisory Board Meeting, November 6, 2008

[2] *A. Neidhardt*: Manual for the remote procedure call generator idl2rpc.pl, Geodetic Observatory Wettzell, 2009

[3] *Ettl, M.; Neidhardt, A.; Mühlbauer, M.; Plötz, C.; Beaudoin, C.*: The Wettzell system monitoring concept and first realizations; in: Behrend, D.; Baver, K. D. (eds.) VLBI2010: From Vision to Reality, IVS 2010 General Meeting Proceedings, NASA/CP–2010–215864, pp 444-448, NASA, Goddard Space Flight Center, 2010

## Correspondence

Eckl Johann
Geodätisches Observatorium Wettzell
Sackenrieder Str. 25
D-93444 Bad Kötzting

eckl@fs.wettzell.de

Ettl Martin
Geodätisches Observatorium Wettzell
Sackenrieder Str. 25
D-93444 Bad Kötzting

ettl@fs.wettzell.de

# Session 16:
# System Automation

# Introduction to the session about automation

*Alexander Neidhardt, Chris Moore, Martin Ploner*

ABSTRACT
This session addresses the technical issues that are important for the development of greater levels of automation in SLR systems. Optimized scheduling, efficient use of resources and the reduction of staff for operations are profitable goals. However there are many constraints and difficulties that must be considered when systems are to be run unattended. For example, in-sky or aircraft safety is a particularly important factor that must be addressed before a system can run unmanned, This following papers describe current development, ideas and possible difficulties, which are relevant for the development of automation of any SLR site or analysis center.

## 1. Automation – a short overview

Automation allows the possibility to run unmanned operations for useful periods, which reduces the need of permanent operating staff. Nevertheless, competent staff is required to maintain hardware and ensure on-going operational performance, to check security and environmental conditions. Reliable computer systems must offer the functionality of a flexible scheduling, automated tracking and data management. Alerts and alarms must be raised and distributed to appropriate remote and accessible monitoring systems. This is only possible with a suitable level of standardization especially of the interfaces that can access different proprietary systems. Such standardization may support a further goal of sharing observations and resources between different observatories. Code sharing may optimize the synergies within the communities. The result of such improvements and increasing level of automation should lead to improved data productivity, consistent quality and ultimately to better scientific results.

Automation is also possible in the data centers, as demonstrated by the European Data Center (EDC). Here, current improvements based on the use of two parallel servers with internal synchronization offer a 24/7 access to FTP accounts for each station and provider. Hourly and daily exchanges with CDDIS and ITT keep the databases consistent, and notification of data problems are automatically generated and distributed. Mailing lists as SLRMail, SLRReport and UrgentMail and a new webpage help to coordinate the network operations and data center states.

The experience of using real-time Linux systems for the control systems at some SLR stations was reported. Pathfinder technologies are currently being developed at fundamental stations such as GGAO to support their multi-technique environments and integration of NGSLR. In these environments it is been found necessary to avoid operational conflicts, where real-time techniques and systems are needed (e.g. for the antenna pointing). It is necessary to monitor site ties and to take care of constraints such as sun avoidance, cloud coverage and other weather conditions. The systems at NGSLR allow a sophisticated scheduling, signal processing and remote operation. In-sky safety is being addresses by the integration of a radar based Laser Hazard Reduction System (LHRS).

Other fundamental stations are also developing new software and hardware to integrate SLR operations and improve automation. A new approach is under development at the Geodetic Observatory Wettzell with the SLR2.0 software based on generalized Wettzell telescope control software. Using generic programming techniques for the communication interfaces of a classic client-server-architecture, interfaces between the hardware, the scheduler and the graphical user interface have been developed. It is planned to offer the whole software under the terms of open source.

## Correspondence

Alexander Neidhardt
Forschungseinrichtung Satellitengeodäsie, TU München
Geodätisches Observatorium Wettzell
Sackenrieder Str. 25
D-93444 Bad Kötzting
Germany

neidhardt@fs.wettzell.de

Christopher Moore
EOS Space System. Pty Limited
Mount Stromlo Observatory,
ACT, Australia.

cmoore@eos-aus.com

Martin Ploner
Astronomical Institute
University of Bern
Sidlerstr. 5
CH-3012 Bern
Switzerland

martin.ploner@aiub.unibe.ch

# Automated Data Management of SLR-Data and Products at the EUROLAS Data Center (EDC)

*Christian Schwatke*

ABSTRACT

Within the ILRS, the EUROLAS Data Center (EDC) at the DGFI operates as ILRS Data Center adjacent to the CDDIS. Over the last years the data volume of SLR observations, predictions and products increased. An additional hourly and daily data exchange between CDDIS/HTSI and EDC demands an automated system for the management of data. This automated system checks the formats of incoming data (quick-look, full-rate, CRD, CPF). All valid data sets are published on FTP. Additionally all valid predictions are distributed via mail. The permanent upload of data to the EDC requires also a high available server structure consisting of two servers to minimize the downtime of FTP, web server, etc. The distribution of users to the available services on the servers is realized by using port forwarding of Iptables. This requires an additional timely synchronization between FTP and especially databases for the data management. Furthermore the mailing lists (SLR-Mail, SLR-Report) are automated by using the open source tool Mailman.

## 1. Introduction

The DGFI operates as EUROLAS Data Center (EDC) since 1994. The main task is to assure that the SLR data and products are available for the stations, analysis centers, combination centers, prediction providers and users. In Addition to the Data Center, the EDC runs the Operation Center. The task of the Operation Center is to check all kind of SLR observations such as Normal Point and Full-Rate data for format errors. Also products such as predictions have to be checked by the Operation Center.

## 2. System Architecture

The continuously uploading and downloading of data sets by stations, analysis centers, combination centers, prediction providers and users to the EDC requires an operational system which has as few as possible outages. To achieve this objective the system architecture has changed.

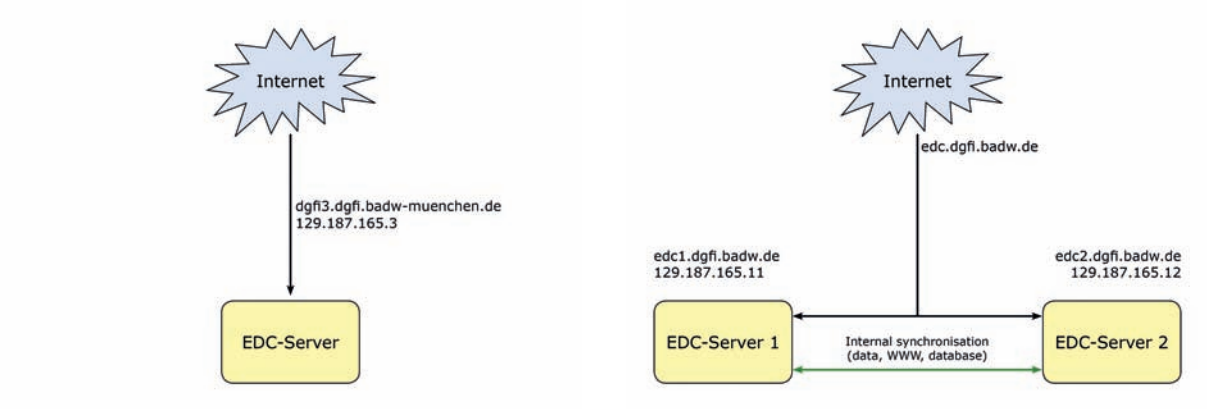


**Figure 1: Past and current system architecture**

In the past there was only one operational system available at the EDC. The backup of this system happened by saving the complete data holding on an internal server.

The system architecture has changed in the following way. There are now two identical mirrored systems available. The address of the FTP is ftp://edc.dgfi.badw.de. The user will be directed automatically to one of the FTP servers. By using techniques such as port forwarding the failing of individual services (FTP, WWW) can be handled by redirecting requests to different servers. This procedure minimizes the downtime of the EDC.

# 3. Data Flow of EDC within the ILRS

In last years the data exchange becomes more important. Especially the data transfer between the data centers EDC and ITT/CDDIS has changed. For Low earth orbit (LEO) satellites such as GRACE, GOCE are sub-daily predictions necessary. An additional hourly data exchange of data sets in the new Consolidated Laser Ranging Data (CRD) format and the Consolidated Prediction Format (CPF) was realized.

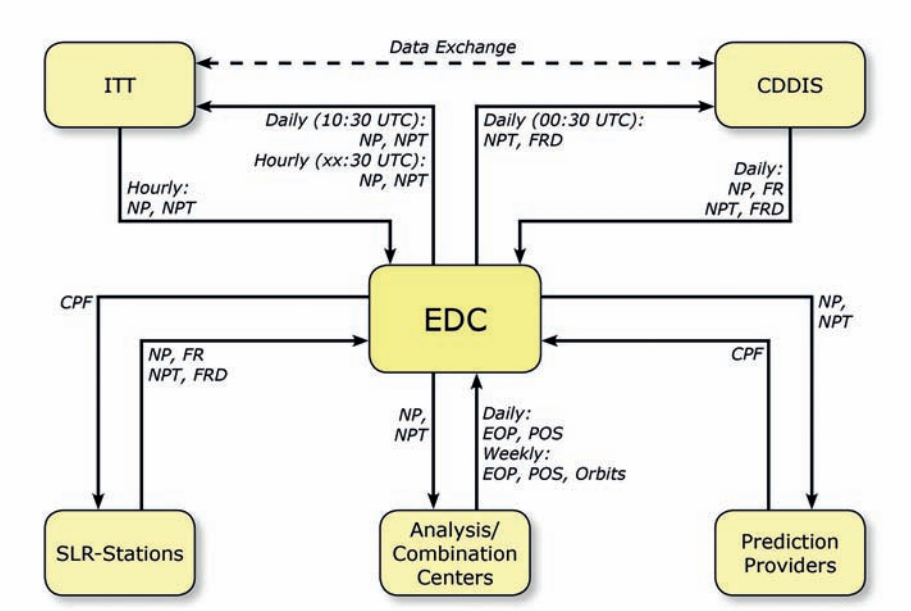


**Figure 2: Data Flow of EDC within the ILRS (NP: Normal Points (CSTG), NPT: Normal Points (CRD), FR: Full-Rate (MERIT-II), FRD: Full-Rate (CRD) and CPF: Predictions(CPF))**

The data flow in the ILRS begins at the SLR-stations, which send Normal Point and Full-Rate data sets to the Data Centers. In the Operation Center, all incoming SLR observation will be checked. All valid Normal Point data sets are sent to ITT the Operation Center of CDDIS every hour. Additional to the hourly file, a daily file is send to ITT at 10:30 UTC. Independently from ITT, EDC sends daily files with Normal Point and Full-Rate data sets at 00:00 UTC to CDDIS. On the other side, the EDC receives hourly Normal Points from ITT and daily Normal Point and Full-Rate data sets from CDDIS.

All SLR observations are available on the FTP server of the EDC (ftp://edc.dgfi.badw.de) for the ILRS-Community. Normal Points are used by the Analysis and Combination Centers for the estimation of EOPs, POS and Orbits. Normal Points are also used by Prediction Centers to estimate predictions of satellites. All of these products are also delivered to the EDC and are available on FTP. Additionally, predictions are forwarded via mail to SLR stations.

# 4. Data Management at the EDC

The EDC changes the procedure of managing SLR data and products with the introduction of the new Consolidated Laser Ranging Data (CRD) format, the Consolidated Prediction Format (CPF) and the change to a hourly data exchange.

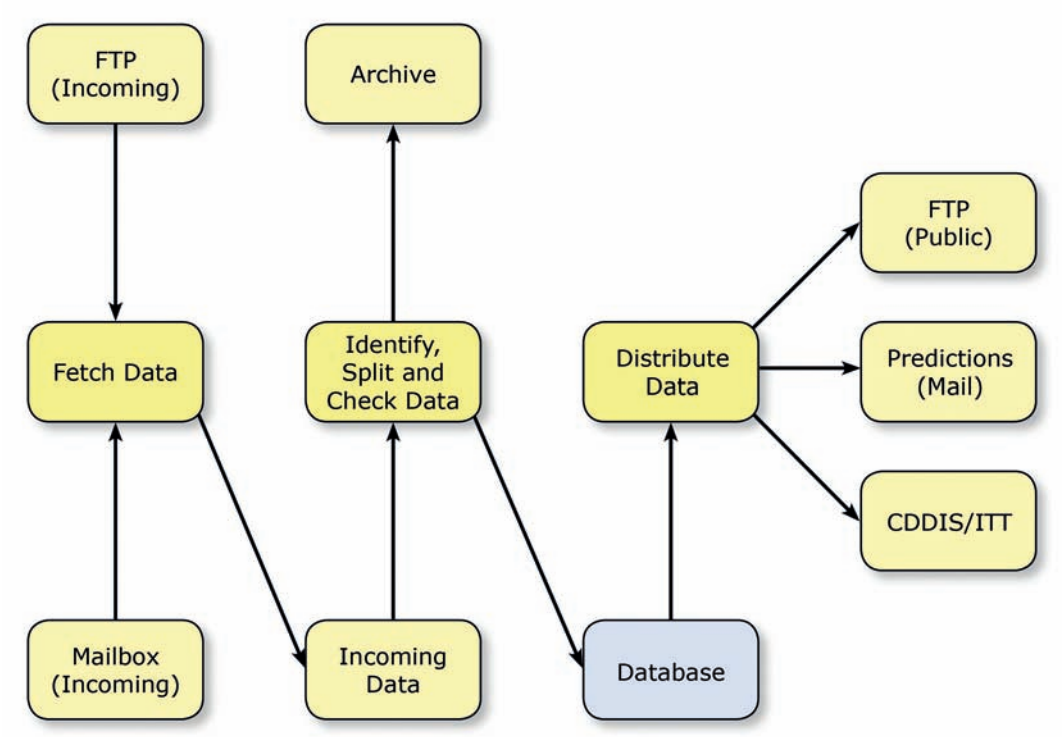


**Figure 3: Data flow at the EDC**

At the EDC, all kind of data sets are delivered by mail or ftp. The first step in the data flow is to fetch all data sets from the ftp and mailbox and move them into an incoming folder. Afterwards, a type-identification (NPT, NP, FRD, FR, CPF, etc) occurs. The original data set will be kept untouched with the original timestamp in an archive. Within the Operation Center all data sets are checked to detect format errors. If erroneous data is found the station manager will be informed to correct them. Multi pass files are split in single pass files. Every single pass file is now saved as a new data set in the data base. Every Normal Point and Full-Rate data set can be identified exactly by satellite id, station id, start date of measurement, end date of measurement and version. Predictions can be identified exactly by satellite id, provider, start date and end date.

The last step in the data flow at the EDC is the distribution of data. All valid data sets are published on the FTP for the ILRS-Community. Additionally CPF-Predictions are sent to the stations as fast as possible after the submission. Finally, the data exchange between EDC and CDDIS/ITT is made as described in the last chapter “Data Flow within the ILRS”.

# 5. ILRS-Mailing Lists

The EDC maintains the following mailing lists within the ILRS:

- *SLR-Mail* (http://slrmail.dgfi.badw.de)
- *SLR-Reports* (http://slreport.dgfi.badw.de)
- *Urgent-Mail* (http://urgent.dgfi.badw.de)
- *Rapid Service Mail* (http://rapidservicemail.dgfi.badw.de)

The SLR-Mail is used to communicate a message to the full ILRS membership (ILRS associates and correspondents). The SLR-Reports are usually computer generated reports to communicate a periodic status report to interested parties, which are suitable for automated processing. The Urgent-Mail informs station operators about upcoming satellite maneuver, urgent modification of satellite priorities, etc. The Rapid Service Mail informs stations and analysis centers about detected errors in SLR observations.

All mailing lists were handled by own scripts. They worked semi-automatic and required special tags for the handling of messages. A transition to the open source software "Mailman" was made. The mailing lists are now working automatically and don't need any special tags for the processing.

# 6. EDC-Website

The EDC has redesigned their website (http://edc.dgfi.badw.de).

This website provides near real time access to the data flow at the EDC. The current status of incoming Normal Points, Full-Rate data and Predictions are available. If erroneous data sets were submitted, information about the error is available.

There are also statistics about the data holdings of Normal Points, Full-Rate Data and Predictions available.

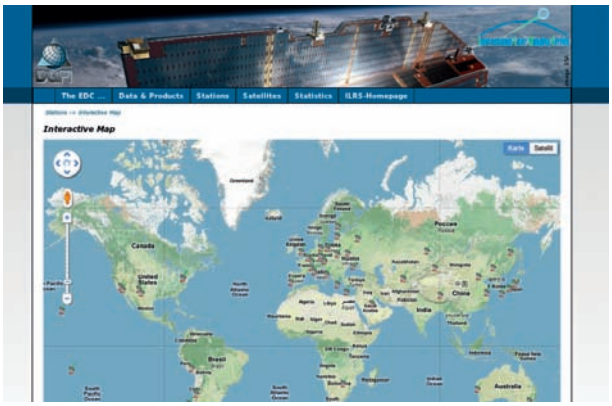


**Figure 4: Website of EDC**

## Correspondence

Christian Schwatke
Deutsches Geodätisches Forschungsinstitut (DGFI)
Alfons-Goppel-Str. 11
80539 München
Germany

schwatke@dgfi.badw.de

# Controlling Laser Ranging with RTAI-based Real-Time Linux

*Evan Hoffman, Randall Ricklefs*

ABSTRACT

Currently, many laser ranging systems, such as NASA's MOBLAS systems and the McDonald Laser Ranging Station (MLRS), use proprietary Unix-like real-time operating systems for time-sensitive ranging control software. Such OS's are expensive to maintain and often carry a risk of vendor lock-in. We outline a method of controlling an SLR system using the Linux operating system with the RealTime Application Interface (RTAI) hard real time extension. Linux provides a wide variety of software packages that have low operating cost, are under active development, and are open source. Two flavors of Linux are discussed: Arch Linux and CentOS. Both of these flavors have strengths and weaknesses when being used in a real time environment. Choosing which real time scheduler to use is important for programming considerations. Our approach uses the LXRT scheduler which allows real time control in user mode. We show effective control of an LR system using modest hardware. The current status of conversions of the Goddard Geophysical and Astronomical Observatory (GGAO) 48" telescope and MLRS is presented.

## 1. Introduction

Accurate satellite laser ranging requires a reliable and predictable method of controlling hardware. This is usually achieved through the use of software running on real time operating systems (RTOS), that is, operating systems whose response time to user-provided interrupts can be guaranteed to be in a given threshold regardless of other software running on the system. Currently, many SLR stations around the world use proprietary, Unix-like RTOS's for hardware control. At the time of implementation, these were the most efficient choices available. However, they are often times very expensive, and software developed for them is not always portable to other RTOS's, creating a risk of vendor lock-in. NASA's MOBLAS systems, and the McDonald Laser Ranging Station at the University of Texas, are examples of systems using proprietary RTOS's.

We propose replacing these proprietary RTOS's with an open source alternative, specifically, Linux. The 2.6 kernel, released in late 2003, provided a significant reduction of overhead thread processing over its 2.4 predecessor. In addition, it allowed processes running kernel mode to be partially preemptable [1]. An additional patch to the stock kernel, the RealTime Application Interface (RTAI), allows complete premption of kernel running processes [2].

We intend to use the 48" telescope facility at the Goddard Geophysical and Astronomical Observatory (GGAO) and the McDonald Laser Ranging Station (MLRS) as test stations using this new software.

## 2. Available Linux and Real Time Linux options

Linux has a large array of distributions suited for a variety of purposes. When selecting a distribution for our systems, we considered stability, quality of software repositories, and ease of maintainability. Arch Linux[3] was chosen for the 48" facility, while CentOS[4] was chosen for MLRS. Both have feature rich package managers for easy installation of software. A brief discussion of each follows. As development continues, these are subject to change.

## 2.1 Arch Linux

Arch Linux is a general purpose Linux distribution that focuses on simplicity and minimalism.

### 2.1.1 Advantages

- Arch is a rolling release distribution, that is, each software package is kept at the latest version available. This provides the system with the latest feature updates and bug fixes.
- Arch has an easy to use software package manager with a large library of free software.
- Arch is minimalist. Its base install has little software and low overhead. This allows the system to be lean and bloat free.
- Arch is designed for simple and centralized configuration (BSD style).

### 2.1.2 Disadvantages

- Being a rolling release, updates to the system should be done carefully as to not jeopardize the stability of the system. Latest software can introduce new bugs.
- Arch requires some knowledge about Linux/OpenBSD system management. It is not the most user friendly distribution on the market.

## 2.2 CentOS

CentOS is a distribution based on the popular Red Hat Enterprise Linux.

### 2.2.1 Advantages

- Similar to Arch Linux, CentOS has an easy to use software package manager with a large library of software.
- CentOS has a long term release based on Red Hat Enterprise Linux. It will be supported with security updates for years.

### 2.2.2 Disadvantages

- CentOS is not as lean as other distributions.
- The current CentOS kernel is 2.6.22.1, a couple versions behind the latest (as of this writing, 2.6.39.3).
- Latest software is not always available in the software repositories, as there is an emphasis on stability.
- Clean shutdown and reboot times are slower when compared to current proprietary RTOS's in use, such as LynxOS as well as other distributions such as Ubuntu.

## 2.3 Other Linux Options

A full discussion of available Linux options is beyond the scope of this paper. Several other popular distributions were considered. Ubuntu is very popular and user friendly, but suffers from significant bloat. Debian has a reputation for rock solid stability and a very long release time, though its software is usually held several versions back.

# 3. RTAI: What is it and how does it work?

There are several different real time Linux options. RTLinuxFree, Xenomai, RTAI are free examples, while commercial options such as RTLinuxPro and BlueCat Linux are also available. A complete discussion of them is beyond the scope of this paper. RTAI was selected as it has a very active user base and is free.

RTAI is an real time extension of the vanilla Linux kernel, allowing hard real time. After the patch is applied, it runs as a second kernel alongside the regular Linux kernel. In addition, a nanokernel abstraction layer called Adeos [5] runs as an interface between the Linux kernel and the RTAI kernel. This allows RTAI to take over real time interrupts, while passing regular ones to the regular Linux kernel. The RTAI API is POSIX compliant, which means that much code that has already been written for the proprietary RTOS's can be reused.

RTAI has two process schedulers available to it. The one we have selected, LXRT, provides hard real time in user space, allowing non-root users the ability to run hard real time dependent programs. The advantage is that it allows programs to run without touching the kernel code, which allows for easier programming. It also more closely models how current proprietary RTOS's are used at the NASA stations.

# 4. Advantages and Disadvantages of Real Time Linux

Here we briefly discuss predicted advantages and disadvantages to using RTAI based real time Linux, in an SLR context, over current proprietary RTOS's.

## 4.1 Advantages

- RTAI is completely free and open-source. This will allow SLR stations greater control over software and give them the ability to modify it to suit specific needs that may be unique to SLR work. It also reduces possible licensing costs associated with proprietary software.
- Many distributions of Linux have a proven record of stability and security.
- There is a large (and often free) software library available for Linux. Since RTAI runs alongside the regular Linux kernel, a system using it can run any software that was designed for Linux.
- RTAI has an active community for collaboration and support.

## 4.2 Disadvantages

- Commercial support is unavailable.
- Up to date documentation can sometimes be difficult to find. Conflicting versions of API documents can cause confusion.

# 5. At MLRS

The Linux/RTAI upgrade at MLRS steals time when the ranging crews are not at work to slip a disk drive with the new operating system and software into the operational ranging system. Thus far, the RTAI/Linux system properly controls all the existing hardware from meteorological sensors, to timing electronics, to the laser and telescope. Hardware-based simulation of tracking can run for hours without unexpected problems. Tests tracking stars and satellites show the system can properly handle the telescope mount. Real satellite ranging was only attempted once so far, with internal calibrations working properly. No satellite data was obtained, but that was not surprising since the engineering staff and not an observing crew made the attempt.

A couple major issues remain. The software could probably be used in production as is, although that won't be done because the CAMAC device driver is not yet running in hard real time mode. The result is that any major disk accesses, such as starting a web browser or compiling software will temporarily drop real time interrupts and therefore prevent ranging.

The other issue is that shutting down or booting CentOS takes much longer than with the proprietary real time OS or other Linux distributions such as Fedora or Ubuntu. Tests will be made with the latest Ubuntu long term support (LTS) version with the aim at replacing CentOS. Initial results are encouraging.

# 6. At GGAO

The upgrade to RTAI for the 48" facility is part of an ongoing modernization effort. Currently the facility uses a CAMAC interface with ISA computer boards for its hardware/software interface. Using a modern computer with a PCI and PCI Express bus, it is intended that the entire console and control logic be replaced, as well as the optical encoders and the servo pre-amplifiers. PCI and PCI express I/O cards are planned to replace the entire CAMAC interface.

Much of the software code structure is being maintained for the new system, however, the old Motif GUI is being replaced using the GTK+ toolkit. In addition, as RTAI runs as its own kernel, it must communicate with the regular Linux kernel through shared memory and RTAI FIFOs. A major software re-write is underway.

Currently, much of the GUI software has been written. Timing signals and analog out signals are being controlled and read in real time using RTAI. Encoders have been read in soft real time, and conversion to hard real time is underway. These are significant steps to producing a real time system capable of controlling the telescope; an encoder-in analog-out system provides the basic feedback loop necessary.

Due to the large scale of the upgrading effort, progress with the RTAI portion has been slower than hoped, but steady. New optical encoders have been installed into the system, and a logic interface is being tested to read them reliably with the new hardware.

## Conclusion

We believe that, given the results of our expermients at the 48" facility and MLRS, RTAI based real time Linux is a good candidate for replacement of proprietary RTOS's involving the control of SLR systems. There is still much work to be done to prove the concept. Progress speed is dependent on available funding and hours to devote to the project. The ultimate goal will be to acquire good data using an RTAI based system. We hope to make significant progress towards this goal in the coming months.

## Acknowledgments

Ricklefs would like to thank NASA for support through NASA contract NNG06DA07C and others in the laser ranging community for their encouragement.

Hoffman would like to thank Jan McGarry, Tom Zagwodski, Jack Cheek, Howard Donovan, and many others at NASA , HTSI, and the ILRS community for their continuing support.

## References

[1] "Real-Time and Performance Improvements in the 2.6 Linux Kernel | Linux Journal." *Linux Journal | The Original Magazine of the Linux Community*. Web. 29 July 2011. <http://www.linuxjournal.com/article/8041>.

[2] *Di Milano, Politecnico*. RTAI - Official Website. Web. 29 July 2011. <http://www.rtai.org>.

[3] *Arch Linux*. Web. 31 July 2011. <http://www.archlinux.org/>.

[4] *The Community* ENTerprise Operating System. Web. 31 July 2011. <http://www.centos.org/>.

[5] "Adeos." Web. 31 July 2011. <http://home.gna.org/adeos/>.

## Correspondence

Evan Hoffman
Honeywell Technology Solutions, Inc.
7515 Mission Drive
Lanham
MD 20706

Evan.Hoffman@Honeywell.com

Randall Ricklefs
The University of Texas at Austin, Center for Space Research
3925 W. Braker Lane
Suite 200
Austin
TX 78759-5321

ricklefs@csr.utexas.edu

# SLR Automation for the New Space Geodesy Multi-Technique Sites

*Jan McGarry[1], Scott Wetzel[2], John Cheek[3], Thomas Zagwodzki[4], Christopher Clarke[5], Howard Donovan[5], Julie Horvath[5], Anthony Mann[5], Donald Patterson[5], Randall Ricklefs[6]*

ABSTRACT

The original NGSLR plan was for a completely automated stand alone system using an eye-safe laser. Since then the requirement for daylight GNSS ranging has been added, and NGSLR is now part of a larger multi-technique facility which includes VLBI, GNSS, and DORIS. Because of this the automation needs have also changed. NGSLR must now interface with and potentially automate much of the Laser Hazard Reduction System (LHRS). Daylight GNSS tracking has made the signal processing and automated closed-loop tracking more challenging. Automated real-time coordination between VLBI and SLR has now become a requirement, and automated surveys between all of the systems are being planned. A brief discussion of the status of NGSLR automation will be presented along with some preliminary thoughts on near term station automation design work.

## 1. Background

NASA's Next Generation Satellite Laser Ranging System (NGSLR) was originally designed to be a completely autonomous satellite laser ranging system, with the capability of ranging to low Earth orbiting satellites and LAGEOS during both night and day [1] [2]. Ranging to satellites at altitudes higher than LAGEOS was to be a night-time only requirement with daylight ranging a best effort.

NGSLR is now part of the new NASA Space Geodesy Project's Multi-Technique Fundamental System which includes Very Long Baseline Interferometry (VLBI), Global Navigational Satellite System Receivers (GNSS), and Doppler Orbitography and Radiopositioning Integrated by Satellite (DORIS). Coordination between NGSLR and the other techniques as well as daylight ranging to the high altitude GNSS satellites [3] have both become a requirement.

## 2. Planned Automation

To operate completely autonomously NGSLR needed to transmit at eye-safe laser energies (60 microJoules at 300 picosecond pulsewidth) because of Federal Aviation Administration (FAA) regulations in the United States regarding hazardous laser transmissions skyward. To maintain a similar return rate to existing NASA systems and to facilitate system automation, the laser pulse repetition frequency (PRF) was chosen to be 2 kHz.

The software was designed to make all of the decisions that are normally made by the system operator, including closing the system for inclement weather, determining what to track based on cloud cover, determining when signal is being received from the satellite, and closing the tracking loop to optimize the signal response.

In addition it was planned for the software to continuously monitor the sun angle and prevent the telescope from getting within 15 degrees of the sun. The software was to configure all of the hardware including optics on the transceiver bench and was to completely control switching from satellite tracking to ground calibration to star calibration. The transceiver bench controls include:

[1] NASA Goddard Space Flight Center
[2] Honeywell Technology Solutions Incorporated
[3] Sigma Space Corporation
[4] Cybioms Corporation
[5] Honeywell Technology Solutions Incorporated
[6] University of Texas at Austin

- Laser divergence
- Receiver FOV
- Risley point-ahead
- System focus
- Daylight / twilight filters
- ND filters
- Shutters for camera and detector
- Blocks for laser

As in other NASA systems the data processing was to occur automatically after each pass with the standard SLR products delivered within two hours of data collection.

A Remote Access Terminal (RAT) was designed to provide the interface for a human to monitor and control the system, either locally or remotely. The RAT laptop was not required when the system was running autonomously.

The original system design included hardware and software to monitor the health and safety of the system. The Health and Safety subsystem as planned consisted of:

- Remote monitoring and alerts
- System security
- HVAC monitoring
- Prime voltage monitoring
- Interior and exterior cameras
- Motion and vibration sensors, door/gate interlocks
- Temperature and humidity sensors
- Water sensors
- Emergency shutdown

# 3. Automation Status

Much of the operator decision making software is written and tested. The weather monitoring software and hardware is mature. The cloud cover monitoring station is complete and the decision software to make use of the sky information is in progress. The real-time signal processing algorithm works well for LAGEOS and LEO in both night and day. Closed loop tracking automation is in progress.

The system scheduling software is finished and in use for many years, and the data processing and product delivery is nearing completion. The sun avoidance software is tested and has been operationally working well for almost two years. Software to control all the optics in the system is nearing completion, and control of the system configuration settings is underway.

The Remote Access Terminal software is mature and has been in use for many years. Currently monitoring and control of the system requires access from within the Goddard firewall.

The Health and Safety subsystem will still be needed for completely autonomous operation, however, this subsystem is not in the NGSLR prototype as the current plans are for semi-autonomous operation. This is due to FAA requirements to have an operator present during all non-eye-safe laser operations.

# 4. New Requirements for GNSS Daylight Ranging

Because of the daylight GNSS requirements, NGSLR will require the use of a laser with a minimum of 1 milliJoule per pulse output at a pulse repetition frequency of 2 kHz which is non-eye-safe. Ranging with this laser will require the use of an aircraft avoidance radar and its associated beam blocks and ND inserts. This system, called the Laser Hazard Reduction System (LHRS), will require a new interface which will give the software the ability to both monitor and control the LHRS.

GNSS daylight ranging poses challenges for the signal processing. The high daylight noise rates combined with the low signal return rates will likely require an upgraded signal processing technique. The current software can find signal with return rates as low as 0.0005 per shot, but to date GNSS ranging has generally been less than this.

# 5. New Automation for the Multi-Technique Site

The multi-technique site will need to automatically coordinate the day to day scheduling to provide seamless non-conflicted operations between all of the system, to support remote or unmanned operations of each technique, to maximize performance and reduce cost, and to allow for site surveys between systems to monitor site ties.

# 6. Coordination between VLBI and SLR

Some analysis has been performed on the coordination of VLBI2010 and NGSLR where damage to the VLBI2010 receiver could occur if the two systems were pointed at or close to each other. In 2010 a study was performed to determine the overload threshold of VLBI2010 Broadband receiver from RFI from the SLR LHRS [4]. Currently NGSLR has implemented a telescope mask to restrict pointing its radar within the calculated damage region of VLBI2010.

Real-time knowledge of the antenna and telescope pointing will allow for the highest individual system performance while protecting the VLBI2010 system from damage. The real-time pointing avoidance model used on Mauna Kea and Maui [5] will be reviewed as a potential starting point for this work.

## Conclusion

Requirements for NGSLR have changed over the past decade. Continued evolution of NGSLR into the Fundamental Station concept will improve the science product but introduces new challenges. NGSLR automation and fulfilling the Fundamental Station requirements will be the major tasks to be completed at Goddard under the newly awarded Space Geodesy Proposal.

## Acknowledgements

NGSLR SLR development is funded by the NASA/HQ Science Mission Directorate. The authors would like to thank John LaBrecque of NASA/HQ for his continued support of the NGSLR SLR work.

## References

1- *Degnan, J., J. McGarry, and T. Zagwodzki,*1996: SLR2000: An Inexpensive, Fully Automated, Eyesafe Satellite Laser Ranging System, Proceedings of 10th International Laser Workshop on Laser Ranging Instrumentation, Chinese Academy of Sciences, Yang Fumin (ed.), 367-377, Shanghai.

2- *McGarry, J. and T. Zagwodzki,* 2006: SLR2000: The Path toward Completion, Proceedings of the 15th International Workshop on Laser Ranging, pp 265-269, October 15-20, Canberra, Australia.

3- *McGarry, J., T. Varghese, T. Zagwodzki, J. Degnan, J. Cheek, et al, 2011*: Improvements at NASA's NGSLR in Support of GNSS Ranging, in this Proceedings.

4- *Beaudoin, C.J., and S. Cappallo:* 2010, MOBLAS 7 and NGLR Radar Power Level Measurements Collected at GGGAO, BBDEV internal memorandum #037, Massachusetts Institute of Technology.

5- *O'Gara, D., E. Kiernan-Olson, C. Giebink, and D. Summers,* 2011: Implementation of the LASER Traffic Control System at the Haleakala Observatories, in this Proceedings.

## Correspondence

Jan McGarry
NASA Goddard Space Flight Center
Code 694
Greenbelt
Maryland 20771
USA

Jan.McGarry@nasa.gov

# SLR-2.0: An overview about the new SLR/LLR control software from Wettzell

*Martin Ettl, Alexander Neidhardt, Pierre Lauber, Andreas Leidig, Johann Eckl, Martin Riederer, Lea Schreiber, Reiner Dassing*

ABSTRACT

This paper gives an overview about how the new developed software SLR-2.0 from Wettzell works. It reveals the internal structure and architecture of the software. This new approach is very flexible and adaptable to future needs and requirement. One of the key features is fast interleaving between satellite passages, which was not available at the former system. The new software is written in C/C++ and is based on a client/server architecture which is extraordinary flexible. Furthermore, it is organized in several layers with a strict separation between the data representation and the data processing. According to Wettzell's approach, all the processing is done at the server side and the user interface acts only as client. This graphical user interface (GUI) is based on wxWidgets, a platform independent framework. Based on this, a set of extensions were developed, which are the basic components for our software at the representation layer.

## 1. Introduction

The former SLR software, running at the Wettzell Laser Ranging System (WLRS), is historically grown and therefore written in several programming languages: LabVIEW [1] , Python, C, Perl and Fortran. An impression of the former SLR software structure is shown in fig. 1, which it has been operational successfully since the 1990th. Therefore it was a stable software infrastructure. Never the less, problems in maintainability and changeability motivated us to start the development of new software for the Satellite Observing System Wettzell (SOSW). Therefore, a new software approach based on state-of-the-art techniques was started.

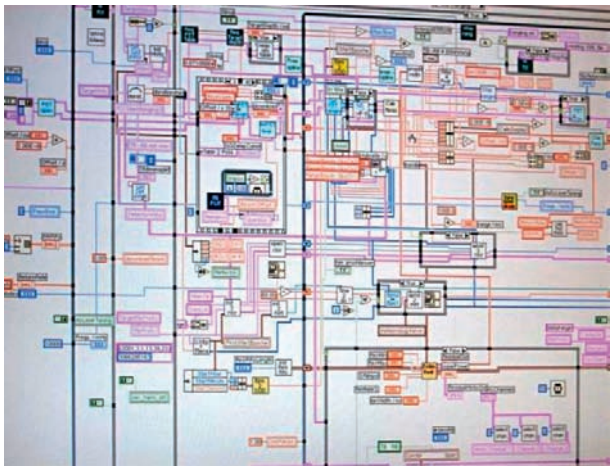

**Figure 1: Screenshot of the former SLR software written mainly with LabVIEW**

[1] http://sine.ni.com/np/app/flex/p/ap/global/lang/de/pg/1/docid/nav-77/

# 2. SLR2.0 as a complete redesign

Using C/C++ and Perl in combination with modern software development methods, the whole control system was redesigned and rewritten. The idea was to solve the following disadvantages of the former SLR software:

- The LabVIEW code was based on National Instruments LabVIEW version 5. Because of release jumps of the licensed LabVIEW environment the existing, older hardware access was not supported anymore or was only possible with big changes in the software. Newer hardware is only supported by the ne wer releases. Therefore it caused problems in upgrading the controlling computer (wlrctrl), for which spare parts are almost not available anymore.
- There is almost no documentation available about the software internals. A lot of experience was necessary to do changes in the system, without damaging the functionality.
- The setup and shutdown times for satellite observations were too long, so that switching between satellites (interleaving) had large time constraints.
- The software didn't include Lunar Laser Ranging.
- The software interaction is not comfortable and flexible enough for operators.
- The whole observation is interactive. For example, the selection of the satellite and long-/cross-tracking of the satellite position are done manually.
- The whole software design is not flexible and extensible enough for future needs, such as time transfer or transponder missions or at least just for new Linux operating systems (32-, 64-bit).
- Too many different languages were used. This caused problems in interfacing between the different pro gramming languages.
- The communication between the devices is not standardized and uses proprietary protocols, which are not always error-proven.

Therefore the new design realizes a classic client-server-model on the basis of a communication with Transmission Control Protocol over Internet Protocol (TCP/IP) or User Datagram Protocol over Internet Protocol (UDP/IP). Each hardware device is represented as a service-offering server. A service requesting client starts the communication and sends an order request via message communication to such server. At the server side, the order is processed and an answer message is returned to the client [1].

Another attempt reduces the efforts of communication programming by defining a standardized way for the transmission of remote procedure calls (RPC). RPCs are comparable to local calls of procedures in a structured program but realized as control and data flows over a communication network to allow a standardized interaction between a requesting client and a service offering server [1]. Then the client just calls a procedure or function without the knowledge of the processing location and an additional RPC communication layer realizes the transfer between the remote processing server and the client. The response follows the same way back to the client, so that the procedure call appears to be local [2].

The complete system itself is then a direct representation of identified, independent, but interacting hardware and software components. In general a modern laser ranging systems can be described as a distributed system in terms of computer science. Several independent processes partly on different computers are connected together to solve a collective task in a cooperative way. They communicate information while transferring messages via a computer network. [2]

The system is hierarchically structured where each communication stack has the similar layers:

- the presentation layer with the graphical user interface
- the communication layer using RPCs and
- the processing layer with the server functionality and device control

The complete stack for a single communication in the new SLR-2.0 is shown in fig. 2.

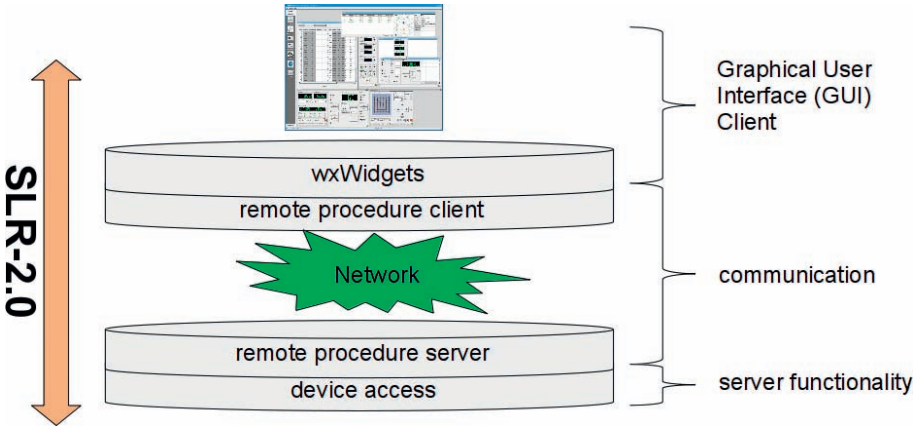


**Figure 2: The client/server architecture and multilayer design of SLR-2.0**

To simplify the RPC usage a self-made additional generator on the basis of the SunRPC generator "rpcgen" was developed, which could be continuously improved. It converts an interface description in a C style format into all needed modules for the RPC communication. The generator also adds safety mechanisms as server watchdogs or an automatic safety device. This device acts similar to a "dead man's handle" in trains, with the difference that it can run dedicated actions if no responsible client is available anymore. [3] The generator is currently used as a basic mechanism for all standardized communication tasks within distributed systems. Therefore it creates also the communication for the remote control of the telescopes for the Very Long Baseline Interferometry at Wettzell, Concepción/Chile and O'Higgins/Antarctica [4].

According to the new RPC philosophy, the graphical user interface plays the role of a remote procedure client, which just presents the requested information. It is written in wxWidgets , which is a toolkit for creating user interfaces on several platforms. A lot of extensions have been developed in addition to the standard library of wxWidgets[2]. These features are also under the terms of open source software. As visible in fig. 2, the graphical user interface is a separate layer, which is independent from the communication model. This makes it easy for adaption to changing requirements in case of future graphical user interfaces or communication methods.

# 3. The new central GUI component

In combination with new graphical user interaction features a new component becomes one of the central elements: the skyplot. It replaces the former alert list and contains several satellite and control information in just one, graphical presentation. Fig. 3 shows a screenshot of the new skyplot in SLR2.0.

As replacement of the former alert list the skyplot shows current satellite passages printed graphically over a 360 degree azimuth (with north on top) and 90 degree, ring-based elevation (with 90 degree in the center and 0 degree at the utmost ring) coordinate system. Passages are updated regularly. Rectangles show the current position of the satellite while solid lines represent the future passage segment and doted lines show the past segments. The current telescope position is shown as a blue line from the center with a cikrcle at the end. It shows where the telescope currently points to.

Another helpful information is the sun avoidance area, which marks a restricted region, where should not be pointed to, to protect the telesope and optics from damages because of direct sun light injection. In combination with a transponder based aircraft tracking system the positions of the aircraft over the observatory are printed (red crosses). This additional information helps operators to manually check in-sky-safety constraints beside the interlock mechanism based on an Laser Hazard Reduction System radar.

[2] http://www.wxwidgets.org/

A further nice extension would be a fish eye camera, using the visible and infrared light. With such an equipment it would be possible to show the cloud coverage at day and night. This improves the usability of the system and simplifies the scheduling decisions for operators. Therefore the skyplot offers a complete tracking information and can be used for automation implementations in the future.

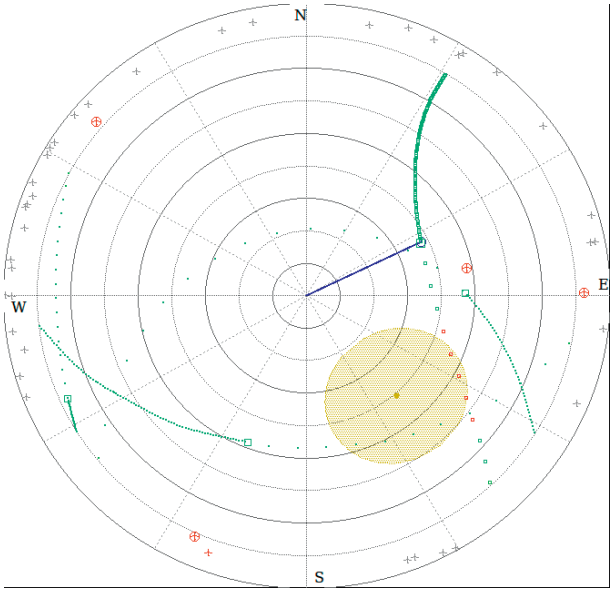


**Figure 3: The central, graphical skyplot component of the SLR2.0 software**

# 4. Conclusion and outlook

The software is currently in the process of integration tests [5], done in parallel along with the former system. First observations with the new system showed the correctness of the measured passages and the resulting normal points. Switching between the two systems is quite fast and straight forward, as the modular and flexible design of the new software allows direct combinations of both systems. In the near future the software will be also extended with LLR observation capabilities. First feasibility studies were already made in a diploma work [6]. The prediction calculation is already tested and compared to other solutions from the observatory Grasse/France and Texas and first pointing tests with the real hardware confirmed the correctness by pointing to the region of the lunar reflector of Apollo 15. The next steps are, installing the software on the new Satellite Observing System Wettzell and preparing everything for remote operations from the current Wettzell Laser Ranging System.

## References

[1] *Singhal, Mukesh; Shivaratri, Niranjan G.*: Advanced Concepts in Operating Systems. McGraw-Hill, Inc. 1994

[2] *Neidhardt, A.; Ettl, M.; Lauber, P.; Leidig, A.; Dassing, R.; Mühlbauer, M.; Plötz, C.*: New concepts in control systems for SLR with remotely accessible, autonomous process cells; in: Schillak, S. (eds.) Proceedings of the 16th International Workshop on Laser Ranging, SLR – the Next Generation, Vol. 2, pp 456-461, Space Research Centre, Polish Academy of Sciences, 2009

[3] *Neidhardt, Alexander*: Manual for the remote procedure call generator “idl2rpc.pl”. Geodetic Observatory Wettzell 2008 (latest stable version)

[4] *Neidhardt, A.; Ettl, M.; Rottmann, H.; Plötz, C.; Mühlbauer, M.; Hase, H.; Alef, W.; Sobarzo, S.; Herrera, C.; Himwich, E.*: E-control: First public release of remote control software for VLBI telescopes; in: Behrend, D.; Baver, K. D. (eds.) VLBI2010: From Vision to Reality, IVS 2010 General Meeting Proceedings, NASA/CP–2010–215864, pp 439-443, NASA, Goddard Space Flight Center, 2010

[5] *Ettl, M.; Neidhardt, A.; Dassing, R.*: Continuous integration and quality control during software development; The Growing Demands on Connectivity and Information Processing in Radio Astronomy from VLBI to the SKA, Aveiro, Portugal, 25.05.2011

[6] *Schreiber, L.*: Integrating Lunar Laser Range Prediction into the Wettzell Laser Ranging System Operations, 2011

## Correspondence

Martin Ettl
Forschungseinrichtung Satellitengeodäsie
TU München
Geodätisches Observatorium Wettzell
Sackenrieder Str. 25
D-93444 Bad Kötzting

ettl@fs.wettzell.de

Alexander Neidhardt
Forschungseinrichtung Satellitengeodäsie
TU München
Geodätisches Observatorium Wettzell
Sackenrieder Str. 25
D-93444 Bad Kötzting

neidhardt@fs.wettzell.de

(Correspondence to the other authors will be forwarded)

# Automation and remote control as new challenges on the way to GGOS

*Alexander Neidhardt, Martin Ettl, Pierre Lauber, Andreas Leidig, Johann Eckl, Martin Riederer, Reiner Dassing, Matthias Schönberger, Christian Plötz, Ulrich Schreiber, Iain Steele*

ABSTRACT

The ideas of a Global Geodetic Observing System (GGOS) need technical realizations as pathfinder technologies. In the future more observatories with co-located techniques will observe much more than now. To be able to follow these goals it is necessary to realize automation techniques and new technical observation strategies. The paper points out the chances and possibilities of new workflows and shows a realization of similar structures in the astronomical community.

## 1. Introduction

The Global Geodetic Observing System (GGOS) and its proposed network of Fundamental Stations is a vision for the future in geodesy and Earth science [1]. To implement this network and realize these benefits, it is necessary to understand the technical requirements and possible options to address them. It is essential to consider the needs of each of the space techniques at a site as well as solutions to optimize operation work and data flows over the sites, among network sites, and with any central control and reporting facility within the network. New technical possibilities are available, which might improve the network of SLR stations as well to interact as one global SLR observing system.

## 2. Interactive real-time workflows

It is essential to think about optimizations of the current workflows. Higher observation loads need more cooperation among the observatories and a sophisticated feedback structure in real-time. In future GGOS scenarios it might be useful if the ILRS data and analysis centers also offer input to coordinate observations. Observation restricted targets and time transfer requires a pre-defined scheduling, where priorities and go-nogo-flags are defined by the centralized data centers. Therefore it is not only necessary for telescope sites to fetch the prediction files but also the operation relevant scheduling information. Optimized to dedicated research needs it could be helpful to force observations of special targets in future scenarios. Special telescope sets and combinations could be selected for a dedicated time period to realize a temporarily required task in the global network of telescopes.

In general the main modules of the workflows can normally be found in similar ways in all the systems of the geodetic space techniques with more or less extensive subsections. The main workflow parts for SLR observations can be seen in figure 1. The first step of SLR control is the fetching of the prediction files, which includes the preparation of the ranging relevant passage information for the dedicated site. A crude scheduling offers a sequence of possible satellite passages, which must be rescheduled with finer granularity during the ranging. Currently this is mostly done by a human operator manually. The actual ranging normally lasts a few minutes and produces system specific observation files. These intermediate files are stored and processed to calculate the normal point files, which are sent to the data centers, where the analysis centers have access on it.

Currently the near real-time knowledge about the operations in the network is given by the EUROLAS status information as EUROLAS near-real-time display since 2002 [2], which is sent by several ranging sites. This rudimentary network status can be requested and offers information as the currently observed satellites, hit rates or sequence numbers of the used prediction of the different ranging stations. In future it might be interesting to include the status information into the scheduling procedure. This could improve the network performance as it would become possible that different telescopes observe different pass segments of the same satellite or different passages in a remotely controlled way. Another interesting aspect might be to increase the status information. Raw data from the telescopes can be sent to analysis centers, which can perform standardized quality checks and offer immediate feedback to the telescopes in real-time, which is interesting for future time transfer scenarios.

For the SLR control itself it is necessary, that the operator is supported by dedicated protocol logs, checklists and history graphs of monitoring data. These additional data sets offer a general overview about the system. They can be organized in data for science and analysis (e.g. meteorological data or clock offsets), data for system operations (as emergency stops or laser or rack temperatures) and data for diagnosis (as servo currents or contouring errors). The data are collected by a system monitoring equipment with sensors and actuators. Also the safety system to protect human operators is included to such a system. To support the operator with needed monitoring data it is necessary to present the checklist details and operating states as well as the historic data over time in an ergonomic way.

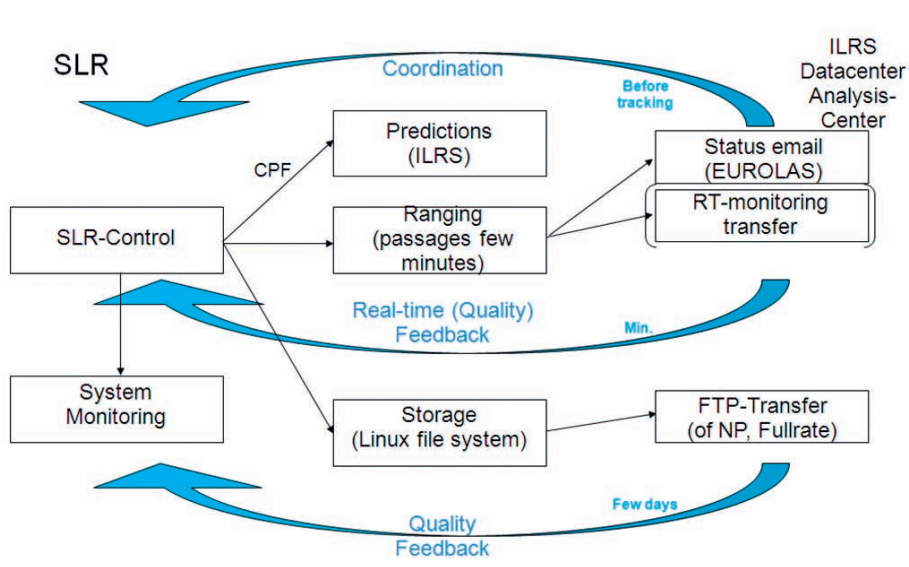


**Figure 1: The design principle**

The control software should be separated into such general, re-usable modules. Standardized communication access points also to the observatories on save and secure networks allow a better interaction to realize one global SLR observing system. New techniques allow to realize new, technical observation strategies.

# 3. Possible, technical observation strategies

The standard case to control operations for a laser ranging observation is that an observer controls the system locally on site at the telescope (local observation). He has direct access to the control system, the hardware, as the laser, the optics and the telescope itself. In case of an error the operator can directly interact and stop the system manually. It is important, that well educated personnel can detect problems immediately by using all human senses. But this operation mode is also the most time consuming one in case of operator manpower.

With new remote control technologies it is no longer necessary for the operator to be on location (see figure 2). An operator can control the system from remote (remote observation). On stable Internet connections and with intelligent and self-controlling mechanisms on location of the telescopes critical situations can automatically be detected. Autonomous, redundant systems can check system states and stop the operation in case of an error. The important system information can be transferred to responsible operators over the Internet to each place all over the world. As the operator just gets the information, which is offered by the system, an additional monitoring on location of the telescope must replace the senses of a local operator. These monitoring data allow an automatic detection of critical states and situations, either automatically taking action or informing the remote operator.

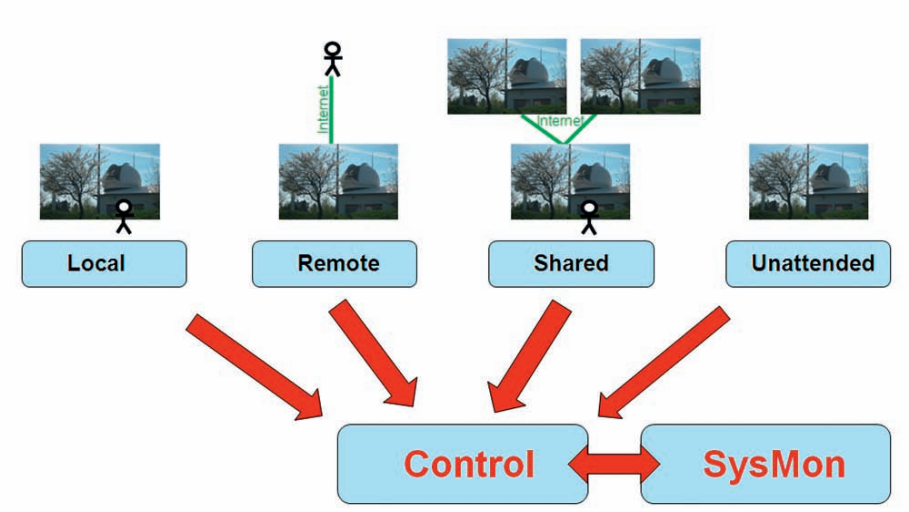


**Figure 2: Possible, technical observation strategies using a standardized control access and a separated system for monitoring of the telescope environment**

A big issue within this context is to realize the laser safety on earth and also in sky, to protect human operators and also participants in air traffic. Currently the laser observations are normally protected by a radar system. But the used, pulsed radar frequencies are not compliant with the broadband concept for future radio telescopes of the VLBI2010 series of the International VLBI Service for Geodesy and Astrometry (IVS). Therefore it is necessary to realize new technologies for the in-sky-safety in case of future GGOS stations. Reduced, eye-safe laser power, the usage of radio transponders of the aircrafts or alternative, optical systems as LIDAR are possible starting points. Combinations of these techniques may offer the necessary operational and functional safety, which is necessary for the remote and automated observing.

If the technical issues for laser safety are solved the new control technology can also be used to operate more than one telescope by a single operator. This is required for the operation of the two laser ranging telescopes at the observatory Wettzell, as a single operator should be able to control both telescopes from one operations desk. Furthermore the control can be shared between different operators on different sites (shared observation). Therefore sophisticated graphical user interactions with the control system are as important as reliable communication systems. Communication losses must be detected, reestablished and proofed. During blackouts the systems must be able to run autonomously. With reliable autonomous techniques it might also be possible to run operations completely unattended (unattended observations). But to realize this it is necessary to investigate more on scheduling mechanisms and intelligent decision strategies during the ranging and for the startup of an observation of a following satellite passage.

These remote and shared observations offer many possibilities: A passive data access can be granted for live monitoring. There are possibilities for tele-working with full control access. Specialists can assist local operators by remote. Shared observations can reduce the manpower for shifts or help react to current research requirements. These shared observations are not restricted to systems of one dedicated space technique but can partly be arranged over system borders. Tests at Wettzell are already performed, where student operators at the laser ranging system also take care of the weekend sessions at the radio telescope.

In general well maintained and stable telescopes are needed. It is also helpful to have an on-call service, where especially trained staff can be activated on time to react on critical, automatically or from remote not solvable situations. The most important implementation of the system to detect such situations is a functional and detailed system monitoring (Neidhardt et. al., 2010).

# 4. An example from astronomy: the fully robotic Liverpool telescope

Which impact new observation strategies can have, is shown by a realization of a fully robotic, optical telescope: the Liverpool telescope. Located at La Palma on the Canary Island it operates completely unattended. It means that no staff at all is on site. The telescope offers different sensors, as CCD imagers, a polarimeter and a spectrograph, which can be selected by the users individually. Therefore about 50 common users from about 20 institutions can use the instrument for their individual research needs according to budget levels and priority settings. The total operating budget per year is 600,000.- Euro. Using such a robotic telescope increased the number of relevant publications from lower than 5 to over 30 during the last years while the technical downtime could be decreased to about 4% per year. All of these competing user interactions are only possible by using a sophisticated web interface, where users can place their orders for observation time.

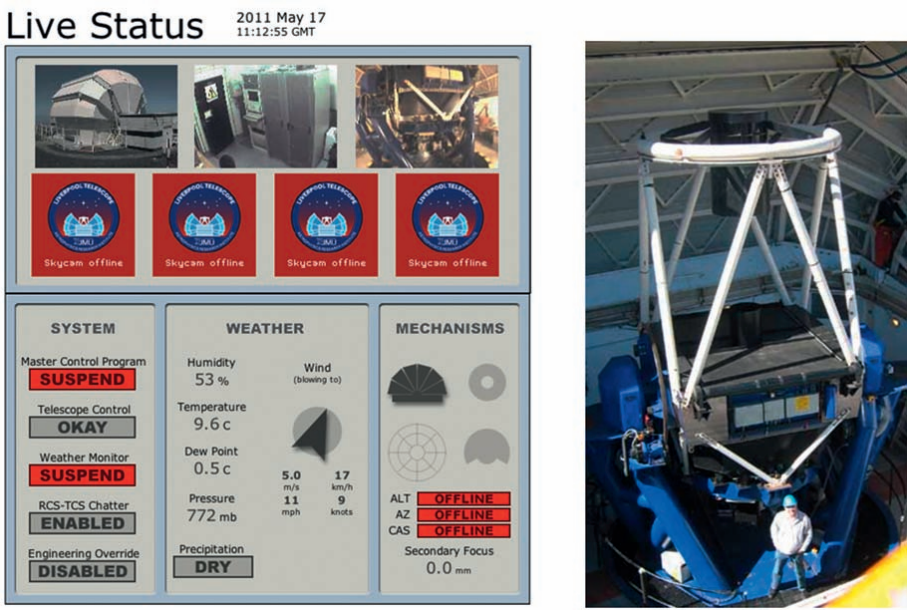


**Figure 3: The 2.0 meter Liverpool telescope on the Canary Island (r.) and its web-based live status display (l.)**

The users can define fixed timing constrains or observing constraints as solar elevation constraints, seeing constraints or lunar distance constraints. Once an observation is scheduled the remote user is informed about the system status via a live status display on the web (see figure 3). Several webcams offer different views into the operational building. Meteorological data, information about the mechanics and system states complete the live display. Even when the remote user is informed about the current states he can't interact or control the system by remote. Only the super-user can directly influence the system behavior from Liverpool. But the scheduling is flexible enough to follow high prioritized orders, for example when immediate observations of a dedicated space event are needed. The taken images are stored after the observation and can be retrieved via web to analyze the results [4].

Of course the Liverpool telescope is not a laser telescope and therefore doesn't send actively high power laser beams into space, which increases the needed safety issues. But the realized software techniques, including the system monitoring sensors, are similar to those, needed also for SLR telescopes. Scheduling techniques can maybe be copied and a similar optimization of operation times maybe could be achieved.

# 5. Conclusion

Already now available techniques and implementations offer additional and new possibilities to control SLR telescopes. Astronomical sites with fully automated workflows show the possibilities. New technical observation strategies as shared observations or an optimized scheduling can improve the network behavior and could lead to a global SLR observation system. By using similar techniques all over the different systems of the space techniques it might become possible, to share code, to reduce implementation costs and to improve the performance of combined fundamental stations.

But improving the control of a system includes also to define new interfaces as access points from outside, establishing new protocols and communication styles, optimizing the workflows, increasing the safety and security, using standardized data formats and software/hardware techniques and realizing consequently the new strategies as pathfinder technologies to future GGOS sites. Even when safety issues are not easy only the synergies during development and the optimization according to live status information may be useful enough to show a great impact into the daily work and into the scientific results.

(Acknowledgment: Thanks to Iain Steele and Carole Mundell from the Astrophysics Research Institute of the Liverpool John Moores University for their warm welcome in Liverpool and the interesting discussions about the Liverpool telescope)

## References

[1] *H.-P. Plag, M. Pearlman*. Global Geodetic Observing System. Meeting the Requirements of a Global Society on a Changing Planet in 2020. Springer, 2009.

[2] ILRS: EUROLAS Workshop. Detecting and eliminating errors in the EUROLAS network. http://ilrs.gsfc.nasa.gov/reports/special_reports/eurolas_workshop.html, 2002 (Download 2011-07-26).

[3] *Neidhardt, A.; Ettl, M.; Plötz, C.; Mühlbauer, M.; Hase, H.; Sobarzo, S.; Herrera, C.; Alef, W.; Rottmann, H.; Himwich, E.*: Interacting with radio telescopes in real-time during VLBI sessions using e-control. 10th European VLBI Network Symposium and EVN Users Meeting: VLBI and the new generation of radio arrays,10th EVN Symposium, PoS(10th EVN Symposium)024,http://pos.sissa.it/archive/conferences/125/024/10th%20EVN%20Symposium 024.pdf, 2010 (Download 2011-05-29).

[4] *Steele, I. et.al.*: The Liverpool Telescope. Observing robotically since 2004. http://telescope.livjm.ac.uk/, (Download 2011-07-26).

## Correspondence

Alexander Neidhardt
Forschungseinrichtung Satellitengeodäsie
TU München
Geodätisches Observatorium Wettzell
Sackenrieder Str. 25
D-93444 Bad Kötzting

neidhardt@fs.wettzell.de

(Correspondence to the other authors will be forwarded)

# Proceedings of the 17th International Workshop on Laser Ranging

# -Posters-

# Recent and future operation of Helwan-SLR station

*Makram Ibrahim, Khalil I. Khalil, and A. T. Roman*

ABSTRACT

We concerned on the recent Satellite Laser Ranging (SLR) from the Helwan station. The recent equipments used for the operation of the Helwan SLR-station are described. A new Laser Radar Control (LRC) system had been tested theoretically and will apply during august, 2011 to the Helwan station. The results and the analysis of the data obtained recently using the cpf-formats are given. The future operation of the Helwan-SLR station which is expected to improve after the upgrading with the LRC, is also discussed.

## 1. The description of the present Helwan SLR-station

The tracking of the artificial earth satellites from the Helwan has started in the year 1974. A lot of modifications and upgrading have been applied to the Helwan-SLR station in order to improve its accuracy and performance (Hamal, K. , 1978, Jelinkova, H., 1984, Prochazka, I., 1989, Tawadros, M. et. al, 2000, Ibrahim, M. ,2005). For this end, a brief description of the H-SLR station is given.

The mount configuration is Azimuth/Elevation with a coude system of mirrors for the transmitted beams as shown in fig. 1(a). The movement drive is consisting of 2 step drive motors, and the maximum tracking rate is 2 deg./sec. The guiding of the mount is a computer controlled. The receiving system of the mount is a spherical mirror lens of diameter 40 cm, and optical filter of 6 nm with 80 % transmission. The type of the detector is a Photomultiplier (PMT) manufactured by Hamamatsu model H6533. The quantum efficiency of this PMT is 10 % at 532 nm and of normal gain equal 5.6 million. The mode of the PMT is single photoelectron detection (Cech, M., et.al, 1998).

The laser transmitter (as shown in fig.1b ) is composed of Nd: YAG oscillator, Pulse selector, three amplifiers system and a Second Harmonic Generator (SHG); it produces a semi train of pulses. The wavelength of the laser is 0.53μm with output energy of 80 millijoule, the pulse width is 20 psec and its repetition rate is nearly 5 Hz. The divergence of the laser beam is adjustable and can reach to 0.1 mill radians. The laser transmitter is placed outside the mount and then the laser beam is directed to the satellite through the mount via a four coude of mirrors.

The ranging electronics of the system consists of a time interval counter of type a Stanford SR620 of resolution equal 4 ps. The time and frequency system, is GPS Time/Frequency standard, manufactured by Helwlett-Packard of model 58503B, and it measures the time with accuracy below than 110 nsec.

The meteorological station (MET-3) is installed to improve temperature, humidity and atmospheric pressure s' measurements. The pressure sensor model is a Digiquartz MET3 and it measures with accuracy of 0.1 mbar. The temperature sensor model is Platinum resistance temperature probe and it measures with accuracy ~ 0.5 deg C. As for the model of the humidity sensor, it is a capacitance probe and its accuracy is 2 % at 25 deg C. The Laser Radar Control (LRC) unit used at the Helwan station is used since 20 years and will replace by a new one as explained in section3.

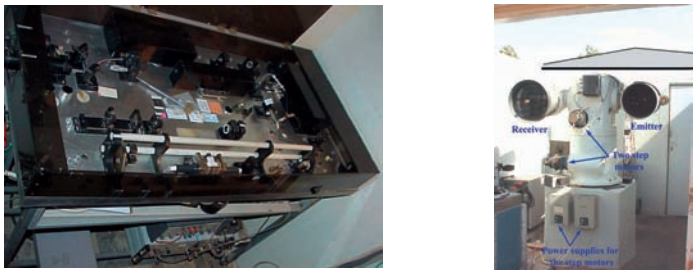


(a) (b)

**Fig1: The mount of the H-SLR Station in (a) and the used Nd:YAG laser transmitter in (b)**

# 2. Recent satellites tracking

The data obtained from satellite tracking is the distance between the satellite under observation and the station. The most recent data of the satellites tracked from Helwan SLR station has been obtained during the years 2008 and 2009. The observations are carried out for low orbit satellite only; by the way during 2007 we started observation of the satellites using the CPF-formats as a prediction of their positions (Blazej, J. et al, 2008).

The analysis of the data is based on calculating the difference between the observed and the predicted ranges of the satellites. To analyze and remove the noise of the Helwan satellite laser ranging data, a procedure has been used. The principal phases of the analysis as explained (Tawadros, M. et al, 2000, Ibrahim, M., 2005).

Due to the upgrading of the station, the precision of it measurements had been improved. In this part, an example has been given for the satellite Champ tracked during the year 2008. The observed range of the satellite as well as the range residuals after the polynomial fitting is plotted versus the number of laser shots and the results are shown in Fig.2. The histograms of the range residuals of the polynomials are computed and plotted in Fig.3. (after removing the points with weight 0), for the same satellite represented in Fig.2. Using the results of the 2.5 Sigma, which is the general standard in SLR on-site data processing, gives nearly the accuracy of the measurements of this satellite is 0.084 nsec.

The primary output of the satellite laser ranging stations is the normal point's data. The method used for the generation of the normal points as well as the selection of the value of the bin size are given in details (Ibrahim et al., 2001, Sinclair, 1997). The normal points are computed for each observed satellite. As an example Tab.1 represents the normal points as computed for the same satellite Champ. It gives average precession of 88 ps.

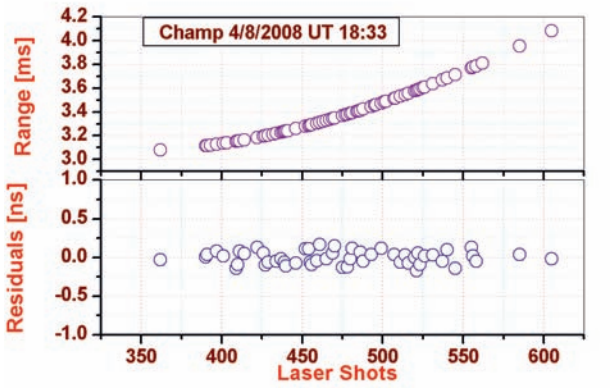


**Fig 2: The number of laser shots are plotted vs. the observed range in ms in the upper part and vs. the residuals in nsec in the lower part for the satellite Champ.**

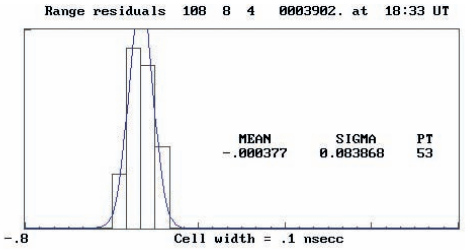


**Fig.3: Histogram of the range residuals as computed for Satellite Champ observed at 4/8/2008.**

**Tab.1: The number of normal points as computed for the satellite Champ Observed at 4/8/2008.**

| Ser. | H | M | S | Range(ms) | Psec | PT/PNT |
|---|---|---|---|---|---|---|
| 1 | 18 | 33 | 56.8003 | 3.0783 | 88 | 1 |
| 2 | 18 | 34 | 3.80031 | 3.12706 | 31 | 4 |
| 3 | 18 | 34 | 8.8003 | 3.18521 | 105.7 | 7 |
| 4 | 18 | 34 | 12.4003 | 3.23847 | 70.2 | 7 |
| 5 | 18 | 34 | 17.4003 | 3.32732 | 109.1 | 9 |
| 6 | 18 | 34 | 22.0003 | 3.42327 | 90.3 | 7 |
| 7 | 18 | 34 | 28.4003 | 3.57729 | 75.5 | 9 |
| 8 | 18 | 34 | 32.4003 | 3.68449 | 103.4 | 4 |
| 9 | 18 | 34 | 36.0003 | 3.78745 | 90.7 | 3 |
| 10 | 18 | 34 | 41.4003 | 3.95233 | 88 | 1 |
| 11 | 18 | 34 | 45.4003 | 4.08175 | 88 | 1 |

By the way, Fig.4 shows the range in ms as measured for the satellite Envisat observed from H-SLR station during 2009. What we want to show here is the few number of the observed points. That is due to the LRE errors message which we receive usually during the recent observations. So, our hope is, by the change to a new LRC, we get rid of the majority of problems produced by the LRE.

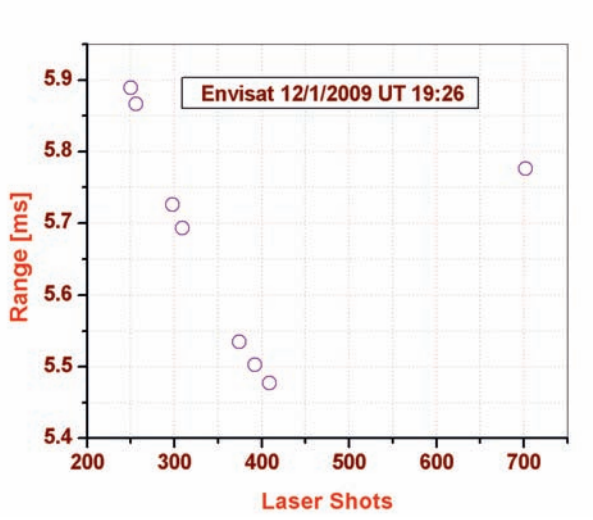


**Fig. 4: The laser shots as measured for the observed range in ms for the Envisat observed at at 12/1/2009.**

The precision of the measurements of the Helwan SLR station are compared with the precision of other SLR stations, and the results are given in Fig.5 as computed for the satellite Starlette in the period from October 1, 2007 till December 31, 2007 (http://ilrs.gsfc.nasa.gov/images/2007_12_str_rms.html). It shows that the root mean square value from H-SLR station is 8.4 mm.

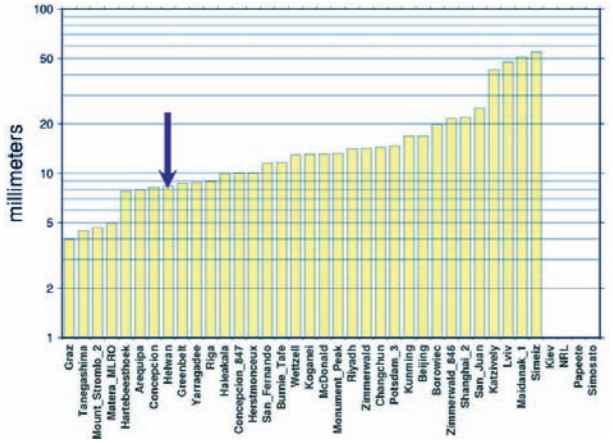


**Fig. 5: The deduced precession of the satellites passes tracked during 2000 for the satellites Lageos-1 and Lageos-2.**

# 3. New Laser Radar Control (LRC)

A satellite laser radar in Helwan has been operating since 1981 with full computer control based on minicomputer system HP 2100. In the period 1987-1989 IBM-PC computer and special control electronics based on Z80 microprocessors were implemented to the laser radar (Cech, M. & Novotny, A., 1989). The control system covers all important functions for satellite ranging and calibration - two axes mount control with stepper motors, range and epoch counter, laser trigger, HP-IB interface for HP5270 or Stanford SR620 counters, arming and gate control. A new servo motor control system was developed in 1994 (Cech, M., 1994).

In the 2009 the laser radar control system was completely redesigned. The new system is based on powerful 80C188EB microprocessor operating with 1MB memory. Special circuits for range and epoch reading are included. The control system is connected to the main station computer via fast RS232C interface based on 16550 chips. A second serial port is used for high accurate meteorological station MET-3. Two DC servo motors (for azimuth and elevation) are controlled in closed loop feedback. Special microchips HP HCTL-1100 are used. HCTL-1100 is a high performance, general purpose motion control IC. A very precise time interval counter (resolution 20 ps) HP5370B or Stanford SR620 is connected via HP-IB interface based on second generation of HP-IB micro controller Ines i7210. The control system consists of two printed boards in Camac unit with a size 14x22x30 cm, as sown in Fig. 6 (a). A firmware is written in C language and Assembler and it is very flexible. Firmware is compatible with old LRCS system on command level (Dr. Mirosalv Cech, private information). A computational power of microprocessor is sufficient to implement simple real time operating system (in future).

The new system will increase the reliability of the laser station. Special circuits for range and epoch reading are included. The control system is connected to the main station computer via fast RS232C interface based on 16550 chips. A second serial port is used for high accurate meteorological station MET-3. Two DC servo motors (for azimuth and elevation) are controlled in closed loop feedback. Special microchips HP HCTL-1100 are used. HCTL-1100 is a high performance, general purpose motion control IC. A very precise time interval counter (resolution 20 ps) HP5370B or Stanford SR620 is connected via HP-IB interface based on second generation of HP-IB micro controller Ines i7210.

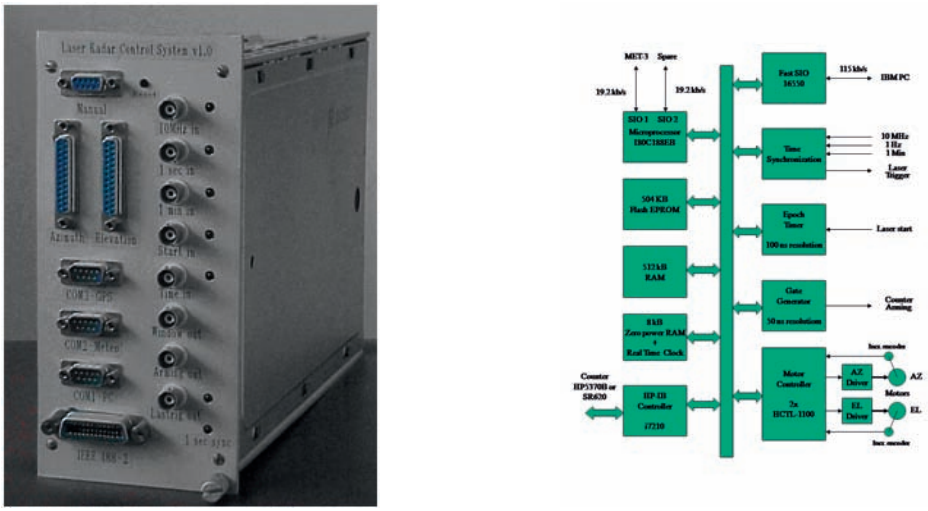


(a) (b)

**Fig.6: A new laser radar control in Camac unit in (a) and its Block diagram in (b)**

A block diagram of the LRC is shown in Fig. 6(b). The control system consists of two printed boards in Camac unit with a size 14x22x30 cm . A firmware is written in C language and Assembler and it is very flexible. Firmware is compatible with old LRCS system on command level. A computational power of microprocessor is sufficient to implement simple real time operating system (in future).

## References

*Blazej, J., Prochazka, I., Novotny, A, Matlas, P., Ibrahim,M. and Khalil I. Kh.,*2008: Implementation of Consolidated Prediction format at satellite laser ranging Helwan" CTU Reports, Proceedings of workshop 2008, Part A Vol. 12, PP. 210.

*Cech, M. and Novotny, A.,* 1989: A Satellite Laser Radar Electronics Based on IBM PC Computer. In: The Seventh International Workshop on Laser Radar Instrumentation, Matera, Italy, 1989.

*Cech, M.,* 1994: Compact Laser Radar Control System with Auto tracking Capability. In: The Ninth International Workshop on Laser Radar Instrumentation, Canberra, Australia, 1994.

*Cech, M., Hamal, K., Jelinkova, H., Novotny, A., Prochazka, I., Helali, Y.E. and Tawadros, M. Y.,* 1998: Upgrading of the Helwan Laser Station (1997-98), Proc. of the 11th International Workshop on Laser Ranging, Deggendorf, Germany, September 21-25,(1998), pp. 197.

*Ibrahim, M., Tawadros, M.Y., Helali, Y.E., El-Saftawy, M., Fahim, G. and Yousry S. Hanna,* 2001: Results of on site data processing after upgrading of Helwan SLR station, Bull. National Research Institute of Astronomy and Geophysics, ser. A., pp. 51- 67.

*Ibrahim, M.,* 2005: ranging to new satellites from Helwan laser tracking station", Journal of the Astronomical Society of Egypt., vol. 13. No I., pp. 52.

*Jelinkova, H.,* 1984: Mode Locked Train Laser Transmitter, Proc. of the 5th International Workshop on Laser ranging Instrumentation, Herstmonceux, U.K., published by Geodetic Institute, Univ. Bonn,(1984), pp. 224

*Prochazka, I,* 1989: Mode locked semitrain laser ranging data processing software, Proc. of the 7th International Workshop on Laser Ranging Instrumentation, Matera, Italy October 2-8, published by OCA/CERGA, Grasse, France,(1989), pp. 405 .

"This research has been partially supported by the grant of the Czech Scientific Foundation GA205/05/0110 and by the research framework MSM6840770022 of Ministry of Education of Czech Republic."

## Conclusion

The results and the analysis of the data obtained recently using the cpf-formats are given and shows a high precision of the measurements. The total number of passes observed during 2007, 2008 and 2009 are, 54, 21 and 6. It shows that, although the precision of the measurements of the Helwan SLR-Station is good, its performance became bad especially during the previous years. That is the reason why the observations from H SLR station are reduced. That performance is referred in fact to some reasons; one of them is the old LRE unit which installed at the station 20 years ago. There is upgrading of new equipment (LRC) of the satellite laser ranging station at Helwan-SLR station. It will be installed to the station during august 2011. It is expected to improve the performance of the Helwan SLR-Station in the near Future.

## Correspondence

Makram Ibrahim
National Research Institute of Astronomy and Geophysics (NRIAG)
Helwan, Cairo
Egypt.

makikh@yahoo.com

# Testing a Phillips 7186 16-Channel Time-to-Digital Converter

*Jerry R. Wiant, Randy L. Ricklefs, Judit Györgyey Ries, and Peter J. Shelus*

ABSTRACT
A Phillips 7186 16-channel time-to digital-converter has been modified and is being tested during times when the MLRS station is not actively gathering ranging data. The Phillips 7186 has the potential of becoming a critical component in the time-of-flight timing system. Eventually the Phillips 7186 will be used in a test satellite pass. If the data quality is improved using the Phillips 7186 it will replace the Ortec TD811 8-channel time digitizer.

## 1. Motivation

The Phillips 7186 was given to MLRS as a gift from the Next Generation SLR, Greenbelt, Maryland (NGSLR) project. NGSLR had hoped to use the Phillips 7186, but it did not meet the project's needs. The similarity between the Ortec TD811, in use at MLRS, and the Phillips offered the possibility of improving the MLRS data, without additional cost to our station.

Both the Ortec TD811 and the Philllips 7186 digitize the time between zero and 100 nanoseconds. The Ortec TD811 gives 50 picoseconds per count where the Phillips 7186 is about 25 picoseconds per count, thus offering better time resolution. Our hope is that the 16-channel Phillips 7186 will produce better data RMS than the 8-channel Ortec TD811.

## 2. Technical Challenges

Both the Ortec and the Phillips are Computer Automated Measurement And Control (CAMAC) units, which can be plugged into individual crates that are controlled by slave units. However, a lot has to be done to consider using the Phillips 7186. Before testing on a satellite pass we need to accomplish the following tasks:

Hardware
The unit needs to be:

- Configured for Common Start
- Configured for 100 nanoseconds range

The unit needs to be modified to allow inputs:

- Channel 1 - Channel 8 bridging
- Channel 9 - Channel 16 bridging

All gains need to be reduced for a maximum range of only a few nanoseconds more than 100 nanoseconds Heater and Resistance Temperature Detector need to be installed.

We also need to discover:

- Best operating temperature
- Best percent applied heat
- Best load resistor in series with heater
- Best operating parameters for the temperature micro-controller.

Software
We need to:

- Create a special ranging program that will accept 16 instead of 8 channels using slightly different CAMAC commands.
- Create a special slope-determining program to determine the individual slopes of the 16 channels.

- Modify several diagnostic programs for use in testing the Phillips 7186.
- Brain-storm to figure out why weird results were being produced.
- Review satellite data for accuracy and low rms.

If the Phillips 7186 produces lower RMS values and we decide to install it for all ranging, many more modifications have to be implemented to integrate the Phillips into the "production" system.

The 16 channels of the Phillips 7186 must be calibrated at a chosen temperature and satellite ranging must be done at the same. The temperature sensor, which is almost a point source sensor, is placed directly on top of the most temperature-sensitive elements in the Phillips 7186. Maintaining a constant temperature is necessary, but not sufficient, since there will always be a temperature gradient (the unit is over 6 inches high). Thus the controller will only keep one spot at the specified temperature, which does not keep the gradient from changes. If the room heats up, the gradient change will cause the RMS to grow.

One way to establish a constant thermal gradient within the converter, is to visually monitor the percent heat being delivered to the unit by the temperature controller. The crew changes the temperature of the equipment van room manually to keep the percent heat delivered to within a few single digit units of percent heat. This procedure has worked well with the TD811 for many years. We have learned that when the percent heat is off by more than four units of percent for the TD811, our range data is not usable.

Until the Phillips 7186 demonstrates sufficient thermal stability, that is, stays in a narrow range of percent heat delivered, ranging to a satellite is meaningless. So... Stay tuned!

## Acknowledgements

This work is supported by NASA Contract # NNG06DA07C.

## Correspondence

Jerry R. Wiant
9 Lunar Cir
McDonald Obs
Texas 79734
USA

jrw@astro.as.utexas.edu

# On use of Starlette and Stella Laser measurements in determination of Earth Orientation Parameters (EOP) and SLR stations' coordinates

*Bachir GOURINE*

ABSTRACT

The present work deals with the calculation of Laser stations coordinates and Earth Orientation Parameters (EOP) based on observations of Low Earth Orbit (LEO) satellites, namely Starlette (STL) and Stella (STA). The orbits of these satellites are less accurate because they are more affected by the gravitational and non-gravitational forces than those of high satellites as LAGEOS-I (LA1) and LAGEOS-II (LA2). The objective is to achieve good quality on the geodetic products by inter-satellite combination of Low and High satellites data. The orbit computation of the different satellites is performed with GINS software and the laser data processing is carried out by MATLO software, with consideration of a recent GRACE gravity model (Eigen_Grace-03s) in the processing, for a period of four years (between January 2002 and December 2005). The time series of the results are projected according to ITRF2000, by CATREF software, where the Helmert transformation parameters are obtained. We compare two series of solutions: LA1+LA2 (LL) only, and a four-satellite combination based on LA1+LA2+STL+STA (LLSS), in terms of quality of the weekly stations positions, EOP and Geocentre variations. The results presented show that the data obtained from LEO satellites such as Starlette and Stella can be successfully used for precise determination of the SLR geodetic products.

## 1. Introduction

Satellite Laser Ranging (SLR) is one of the main techniques of the calculation of the International Terrestrial Reference Frame (ITRF). It contributes to the frame determination by providing time series of laser stations coordinates and Earth Orientation Parameters (EOPs). The laser observations of LAGEOS-I (LA1) and LAGEOS-II (LA2) are generally used for such determination. However, what is the contribution in this determination of other satellites like Low Earth Orbit (LEO) ones?. The twins Starlette (STA) and Stella (STL), orbiting at 800 km altitude, were launched by the CNES, on 1975 and 1993, respectively. The main tasks of these LEO satellites are the determination of Earth's gravity field coefficients, Earth rotation parameters, and investigation of Earth and ocean tides. So, the computation of the laser ranging stations coordinates on the basis of data other than those from LAGEOS-I/-II observations is desirable for the following reasons: (1) significantly increases the number of observations used for determination of the stations coordinates and EOPs, (2) permit verification of results obtained from the LAGEOS-I/-II data, (3) permit determination of coordinates of the stations that cannot range to LAGEOS satellites.

Promising results of the stations coordinates determination were obtained for LEO satellite for short period [Lejba et al., 2008] & [Lejba et al., 2007]. The objective of the study is to check if the laser ranging observations of Starlette and Stella can be used for a precise determination of the laser ranging stations coordinates and EOP, and to investigate the contribution of these LEO data for the geodynamic study of the stations behaviour, pole and Geocenter motions. So, the work concerns the computation of a laser network based on both LAGEOS satellites measurements with those of Starlette and Stella over 04 years period (between January 2002 and December 2005), according to two data combination solutions, namely LA1+LA2 (LL) and LA1+LA2+STL+STA (LLSS).

## 2. Results Analysis

According to table (1), it is clear that the orbits of the high satellites (LAGEOS-I/-II) have a better precision than those of the low satellites (Stella and Starlette), because they are less perturbed. The SLR time series of positions of 34 stations expressed in the local coordinates (NEH); obtained from the LL and LLSS combinations; are projected on ITRF2000 reference frame and are statistically equivalents, according to table (2). The addition of the low satellites to the high satellites did not deteriorate the results quality, in particular for the estimates of EOP and Geocenter parameters, see table (2).

| Satellite | Length of the arc *(days)* | WRMS *(mm)* |
|---|---|---|
| LAGEOS-I | 7 | 11.1 |
| LAGEOS-II | 7 | 9.5 |
| Starlette | 3.5 | 16.1 |
| Stella | 3.5 | 15.5 |

**Table 1: Length of arcs and weighted RMS of orbital arcs residuals**

| Combination | N*(mm)* | E*(mm)* | U*(mm)* | Xp*(mas)* | Yp*(mas)* | TX*(mm)* | TY*(mm)* | TZ*(mm)* |
|---|---|---|---|---|---|---|---|---|
| LL | -20±35 | 21±23 | -6±26 | -0.12±0.32 | 0.30±0.32 | -1±6 | 1±5 | 1±7 |
| LLSS | -21±36 | 20±21 | -5±28 | -0.10±0.30 | 0.33±0.32 | 0±6 | 1±5 | 1±7 |

**Table 2: Statistics of stations coordinates' residuals, pole coordinate updates (Xp, Yp) and Geocenter parameters time series.**

## 2.1 Pole motion

The figure (1) illustrates the residuals time series of pole coordinates ($X_p$, $Y_p$) and of the Length of Day (LOD), with respect to the standard solution EOPC04 of IERS. In the table (2), the values and their RMS of pole coordinates, according to LL and LLSS solutions are practically the same. In addition, the estimation of pole parameters is satisfactory for the SLR technique and the obtained values are coherent with published values of IERS [Gambis, 2004].

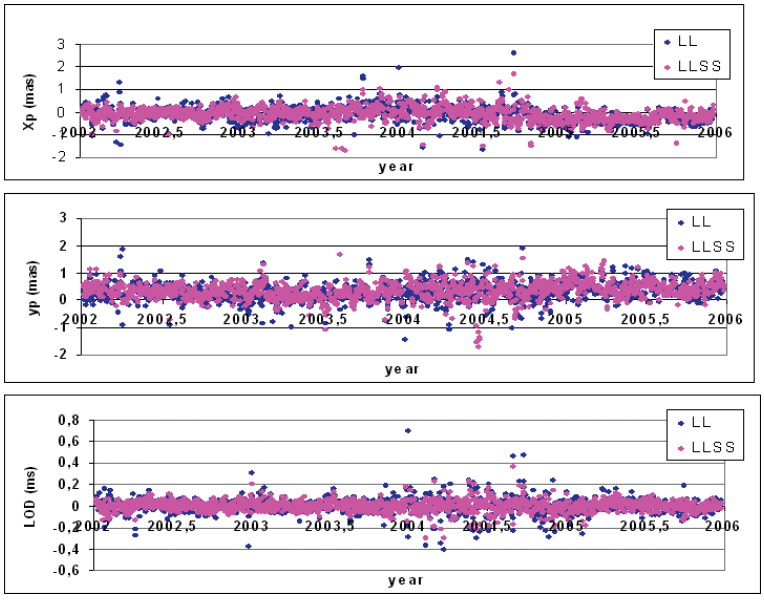


**Figure 1: Parameters of pole motion according to LL and LLSS combinations.**

The frequency analysis of pole time series is performed by FAMOUS software [Mignard, 2005]. The related periodic signals are decomposed, with respect to three periods [Frède, 1999]: inter-annual, annual and short periods (from few days to few months < 100 days). The amplitude values of pole coordinates, according to LL and LLSS combinations, are very closed, because the maximal difference does not exceed 22µas (i.e., 0.7 mm). In other hand, the amplitudes are small of about few mm. For LOD, the average amplitude is around 10µs (i.e., 5mm). Generally, these values remain very small because they describe the residual signals of the geophysical phenomena. The study of the noise, affecting the

pole time series is based on Allan variance method. The dominant noise, for LL and LLSS solutions, is the flicker noise with a slope of the Allan diagram of -0.4 and -0.6. The noise level is of about 106 - 115µas or 3mm, for pole coordinates and it is around 11 and 16 µs (6 and 8mm), for LOD, according to LL and LLSS, respectively.

## 2.2 Geocenter variations

The Geocenter variations are mainly due to the redistribution of masses in atmosphere, in oceans and also in hydrological reservoirs. Table (3) displays the values of amplitudes and phases of annual terms of our solutions, and of two geodynamic models of (Dong et al., 1997) & (Chen et al., 1999). One can observe a coherence in the amplitudes values for LL and LLSS solutions and in comparison of our solutions with geodynamical ones.

| | | LL | LLSS | Dong et al. 1997 | Chen et al. 1999 |
|---|---|---|---|---|---|
| TX | A | 2.9 ± 0.8 | 2.6 ± 0.8 | 4.2 | 2.4 |
| | φ | 139 ± 15 | 131 ± 18 | 224 | 244 |
| TY | A | 2.3 ± 0.5 | 4.1 ± 0.6 | 3.2 | 2.0 |
| | φ | 168 ± 22 | 183 ± 16 | 339 | 270 |
| TZ | A | 2.3 ± 2.6 | 1.9 ± 2.1 | 3.5 | 4.1 |
| | φ | 246 ± 67 | 218 ± 71 | 235 | 228 |

**Table 3: Annual terms of the Geocenter variations components (TX, TY, TZ) according to the LL and LLSS combinations**

The white noise is the dominant noise for the X and Y Geocenter components, with noise level of about 1.8 mm (according to the LL and LLSS combination but it is about 2.3 mm for Y-component of LLSS solution). However, the Z-component is affected by a flicker noise at level of 2.8mm.

## 2.3 Coordinate updates of SLR stations

Figure (2) shows the average RMS of topocentric coordinates (NEU) of 34 SLR Stations over four years (2002-2005), according to the LL and LLSS combination solutions, which are equivalents.

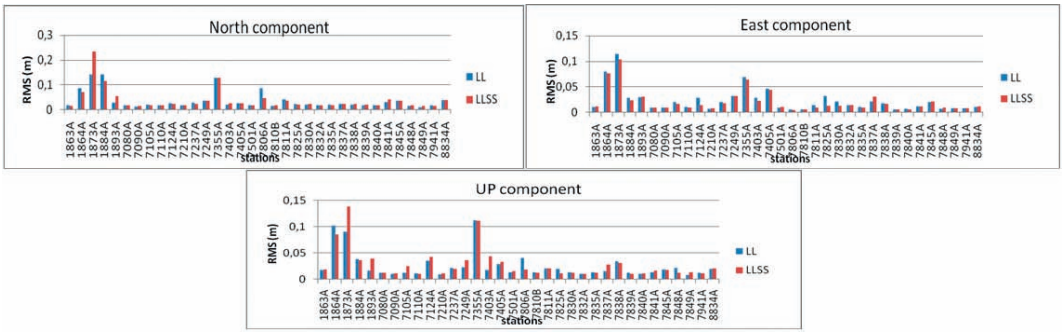


**Figure 2: RMS of topocentric coordinates of SLR stations, according to LL and LLSS combination solutions.**

Figure (3) shows an example of the position time series of two best stations (7080-McDonald, USA) and (7090-Yarragadee, Australia). We focused on vertical component because it is important for the geodynamical studies since it holds 2/3 amplitude of signals acting on the station motion [Coulot, 2005]. Seasonal signals with amplitudes of about few mm were estimated. Since, the effects of ocean loading were considered in the model a priori of restitution, the signals detected are probably related to residual loading effects, which typically have amplitudes of mm level.

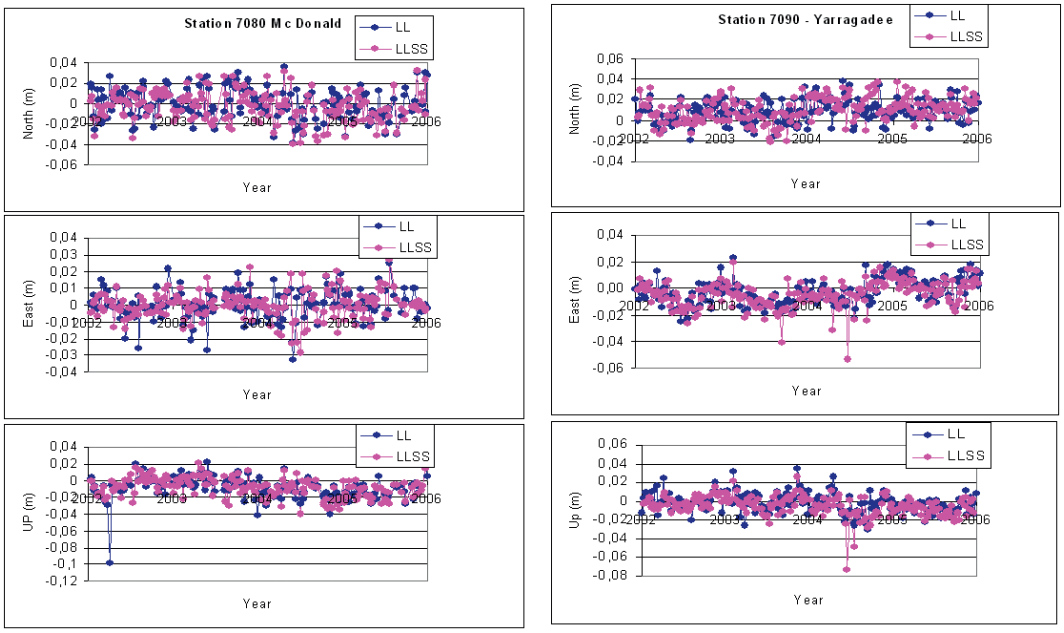


**Figure 3: Coordinates Time series of McDonald (7080) and Yarragadee (7090) stations.**

# 3. Conclusion

This study has showed, in one hand, the feasibility of precise calculation of a SLR network, Earth orientation parameters (EOP) and transformation parameters, by using four years observations of low satellites namely Starlette and Stella and, in other hand, the methodology of analysis adopted for this work. It will be useful and interesting to consider more observations of LEO satellites (such as, Ajisai, TopexPoseidon, Jason-1&-2,...), during a long period, for: (i) Contribution to the realisation of new SLR reference frame and SLR solution for future version of ITRF, and (ii) Analysis of geodetic products variations (Stations motions, EOP, Geocenter) with the adopted methodology.

## Acknowledgements

Special thanks to GMC team (Exertier, Berio, Deleflie, etc.) from (GEMINI/OCA, France) for scientific and technical helps.

## References

*Chen, J. L., Wilson, C. R., Eanes, R. J. & Nerem, R. S,* 1999: Geophysical interpretation of observed geocenter variations. Journal of Geophysical Research, 104(B2) : 2683-2690.

*Coulot, D.*, 2005: Télémétrie laser sur satellites et combinaison de techniques géodésiques. Contributions aux systèmes de référence terrestres et applications. PhD thesis (in French), Observatoire de Paris.

*Dong, D., Dickey, J. O., Chao, Y & Cheng, K.*, 1997: Geocenter variations caused by atmosphere, ocean and surface ground water. Geophysical Research Letters, 24(15) : 1867-1870.

*Frède, V.*, 1999: Apport de l'analyse non linéaire à l'étude géophysique de la rotation de la Terre. PhD thesis (in French), Observatoire de Paris, France.

*Gambis, D.*, 2004: Monitoring earth orientation using space-geodetic techniques: state-of-the-art and prospective. Journal of Geodesy, 78: 295-305.

*Lejba, P., Schillak,* 2008: Determination of the SLR station coordinates and velocities on the basis of laser observations of low satellites, Proceedings of the 16th International Workshop on Laser Ranging, Poznań - Poland, October 13-17.

*Lejba, P., Schillak, S., Wnuk, E.,* 2007: Determination of orbits and SLR stations' coordinates on the basis of laser observations of the satellites Starlette and Stella, Advances in Space Research, Vol. 40, Issue 1, p.143-149.

*Mignard, F.,* 2005: Guide d'utilisation du logiciel FAMOUS. OCA Internal Report (in French) - France.

## Correspondence

Bachir GOURINE
Centre des Techniques Spatiales, Division de Géodésie Spatiale.

BP n° 13, 31200
Arzew – Algérie
Tél. +213 41 472217
Fax. +213 41 473665.

Email: bachirgourine@yahoo.com

# Adjustment of EOP and gravity field parameters from SLR observations

*Mathis Bloßfeld, Horst Müller, Detlef Angermann*

ABSTRACT

Satellite Laser Ranging (SLR) provides the potential to estimate consistently station positions, Earth Rotation Parameters (ERPs) and gravity field parameters of low degree and order. Additionally, parameters which are related to the satellites orbit like the Keplerian elements or empirical accelerations could be estimated within one common adjustment. Since there are high correlations of these parameters among each other, the combined adjustment is a big effort. Although SLR provides highly accurate measurements of the first derivative of UT1-UTC, the Length-of-Day (LOD), the correlation between LOD and the ascending node $\Omega$ distorts the estimated parameters systematically. The estimatedUT1-UTC values show a significantdrift relative to theInternational Earth Rotation and Reference Systems Service (IERS) 08 C04 time series which is not strictly linear over time.

In this study we quantify the systematic effects on the estimated UT1-UTC values using observations of the satellites LAGEOS1 and LAGEOS2. Furthermore, we discuss how the high correlations could be reduced by firstly using longer arc lengths or secondly including observations to more than one satellite in the solution. The gained values of UT1-UTC are vali-dated w.r.t. the IERS 08 C04 time series. Within the solution, gravity field parametersof degree and order two are estimated. For validation, the estimated $C_{20}$ coefficients arecompared to atime series of the Center for Space Research (CSR).

## 1. Correlation factors of LOD, $\Omega$ and $C_{20}$

Satellite Laser Ranging (SLR) is the primary technique to estimate consistently station positions, ERPs and orbit parameters of the satellites together with the spherical harmonics of low degree and order of the Earth gravity field. The big effort of the consistent estimation are the high correlations of the satellite-dependent parameters like Keplerian elements or empirical accelerations, the first derivative of UT1-UTC, called length of day(LOD), and the gravity field parameter $C_{20}$. The relationship between the ERPs and the orbital elementsare given in equation (1)[Rothacher et al., 1999].

$$(UT1 \dot{-} UTC) = -LOD = -\left(\dot{\Omega} + \cos i \cdot \dot{u}\right)\rho^{-1} \qquad (1)$$

The rate of change of the argument of latitude $\dot{u}$ of a satellite is calculated by $\dot{u}=\dot{\omega}+\dot{M}$ with $\dot{\omega}$ being the rate of change of the argument of perigee and $\dot{M}$ being the rate of change of the mean anomaly. $\rho$ is the ratio of universal time to sidereal time ($\rho\approx1.0027379$). The secular rate of change of these quantities is caused inter alia by (i) the even zonal spherical harmonics $C_{nm}$ with $n,m$=2,4,..., (ii) by the sine term of the cross-track empirical acceleration or (iii) by relativistic effects like the *Geodetic Precession* or the *Lense-Thirring Effect*. The secular rate of $\Omega$ due to $C_{20}$ is calculated with [Beutler, 2005]

$$\dot{\Omega}\Big|_{secular} = \frac{3}{2}\sqrt{\frac{GM}{a_e^3}}\left(\frac{a_e}{a}\right)^{\frac{7}{2}}\frac{C_{20}}{(1-e^2)^2}\cos i \qquad (2)$$

Satellite-dependent variables are the semi-major axis $a$ and the eccentricity $e$ which define the geometry of the orbital ellipse and the inclination $i$ which is the angle between the orbital plane and the equatorial plane. Variables of the Earth gravity field are the semi-major axis $a_e$ and the gravitational constantmultiplied by the mass of the Earth$GM$ (the mass $m$ of the satellite is negligible) and the spherical harmonic coefficient $C_{20}$ which is related to the Earth oblateness.

In order to quantify the correlations, several solutions are calculated. One type of the solutions contains only observations to a single satellite (LAGEOS1 or LAGEOS2), whereas the other type contains observations to both satellites (multi-satellite solution).The arc length of both solution types is varied between 7 days and 28 days. The mean values of the orbit fits of the 7-day arc solutions are below 5mm whereas the mean values of the 28-day arcs are around 1cm. For calculating the root mean square (RMS) values, only observations to official core stations of the International Laser Ranging Service (ILRS) are considered.If the arc length of the solution is increased from 7 days to 28 days, the correlations between $\Omega$ and $C_{20}$ are strongly decreased. Fig. 1 shows themean correlation factors for the different solution types. On the left side of Fig. 1, the factors for single-satellite and multi-satellite solutions with an arc length of 7 days

are displayed whereas the right side shows the values for single- and multi-satellite solutions with an arc length of 28 days. The mean correlation factors of the single-satellite solutions are around ±1.0, the mean correlation factors for the multi-satellite solutions are between -0.6 and 0.15, respectively. The mean inclinations of the two LAGEOS satellites ($i_{LA1}$ ≈110°, $i_{LA2}$ ≈53°) allow a decrease of the correlation factors.The most uncorrelated solution could be obtained by calculating a multi-satellite solution with observations to both satellites and an arc length of 28 days. The remaining correlation factors are then 0.15 for $C_{20}$and $\Omega_{LA1}$ and 0.3 for $C_{20}$ and $\Omega_{LA2}$. These low correlation factors allow to stably estimate both parametersin one common adjustment.

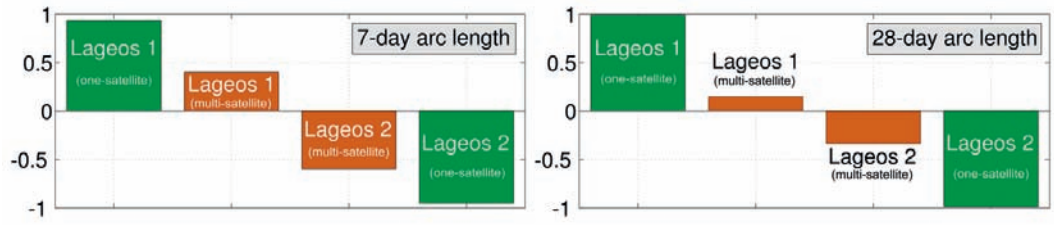


**Fig. 1: Mean correlation factors of $C_{20}$ and $\Omega$ for single-satellite and multi-satellite solutions.**

# 2. SLR solution (1st iteration)

The DGFI SLR solutions contain various different parameter types. Tab. 1 gives an overview over the different estimated parameters. Every solution contains the station coordinates, the Earth Rotation Parameters (ERP), namely the coordinates of the terrestrial pole ($x, y$) and UT1-UTC, and the spherical harmonics of degree two. In order to minimize the Observed-Computed residuals,additional parameters like empirical accelerations are set up in the solution in cross-track direction and in along-track direction.The vector of the cross-track acceleration is pointing in perpendicular direction to the orbital plane, the vector of the along-track acceleration points towards the instantaneous flight direction of the satellite (tangential to the orbital ellipse). If the empirical accelerations are not estimated, the orbit fit would get much worse than it is described above.

**Tab. 1: Estimated parameters within the DGFI SLR solution.**

| parameters | temporal resolution (arc length: 7-day/28-day) |
|---|---|
| **station coordinates** $(X,Y,Z)$ | 1 per arc (+ bias if necessary) |
| **pole coordinates** $(x,y)$**, UT1-UTC** | piecewise linear polygon at 0h epochs (8/29 per arc) |
| **spherical harmonics d/o 2** $(C_{20},C_{21},S_{21},C_{22},S_{22})$ | 1 per arc |
| **Keplerian Elements (a,e,i,ω,Ω,M)** | 1 per arc (starting element) |
| **factor for solar radiation pressure** | 3 per arc (start, mid, end of arc) |
| **empirical acceleration (along-track), once-per-revolution** | 1 per arc (sine-/cosine term) |
| **empirical acceleration (along-track), offset** | 3 per arc (start, mid, end of arc) |
| **empirical acceleration (cross-track), once-per-revolution** | 1 per arc (sine-/cosine-term) |

The temporal resolution of the empirical accelerations is a very sensitive part in the SLR solution. Although the once-per-revolution cross-track acceleration stabilizes the estimated orbit, high correlations with the rate of change of the ascending node and therefore with LOD falsify the correlated parameters. To describe the impact of the cross-track acceleration $W'$ on the rate of change of $\Omega$, $W'=s\cdot sinu+c\cdot cosu$ is introduced in equation (3) [Beutler, 2005].

$$\dot{\Omega} = \frac{r \cdot sinu}{na^2\sqrt{1-e^2}sini} W' = \frac{r \cdot s}{na^2\sqrt{1-e^2}sini} + \frac{r \cdot c \cdot sinu \cdot cosu - r \cdot s \cdot cos^2 u}{na^2\sqrt{1-e^2}sini} \qquad (3)$$

The variable $n=\sqrt{GM/a^3}$ describes the mean motion of the satellite. Thecross-track force $W'$ is acting periodically (once-per-revolution)on the satellite (see Tab. 1). This perturbing accelerationcauses a secular rate of change of $\Omega$ (1st part on the left side in equation (3)) and a periodical rate of change (2nd part on the left side in equation (3)). Also the temporal resolution of the along-track acceleration causes instabilities of the estimated parameters, but these effects are not discussed in this study. To prevent an impact of the cross-track acceleration on the rate of the node, the sine coefficients is constrained to zero.The typical order of magnitude is $10^{-12}$ $ms^{-2}$.

## 2.1. Earth Rotation Parameters

The parameterization of the ERPs (namely the coordinates of the terrestrial pole in x- and y-direction and the rotation angle of the Earth around its rotation axis UT1-UTC) is within all solutions the same. Since SLR is only able to determine LOD, the UT1-UTC values are extrapolated via the estimated LOD values to 0h epochs, which means that a 7-day arc solution contains eight UT1-UTC values representing a piecewise linear polygon.To eliminate the remaining degree of freedom (the offset of the polygon is not defined), the UT1-UTC value at the mid-arc epoch is fixed to its apriori value (IERS 08 C04). Because of the correlations described in the previous equations, errors or non-modeled perturbations of the satellites systematically affect the estimated LOD and the UT1-UTC polygon respectively. Fig. 2 shows the systematic drifts of weekly/4-weekly Δ(UT1-UTC) values which are accumulated over 16.5 years w.r.t. the IERS 08 C04 time series. The spurious drifts of the 7-day single-satellite solutions have an opposite sign and a specific ratio which could be explained with equation (2). Since all satellite independent parameters in equation (2) are nearly the same for both satellites the sign and ratio depend on the ratio of the satellite dependent parameters and thereby mainly on the cosine terms of the inclination. LAGEOS1 shows a mean drift of 8.23 ms/yr whereas LAGEOS2 shows a mean drift of -17.57 ms/yr. The ratio is -0.47. The ratio of the cosine terms of the two inclinations is -0.56. Except a small offset, the agreement is quite good. The single-satellite solutions with an arc length of 28-days are not displayed because their values are much more inaccurate than the values for the 7-day arc solution (-38.02 ms/yr for LAGEOS1 and -26.93 ms/yr for LAGEOS2) [Rothacher et al., 1999].

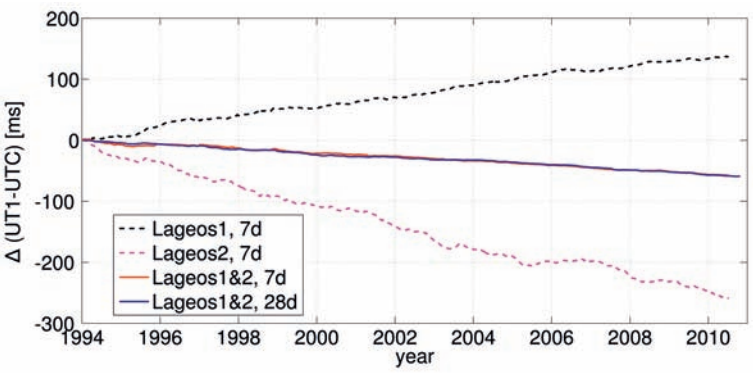


**Fig.2: Accumulated differences of Δ(UT1-UTC) w.r.t. the IERS 08 C04 time series over a time span of 16.5 years.**

The mean drifts of the multi-satellite solutions in Fig. 2 are for both arc lengths nearly the same (-3.63/-3.97 ms/yr). These mean drifts are much smaller because the correlations between $C_{20}$ and $\Omega$ are reduced significantly (Fig. 1).

## 2.2. Gravity field parameters

Together with the UT1-UTC values the SLR solutions contain consistently estimated gravity field parameters. The $C_{20}$ coefficients of the two multi-satellite solutions estimated between 1994.0 and 2010.5 are displayed in Fig. 3. All other degree two coefficients are estimated but not discussed here. The 7-day solution and the 28-day solution show a good agreement with the external CSR solution although the CSR solution (monthly mean values; 2002.0 to 2010.5) contains additional observations to Stella, Starlette and Ajisai.The CSR solution is available at ftp.csr.utexas.edu/pub/slr/degree_2 (28.06.11). The $C_{20}$ coefficients show a clear non-linear behavior.In contrast to the estimated parameters the apriori model GGM02S [Tapley et al., 2005] is parameterized as an offset with a rate.

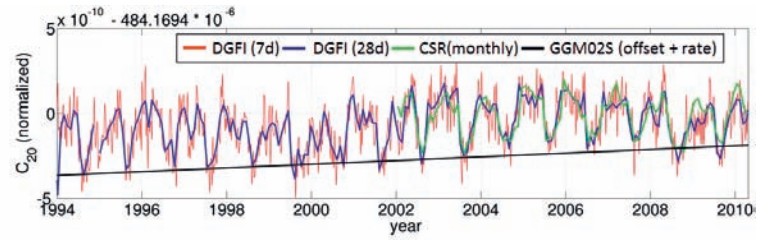


**Fig. 3: Estimated normalized $C_{20}$ coefficients of the Earth gravity field. The two DGFI solutions, the CSR solution and the apriori values (gravity field model GGM02S) are shown.**

# 3. SLR solution (2nd iteration)

The high correlations between $C_{20}$ and the rate of change of the ascending node (Fig. 1) cause errors in the estimated gravity field coefficients of the single-satellite solutions. Therefore, a second iteration step is performed. Within this step, the $C_{20}$ coefficients of the multi-satellite solutions of the first iteration step are introduced as new apriori values for the single-satellite solutions. The estimated coefficients are fixed to these apriori values in order to reduce the drift of the estimated UT1-UTC values in the single-satellite solutions which result from the wrong estimated $C_{20}$ coefficients [Rothacher et al., 1999]. The results for the accumulated Δ(UT1-UTC) values are displayed in Fig. 4. The drifts of all single-satellite solutions (LAGEOS1 and LAGEOS2, 7-day arc and 28-day arc) are reduced significantly and are now nearly the same as the drifts of the multi-satellite solutions. The mean values for these drifts are now between -2.8 ms/yr and -3.9 ms/yr. Nevertheless there is still a remaining drift in all solution types. This main part of this remaining drift is caused by neglecting the relativistic corrections due to the *Geodetic Precession* and the *Lense-Thirring Effect* [Ciufolini, 2004], which are, at the moment, not modeled within the SLR solution discussed in this paper. The sum of these two drifts is approximately -3.2 ms/yr and therefore in good agreement with the remaining drifts.

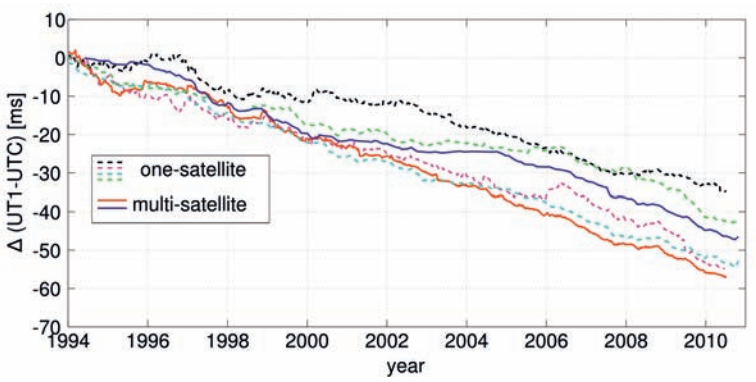


**Fig. 4: Accumulated differences of Δ(UT1-UTC) w.r.t. the IERS 08 C04 time series.**

# 4. Conclusions

Within the DGFI SLR solution, station coordinates are consistently estimated together with ERPs and spherical harmonics of the Earth gravity field. This combined adjustment provides the opportunity to study the correlations between the different parameter types. For instance the correlation between $C_{20}$, Ω and LOD plays a very important role. To reduce the correlation of these three parameters, different solution types were calculated. The multi-satellite solution with an arc length of 28 days shows the smallest correlation factor. In the first of two iterations the observations to LAGEOS1 and LAGEOS2 were combined in order to get a stable estimation of the $C_{20}$ coefficients. These coefficients were introduced in the second iteration step as apriori values for the single-satellite solution to reduce the spurious drifts of the estimated UT1-UTCvalues within these solutions in order to proof that the main drift in the single-satellite solutions is caused by a wrong estimated $C_{20}$ coefficient. At the end a small drift in the accumulated Δ(UT1-UTC) values remains in all solution types. This drift is related to the not modeled relativistic corrections due to the *Geodetic Precession* and the *Lense-Thirring Effect*.

## Acknowledgements

The previously presented results are worked out in a project funded by the German Research Foundation DFG within the research group “Earth rotation and global dynamic processes”.The authors want to thank the DFG for making the work in this project possible. The authors also want to thank Univ.-Prof. Dr.phil.nat. Urs Hugentobler from the Technical University of Munich (TUM) for various very fruitful discussions.

## References

*Beutler, G.:* Methods of Celestial Mechanics; *Vol. 1*: Physical, Mathematical and Numerical Principles& Vol. 2: Application to Planetary System, Geodynamics and Satellite Geodesy, Springer-Verlag, Berlin Heidelberg, 2005

*Bloßfeld, M., Müller, H., Seitz, M., Angermann, D.*: Benefits of SLR in epoch reference frames, Proceedings of the 17th International Workshop on Laser Ranging, Bad Kötzting, Germany, May 16-20, 2011

*Ciufolini, I., Pavlis, E.C.*: A confirmation of the general relativistic prediction of the Lense-Thirring effect, Letters to Nature, Vol. 431, 958-960, doi: 10.1038/nature03007, 2004

*Rothacher, M., Beutler, G., Herring, T. A., Weber, R.*:Estimation of nutation using the Global Positioning System,Journal of Geophysikal Research, 104(B3), 4835–4859, doi:10.1029/1998JB900078, 1999

*Tapley, B., et al.*: GGM02 – An improved Earth gravity field model from GRACE, Journal of Geodesy, Vol. 79, Nr. 8, 467-478, DOI:10.1007/s00190-005-0480-z, 2005

## Correspondence

Mathis Bloßfeld
Deutsches Geodätisches Forschungsinstitut
Alfons-Goppel-Straße 11
80539 München

blossfeld@dgfi.badw.de
http://www.badw.dgfi.de

# The EUROLAS Data Center (EDC) Status Report 2009-2011

*Christian Schwatke, Beate Forberg*

ABSTRACT
The EUROLAS Data Center (EDC) operates as ILRS Data Center for many years. In 2007 the new "Consolidated Laser Ranging Data (CRD)" format was introduced. The first stations started converting their quick-look and full-rate data to the new CRD in 2009. The conversion hasn't finished until now. Statistics show the development of the data holding of quick-look, full-rate, CRD, predictions and products at the EDC.

## 1. Introduction

Since 1994 the DGFI operates the EUROLAS Data Center (EDC) as ILRS Data Center. The major task is the provision of SLR/LLR data to the ILRS-Community. The data holding of the EDC contains full-rate data, normal point data, predictions and ILRS-products. All data sets of the EDC are available on FTP: ftp://edc.dgfi.badw.de

## 2. Full-Rate Data

Full-Rate data was the first SLR product in the 1970's. At the beginning these data sets were published in the MERIT II format of version 2 and later until today in the extended MERIT II format of version 3. In April 2008, the first data sets were published in the new Consolidated Laser Ranging Format (CRD). The new format consolidates full-rate and normal point data in one format.

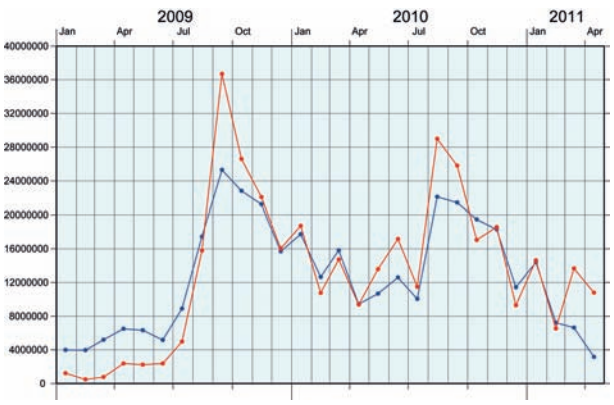


Figure 1 shows the development of the data holding at the EDC since January 2009 until April 2011. The peak of the maximum number of Full-Rate data in the MERIT II as well as in CRD format was reached in September 2009. Since then the number of measurements is decreasing. Especially between January 2011 and April 2011 a decreasing of Full-Rate data in MERIT-II format can be observed.

Since January 2009, 40 stations delivered normal point data in the new CRD format. At this time 71 satellites were observed. The table 2 shows the number of normal point observations (CRD) between January 2009 and April 2011.

**Figure 1: Number of observations every month from January 2009 until April. The blue line shows full-rate data in the MERIT-II format and the red line shows full-rate data in CRD format.**

| Satellite | 2009 | 2010 | 2011 |
|---|---|---|---|
| Ajjisai | 67451 | 117680 | 49429 |
| Andec | 2277 | 2969 | - |
| Andep | 1325 | 328 | - |
| Anderrp | - | 10 | - |
| Apollo 11 | 26 | 2 | - |
| Apollo 14 | 25 | 2 | 1 |
| Apollo 15 | 73 | 56 | 24 |
| Beacon-C | 51181 | 69217 | 32506 |
| Blits | 2890 | 15341 | 7258 |
| Champ | 12164 | 9001 | - |
| Compass-M1 | 2116 | 7246 | 2992 |
| Cryosat-2 | - | 37708 | 17913 |
| Envisat | 34289 | 59965 | 26254 |
| ERS-2 | 38213 | 64373 | 24518 |
| Etalon-1 | 4597 | 7813 | 2758 |
| Etalon-2 | 3434 | 8079 | 3121 |
| ETS8 | 181 | 185 | - |
| Giove-A | 922 | 2739 | 1500 |
| Giove-B | 2405 | 3997 | 1541 |
| Glonass-95 | 20 | 204 | 22 |
| Glonass-99 | 384 | - | - |
| Glonass-100 | 579 | 35 | 83 |
| Glonass-101 | 7 | 128 | 37 |
| Glonass-102 | 4100 | 7825 | 3268 |
| Glonass-103 | 15 | 163 | 74 |
| Glonass-104 | 5 | 155 | - |
| Glonass-105 | 10 | 181 | 80 |
| Glonass-106 | 11 | 201 | 70 |
| Glonass-107 | 11 | 168 | 100 |
| Glonass-108 | 18 | 86 | 33 |
| Glonass-109 | 3562 | 3960 | 3773 |
| Glonass-110 | 13 | 1982 | 1659 |
| Glonass-111 | 9 | 183 | 91 |
| Glonass-112 | - | 27 | - |
| Glonass-113 | 13 | 177 | 22 |
| Glonass-114 | 13 | 191 | 39 |

| Satellite | 2009 | 2010 | 2011 |
|---|---|---|---|
| Glonass-115 | 4881 | 8560 | 2124 |
| Glonass-116 | - | 136 | 17 |
| Glonass-117 | - | 170 | 15 |
| Glonass-118 | - | 2574 | 2082 |
| Glonass-119 | - | 141 | 82 |
| Glonass-120 | - | 4840 | 2528 |
| Glonass-121 | - | 148 | 77 |
| Glonass-122 | - | 50 | 69 |
| Glonass-123 | - | 66 | 121 |
| Glonass-124 | - | 56 | 78 |
| Glonass-125 | - | - | 26 |
| GOCE | 3336 | 10176 | 5663 |
| GPS-35 | 595 | 92 | - |
| GPS-36 | 1121 | 2928 | 660 |
| GRACE-A | 17749 | 31605 | 13245 |
| GRACE-B | 16919 | 30840 | 12073 |
| IceSAT | 15576 | 11444 | - |
| Jason-1 | 75382 | 141192 | 58583 |
| Jason-2 | 88678 | 185412 | 65125 |
| Lageos-1 | 38622 | 71198 | 27005 |
| Lageos-2 | 36806 | 63373 | 25304 |
| Larets | 14191 | 24785 | 10839 |
| LRO | 78605 | 191861 | - |
| Luna-17 | - | 1 | - |
| Luna-21 | 6 | - | - |
| Oicets | 245 | - | - |
| Proba2 | - | 2388 | 4634 |
| QZS-1 | - | 251 | 647 |
| Reflector | - | 253 | 386 |
| Sohla1 | 605 | - | - |
| Starlette | 43005 | 69340 | 29190 |
| Stella | 20066 | 34300 | 14361 |
| Tandem-X | - | 20813 | 12472 |
| Terrasar-X | 34918 | 43428 | 12472 |
| Westpac | - | 12 | 15 |

**Table 1: Number of observations in Full-Rate data (CRD) sorted by satellite from January 2009 until April.**

# 3. Normal Point Data


Normal point data is the primary product of ILRS stations product replacing on-site sampled data and subsequently full-rate data. In 2006 the first data sets were published in the new Consolidated Laser Ranging Format (CRD). Since then there is a continuously increasing amount of normal points in the new CRD format.

**Figure 2: Number of observations every month from January 2009 until April 2011. The blue line shows normal point data in the cstg format and the red line shows normal point data in CRD format.**

Since January 2009, 40 stations delivered normal point data in the new CRD format. At this time 71 satellites were observed. The table 2 shows the number of normal point observations (CRD) between January 2009 and April 2011.

| Satellite | 2009 | 2010 | 2011 |
|---|---|---|---|
| Ajjisai | 67451 | 117680 | 49429 |
| Andec | 2277 | 2969 | - |
| Andep | 1325 | 328 | - |
| Anderrp | - | 10 | - |
| Apollo 11 | 26 | 2 | - |
| Apollo 14 | 25 | 2 | 1 |
| Apollo 15 | 73 | 56 | 24 |
| Beacon-C | 51181 | 69217 | 32506 |
| Blits | 2890 | 15341 | 7258 |
| Champ | 12164 | 9001 | - |
| Compass-M1 | 2116 | 7246 | 2992 |
| Cryosat-2 | - | 37708 | 17913 |
| Envisat | 34289 | 59965 | 26254 |
| ERS-2 | 38213 | 64373 | 24518 |
| Etalon-1 | 4597 | 7813 | 2758 |
| Etalon-2 | 3434 | 8079 | 3121 |
| ETS8 | 181 | 185 | - |
| Giove-A | 922 | 2739 | 1500 |
| Giove-B | 2405 | 3997 | 1541 |
| Glonass-95 | 20 | 204 | 22 |
| Glonass-99 | 384 | - | - |
| Glonass-100 | 579 | 35 | 83 |
| Glonass-101 | 7 | 128 | 37 |
| Glonass-102 | 4100 | 7825 | 3268 |
| Glonass-103 | 15 | 163 | 74 |
| Glonass-104 | 5 | 155 | - |
| Glonass-105 | 10 | 181 | 80 |
| Glonass-106 | 11 | 201 | 70 |
| Glonass-107 | 11 | 168 | 100 |
| Glonass-108 | 18 | 86 | 33 |
| Glonass-109 | 3562 | 3960 | 3773 |
| Glonass-110 | 13 | 1982 | 1659 |
| Glonass-111 | 9 | 183 | 91 |
| Glonass-112 | - | 27 | - |
| Glonass-113 | 13 | 177 | 22 |
| Glonass-114 | 13 | 191 | 39 |

| Satellite | 2009 | 2010 | 2011 |
|---|---|---|---|
| Glonass-115 | 4881 | 8560 | 2124 |
| Glonass-116 | - | 136 | 17 |
| Glonass-117 | - | 170 | 15 |
| Glonass-118 | - | 2574 | 2082 |
| Glonass-119 | - | 141 | 82 |
| Glonass-120 | - | 4840 | 2528 |
| Glonass-121 | - | 148 | 77 |
| Glonass-122 | - | 50 | 69 |
| Glonass-123 | - | 66 | 121 |
| Glonass-124 | - | 56 | 78 |
| Glonass-125 | - | - | 26 |
| GOCE | 3336 | 10176 | 5663 |
| GPS-35 | 595 | 92 | - |
| GPS-36 | 1121 | 2928 | 660 |
| GRACE-A | 17749 | 31605 | 13245 |
| GRACE-B | 16919 | 30840 | 12073 |
| IceSAT | 15576 | 11444 | - |
| Jason-1 | 75382 | 141192 | 58583 |
| Jason-2 | 88678 | 185412 | 65125 |
| Lageos-1 | 38622 | 71198 | 27005 |
| Lageos-2 | 36806 | 63373 | 25304 |
| Larets | 14191 | 24785 | 10839 |
| LRO | 78605 | 191861 | - |
| Luna-17 | - | 1 | - |
| Luna-21 | 6 | - | - |
| Oicets | 245 | - | - |
| Proba2 | - | 2388 | 4634 |
| QZS-1 | - | 251 | 647 |
| Reflector | - | 253 | 386 |
| Sohla1 | 605 | - | - |
| Starlette | 43005 | 69340 | 29190 |
| Stella | 20066 | 34300 | 14361 |
| Tandem-X | - | 20813 | 12472 |
| Terrasar-X | 34918 | 43428 | 12472 |
| Westpac | - | 12 | 15 |

**Table 2: Number of observations in Normal Point data (CRD) sorted by satellite from January 2009 until April 2011.**

# 4. Predictions

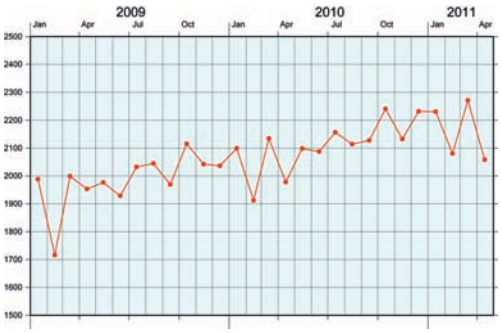


Since June 30, 2006 the Consolidated Prediction Format (CPF) is the official ILRS format for satellite predictions. Elder predictions in the Tuned Inter-Range Vectors (TIRV) format were detached by the new CPF.

In the period between January 2009 and April 2011, predictions (CPF) of 44 satellites were computed by 12 providers.

**Figure 3: Monthly number of predictions (CPF) from January 2009 and April 2011.**

| Satellite | 2009 | 2010 | 2011 |
|---|---|---|---|
| Ajjisai | 1090 | 1082 | 357 |
| Andec | 202 | 217 | - |
| Andep | 153 | 85 | - |
| Apollo 11 | 359 | 361 | 120 |
| Apollo 14 | 359 | 361 | 120 |
| Apollo 15 | 359 | 361 | 120 |
| Beacon-C | 726 | 718 | 237 |
| Blits | 160 | 600 | 183 |
| Champ | 1452 | 1139 | - |
| Compass-M1 | 460 | 453 | 128 |
| Cryosat-2 | - | 476 | 219 |
| Envisat | 995 | 1000 | 307 |
| ERS-2 | 994 | 1048 | 323 |
| Etalon-1 | 727 | 726 | 236 |
| Etalon-2 | 725 | 727 | 238 |
| ETS8 | 26 | 15 | - |
| Giove-A | 504 | 567 | 204 |
| Giove-B | 711 | 691 | 225 |
| Glonass-99 | 179 | - | - |
| Glonass-100 | 152 | - | - |
| Glonass-102 | 709 | 717 | 220 |
| Glonass-109 | 707 | 421 | 220 |
| Glonass-110 | - | 229 | 220 |
| Glonass-115 | 526 | 721 | 220 |

| Satellite | 2009 | 2010 | 2011 |
|---|---|---|---|
| Glonass-118 | - | 230 | 220 |
| Glonass-120 | - | 517 | 220 |
| GOCE | 481 | 877 | 330 |
| GPS-35 | 316 | 70 | - |
| GPS-36 | 709 | 726 | 234 |
| GRACE-A | 723 | 735 | 269 |
| GRACE-B | 726 | 720 | 268 |
| IceSAT | 1 | 14 | - |
| Jason-1 | 1050 | 1052 | 355 |
| Jason-2 | 1093 | 1087 | 357 |
| Lageos-1 | 1091 | 1079 | 355 |
| Lageos-2 | 1091 | 1091 | 357 |
| Larets | 962 | 963 | 314 |
| Luna-17 | 359 | 361 | 120 |
| Luna-21 | 359 | 361 | 120 |
| Luncenter | 359 | 361 | 120 |
| Oicets | 31 | - | - |
| Proba2 | - | 32 | 36 |
| QZS-1 | - | 17 | 114 |
| Sohla1 | 16 | - | - |
| Starlette | 727 | 727 | 237 |
| Stella | 709 | 465 | 239 |
| Tandem-X | - | 381 | 241 |
| Terrasar-X | 720 | 728 | 241 |

**Table 3: Number of predictions (CPF) sorted by satellite from January 2009 until April 2011.**

## Correspondence

Christian Schwatke
Deutsches Geodätisches Forschungsinstitut (DGFI)
Alfons-Goppel-Str. 11
80539 München, Germany

schwatke@dgfi.badw.de

# Validation and estimation of low-degree gravity field coefficients using LAGEOS

*A. Jäggi, K. Sośnica, D. Thaller, G. Beutler*

ABSTRACT

Precise orbit determination is an essential task for analyzing satellite laser ranging (SLR) data. The quality of the satellite orbits directly depends on the background models used for dynamic orbit determination, e.g., on the underlying model of the Earth's gravity field. We investigate the influence of more than ten recent and well known gravity field models on the quality of a combined LAGEOS-1 and LAGEOS-2 orbit determination by analyzing orbital fits. For this purpose we process the SLR data collected by the stations of the International Laser Ranging Service (ILRS) to both LAGEOS satellites in 2008 and show that not only the type and maximum degree of the underlying gravity field model is essential, but also the proper choice of a limited number of empirical orbit parameters that have to be estimated together with all other relevant parameters like station coordinates, Earth orientation parameters, and the satellite's initial conditions on a weekly basis. Based on the experience gained from such validations, the LAGEOS SLR data collected by the ILRS in 2009 are used to estimate weekly corrections to the $C_{20}$ values of the underlying a priori gravity field model, and to accumulate the estimates to monthly corrections.

## 1. Introduction

The satellite laser ranging (SLR) data to both LAGEOS satellites are processed in a combined analysis based on 7-day arcs using the gravity field models listed in Table 1 (ICGEM, 2011) according to two different solution strategies. For solution (a) one constant empirical acceleration is estimated per 7-day arc for each LAGEOS satellite in the along-track direction in addition to the initial conditions, as well as once-per-revolution (OPR) accelerations in the along-track and cross-track directions. The OPR accelerations in the respective directions are set up as coefficients scaling the cosine and sine of the argument of latitude, i.e., of the angle between the nodal line and the satellite's geocentric position vector as measured from the ascending node. For solution (b) essentially the same parametrization is used, but without estimating the coefficients of the OPR cross-track accelerations. For both solutions the coordinates of the ILRS tracking stations, the Earth orientation parameters, and range biases for selected sites are co-estimated on the same weekly basis.

| Gravity field model | Year | Max. degree | Drift | SLR | CHAMP | GRACE | GOCE | Ground data |
|---|---|---|---|---|---|---|---|---|
| JGM3 | 1994 | 70 | | X | | | | X |
| EGM96 | 1996 | 360 | | X | | | | X |
| EIGEN-GL04C | 2006 | 360 | 4 | X | | X | | X |
| EGM2008 | 2008 | 2190 | | | | X | | X |
| EIGEN51C | 2010 | 359 | 4 | X | X | X | | X |
| ITG-GRACE2010 | 2010 | 180 | | | | X | | |
| AIUB-CHAMP03S | 2010 | 100 | | | X | | | |
| AIUB-GRACE03S | 2011 | 160 | 30 | | | X | | |
| GO-CONS-2-DIR-R2 | 2011 | 240 | | | | | X | |
| GOCO02S | 2011 | 250 | | X | X | X | X | |
| AIUB - SST - only | 2011 | 120 | | | X | | X | |

**Table 1: Gravity field models and their characteristics**

## 2. Validation of gravity field models

The LAGEOS orbits are sensitive only up to about degree and order 20 of the Earth's gravity field. Orbit solutions only differ slightly when the gravity field coefficients are taken into account up to higher degrees than 14, e.g., on a level of about 0.5 mm for a spherical harmonic expansion up to degree 20. Coefficients above degree 20 do not significantly impact the LAGEOS trajectories.

## 2.1 Standard solution

Figure 1 shows the root-mean-square (RMS) of the SLR observation residuals obtained from the weekly solutions when using the gravity field models listed in Table 1 and adopting the solution strategy (a). Similar results of good quality are obtained for the majority of the models, apart from EGM96 showing a slightly inferior performance. JGM3 and ITG-GRACE2010 also show a very small degradation with respect to other models. Smallest RMS values are obtained for EGM2008, GO-CONS-2-DIR-R2, AIUB-GRACE03S, EIGEN-51C, and EIGEN-GL04C (7.13, 7.14, 7.15, 7.16, and 7.17 mm, respectively). The RMS of ITG-GRACE2010 may be reduced to 7.18 mm as well, provided that the degree-one coefficients are set to zero. This modified model is labeled as "ITG-GRACE2010 mod" in Fig. 1.

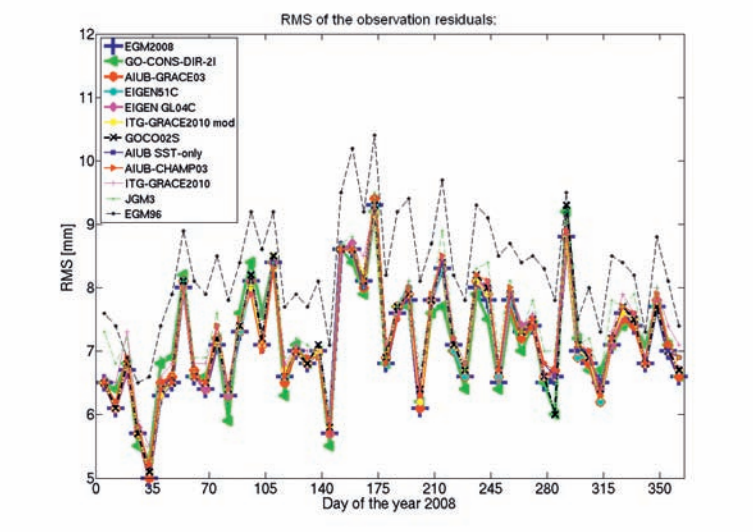


**Figure 1: RMS of weekly LAGEOS solutions with the full set of OPR accelerations estimated (solution (a))**

## 2.2 Omission of OPR cross-track accelerations

Figure 2 shows the RMS of the SLR observation residuals obtained from the weekly solutions when using the gravity field models listed in Table 1 and adopting the solution strategy (b). A very pronounced discrimination between the different models is obvious. AIUB-GRACE03S, among the best models when adopting solution strategy (a) (see Fig. 1), is now showing an exceptionally poor performance. Smallest RMS values are obtained for the GPS-only models AIUB-CHAMP03S and AIUB-SST-only (10.51 and 10.52 mm, respectively), where the latter is an extension of the CHAMP-based model with GPS data from GOCE. The best performance of the GRACE-based models is obtained for EIGEN-GL04C with an RMS of 12.56 mm.

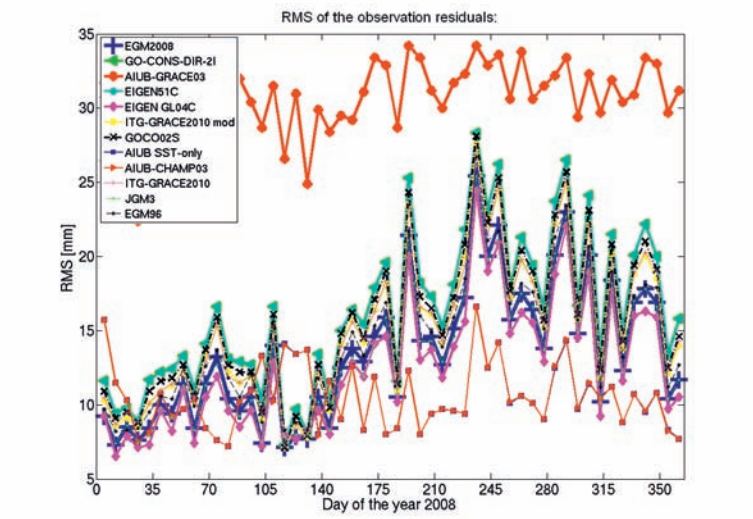


**Figure 2: RMS of weekly LAGEOS solutions without OPR cross-track accelerations estimated (solution (b))**

### 2.2.1 Correlation of OPR accelerations with $C_{20}$

Equation 1 shows the acceleration due to $C_{20}$ in the radial ($R$), along-track ($A$), and cross-track ($C$) directions as a function of the argument of latitude $u$, the geocentric distance $r$, the orbital inclination $i$, and the equatorial radius of the Earth $a_e$:

$$\begin{pmatrix} R \\ A \\ C \end{pmatrix} = \frac{3}{2}\frac{GMa_e^{\,2}C_{20}}{r^4}\begin{pmatrix} 1-\frac{3}{2}\sin^2 i+\frac{3}{2}\sin^2 i\cos 2u \\ \sin^2 i\sin 2u \\ \sin 2i\sin u \end{pmatrix}$$

**Equation 1: Acceleration due to $C_{20}$**

Since only the cross-track component is governed by a OPR periodicity, Eq. 1 illustrates a full correlation between $C_{20}$ and the sine coefficient of an empirically determined OPR cross-track acceleration per arc. The results of the solution strategy (a) are thus almost insensitive to the quality of the $C_{20}$ coefficient of the used gravity field model. Deficient $C_{20}$ coefficients, such as for AIUB-GRACE03S where $C_{20}$ is derived from GRACE-only, may be perfectly absorbed by the sine coefficient of the empirical OPR cross-track acceleration. Solution strategy (b) is thus well suited to mainly validate the quality of the $C_{20}$ coefficient, whereas solution strategy (a) is well suited to essentially overcome the impact of bad $C_{20}$ coefficients in the analysis. As a consequence, solution strategy (a) cannot be used to estimate $C_{20}$ from SLR data on a weekly basis as it is performed in Sect. 3.

# 3. Estimation of low-degree gravity field coefficients

Figure 3 shows normalized and unconstrained weekly estimates of $C_{20}$ when using the a priori gravity field model GGM02S and when adopting the solution strategy (b). For comparison with the monthly series from the Center for Space Research (CSR), the weekly estimates are accumulated to monthly solutions as well, and the a priori values of GGM02S are shown as reference. The first result of $C_{20}$ estimates obtained with the Bernese Software (Dach et al., 2007) shows a fair agreement with the series from CSR, including data from Stella, Starlette, and Ajisai in addition.

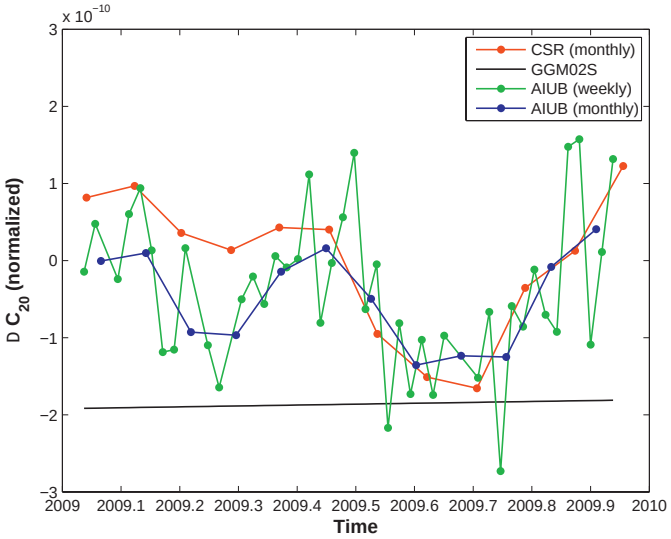


**Figure 3: Weekly and monthly estimates of $C_{20}$ w.r.t. 4.84169411.10-4**

# 4. Conclusions

The smallest RMS of fit to the SLR data from LAGEOS-1 and LAGEOS-2 are obtained for the gravity field models EGM2008, GO-CONS-2-DIR-R2, AIUB-GRACE03S, EIGEN-51C, and EIGEN-GL04C when estimating the full set of OPR accelerations. Without estimating OPR cross-track accelerations, the validation results are mainly dominated by the quality of the $C_{20}$ coefficients, e.g., revealing an exceptionally poor quality of $C_{20}$ for AIUB-GRACE03S and best results for the GPS-only models AIUB-CHAMP03S and AIUB-SST-only. First results of $C_{20}$ estimates obtained with the Bernese Software show a fair agreement with the series from CSR when omitting OPR cross-track accelerations. Longer data series will be processed in the near future.

## References

*Dach, R, Hugentobler U, Fridez P., Meindl M.*, 2007: Bernese GPS Software Version 5.0. Astronomical Institute, University of Bern.

*ICGEM*, 2011: International Centre for Global Earth Models. GFZ Helmholtz Centre Potsdam, http://icgem.gfz-potsdam.de/ ICGEM/

## Correspondence

Adrian Jäggi
Astronomical Institute, University of Bern
Sidlerstrasse 5
3012 Bern
Switzerland

adrian.jaeggi@aiub.unibe.ch

# Fulfillment of KHz SLR daylight tracking of Changchun station

*Xingwei Han, Xue Dong, Qinli Song, Haitao Zhang, Jianyong Shi*

ABSTRACT:
This paper presents the solution of one key problem of too much background noise in daylight SLR tracking, which incorporates smaller receiver field of view, application of narrowband interference filter and higher pointing stability. We successfully accomplished the KHz daylight tracking SLR system, and some results in daylight tracking of KHz system are shown in the paper and the observation results are analyzed.

Key words: KHz SLR, daylight SLR, background noise

## 1. Introduction

Changchun SLR station upgraded the original system in order to adapt the new technology—Daylight KHz SLR. Using independent research software and hardware, Changchun SLR station successfully achieved Routine kHz SLR and daytime tracking. It includes kHz laser system, Event Timer, designing nanosecond accuracy of Range Gate Generator with event mode and back-scattering avoiding circuit, using smaller receiver field of view, applying narrowband interference, confirming higher pointing stability, developing real-time control software and data pre-processing software. The paper presents the progress in KHz SLR at Changchun station, including ranging to the LEO and HEO satellites at night and daylight tracking. In addition, some new measuring results also showed in this paper.

## 2. The main upgrade of kHz Daylight Tracking

Changchun SLR station successfully achieved Routine kHz SLR and daytime trackong. It includes kHz laser system, Event Timer, designing nanosecond accuracy of Range Gate Generator with event mode and back-scattering avoiding circuit, using smaller receiver field of view, applying narrowband interference filter, higher pointing stability, developing real-time control software and data pre-processing software.

### 2.1 Back-scattering avoiding circuit

Back-scattering is a special phenomenon that occurs when radiation is scattered predominantly backwards along its original path. For the high frequency of Changchun SLR system, the echo from the satellite might be quite near from the main pulse transmit to the satellite, the system could not distinguish them. So the main pulse which should be transmitted being delayed, the delayed time is a few hundred microseconds.

### 2.2 The smaller receiver field of view

In Changchun SLR System, remote control is used in the adjustable iris (0.5mm-7mm). The field of view is in a rang of 30"-- 420“. The smaller receiver field of view is for daylight tracking. Fig. 1 shows the machine frame of the adjustable iris.

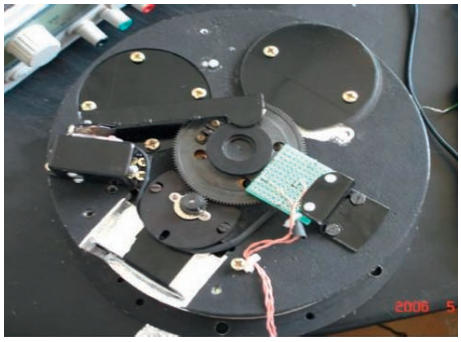

**Fig. 1: The machine frame of the adjustable iris**

## 2.3 Spectrum Filter

The narrow interference filter in Changchun Observatory is from BARR Corporation. The performances listed below.

| Tab.1 BARR Filter Performances | |
|---|---|
| Center Wavelength | 531.955nm |
| Transmission | >70% |
| Bandwidth | 0.15nm |
| Size | Φ 25.0+0/-0.25nm |
| Operating Temperature | 23°C |

The application of 0.15nm narrow interference filter and the constant temperature box could cut more background noise and make the filter working in a constant temperature environment. (shown in Fig. 2).

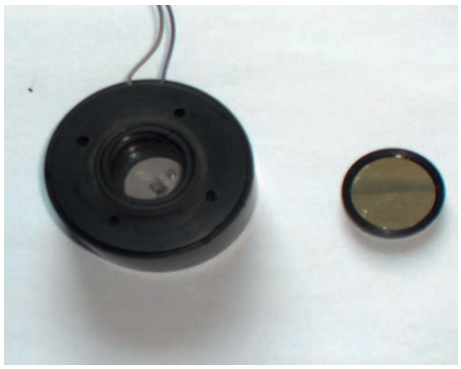

**Fig.2: Spectrum filter in constant temperature box**

## 2.4 Pointing stability

The mount model is applied to modify the pointing of telescope. The result in application of mount model is quite fine. The RMS of Azimuth is 5.5“,and the RMS of Altitude is 4.8“.

# 3. Results

After upgrade of Changchun SLR System, the quantity of data in routine operation is quite fine. Also, the observation of HEO (Glonass 115) satellite in daylight with the kHz SLR system is successful. The details from Jan 2009 to Dec 2010 in kHz ranging and daylight tracking are shown in table 2 and table 3. The upgrade of Changchun Observatory is successful, and the system runs well since then. Changchun Observatory ranks No.2 of 40 stations in ILRS network owing to the daylight observation (Fig. 3).

**Tab.2: Passes in 2009 and 2010**

| | | |
|---|---|---|
| 2009 | Total | 6158 passes |
| | Daylight | 1141 passes |
| 2010 | Total | 7789 passes |
| | Daylight | 2159 passes |

**Tab. 3: Data quality table**

| | |
|---|---|
| Single shot precision | <13 mm (Lageos) |
| Normal Point (RMS) | <1mm (Lageos) |
| Far target calibration | 6.0mm |

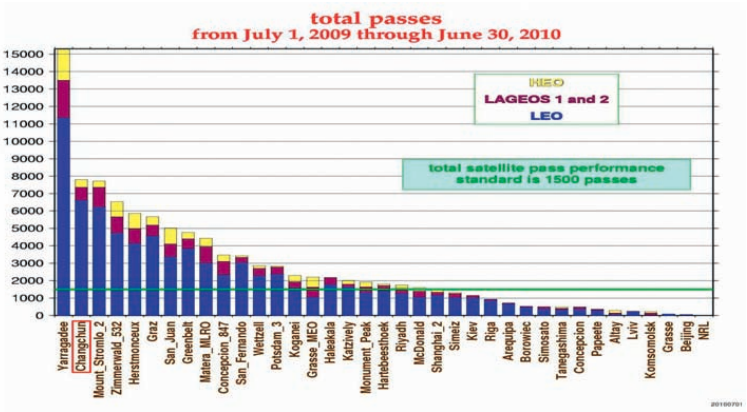


**Figure 3: No.2 of 40 stations in ILRS network**

## References


1. *G. Kirchner, F. Koidl*, Low Cost laser Beam Imaging for Daylight Tracking, 12th International Workshop on Laser Ranging Instrumentation, Matera, Italy

2. *Werner Gurtner, Ulrich Schreiber*, Daylight Tracking, 13th International Workshop on Laser Ranging Instrumentation, San Fernando, Spain


## Correspondence


Xingwei Han
Changchun Observatory/NAOC
Jingyue Lake
Changchun, Jilin
CHINA 130117

hanxw@cho.ac.cn

# Progress in KHz SLR and Daylight Observation at Changchun Station

*Chengzhi Liu, Xingwei Han, Cunbo Fan, Ziang Zhang, Qingli Song*

Abstract: Changchun Station completed Kilo Hertz SLR and daylight tracking system upgrade the year before last. Routine operation has been over 22 months since July, 2009. We have obtained about 14 thousand passes in total, including more than 38 hundred passes in daylight. The main upgrades of Kilo Hertz SLR and daylight tracking in Changchun observatory includes new Kilo Hertz Laser, Event timer, Ranging control system, Spectrum filter, Higher pointing stability and optic route adjust etc. these contain related research contents such as optics, machinery, electron and automatic control and so on.

## 1. The main upgrades of Kilo Hertz SLR system

The main upgrades of Kilo Hertz SLR in Changchun Station include the following 3 parts: A new Kilo Hertz Laser; Event timer; Ranging control system.

### 1.1 The Kilo Hertz Laser

Our laser is from Photonics Industries (PI) Corporation in USA. Typical lifetime of pump diode exceed 5000 hours, From July 2009, Changchun has been using this laser at low power for more than 6850 hours, about 22 months, with an average 10 hours per day. Laser specification is as follow.

| | |
|---|---|
| Pulse energy | 3mJ @ 532nm/1kHz |
| Pulse width | 10ps FWHM |
| Repetition rates | 500 to 10KHz |
| Beam quality – TEM00 | M2<1.3 |
| Divergence | 0.4 mrad |
| Pointing stability | <10 urad (typical 5urad) |

### 1.2 Event timer

We use A-032 ET Event Timer to get epochs of laser firing and return signals, which can get to an accuracy of a few picoseconds.

### 1.3 Ranging control system

The main part of the control system is RGG. It can generate Range Gate and laser fire signal, and avoid backscatter. Frequency is from 1 to 3000 Hz. Precision is 10 nanoseconds

We use Single Windows PC to manage Kilo Hertz Laser ranging control, such as reading ET, driving telescope, controlling laser, data identifications, display data, etc.

## 2. The main upgrade of Kilo Hertz Daylight Observation

When we operate in Kilo Hertz, there is much more background noise in daylight tracking. So we adopt the following methods.1, Smaller Receiver field of view. Iris can be Adjusted from 0.5mm to 7mm and field of view is 30 arc-seconds. 2, Spectrum filter. Narrow Band Interference Filter from the U.S BARR Corporation is used. Bandwidth is 0.15nm. Trans-

mission of Center Wavelength is more than 70%. 3,Higher pointing stability. We have no camera for laser beam in daylight,The pointing is stable and the alignment of transmitting and receiving paths is  better than 5" by means of adjustment.

# 3. Routine Operation

SLR is routine Operation in KHz ranging and daylight tracking from Aug 2009. We have obtained about 14 thousand passes in total, including more than 38 hundred passes in daylight until May 2011. Someday we got 75 passes including 34 pass in daylight. Our Data quality is also very good. The Single shot precision is better than 13 mm for Lageos and Normal Point RMS is less than 1mm (Lageos). Far target calibration precision is less than 6.0mm.

The following figure is the first day of Kilo Hertz daylight tracking interface. It's August the twenty-first, 2009 and the local time is four thirty p.m. and the satellite is Lageos-2. The Interface maintain the original style

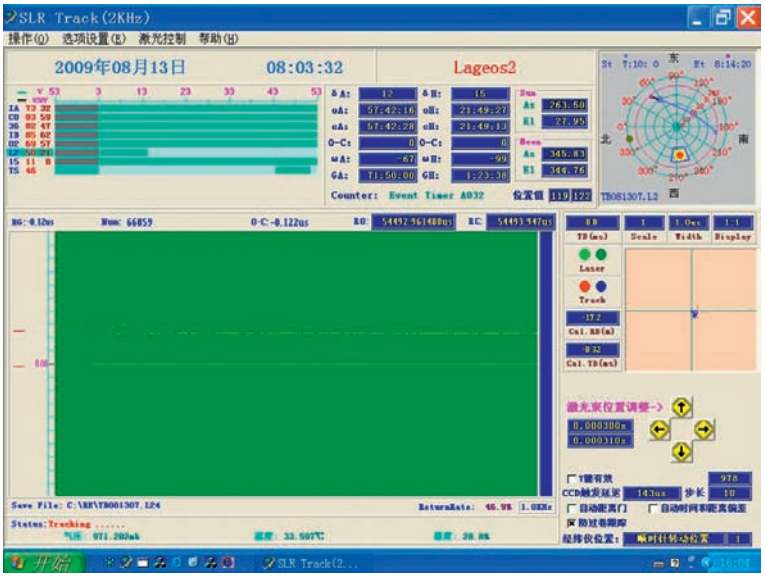


**Figure1: First day of KHz daylight tracking interface(Lageos-2)**

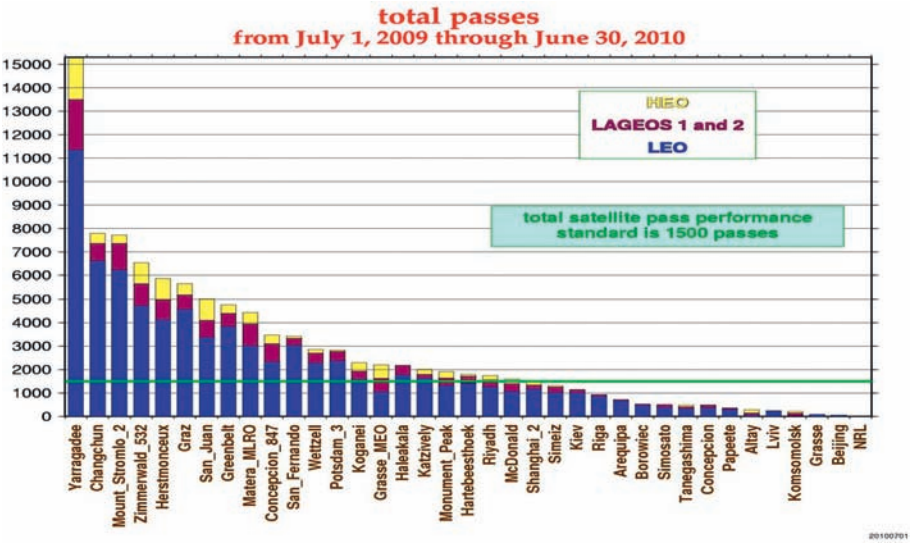


**Figure 2:  global report card**

This is the global report card of the second Quarter last year. Changchun Station ranks the second and still keeps in the former third position up to now.

# 4. Future Plan

For obtaining more and better data, we prepare to develop the following work. 1, establish the near target. 2, KHz laser beam imaging in daylight. 3, Improve the telescope pointing accuracy. 4, Ranging HEOs in Daylight: High Earth Orbits Satellites such as : Compass(Beidou), Galileo, Etalon, GPS, Glonass, etc.

Recently, we tested a new sensitive camera for watching the laser beam, which is very good at daylight. The camera is made in Germany. This page Background is Continuous imaging of five percent backscatter. It is the remaining reflection of our dichroic mirror.

**Figure3: Laser Beam Imaging in Daylight**

## Correspondence

Liu Chengzhi
Changchun observatory, National astronomical observatories , Chinese Academy of Sciences
Jing Yue Tan Xi Shan
Changchun 130117
China

e-mail: lcz@cho.ac.cn

# A CCD System of Monitoring KHz Laser in Daytime

*Zhang Ziang, Han Xingwei, Song Qingli, Zhang Haitao*

ABSTRACT

On account of intensive background noise in daytime, we put forward a monitoring KHz laser solution with CCD system. This solution use high-speed CCD camera, modify the exposure time and integral exposure numbers etc. We successful obtained clear image of back scatter laser in this experiment and measured the key factor of this kind system. It means a lot to improve KHz satellite laser rang (SLR) system in daytime, and increase rang ability.

## 1. Introduction

Separation light path telescope system is widely used in many SLR station. Use an isolate telescope to transmit laser pulse. As to the changes in ambient temperature, it's hard to keep parallel of transmit and receive telescope exactly in this kind of mechanical structure for a long time. So it's necessary to modify the laser pointing direction, especially in the daytime. Ordinary, we apply an EMCCD to monitor the laser backscatter from the main telescope in the night and modify the laser pointing direction timely. But in the daytime, the backscatter laser has embedded in the strong background noise. Furthermore, in the high repetition SLR system, the single laser pulse energy is low to the 1-2 mJ, it produce even weaker of the backscatter intensity. Classical way can't meet the need of daytime SLR. To address this problem, we introduce a new CCD system and got some encouraging result.

## 2. System description

In this experiment, we installed the CCD camera (PCO 1600) in our SLR system at the monitoring channel, replace previous EMCCD. Use a pulse signal generator (DG535) to synchronize the CCD camera exposure and the laser pulse emission. The system setup as bellow.

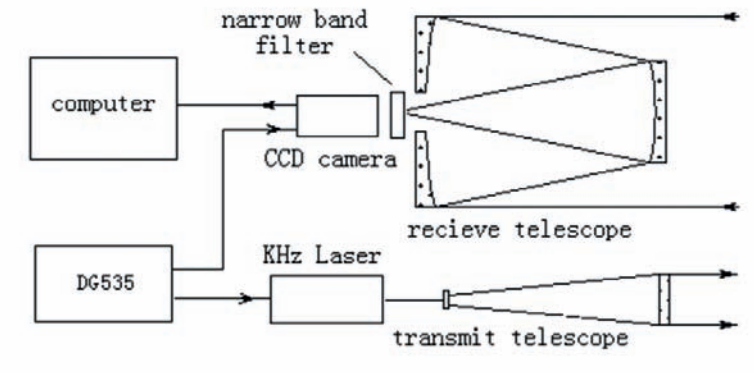


**Fig.1: experiment setup**

**Fig.2: Photograph of experiment equipment**

**Table 1: indicate the main specialty of the CCD camera that we tested.**

**Table 1. CCD camera specialty (PCO 1600)**

| | |
|---|---|
| resolution (hor x ver) | 1600×1200 |
| pixel size (hor x ver) | 7.4μm × 7.4μm |
| sensor format(mm²) | 12.2×9.0 |
| spectral range (nm) | 320—1000 |
| peak quantum efficiency | 55% (500nm) |
| exposure time (s) | 500ns—47days |
| max. exposures in one image | 500000 |
| max. modulation frequency | 50KHz |
| data interface | IEEE1394 |

This diagram has described the sequential relationship. The emitted laser pulse will produce backscatter coursed by suspended particle in the lower atmospheric layer. This backscatter will last about 60 microseconds (according to changchun weather condition) along with laser transmit. So the CCD camera should exposure at this time interval.

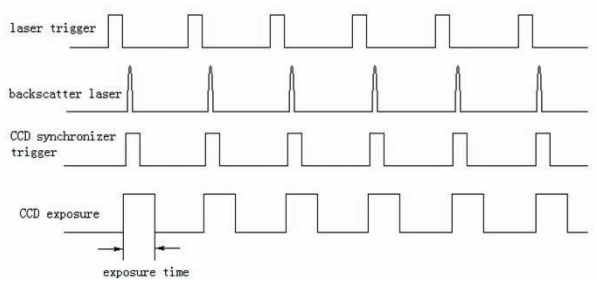


**Fig.3: sequence chart**

# 3. Experiment result

Figures underneath are the representative result we got.

**Fig.4. 100 times exposure modulation, exposure time 50 μs**

**Fig.5. 200 times exposure modulation, exposure time 67 μs**

**Fig.6. 1000 times exposure modulation, exposure time 67.5μs**

# 4. Conclusion

After repeatedly experiment, compared with the image we got, the result of Fig.5 is very exciting. The laser beam in this image we got in the daytime is clear as the one obtain at night. The parameters we set to this camera are suitable for ChangChun station satellite laser ranging in the daylight. According to the experiment result, we find that for monitoring the laser beam in the daylight, a camera should have these specialties below:

a. short exposure time achieve scores of microsecond and variable.

b. can exposure many times in one image, the number of that maybe up to thousands.

c. There will be a narrow band filter in front of the CCD camera.

## Reference

*G. Kirchner, F. Koidl, SLR Graz*: Daylight CCD, Graz KHz SLR Meeting, Graz

## Correspondence

Zi'ang Zhang
Changchun Observatory/NAOC
Jingyue Lake, Changchun, Jilin
CHINA 130117

zhangza@cho.ac.cn

# Software Design and Development Status of ARGO-M Operation System

*Yoon-Kyung Seo[1], Hyung-Chul Lim[1], Eun-Seo Park[1], Jong-Uk Park[1], Seung-Cheol Bang[1], Jin-Young Lee[1], Sung-Yeol Yu[1], Dong-Young Rew[2], Cheong Youn[3]*

ABSTRACT

A satellite laser ranging system named ARGO-M, Accurate Ranging System for Geodetic Observation-Mobile, is being developed by Korea Astronomy and Space Science Institute (KASI) and critical design review was finished on 31 March, 2011. During the design phase, SLR software logic for the ARGO-M operation was established with the aid of Graz SLR observatory in Austria. Software analysis and design include real-time control algorithm for laser ranging, data screening and processing algorithm for normal point formation. This paper describes software design feature and test results performed in order to examine the function of ARGO-M operation system. Furthermore, status of installation of operation support equipment and test running results of that equipment are presented in this paper.

## 1. ARGO-M Operation System(AOS) Overview

ARGO-M consists of five main subsystems including optical subsystem (OPS), opto-electronics subsystem (OES), laser subsystem (LAS), tracking and mount subsystem (TMS) and ARGO operation system (AOS) in additions to a dome and a mobile container (Lim et al. 2010). Among these, AOS is the system that controls the entire subsystems needed for the laser observation, make a comprehensive judgment regarding the environment and eventually reflects the judgment to the observation (Seo et al. 2009). Moreover, it plays the role of integrating and processing the data obtained from actual observation. AOS can be considered as the core subsystem since it controls the overall observation operation and produces the result data based on a number of interfaces combining the components necessary to operate the SLR normally. This AOS can be divided into developed items in detail and the main categories are the operation and control system and the operation equipment. The software configuration items that belong to the operation and control system part are interface control system (ICS), observation control system (OCS), data analysis system (DAS) and remote operation system (ROS). The operation equipment part is composed of the radar for aircrafts detection, weather monitoring system, timing system, network system, network security solution, and surveillance camera.

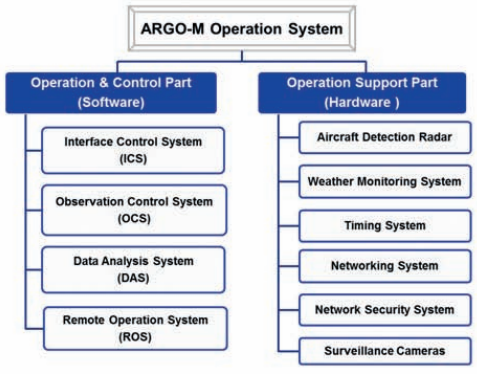


| Part | Sub-part | Q'ty | Assemblies |
|---|---|---|---|
| Operation & Control Part | Interface Control System (ICS) | 1 | Software development & installed computer |
| | Observation Control System (OCS) | 1 | |
| | Data Analysis System (DAS) | 1 | |
| | Remote Operation System (ROS) | 1 | |
| Operation Support Part | Timing System | 1 | GPS Receiver & Antenna, Oscillator, Extended Modules |
| | Weather Monitoring System | 1 | Real-time Weather Transmitter, Visibility & Precipitation Sensor, Rain Sensor, Cloud Sensor |
| | Aircraft Detection Radar | 1 | Pedestal Assembly, Radar Transmitter, Radar Receiver, Parabolic Antenna |
| | Networking System | 1 | Router, Switch |
| | Network Security System | 1 | Firewall, VPN |
| | Surveillance Camera | 1 | Network Camera (5ea) Workstation & Software |

**Figure 1: ARGO-M Operation System (AOS) development item**

[1]Korea Astronomy and Space Science Institute, Korea
[2]Korea Aerospace Research Institute, Korea
[3]Chungnam National University, Korea

## 2. Operation Scheme & Scenario

The operation status of AOS was distinguished into three statuses in terms of the functions that should be realized in the design process: pre-observation status, ground calibration status or actual observation status, and post-analysis status. In the pre-observation status, the operator who has undergone the previously permitted authentication procedure approaches ICS and OCS, and checks the operating state of the entire subsystem. Then, the calibration mode or observation mode is chosen through the mode control. In addition, the initial procedure is performed to verify the setting values including the previously prepared orbit data of the tracking target satellite. In the ground calibration status or the actual observation status, the ground target is managed under the setting that has been already completed or the real-time scheduling is performed for the satellite to observe. Additionally, initialization of the system that needs maneuvering or that is controlled by the AOS is carried out. After finishing the initialization, the mission is carried out or the observation is conducted with the input from the manual control of the operation, if necessary.Following the time of predetermined ground calibration or the time when satellite observation is possible, the observation result and the mode values are saved and then the system is shut down or the next task is performed in the same manner. In the post-analysis status, after a path of the satellite to observe is finished, the observation data save in OCS is transferred to DAS which independently performs analytical task including removal of noise. Following this, the normal point, the final output of the SLR observation, is generated and it is reported to international laser ranging service (ILRS) to complete the after-analysis procedure(Seo et al. 2010).

## 3. Operation Support Part

Complete products will be introduced for most of the operation equipments, and only the interface of the computer in the operating system that will communicate with the equipments will be developed for the establishment of the part. The establishment time depends on the time needed for the development, the time when the equipment is required and the installation environment and conditions of different equipments. Figure 2 and 3 show the timing system and weather sensors installed in KASI for ARGO-M development. Besides, other operational equipment such as the aircraft detection radar, network system, network security solution, and surveillance camera will be established according to the time to complete the mobile container.

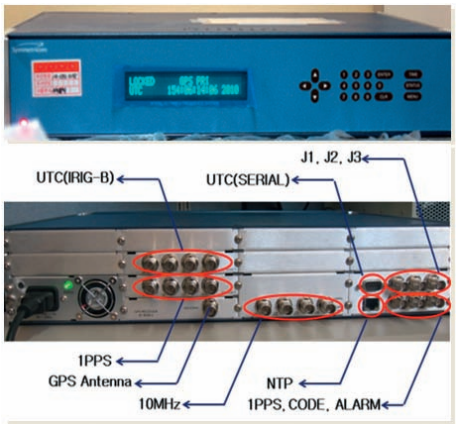


**Figure 2: Front panel(upper) & rear panel(lower) of timing system(Xli, SYMMETRICOM INC. 2008) installed in KASI**

**Figure 3: Pre-installed weather monitoring system in KASI: Total weather transmitter (WXT520), Rain detector (DRD11A), Visibility sensor (PWD52)**

# 4. Interface Check with Tracking Mount System

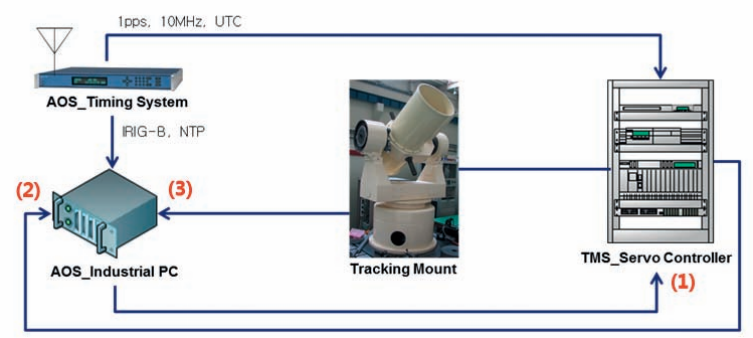


**Figure 4: Test set-up for Interface check with tracking mount system**

(1) Commended position data for TMS

- Check stored data in AOS local HDD
- Store commanded data(1) to the AOS local HDD before transferring to TMS
- Compare data(1) with (2) after finishing the test

(2) Actual tracking data from TMS

- Check stored data in AOS local HDD
- Store received data(2) from the TMS_Servo controller to the AOS local HDD
- Compare data(1) with (2) after finishing the test

(3) Status information from TMS sensors

- Monitor GUI in real-time
- Run a test to change each status value of TMS sensors subsequently
- Check if status changes are reflected on the GUI of the AOS_industrial PC

**Test Result 1.** Difference between commanded and actual position is less than 0.1arcsec.

**Test Result 2.** We checked the exceptional operation in Key-hole zone (El. > 87deg.). Figure 5 and 6 show the result data.

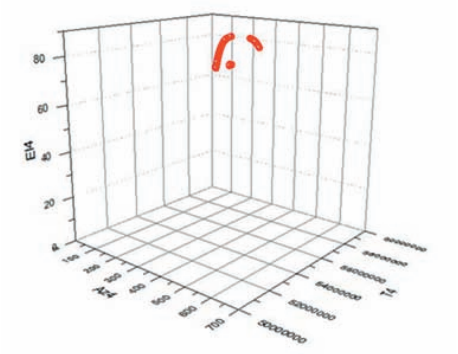

**Figure 5: Commanded position data(AOS->TMS) : Azimuth vs. Elevation with time**

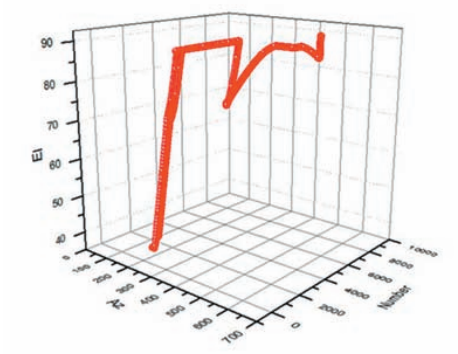

**Figure 6: Actual position data(TMS->AOS): Azimuth vs. Elevation with time**

# 5. Pilot Test – Ground Target Detecting

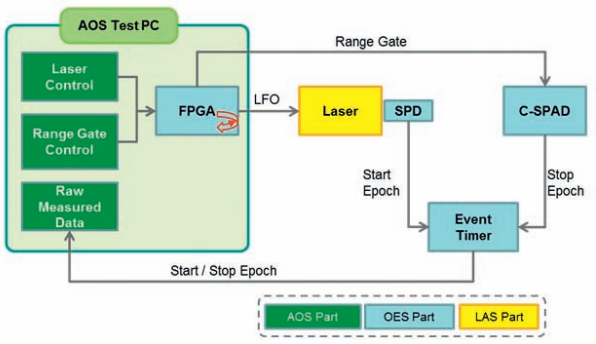


**Figure 7: Test configuration for ground target detecting**

**Test Result**.Function of newly developed AOS data processing software is checked by a ground target detecting test. The result showed that the average residual is about 128ns. This result is verified by comparing with the vendor supplied Event Timer(A032-ET) client software (Institute of Electronics and Computer Science Riga, Latvia 2009).

## Acknowledgements

This study was supported by "SLR system development program for space geodesy" project of KASI funded by the Ministry of Education Science and Technology (MEST). We also express our gratitude to Dr. Georg Kirchner of Graz SLR observatory, Austria.

## References

Institute of Electronics and Computer Science Riga, Latvia 2009, "Event Timer A032-ET Manual"

*Lim, H. C., Seo, Y. K., Na, J. K., Bang, S. C., Lee, J. Y., Cho, J. H., Park, J. H., & Park, J. U.* 2010, "Tracking Capability Analysis of ARGO-M Satellite Laser Ranging System for STSAT-2 and KOMPSAT-5", JASS, 27, 245

*Seo, Y. K., Rew, D. Y., Lim, H. C., Park, I. K., Yim, H. S., Jo, J. H., & Park, J. U.* 2009,"A study on the deriving requirements of ARGO Operation System", JASS, 26, 279

*Seo, Y. K., Lim, H. C., Rew, D. Y., Jo, J. H., Park, J. U., Park, E. S., & Park, J. H.* 2009,"Study on the Preliminary Design of ARGO-M Operation System", JASS, 27, 393

*SYMMETRICOM INC.* 2008, SYMMETRICOM INC. "Technical Document (Xli Time and Frequency System)"

## Correspondence

Yoon-Kyung Seo
Korea Astronomy and Space Science Institute 776
Daedeokdae-ro, Yuseong-gu, Daejeon
Republic of Korea 305-348

ykseo@kasi.re.kr

# Status and Progress of Korean SLR Program, ARGO

*Hyung-Chul Lim, Eunseo Park, Yoon-Kyung Seo, Seung-Cheol Bang, Seong-Yeol Yu, Jin-Young Lee, Kwang Dong Kim, Jakyoung Nah, Jeong Gyun Jang, Bi-Ho Jang, Jong-Uk Park*

ABSTRACT

KASI (Korea Astronomy and Space Science Institute) has fulfilled a governmental program named ARGO (Accurate Ranging system for Geodetic Observation) since 2008 to develop one mobile and one fixed SLR systems, ARGO-M and ARGO-F respectively. ARGO-M, which will be completely developed in 2011, has the separate optical path that employs the 40cm receiving and 10cm transmitting telescopes. Some essential components effecting on ranging accuracy came from the foreign institutes, which include the timing system, photon detector, laser and optoelectronic controller developed by Graz station in Austria. The CDR (Critical Design Review) of ARGO-M was carried out on March 2011 and it is now in the phase on a fabrication and system integration. ARGO-F, which is equipped with a telescope of 1 m diameter, has the common optical path and its development will actually begin from 2012 after ARGO-M completion. Its basic function is also laser ranging to satellites with the laser retro-reflector array and it can have an additional function such as optical tracking using laser illumination, satellite imaging using an adaptive optics and space debris laser ranging. None of these additional functions are determined yet but KASI is going to make development strategies including these additional functions by 2011.

## 1. Overview of ARGO Program

KASI (Korea Astronomy and Space Science Institute) had tried to construct SLR (Satellite Laser Ranging) station from 1986 for satellite tracking and its orbit determination. To develop the Korean SLR system, KASI also did the feasibility study in 2005 in which the development strategies, system requirements and some specifications were provided. Eventually, KASI started the development program of two SLR systems from 2008 with the Korean government fund. The program was named of the Accurate Ranging System for Geodetic Observation (ARGO) from the ancient Greek mythology. The final goal of ARGO program is to develop two SLR systems, one 40cm mobile system and one 1m fixed system. The planned program period is from 2008 to 2014, which can be adjusted by the budget profiles of upcoming years from the government. The objectives of ARGO program can be categrorized into three items; i) space geodesy research and GEOSS/GGOS contribution by laser ranging for satellites with LRA, ii) precise obit determination(POD) through laser ranging measurement with mm level accuracy, iii) contribution to international SLR societies and ILRS network participation.

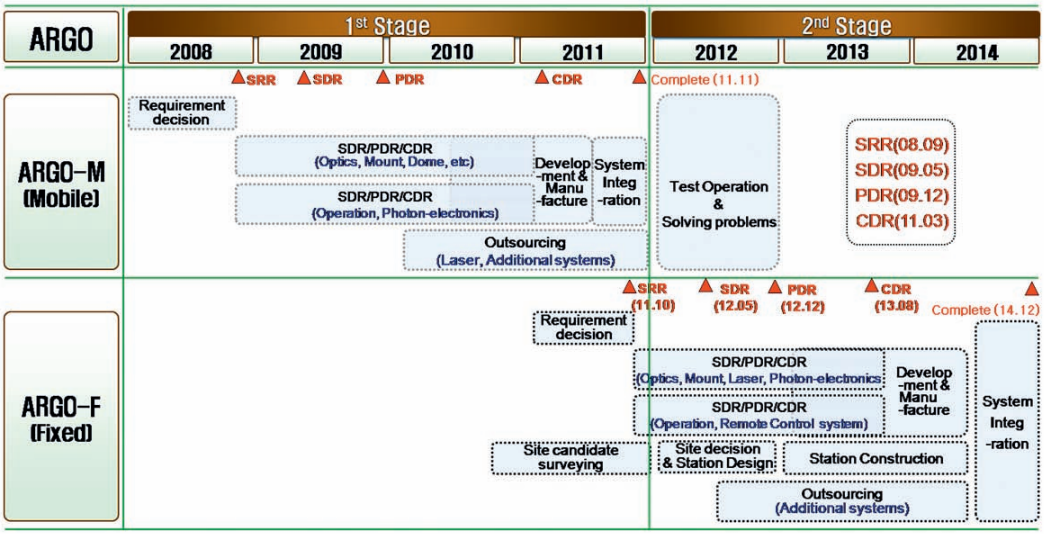


**Figure 1: Milestone of ARGO development**

The mobile SLR system (ARGO-M), which will be completely developed in 2011, is the separate optical path type that employs a 40 cm-receiving telescope and the laser with the repetition rate of KHz. In addition, it is equipped with an event timer as the time measurement equipment that can measure the KHz laser, the compensated single photon avalanche diode (C-SPAD) detector that calibrates the time-walk error, and the spatial and band-pass filters for daylight tracking. In particular, it allows observation in different location because it is established in a container structure. It provides precise tracking and high pointing capabilities because the telescope, the tracking mount and the laser system are designed to block vibrations coming from the container during observation. The stationary SLR system (ARGO-F), which is equipped with a telescope of 1 m diameter, has the common optical path and its development will begin after completing ARGO-M. The milestone of ARGO development is shown in the Figure 1.

ARGO-M is a remotely controllable and kHz laser ranging system with the single shot range precision less than one centimeter and NP precision better than 5 mm for LAGEOS satellite. ARGO-M will be capable of tracking satellites with LRA up to the altitude of 25,000 km and provides 24 hour tracking coverage including daylight tracking. ARGO-M uses a diode pumped laser with 532 nm wavelength, the original output energy of 2.8 mJ at 2 kHz, 15 ps pulse width. In contrast, ARGO-F has the common coude optical path using the telescope of 100 cm aperture, whose requirements are not fixed yet because its development is planned to be started from 2012 and finished in 2014. The detailed specifications of ARGO-M and ARGO-F are shown in the Table 1.

**Table 1: Major specifications of ARGO-M and ARGO-F**

| Item | Parameter | ARGO-M | ARGO-F |
|---|---|---|---|
| Telescope | Path type | Seperate | Common Coude |
| | Rx and Tx telescope | 40/10 cm | 100 cm |
| | Primary mirror F-ratio | 1.5 | N/A |
| | Beam divergence | 5 ~ 200 arcsec | N/A |
| | Max slew rate | 20 deg/sec (Az), 10 deg/sec (El) | N/A |
| | Tracking & pointing accuracy | < 5 arcsec | < 1 arcsec |
| Detector | Type | C-SPAD | N/A |
| | Quantum efficiency | 20% | N/A |
| Laser | Wavelength | 532 nm | 532 nm |
| | Pulse energy | 2.8mJ @2KHz | N/A |
| | Pulse width | 15 ps | N/A |
| | Repetition rate of operation | 2 KHz | N/A |
| | Beam diameter @ Tx telescope | 6 cm | 80 ~ 100 cm |

# 2. Development Status of ARGO-M

ARGO-M is composed of five sub-systems that are the optical system, the optoelectronic part, laser system, tracking mount and operating system. The optical system shoots laser pulse to satellites and collects the reflected optical signals. The photoelectronic part detects the optical signals and precisely measures the time of flight of the laser pulse at the pico-second level. The laser system generates the ultra-shot laser pulse of 532 nm wavelength and the tracking mount is the mechanical system that performs precise tracking of satellites, supporting the optical telescopes and the peripheral devices. The operating system controls various sub-systems needed for the laser observation, performs actual observation after comprehensively judging the observation environment and reflecting the results, and integrates, processes and transmits the data obtained by the actual observation.

The optical subsystem was designed and manufactured by KASI, whose configuration are shown in Figure 2. The iris behind the primary mirror is on the focal pland and has three holes and one blocked hole for the spatial filters and the sun shutter. The collimating lens is used for focusing of C-SPAD and two camers of day and night tracking.

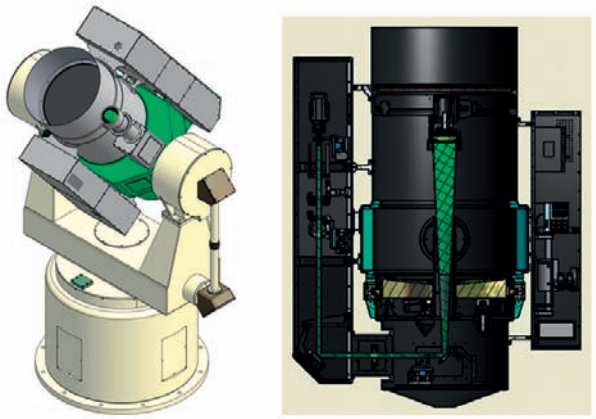

**Figure 2: Shape of the optical subsystem(left) and its configuration(right)**

As shown in Figure 2(right), the detecting optics is located on the telescope and its components including C-SPAD and cameras are in the box. Its beam path and optical design is shown in Figure 3. Two bandpass filters are used for night(1nm band width) and for daytime(0.3nm band width). The swithing mirror(M3 in Figure 3) changes the beam path for daytime camera and C-SPAD. The daytime camera is activated when it is inserted in the beam path, and the nighttime and C-SPAD are activated when it is removed from the beam path. C-SPAD made by Peso Consulting(Austria) is used and PCO 1600 and Watec WAT-120N are also used for day and night, respectively.

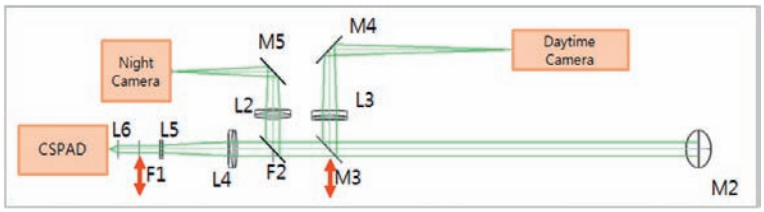


**Figure 3: Design of the detecting optics**

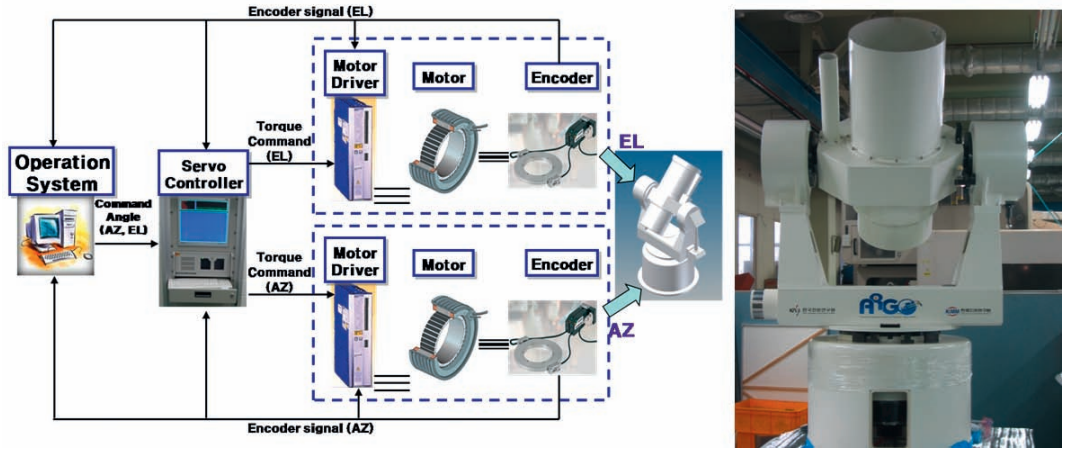


**Figure 4: Block diagram of the servo system(left) and the prototype of the tracking mount(right)**

The tracking mount subsystem was designed and manufactured by KIMM (Korea Institute of Machinery and Materials) in Korea. The direct drive motors made by ETEL are used and the encoder is REXM model of Reishaw. KIMM alrady manufactured the prototype of tracking mount for the performance experiments in February 2011. For the test results of mount prototype, the repetition accuracy is less than 0.9 arcsec for azimuth and 0.6 arcsec for elevation.

RGL-532 model made by Photonics Industries(USA) is used for the laser system, which has about 2.8mJ at 2KHz repetition rate and 15 ps of pulse width. The beam diameter is 1.9 mm at the exit of the laser head, which is expanded to 30 mm by two beam expanders on the optical table. The optoelectronic and operating subsystems were given by the 17th laser ranging workshop. The experiment of the integrated optoelectronic system was performed with 2 kHz repetition rate on the optical table in the laboratory to validate the performance of the optoelectronic system. As shown in Figure 5, it has the block diagram similar to the ground calibration or ground laser ranging to correct the system error. The experiment shows about 33 ps RMS of accuracy after post-processing, whose performance is expected to be increased aftter the system integration.

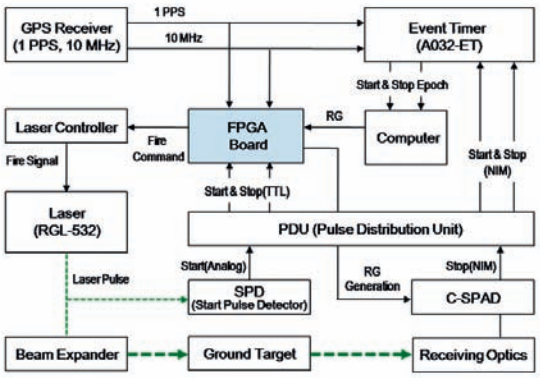


**Figure 5: Block diagram of the experiment of the integrated optoelectronic subsystem**

## Acknowledgements

This work was supported by the Korea Astronomy and Space Science Institute through the SLR system development program for space geodesy funded by the Ministry of Education Science and Technology (MEST).

## References

*Lim, H. C., Seo, Y. K., Na, J. K., Bang, S. C., Lee, J. Y., Cho, J. H., Park, J. H. and Park, J. U.*, 2010,Tracking Capability Analysis of ARGO-M Satellite Laser Ranging System for STSAT-2 and KOMPSAT-5, Journal of Astronomy and Space Sciences, Vol. 27, No. 3, pp. 245-252

*Lim, H. C., Seo, Bang, S. C., Yu, S. Y., Seo, Y. K., Park, E., Kim, K. D., Nah, J., Jang, J. G., Jang, B. H., Park, J. H. and Park, J. U.*, 2011,Study on the Optoelectronic Design for Korean Mobile Satellite Laser Ranging System, Journal of Astronomy and Space Sciences, Vol. 28, No.23, pp. 155-162

## Correspondence

Hyung-Chul Lim
Korea Astronomy and Space Science Institute
776 Daedeok-Daero
Yuseong-gu, Daejeon, 305-348
South Korea

hclim@kasi.re.kr

# Configuration of ARGO-M Optoelectronic Subsystem and Its Performance Experiments

*Seung-Cheol Bang, Seong-Yeol Yu, Nung-hyun Ka, Yoon-Kyung Seo, Eun-Seo Park, Jin-Young Lee, Hyung-Chul Lim, JongUk-Park*

ABSTRACT

The optoelectronic subsystem of ARGO-M, Korean mobile SLR system, measures the start and stop epoch of laser pulses to compute the distance from a station to satellites, which includes SPD (Start Pulse Detector), C-SPAD, PDU (Pulse Distribution Unit), Event Timer and ISA card. The SPD developed by KASI (Korea Astronomy and Space Science Institute) and detects start laser signals on the transmitting optical table. C-SPAD from Peso-consulting in Czech is used to detect the returns from satellites. A032-ET from Institute of Electronics and Computer Science in Latvia measures the precise start and stop epoch. The PDU receive signals from SPD and C-SPAD deliver to A032-ET and ISA card, which was developed by KASI and performed various tests. ARGO-M runs KHz laser ranging which requires a fast optoelectronic control of RG generation and laser fire command. For these missions, ARGO-M uses the ISA card which was developed by Graz in Austria and consists of 500ps internal Event Timer, RG generator and the laser fire controller. The experiment based on components was performed to guarantee and validate the performance of all components belonging to the optoelectronic subsystem. In addition, the experiment of the integrated optoelectronic subsystem including the ground target was also carried out for the functional and performance verification of ARGO-M in the laboratory by using the laser with 15ps pulse width. In this study, the design and performance test results are provided for SPD, PDU and Event timer. And the test results of the integrated optoelectronic subsystem is also presented with its configuration and analyzed.

## 1. Block diagram of optoelectronic

As shown in Figure 1, the optoelectronic system of ARGO-M consists of three components: event timer, optoelectronic controller and transmitting/receiving photon detectors.

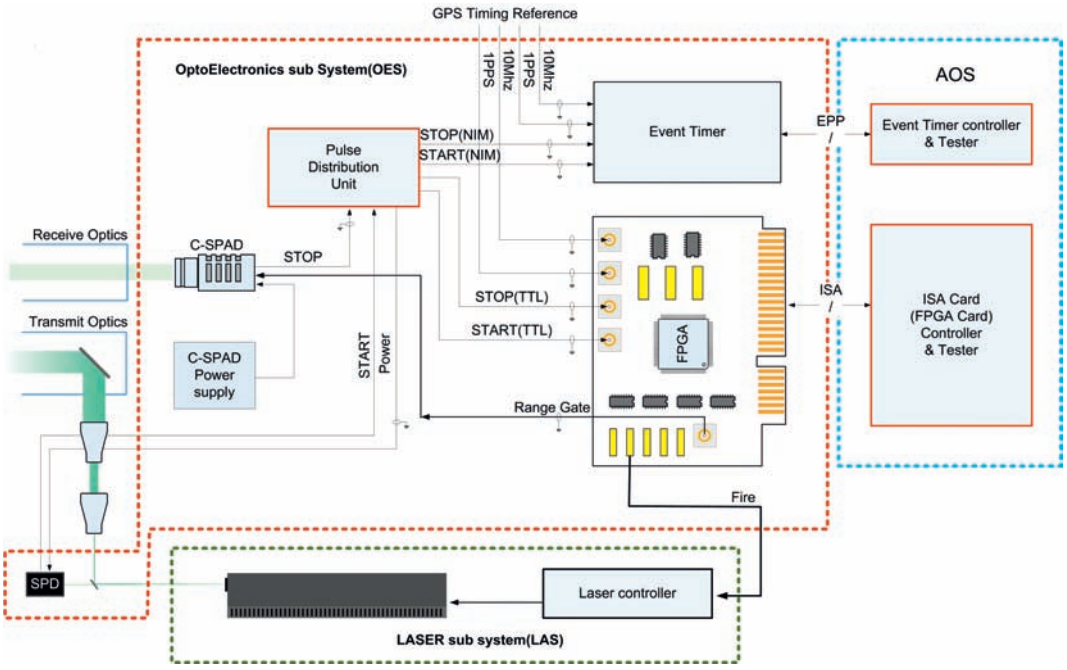


**Figure 1: Block diagram of optoelectronic subsystem**

# 2. Start Pulse Detector (SPD)

The SPD made by KASI detects the start laser pulse which is located in transmit optical table. The SPD is placed behind the 2nd laser reflecting mirror, which uses penetrated beam through the mirror to maximize the transmit efficiency of laser beam. The SPD has a focus lens to adjust input light intensity for optimal performance. The PIN diode in SPD uses FCI-125G-006HRL made by OSI optoelectronics.

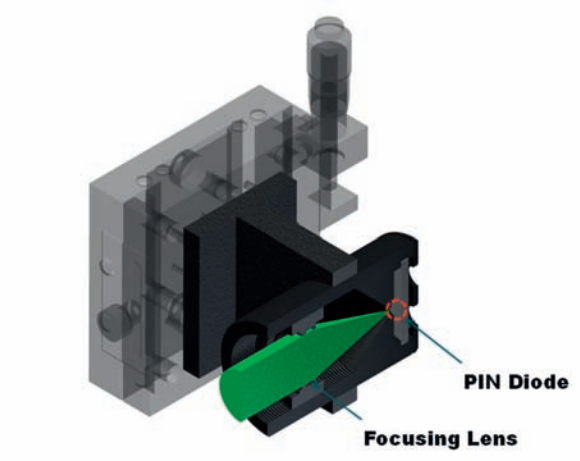


Figure 2: SPD structrure

| Part No | SFH229 | FCI-125G-006HRL [KASI] |
|---|---|---|
| Company | OSRAM | OSI optoelectronics |
| Reverse voltage[max, V] | 20 | 20 |
| Capacitance [pF/$V_R$,V] | 13/0 | 0.65/5 |
| Rise time [s/$V_R$,V] | 10ns/10 | 35ps/5 |
| Peak sensitivity[nm, peak] | 380~1100(860) | 400~1100(750) |
| Spectral sensitivity[A/W] | 0.62/850nm | 0.36/850nm |
| Dark current[pA/$V_R$] | 0.05nA/10 | 0.02pA/5 |
| Active area diameter | 0.3 mm² | 150 um² |

Figure 3: PIN Diode specifications

# 3. Pulse Distribution Unit (PDU)

The PDU delivers start and stop signal to Event Timer and ISA card. The pulse width of the start and stop signal is expanded using R-C time-constant circuit at first stage of this unit. The PDU circuit is connected by one-to-one between the transmitter and the receiver using Emitter-Coupled-Logic(ECL). This unit has three kind of output port. Primary output port is for event timer, secondary output for signal monitoring and TTL output for ISA Card. The PDU with 1U height was developed by KASI. It supplies the SPD power and It has also the LED indicator on the front panel to check start and stop signal status.


Figure 4: Front panel of Pulse Distribution Unit

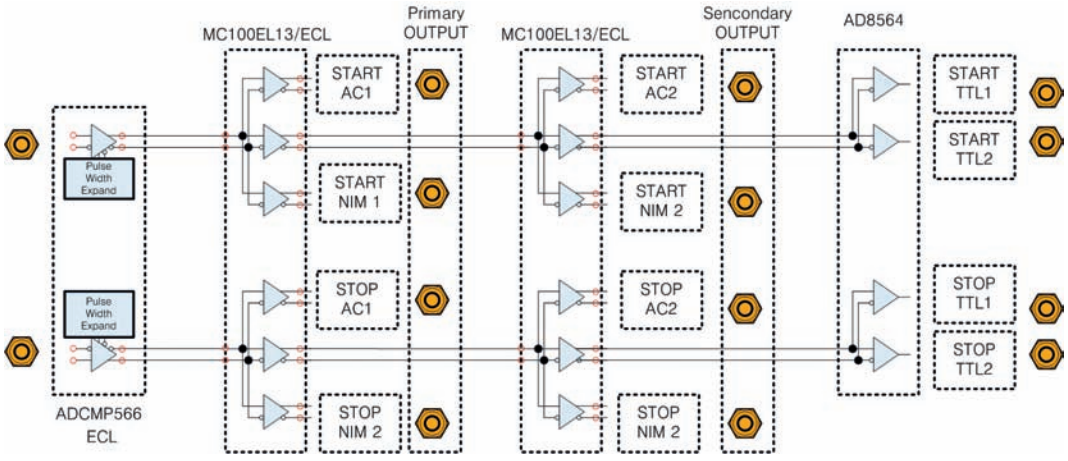


Figure 5: Block diagram of Pulse Distribution Unit

# 4. C-SPAD & ISA card

The C-SPAD(Peso consulting) is used for stop signal detector of ARGO-M. KASI performed the function and performance test of the C-SPAD by various means. Test results are presented in the integrated test results of this poster.

This ISA card was designed by Graz in Austria and also manufactured by KASI. ARGO-M operates KHz laser ranging which requires a fast optoelectronic control to generate RG and to execute laser fire command.

**Figure 6: C-SPAD**

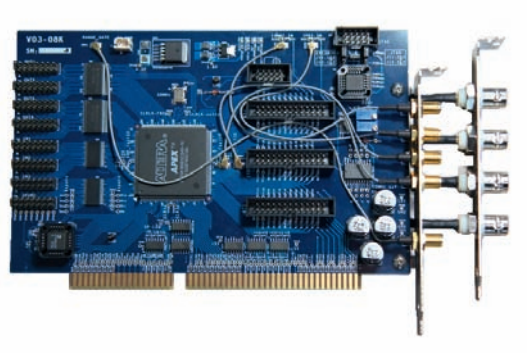

**Figure 7: ISA card**

# 5. Event timer performance test

ARGO-M uses Riga A032-ET to measure start and stop epoch. KASI performed A032-ET performance test using Symmetricom GPS receiver for timing reference and SRS DG-645 delay generator to generate start and stop signal. The left picture below represents configuration for this test and the right graph shows the test result of A032-ET. The legend of 01, 02 and 03 means no connection between GPS receiver and delay generator. But the last legend of 01(10MHz) means the connection between the GPS receiver and the delay generator to supply 10MHz clock. KASI also checked 60ns dead time period through the test.

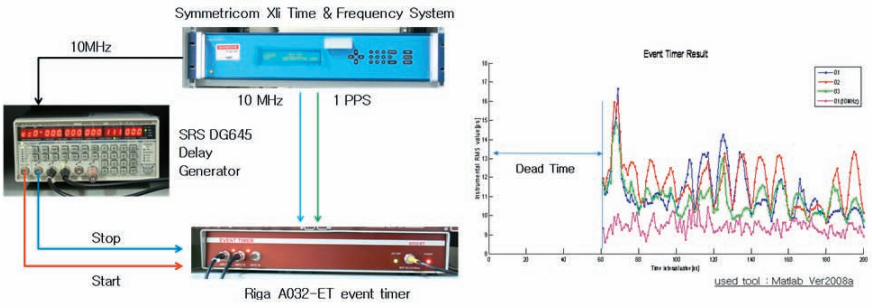


**Figure 8: Configuration of event timer test(left) & its result(right)**

# 6. Conclusion

Besides components of optoelectronic subsystem such as SPD, C-SPAD, PDU, ISA Card and event timer, RGL-532 laser, transmitting optics, ground target and receiving optics are also used for the integrated test of optoelectronic subsystem in the laboratory. Especially, we made the ground target consisting of a prism and a aluminum reflector to verify C-SPAD performance as well as the receiving optics similar to telescope.

The test measurement of integrated optoelectronic subsystem was done by using A032-ET event timer. Figure 9 shows the integrated test results with 13.5ps RMS accuracy which actually depends on the laser beam strength coming to C-SPAD.

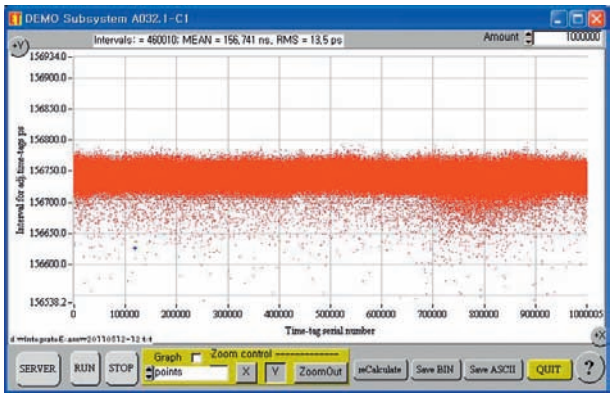


**Figure 9: The test result of the integrated optoelectronic subsystem**

## Acknowledgements

This study was supported by "SLR system development program for space geodesy" project of KASI funded by the Ministry of Education Science and Technology(MEST).

## References

*Park, P.H., Park, J.U., Lim, H.C. Cho, S.K., Jang, J.K., Min B.H. & Han, J.Y.* 2005, Development of fundamental technology of satellite tracking and space surveillance system using SLR(Korea Astronomy and Space Science Institude Project Document)

*Lim, H.C., Seo, Y.K., Na, J.K., Bang, S.C., Lee,J.Y., Choi, J.H., Park, J.H., & Park, J.U.* 2009, Tracking capability analysis of ARGO-M satellite laser ranging system for STSAT-2 and KOMPSAT-5, Journal of Astronomy and Space Sciences ,Vol. 27, No. 3, pp 245-252

*Lim, H.C., Bang, S.C.,Yu, S.Y., Seo, Y.K., Park, E.S., Kim, K.D., Nah., J.K., Jang, J.K., Jang, B.H., Park, J.H.,Park, J.U.,* 2010, Study on the Optoelectronic Design for Korean Mobile Satellite Laser Ranging System, Journal of Astronomy and Space Sciences, Vol. 28, No. 3, pp 155-162

## Correspondence

Seung-Cheol Bang
Korea Astronomy and Space Science Institute
776 Daedeok-Daero
Yuseong-gu, Daejeon, 305-348
South Korea

scbang@kasi.re.kr

# New fpga based SLR controller in Metsähovi

*Kirco Arsov*

ABSTRACT

Metsähovi SLR system is currently going through a major renovation. A new 2KHz laser has been bought together with the timing devices, C-SPAD and other necessary electronics. This change from old 1Hz system to our new 2KHz SLR requires improvement in all the hardware and software accordingly. Since in 2kHz scenario there are many time critical tasks to be managed due to this high observations rate, we found for the software impossible to handle some of these tasks. Even with real time operating system this was not possible. We therefore started to look for alternatives, and at the end came up that this tasks could be performed successfully in one fpga board. A product of that is one fpga-based SLR controller developed in Metsähovi that is main topic of this paper. It is conceptually based on the Graz ISA controller, but offers some more elegant manipulation of the operations through the PCI bus. Also, some improvements are introduced, such as fifos for all time critical operations as well as another approach in the overlapping avoidance of the start and stop pulse. It is furthermore fully implemented in the windows as well as linux operating system by proper programming of the necessary drivers. The project is developed in the already commercially available PCI development boards by Altera. Some registers as well as operations are reviewed and explained in more detail. A test software to test the functionality of the board is also programmed and presented.

## 1. Introduction

This paper deals with the new FPGA-based Satellite Laser Ranging system controller developed at the Finnish Geodetic Institute. In its current version it offers 5ns timing resolution on the low-cost Cyclone II fpga. A smaller project targeting the Altera MAX II development board of 120 EUR is also compiled and works with the minimum requirements for 2KHz SLR (controlling the laser, event timing as well as RG and overlapping avoidance with 5ns and only fractional seconds) and its design document is currently being under preparation. Although the system is primarily a replacement for the old ISA Card and replicates and extends the critical functions of the old card, the developed SLR code base with its extremely popular Wishbone interface is highly portable and can be re-used on other commercial PCI or PCIe development boards from Altera or Xilinx with little effort. The unmodified project runs on Cyclone II fpga. Future systems may use newer Stratix, Spartan or Virtex FPGAs and their high-speed transceivers to achieve a timing resolution between 1ns-100ps or better. In the following we describe the controller system functions and registers in more details and give some examples where necessary.

## 2. Principle of operation

**Basic tasks:** The board is foreseen to manage most of the necessary tasks in the new 2KHz SLR system in Metsähovi. Among other tasks, its basic functionality is also to manage the Range Gate pulses which are sent to the C-SPAD. For that purpose, an integer and fractional part of the expected RG is written in the PCI registry and at desired time the RG pulse is output from the board. For that a FIFO of 1024 points is used inside the board. Other functionality is controlling of the laser fire frequency, where the user might change on-the-fly the laser frequency. Also a calibration and CCD control is programmed, and fully automatic. One other application implemented in the board is Event timing with 5ns resolution. The start as well as stop events are timestamped and put into 1024 FIFOs in the board having integer and fractional part, so absolute reading is possible. It also has couple of counters readable, for example one 10MHz counter giving the time as well as its rollovers counter, so the board gives absolute time and it is not necessary to read the clock with the software here and there not to loose the track of the absolute timing. It has also internal secs counter who is counting the integer seconds and it is implemented as a 24 bit value alowing idle time of the board for couple of years. Also it has implemented overlapping avoidance of start and stop signals and the user might adjust on-the-fly the intervals of overlapping etc. It has calibration mode as well as CCD mode where appropriate pulses are generated when necessary, dependant on different configuration. The board is fully implemented into our SLR software and up to now very good results have been obtained in the testing. We also provide one demo program to test the functionality of the board for windows as well as for Linux operating system. It has extended documentation so the users might get familiar with the functionality of the board. The main motivation in starting the project is that nowadays many open cores for fpga exist.

One place where one might take a look is www.opencores.org for example. Initially we bought the ISA Graz board and at the beginning it was not so easy to find one computer having ISA slot. It was possible only to use backplane industrial computer for that purpose. These indutrial computers, although very robust, having all the nowadays obsolete slots do not at the moment support the best CPUs. Our intention in development of the new 2KHz SLR was however to make use of all the most current up to date hardware. Deciding moment was when we noticed that there is already available open core for PCI bus manipulation. We also noticed that some of our old ISA board functionality could be maybe improved and slightly better. On the other hand designing our own PCB PCI fpga board is pretty expensive. For that purpose, we decided to use already available commercial development boards who are relatively cheap but on the other hand provide great flexibility regarding available options.

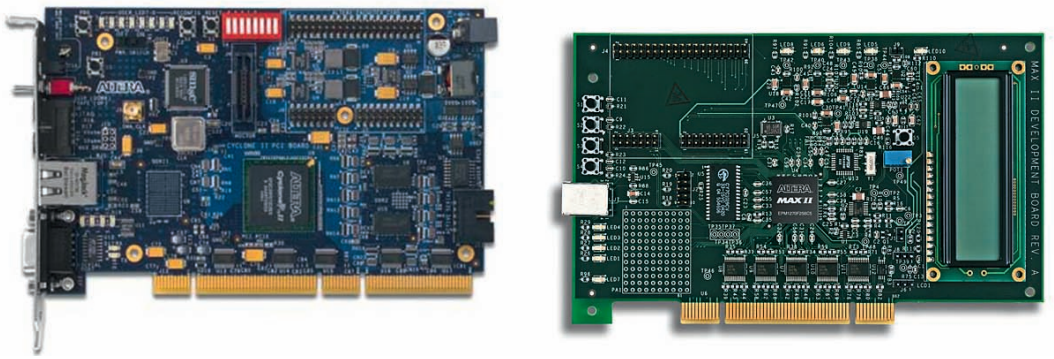

**Figure 1: fpga boards used for the SLR controller project**

**Verilog Software**: The majority of the SLR code has been implemented as generic parameterized verilog modules. Emphasis was taken on cross-platform portability, such that none of the modules are specific to Xilinx, Altera or the FPGAs of other companies. The code is also largely independent of the particular hardware evaluation kit used. The SLR project files are intended for Altera Quartus 9.1 and later. The project is configured for the Cyclone II EP2C35 PCI Development Board. This makes then very easy later modification of the code, implementation of different fpga etc. We did not use any graphics programming, but the whole code is written in verilog. However, due to the particular development board used, we have to use also some particular IPs that are chip dependant, in our case Altera's Cyclone II fpga. Those IPs are designed with the Quartus MegaCore IP library. This includes the PLL management, the FIFO design etc. If at some point the project is changed to other fpga, these IPs should be replaced with appropriate for that particular fpga used later.

For the PCI bus communication the design uses the 'pci32lite' 32-bit PCI Target to Wishbone bridge available at OpenCores.org under a GNU LGPL license. The Target is light-weight, fully self-contained and thus portable to Xilinx, Altera etc. We decided further to make all the **code freely available** to the SLR community for non-profit usage. In the meantime the Cyclone II development board is unfortunately obsolete due to the rapid development of the PCIe as well as transceivers technology, so we implemented one lightweight project who can support the complete 2KHz SLR in the MAXII development board, the second board shown in Figure 1. This second project has some restrictions as compared with Cyclone II board, but still most of the 2KHz SLR critical tasks, such as Overlap avoidance, laser control, event timing are supported. For the fifos we could not use the logical elements due to their small number (there is also no block RAM inside the board) but developed one FIFO SRAM controller and used the already implemented SRAM in the MAX II development board for fifos. We implemented this only for the Overlapping avoidance fifos. For event timing unfortunately due to the limited number of logical elements we do not use FIFOS but simply whenever event comes, flag in the PCI registry is set and if fast enough one may read this event via the PCI bus. Also many tasks that we set via the PCI registry, such as Overlapping avoidance border, pulse width, laser frequency, integer seconds etc are not implemented or hard coded in the MAXII project in order to save as much as possible memory. For example, the Cyclone II board has about 30 000 logical elements, whereas MAX II cpld has about 1400, so it is evident that one has to take care to save as much as possible logical elements. There is also extensive documentation about this MAXII SLR controller so if someone interested might take a look for more details.

**Board PCI registry**. The overview of the PCI registry used is presented in Figure 2. In the current version we use 20 words in the PCI registry I/O space. Each registry is 32 bits. The I/0 registers are shown in the first table. From there one might see the basic functionality of the board. Some registers are read only, some write only and some are read and write. For example, the RG registry is read/write. This is one option where the software by reading the RG might see for

what time value the board is waiting for control purposes. In the board however is also implemented that if the written time for RG is larger then the current time, the RG value is automatically deleted and the new value is red from the RG fifo. The reading RG registry option has been implemented in the early design phases and is not really necessary, but is left as it is as an option. The I/0 registry has registers for reading the counters, reading the start as well as stop events, reading the 200MHz clock, reading/writing the RG values, setting the OA window, setting the laser frequency, calibration delay setting etc. Two of the most important registers are the configuration register and the global status register since they control and manipulate the

| Port | R/W | Description |
|---|---|---|
| Base+w0 | R | Firmware Version |
| Word 1 | R/W | Configuration Register |
| Word 2 | R | Global Status Register |
| Word 3 | R | RTC Seconds Counter |
| Word 4 | R | 10 MHz Software Timing |
| Word 5 | R | 10 MHz Rollovers |
| Word 6 | R | 10 MHz Fractional (debug) |
| Word 7 | R | 200 MHz Fractional (dbg) |
| Word 8 | R | Start Time Integer FIFO |
| Word 9 | R | Start Time Fraction FIFO |
| Word 10 | R/W | Range Gate Integer FIFO |
| Word 11 | R/W | Range Gate Fraction FIFO |
| Word 12 | R | Stop Time Integer FIFO |
| Word 13 | R | Stop Time Fraction FIFO |
| Word 14 | R/W | Laser PWM Configuration |
| Word 15 | R/W | Target Calibration Delay |
| Word 16 | R/W | 1PPS pulse width register |
| Word 17 | R/W | debug |
| Word 18 | R/W | Overlap Avoidance Window |
| Word 19 | R/W | Range Gate to CCD Enable |
| Word 20 | R | Vernier Delay bits |

MSB-LSB: cccccccc||cccccccc||EFGHefgh||xxVSRLAB

| Bit # | Description |
|---|---|
| 31-24 | [C] Start FIFO element count[1] |
| 23-16 | [c] Stop FIFO element count[1] |
| 15 | [E] Start Time Int FIFO Empty |
| 14 | [F] Start Time Int FIFO Full[2] |
| 13 | [G] Start Time Fract FIFO Empty |
| 12 | [H] Start Time Fract FIFO Full |
| 11 | [e] Stop Time Int FIFO Empty |
| 10 | [f] Stop Time Int FIFO Full[2] |
| 9 | [g] Stop Time Fract FIFO Empty |
| 8 | [h] Stop Time Fract FIFO Full |
| 7-6 | (Unassigned) |
| 5 | [V] Configuration not Valid[3] |
| 4 | [S] 1PPS is GPS-synched |
| 3 | [R] SLR is reset (disabled) |
| 2 | [L] Locked to 10 MHz |
| 1 | [A] Locked to 100 MHz |
| 0 | [B] 10 MHz counter synched |

MSB-LSB: xxxxxxxx||xxxxxxxx||xxxxxxxx||xOSRFFLE

| Bit # | Description |
|---|---|
| 31-9 | (Unassigned) |
| 8 | [f] Clear the Stop FIFO[5] |
| 7 | [f] Clear the Start FIFO |
| 6 | [O] Enable Overlap Avoidance |
| 5 | [S] Use only fractional seconds[1] |
| 4 | [R] Clear the Range Gate FIFO |
| 3 | [F] Enable internal feedback[2] |
| 2 | [P] Use fake 1PPS signal[3] |
| 1 | [L] Enable Laser Firing generator |
| 0 | [E] Enable all SLR functions[4] |

**Figure 2: Some PCI registry; first table is the overall PCI I/O registry space used, second is the global board status register, the third table is board configuration register.**

overall board functionality. If one takes a look in the second table in Figure 2 which represents the status register (word2 of the first table) one might see that it allows the determination of start or stop events, the count of them in the fifos etc. One important bit there is bit 5 telling if the current configuration set is OK or not. In the board there are implemented many loops checking the proper values of RG, RG windows, laser frequency etc. So if there is any conflict, by checking this bit one is sure that the configuration is ok. In the configuration registry, also the global reset of the board is performed as well as check of the different counters, PPS synchronization etc is performed. We would like here also to mention that as input the board uses 10MHz signal as well as 1PPS, and all other frequencies are generated inside the board by usage of the 10MHz reference which in our case comes from the H. maser. We also designed one additional board who serves mainly to produce 50 Ohm terminated input/output signals to be used by the board. We mention also that in order to produce NIM signal we used commercially available TTL to NIM converter provided by the company Micro research Finland at www.mrf.fi. In the early development phase we also used a fake PPS signal generated inside the board, and this is bit 2 in the configuration register, so if one uses real PPS then this bit should be set to 0. For fast enabling of all functions, one might set bit 0 in the configuration registry. As far as the bit 0 in the configuration register is enabled, the board resets itself (including all fifos etc) and waits for the first PPS to come, and then synchronizes all counters etc to this epoch.

**Demo software**. The whole fpga project is developed to serve our SLR operational software. For that purpose, some libraries for reading/writing and remapping the PCI registry as well as the libraries for reading the hardware ports are used. However, in the project we decided to write also one program who can test the overall functionality of the board without needing our SLR software. In Figure 3 we present the demo program written for the Windows operating system. We also designed one demo program which might be used for the Linux system. The main purpose of the program as one might see from the Figure 3 is testing the laser, OA, calibration, CCD, event timing etc of the board. This program together with the Linux version is also freely available to the SLR community for testing the board for non commercial purposes by the author. The above mentioned libraries are also included in the code as dll files, but we advice if someone uses this test program later to purchase its own licenses for these libraries (cost about 50 EUR). For Windows, we

also developed one driver who should be used in order to install the board in the computer. It does not do a lot, it just remaps the board address space and tells the system what is the main functionality of the board by reading the board's PCI registry values. The further board operation such as registry reading/writing is done by the abovementioned libraries. Reading of the board on i9 processor takes about 2 micro seconds, so it fulfills fully the 2Khz requirements.

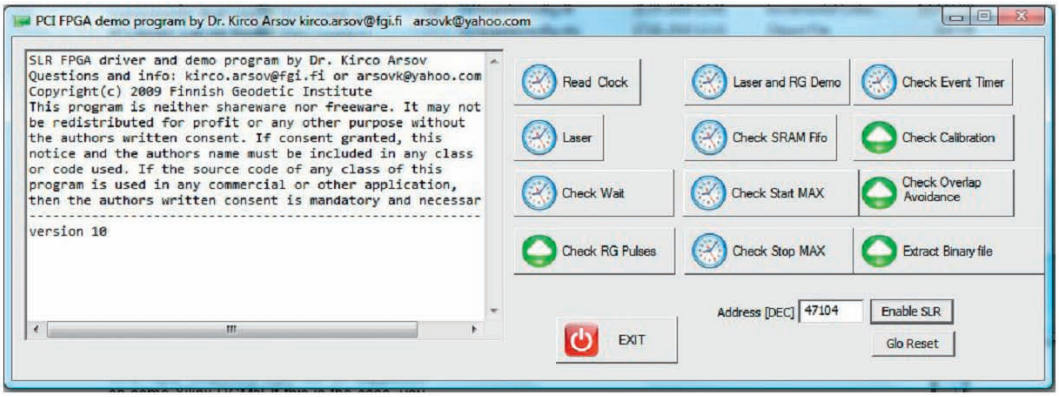


**Figure 3: Windows demo software**

# 3. Overview and future work

So far we have presented one fpga based SLR controller capable of doing most of the time critical operations inside the board. However there is always something to be improved, updated or replaced. In this version, for board-PC communication we use the PCI bus. Nowadays however PCI is already becoming obsolete. The PCIe bus offers much higher transfer rate as well as more flexibility in usage of the board. However, there is still not available open core IP for the PCIe bus. Some companies offer this IP, but we still consider the price of around 5-7000 EUR relatively high. Anyway, for the future we would like to continue this project on the PCIe.

We used as the fpga host commercially available development board. We would be interested in the future if someone from the SLR community is interested in developing together the PCB board for some particular fpga.

At the moment pico-second Event Timing is performed on external purpose-built devices (in our case A032-ET). Modern transceivers available on FPGAs and used for 10G/40G/100G network links may be applicable as an easy replacement for such extra devices (see Arria GX transceiver pdf document). It may be possible to achieve sub-picosecond resolution.

Additional timing options are provided by various Time To Digit Converter (TDC) implementations using FPGA slices or logic elements. The do coarse resolving using a 200 MHz or faster (500MHZ with pos and neg clocking) clock with additional fine resolving along on-FPGA delay lines implemented using fast carry logic as explained in High-Resolution Time-to-Digital Converter in Field Programmable Gate Array reference. The current resolution is rather poor at only around 50-100ps. Such TDCs with "free" resources already on the FPGA may nevertheless be attractive for coarse timing purposes and can replace our current 5ns course timing resolution within the fpga.

## Acknowledgements

Author would like to acknowledge all the great help he got from Graz Observatory in general and from Georg Kirchner And Franz Koidl in particular. All the fruitful discussions and all the great help Georg and his team offered during my few visits in Graz are herewith greatly acknowledged.

## References

*OpenCores.org* pci3 2lite PCI Target with Wishbone interface, Release 03, GNU GPL, Peio Azkarate. http://www.opencores.com/project,pci32tlite_oc

*Arria GX transceiver* http://www.altera.com/literature/hb/agx/agx_51004.pdf

High-Resolution Time-to-Digital Converter in Field Programmable Gate Array. http://cdsweb.cern.ch/record/1158663/files/p383.pdf

*Kirchner, G., Koidl, F.,* 2004 Graz KHz SLR System: Design, Experiences and Results, 14th ILRS Workshop

*G. Kirchner,* 2004, Range Gate Generator at Graz, Proceedings of KHz SLR Meeting, Graz, Austria

## Correspondence

Dr. Kirco Arsov
Finnish Geodetic Institute
Geodeetinrinne 2
02431 Masala
Finland

Kirco.arsov@fgi.fi

# LAGEOS-ETALON solutions using the Bernese Software

*D. Thaller, K. Sośnica, R. Dach, A. Jäggi, G. Beutler*

ABSTRACT

During the last three years, the Bernese Software has been extended with the capability to analyze SLR data to geodetic satellites, e.g., LAGEOS and ETALON. SLR data to LAGEOS and ETALON have been processed to obtain weekly solutions including station coordinates, satellite orbits, Earth rotation parameters (ERPs), and range biases.

Different background models and parameterizations are used in the analysis and their impact on the weekly solutions is studied. The models of interest are, e.g., ocean tidal loading (OTL) and atmospheric tidal loading (ATL). The impact of OTL was found to be larger than the impact of ATL. The differences in the LAGEOS orbits are at the level of 4 mm and 1 mm when ignoring OTL and ATL, respectively.

In addition, different parameterizations of the ERPs have been tested and compared: the standard ILRS parameterization using constant pole offsets per day (resulting in jumps at the day boundaries), and the piece-wise linear parameterization used in the Bernese Software for the GNSS solutions (including continuity at the day boundaries). When comparing with the IERS-08-C04 series, the RMS of the differences is smaller by almost 10% if a piece-wise-linear parameterization is chosen for the ERPs instead of a piece-wise-constant parameterization.

## 1. Introduction

The Bernese Software (Dach et al., 2007) recently has been extended with the capabilities of analyzing SLR observations to spherical satellites, e.g., LAGEOS and ETALON satellites. We processed five years of data to these satellites (2006 - 2010) and generated weekly solutions following the recommendations of the ILRS Analysis Working Group (AWG). The observations to LAGEOS and ETALON are weighted against each other by a factor of 9 using a priori sigmas for the observations of 1 cm and 3 cm, respectively.

SLR station coordinates are estimated together with satellite orbits for LAGEOS and ETALON, daily Earth Rotation Parameters (ERPs), i.e., polar motion and universal time/ length of day (LOD), as well as range biases for a few selected SLR sites.

The weekly satellite orbit is represented by six initial osculating elements at the first epoch of the weekly arc, and five empirical parameters: a constant acceleration in along-track direction, and once-per-revolution accelerations (represented as sine and cosine terms) in along-track and cross-track direction. The empirical parameters are valid for the entire orbital arc of 7 days.

## 2. Impact of background models

A priori models have a big impact on the solution generated. As the orbits of spherical satellites like LAGEOS and ETALON can be modeled rather simple so that only a few empirical parameters have to be estimated (see Sec. 1), the SLR solutions are well suited to test the impact of several a priori models.

The impact of different Earth's gravity field models on the LAGEOS solutions has been presented by Jäggi et al. (2011).

The impact of applying or ignoring ocean tidal loading (OTL) and atmospheric tidal loading (ATL) corrections to the Earth's center of mass is analyzed for weekly LAGEOS solutions of the year 2008. The weekly RMS of the observation residuals are displayed in Fig. 1 (left). Comparing the different solutions reveals that ATL has almost no impact on the solution, whereas omitting OTL slightly decreases the quality of the solution, i.e., about 10% of the RMS value itself.

We also studied the impact of OTL and ATL on the estimated LAGEOS orbits and compared the orbits with each other. Taking the orbit of the solution with both, i.e. OTL and ATL, applied as a reference, Fig. 1 (right) shows the RMS of the orbit differences for each weekly comparison. Table 1 summarizes the median of the weekly RMS values of the orbit

comparisons for the entire year. Generally speaking, the impact of OTL and ATL in terms of RMS of orbit differences are at the level of several millimeters. Similar to the RMS of the observation residuals, the impact of ATL on the resulting orbits is clearly smaller than the impact of OTL, i.e., about 1 mm and 4.5 mm, respectively.

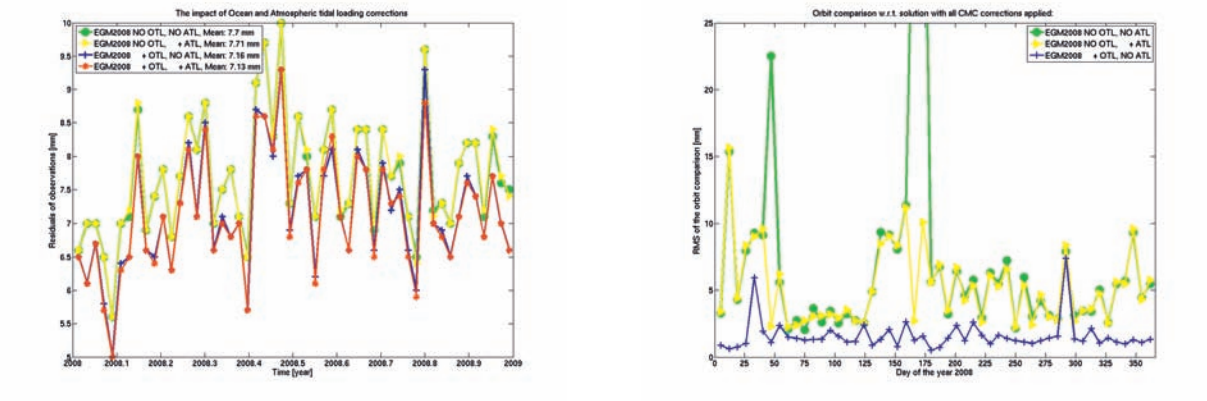


**Figure 1: Impact of ocean and atmospheric tidal loading on the SLR solutions. Left: RMS of the observation residuals; Right: RMS of orbit comparison w.r.t. the solution with OTL and ATL applied.**

| | No OTL, + ATL | + OTL, No ATL | + OTL, + ATL |
|---|---|---|---|
| **No OTL, No ATL** | 1.17 | 4.43 | 4.96 |
| **No OTL, + ATL** | | 4.06 | 4.54 |
| **+ OTL, No ATL** | | | 1.33 |

**Table 1: Impact of ocean and atmospheric tidal loading on the SLR solutions: Median values of RMS of orbit differences for weekly orbit comparison (in mm).**

# 3. Impact of different parameterizations of ERP

We tested different parameterizations for the ERPs. First, the standard parameterization as it is used within the ILRS AWG was chosen, i.e., piece-wise-constant daily polar motion estimates, daily LOD estimates and UT1-UTC fixed to IERS-08-C04. The disadvantage of this parameterization is that the resulting time series of ERPs have discontinuities at the day boundaries, whereas the orbit is parameterized as continuous arc over the entire week. Therefore, a second parameterization was chosen: piece-wise-linear (PWL) with offset and drift parameters per day for polar motion and UT1-UTC and additional continuity conditions at the day boundaries. The first value of UT1-UTC is fixed to the IERS-08-C04 series. This type of parameterization is similar to that used in the GNSS data analysis at the IGS Analysis Center CODE (Center for Orbit Determination in Europe).

The comparison of both SLR-based polar motion series w.r.t the IERS-08-C04 series is shown in Fig. 2, and the corresponding mean and weighted RMS values are given in Table 2. The comparison is done for the epochs at 12:00 UTC. It can be seen that the agreement with the IERS-08-C04 series is slightly better for the SLR-derived polar motion series using the piece-wise-linear parameterization than the piece-wise constant parameterization.

Additionally, a polar motion series based on microwave GNSS observations are compared to IERS-08-C04. The GNSS series result from the weekly analysis performed at the IGS analysis center CODE. The ERPs are parameterized as piece-wise-linear polygons with polygon values estimated at 00:00 UTC. For the comparison with IERS-08-C04, the polygon values are interpolated to the epochs 12:00 UTC. We can see from Fig. 2 as well as from Table 2 that the polar motion series derived from GNSS observations are much more stable than the polar motion series based on SLR data. The difference is about a factor of 10 in terms of RMS.

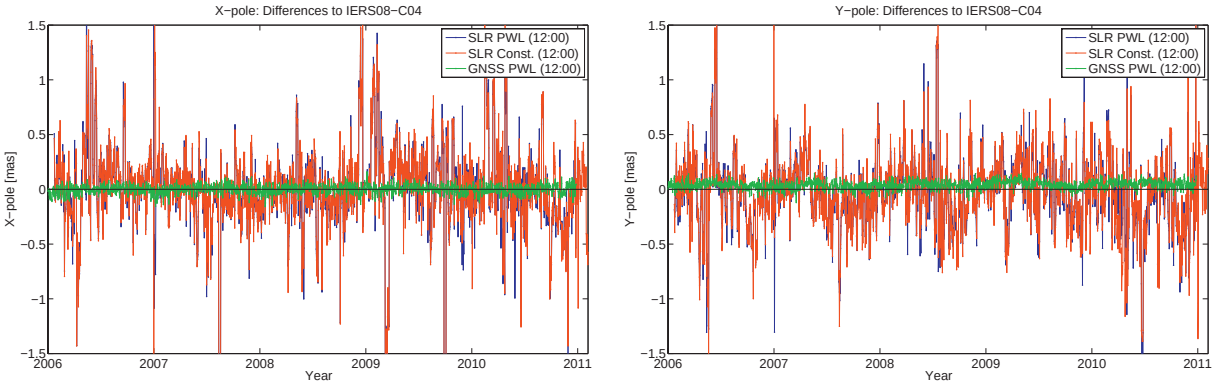


**Figure 2: Comparison of polar motion derived from SLR and GNSS solutions with the IERS-08-C04 series at 12:00 UTC epochs. Left: X-pole; Right: Y-pole.**

| | | LAG+ETA: constant ERP | LAG+ETA: pwl ERP | GNSS: pwl ERP |
|---|---|---|---|---|
| **Mean Bias** | **X-pole [µas]** | 13.8 | -4.1 | -0.1 |
| | **Y-pole [µas]** | -37.7 | -41.4 | 40.5 |
| **Weighted RMS** | **X-pole [µas]** | 459.9 | 428.9 | 41.0 |
| | **Y-pole [µas]** | 371.3 | 334.7 | 36.6 |

**Table 2: Comparison of polar motion derived from SLR and GNSS solutions with the IERS-08-C04 series at 12:00 UTC epochs: Mean bias and weighted RMS.**

# 4. Impact of ETALON observations on ERP

The number of SLR observations to ETALON satellites is clearly smaller than to LAGEOS, i.e., in average only about 10% of the amount of LAGEOS data. But due to different orbital characteristics of the ETALON satellites, they could stabilize the ERP estimates. Therefore, we wanted to study the impact of the ETALON observations on the ERP time series. For the comparison of the ERP series derived from LAGEOS-only solutions and the ERP series derived from combined LAGEOS+ETALON solutions we have chosen the piece-wise-linear parameterization as explained and analyzed in Sec. 3.

The differences for the polar motion and LOD estimates are shown in Fig. 3. As expected, the impact of the ETALON observations on LOD is larger than the impact on polar motion. The mean difference in the polar motion time series is negligible, although the differences can reach up to 0.1 mas for some epochs. The differences in LOD seem to be rather systematic with a mean bias of about 0.348 ms/d.

Compared to the GNSS-only solution, the bias in LOD is slightly reduced for the combined LAGEOS-ETALON solution, i.e., 20 µs, compared to 55 µs for the LAGEOS-only solution.

# 5. Conclusions

The impact of a priori models for ocean and atmospheric tidal loading has been tested for weekly LAGEOS solutions of the year 2008. We found that neglecting OTL slightly degrades the solution by increasing the RMS of the observation residuals by about 10%, whereas there is almost no negative impact on the RMS seen when neglecting ATL. The differences in the estimated orbits are at the level of several millimeters when neglecting OTL or ATL, with OTL having a bigger impact on the orbit.

We addressed several aspects concerning the ERPs derived from SLR solutions: the comparison of the SLR-derived ERPs with the IERS-08-C04 series, the impact of different parameterizations for the ERPs, and the impact of ETALON observations on the ERP estimates.

We have seen an agreement of the SLR-based polar motion series with IERS-08-C04 at the level of 0.3 – 0.4 mas in terms of weighted RMS. The RMS of the differences w.r.t. IERS-08-C04 is smaller by almost 10% if a piece-wise-linear parameterization is chosen for the ERPs instead of a piece-wise-constant parameterization.

A systematic impact on the LOD estimates is seen when additionally including ETALON observations. The polar motion series do not show any systematic differences between LAGEOS-only and combined LAGEOS-ETALON solutions.

We intend to extend the time series of combined LAGEOS-ETALON solutions in order to approve the findings described in this contribution.

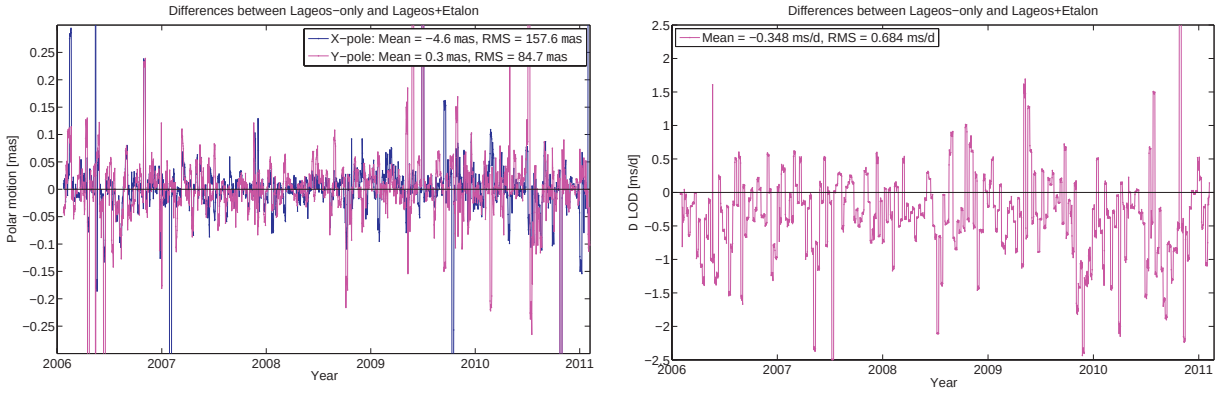


**Figure 3: Comparison of ERPs derived from LAGEOS-only solutions and combined LAGEOS+ETALON solutions. Left: Polar motion; Right: LOD.**

## Acknowledgements

The IGS and ILRS are acknowledged for providing microwave and SLR tracking data. Bundesamt für Kartographie und Geodäsie (BKG) is acknowledged for the financial support.

## References

*Dach, R., Hugentobler U, Fridez P, Meindl M* (2007): Bernese GPS Software Version 5.0. Astronomical Institute, University of Bern.

*Jäggi, A., Sośnica K, Thaller D, Beutler G* (2011): Validation and estimation of low-degree gravity field coefficients using LAGEOS. Proceedings of the 17th International Workshop on Laser Ranging, Bundesamt für Kartographie und Geodäsie (BKG), Germany.

## Correspondence

Thaller Daniela
Astronomical Institute
University of Bern
AIUB, Sidlerstrasse 5
CH-3012 Bern
Switzerland

thaller@aiub.unibe.ch

# A Preliminary Research of Precise Orbital and Geodetic Parameter Estimation System Using SLR Data

*Eunseo Park[1], Young-Rok Kim[2], Hyung-Chul Lim[1], Sang-Young Park[2]*

ABSTRACT

Korea Astronomy & Space Science Institute (KASI) has been developing SLR system. The name of the Korean SLR system is ARGO(Accurate Ranging system for Geodetic Observation) and the final goal of ARGO project is to develop two SLR systems, a 40cm mobile SLR system (ARGO-M) and a 1m fixed system (ARGO-F). ARGO-M will be developed by 2011 and then ARGO-F by 2014. The main applications of ARGO are precise orbit determination, space geodesy and space tracking. For the applications, we performed a preliminarily research to develop a precise orbital and geodetic parameter estimation system using SLR data, which was cooperated with ACL(Astrodynamics and Control Lab.) in Yonsei University. The feasibility study of estimation system development was implemented and we conducted a precise orbit determination system. The estimation system is consisted of dynamic, measurement models, and estimation algorithms. The dynamic models include geopotential perturbation, gravity of planets, solid earth tide, ocean tide, dynamic polar motion, relativistic effect, empirical acceleration, atmospheric drag, solar radiation pressure, and earth albedo pressure. A tropospheric delay and satellite body-fixed offset of the SLR array phase center are also considered as measurement models. The batch filters based on the least squares and the unscented transformation are used for estimation algorithm. In this presentation, the structure of the developed estimation system is described and the orbit determination results using SLR data are analyzed.

## 1. Orbit Determination System

The orbit determination problem is to estimate accurately the ephemeris of an orbiting satellite at a chosen epoch. To achieve this goal, estimations of the state and the model parameters of the satellite are made based on a sequence of observations. The dynamic models of the equations-of-motion are usually integrated from a chosen epoch to each observation times to produce predicted observations. The differences between the predicted observations and true observations are defined as the observation residuals. Then, components of the state vector at a chosen epoch are corrected to minimize the observation residuals in a least squares sense. Thus, solving the orbit determination problem requires (a) dynamic model (describing the forces acting on the satellite), (b) measurement model (the relationship between the observed parameters and the satellite's state vector), and (c) an estimation algorithm.

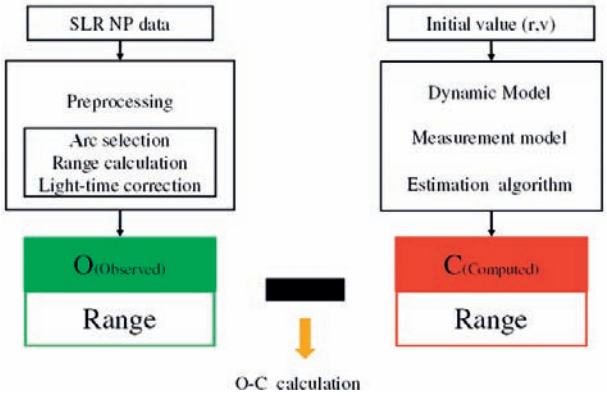


**Figure 1: Orbit determination system structure.**

[1]SLR Research Group, Space Science Division, Korea Astronomy & Space Science Institute, South Korea
[2]Astrodynamics and Control Lab. Dept. of Astronomy, Yonsei University, South Korea
skel93@kasi.re.kr / Fax: +82-42-861-5610

## 1.1 Dynamic Model

- Mean equinox and equator of J2000, ITRF2005 station coordinates and velocities
- TDT, UTC Reference time
- ADAMS-COWELL 11th Predictor-Corrector numerical integration
- Geopotential perturbation (JGM 1, 2, 3, EGM96: selectable, EGM96 (70×70) for test)
- Gravity of SUN, MOON, and planetary (DE405: Standish et al. 1998)
- Solid earth and ocean tide (Colombo 1984)
- Dynamic polar motion
- Relativistic effect (Huang et al. 1990)
- Empirical acceleration (Colombo 1989)
- Atmospheric drag (MSIE-90 : Hedin 1991, Box-wing macro model : Marshall & Luthcke 1994)
- Solar radiation pressure (Box-wing macro model : Marshall & Luthcke 1994)
- Earth albedo pressure (Box-wing macro model : Marshall & Luthcke 1994)

## 1.2 Measurement Model

- Tropospheric delay model (Mendes et al. 2002)
- Satellite body-fixed offset of the SLR array phase center (ILRS)

## 1.3 Estimation Algorithms

- Estimate state at chosen epoch using all the data for a fixed period and processes non-recursively

### 1.3.1 Weighted Least Squares filter

- Most widely used method.
- The filter is applied to non-linear system by simply linearizing and approximating all the non-linear models, which can cause a large error, instability, and divergence in estimation process in highly non-linear situations (large initial error in position and velocity, sparse measurement)

### 1.3.2 Batch filter based on the Unscented Transformation (UT, Julier & Uhlmann, 1995)

- UT contains no linearization process and yields superior performance in highly non-linear situations
- Therefore, UT was applied to batch estimation and compared with the result of the weighted least squares filter

# 2. Orbit Determination System Configuration

- Satellite : CHAMP

| | |
|---|---|
| Sponsor | GFZ (Germany) |
| Primary Applications | geodesy |
| Primary SLR Application | precision orbit determination, geodesy |
| Launch Date | July 15, 2000 |
| NP Bin Size | 5 seconds |
| Reflectors | 4 corner cubes |
| Orbit | circular, near polar |
| Inclination | 87.27 degrees |
| Eccentricity | 0.00396 |
| Perigee | 474 km |
| Period | 94 minutes |
| Weight | 400 kg |

- SLR measurement: NP data
- Measurement(NP data) Information

| Arc | Time(UTC) (YYYMMDD HH:MM:SS) | Station | NP # |
|---|---|---|---|
| 1 | 20010520 22:07:11 - 22:14:58 (0520B) | 7839(GRZL),7840(HERL)7810(ZIML),7824(SFEL) | 129 |
| 2 | 20010523 10:26:18 - 10:27:59 (0523B) | 7840(HERL),7810(ZIML) | 29 |
| 3 | 20010523 21:38:14 - 21:43:11 (0523F) | 7840(HERL),7839(GRZL),7824(SFEL) | 99 |
| 4 | 20010728 03:44:42 - 03:48:47 (0728) | 7810(ZIML),7836(POTL) | 40 |
| 5 | 20010808 02:17:08 - 02:22:20 (0808) | 7835(GRSL),7839(GRZL),7836(POTL) | 119 |
| 6 | 20010814 01:14:01 - 01:17:06 (0814G) | 7839(GRZL),7835(GRSL) | 50 |

- Estimation states and parameters
  - State position, velocity, true pole Xp, Yp, TAI-UT1
  - Atmospheric drag coefficient (Cd), Solar radiation pressure coefficient (Cr), Empirical general acceleration scale factor

# 3. Orbit Determination Test

The CHAMP precision orbit ephemeris (POE) data from NASA are considered as a true orbit, and is also used for verifying the accuracy of the orbit determination. The states at a chosen epoch are determined using the batch least squares filter(LS) and the batch filter based on the unscented transformation(UT). From the estimated states at a chosen epoch, the orbit ephemeris data are generated from a specified epoch to a final time and compared with the reference POE data. The RMS differences between the generated orbit and reference orbit in radial, along track, cross track, and position are applied for the performance assessment of both the filters. The effects of the initial errors in are tested and compared in two cases for the two estimation algorithms. The initial errors in position are assumed to be added [10 m, 10 m, 10 m] for Case-1, [100 m, 100 m, 100 m] for Case-2.

# 4. Orbit Determination Test Results

## 4.1 Effect of initial orbit error: Case 1

- Initial value = true initial orbit value $(x_0,y_0,z_0)$ + $(x_0$ +10m, $y_0$+10m, $z_0$+10m error)
- True initial orbit value: CHAMP (NASA JPL POE)
- Compared results of both the filters with POE
- For relatively small initial orbit errors, results of two filters are similar

| ARC (CHAMP) | | NP# | RMS (cm) | | | | | | | | | |
|---|---|---|---|---|---|---|---|---|---|---|---|---|
| | | | O-C | | Radial | | Along | | Cross | | Position | |
| | | | LS | UT | LS | UT | LS | UT | LS | UT | LS | UT |
| 1 | 0520B | 129 | 5.2 | 6.0 | 6.5 | 5.4 | 6.0 | 9.4 | 6.4 | 2.3 | 10.9 | 11.1 |
| 2 | 0523B | 29 | 1.4 | 3.7 | 2.8 | 3.6 | 4.4 | 9.2 | 3.1 | 1.1 | 6.1 | 9.9 |
| 3 | 0523F | 99 | 4.5 | 2.9 | 4.1 | 1.5 | 5.7 | 3.7 | 6.2 | 1.3 | 9.4 | 4.2 |
| 4 | 0728 | 40 | 2.9 | 1.5 | 2.1 | 1.1 | 3.5 | 3.0 | 9.1 | 6.2 | 10.0 | 7.0 |
| 5 | 0808 | 119 | 2.8 | 4.0 | 3.5 | 2.1 | 9.9 | 7.4 | 9.3 | 0.8 | 14.0 | 7.7 |
| 6 | 0814G | 50 | 1.6 | 2.6 | 1.3 | 2.6 | 6.7 | 4.5 | 6.3 | 4.6 | 9.3 | 6.9 |

## 4.2 Effect of initial orbit error: Case 2

- Initial value = true initial orbit value $(x_0,y_0,z_0)$ + $(x_0$ +100m, $y_0$+100m, $z_0$+100m error)
- True initial orbit value: CHAMP (NASA JPL POE)
- Compared results of both the filters with POE
- For relatively large initial orbit errors(highly non-linear situation), results of the batch filter based on the unscented transformation are more accurate and stable
- It can be concluded that the batch filter based on the unscented transformation has advantage over the batch least squares for large initial errors(Park et al. 2007, Park et al. 2010)

| ARC (CHAMP) | | NP# | RMS (cm) | | | | | | | | | |
|---|---|---|---|---|---|---|---|---|---|---|---|---|
| | | | O-C | | Radial | | Along | | Cross | | Position | |
| | | | LS | UT | LS | UT | LS | UT | LS | UT | LS | UT |
| 1 | 0520B | 129 | 30.7 | 7.3 | 45.0 | 2.8 | 63.0 | 9.3 | 71.7 | 6.1 | 105.5 | 11.5 |
| 2 | 0523B | 29 | 7.3 | 3.1 | 19.0 | 5.5 | 25.3 | 3.1 | 25.5 | 5.4 | 40.6 | 8.3 |
| 3 | 0523F | 99 | 40.3 | 6.3 | 34.9 | 5.1 | 52.1 | 3.9 | 67.7 | 2.7 | 92.3 | 7.0 |
| 4 | 0728 | 40 | 12.9 | 16.7 | 26.2 | 1.8 | 47.1 | 5.9 | 77.3 | 2.0 | 94.2 | 6.5 |
| 5 | 0808 | 119 | 25.0 | 8.9 | 40.3 | 3.3 | 41.3 | 8.2 | 94.0 | 4.9 | 110.3 | 10.1 |
| 6 | 0814G | 50 | 13.3 | 1.6 | 30.1 | 3.6 | 98.0 | 6.1 | 78.0 | 2.3 | 128.8 | 7.4 |

# 5. Summary and Future Work

- Performed a preliminary research for developing a precise orbital and geodetic parameter estimation system using SLR data
- Test system design for precise satellite orbit determination
  - Batch filter based on the unscented transformation is applied to batch estimation and compared with the result of the weighted least squares filter
  - In the case of the relatively small initial position errors, results in both the filters are similar
  - The nonlinearity is strengthened, in other words, as the large initial errors are considered, the batch filter based on the unscented transformation is more robust and accurate than the weighted least squares filter
- Present test system is inchoate,
  - More considerations for system design and construction
  - States and parameters, numerical models (dynamic/measurement), estimation method, test procedure, accuracy enhancement

## Acknowledgements

This work was supported by the Korea Astronomy and Space Science Institute through the SLR system development program for space geodesy funded by the Ministry of Education Science and Technology (MEST).

## References

*Colombo, O.,* 1984, NASA Technical Memorandum/Altimetry, Orbits and Tides, NASA-TM-86180.

*Hedin, A. E.,* 1991, Extension of the MSIS thermosphere model into the middle and lower atmosphere, J. Geophys. Res., 96, 1159–1172.

*Julier S. J., Uhlmann J. K. and Durrant-Whyte H. F.,* 1995, A New Approach for Filtering Nonlinear systems, Proceedings of the American Control Conference, American Automatic Control Council, Evanston, IL, pp. 1628-1632.

*Marshall, J.A. and S.B. Luthcke*, Modeling Radiation Forces Acting on TOPEX/Poseidon for Precision Orbit Determination, Journal of Spacecraft and Rockets, Vol. 31, 99-105.

*Mendes, V.B., G. Prates, E.C. Pavlis, D.E. Pavlis, and R.B. Langley,* 2002, Improved mapping functions for atmospheric refraction correction in SLR, Geophysical Research Letters, Vol. 29, 1414.

*Park E.-S., Roh K.-M., Park S.-Y., and Choi K.-H.,* 2007, Satellite Orbit Determination Using a New Batch Filter, AAS 07-101, AAS/AIAA Astrodynamics Specialist Conference, Mackinac Island, Michigan.

*Park E.-S., Park S.-Y., Roh K.-M., and Choi K.-H.,* 2010, Satellite Orbit Determination Using a Batch Filter Based on the Unscented Transformation, Aerospace Science and Technology, 387-396.

*Standish, E. M.,* 1998, JPL Planetary and Lunar Ephemerides, DE405/LE405, JPL, 1-6.

## Correspondence

Eunseo Park
Space Science Division
Korea Astronomy & Space Science Institute
South Korea

skel93@kasi.re.kr

# Recent upgrades of the Metsähovi SLR telescope

*(A.Raja-Halli[1], J. Näränen[1], K. Lapushka[2], K. Arsov[1], M. Poutanen[1])*

ABSTRACT

Metsähovi satellite laser ranging station (Kirkkonummi, Finland) has been under renovation since 2005. In 2006 a new 2 kHz laser was purchased and simultaneously upgrades for the telescope control and pointing mechanism were planned. Faster and more accurate operation of the telescope will be achieved by upgrading the motors and by installing highly accurate incremental encoders. The telescope was fully disassembled in 2007 and vigorous work for the restoration and upgrading of the telescope was started. In 2008 it became evident that the old optical system couldn't operate with a 2 kHz laser due to outgoing and incoming beams using a single optical path. Hence a new optical scheme was planned. In the old system the separation of the beams was controlled with rotating mirrors. The old mechanism was only capable to approximately 100Hz repetition rate. In the new system the beams will travel through separate paths. Currently, the optical and mechanical updates are in implementation phase and we will give a short presentation of the recent work done and future plans for the Metsähovi SLR telescope.

# 1. The Metsähovi SLR telescope

## 1.1 Overview

The Metsähovi satellite laser ranging telescope was designed and built by the University of Latvia, Riga, in 1992-1993. Observations were made during 1998-2005. The alt-az telescope has a main mirror of 1m (recoated in 2009 at Jena, Germany) and is a Cassegrain-Mangin type with a focal length of 11.6m. It is the same type as used in e.g. Riga, several Ukraine stations and in Potsdam (old telescope). The old telescope motors were stepper motors with one step corresponding to one arcsecond. As encoders microscope-readable glass rings were used. However, these were only used for zero pointing and for position information the steps made by the motors were counted and no independent pointing information was available. This system will be improved by the implementation of the new drive mechanics.

## 1.2 New optical system

To enable 2 kHz observations a new optical design was necessary for separating the two parallel beams (outgoing laser and incoming returns). In 2009 a new optical solution was designed in co-operation with the original designers of the telescope at the University of Latvia in Riga. In the new system the transmitted beam is guided outside of the main aperture to a separate beam expander (Fig. 1.). To make this possible the prime focus of the telescope had to be changed. This fundamental modification brings the focal point of the telescope from the Coudé-focus into Cassegrain-focus and reduces focal length to a quarter, while also reducing slightly the effective aperture. Before these modifications, the focus and the PMT-detector were located in a separate room next to the telescope and the visual channel for the CCD was separated to the other side of the telescope by use of rotating mirrors. These mirrors were also used for guiding the beams to travel in parallel directions. With the new design the rotating mirrors will be discarded. Wavelength of 532 nm will be guided to a newly acquired C-SPAD detector and the other wavelengths will be separated with a dichroic mirror into the CCD-camera. The detector and the camera will be now mounted inside the telescope, in the Cassegrain-focus. The new custom-made lenses are at the time of writing being tested and the precision mounts are being manufactured in Riga. The new optical setup can be seen in the Fig. 1. It shows the transmitted beam on the right, outside the main aperture.

[1] Finnish Geodetic Institute

[2] Institute of Astronomy, University of Latvia

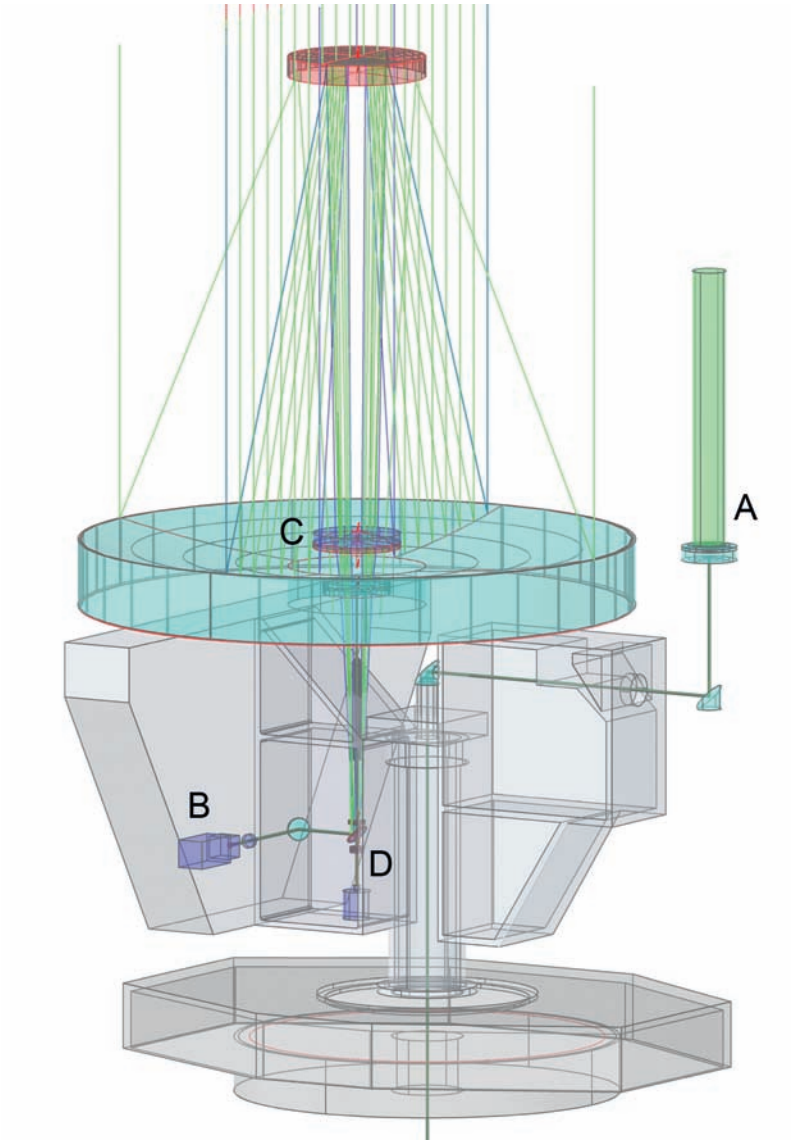


**Figure 1: CAD-drawing representing the new optical setup: A is the transmitted beam; B is the C-SPAD detector; C shows the new optical elements i.e. the focal reducer; D represents the camera for visual band.**

## 1.3 New drive mechanics

Updating of the telescope pointing and control system is ongoing. The previously used non-servo stepper motors and optical encoder rings will be replaced by a servo-motor system and electronic incremental encoders, respectively. In summer 2010 Heidenhein ERA8480C encoder was installed on the azimuth mount (Figure 2.). The new encoder provides a sub-arcsecond accuracy on the azimuth axis, depending on the final achievable quality of the readout signal. In summer 2011, the encoder will be calibrated. On the elevation axis a Heidenhein ERA4481C, with similar angular measurement accuracy, will be installed.

The old telescope drive motors will be replaced with Maxon servo-motor system, controlled with EPOS position-control units. This will enhance the speed of the telescope as well as give additional pointing-modelling data (with feedback from the incremental encoders installed in the motors).The motors will be installed using the old gear system.

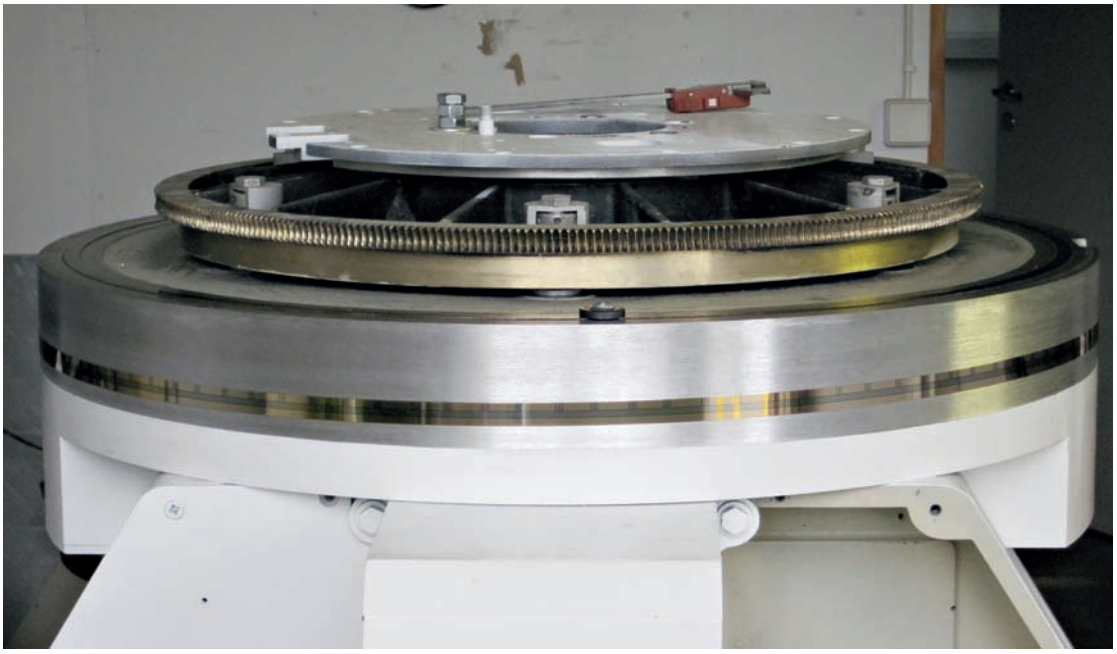

**Figure 2: The new Heidenhein incremental encoder scale tape mounted on the azimuth mount. Above it, is the azimuth gear wheel.**

# 2. Levelling

## 2.1

The telescope mount was levelled with a digital level to discover any possible tilt due to accidental movements of the mount during the disassembling. The flatness of the azimuth rail (i.e., the level on which the telescope performs its azimuth turns) (Figure 3.) was also checked. It was found out that there were bumbs with maximum amplitude of ~0.1 millimeter on the rail and a tilt of ~0.2mm on the North-South axis. The tilt is easily removed but individual bumps may need to be included in the telescope pointing model. In the Fig. 4 the coarse model of the anomalies on the rail can be seen. Measurements were taken in 10 degree steps on the rail i.e. every 6cm as seen on the Figure 3. Three separate measurements were taken in every point with the rod in place. The whole measurement was repeated three times, hence we got nine measurements for every point. We examined only the height differences, not absolute heights. The measurements will be repeated with greater accuracy when the telescope is assembled.

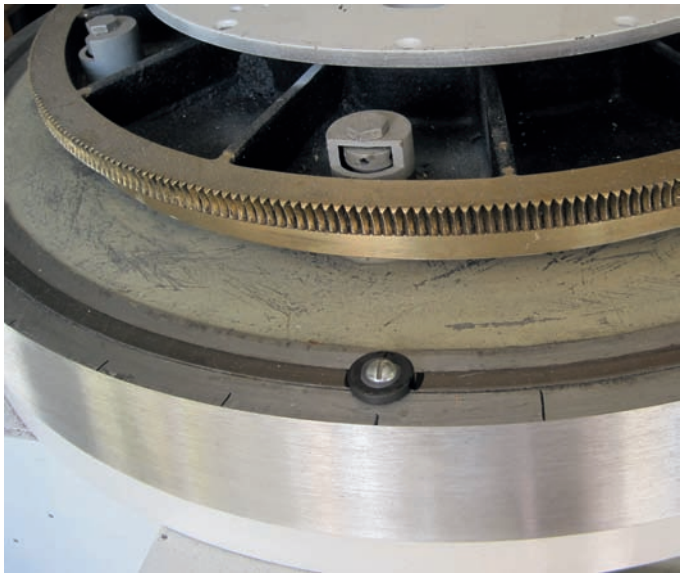

**Figure 3: The azimuth rail. Black marks on the circle show the levelled points on the rail. The rod was placed on the magnet button to reduce error due to placing of the rod on the rail.**

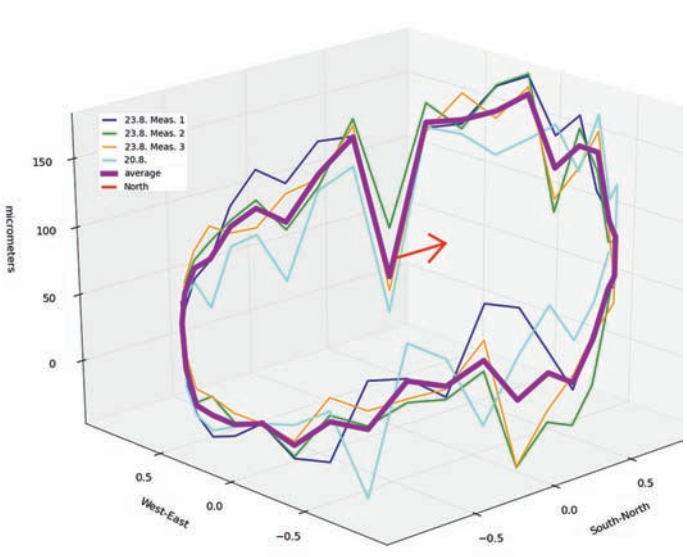


**Figure 4: Plot showing levelled height differences on the azimuth rail. The starting point is set to zero. Magenta is the total average, other colors are the averaged separate measurements.**

# 3. Future plans

After installing the new optics, motors and encoders we will start to build the telescope control software. The motors and encoders need to be calibrated and new calibration targets for the telescope has to be made. For precise pointing a pointing model will be done. Metsähovi is a fundamental station, hence new local tie measurements are important and will be made when the telescope is assembled. Ongoing research is done for the local tie measurements of the Metsähovi VLBI antenna. This research will help us pursuing towards the 1 mm level on the local ties of the SLR telescope as well. Together with the telescope upgrades we are simultaneously working with upgrades of our observing electronics and observing software. The whole observing software will be rewritten and made compatible with the 2 kHz laser.

Parallel to this work we are seeking funding for a new telescope for the kHz laser. This system would use smaller and faster telescope for LEO observations. The old telescope could be used with a slower but more powerful laser to observe HEO satellites e.g. GNSS satellites.

## Correspondence

Arttu Raja-Halli
Finnish Geodetic Institute
Geodeetinrinne 2 PL15
02431 Masala
Finland

arttu.raja-halli@fgi.fi

# Container and Dome Development of Korean Mobile SLR System

*Sung Yeol Yu, Hyung-Chul Lim, Eunseo Park, Seung-Cheol Bang, Yoon-Kyung Seo*

ABSTRACT

Korea Astronomy and Space Science Institute (KASI) has been promoting the first SLR system development project named ARGO(Accurate Ranging system for Geodetic Observation) in Korea since 2008. The ARGO's final goal is to make one mobile SLR system and one fixed SLR system. Currently we are developing the 40 cm mobile SLR system, ARGO-M. The ARGO-M is composed of five subsystems: optical subsystem, Opto-electrical subsystem, laser subsystem, tracking mount subsystem, operation subsystem and container/dome subsystem (CDS). The CDS is consist of dome, container and ground target, which is designed to protect inner devices such as telescope and laser system from outer environments and transport them easily from one to the other site. The dome is an astronomical clamshell type and is made up 6 pieces, whose four pieces open and close by a winch system using iron cables except for 2 bottom pieces that are fastened on the base. The container is divided into 3 rooms, a laser room, an operation room and an accessory room. ARGO-M container has a similar type to the commercial one but its size is a little larger than the commercial product only in the length and width. The ground target is installed in the dome for the precise ground calibration. In this paper, the requirements and detailed design of CDS are provided and current status and future plan are also discussed

# 1. Introduction

Korean Astronomy and Space Science Institute (KASI) has been promotion the first SLR system development project named ARGO (Accurate Ranging system for Geodetic Observation) in Korea since 2008. The ARGO's final goal is to make one 40cm mobile SLR system (ARGO-M) and one 1m fixed SLR system (ARGO-F). The objectives of ARGO program can be divided into three types; 1) space geodesy research and GEOSS/GGOS contribution by laser ranging for satellites with LRA, 2) precise orbit determination (POD) through laser ranging measurement with mm level accuracy, 3) contribution to international SLR societies and ILRS network participation. Currently we are developing the ARGO-M. The ARGO-M is composed of five subsystems: optical subsystem (OPS), opto-electrial subsystem (OES), laser subsystem (LAS), tracking mount subsystem (TMS), operation subsystem (AOS) and container/dome subsystem (CDS). The CDS is consist of dome, container and ground target, which is designed to protect inner devices such as telescope and laser system from outer environments and transport them easily from one to the other site. This paper will discuss the requirement and design of CDS subsystem.

# 2. Dome

## 2.1 Dome Requirement

In order to design the dome, we have derived a variety of requirements. The following are important requirements

- It should be the half-spherical type (clamshell type) and the fully open dome.
- It is installed on the top of the container.
- It should have no obstruction to observe satellite more than 20 degree elevation (Figure 1).
- It should has the hand-operated opening and closing device to prepare for an emergency of broken switching device.
- For emergency situations, emergency stop switches are installed in dome and container.
- It should prepare with the human sense to alert people in the dome.
- It should withstand in the environment less than 250km/h wind speed.

- It should have so sufficient torque that it is operated under the frozen environment.
- The operating temperature ranges from -20 °C to 60°C
- The closing operation is so fast that rains don't come into the dome

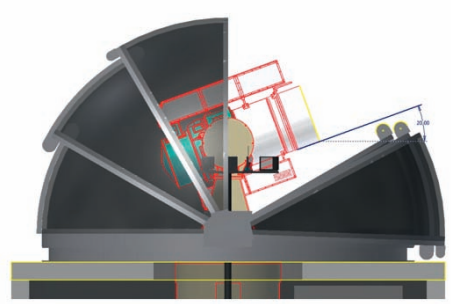

**Figure 1: Dome limit elevation**

## 2.2 Dome Design

### 2.2.1 Size

We decided the size of dome with its moving in mind. The size of dome is 2000mm high X 3600mm diameter(Figure 2). The dome weight is approximately 2000kg.

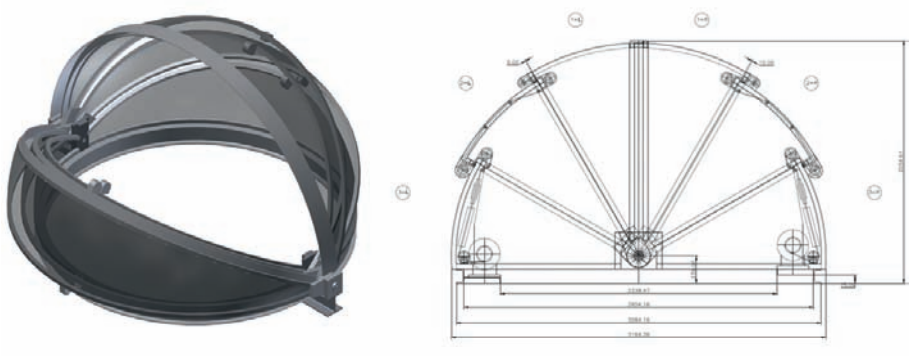

**Figure 2: Dome design**

### 2.2.2 Configuration

The dome is an non-rotating astronomical clamshell type and is made up 6 pieces, whose four pieces open and close by a winch system using iron cables except for 2 bottom pieces that are fastened on the base.

# 3. Container

## 3.1 Container Requirement

We drew the container requirements from general requirements of the other SRL sites and included additional requirements.

- It should be designed and manufactured in order to support SLR measurement in anytime and anyplace.
- It should be designed to is supplied with power in the ground.
- It is able to transported by commercial trailer.
- It is able to lifted with a crane and forklift.
- The Operation room and Laser room should be isolated for safety.
- There is a sally port to handle emergency case of the dome.
- It should be installed on concrete for vibration isolation of circumstance and strength.
- It should insulation structure for the sake of sheltering from the surrounding environment (rain, snow, wind etc.).
- There is an air-conditioning and heating equipment to maintain an constant room temperature.
- There is the solid base to install subsystem racks in container.

## 3.2 Container Design

### 3.2.1 Size

The container is designed to move on the general road. ARGO-M container has a similar type to the commercial one but its size is a little larger than the commercial product only in the length and width. The size of the container is 2600mm high X 3600mm width X 9000mm length. Also, the container uses many stiffeners to bear the weight of the dome (Figure 3).

### 3.2.2 Configuration

The container is divided into 3 rooms, a laser room, an operation room and an accessory room. The laser room is composed to a laser subsystem, a transmit optical system and a ground target. The operation room is consisted of a tracking mount subsystem controller, a opto-electrial subsystem and operation subsystem. The accessory room is composed of UPS, AVR, shelf and switchboard.

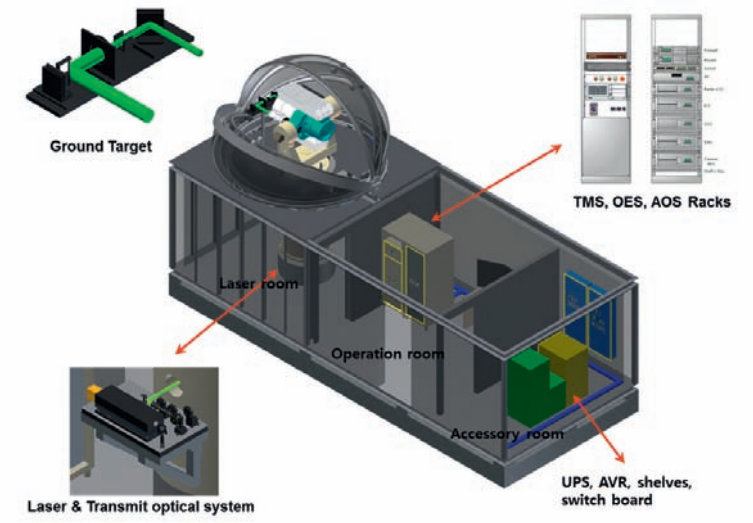


**Figure 3: Container configuration**

# 4. Ground Target

## 4.1 Ground Target Design

The ground target is composed of a prism, an iris, a filter bank and black diffuser (Figure 4). The prism is a wedge prism. The iris and filter bank are used to adjust light intensity. The ground target is designed by Gratz's recommendation

The ground target configuration is :

- Prism : 1 unit 100mm X 120mm, 0.1% reflectivity
- Iris : 1 unit 120mm outer diameter
- ND filter bank : 1 unit 100mm x 100mm (5 slot)
- Black Al diffuser : 1 unit 100mm X 135mm, < 3% reflectivity

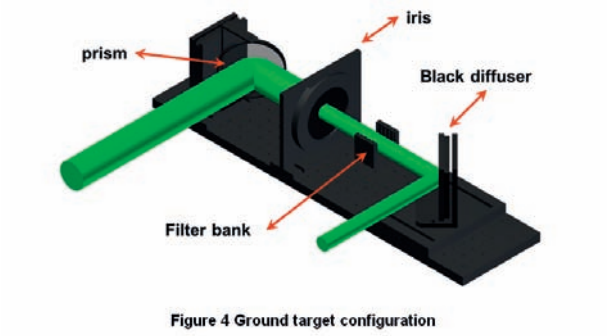


**Figure 4: Ground target configuration**

## References

*Park, J., Lim, H., Seo, Y., Park, J., Kim, Y., Son, Y., Kim, Y.,* 2008: Status and Progress of ARGO, Proceedings of the 16th International Workshop on Laser Ranging

## Correspondence

Sung Yeol, Yu
Korea Astronomy and Space Science Institute 776
Daedeokdae-ro, Yuseong-gu, Daejeon
Republic of Korea 305-348

syyu@kasi.re.kr

# Method of comparison laser locator with standard of length

*Igor Yu. Ignatenko*[1]

There is description of method of comparison laser location station with national standard of length.

National standard of length of the Russian Federation is the interferometric line length of 60 meters. The standard is in "National Research Institute for Physical-Technical and Radio Engineering Measurements" (VNIIFTRI). The interferometer is supported by a national standard time and frequency. The standard is located in a special room in which are supported by the necessary climatic conditions. Therefore, direct comparison of laser ranging system and the standard of length is possible. To overcome these difficulties was developed which technique. Directly on the national standard calibrated precision standard of comparison. As a standard of comparison is used Leica TDA 5005. Also, with the national standard is calibrated retroreflector.

Then we produce comparison by comparison standard in several steps:

- Transfer comparison standard and retroreflector on calibrating basis;
- Placing retroreflector in reference point of laser range;
- Put the comparison standard comparison on the geodetic point;
- Direct the telescope to the geodetic point, and measure the distance by Leica TDA 5005;
- Transfer the reflector on the geodetic point and measure the distance of the laser range.

After this, final distance between reference point of laser range instrumentation and geodetic point, which determine calibrating basis, measured. By results of measurements, additive constant of SLR-system is determined. Later measured basis used for calibration operations in the process. This operation is repeated at least four times a year, in the most typical for each season.

## Correspondence

Igor Yu. Ignatenko

e-mail: IgIg@vniiftri.ru

[1]Federal State Unitary Enterprise "National Research Institute for Physical-Technical and Radio Engineering Measurements" (VNIIFTRI), 141570 Mendeleevo, Moscow region, Russia

# Progress in kHz SLR and laser ranging to un-cooperative space targets at Shanghai Station

*Zhang Zhongping, Wu Zhibo, Zhang Haifeng, Chen Juping, Li Pu, Meng Wendong, Yang Fumin*

ABSTRACT

From October 2009, Shanghai SLR station implemented routinely kHz repetition SLR by using kHz repetition laser with picosecond pulse-width and high-precision Event Timer, designing nanosecond accuracy of Range Gate Generator with event mode and back-scattering avoiding circuit, developing real-time control software and data pre-processing software. The paper presents the progress in KHz SLR at Shanghai station, including ranging to the low-Earth and high-Earth orbit satellites at nighttime and daylight laser ranging for low-Earth orbit satellites, tracking geostationary orbit satellite. In addition, some new measuring results and progresses of un-cooperative space targets laser ranging are also showed in this paper.

## 1. Introduction

Shanghai Observatory has investigated the key technologies of kHz repetition SLR since 2006. In 2008 some experimental results was obtained and Zhang reported the measuring results at Last workshop in Poznan (2008), named "the Experiment of kHz Laser Ranging with Nanosecond Pulses at Shanghai SLR station". It presented Shanghai SLR station had the capability to track satellites up to Lageos with 1~2 kHz laser. Yang also reported "Preliminary Results of Laser Ranging to Un-cooperative Targets at Shanghai SLR Station". It means that Shanghai SLR station have solved some key technologies of un-cooperative targets laser ranging. Recent years Shanghai Observatory got some supports from national projects to develop kHz repetition SLR and un-cooperative targets laser ranging technology. This report will introduce the new progresses on the above two fields.

## 2. Advance of kHz SLR

The major technical upgrading for the kHz SLR is following: 1) Adopt new kHz Laser with 15-20ps pulse width, 3mj energy made by PI company of USA, instead of the experimental laser with 50ns pulse width borrowed from NCRIEO (North China Research Institute of Electro-optics); 2) Develop our KHz Range Gate Generator (RGG) with 5ns resolution; 3) Improve and perfect KHz software system by ourselves.

### 2.1 New kHz Laser

In 2009, Shanghai SLR station imported the new kHz repetition laser from PI Company. The main performances of this laser are following: 1k~2kHz repetition rate; 1-2mJ per shot; 532nm wavelength; 15~20ps pulse-width; 0.5mrad diverge. Figure1 show the inner optic principle and view of new kHz laser. According to the results of measuring near target on ground, the measuring precision is 5~8mm.

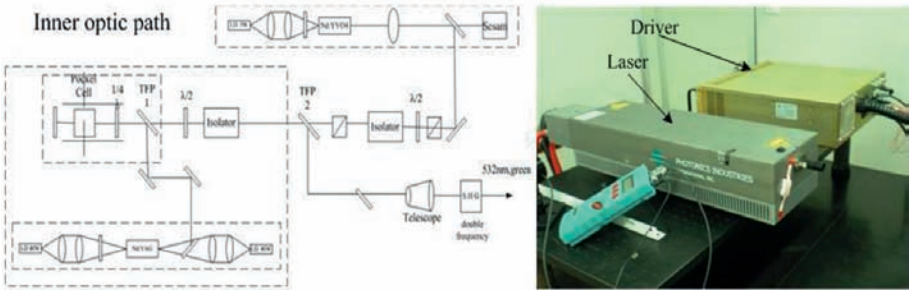


**Figure 1: New kHz Laser from PI of USA**

## 2.2 kHz Range Gate Generator

The kHz Range Gate Generator (RGG) is designed by our group based on FPGA and consists of four modules: serial port control module, real-time clock module, comparator module, enhanced parallel port (EPP) control module and laser firing module. Figure 5 shows the diagram of kHz RGG. The serial port control module receives the 1PPS epoch time from GPS to make the real-time clock module synchronized UTC. The PC calculates the return time of laser signal according to the prediction and sends the timing data to the FIFO of kHz RGG. The comparator module reads the times from real-time clock module and the FIFO respectively and compares to each other. If the time from the real-time clock is equal to the one from the FIFO and then generates the range gate signal to open the photo-detector. The laser firing module is responsible for generating laser fire signal and backscatter avoiding. The main characteristics of kHz RGG are following: 5ns resolution, 1024 buffers and EPP interface.

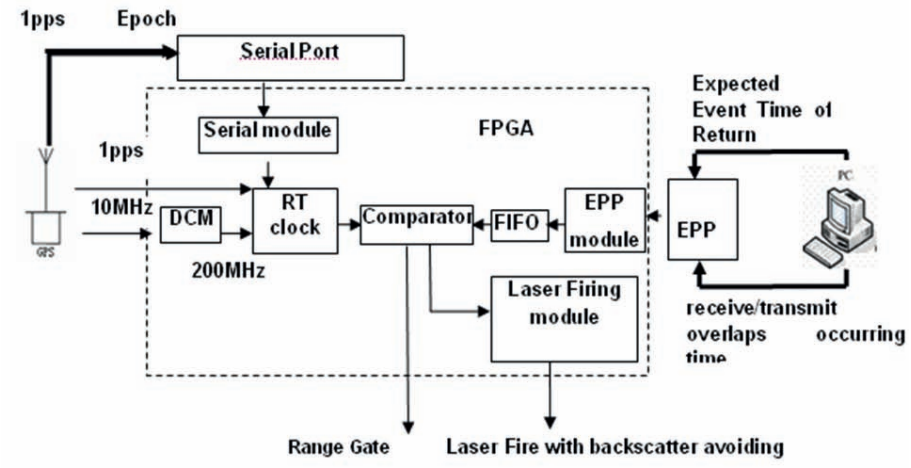


**Figure 2: the diagram of KHz RGG**

## 2.3 Some kHz measuring results

After finishing the kHz laser, RGG, the control software, Shanghai SLR station has been the routine kHz SLR measurement since Oct. 2009 and got 2990 passes in 2010. In Aug. 2010, Shanghai station successfully ranged to geostationary orbit satellite (GEO) by using laser with 1.8mJ@1kHz. Figure 3 show the kHz SLR measuring results for compass M1 and GEO satellites. Comparing with low repetition rate laser ranging, the returns and data density per normal points are greatly increased.

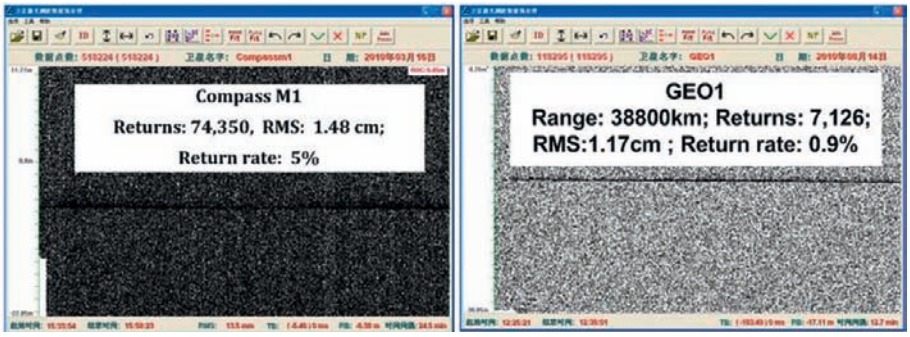


**Figure 3: kHz repetition rate SLR measuring results**

## 2.4 KHz SLR daylight tracking

Based on the routine kHz SLR repetition at nighttime, some key technologies of daylight laser tracking are adopted: 1) Space filter: receiving field of view of 30"- 45"; 2) Spectrum filter: Narrower filter with 0.15nm band width; 3) Transparency of central wavelength of over 50%; 4) Parallelism of transmitting and receiving paths with better than 5"; 5) Real-time return detection; 6) Measurement of telescope sighting error; 7) Increasing tracking and pointing accuracy of telescope mount. Shanghai SLR station has got returns from the LEO satellites at daylight Since Aug. 2010. Figure 4 show some passes of daylight SLR measuring results from Low Earth Satellites (LEO).

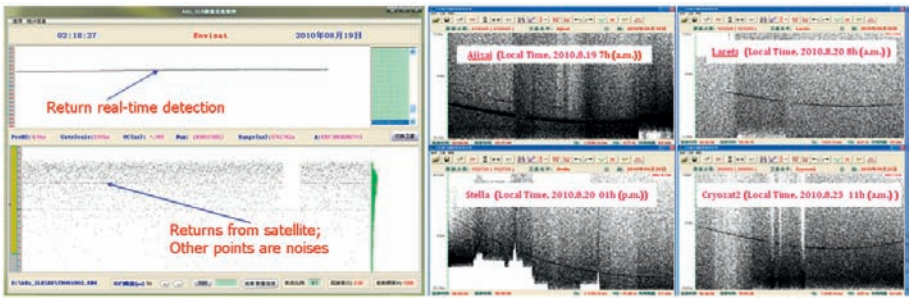


**Figure 4: Daylight SLR measuring results for LEO satellites**

# 3. Advance of Un-cooperative space target laser ranging

In July 2008, Shanghai SLR station successfully ranged to un-cooperative space targets by borrowing high power laser with 2J@20Hz from NCRIEO. For further studying un-cooperative space targets ranging technology, we have been upgrading the experimental system in 2010, including: 1) adopting stable high power laser; 2) improving the capability of servo-tracking system; 3) adjusting Multi step range-gate automatically; 4) adopting Two Line Elements (TLE) predict.

## 3.1 10W High power Laser

Due to the stability of the 40W laser borrowed from NCRIEO is very poor, so we imported a set of high stable 10W laser from the Spectra physics, Inc of USA and continuous working time is more than 1 hour. The main performances of high power laser are following: 10Hz repetition rate; 1J per shot; 8ns pulse-width; 532nm wavelength; 0.5 micrad diverge.


**Figure 5: The view of 10W power laser**

## 3.2 Tracking ability of servo control system

The tracking precision of telescope mount plays an important role in laser ranging to the un-cooperative targets. So we adopted the high accuracy optical RESM angle encoders that offer high speed, reliable operation and open, non-contact performance with excellent immunity to dirt and electrical noise with the resolution to 0.02 arc second. At the same time, the high efficient driver system was installed to insure the ability of telescope tracking. Figure 6 shows the tracking precision of telescope mount and the tracking precision is less than 1 arc second.

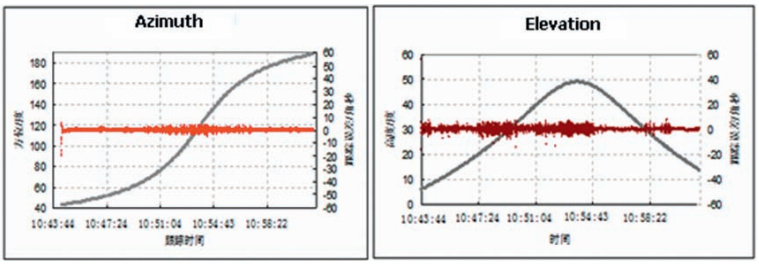


**Figure 6: Tracking capability of telescope mount**

## 3.3 Other upgrading

In our un-cooperative target laser ranging experimental system there are other upgrading, such as close loop tracking mode, multi range gate adjust, two line element (TLE) predict. Through the above upgrading, the measuring efficiency of laser range system is obviously increased.

## 3.4 Measuring results

In 2010, the performances of un-cooperative target laser ranging system were improved and several passes of un-cooperative laser ranging were obtained. Figure 7 shows some measuring results of un-cooperative targets. The ranging precision is about 50~80cm and the max range is up to 1200Km.

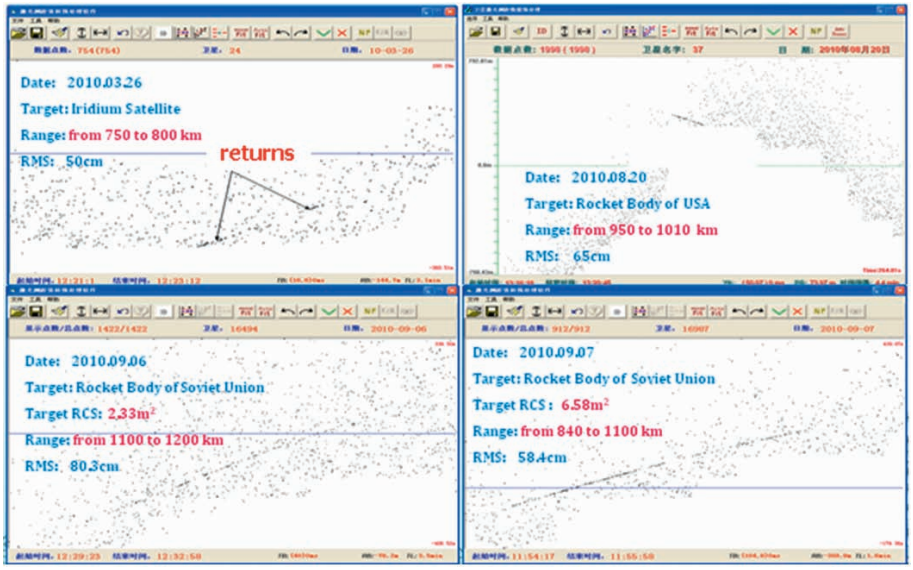


**Figure 7: some results of un-cooperative target laser ranging**

# 4. Summary

Shanghai SLR station has been the ability of routine kHz SLR at night-time and realized daylight laser ranging. Next stage we will improve our kHz SLR system and track to HEO satellite at daylight. For un-cooperative target laser ranging, some technologies will be implemented in the future: 1) Increasing the laser power (40W-50W); 2) Improving orbit predicting precision for un-cooperative target; 3) Adopting closed loop tracking mode; 4) Identifying laser beam automatically.

## Reference

*Zhang Zhongping,* 2008: The Experiment of kHz Laser Ranging with Nanosecond Pulses at Shanghai SLR, Proceedings of the 16th International Workshop on Laser Ranging

*Yang Fumin,* 2008: Preliminary Results of Laser Ranging to Un-cooperative Targets at Shanghai SLR Station, Proceedings of the 16th International Workshop on Laser Ranging

## Correspondence

Zhang zhongping
No.80, Nandan Road, Shanghai
China

zzp@shao.ac.cn

# Installing SLR systems at the “Quasar” VLBI network observatories

*A.Finkelstein [1], I.Gayazov [1], V.Shargorodsky [2], S.Smolentsev [1], V.Mitryaev [1]*

ABSTRACT

The Russian VLBI network “Quasar” consisting of three observatories (Svetloe, Zelenchukskaya and Badary) carries out regular VLBI observations under both IVS and national programs. There are co-located IGS stations performing continuous GPS and GLONASS observations at the observatories and DORIS system at the Badary observatory. In 2011 the Russian satellite laser ranging system “Sazhen-TM” will be installed at all observatories of the “Quasar” network. “Sazhen-TM” has the optical system with a 25 cm diameter and is supplied with the laser system producing a laser pulse with duration 150 ps and frequency 300 Hz. The system is capable of ranging laser retroreflector satellites at 400-23000 km height. The accuracy of normal point range data is expected to be at 1 cm level. The technical characteristics of the “Sazhen-TM” system, the timeline of the installation process, and the co-location of observational instruments at Zelenchukskaya observatory are presented.

## 1. VLBI network “Quasar”

Russian VLBI network “Quasar” (IAA RAS)[1] includes three observatories (Fig.1) with various observational instruments:

- Badary (VLBI, GPS/GLONASS, DORIS),
- Zelenchukskaya (VLBI, GPS/GLONASS),
- Svetloe (VLBI, GPS/GLONASS).

The observatories carry out regular VLBI observations under both IVS and domestic programs. There are co-located IGS stations performing continuous GPS and GLONASS observations at all observatories. DORIS-system at the Badary observatory is operating. Local-ties between different space geodetic instruments at the observatories are regularly measured by classical geodetic methods.

In the framework of IAA EOP Service the processing of different types of space geodetic observations is performed:

- VLBI observations (IVS programs: 24h- and Intensive-sessions);
- VLBI observations (Domestic programs: 24h- and 1h-sessions, weekly);
- GPS observations (IGS sub-network consisting of 35-40 stations, 24h-arcs, daily);
- SLR observations (ILRS network, 96h-arcs, daily).

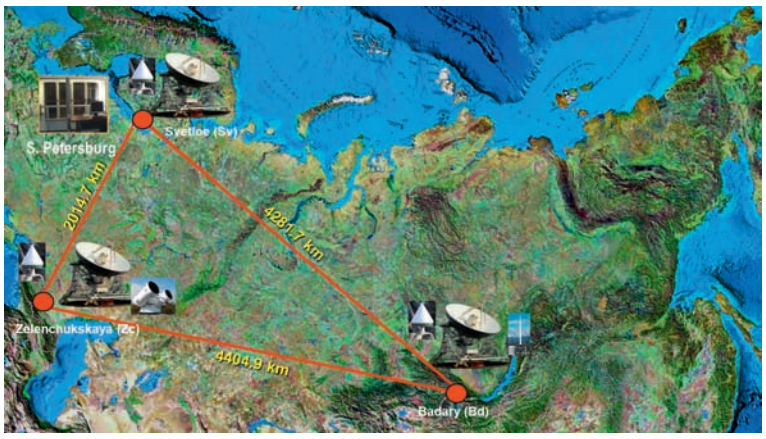


**Figure 1: “Quasar” network geometry**

1) Institute of Applied Astronomy RAS, Russia
2) Research-and-Production Corporation “Precision Systems and Instruments”, Russia

In 2011 the Russian SLR system "Sazhen-TM" (Research-and-Production Corporation "Precision Systems and Instruments") will be installed at all observatories of the "Quasar" network. The timeline of the installation is shown in Fig.2.

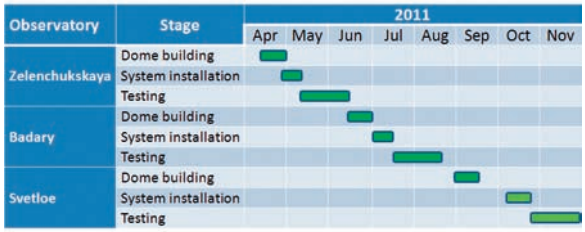


**Figure 2: Timeline of the SLR system installation at the observatories**

# 2. "Sazhen-TM" SLR system

Main technical characteristics of the "Sazhen-TM" system are given in the table below.

| Parameter | Value |
|---|---|
| Ranging distance | |
| Day | 400-6000 km |
| Night | 400-23000 km |
| Aperture | 25 cm |
| Wavelength | 532 nm |
| Beam divergence | 12" |
| Laser pulse frequency | 300 Hz |
| Laser pulse width | 150 ps |
| Pulse energy | 2.5 mJ |
| Mass | 170 kg |
| Normal points precision | 1 cm |
| Angular precision | 1-2" |

# 3. Exploring location variants

Roofs of the laboratory buildings at the observatories were considered as primary installation places for SLR systems. The horizontal stability of the roofs has been measured in 2010 with the precise inclinometer NIVEL-210 (Leica). Variations of the inclination angles of the laboratory building roof at Badary observatory for interval 05.05.2010 – 18.06.2010 are shown in Fig. 3.

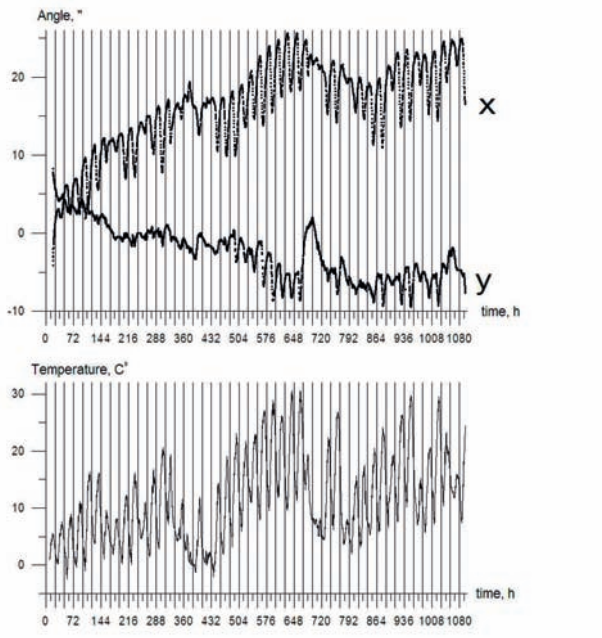


**Figure 3: Variations of the roof inclination angles at the Badary observatory**

There were obvious correlations of inclination angles with the air temperature. Daily variations up to 10" arise due to uneven heating of the building walls by the sun. Therefore final decision was to install the SLR system on the special concrete pillar.

# 4. Installation of "Sazhen-TM" system at Zelenchukskaya observatory

Installation of SLR system at Zelenchukskaya observatory has been finished by 11th of May 2011. Disposition of observational instruments at Zelenchukskaya observatory is shown in Fig. 4 and measured cut-off angles for installed SLR system are illustrated in Fig. 5. The laboratory building cuts ~19° from the south-west side and the radio telescope RT-32 cuts ~20° from south.

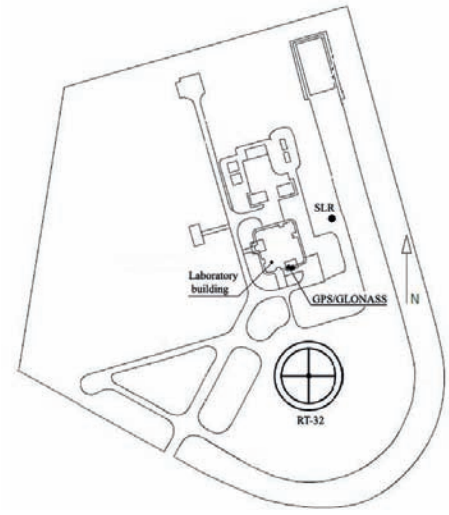


**Figure 4: Disposition of observational instruments**

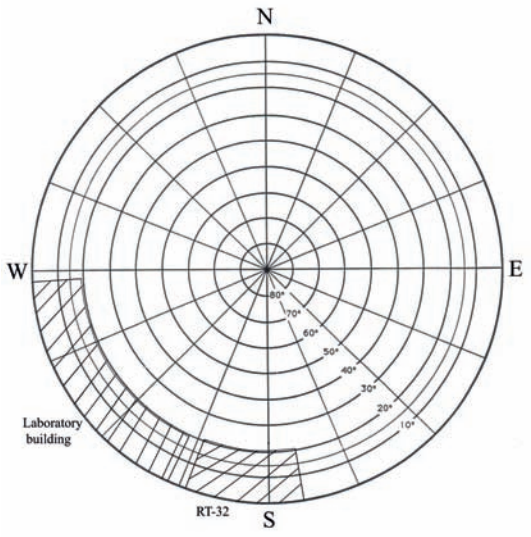


**Figure 5: Cut-off angles for installed SLR system**

Preliminary coordinates of the SLR system reference point were calculated from local geodetic measurements taking into account the instrument height as shown in Fig 6.

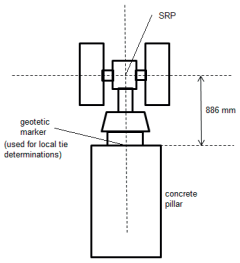


**Figure 6: Reference point of the SLR system and surveyed geodetic marker**

The "Sazhen-TM" system in dome, the laboratory equipment of the system and test ranging of satellites at Zelenchuks-kaya station are shown in figures 7, 8 ,9 and 10.

**Figure 7: "Sazhen-TM" and RT-32 antenna**

**Figure 8: Laboratory equipment of "Sazhen-TM" system**

**Figure 9: "Sazhen-TM" with dome**

**Figure 10: Test ranging of satellites**

The first successful ranging of LAGEOS satellites with "Sazhen-TM" system at Zelenchukskaya station has been carried out 18.05.2011. The results demonstrate the normal point data RMS at the level of 5 mm.

## References

*1. Finkelstein A., Ipatov A., Smolentsev S.,* 2008: The Network "Quasar": 2008-2011. The 5th IVS General meeting Proceedings, p. 39-46.

## Correspondence

Iskander Gayazov
nab.Kutuzova 10
Saint Petersburg, 191187
Russia

gayazov@ipa.nw.ru

# New generation of the SLR station “Mendeleevo”

*Igor Yu. Ignatenko, Vitaliy G. Palchikov, Anatoly G. Zhestkov*

Now in National Research Institute for Physical-Technical and Radio Engineering Measurements (VNIIFTRI) station of laser location «Mendeleevo-1874» is recreating. At the same time collocation station in East-Siberian Branch of VNIIFTRI in Irkutsk city is creating.

Federal State Unitary Enterprise (FSUE) “National Research Institute for Physical-Ttechnical and Radio Engineering Measurements” has the status of the State scientific metrological center and is one of the main Centers of the State standards of Russia. VNIIFTRI performs the duties of the Main metrological center of the State service of time, frequency and the Earth rotation parameters determination (SSTF). At present, VNIIFTRI supports and improves 38 State standards, 19 secondary standards, 23 rigs of highest accuracy, over 120 working standards and calibration rigs for various fields of measurement.

The East-Siberian branch of FSUE «VNIIFTRI» is an autonomous structural subdivision of FSUE «VNIIFTRI» and acts in accordance with The Rules of FSUE «VNIIFTRI», The Branch Regulations and Russian legal system. The major aim of foundation of the East-Siberian branch is carrying out of technical-scientific activity of measurement assurance either in the territory of Eastern Siberia or the whole country.

These stations have the similar equipment, in particular:

- The laser location system produced by Company «Research-and-Production Corporation «Precision Systems and Instruments» (Moscow);
- Time and frequency standards (H-masers);
- Precise gravimeters;
- GPS/GLONASS receivers;
- Local Geodetic Network.

Metrological support:

- National time and frequency standard in Mendeleevo UTC(SU);
- National standard of length in Mendeleevo;
- Secondary time and frequency standard in Irkutsk city.

Additional equipment:

- Mobile laboratory with mobile TWSTFT station and activ H-maser;
- Fixed TWSTFT station in Mendeleevo;
- Standard of comparison - Leica TDA 5005;
- Other accessories.

Plans and perspectives:

- Metrological support of GNSS GLONASS;
- Support of reference line Mendeleevo – Irkutsk (~ 4200 km);
- Earth rotation parameters determination (SSTF);
- Time transfer;
- Work on the global SLR Network.

## Correspondence

Igor Yu. Ignatenko
e-mail: IgIg@vniiftri.ru

Vitaliy G. Palchikov
e-mail: palchikov@vniiftri.ru

# Availability of SLR Normal Points at ILRS Data Centers

*Krzysztof Sośnica, Daniela Thaller, Rolf Dach, Adrian Jäggi, Gerhard Beutler*

ABSTRACT

SLR observations in normal point format are available from two ILRS global data centers, namely CDDIS and EDC. The data are organized in daily and monthly files. The centers have different management philosophies. In CDDIS the files contain data released within one day, whereas EDC publishes the data in daily and monthly batches, containing observations stemming exactly from one particular day and month, respectively.

In this paper, we present the statistics concerning data availability in the two data centers for the period 1994-2010, as well as inconsistencies in quantity of normal point observations from EDC and CDDIS. The total number of measurements to LAGEOS -1, -2, ETALON -1, -2, GPS -35, -36, and to about 50 GLONASS satellites is also presented. We address the number of observations gathered by every ILRS station for the particular year and the global distribution of the stations with the statistics concerning the amount of data. In conclusion we show the data distribution along the groundtracks of geodetic satellites.

## 1. Inconsistencies at ILRS Data Centers

The organization of normal point files differs due to different management philosophies at the two ILRS global data centers (*Pearlman et al.* 2002). At CDDIS (Crustal Dynamic Data Information System) data are labeled with the release date (i.e., independent of the measurement epoch), whereas EDC (Eurolas Data Center) publishes data files containing observations stemming exactly from one particular day. After station upgrades, laser or telescope repairs, data from those stations are sent into "quarantine", which may last for half a year or even longer. CDDIS publishes SLR observations from several previous months in one file (labeled with the release date), whereas EDC updates the observations to the files labeled with the date of the measurement.

Problems may occur with the second and third release of data (for instance after reducing the station's time bias): the same observations are available twice, three or even more times in normal point files (correctly labeled with increased data release flag in the data record). One has to pay special attention in order not to use bad data but to use only the latest release. The above mentioned aspects must be considered in particular when reprocessing SLR data, because all observations should be considered in the correct way in order to achieve best possible results.

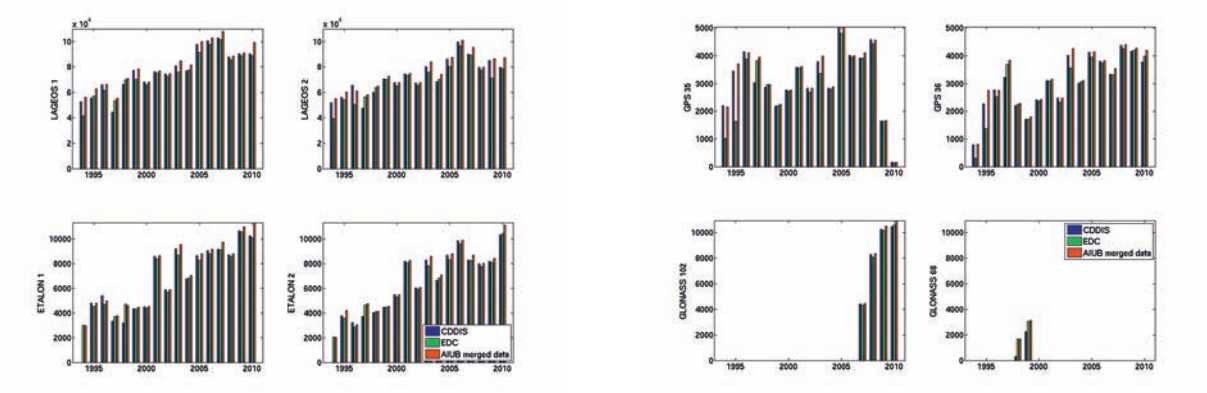


**Figure 1: Number of available normal points in CDDIS, EDC and in the merged AIUB files for the time span 1994-2010. Note the different scales.**

Fig. 1 shows the number of data gathered by CDDIS and EDC as well as the data merged at AIUB by taking into account both data pools. One can notice significant differences between the amount of data which is caused not only by different management philosophies, but also by missing or multiple data. For the satellite GPS -35 the differences in the number of observations in 1994 and 1995 are about a factor of two, whereas in 2009 and 2010 the number of available data is almost the same. For the satellite GLONASS 68, which was tracked during the IGEX campaign (The International

GLONASS Experiment, 1998-2000), taking into account data only from CDDIS would lead to a loss of half of all observations. In this case EDC contains the full set of measurements to this satellite, whereas the CDDIS data pool is incomplete. One has to pay attention that the files from CDDIS may include also observations from the previous year (or even older data). In general, we can conclude that a slightly bigger amount of data is available from CDDIS, but for some satellites this may be vice versa. The highest consistency between both data centers in observed for the period 2000-2009.

# 2. Observation Statistics

It is well known that the global distribution of the ILRS stations is imbalanced. Moreover, the stations differ in the quantity of delivered data (see Fig. 3), quality of normal points, types of observed satellites, and in the capability of tracking specific satellites during daytime or nighttime. The irregularities in the global coverage of the SLR stations result in the better fit to the limited regions. It may imply some problems when generating Earth gravity field models based on SLR observations. Fig. 4 shows the development of the SLR network by taking into account the groundtrack of LAGEOS satellites. From 1994 till 2009 one can observe a big improvement, especially in the African, South American and Asian regions. The quality of European and Asian stations was also significantly improved. On the other hand, there is nowadays a smaller number of observations over North America than in 1994. Even if the general improvement of the SLR network is noticeable, there are still some gaps, especially over India, the Pacific and Atlantic Ocean, and the obvious gaps over Polar Regions due to the satellites' inclinations.

Fig. 2 shows the number of observations from 1994 to 2010 to four groups of satellites, namely LAGEOS -1 and -2, ETALON -1 and -2, GPS -35 and -36 and all tracked GLONASS satellites. In the case of LAGEOS, ETALON and GPS two satellites were tracked; in the case of the GLONASS satellites the number of observed satellites is indicated by the red bars. This number is usually 3-4 satellites per year with two exceptions: during the IGEX campaign all GLONASS satellites were tracked and from December 2009 Herstmonceux observes all active GLONASS satellites.

The number of observations to the LAGEOS satellites amounts from about 110,000 normal points in 1994-1998 to 200,000 in 2006-2007 (see Fig. 2). The number of observations was increasing till 2006. In 2008 there are about 40,000 less normal points than in 2007, but the situation is slowly improving again. According to Fig. 3 and Fig. 2 about 43% of all LAGEOS observations in 2005-2007 were collected by only 3 stations, namely Zimmerwald (7810), Mt Stromlo (7825), and Yarragadee (7090). In case of the ETALON satellites, there are about 5,000 observations in 1994 and 20,000 in 2010, implying that the number of normal points to the ETALONs is about 10 times smaller than to the LAGEOS satellites. One reason is that many SLR stations have problems with tracking high satellites with altitudes above 20,000 km (see Fig. 5). For GPS and GLONASS satellites the average number of observations is 6,000 and 35,000, respectively. The higher number of observations to GLONASS is not only due to bigger number of tracked satellites, but also due to the size of the retroreflector arrays (*Flohrer,* 2008). The Laser Retroreflector Array carried by GPS satellites are 19x24 cm (32 fused-quartz corner cubes), whereas GLONASS satellites have bigger reflectors, e.g. 120x120 cm (396 fused-quartz corner cubes). The larger arrays ease the tracking so that more stations are capable to track GLONASS satellites.

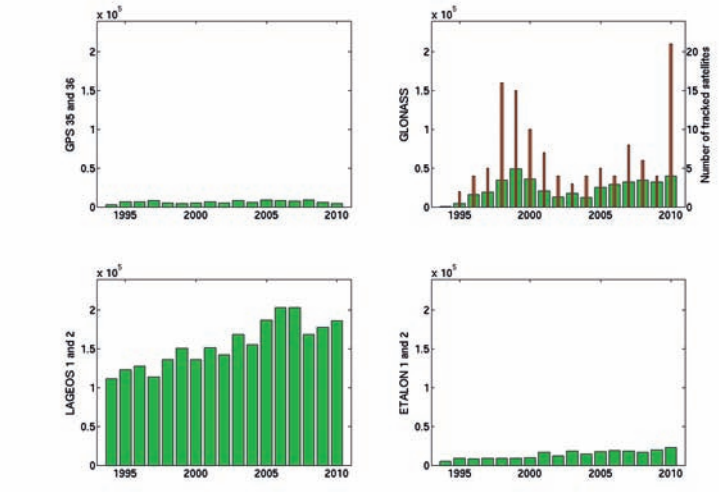


**Figure 2: Number of SLR observations to LAGEOS, ETALON, GPS, and GLONASS satellites in 1994-2010.**

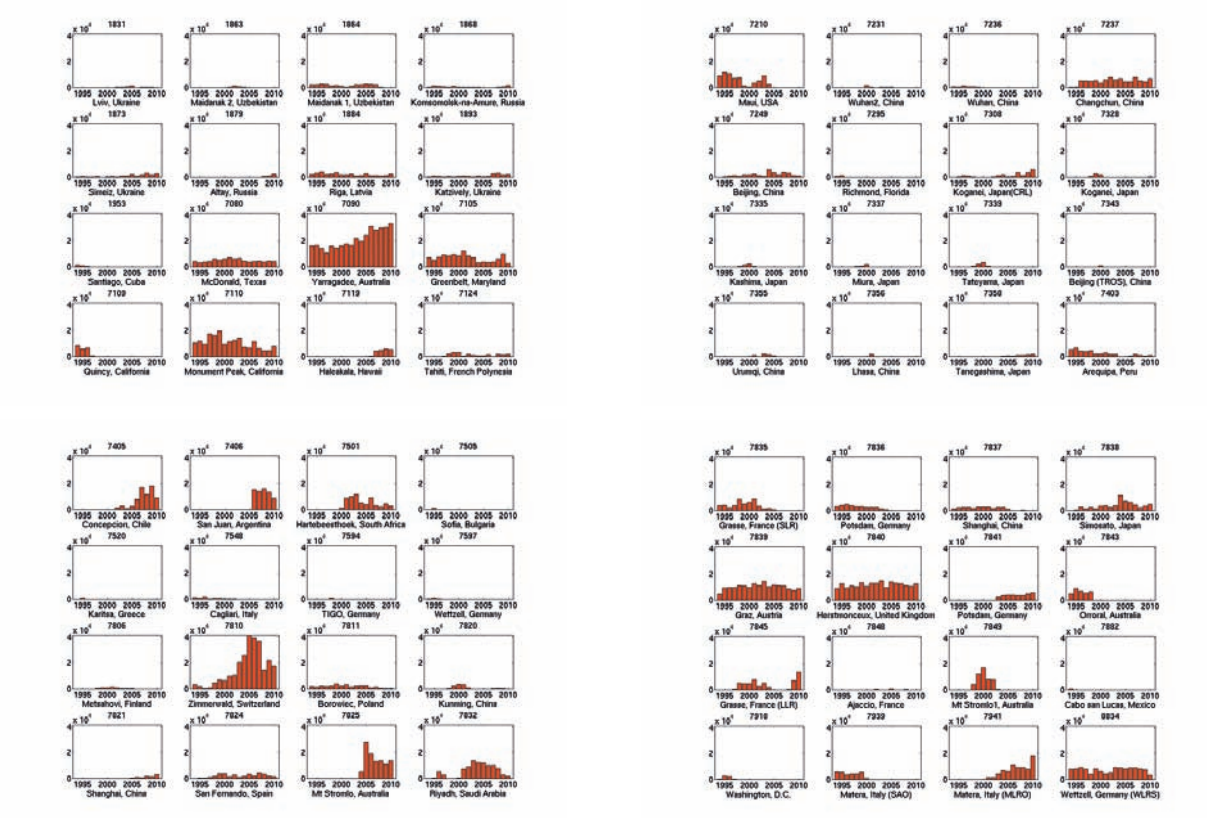

**Figure 3: Total number of LAGEOS -1, -2 and ETALON -1, -2 normal points for the best performing SLR stations**

## Conclusions

The ILRS data centers differ in the number of available observations. Some observations are missing in one or the other center. Multiple entries for normal points can be found in CDDIS. The geometry of ILRS network has been improved since 1994 but the distribution of stations is still imbalanced. The stations differ w.r.t. the quantity of delivered normal points.

## Acknowledgements

The ILRS (*Pearlman et al.* 2002) is acknowledged for providing SLR data.

## References

*Flohrer, C.* 2008: Mutual Validation of Satellite-Geodetic Techniques and its Impact on GNSS Orbit Modeling. Geodätisch-geophysikalische Arbeiten in der Schweiz, vol. 75, ISBN 978-3-908440-19-2

*Pearlman MR, Degnan JJ, Bosworth JM,* 2002: The International Laser Ranging Service. Adv Space Res. 30(2):125–143

## Correspondence

Krzysztof Sośnica
Astronomical Institute, University of Bern
Sidlerstrasse 5
CH-3012 Bern
Switzerland

sosnica@aiub.unibe.ch

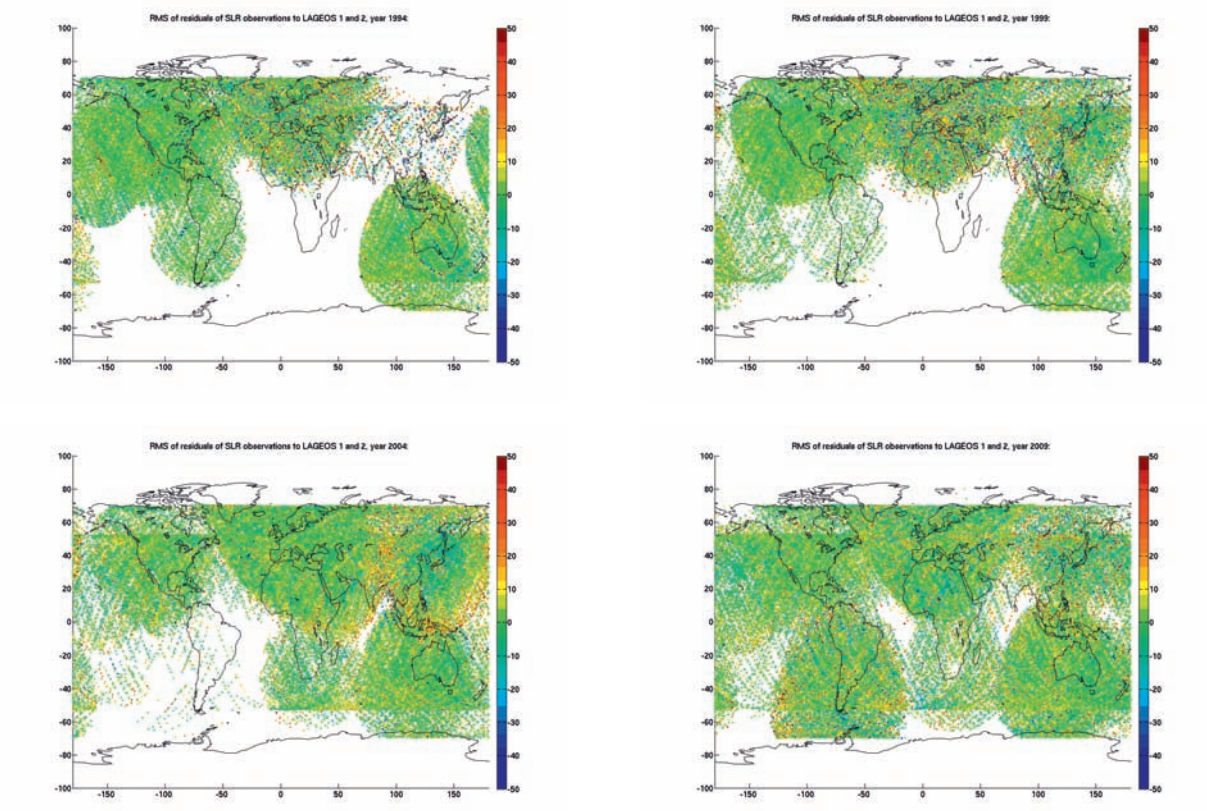


**Figure 4: Groundtracks of observation residuals in mm for LAGEOS -1 and -2 in 1994, 1999, 2004 and 2009.**

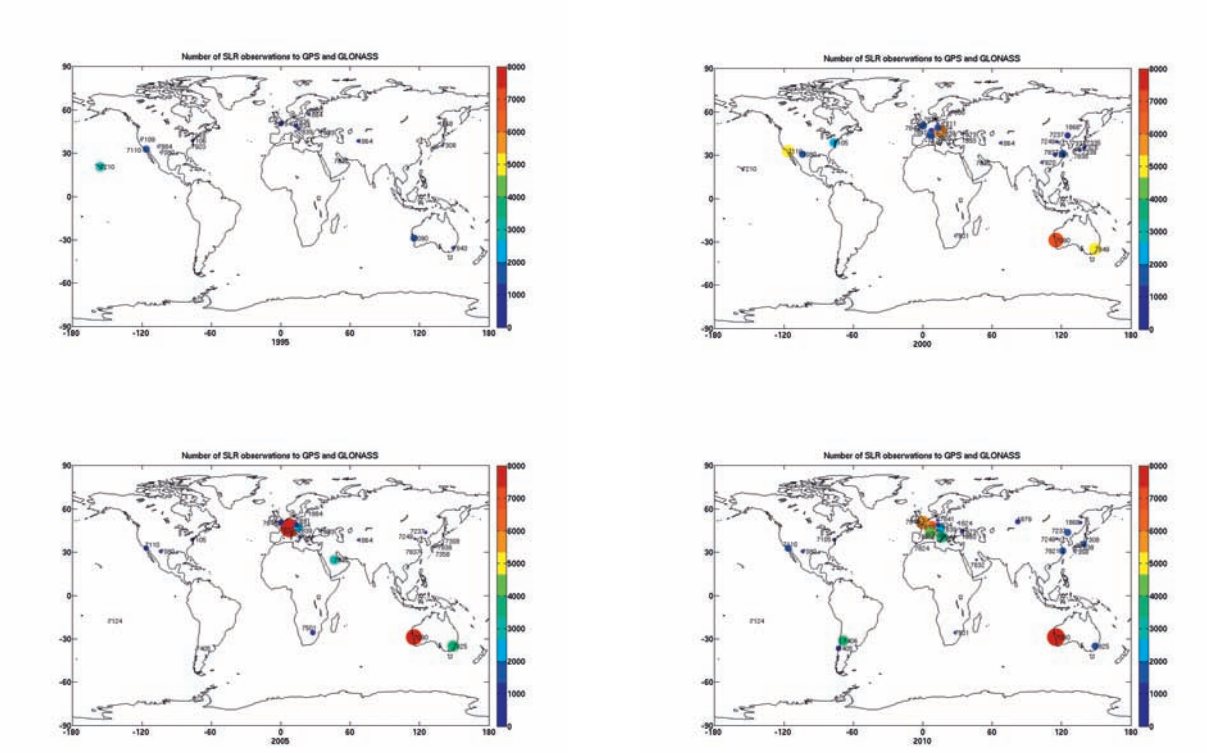


**Figure 5: Number of SLR observations to GPS -35, -36 and all GLONASS satellites in 1995, 2000, 2005 and 2010.**

# SLR providing low-degree gravity field coefficients for the new combined gravity field model GOCO02S

*Maier, A., Krauss, S., Hausleitner, W., Baur, O.*

ABSTRACT

We computed low-degree spherical harmonic coefficients of the Earth's gravity field by means of SLR measurements for a new combined gravity field model. In this context, we conducted a series of closed-loop simulation studies to demonstrate up to which degree and order the gravity field can be resolved by SLR data analysis. Both, for simulation and real data analysis, we analyzed observations to LAGEOS 1 and 2, Ajisai, Stella, and Starlette. For each month, normal equations of all satellites were combined to get geopotential coefficients. We compared the temporal variation of our degree-two terms to two solutions provided by an other research group.

## 1. Introduction

A new global gravity field model – GOCO02S (Goiginger, 2011) – has been computed by combining recent GOCE observations with GRACE, CHAMP, and SLR data. This contribution deals with the determination of the very long wavelengths (low degrees) of the Earth's gravity field, which has been accomplished by means of precise orbit determination (POD) of five dedicated SLR satellites. POD and gravity field parameter estimation have been performed with the GEODYN-II (Long, 1989) and SOLVE software packages.

## 2. Satellite data

The data set consists of Normal Points (NPs) to LAGEOS 1 and 2, Ajisai, Stella and Starlette (Pearlman et al., 2002) gathered over a period of exactly five years (January 2006 to December 2010). Figure 1 shows a typical coverage of NPs for one month. As a consequence of the SLR station distribution and the orbital design of the satellites, there are large data gaps over oceanic areas and polar regions. Additionally, the network is less dense in the southern hemisphere.

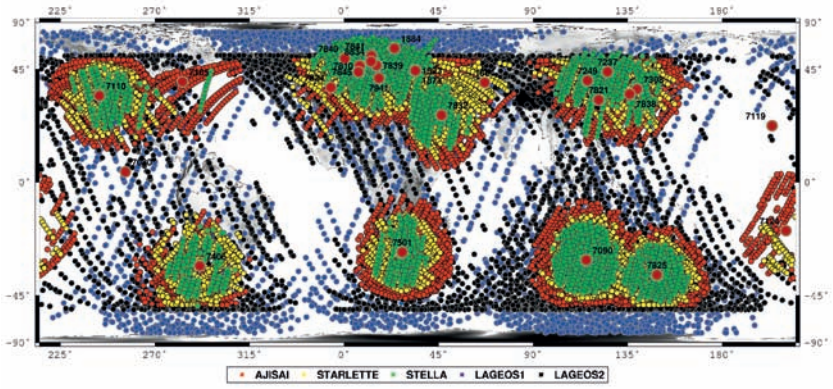


**Fig. 1: Observed ground tracks of all five satellites during one month. Stations are marked with red circles.**

## 3. Closed-loop simulation

We conducted a series of closed-loop simulations with EIGEN-5S assumed as the 'true' model to demonstrate up to which degree and order the gravity field can be resolved by SLR. Observations, superposed with white Gaussian noise, have been generated to all five satellites. Figure 2 (left, middle) shows the reproduced number of digits using one and twelve months of data, respectively. Generally, the number of reproduced digits is lower for the zonal and near-zonal terms. A better performance can be achieved by extending the time span. As the $C_{20}$ term is of special interest,

its temporal variation with respect to EIGEN-5S is depicted in Figure 2 (right). Due to ill-conditioning, the time series of maximum degree and order (d/o) 15 differs quite clearly from zero. In addition, the standard deviations are one order of magnitude higher compared to the solution of the Centre for Space Research (CSR) at the University of Texas at Austin (Cheng and Tapley, 2004). By reducing the maximum d/o to 5, however, deviations from zero and standard deviations get considerably smaller.

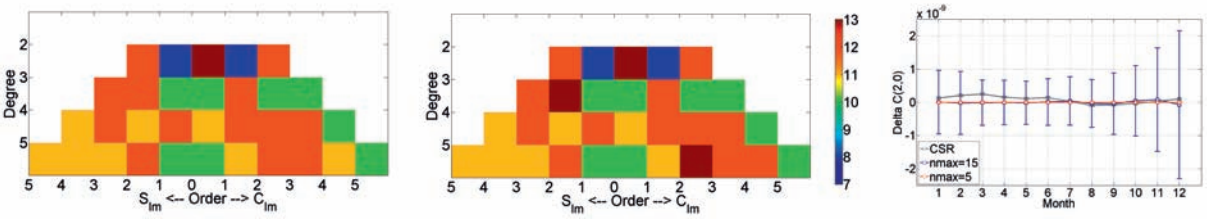


**Fig. 2: Number of reproduced digits with respect to the 'true' gravity field based on data collected over one month (left) and twelve months (middle). Variation of $C_{20}$ with respect to EIGEN-5S and standard deviations (right) for maximum d/o 15 (blue line) and maximum d/o 5 (red line). Variation and standard deviations of CSR (gray line) are depicted as well to be able to rate the range of standard deviations.**

# 4. Parameter settings

We subdivided the time span of five years into monthly arcs. From data of each arc a set of arc-dependent parameters such as drag and solar radiation pressure coefficients has been estimated. A combination of these arcs yields the global parameters, i.e., gravity field coefficients and station coordinates. The complete list of estimated parameters can be found in Table 1. EIGEN-5S served as a priori gravity field model.

**Tab. 1: Measurement model and estimated parameters**

| |
|---|
| **Measurement model** |
| Observations: 120s NPs to LAGEOS and 30s NPs to Ajisai, Stella, and Starlette |
| Tropospheric refraction: Marini-Murray model |
| Data weighting: 1.0m |
| Editing criteria: 3.5σ, cut-off elevation angle of 20°, minimum number of NPs per station and arc: 50 |
| **Estimated parameters** |
| State vector: once per arc |
| Solar radiation pressure coefficient: once per day |
| Atmospheric drag coefficient: once per day |
| Constant acceleration along track, cross track and radial: once per day |
| Measurement bias: once per station and arc |
| Gravity field coefficients up to degree and order 5 |
| Geocentric station coordinates |

# 5. Results and Discussion

One indicator for the precision of the POD process is the RMS of range residuals (*o-c*). The mean RMS over five years for each satellite is listed in Table 2. Due to the long arcs varying between 28 and 31 days, it is not surprising that the fits are at the centimetre level. Nevertheless, additional pass by pass measurement biases (pbiases) have been estimated as an attempt to reduce the residuals. Indeed, the RMS becomes smaller, especially for Ajisai and Starlette (Table 2). On the other hand, the estimated gravity field coefficients are nearly identical. For this reason it has been decided not to estimate additional bias parameters.

**Tab. 2: Mean RMS of orbital fit. The first line of RMS values corresponds to the parameter settings listed in Table 1. The second line refers to the orbit solution where additionally pass by pass measurement biases adjusted.**

| | LAGEOS 1 | LAGEOS 2 | Ajisai | Stella | Starlette |
|---|---|---|---|---|---|
| RMS [cm] | 4.5 | 3.9 | 7.6 | 10.7 | 10.3 |
| RMS [cm] (pbias) | 3.5 | 3.2 | 2.5 | 7.4 | 5.5 |

To detect temporal variations, one set of coefficients has been estimated for each month. Figure 3 depicts the variation of all degree-two terms. Especially the degree-two terms contribute to GOCO02S, since the formal errors of the other coefficients are slightly larger than those resulting from GRACE benefitting from more and more uniformly distributed observations.

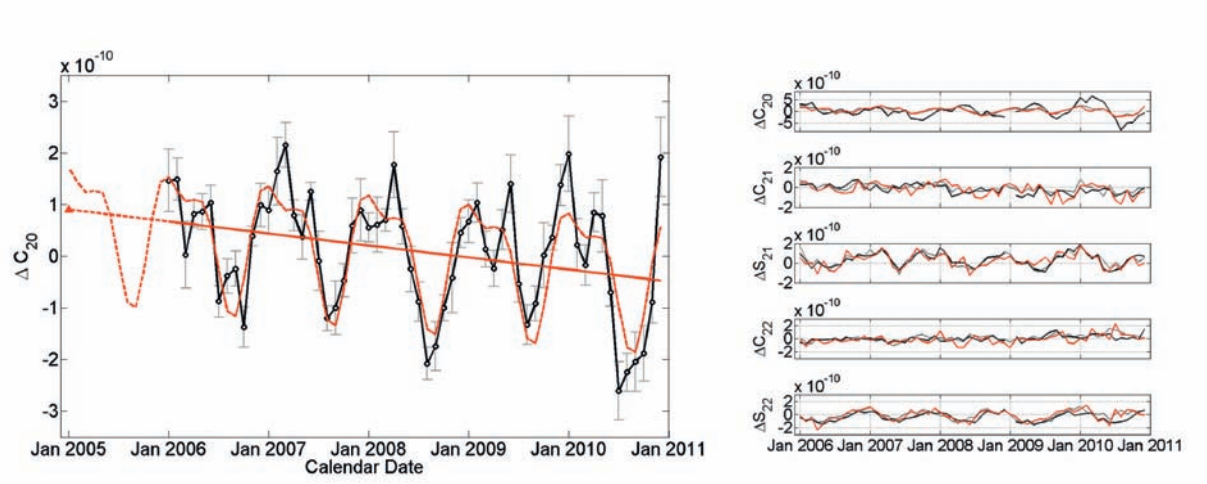


**Fig. 3: Monthly values of $C_{20}$ (left side) with respect to EIGEN-5S (black circles) and standard deviations (gray error bars). The variation has been fit by a regression line (straight red line) together with annual and semi-annual sinusoids (curved red line). The coefficient has been extrapolated (red triangle) along the extrapolated regression line (dashed red line) to January 1, 2005 to be consistent with the reference epoch of GOCO02S. Monthly values of degree-2 terms (right side) estimated from SLR (in red our solution, in gray the one of CSR) and GRACE data (in black, solution of CSR).**

We computed the average geoid height from zonal coefficients (up to degree 5) by dividing latitude into three bands: (1) equatorial band, (2) mid-latitude band and (3) polar band. The change of geoid height was obtained by subtracting the mean geoid height over 60 months from the averaged geoid height per band (Figure 4). The geoid height of the mid-latitudes remains nearly constant. Equatorial and polar geoids, however, experience a significant change. While the geoid in polar regions decreases, the equatorial one increases. This means that during the investigation period a large-scale mass redistribution from polar regions to the equatorial band has taken place. The cause of this shift is not yet fully understood.

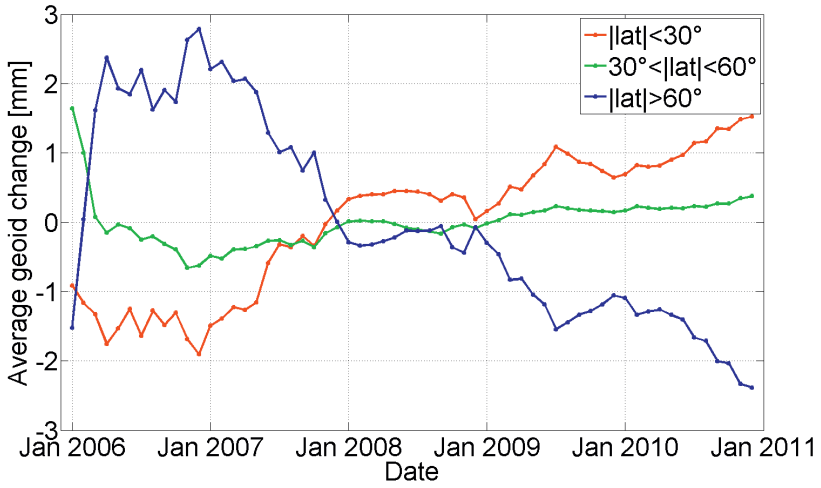


**Fig. 4: Zonal changes in average geoid height over the equatorial (|lat|<30°), mid-latitude (30°>|lat|<60°) and polar region (|lat|>60°) in red, green and blue color, respectively.**

# 6. Conclusion and Outlook

Irregular data distribution, downward continuation and number of estimated parameters influence the condition of the normal equations. Extending the time span and the usage of data of different satellites has a positive effect on gravity field recovery. Due to aliasing effects in GRACE data, SLR is still the most suitable technique to determine the C20 term. The coefficients of higher degree and order can be determined more precisely by other measurement techniques. By including more satellites at different inclinations the precision can be increased.

## Acknowledgements

The studies of the Austrian Academy of Sciences were funded by the Austrian Space Application Programme No. 6 of FFG, charged by BMVIT (project ID 819685).

## References

*Cheng, M. and Tapley*, B.D.: Variations in the Earth's oblateness during the past 28 years. Journal of Geophysical Research, 109(B09402):1–9, 2004.

*Goiginger, H., Rieser, D., Mayer-Gürr, T. Pail, R., Schuh, W.-D., Jäggi, A., Maier, A. and GOCO Consortium*: The combined satellite-only global gravity field model GOCO02S. In EGU General Assembly 2011, volume 13, 2011.

*Long, A.C., Cappellari Jr, J.O., Velez, C.E. and Fuchs, A.J.*: Goddard Trajectory Determination System (GTDS) Mathematical Theory Revision 1, 1989.

*Pearlman, M., Degnan, J.J. and Bosworth, J.M.*: The International Laser Ranging Service. Advances in Space Research, 30(2):135–143, July 2002.

## Correspondence

Andrea Maier
Space Research Institute, Austrian Academy of Sciences
Schmiedlstraße 6
8042 Graz

andrea.maier@oeaw.ac.at

# Construction Progress in the Photon Counting Detector for the European Laser Timing Experiment

*Jan Kodet, Ivan Prochazka, Josef Blazej, Jan Brinek*

ABSTRACT
We are presenting a progress in a construction and indoor tests of the photon counting detector for the European Laser Timing (ELT) experiment. ELT is an optical link prepared in the frame of the ESA mission "Atomic Clock Ensemble in Space" (ACES). The objective of this laser time transfer is the synchronization of the ground based clocks and the clock on board the space station with precision of the order of units of picoseconds and the accuracy of 50 ps. The requirements put on the detector package are quite high – temperature stability of the delay better than 20 ps peak to peak within one satellite orbit, operation within a broad temperature, absolute calibration of the photon to electrical signal delay with precision 25 ps and others.

# 1. Introduction

The laser time transfer link is under construction for the European Space Agency (ESA) for its application in the experiment Atomic Clock Ensemble in Space (ACES). The device is expected to be launched toward the International Space Station (ISS) in 2014. The objective of this laser time transfer is the synchronization of the ground based clocks and the clock on board the space station with precision of a few picoseconds and the accuracy of 50 picoseconds [1].

Although the signal photon flux at the ISS orbit is of the order of $10^{13}$ photons per square meter per one laser shot and multi-photon signal strength may be obtained, the photon counting approach to the optical signal detection has been selected in order to reduce the systematic biases as much as possible.

The project is a spin-off of the existing projects of laser ranging to artificial Earth satellites [2] (SLR). The on-board hardware consists of a Comer Cube Retro-reflector (CCR), an optical receiver based on a Single Photon Avalanche Diode (SPAD) and an event timing device connected to the local time scale, see Fig. 1. The ultra short laser pulses fired towards the satellite by a ground laser ranging station will be time tagged with respect to the ground time scale $T$. They will be detected in space and time-tagged in the local time scale $E$. At the same time, the CCR will re-direct the laser pulse towards the ground station providing precise ranging information $D$ and hence providing the information about the ground-to-space signal propagation delay. This procedure should provide, among others, the time transfer ground to space with precision and accuracy outperforming the radiofrequency techniques.

Because of the ISS is at low orbiter (400-500 km) the signal photon flux at the detectors input optics is of the order of $10^{13}$ photons per square meter per one laser shot and multi-photon signal strength may be obtained, the photon counting approach to the optical signal detection has been selected in order to reduce the systematic errors as much as possible. Hence the requirements put on the detector optics are large attenuation of the receiving signal and the compensation of the radar equation. The input optics must not influence the timing and stability properties.

It is required that the detection timing resolution must be 25 ps with the timing stability of 1 ps per day. The entire ELT package must be able to operate at temperatures from -10 to +40°C and the maximum mass can not exceed 0.5 kg with maximum power consumption 1 W. The ELT project is planned for three years mission in space and there will be no sun protection included.

The absolute calibration of the signal delays within the laser time transfer signal chain is very challenging. Among others the optical to electrical detection delay of the photon counting receiver itself should be calibrated with the uncertainty of 25 ps maximum.

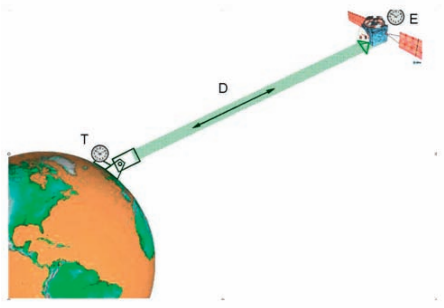


**Figure 1: The principle of the laser time transfer ground to space and vice versa.**

# 2. ELT construction

The detector under construction is based on the Single Photon Avalanche Diode (SPAD) having an active area of 100 µm in diameter. The detection chip is manufactured by the K14 technology and is mounted in un-cooled socket and is operated in active quenching and gating mode. Designing the detector electronics with detection delay stability of 20 ps peak to peak (with the goal of 10 ps) over one satellite orbit, the operating temperature range of -10 °C to +40 °C and last but not least the radiation stability in a near Earth orbit environment were rather challenging. The classical schemes used until now could not be used. The space qualified electronic components had to be used whenever possible. The electronics block diagram is in Fig. 2 a).

Two linear stabilizers provide the biases +5.0 V and +3.3 V for the detector logic. The DC - DC converter provides +35 V, 10 mA for the SPAD bias stabilizer. The SPAD bias stabilizer is stabilizing the SPAD reverse bias according to the detector temperature hence the detector delay temperature dependence is compensated. The ultra-fast PECL comparator is sensing the SPAD break down after a photon is detected. The gate and quenching logic is based on LVDS and CMOS circuits. The circuit enables to operate the SPAD chip 0.1 V up to 2.0 V above its break down.

The photograph of the bread board (BB) version of the active quenching and gating circuit is in Fig. 2 b). The detection chip is connected in the centre from the bottom side of the printed circuit board. The power, gating signal, and test signals are connected via a multi-pin connector (left). The DC-DC converter providing the SPAD bias voltage is in the lower part, the SPAD bias stabilizing and temperature control circuit is in the left. The +5.0 V and +3.3 V power stabilizers are on the top, the fast comparator sensing the SPAD electrical output is in the center with the gating and level converting circuits on the right. The total board dimensions are 74 × 74 mm, its mass is 42 g.

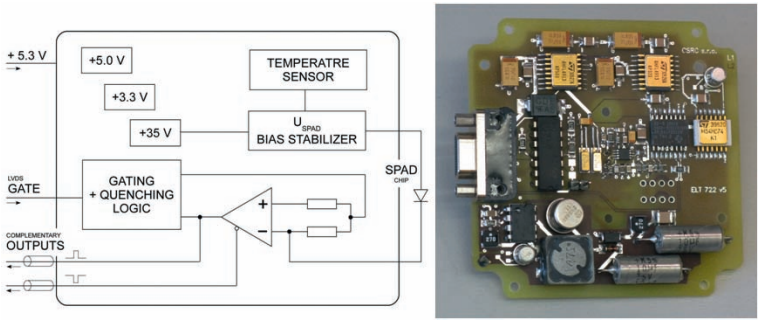


**Figure 2 a): The ELT detector eletronics block diagram. b) Bread board version of the active quenching and gating circuit. Entire components are space qualified or their military specified pin to pin compatible versions.**

The entire components which are used for ESA ELT mission are space qualified and where approved by ESA except of the fast comparator sensing the SPAD breaks down. Due to extreme requirements on the propagation delay stability over a broad temperature range the Analog Devices ADCMP 553 was selected for our purpose. The manufacturer claims

propagation delay of 500 ps with the temperature coefficient of 0.2 ps / K. We were allowed to test the comparator by ourselves by ESA approved radiation test procedure. The comparator survived three times larger radiation dose then it was prescribed and any of the comparator parameters had changed.

# 3. Receiver Optics

The ELT detector front-end consists of input aperture with diffuse polycarbonate 3 mm in diameter, narrow bandwidth interference filter, stack of pinholes and SPAD, as it is shown in Fig. 3. Because the entire experiment will work only with optical signal strength in single photon level, the impacting energy level must be kept as constant as it is possible for entire range of angles. It is not possible to range in angle interval form 0 to 5 degree, hence the detector should be blind in this angle interval otherwise the background photon noise scattered from the Earth will undesirably increase the detector effective dark count rate on the other side the angle interval is limited by the SLR station minimum ranging elevation, in most of the stations it is possible to range up to 60 degree from the zenith in all directions.

When the previous limitations will be taken on account, the detector optics Field of View (FoV) should be designed from 5 to 60 degree. The main advantage, which should be considered in designing the ELT optics, is that the signal must be attenuated by the optics. The expected signal strength is to be 1013 photons/m2 in pulse length of 10 to 100 ps FWHM and the signal must be attenuated to the single photon level. The main attenuation is set by the distance between front aperture and SPAD.

The narrow bandwidth interference filter is used to effectively filter the background photon noise scattered from the Earth and coming from the sunlight. SLR stations work with second harmonic Nd:Yag laser - 532 nm thus the interference filter is centered at 532 nm with bandwidth of 3 nm. It should be pointed out, for several tests at CTU laboratory picoseconds laser of wavelength 778 nm was used, hence the 532 nm interference filter was replaced by 778 nm filter. However the interference filter has narrow FoV in units of degrees. The stack of pinholes is used for blocking the signal coming from larger angels and which do not propagates alongside the optical axis. The diffuse polycarbonate is used to increase the detector FoV, but it still prefers the perpendicular light. To increase the signal to noise ration the steal shield is used to block out the scattered photons from the Earth atmosphere. To minimize the angle dependency for angels from 5 to 60 degrees the circular shield was improved with conical cuts. The relative intensity varies only from 0.05 to 0.8 through entire interested interval with en-counted radar equation. The construction overview of the ELT optics can be find in [3].

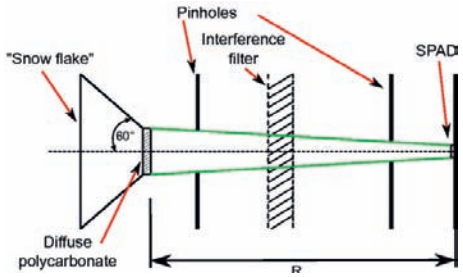


**Figure 3: Schematic drawing of the receiver front-end optics.**

## References

[1] *Schreiber, U. - Procházka, I. - Lauber, P. - Hugentobler, U. - Schäfer, W.* - et al.: Ground-Based Demonstration of the European Laser Timing (ELT) Experiment. IEEE Transactions on Ultrasonics, Ferroelectrics, and Frequency Control (UFFC). 2010, vol. 57, no. 3, p. 728-737

[2] *Procházka, I. - Yang, F.*: Photon counting module for laser time transfer via Earth orbiting satellite. Journal of Modern Optics. 2009, vol. 56, no. 2&3, p. 253-257

[3] *Jan Kodet, Michael Vacek, Petr Fort, Ivan Prochazka and Josef Blazej,* "Photon counting receiver for the laser time transfer, optical design, and construction", Proc. SPIE 8072, 80720A (2011); doi:10.1117/12.883701

## Correspondence

Czech Technical University in Prague
Prague 1
Czech Republic

kodet@fjfi.cvut.cz

# Isothermal FFDP-Test and SCF-Test of Flight-quality Uncoated Cube Corner Laser Retroreflectors

*S. Dell'Agnello[1], G. O. Delle Monache[1], D.G. Currie[2], R. Vittori[3], C. Cantone[1], M. Garattini[1], A. Boni[4], M. Martini[1], C. Lops[1], N. Intaglietta[1], G.Bianco[5], M. Maiello[1], S. Berardi[1], L. Porcelli[1], G. Patrizi[1]*

ABSTRACT

Using dedicated facilities of INFN-LNF in Frascati, Italy, including the "Satellite/lunar laser ranging Characterization Facility" (SCF,[1]), we characterized the detailed thermal behaviour and/or the optical performance of many flight units of coated and uncoated cube corner laser retroreflectors (CCRs). As a reference for the ILRS community, with this article we provide a compilation of the many tests carried out in the last years on uncoated CCRs (tests on coated CCRs are reported in detail in [1]).

## 1. Industrial optical acceptance test of 110 LARES Flight CCRs (ASI reference document: DC-OSU-2009-012)

The work reported in this section was performed by INFN-LNF authors only. At the end of 2008 INFN-LNF was requested by ASI[1] to perform an industrial acceptance test of all of the 110 CCRs of the LARES satellite. LARES is a tungsten sphere passive satellite of about 18 cm radius, covered with 92 CCRs made of fused silica. It will orbit at a nearly circular orbit with semi-major axis of about 7900 Km. The CCRs used for the satellite were manufactured by ZEISS, but in order to asses the compliance with their specification ASI requested INFN-LNF to do FFDP (Far Field Diffraction Pattern) measurements of those CCRs. Specifications of LARES CCRs were:front face aperture of 1.5", DAOs[2] = 1.5±0.5 arcsec. We performed FFDP measurements at the SCF, in air at room temperature, in 3 working weeks before Christmas 2008, on a red laser optical table (He-Ne, λ=632.8 nm) [2], since CCRs were designed by ZEISS at this wavelength. In Fig. 1 we can see one of the measured CCRs. In order to define a criterium of acceptance for the CCRs, we referred to the shape of the FFDP of an uncoated CCR with front face aperture of 1.5" and DAOs as specified before, oriented with a physical edge vertical and an horizontally polarized beam.

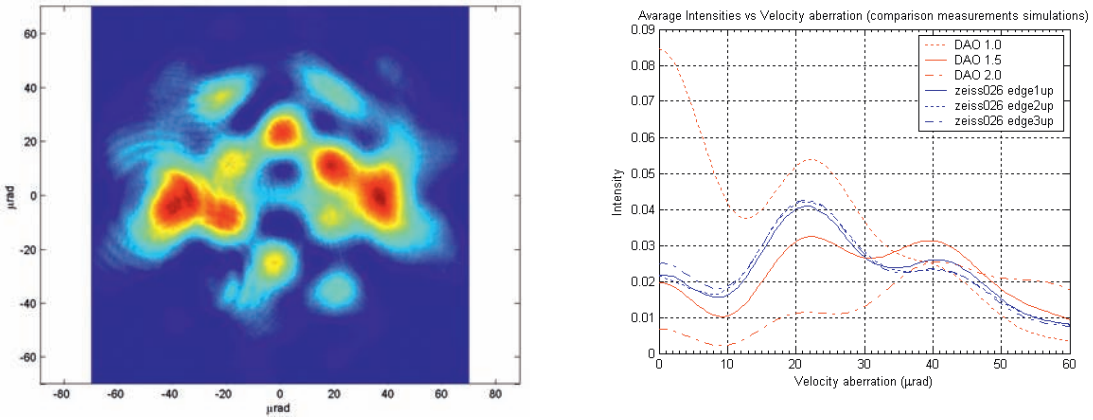


**Figure 1: (left) Measured FFDP of one of LARES CCRs. (right) Average intensity vs velocity aberration, comparison measurements simulations. Measured intensity has ±25% relative intensity error not shown**

[1] Laboratori Nazionali di Frascati (LNF) dell'INFN, Frascati (Rome), Italy

[2] University of Maryland (UMD), College Park, MD, USA and NASA Lunar Science Institute, NASA Ames Research Center, Moffett Field, CA, USA

[3] Aeronautica Militare Italiana (AMI) and Agenzia Spaziale Italiana (ASI), Rome, Italy

[4] University of Rome "Tor Vergata" and INFN-LNF, Rome, Italy

[5] ASI, Centro di Geodesia Spaziale "G. Colombo" (ASI-CGS),

[1] Italian Space Agency

[2] Dihedral Angle Offset

The FFDP has a very distinctive shape with two peaks distributed horizontally, symmetric with respect to the center. We therefore compared the distances between those peaks and their intensities with measurements. Simulations (peaks distances and intensities), defined a band, in red in Fig. 2, in which measured values should be delimited. In Fig. 2 we present the results of the tests on all of the 4 lots in which were divided the 110 CCRs.

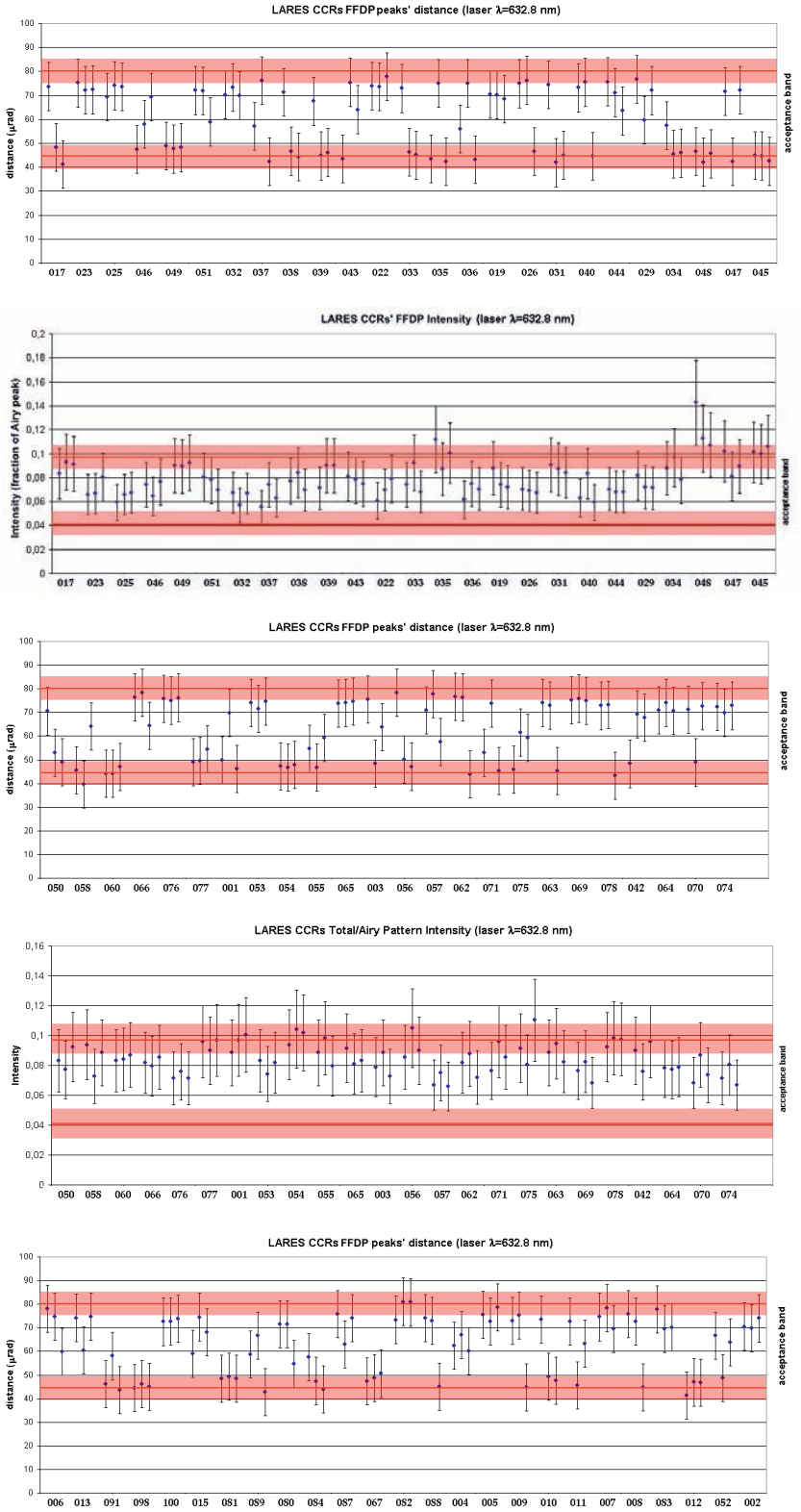

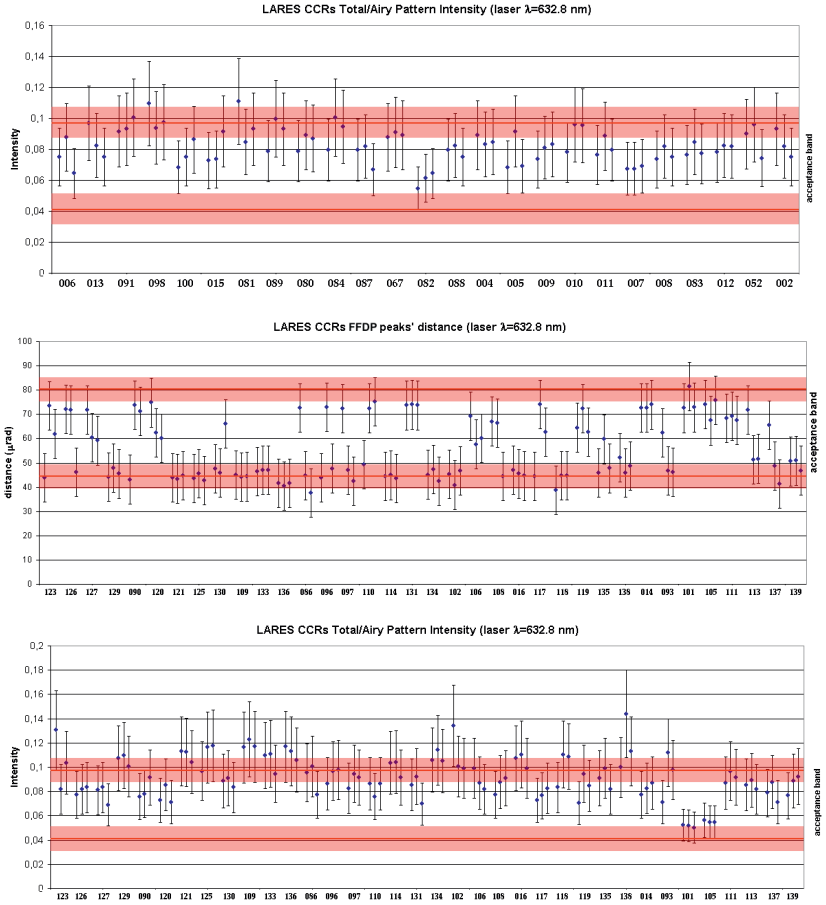


**Figure 2: Industrial acceptance test performed on all of the LARES flight CCRs, by INFN-LNF authors only, at a red optical table. Error on measured peaks distance is ±10 μrad. Error on measured intensity is ±25% relative**

This work was completely successful and approved by ASI with ASI reference document: DC-OSU-2009-012. Right plot of Fig. 1 shows another analysis we started to perform, involving the evaluation of the average intensity of the FFDP vs. the velocity aberration. This is a better way to compare measurements with simulations as we will explain in section 3. Figure one shows, for example, that the CCR, within errors, is in very good accordance with DAO specs. Results of this analysis will be subject of a future work.

# 2. LLRRA-21[3] /MoonLIGHT[4] an uncoated lunar CCR

Here we present the SCF-Test performed on a 100 mm front face aperture uncoated CCR, LLRRA-21, for the next generation of lunar laser ranging. Full description of CCR characteristics can be found in [3]. The CCR was installed with its housing inside the SCF, on the rotation positioning system, see Fig. 3. The housing was controlled in temperature with tape heaters. An IR (InfraRed) camera measured CCRs' front face temperature. Platinum RTD sensors recorded housing and gold cans temperatures while two precise diode sensors recorded the temperature of one of the faces of the CCR, in order to have a third dimension on the thermal gradient of the CCR. These last one were put one on the center of this face and one close to the front face.

[3] Lunar Laser Ranging Retroreflector Array for the 21st century, funded by NASA with Contract NASA NNX07AV62G for the LSSO (Lunar Sortie Scientific Opportunities) and by the LUNAR (LUnar Network for Astrophysics Research) via Cooperative Agreement NNA09DB30A.

[4] Moon Laser Instrumentation for General relativity Hugh-accuracy Tests (an INFN R&D experiment).

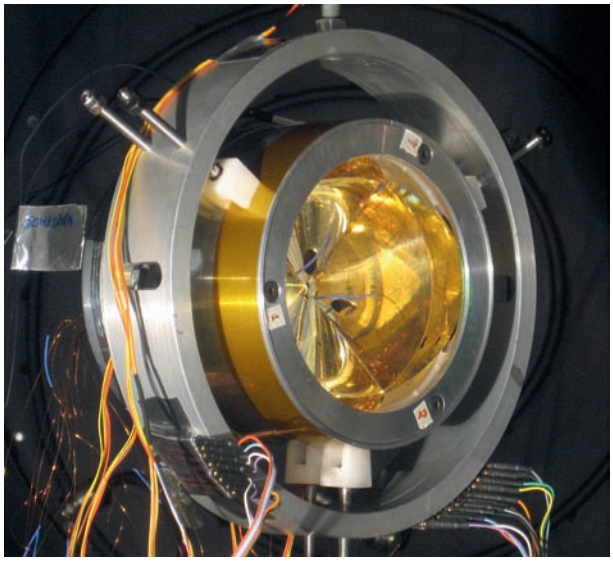

**Figure 3: MoonLIGHT/LLRRA-21 flight CCR hold inside the SCF, ready for the test**

The CCR had an orientation inside the housing such that one physical edge was horizontal. The procedure of the SCF-Test was the same as described in [1]. Created the simulated space environment we heated the CCR with the Solar Simulator (SS), with the beam orthogonal to the CCR. After this condition, which, thermally, is the best for an uncoated CCR, we simulated also an illumination of the Sun at lower elevations. In order to do this the CCR was rotated of 30° clockwise and 30° counterclockwise with respect to the SS. In one direction we had a Total Internal Reflection breakthrough situation, in the other not. Temperature variation with time of various prototype's parts is in Fig 4.

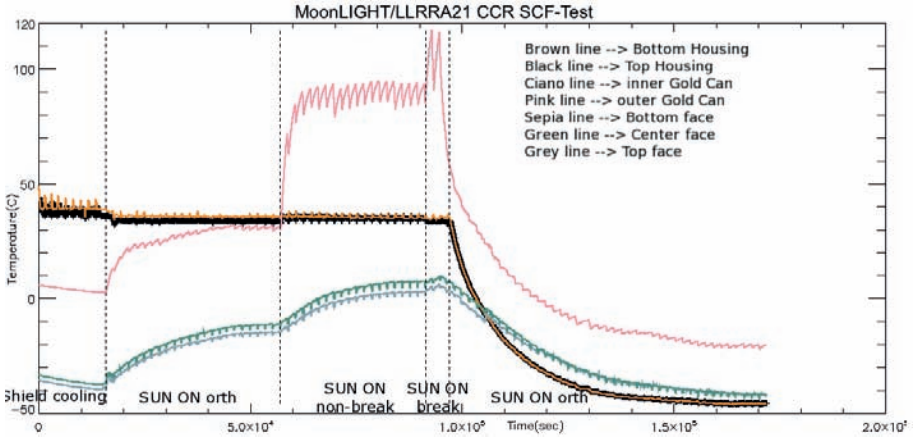


**Figure 4: MoonLIGHT/LLRRA-21 flight CCR temperature variations of various housing parts and of CCR**

As expected, going from an orthogonal SS beam to non-breakthrough position to a breakthrough position increased the temperature of the CCR and most of all the temperature of the gold cans. In particular we noticed an increasing temperature gradient on the CCR face. Until the "SUN ON break" phase the housing was controlled, while on the last phase the housing was left floating. The FFDP measurements reflected this behaviour (see Fig. 5). FFDP measurements were performed with a green laser ($\lambda = 532$ nm), but the diameter of the beam hitting the CCR was only 38 mm, not 100 mm as the front face of the CCR. Future upgrades of the optical table will allow that. As mentioned above, the temperature difference between the two sensors on a reflecting face of the CCR (green and grey lines of Fig. 4) increased; the intensity of the FFDP at Moon velocity aberration decreased until the breakthrough phase. Instead during the last phase the intensity increased, as the temperature difference of temperature sensors on the CCR reduced.

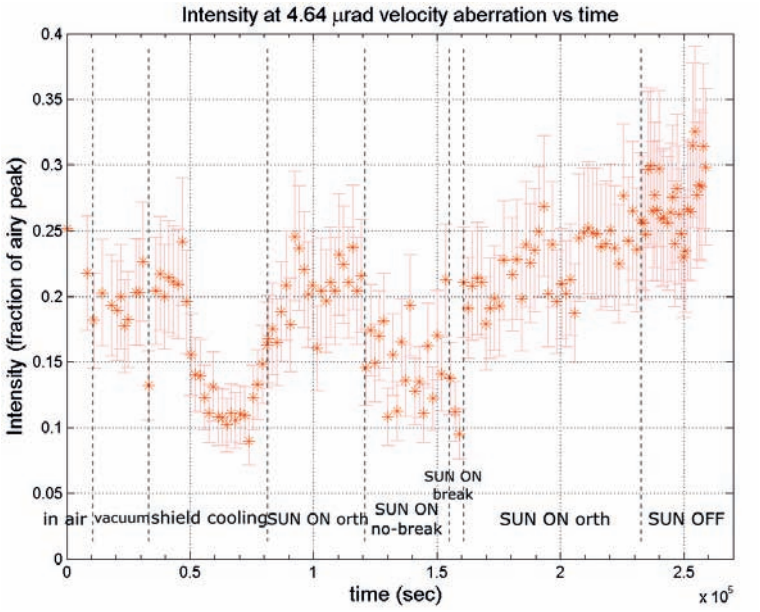


**Figure 5: MoonLIGHT/LLRRA-21 flight CCR average FFDP intensity variation at Moon velocity aberration (2V/c) during tests. Error on intensity is ± 20% relative.**

# 3. Conclusions

The SCF has proven to be the right facility for the test of flight quality uncoated CCRs in an accurate laboratory-simulated space environment and in air for FFDP acceptance tests. In particular LARES flight CCRs FFDP acceptance tests represent a big milestone for our facility, because proved our equipment to be appropriate for such aim. These tests were a good occasion to start thinking on a new approach on FFDP analysis. Future publications will describe in detail such analysis on LARES flight CCRs. Finally we report a complete SCF-Test of a new concept of lunar LRA (described in [3]), which proved useful for the design progress of LLRRA-21. Refinements on hardware is mandatory for an exhaustive test.

## References

*1. Dell'Agnello S., et al.,* Creation of the new industry-standard space test of laser retroreflectors for the GNSS and LAGEOS, Adv. in Space Res., 47 (2011), 822-842

*2. Boni A., et al.,* Optical Far Field Diffraction Pattern test of laser retroreflectors for space applications in air and isothermal conditions at INFN-LNF, INFN-LNF Report LNF-08/26(IR), 2008.

*3. Currie D., et al.,* A Lunar Laser Ranging Retroreflector for the 21st Century, Acta Astronautica, DOI: 10.1016/j.actaastro.2010.09.001.

## Correspondance

Alessandro Boni
alessandro.boni@lnf.infn.it

# Global SLR Tracking Support for HY-2 Satellite Precise Orbit Determination

*Wu Bin[1], Lin Mingsen[2], Zhang Zhongping[1]*

ABSTRACT

The HY-2 Satellite, which will be launched in August 2011, is the first satellite for State Oceanic Administration of China with the microwave altimeter, remote sensing systems for the oceanic environmental monitoring and related scientific researches. For the application of the microwave altimeter measurement, the precise orbit determination of the satellite is a key support. HY-2 satellite will equip with Laser Retro Reflector Array (LRA), Doppler Orbit graph and Radio-positioning Integrated by Satellite (DORIS), Global positioning System (GPS) to implement the precise orbit determination. HY-2 satellite will be tracked by the Chinese SLR network and international SLR network to precisely determinate its orbit and that is very important for environment monitoring and scientific research. This paper will introduce HY-2 satellite, its LRA and the plan of laser tracking.

## 1. Introduction

China has launched two oceanic satellites, HY-1A and HY-1B, on 15 May 2002 and 11 April 2007 respectively. Those two oceanic satellites have played an important role in surveying the variety of Chinese ocean in the passed years. The HY-2 satellite will be launched in Augest 2011, which is the first satellite for State Oceanic Administration of China with the microwave altimeter, remote sensing systems for the oceanic environmental monitoring and related scientific researches. HY-2 satellite will equip with Laser Retro Reflector Array (LRA), Doppler Orbit graph and Radio-positioning Integrated by Satellite (DORIS), Global positioning System (GPS) to implement the precise orbit determination. One of the measuring techniques, SLR will provide the laser tracking data with the better than 2cm for single shot. So, the Chinese SLR network will track HY-2 satellite and Shanghai Observatory as an organizer for the measurement will also call for ILRS to organize International Laser Ranging Tracking Network to observe HY-2 satellite after launched. HY-2 satellite will become the second Chinese satellite tracked by international SLR network following Compass M1. This paper will introduce HY-2 satellite, its LRA and the plan of laser tracking.

## 2. HY-2 satellite Overview

Figure 1 shows the view of HY-2 satellite and the main orbit parameters is following:

- Altitude: 971km
- Eccentricity: 0.00117
- Inclination: 99.35 degree
- The orbit is sun-synchronous: the first 2 years with a 14-day cycle, then one year with geodetic orbit (168-day cycle, 5 day approx. subcycle)

[1] Shanghai Observatory, Chinese Academy of Sciences, China
[2] National Satellite Ocean Application Service, China

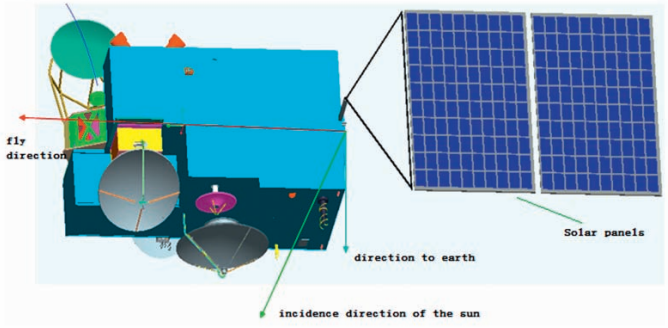


**Figure 1: The view of HY-2 satellite**

HY-2 will have the following instruments onboard:

- microwave altimeter for sea level change monitoring
- microwave scatterometer for sea surface wind measurement
- scanning radiometer for sea surface temperature measurement
- microwave radiometer for measurement of the integrated atmospheric water vapour correction
- GPS receiver for orbit determination with dual frequencies code and phase measurement
- Doris system for orbit determination by CNES
- LRA( Laser Retro-reflector Array) for orbit determination

# 3. Laser Retro-reflector Array for HY-2 satellite

The laser retro-reflector of HY-2 satellite adopted the structure of eight pyramids and the corner cubes made of fused quartz are symmetrically mounted on a hemispherical surface with one nadir-looking corner cube in the center, similar to Envisat, ERS-2, Jason-1/2. The angle between the normal of the center reflector and the side ones is 48 degrees. The size is 250mm×88.5mm and the weight is about 1.41kg. The photo of the LRA is shown in Figure 1.

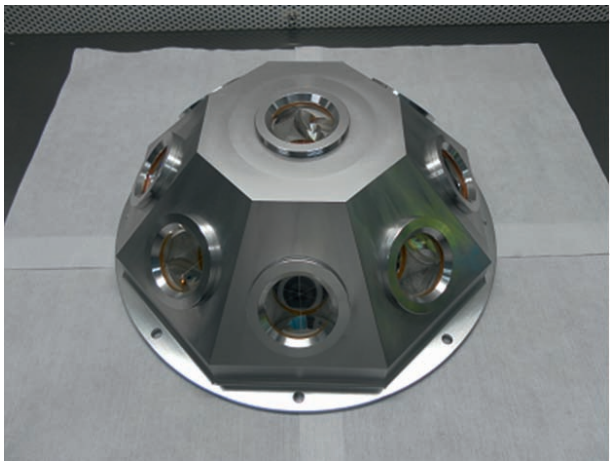

**Figure 2: The photo of LRA for HY-2 satellite**

# 4. Support from China and ILRS SLR network

At last workshop Yang Fumin reported that All of Chinese stations planed to develop kHz ranging under the support of CMONOC (Crustal Movement Observation Network of China). Four stations (Shanghai, Changchun, Beijing, Kunming) in China have been the capability of kHz ranging up to MEO satellites and daylight tracking since last year. Other three stations have been implementing kHz ranging. National Astronomical Observatory of China (NAOC) has got the funding for kHz improving of San Juan SLR station and the upgrading is in process.

In 2008, Chinese Compass M1 satellite was successfully tracked by international SLR stations and the routine SLR tracking data are being provided to precisely determinate its orbit. So, the SLR technique will be also regarded as one of important methods of precise orbit determination for HY-2 satellite.

At the end of 2010, most of Chinese SLR stations finished the systematic improvement and upgrade and the performances were advanced to a great extent. After HY-2 satellite launched, Shanghai Observatory will organize the Chinese SLR network to track it and call for ILRS stations to support global SLR tracking for HY-2 satellite.

Shanghai Observatory will also be the data center of HY-2 satellite to process and analyse the laser tracking data and provide the orbit prediction to SLR stations.

# 5. Summary

HY-2 satellite is the first one with the microwave altimeter, remote sensing systems for the oceanic environmental monitoring and related scientific researches for State Oceanic Administration of China and the accurate orbit parameters are necessary. So, several measuring techniques are adopted on HY-2 satellite to perform the precise orbit determination, such as Laser Retro Reflector Array (LRA), Doppler Orbit graph and Radio-positioning Integrated by Satellite (DORIS), Global positioning System (GPS). And Shanghai Observatory will organize the Chinese SLR network and call for ILRS committee to support global SLR tracking for HY-2 satellite after it launched. HY-2 satellite will become the second Chinese satellite tracked by international SLR network following Compass M1.

## Reference

*Yang Fumin,* 2008:*Upgrading Plan of the Chinese SLR Network*, Proceedings of the 16th International Workshop on Laser Ranging

## Correspondence

Wu Bin
No.80, Nandan Road
Shanghai
China

bwu@shao.ac.cn

# Narrow-band holographic spectral selector for satellite laser ranging: more stability, new spectral range

*V.L. Moshkov, V.D. Shargorodsky, A.P. Popov, Yu.L. Korzinin, A.V. Veniaminov,*

Serial production cycle of narrowband holographic selectors operating at SHG of YAG:$Nd^{+3}$ (532 nm) was discussed before.

New projects of the satellite laser ranging at 1064 nm require extension of the selector range to the near infrared. Hologram registration technology based on the application of UV He-Cd laser radiation in the photorefractive glass material is presented in the report. New selector operating at 1064 nm having 2 Angstroms spectral selectivity and about 80% diffraction effi-ciency was obtained and tested.

Production of narrowband holographic selectors for SLR in visible spectral range (mainly at 532 nm, second harmonic of $Nd^{+3}$ laser emission) has been previously reported [1]. The selectors are made by holographic recording of a reflection-type 3D grating in the polymeric material doped with phenanthrenequinone (PQ)[2-4]. The holograms are self-developed after exposure due to diffusive redistribution of PQ molecules within the polymer bulk at moderately elevated temperatures, without photopo-lymerization. The material is known for large thickness (up to a few millimeters), hence high selectivity and diffraction efficiency of holograms, very low shrinkage, and good stability of grating strength. Half-width of spectral selectivity contour 0.1 nm, diffraction efficiency 90% and lifetime exceeding several years are characteristic of the holographic selectors operating at 532 nm that were made on the basis of PQ-doped polymeric materials.

New projects aimed at SLR using Nd laser emission at 1064 nm require narrowband selectors capable to operate in NIR spectral range. Holograms efficient in this range can be recorded in PQ-based materials, too [2,5]. However, such features of the polymeric materials as photoinduced postexposure relaxation resulting in slight misalignment of Bragg wavelength/angle (though it can be mechanically or thermally compensated) and light absorption in NIR range (attributed to overtones of molecular vibrations) that may reduce the diffraction efficiency encourage the researchers to look for efficient thick light-sensitive materials free from these shortcomings.

In this contribution, we suggest recording spectral selectors for NIR range as reflection-type holographic elements in photo-thermo-refractive glass (PTRG), known also as multichromatic, or polychromatic glass.

The photo-thermo-refractive process invented in 1945 at Corning is based on photoinduced formation of micro- and nano-crystals in the bulk of $SiO_2$-$Al_2O_3$-ZnO-$Li_2O$($Na_2O$) glass doped with silver and cerium. In a few decades after invention, such glasses have drawn attention as holographic materials [6]. Under UV irradiation (e.g. 325 nm, He-Cd laser), photoionization of $Ce^{3+}$ occurs enabling regeneration of silver atoms, without noticeable change of refractive index. The diffraction efficiency of thus created "latent image" is below 0.01%.

Postexposure thermal treatment (development) gives birth to colloidal silver particles that in turn initiate growth of nano-crystals of NaF and NaBr, whose concentration, hence refractive index, reproduce the distribution of intensity in the interference pattern being recorded and form an extremely stable and efficient hologram (Fig.1).

The stability of 3D holograms in PTRG based on physical chemistry of glass matrix makes them promising candidates for the role of selective elements in laser systems.

Typical parameters of the selectors for SLR recorded in PTRG are as follows:

- operation wavelength 1064 nm
- diffraction efficiency 70 ÷ 80%
- diffraction angle 7.5°
- spectral selectivity (contour halfwidth) 0.2 nm
- aperture 20 mm

- thermal drift of wavelength < 0.02 nm/K
- operation/storage temperatures -160 ÷ +400°C
- lifetime (shelf or operation) > 10 years

The selectivity contour of PTRG holographic element is shown in Fig.2:

Hologram registration layout and sample of the registered selector are shown in Fig. 3 and 4 respectively.

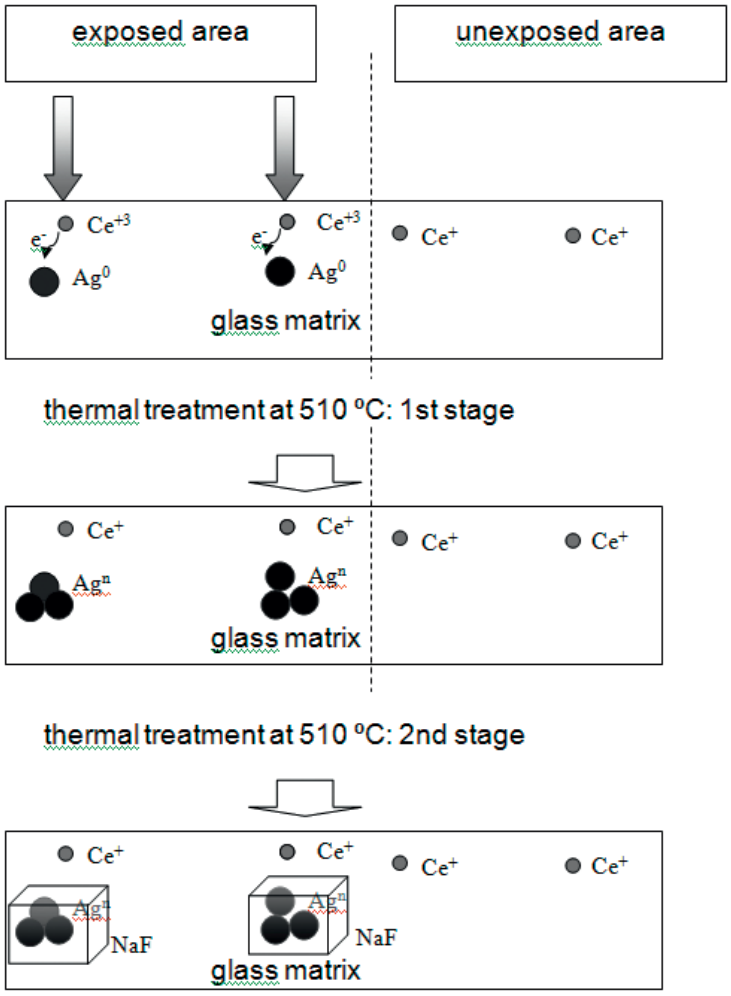


**Fig.1: Mechanism of hologram formation in PTRG**

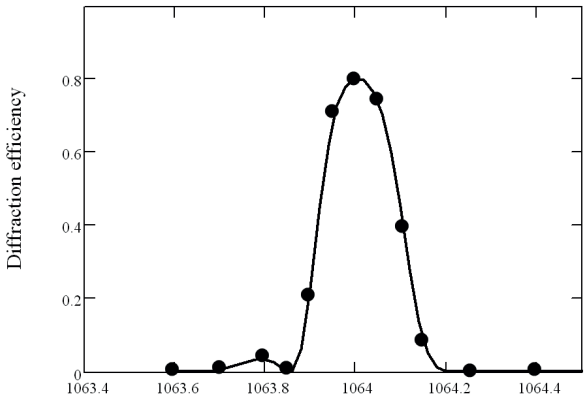


**Fig.2: Exemplary spectral selectivity contour of a holographic element recorded in PTRG**

**Fig. 3: Hologram registration layout**

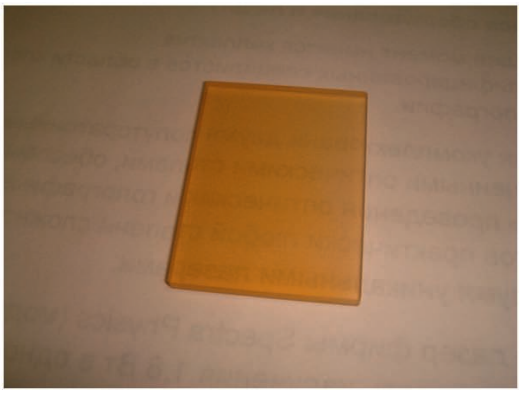

**Fig. 4: Holographic selector recorded in PTRG**

## References:


1. *Shargorodsky V.D., Popov A.P., Korzinin Yu.L., Veniaminov A.V., Moshkov V.L.,* 2008: Production of narrowband holographic selectors for SLR. Proceedings of the 16th International Workshop on Laser Ranging, Poznan, P.435-441.

2. *Semenova I.V., Popov A.P., Veniaminov A.V., Reinhand N.O.* 1999: Narrowband holographic spectral filters for the near-IR spectral range. Proc. SPIE, V. 3698. P. 910-917.

3. *Popov A., Novikov I., Lapushka K., Zyuzin I., Ponosov Y., Ashcheulov Y., Veniaminov A.* 2000: Spectrally selective holographic optical elements based on a thick polymer medium with diffusional amplification. J. Optics A: Pure and Applied Optics. V. 2. P. 494-499.

4. *Burzynski R., Weibel J.F., Casstevens M.K., Billmers R.I., Billmers E.J.,* 2003: Holographic wavelength filters based on MEMPLEX(r) photopolymer. Proc. SPIE. V. 4833. P. 577-583.

5. *Sato A., Kostuk R.K.* 2003: Holographic grating for dense wavelength division optical filters at 1550 nm using phenanth-renquinone-doped poly (methyl methacrylate). Proc. SPIE. V. 5216. P. 44-52.

6. *Glebov L.B., Nikonorov N.V., Panysheva E.I., Petrovskii G.T., Savvin V.V., Tunimanova I.V., Tsekhomski V.A.*1991: New Possibilities of Photosensitive Glasses for 3-Dimensional Phase Hologram Recording. Proc. SPIE. V.1621. P.21-32.


## Correspondence


Vladislav Moshkov
53 Aviamotornaya st. Moscow 111024
Russia OJC “RPC “PSI”

vlad_moshkov@mail.ru

# Russian Laser Tracking Network: Current State and Perspectives

*V.Burmistrov, N.Parkhomenko, M.Sadovnikov, V.Shargorodsky*

The Russian Laser Ranging Network includes 4 stations participating in the ILRS operation: three of them are within the Russian territory – the Altay Optical and Laser Center, the station near Komsomolsk-on-Amur, and the station in the Northern Caucasus – while the fourth is on the Baikonur launching site, in Kazakhstan.

It is intended to create three SLR/VLBI collocation points – in the Northern Caucasus, near Irkutsk, and near St. Petersburg.

It is also planned to create two stations outside the Russian Federation, using serially produced compact SLR systems; inter-state agreements are currently in preparation with Israel, Chile, and SAR.

A distributed control network is now under development, providing centralized control of operation of all Russian SLR stations. The control center should provide tracking planning and spacecraft orbit predictions, SLR network monitoring, and measurement date collection.

The Russian Laser Tracking Network has been established for applications in space geodesy, navigation, geophysics, and geodynamics.

In navigation, the SLR stations are used for determination of high-accuracy ephemeris corrections to GLONASS SC data, as well as for SC clock synchronization.

In geodesy, the stations are used for calibration of on-board RF ranging equipment of the GEOIK spacecraft.

Currently, the network consists of five stations: near Moscow, near Komsomolsk-on-Amur, at the Baikonur launching site, and in the Northern Caucasus (Arhiz). The station near Moscow is used for calibration of RF two-way ranging systems, as well as for clock synchronization within the GLONASS SC constellation.

## 1. Unified SLR station near Moscow (Shelkovo town)

**SLR system** **Telescope dome**

**Figure 1: Unified SLR station near Moscow (Shelkovo town)**

| Ranging | Angular measurements | Photometry |
|---|---|---|
| SC orbit height: up to 36,000km | Star magnitude up to: 14m | Star magnitude up to: 13m |
| | RMS of measurement 1 – 2 arcsec | Brightness measurement RMS error less than 0,2m |
| NP RMS errors: 0,5 to 1 cm | for SC angular velocity up to 40 arcsec/sec | |

## 2. Unified SLR station (transportable version) at the Baikonur launching site

**Figure 2: Working platform with the installed equipment, containers, and a telescope**

| Ranging | Angular measurements | Photometry |
|---|---|---|
| SC orbit height: up to 36,000km | Star magnitude up to: 14m | Star magnitude up to: 13m |
| | RMS of measurement 1 – 2 arcsec | Brightness measurement RMS error less than 0,2m |
| NP RMS errors: 0,5 to 1 cm | for SC angular velocity up to 40 arcsec/sec | |

## 3. SLR station near Komsomolsk-onAmur

**Figure 3: SLR station near Komsomolsk-onAmur**

| Ranging | Angular measurements | Photometry |
|---|---|---|
| SC orbit height: up to 36,000km | Star magnitude up to: 14m | Star magnitude up to: 13m |
| | RMS of measurement 1 – 2 arcsec | Brightness measurement RMS error less than 0,2m |
| NP RMS errors: 0,5 to 1 cm | for SC angular velocity up to 40 arcsec/sec | |

# 4. Altay Optic/Laser Center (AOLC)

**Figure 4: Altay Optic/Laser Center (AOLC)**

| Ranging | Angular measurements | Photometry |
|---|---|---|
| SC orbit height: up to 36,000km | Star magnitude up to: 14m | Star magnitude up to: 13m |
| | RMS of measurement 1 – 2 arcsec | Brightness measurement RMS error less than 0,2m |
| NP RMS errors: 0,5 to 1 cm | for SC angular velocity up to 40 arcsec/sec | |

# 5. The small-size SLR system "Sazhen – TM"

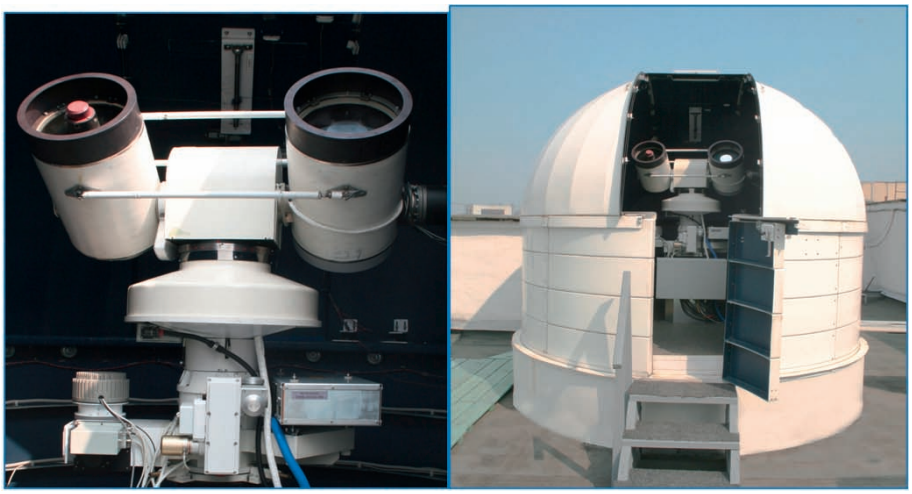

**Figure 5: The small-size SLR system "Sazhen – TM"**

The small-size SLR system is currently in serial production. During the 2011 – 2012, it is planned to install 21 such stations within the Russian territory and abroad. Three such stations will be used in combination with the VLBI systems near St Petersburg, near Irkutsk, and in the Northern Caucasus, to form collocation sites. The site in the Northern Caucasus is in operation since April, 2011

| Ranging | Angular measurements | Photometry |
|---|---|---|
| SC orbit height: up to 23,000km | Star magnitude up to: 12m | Star magnitude up to: 11m |
| | RMS of measurement 1 – 2 arcsec | Brightness measurement RMS error less than 0,2m |
| NP RMS errors: 0,5 to 1 cm | for SC angular velocity up to 40 arcsec/sec | |

**Figure 6: The small-size SLR system on VLBI station "Zelenchukskaya" of Kvazar complex**

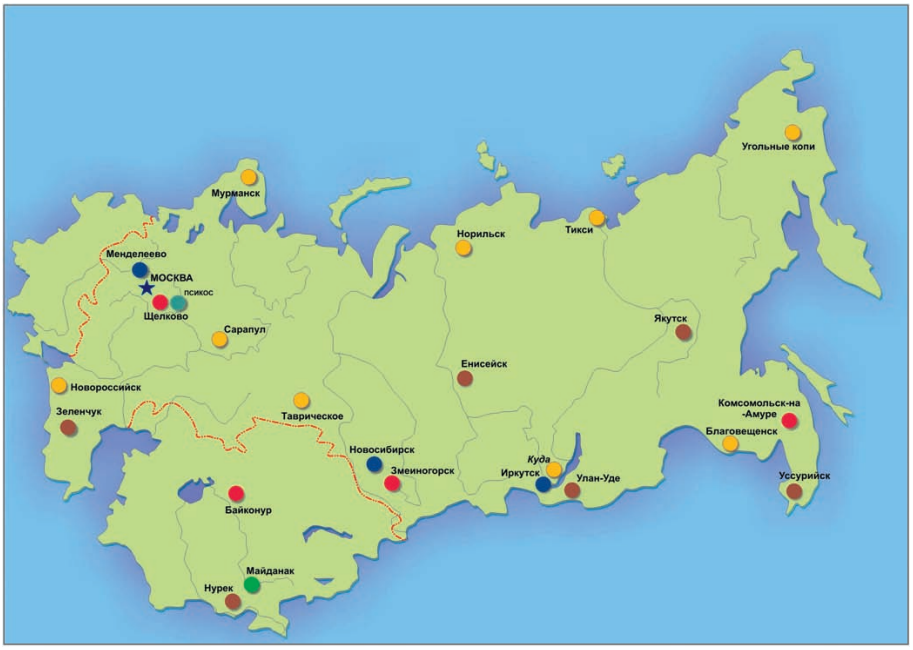


**Figure 7: DEVELOPMENT OF RUSSIAN LASER NETWORK STATIONS TO 2012**

## Correspondence

Natalia Parkhomenko
53 Aviamotornaya st. Moscow 111024
Russia OJC "RPC "PSI"

parknataliya@yandex.ru

# Solving ordinary differential equations with multi-precision libraries

*Martin Ettl, Manfred Schneider, Urs Hugentobler*

ABSTRACT

Modern earth observation techniques require precise knowledge about the position and velocity of observed satellites or other objects in space. Computing the position analytically no longer provides the necessary accuracy owing to the lack of an analytical high accuracy orbital theory. In order to gain accuracy, it is common practice to compute an orbit by solving ordinary differential equations (ODEs). Solving this kind of mathematical equation leads to well-tested standard methods like Runge-Kutta-methods, Burlisch-Stoer, symplectic or power-series integrators. These solvers have been implemented using C++-templates allowing us to change the floating-point data type at compile time. Therefore multi-precision data types with a free-to-choose decimal precision can be used. Based on this approach, each numerical solver can operate with variable internal precision. This, for instance, makes it possible to reveal round-off errors or missing accuracies by simply increasing the precision of the underlying data type. It can be used to verify computed or measured results with hitherto unavailable numerical accuracy. Solving an ODE with high accuracy using a multi-precision library requires more CPU-cycles. This is why the implemented algorithm has been profiled and highly optimized to avoid wasting CPU-cycles on our testing platforms.

## 1. Design and implementation

Numerically solving an Ordinary Differential Equation (ODE), from the programming perspective, is a task that can be split into three parts (*see figure 1, The design principle*). First of all an algorithm is needed, capable of solving an ODE. Each solver has its own characteristics and therefore specific pros and cons. Nevertheless, a standardized interface has been created using object-oriented inheritance, which allows us to plug any ODE into the solver. This design makes it possible to extend the available ODEs without touching the already well-tested implementation of the solving algorithm. The ODE can be implemented by simple derivation from a base class containing pure-virtual functions that must be implemented by the derived class. This separation of algorithm and mathematical problem into separate and independent components massively improves the re-usability of the software components. In general, all algorithms are implemented with basic datatypes, with fixed precision. This is why all the modules have been implemented as C++-template classes, which offers a way to implement the classes without this datatype dependency. Consequently, the corresponding standard or multi-precision datatype, used for the computation can be selected at compile-time. In the case of multi-precision, most of the datatypes used are capable of changing their internal decimal precision during runtime.

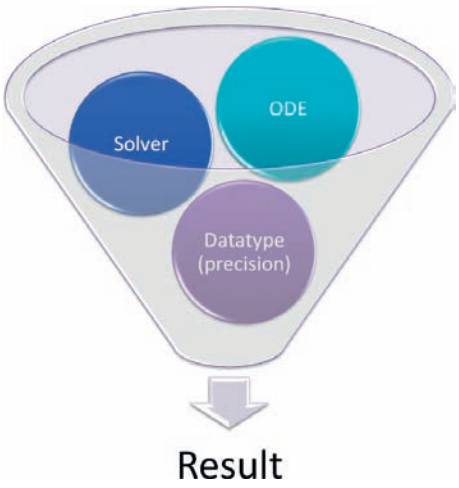


**Figure 1: The design principle**

# 2. Categorization of solvers

In *figure 2*, the implemented solvers are listed and grouped by their specific features. Each solving algorithm has its own characteristics. Some of the solvers have a built-in adaptive step-size control mechanism. This means, before the integration starts, the user can set an absolute and relative error-bound. According to this information, the integration-solver chooses the step-size automatically. Most of the algorithms are designed to solve ODEs of the first order, because an ODE of higher order can be transformed into a system of first-order ODEs. Nevertheless the GJ4 algorithm has been implemented, which is capable of solving second-order ODEs. Computing the next time-step (solving an ODE) can be done using different approaches. The single-step methods use only data from the last step, whereas the multi-step methods take into account former time-steps. The power series methods create and solve at each integration step a power-series, according to recursive laws of power-series composition. In this case, the order of the series is not fixed and can be set by the user. The symplectic solvers are designed to be more energy-conserving than others.

| solver | categorization | | | | | | |
|---|---|---|---|---|---|---|---|
| | adaptive stepsize control | ODE order | | single step | multistep | power series | symplectic |
| | | 1 | 2 | | | | |
| Shampine Gordon (SG) | ☑ | ☑ | | | ☑ | | |
| Burlisch Stoer (BS) | ☑ | ☑ | | | ☑ | | |
| Gauss-Jackson (GJ4) | | | ☑ | ☑ | | | |
| Runge Kutta 4.order (RK4) | | ☑ | | ☑ | | | |
| Runge Kutta 10.order (RK10) | | ☑ | | ☑ | | | |
| Dormand-Prince (DOPRI) | ☑ | ☑ | | ☑ | | | |
| Leap-Frog (LF) | | ☑ | | ☑ | | | ☑ |
| Symplectic (SYMP) 4.-, 6.-and 8.order | | ☑ | | ☑ | | | ☑ |
| Power series (POWSER) | | ☑ | | ☑ | | ☑ | |

**Figure 2: Categorization of available integration methods**

# 3. Results of long time evolution of Earth-Moon distance

In *figure 3* the results of a comparison of two different numerical simulations are shown. Both simulations were computed using the BS-solver with adaptive step-size control. Furthermore, identical settings and initial values were used to compute the orbit based on the LiDIA[1] multi-precision datatype. The first solution was computed with a decimal precision of 16 significant digits and the second with 38 significant digits. The plot shows the absolute errors for each coordinate and the distance along the integration time of 32 years. The plot also shows the absolute error in each coordinate starting to oscillate after approximately ten years' integration time. The absolute error in range increases after approx. 12 years, decreases and then accumulates to 0.5 m at approx. 28 years. During the integration the ODE-function was called ~300000 times. This possibly explains the increase of round-off errors, owing to millions of floating point operations over the whole integration. This possibility of checking for round-off errors using multi-precision methods is a very helpful technique for verifying results.

[1] http://www.cdc.informatik.tu-darmstadt.de/TI/LiDIA/

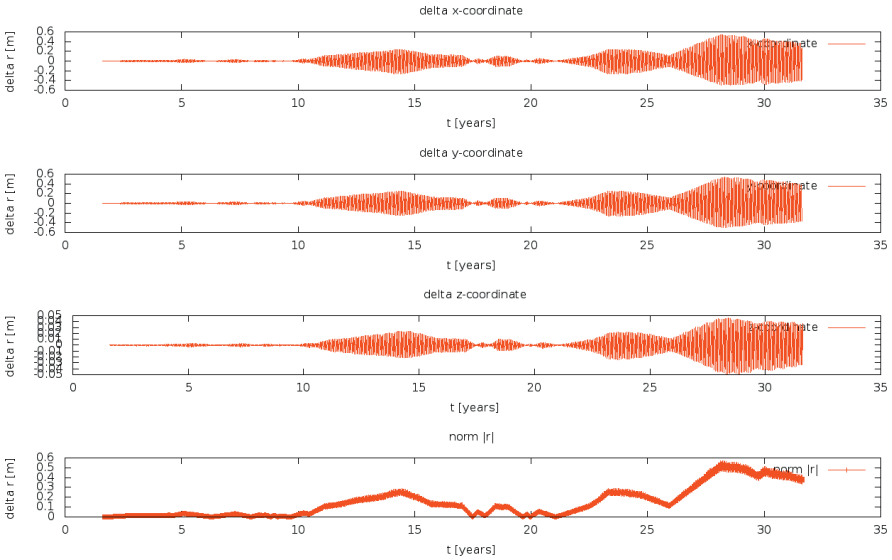


**Figure 3: Results of long time evolution of Earth-Moon distance**

## References

*Montenbruck Oliver*: Ephemeridenrechnung und Bahnbestimmung geodätischer Satelliten mit Hilfe der Taylorreihenintegration, Deutsche Geodätische Kommission, Reihe C, Disseration, Heft Nr. 384, München 1991

*Press H. William, Teukolsky A. Saul, Vetterling T. William, Flannery P. Brian*: Numerical Recipes in C, The Art of Scientific Computing, Third Edition, Cambridge University Press, ISBN 978-0-521-88068-8

*Reichhoff, Burkard*: Verfeinerung und objektorientierte Implementierung eines Modells zur Nutzung von Lasermessungen zum Mond; ISBN (Print) 3-7696-9550-X, 1999

*Schneider Manfred*: Himmelsmechanik Bd. I - Grundlagen, Determinierung, 3., völlig neu bearbeitete und erweiterte Auflage, BI-Wiss.-Verlag, ISBN-3-411-15223-0

*Sutter Herb, Alexandrescu Andrei*: C++ Coding Standards -101 Rules, Guidlines, and best Practices, Pearson Education, 2005, ISBN 0-321-11358-6

*Vandevoorde David, Josuttis Nicolai M.*: C++ Templates - The Complete Guide, Pearson Education, 2008, ISBN 0-201-73484-2

*Yoshida Haruo*: Construction of higher order symplectic integrators, NationalAstronomical Observatory, Mitaka, Tokyo 181 Japan, 1990, Phys. Lett. A 150: 262. doi:10.1016/0375-9601(90)90092-3

## Correspondence

Dipl. Inf. Ettl Martin
Geodätisches Observatorium Wettzell
Sackenrieder Str. 25
D-93444 Bad Kötzting

ettl@fs.wettzell.de

Prof. Dr. Manfred Schneider
Institut für Astronomische und Physikalische Geodäsie
Technische Universität München
Arcisstr. 21
80333 München

mxsx.tum@t-online.de

Univ.-Prof. Dr. phil. nat. Urs Hugentobler
Institut für Astronomische und Physikalische Geodäsie
Technische Universität München
Arcisstr. 21
80333 München

urs.hugentobler@bv.tum.de

# Using Pulse Position Modulation in SLR stations to transmit data to satellites

*G. Kirchner, F. Koidl, D. Kucharski*

ABSTRACT
The laser repetition rates of SLR stations vary from 10 Hz to 2 kHz. At the Graz 2 kHz SLR station, we upgraded the software to modulate the – usually constant – interval between laser pulses; using such a Pulse Position Modulation (PPM) scheme, we successfully transmitted text files via a 4288 m distant CCR back to a Multi-Pixel Photon Counting (MPPC) module in our receiver telescope. With such a setup at any SLR station, and a suitable detector plus simple time tagging electronics at Low Earth Orbiting (LEO; < 1000 km) satellites, it is possible for any kHz SLR station to transmit data to satellites with a rate of up to 2 kBytes/s - even during standard SLR tracking.

As this technique is easy to implement and does not affect routine kHz SLR tracking, it can be applied to upload data to satellites, using the more than 30 available SLR stations around the world, and with higher data rates than some of the conventional microwave uplinks.

## 1. Introduction

The laser repetition rates used at different SLR stations may vary from 10 Hz to 2 kHz (*M.R. Pearlman et al*, 2002). At the Graz 2 kHz SLR station, we upgraded the software to modulate the – usually constant – interval between laser pulses; using such a Pulse Position Modulation (PPM) scheme, we successfully transmitted text files via a 4288 m distant CCR back to a Multi-Pixel Photon Counting (MPPC) module in our receiver telescope. With such a setup at any SLR station, and a suitable detector plus simple time tagging electronics at Low Earth Orbiting (LEO; < 1000 km) satellites, it is possible for any kHz SLR station to transmit data to satellites with a rate of up to 2 kBytes/s - even during standard SLR tracking.

As this technique is easy to implement and does not affect routine kHz SLR tracking, it can be applied to upload data to satellites, using the more than 30 available SLR stations around the world, and with higher data rates than some of the conventional microwave uplinks.

Using laser repetition rates of e.g. 10 kHz – as planned at Graz SLR – it is possible to transmit standard GSM coded speech to a LEO satellite.

## 2. PPM Scheme for Graz 2 kHz SLR Station

### 2.1 Basic principle

The PPM scheme we used for first tests encodes one single byte into each laser firing interval. The routine SLR procedure – without any PPM - uses constant intervals of 500 µs; detecting a minimum of 100 consecutive pulses with such a 500 µs interval (but allowing for the intrinsic ± 7 ns variations of the laser itself) establishes the basic grid for the PPM application (fig. 1, top). To apply PPM, we insert for each laser firing command small additional delays against this basic grid (fig. 1, bottom); the amount of this delay determines the byte value.

### 2.2. Suitable detector for SLR PPM

Our standard detector for SLR is a C-SPAD: A Single-Photon-Avalanche-Diode with time-walk compensation; while this is an excellent device for SLR, it is not suitable as a PPM detector: It is single-photon sensitive, thus reacting on any arriving

background photon; in addition, at 2 kHz gating rate it produces a dark noise of about 400 kHz – when gated, a break occurs after about 2.5 µs average, without any photons involved; all that ends up in a lot of noise points, prohibiting its use as a PPM detector.

Instead, we used a Hamamatsu Multi-Pixel Photon Counter Module (MPPC; C10507-11-050U, ); this device consists of 400 SPAD elements of 50 x 50 µm each, arranged in a square of 20 x 20 SPADs on a single chip (fig. 2); all 400 outputs are summarized on a single pin. Although it produces even more dark noise (up to 800 kHz) than our SLR SPAD, the resulting dark noise pulse amplitudes are according to single photons only; however, if a 10 ps laser pulse from our SLR laser arrives, it triggers many or all of the 400 SPAD elements simultaneously; the combined outputs are superimposed in a much higher – analogue - output pulse; thus, although such a MPPC remains basically single-photon sensitive, it can easily discriminate our laser pulses against very high dark noise and against significant background noise.

The leading edge of the MPPC analogue output is discriminated by a fast comparator with adjustable trigger level; the TTL output of this comparator is connected to the ISA FPGA PC card. A simple 5 ns counter in this FPGA time tags the events; the 5 ns resolution of this counter is sufficient to resolve the number of 80 ns multiples. The PC reads these event times, and decodes the corresponding ASCII values.

## 2.3 Test Setup

The Laser Control PC read one of several ASCII text files, and pointed the telescope to a retro-reflector in a distance of 4288 m. The attenuated laser fired to this target, and on request of the observer it applied PPM to the laser firing epochs to encode the characters of the selected ASCII text file.

The photons reflected from the retro-reflector were detected by the MPPC, which was mounted in the main SLR receiving telescope; with proper attenuation of the incoming photon stream, the MPPC produced the required output pulses, their epoch times were decoded, and the complete ASCII text file recovered and compared with the original file.

## 2.4 Detecting the SLR photons at the satellite

A typical kHz SLR station – example: Graz SLR – tracks LEO (Low Earth Orbiting) satellites with a divergence of the laser beam of about 20 arc seconds; the advantages of such a relatively high divergence are less demanding tracking requirements, and insensitivity against atmospheric seeing effects, beam wander etc.

With a single shot energy of 400 µJ @ 532 nm, the Graz SLR station transmits about $10^{14}$ photons per shot; at a typical LEO distance of 1000 km, the beam diameter will be roughly 100 m; a single 50x50 µm pixel of the MPPC thus will see an average of about 32 photons; this amount of photons will trigger most of the 400 MPPC pixels, resulting in a well determined analogue output pulse of the MPPC module.

At low energy kHz SLR stations, tracking HEO satellites requires the minimum laser beam divergence ($<$ 5 arc seconds for Graz kHz SLR), which than still results in about 14 photons per MPPC pixel in about 6000 km; but this small divergence in turn causes much higher sensitivity to atmospheric turbulence, beam wander etc; while this only reduces SLR results, it is more or less prohibitive for the suggested simple PPM uplink channel.

# 3. Applications

There are more than 30 active SLR stations around the world; within the next few years, about one third of them will use kHz lasers – with repetition rates between at least 0.1 and up to 2 kHz; there are also plans for higher repetition rates on some stations. In principle, many of these kHz SLR stations could be easily and with minimal costs upgraded to perform such PPM based data uploads to satellites. The available data rate is given mainly by the laser repetition rate; the 2 kHz at Graz result in a maximum of 2 kbytes/s, which is already significantly more than e.g. the microwave upload rate to the satellite CHAMP (119 bytes/s).

On the satellite side, the only requirement is the installation of a suitable receiver (e.g. MPPC) and some simple electronics (basically a 5-ns time tagging unit); the energy density of the laser beam at least in satellite orbits up to 1000 km is enough to trigger reliably most elements of such an MPPC, without the need for additional optics or telescopes; the

only requirement would be a 532 nm filter of at least 1 nm bandwidth (to allow for incidence angle variations). Such a satellite add-on would be of low weight (a few 100 g) and low power consumption.

To verify the successful transmission of data to the satellite, all conventional techniques for error detection and / or correction can be applied (parity bits, checksums, cyclic redundancy checks, error correction codes like the Verhoeff algorithm etc.). In addition, a basic check is possible also at the SLR station: If the satellite is equipped also with a CCR, it can be assumed that if a specific shot produced a valid return at the SLR station, this shot DID hit the detector on the satellite, and should have triggered the MPPC there.

In addition, using a standard simple microwave down-link from satellite to a receiver at the SLR station could provide a real-time feedback, allowing immediate re-transmission of any missing or disturbed data.

A simple first test could be with ACES, flying on the ISS within the next years; for time transfers, there will be already a CCR on board; adding the MPPC and the mentioned simple electronics would complete the test setup there.

# 4. Limitations and improvement possibilities

## 4.1 Data Rate Considerations

The data rate is limited by the repetition rate of the laser used at the SLR system; at present, the maximum repetition rates in use are 2 kHz (e.g. Graz, Herstmonceux); some SLR stations are upgrading to 2 kHz (Potsdam, Metsahövi) or use up to 1 kHz laser systems (Shanghai, Changchun, TIGO). Repetition rates of up to 10 kHz are feasible; above that there are limitations due to overlapping transmit / receive pulses, detector noise problems and event timer speeds.

The selected basic value for the PPM delay unit (80 ns chosen in our tests) has to cover mainly the ± 7 ns variations of the laser; and it has to take into account also the motion of the target satellite in orbit between 2 consecutive laser shots; for a 2 kHz SLR station, the minimum value to cover both effects is about 50 ns; the maximum value depends on the chosen encoding system (or number of different values to encode); the maximum resulting delay should not be more than about 10% of the standard laser pulse interval for undisturbed operation of the laser itself (for the Graz 2 kHz laser this would be 50 µs maximum); using a 255 character set for the PPM, the maximum delay unit than is 50 µs / 255 (about 200 ns); however, since this value does not affect PPM data rate nor the basic SLR operation, the exact value is not critical at all.

A slightly modified PPM scheme – the differential pulse-position modulation, or DPPM – encodes each pulse position relative to the previous pulse, such that the receiver has to measure only the difference in the arrival time of successive pulses. This limits the propagation of errors to adjacent symbols, so that an error in measuring the differential delay of one pulse – or errors due to a single missed pulse - will affect only two data bytes, instead of affecting all successive measurements. However, this modified PPM scheme slightly reduces the SLR repetition rate, and was therefore not implemented and tested in Graz.

## 4.2 Problems due to atmospheric seeing, clouds, beam wander ...

Due to the used optical wavelengths (532 nm in almost all SLR stations), optical visibility in the line of sight to the satellite is required; any clouds, fog etc. will prohibit SLR as well as successful data transmission; therefore, the above mentioned conventional techniques for error detection and / or correction should be applied.

Microwave uplinks to satellites use beam divergences in the order of 0.1° to 1° (depending on band, antenna size *(Kumar,2008)*), simplifying the required tracking accuracy; however, the optical wavelengths used in SLR allow – and require - much narrower beams, in the order of a few arc seconds (for High Earth Orbiting satellites, HEO) to several tens of arc seconds (for LEO satellites). Because the suggested PPM data uplink is targeting at LEO satellites only, the tracking requirements for any SLR station are rather reduced. And even with the relatively weak pulses of Graz kHz SLR station (400 µJ per pulse, according to about $10^{14}$ photons), a divergence of up to 20 arc seconds – as used for LEO satellites – is sufficient for about 32 photons for any 50x50 µm pixel of the 400-pixel MPPC.

The relaxed divergence demands for LEO satellites allows neglecting effects of atmospheric seeing (most times between 4 and 10 arc seconds in Graz), which is generally a problem for optical uplink channels to HEO satellites *(Morio Toyoshima, 2008)*. In addition, optical uplinks to satellites are less affected by atmosphere than optical downlinks, mainly due to the relatively smaller beam sizes in relation to the atmospheric inhomogeneity.

## 4.3 Non-constant intervals due to Overlap Avoidance Procedures

In case of kHz SLR, always multiple laser pulses travel simultaneously between station and satellite; if one or few photons from a previous laser shot arrive at the same time when a new laser shot is fired ("overlap situation"), the backscatter of the new laser shot will increase significantly the noise as seen by the detector. To avoid this, most kHz SLR stations use some overlap avoidance procedure; all of these methods are modifying or changing the otherwise constant time intervals between laser pulses.

The overlap periods for LEO satellites are shorter (few seconds), and due to relatively high return signals – up to a few 1000 photons per shot - less severe than for HEO satellites (which are tracked with return quotes of 0.1% average – only 1 out of 1000 shots results in a single detected photon). Therefore, the overlap problem is less perturbing for LEO satellites.

Therefore it can be tolerated for the PPM application to LEO satellites to switch off these overlap avoidance procedures; according to tests at Graz kHz SLR station, the resulting increased noise at the SLR station receiver for several short periods throughout a standard satellite pass can be handled without problem.

## 4.4 Space qualified detectors

If the MPPC is considered as detector for the PPM SLR uplink channel, its space qualification must be proven; according to the manufacturer, this has not been done yet. In case the MPPC it NOT space qualified, any other linear detection device based on a photon detector in linear gain mode may be used; such a space qualified detector is successfully used e.g. for the T2L2 experiment (*E. Samain et al*, 2007) on the LEO satellite Jason-2.

# 5. Conclusion

Applying simple Pulse Position Modulation (PPM) to the firing times of laser pulses at existing and operational kHz SLR stations, offers an opportunity for a new data upload channel to satellites in orbits up to about 1000 km. The only requirement at the satellite side is a simple photon detector without the need of optics – except a simple laser wavelength spectral filter -, a 5 ns resolution time tagging unit, and possibly a CCR; on the kHz SLR station side, the upgrade depends on the specific hardware, but in many cases that would be simply a few more lines of software to control the laser firing times of the SLR station with an accuracy of some nanoseconds.

## References


*M.R. Pearlman, J.J. Degnan, J.M. Bosworth, (2002)*: "The International Laser Ranging Service" Advances in Space Research, Vol. 30, No. 2, pp. 135-143,DOI:10.1016/S0273-1177(02)00277-6.

http://ilrs.gsfc.nasa.gov

http://sales.hamamatsu.com/de/produkte/solid-state-division/si-photodiode-series/mppc-modules

*A. Kumar, V.K. JAIN (2008)*: "Antenna Aperture Averaging and Power Budgeting for Uplink and Downlink Optical Satellite Communication". IEEE International Conference on Signal Processing, Communications and Networking; Madras Institute of Technology, Anna University Chenmai India, Jan 4-6, 2008, pp 126-131

*Morio Toyoshima(2008)*: "Trends in satellite communications and the role of optical free-space communications". National Institute of Information & Communications Technology, Koganei, Tokyo 184-8795, Japan; OCIS codes: 010.0010, 010.1330, 010.3310, 060.4510, 350.6090.

*E. Samain, P. Vrancken, J. Weick, P. Guillemot, 2007:* "T2L2 flight model metrological performances," www.storming-media.us/97/9713/A971305.pdf

## Correspondence

Georg Kirchner
Observatory Lustbühel
Lustbühelstr. 46
A-8042 Graz
AUSTRIA

Georg.Kirchner@oeaw.ac.at

## Captions / Figures

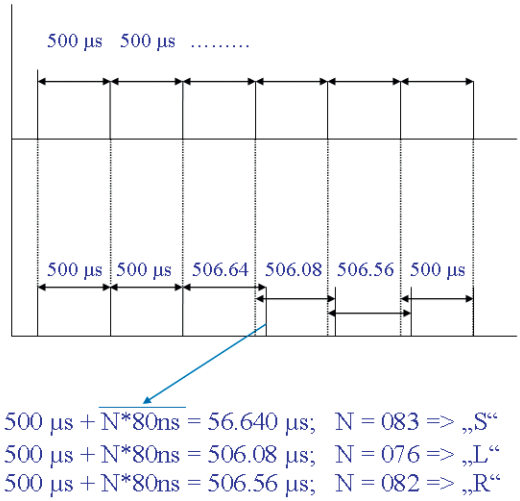


**Fig 1:** **Top: Basic Grid: Constant 500 µs intervals;**
**Bottom: Deviations from grid in 80 ns multiples define the ASCII value of the byte**

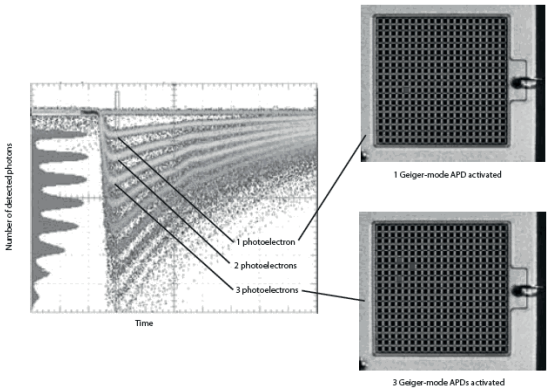


**Fig. 2: Hamamatsu C10507-11-050U MPPC (Multi-Pixel Photon Counter) with 400 pixels, arranged in a 20x20 pixel (each pixel 50x50 µm) matrix, with a common output line (by courtesy of Hamamatsu)**

# SLR for LEO Ranging

*M.Abele, J.Balodis, A.Rubans, G.Silabriedis, A.Zarins*

ABSTRACT

Already 2 years around since SLR for Low Earth Orbiters (LEO) ranging has been operational at the Institute of Geodesy and eoinformation (GGI). The test observations has approved the capability of SLR for LEO ranging, including LAGEOS, ERS2, ENVISAT, Ajisai and others. Regular observations has not been done for different reasons. However, the SLR system is operational.The SLR hardware and control software is designed in GGI by integrating advanced industrially produced components. The experience gained by the SLR personnell in Riga and in Australia has been applied. There is an alt/alt original small size telescope mount, EKSPLA diode pumped 17 mJ laser used with a repetition rate 50Hz and a 35 psec pulse width. A032-ET event timer and the Quartzlock (UK) GPS steered time service applied. Hamamatsu PMT used. SLR is placed on the roof of 150 years old 5 storey University building. The manual corrections for the laser beam poining has been applied by using digital imagery on the screen of computer. The guiding digital imagery of the sky has been obtained using sensitive CCD matrix.

The joint system of both the GNSS network and SLR will be applied for LEO satellite positioning. The system consists of a EUPOS-RIGA GNSS RTK five reference station network. The JAVAD GNSS chock ring antennas calibrated in Garbsen, Germany. The heights of antennas were additionally controlled by levelling to the 1-2 order levelling benchmarks. The analysis centre's server at the Institute of Geodesy and Geoinformation of the University of Latvia (GGI) and the GNSS receivers connected via optical cables. The signal from each receiver is received in GGI with a latency of 1-2 msec. The Geo++ network solution software GNSMART is used. EUPOS-RIGA is operational more than 5 years and its RTCM correction data is widely used by land surveyors.

Recently the construction of the digital zenith camera for the studies of vertical deflection has been commenced in GGI.

## 1. Institute of Geodesy and Geoinformation, University of Latvia

The Institute of Geodesy and Geoinformation (GGI) is a research & development unit of the University of Latvia. The predecessor was Institute of Geodesy established in 1924 which was closed during the Soviet time. The Institute of Geodesy and Geoinformation was established at 1994 on the bases of Astronomical Observatory of University by quitting it. The experienced astrometry software developers switched their activities to digital mapping and geoinformation. The SLR construction experts commenced the development of PSLR (Abele et al., `996).

Currently the Institute consists of two departments:

Department of Geodesy and Department of Geoinformation. The main topics of the activities are:

Department of Geodesy –

- Satellite laser ranging and SLR hardware, and software development;
- Riga multifunctional GNSS positioning system is " *EUPOS*®- RIGA ".(5 GNSS station network) participating in the project *EUPOS*®
- Mobile Zenith digital camera for detection of vertical deflection currently under development;
- Time series calculation of weekly solutions of *EUPOS*®- RIGA and LATPOS (24 station network). SINEX data files forwarded to ECC (*EUPOS*® Combination Centre) in Fomi Geodetic Observatori (Hungary).

Department of Geomatics –

- Development of 2D and 3D country-wide geographical databases,
- Development of large urban geographical databases and DEM,
- Development of highly detailed local geographical databases.

# 2. Satellite laser ranging system

SLR for Low Earth Orbiters (LEO) (Abele et al.,2008) has started operational tests at the Institute of Geodesy and eoinformation (GGI) since 2009. The test observations has approved the capability of SLR for LEO ranging, including LAGEOS, ERS2, ENVISAT, Ajisai and others. Unfortunately, financial shortage has no allowed regular observations.

The SLR mechanical and optical components and control software are designed in GGI. Telescope mount is alt/alt type with a 30 cm main mirror, independent 7 cm guide telescope (equiped with a CCD matrix), and 5 cm laser collimator. Transmitted pulses are provided by EKSPLA diode pumped 17 mJ laser with repetition rate of 50 Hz and 35 psec pulse width. Receiver (a Hamamatsu PMT) is placed directly in the main focus. A032-ET event timer and Quartzlock GPS-disciplined quartz time standard are used for time interval measurement. Presently SLR is installed on the roof of the University building.

The present mechanical construction of mount has been extensively revised during design and should be considered a model and eventually replaced for it does not provide mechanical accuracy needed for blind or day-time observations so that manual corrections of transmitted beam position (collimator alignment) and satellite image position are necessary during tracking.

**Figure 1: SLR mount**

**Figure 2: Collimator and alignment motors**

SLR control software is MS Windows based, communicates with external devices via USB, RS-232 and TCP/IP. All tasks except event timer control (running on a separate computer) are implemented in a single control program. Functionality includes:

- mount position control via USB, using encoders and stepper motors,
- tracking speed up to ~10 dg/s, tracking accuracy up to encoder resolution.
- Real-time mode implemented using multimedia timer, up to 1 kHz control frequency,
- synchronization of tracking events with external time reference using a standard counter-timer extension PCB, about 1mks accuracy,
- communication to time interval counter via TCP/IP, many stop events per each start event supported, multi-pulse mode possible,
- real-time visualization of ranging results with filtering and possibility to adjust range gate and prediction time delay,

- result processing and generation of normal points,
- mount error model and orientation subsystem, Hipparcos star catalog used
- meteo subsystem.

**Figure 3: Tie to local network**

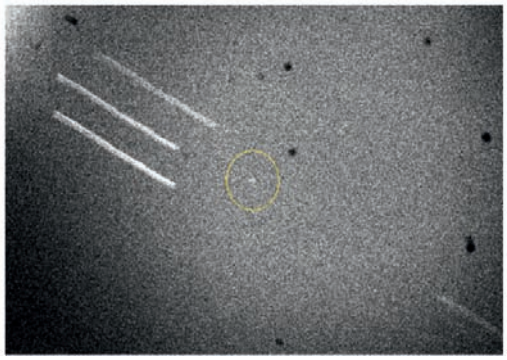

**Figure 4: LAGEOS image using for tracking CCD camera**

Test ranging results confirm SLR ability to reach low and medium (Lageos) range satellites. Return rate for low satellites is up to 50%, for Lageos up to 1-2%. Accuracy, as might be expected for PMT, is 1-4 cm for single shot RMS, 5-10 mm for normal point RMS, probably can be improved adjusting pulse processing and analyzing return pulse amplitude.

**Table 1: Test results**

| | Date | Satellite | Points | RMS (cm) | NP | RMS (cm) |
|---|---|---|---|---|---|---|
| 1 | 2009.04.13. | Ajisai | 661 | 3.1 | 9 | 0.64 |
| 2 | 2009.04.16. | Jason2 | 752 | 4.0 | 9 | 0.54 |
| 3 | 2009.04.16. | Ajisai | 631 | 4.7 | 6 | 0.62 |
| 4 | 2009.10.06. | Ajisai | 1894 | 4.2 | 13 | 0.70 |
| 5 | 2009.10.06. | Jason1 | 9 | 1.7 | | |
| 6 | 2010.04.13. | Lageos1 | 33 | 1.9 | 2 | 1.01 |
| 7 | 2010.04.19. | Lageos2 | 58 | 2.1 | 3 | 0.66 |
| 8 | 2010.04.19. | ERS2 | 368 | 2.7 | 11 | 1.0 |
| 9 | 2010.04.20. | Lageos1 | 97 | 3.4 | 2 | 0.54 |
| 10 | 2010.04.26. | ENVISAT | 1212 | 2.7 | 16 | 0.70 |
| 11 | 2010.04.26. | ERS2 | 1539 | 2.3 | 17 | 0.41 |
| 12 | 2010.04.27. | Jason2 | 210 | 3.1 | 10 | 0.65 |

# 3. GNSS network *EUPOS*®-RIGA

The continuosly operating dense GNSS RTK network has been developed at the countries of Easten Europe named *EUPOS*® (Sledzinsky, Graszka, 2010). GNSS stations situated at a distanves of about 50-70 km covering the area of whole region. *EUPOS*® network consists of subnetworks developed by each national country geodesy and mapping authority. All *EUPOS*® member countries use the common operation standards. The LATPOS subnetwork (24 stations) developed by Latvian Geospatial Information Agency (Zvirgzds, 2007).

The *EUPOS*®-RIGA GNSS subnetwork covers the territory of Riga city and it is surrounding SLR site. The system has been developed in co-operation of Municipal surveying company "Rigas GeoMetrs" and GGI. It consists of a *EUPOS*®-RIGA GNSS RTK five reference station network located at a distances from 20 m to 17 km from SLR. The GNSS chock ring antennas calibrated in Garbsen, Germany (Schmitz and Wubbena, 2008). The heights of antennas were additionally controlled by levelling to the 1-2 order levelling benchmarks. The analysis centre server is placed at GGI, close to the SLR control unit. The Geo++ network solution software GNSMART is used. EUPOS®-RIGA is operational more than 5 years and its RTCM correction data has been used for the research control of the geodetic network of Riga city. In daily routi-

ne they are being used by individual land surveyors. All the collected GNSS observations has been stored for the further research. The computation of the time series of LATPOS and *EUPOS®*-RIGA are in process now by using Bernese software v.5.0. The year 2008 (Jul-Dec), 2009 and 2010 observations are processed already and analyses results reported (Balodis et al., 2011).

# 4. Digital zenith camera

Recently the new construction of the digital zenith camera for the studies of vertical deflection has been commenced in GGI. The project is funded by European structural funding. The aim is to develop the camera for the omprovement of national geoid model and study the gravitational field anomalies.

## References


*M.Abele, J. Balodis, L. Brodie-Hall, W. Decker, U.K. Rao, A. Rubans, O. West, J. Vjaters, A. Zarinjsh*. Field tests of GPS Steered Portable Satellite Laser Ranging System. International Association of Geodesy. Section I - Positioning. Commission X - Global and Regional Geodetic Networks. Subcommission for Europe (EUREF). Publication No. 5. Report on the Symposium of the IAG Subcommission for the European Reference Frame (EUREF) held in Ankara, Turkey, May 22-25, 1996. Munchen 1996. pp. 319-324.

*M.Abele, J.Balodis, M.Caunite, I.Janpaule, Rubans, G.Silabriedis, A.Zarinsjh*. Engineering process of SLR for LEO orbiters. Proceedings. 16th International Laser Ranging Workshop. Poznan, Poland, 13-17 October 2008. pp 641-643. Published December 2009. Publisher: Space Research Centre, Polish Academy of Sciences

*J.Sledzinski, W.Graszka*. The European initiative of establishment of multifunctional satellite reference stations in Central and Eastern Europe.. Proceedings of the International Symposium on Global Navigation Satellite Systems, Space-based and Ground-based Augmentation Systems and Applications. Berlin, ISBN 978-3-938373-93-4. Germany, 1-2 December 2009. pp. 13-16.

*J.Zvirgzds.* 2007. Geodetic surveying by using GPS base station network LatPos. In: Riga Technical University Research. Ģeomātika. Vol.11. No.1. pp.81-89. (In Latvian)

*M.Schmitz, G.Wubbena*. Absolute robot-based GNSS antenna callibration – features and findings. Proceedings of the International Symposium on Global Navigation Satellite Systems, Space-based and Ground-based Augmentation Systems and Applications. Berlin, ISBN 978-3-938373-93-4. Germany, 11-14 November 2008. pp. 52-54.

*Balodis J,, Haritinova D., Janpaule I, Morozova K., Normand M., Silabriedis, G., Zvirgzds J.* GNSS Network Station's Time Series Analyses". Proceedings of the International Symposium on Global Navigation Satellite Systems, Space-based and Ground-based Augmentation Systems and Applications. Berlin, Germany, ISBN 978-3-938373-94-1. Germany, 10-11 October 2011.

# ILRS Website Redesign

*Carey Noll (NASA GSFC, Greenbelt MD, USA)*
*Lisa Lee (SGT, Inc., Wallops VA, USA)*
*Mark Torrence (SGT, Inc., Greenbelt MD, USA)*

ABSTRACT
The ILRS website, *http://ilrs.gsfc.nasa.gov*, is the central source of information for all aspects of the service. The website provides information on the organization and operation of ILRS and descriptions of ILRS components, data, and products. Furthermore, the website and provides an entry point to the archive of these data and products available through the data centers. Links are provided to extensive information on the ILRS network stations including performance assessments and data quality evaluations. Descriptions of supported satellite missions (current, future, and past) are provided to aid in station acquisition and data analysis. The current format for the ILRS website has been in use since the early years of the service. Starting in 2010, the ILRS Central Bureau began efforts to redesign the look and feel for the website. The update will allow for a review of the contents, ensuring information is current and useful. This poster will detail the proposed design including specific examples of key sections and webpages.

## 1. Website Style

The redesigned ILRS website is divided into six main sections (level 1 pages) that are accessible through the top horizontal navigation bar:

- About ILRS
- Network
- Missions
- Science
- Data & Products
- Technology

Horizonally, each page is divided into three sections: Top Banner, Content, and Bottom Footer. The top banner section contains the ILRS branding, a search box, and links to the IAG and GGOS. Clicking on the ILRS' logo or text in the banner will always return the user to the ILRS home page. The middle content section contains the page heading, the navigation (both top and left side) as well as the page content itself. The bottom footer section contains required NASA GSFC content such as contacts, date of last update, and policy statements. The footer also includes the GGOS logo which links to the GGOS website.

The new design for the ILRS website also uses a vertical, multi-column layout. Both horizontal (persistent on all pages) and vertical (on lower level pages) menus are used for navigation through the site. This presentation provides extensive information in an organized fashion allowing the user to easily find main topics of interest. Rotating images are placed on the home page and inital pages of each main section.

Drop-down menus from the horizontal navigation bar allow for quick navigation to the initial, or level 1, pages within each main section. Navigation within these sections, to level 2, 3, etc. pages is accomplished through links on the left vertical navigation column.

All links to pages outside of the ILRS website open a new browser window, which further emphasizes that the user is leaving the ILRS website.

# 2. Site Layout

## 2.1 Home Page

The new design for the ILRS home page (the Level 0 page of the ILRS website), shown in Figure 1, includes three main logical areas: ILRS Overview (left panel), Welcome and Highlights, (center panel), and lists of Recent News/Meetings/ Publications (right panel). Popular pages are included in a "quick links" section to allow users to easily navigate to these important sections of the website. This organization allows for quick access to prime content.

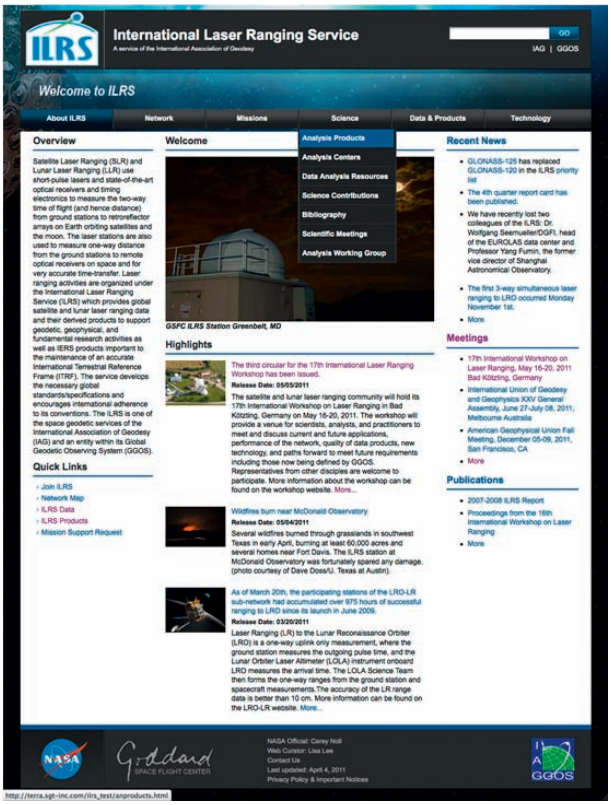


**Figure 1: Design for New ILRS Home Page**

The Highlights section contains brief science, mission, network stories with pictures and links to complete text. Brief lists of recent news, upcoming meetings, and recent publications link to more complete information.

## 2.2 Lower Level Pages

### 2.2.1 Level 1 Pages

The Level 1 pages are the top-most pages for each of the main sections of the ILRS website: About ILRS, Network, Missions, Science, Data & Products, and Technology. Examples of Level 1 pages are shown in Figures 2 and 3.

The Level 1 page of each section contains three colums. The left column provides a list of main navigation areas as well as "quick links" which are links to popular pages within the current section. The center section is the main text area for the page. This includes an image followed by text highlighting important topics of the section. Images on these pages rotate through a selection of content-related photos/diagrams/plots. Finally, the third, right-most column lists recent news (once again, section-specific) meetings, and publications.

Each main section is colored uniquely to further emphasize the content and location within the ILRS website. This convention helps the user locate the page within the site. The colors persist through the shading of the background image, horizontal bars, and background coloring of the drop-down menu items as the user passes their mouse over each selection.

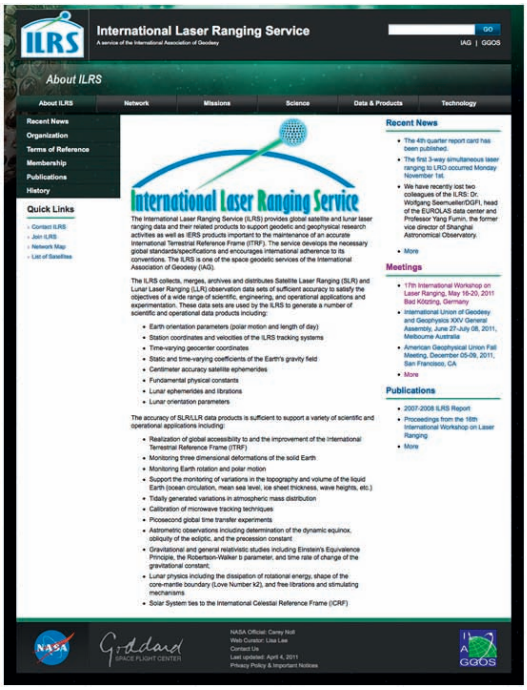


**Figure 2: Design for Level 1 Page (About ILRS)**

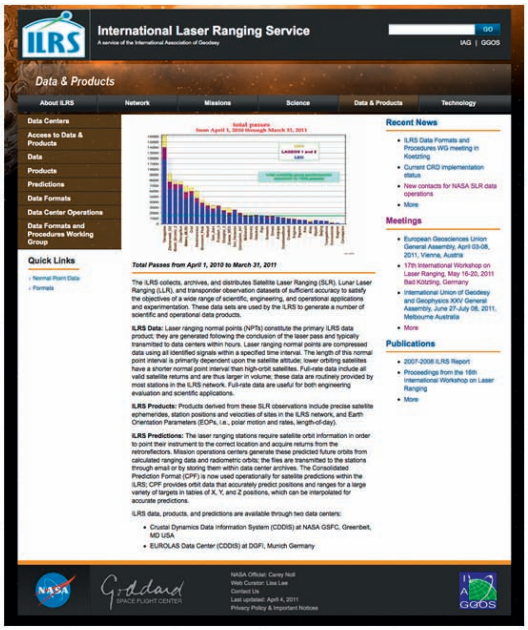


**Figure 3: Design for Level 1 Page (Data & Products)**

### 2.2.2 Level 2 (and Lower) Pages

Level 2, 3, etc. pages use a two-column layout that consists of left column and a main content section. The left column contains a navigation area and a list of "quick links" which are links to popular pages within the current section of the website. The second column contains the main text for the page. An example level 2 page within the About ILRS section of the website is shown in Figure 4.

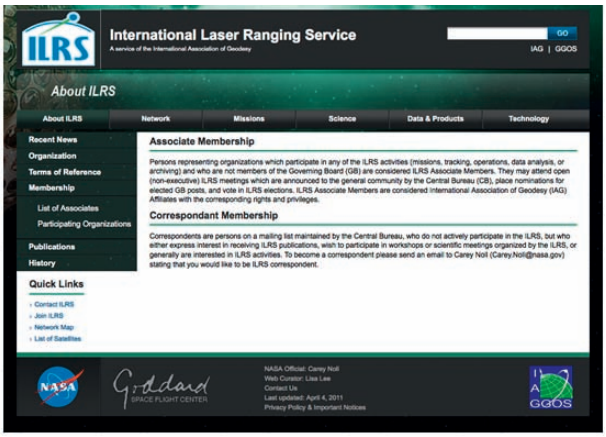


**Figure 4: Design for Level 2 Page within the About ILRS Section**

# 3. Future Plans

The ILRS website redesign team continues to fine-tune various aspects of the look-and-feel for the site. Content from the current website is being migrated to the new site, taking care to validate and update content and links. ILRS colleagues can view the new site at *http://ilrs.gsfc.nasa.gov/new*. Comments on the design are welcome and should be sent to *ilrs-web@lists.nasa.gov*. The team hopes to have an initial draft of the new site available for public testing during the fall of 2011.

## Correspondence

Carey Noll
NASA GSFC
Code 690.1
Greenbelt, MD 20771
USA

carey.noll@nasa.gov

# Borowiec activity in satellite orbit determination

*Paweł Lejba, Stanisław Schillak*

ABSTRACT

The paper presents the results of orbital analysis made for few satellites: Ajisai, CHAMP, GOCE, Larets, Lageos-1/Lageos-2 and Starlette/Stella based on laser data of 20 SLR stations collected during the period from 2001 to 2005 for Ajisai, CHAMP, Lageos-1/Lageos-2, Starlette/Stella, from October 1, 2009 to December 31, 2010 for GOCE and from November 6, 2003 to December 28, 2005 for Larets.

All orbital computations were performed by means of NASA Goddard's GEODYN-II program. The analysis mainly concerns the tests of Earth's gravity field model for Ajisai, Lageos-1/ Lageos-2 and Starlette/Stella. This paper shows which models and parameters are useful for orbital calculations and how depends the *fit* RMS on the altitude of the satellites.

## 1. Determination of orbital arcs

In the first step the orbits of few satellites were determined: Ajisai, CHAMP, GOCE, Larets, Lageos-1/ Lageos-2 and Starlette/Stella. In Table 1 the orbital and technical parameters of satellites are presented.

**Table 1: Orbital and technical parameters of the analysed satellites.**

Table 1. Orbital and technical parameters of the analysed satellites.

| | Ajisai | CHAMP | GOCE | LAGEOS-1 | LAGEOS-2 | Larets | Starlette | Stella |
|---|---|---|---|---|---|---|---|---|
| ID number | 8606101 | 0003902 | 0901301 | 7603901 | 9207002 | 0304206 | 7501001 | 9306102 |
| Launch date | August 12 1986 | July 15 2000 | March 17 2009 | May 4 1976 | October 22 1992 | September 27 2003 | February 6 1975 | September 26 1993 |
| **Technical and physical parameters** | | | | | | | | |
| Number of retroreflectors | 1436 | 4 | 7 | 426 | 426 | 60 | 60 | 60 |
| Shape | spherical | trapezoid | octagonal | spherical | spherical | spherical | spherical | spherical |
| Dimensions [cm] | 214 | 22.4 x 75 x 162.1 | 100 | 60 | 60 | 21.5 | 24 | 24 |
| Mass [kg] | 685 | 542 | 1050 | 407 | 405 | 23.28 | 47.25 | 48.00 |
| CoM [mm] | 1010 | 250 | 2456 | 251 | 251 | 56.2 | 75 | 75 |
| **Orbital parameters of the satellites** | | | | | | | | |
| Inclination [°] | 50.0 | 87.2 | 96.6 | 109.8 | 52.6 | 98.2 | 49.8 | 98.6 |
| Eccentricity | 0.001 | 0.004 | 0.002 | 0.004 | 0.01 | 0.0002 | 0.02 | 0.002 |
| Perigee [km] | 1480 | 370 | 254 | 5900 | 5800 | 690 | 812 | 800 |
| Period [min.] | 116 | 94 | 90 | 225 | 222 | 99 | 104 | 101 |

The orbital computations were performed with the use of NASA Goddard's GEODYN-II program (Pavlis et al.,

1998) based on the observation data from the 20 ILRS stations (Pearlman et al., 2002) in ITRF2005 (Altamimi et al., 2007) collected in the period from 2001 to 2005 for Ajisai, CHAMP, Lageos-1/Lageos-2, Starlette/Stella, from October 1, 2009 to December 31, 2010 for GOCE and from November 6, 2003 to December 28, 2005 for Larets. The list of all stations used presents Table 2.

**Table 2. List of the stations for orbits determination.**

| | Station | | CDP Number |
|---|---|---|---|
| 1 | McDonald | (TX, USA) | 70802419 |
| 2 | Yarragadee | (West Australia) | 70900513 |
| 3 | Greenbelt | (MD, USA) | 71050725 |
| 4 | Monument Peak | (CA, USA) | 71100411<br>71100412 |
| 5 | Tahiti | (French Polynesia) | 71240802 |
| 6 | Haleakala | (HI, USA) | 72102313 |
| 7 | Hartebeesthoek | (RSA) | 75010602 |
| 8 | Zimmerwald | (Switzerland) | 78106801 |
| 9 | Borowiec | (Poland) | 78113802 |
| 10 | Mount Stromlo | (East Australia) | 78259001 |
| 11 | Riyadh | (Sudi Arabia) | 78325501 |
| 12 | Grasse SLR | (France) | 78353102 |
| 13 | Potsdam | (Germany) | 78365801 |
| 14 | Simosato | (Japan) | 78383602 |
| 15 | Graz | (Austria) | 78393402 |
| 16 | Herstmonceux | (UK) | 78403501 |
| 17 | Potsdam | (Germany) | 78418701 |
| 18 | Mount Stromlo | (East Australia) | 78498001 |
| 19 | Matera | (Italy) | 79417701 |
| 20 | Wettzell | (Germany) | 88341001 |

**Table 2: List of the stations for orbits determination.**

In the case of Lageos-1/ Lageos-2 the orbits were determined from the normal equations for the twin satellites combined. This same solution were applied for Starlette and Stella. The following criteria were used for rejection of normal points:

- normal points with orbital residuals larger than 5 sigma,
- normal points lower than 10_ above the horizon.

Orbits of Ajisai, Starlette and Stella were computed with empirical acceleration coefficients (ACCEL) in along-track, cross-track and radial directions determined every 6 or 12 h. In case of CHAMP and Larets the interval of ACCEL parameters were 24 h. Orbits of the lowest GOCE were computed without ACCEL coefficients. Table 3 contains a detailed description of force models and parameters used.

**Table 3. GEODYN II – Force Models and Parameters (THE BEST ORBITAL SOLUTION).**

| |
|---|
| **Force Models** |
| Earth gravity field (coefficients): 20x20 (LAGEOS), 45x45 (Ajisai), 75x75 (Starlette/Stella), 80x80 (Larets), 100x100 (CHAMP), 150x150 (GOCE) |
| Earth gravity field (models): **EGM2008** (Pavlis et al., 2008), **EIGEN-GRACE02S** (Reigber et al., 2005), **GOCE2010s** (Pail et al., 2010) **for all satellites**,**GGM03S** (Tapley et al., 2007) **only for LAGEOS** |
| Earth tides: IERS Conventions 2003 (McCarthy and Petit, 2004) |
| Ocean tides: GOT99.2 (Ray, 1999) |
| Third body gravity: Moon, Sun and all planets – DE403 (Standish, 1995) |
| Solar radiation pressure: $C_R$ coefficient 1.13 (LAGEOS, Starlette/Stella) and 1.0 (Ajisai, CHAMP, GOCE, Larets) |
| Earth albedo (Pavlis et al., 1998) |
| Dynamic polar motion (Pavlis et al., 1998) |
| Relativistic correction (Pavlis et al., 1998) |
| Atmospheric density model: MSIS86 (Hedin, 1987) |
| **Constants** |
| Gravitational constant times the mass of the Earth (GM): $3.986004415 \times 10^{14}$ $m^3/s^2$ |
| Speed of light: 299792.458 km/s |
| Semi-major axis of the Earth: 6378.13630 km |
| Inverse of the Earth's flattening: 298.25642 |
| **Reference Frame** |
| Inertial reference system: true of date defined at $0^h$ of the first day of each arc |
| Stations coordinates: ITRF2005 (Altamimi et al., 2007) |
| Precession and nutation: IAU 2000 |
| Polar motion: C04 IERS |
| Tidal uplift: Love model H2 = 0.609, L2 = 0.0852 |
| Pole tide (Pavlis et al., 1998) |
| **Estimated parameters** |
| Satellite state vector |
| Station geocentric coordinates |
| Atmospheric drag coefficients $C_D$ determined every 1 hour (GOCE), 2 hours (CHAMP), 9 hours (Larets), 12 hours (Starlette/Stella), 15 hours (Ajisai), **no drag parameters for LAGEOS** |
| Acceleration parameters along-track, cross-track and radial at 6 hours or 12-hours intervals (Ajisai, Starlette/Stella), 24 hours (CHAMP, Larets), 5 days for LAGEOS, **no accel parameters for GOCE** |
| **Measurement Model** |
| Observations: 5 seconds normal points (GOCE), 15 seconds (CHAMP), 30 seconds (Ajisai, Larets, Starlette/Stella), 120 seconds (LAGEOS) from Eurolas Data Center |
| Laser pulse wavelength: 532 nm (Zimmerwald 423 nm) |
| Tropospheric refraction: Mendes-Pavlis model (Mendes et al., 2002, Mendes and Pavlis, 2004) |
| Editing criteria: |
| 5σ per arc |
| cut-off elevation 10 degrees for all satellites |
| station coordinates < 50 normal points per station per arc |
| **Numerical Integration** |
| Integration: Cowell's method |
| Orbit integration step size: 20 sec (GOCE), 50 sec (CHAMP), 60 sec (Larets, Starlette/Stella), 90 sec (Ajisai), 120 sec (LAGEOS) |
| Arc length: 1 day (GOCE), 3 days (CHAMP), 7 days (Larets), 10 days (Starlette/Stella), 10 - 14 days (Ajisai), 10 - 30 days (LAGEOS) |

**Table 3: GEODYN II – force models and parameters.**

The results of orbital arcs calculations are presented on Figures 1 and 2. It is clear that the orbital arcs are the shortest for the lowest satellites (Figure 1). Additionally it is very good visible, that the mean RMS of fit depends very strongly on altitude of the satellite (Figure 2).

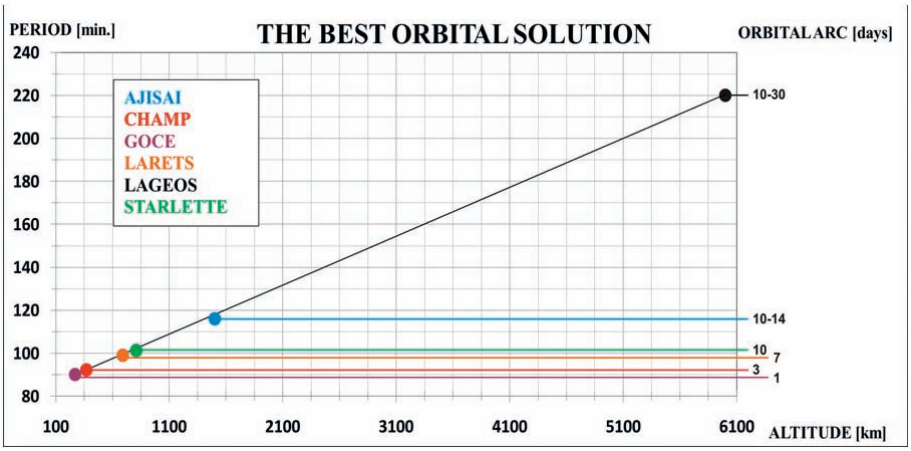


**Figure 1: Dependence of the orbital arcs length on altitude of the satellite.**

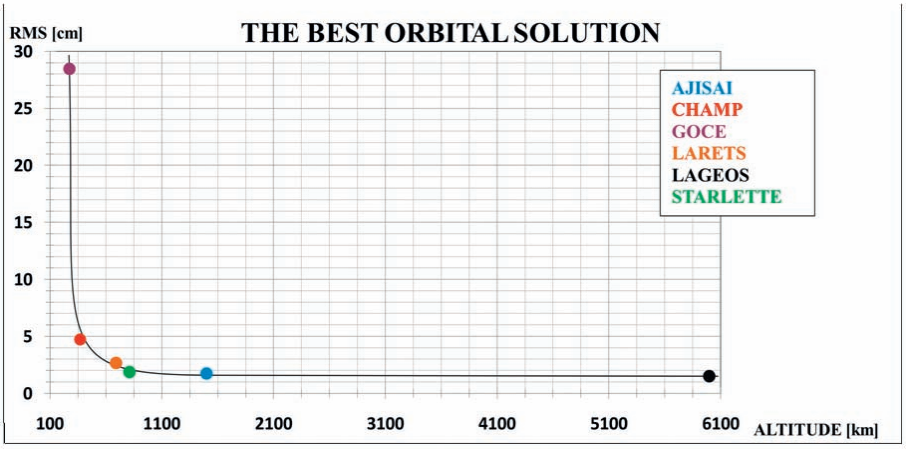


**Figure 2: Dependence of mean RMS of fit on altitude of the satellite.**

# 2. Gravity tests

In the second step in the case of Lageos-1/Lageos-2, Ajisai and Starlette/Stella the orbits were calculated again for five models of Earth's gravity field:

- EIGEN-GRACE2010S,
- GGM03S,
- GOCE2010S,
- IT-GRACE2010S,
- EGM2008.

The data for models were downloaded from http://icgem.gfz-potsdam.de/ICGEM/ICGEM.html. The results of obtained RMS of fit are presented on Figures 3, 4 and 5. The number of gravity coefficients used in each case are listed in Table 3.

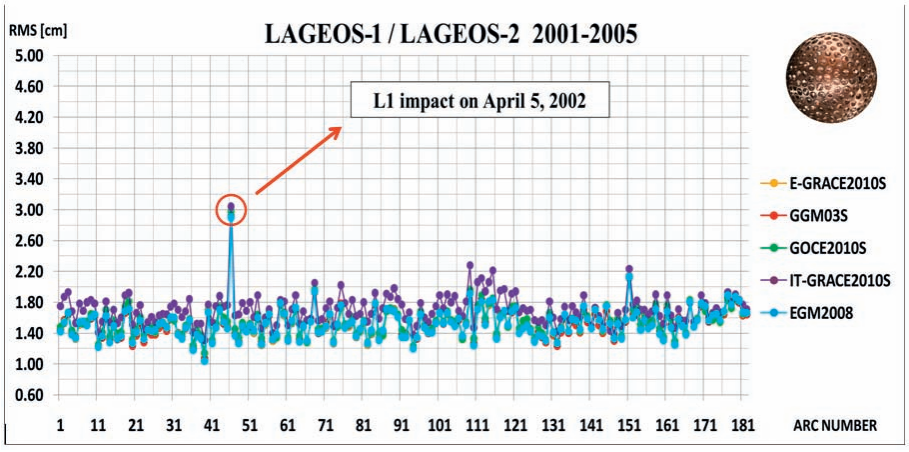


**Figure 3: Dependence of RMS of fit on analysed gravity field models for Lageos satellites.**

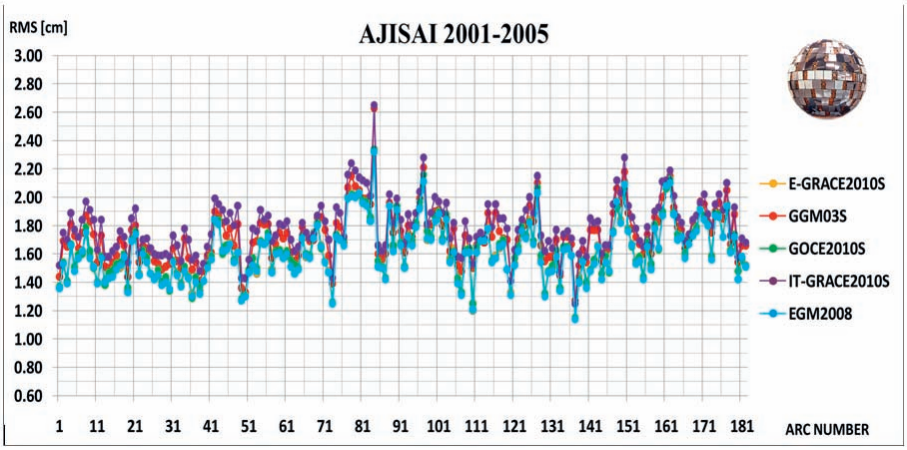


**Figure 4: Dependence of RMS of fit on analysed gravity field models for Ajisai satellite.**

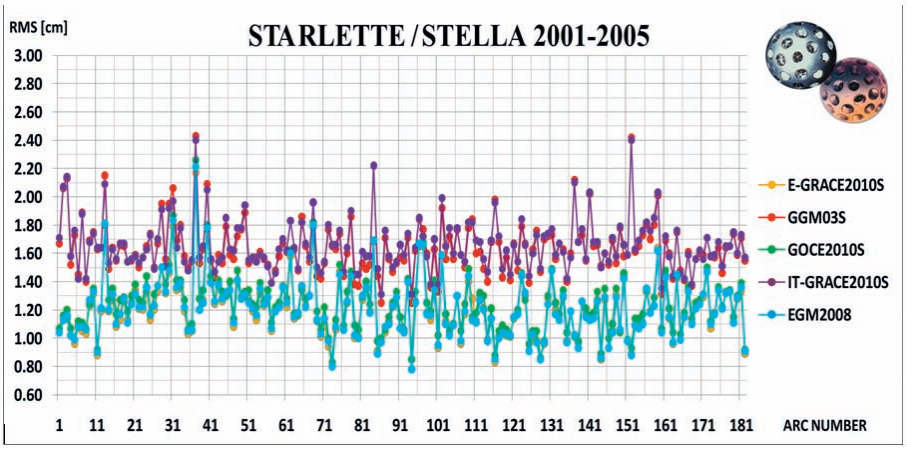


**Figure 5: Dependence of RMS of fit on analysed gravity field models for Starlette/Stella satellites.**

The mean RMS of fit are from 1.54 cm (EIGEN-GRACE2010S, GGM03S, EGM2008) to 1.73 cm (IT-GRACE2010S) for Lageos satellites, from 1.62 cm (EGM2008) to 1.80 cm (IT-GRACE2010S) for Ajisai and from 1.21 cm (EIGEN-GRACE2010S, EGM2008) to 1.66 cm (IT-GRACE2010S) for Sarlette/Stella.

In all analysed cases the best orbital results were obtained for EIGEN-GRACE2010S and EGM2008 models.

## Summary

Based on the results presented in this paper three conclusions should be noticed:

1. The higher orbit of the satellite the lower RMS of fit.

2. The results obtained for the tested Earth gravity field models shows that the best orbital solution ensure the following models:

- EGM2008, EIGEN-GRACE02S and GOCE2010S for all satellites from GOCE to LAGEOS,
- GGM03S for LAGEOS only,
- IT-GRACE2010S should not be used in calculations.

3. A substantial increase in the accuracy of laser observations, new force models and improvement in the quality of the station coordinates over the last years allows determination of station positions and velocities also from LEO satellites.

Please see (Lejba et al., 2007; Lejba et al., 2011) for more details.

## Acknowledgements

This work has been supported by National Science Centre (NCN) as a research project No.N N526 231839.

## References

*Altamimi, Z., Collilieux, X., Legrand J., et al.* ITRF2005: A new release of the International Terrestrial Reference Frame based on time series of station positions and Earth Orientation Parameters. J. Geophys. Res. 112, B09401, 2007.

*Bianco, G., Devoti, R., Fermi, M., et al*. Estimation of low degree geopotential coefficients using SLR data. Planet Space Sci. 46(11/12), 1633-1638, 1997.

*Borkowski, K.M.* Accurate algorithms to transform geocentric to geodetic coordinates. Bull. Geod. 63, 50-56, 1989.

*Burmistrov, V.B, Parkhomenko, N.N., Shargorodsky, V.D., et al.* Reflector, Larets and Meteor-3M(1), what did we learn from tracking campaign results, in: Garate J., Davila J.M., Noll C., Pearlman M. (Eds), Proceedings of 14th International Workshop on Laser Ranging, San Fernando, Spain, pp. 449-452, 2004.

*Cheng, M.K., Shum, C.K., Eanes, R.J., et al.* Long-period perturbations in Starlette orbit and tide solution. J. Geophys. Res. 95(B6), 8723-8736, 1990.

*Cheng, M.K., Shum, C.K., Eanes, R.J., et al.* Observed temporal variations in the Earth's gravity field from 16-years of Starlette orbit analysis, in: Proceedings XX General Assembly of the IUGG, IAG Symp. 3, Vienna, Austria, August, 1991.

*Hedin, A. E.* MSIS-86 thermospheric model. J. Geophys. Res. 92, 4649-4662, 1987.

*Kirchner, G., Hausleitner, W., Cristea, E.* Determination of Ajisai spin parameters using Graz kHz SLR data, in: Luck, J., Moore, C., Wilson, P. (Eds.), Proceedings of 15th International Workshop on Laser Ranging, Canberra, Australia, pp.270-275, 2008.

*Lejba, P., Schillak, S., Wnuk, E.* Determination of orbits and SLR stations' coordinates on the basis of laser observations of the satellites Starlette and Stella. Adv. Space Res. 40(1), 143-149, 2007.

*Lejba, P., Schillak, S.*, Determination of station positions and velocities from laser ranging observations to Ajisai, Starlette and Stella satellites, Adv. Space Res. 47(4), 654-662, 2011.

*McCarthy, D. D., Petit, G.*, (Eds.), IERS Conventions (2003). IERS Technical Note No. 32, Central Bureau of IERS, Bundesamt für Kartographie und Geodäsie, Frankfurt am Main, 2004.

*Mendes, V. B., Prates, G., Pavlis, E. C., et al.* Improved mapping functions for atmospheric refraction correction in SLR, Geophys. Res. Lett., 29(10), 1414, doi:10.1029/2001GL014394, 2002.

*Mendes, V.B., Pavlis, E.C.*, High-accuracy zenith delay prediction at optical wavelengths. Geophys. Res. Lett., 31, L14602, doi:10.1029/2004GL020308, 2004.

*Otsubo T.*, Appleby G. System-dependent center-of-mass correction for spherical geodetic satellites. J. Geophys. Res. 108(B4), 2201, 2003.

*Pavlis, D. E., Luo, S., Dahiroc, P., et al.* GEODYN II System Description. Hughes STX Contractor Report, Greenbelt, Maryland, July, 1998.

*Pavlis, E. C.*, Kuzmicz-Cieslak, M. SLR and the next generation global geodetic networks, in: Schillak, S. (Ed.), Proceedings of 16th International Workshop on Laser Ranging, Poznan, Poland, pp. 183-189, 2009.

*Pavlis, E. C., Kuzmicz-Cieslak, M., Hinkey, P. M.*, Improved modeling approaches towards the mm SLR, in: Schillak, S. (Ed.), Proceedings of 16th International Workshop on Laser Ranging, Poznan, Poland, pp. 233-240, 2009.

*Pearlman, M.R., Degnan, J.J., Bosworth*, J.M. The International Laser Ranging Service. Adv. Space Res. 30(2), 135-143, doi:10.1016/S0273-1177(02)00277-6, 2002.

*Ray, R., D.*, A Global Ocean Tide Model from TOPEX/POSEIDON Altimetry: GOT99.2, NASA/TMm1999-209478, 1999.

*Schutz, B. E., Cheng, M. K., Shum, C. K., et al.* Analysis of Earth rotation solution from Starlette. J. Geophys. Res. 94, 10167-10174, 1989.

*Sengoku, A.*, A plate motion study using Ajisai SLR data. Earth, Planets and Space, 50(8), 611-627, 1998.

*Standish, E.M.*, Newhall, X X, Williams, J.G., et al. JPL Planetary and Lunar Ephemerides, DE403/LE403, JPL IOM 314.10-127, 1995.

*Tapley, B., Ries, J., Bettadpur, S.*, et al. The GGM03 Mean Earth Gravity Model from GRACE, AGU, Fall Meeting 2007, (Abstract) #G42A-03, 2007.

## Correspondence

Paweł Lejba
Space Research Centre, Polish Academy of Sciences, Astrogeodynamic Observatory, Borowiec
ul. Drapałka 4
62-035 Kórnik
Poland

plejba@cbk.poznan.pl

# Continuous integration and quality control during software development

*Ettl Martin, Neidhardt Alexander*

ABSTRACT

Modern software has to be stable, portable, fast, and reliable. This requires a sophisticated infrastructure supporting and providing the developers with additional information about the state and the quality of the project. That's why we have created a centralized software repository where the whole code-base is managed and version-controlled on a centralized server. Based on this, a hierarchical build system has been developed where each project and its sub-projects can be compiled by simply calling the top level makefile. On top of this, a nightly build system has been created where the top level makefiles of each project are called every night. The results of the build, along with the compiler warnings, are reported to the developers using generated html pages. In addition, all the source code is automatically checked using a static code analysis tool called Cppcheck. This tools produces warnings similar to those of a compiler but more pedantic. The reports of this analysis are translated into html and, similarly to the nightly build, reported to the developers. Armed with this information, the developers can reveal issues in their projects at an early development stage. Altogether, this reduces the number of possible issues in our software to ensure the quality of our projects at every development stage.

## 1. What does continuous integration mean?

During the development of a software project it is hard to determine the current state and stability of the current development version. Neither side-effects nor portability issues can be detected in this development phase, especially when multiple developers are working on resources affecting the behavior of several projects. The first attack on this problem was setting up a centralized version control management system where each developer commits his changes regularly to a centralized software repository. All the different versions are stored in this repository and can be restored easily. This makes it very convenient to revert to an older version of the source code, for instance. Based on this, the newest version of the source code is always available and can therefore be tested intensively. The whole workflow of the continuous integration concept is depicted in the figure (right). First of all, the developer team works on the project and commits its changes to the software repository. Because the changes are committed frequently – at least once a day – the repository stores the latest version of the project. Based on the newest version of the software, every night a bunch of separated tests is run against the source code (see red circles). Then, the results of the tests are converted into html pages. These results will be published in our local network. Therefore each developer can use this information to detect and fix possible issues of the latest changes to the code. This kind of workflow reduces the amount of severe issues during the whole development phase and helps the developers to find bugs at an early development stage.

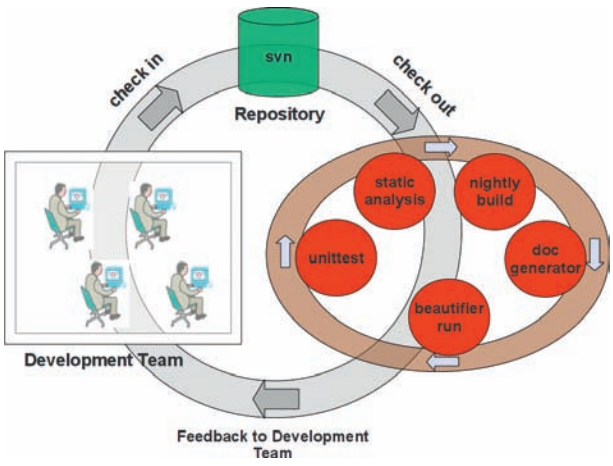


**Figure 1: The continuous integration principle**

# 2. Different methods of quality control

## 2.1 What is static code analysis?

Static program analysis is done without executing or compiling the source code. For our analysis we are using Cppcheck[1], an open source analysis tool for C/C++-source code that finds bugs that a compiler does not detect. It checks our code for memory leaks, null pointer dereferencing, unused variables, not initialized variables, mismatched allocation–deallocation, buffer overrun, memory out of bounds checking, and many more issues. The analysis report is converted into an html-page and published to enable the developers to react to problems found. We are considering using other static analysis tools like Flawfinder[2] and Splint[3] in future.

## 2.2 Why nightly builds?

We have created an automated build-system based on standardized GNU makefiles, where every project has its own makefile. Projects that contain several sub-projects have a top level makefile capable of building all sub-projects at once. Therefore the whole code base can be compiled by simply calling the top-level makefile. This is done automatically every night on our Linux servers. Then all the compiler warnings will be piped to a text file and converted into a build report. This report containing possible errors and warnings is forwarded to our development team.

## 2.3 Why unit tests?

Unit tests are small test programs for checking the results at function or module level. For this, we have created a programming based environment for collecting all these small testing programs (simple_testsuite). This suite offers a way to create such validation tests for all our basic software components and the generated code. These tests can be run on different architectures (32/64-Bit) with different compilers on different Linux operation systems to reveal portability issues. Furthermore the test-coverage is measured using the Intel compiler suite for Linux. The information about the test-coverage as well as the unit-test report is also provided to the developers. With this information it is now possible to measure the quality of the tested source code, which is very convenient.

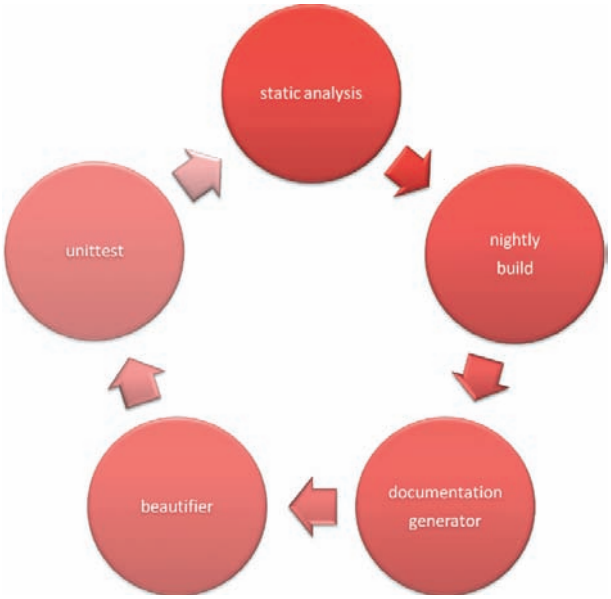


**Figure 2: Several methods of quality control for rapid prototyping**

[1] http://sourceforge.net/apps/mediawiki/cppcheck/index.php?title=Main_Page
[2] http://www.dwheeler.com/flawfinder/
[3] http://www.splint.org/

## 2.4 What is a documentation generator?

Our developer documentation is created by an open source documentation generator called *doxygen*[4]. This tool reads the source code with all the comments, extracts the needed information, and generates developer documentation in several formats along with call-graphs and Unified Modelling Language (UML)-diagrams. Running the documentation generation automatically is a great help for our developers. This makes it simpler to share information between several developers. Furthermore, this generated documentation can be used to get an overview of the object-oriented software structure and the relationships of our software components in our projects. This makes it easier for beginners to understand how a specific module operates and how it can be used, for instance.

## 2.5 What is a code-beautifier?

We are using a tool called Artistic Style[5] , which formats our source code automatically every week according our design rules. This is done frequently and ensures that the same syntax is used in our whole software. This therefore improves readability and reduces maintenance time for developers. Furthermore the takeover and sharing of source code between developers is simplified.

# 3. Future work

This methods have increased the quality of our software to a notable extend. This is why we continuously work to improve our techniques of automatically control and evaluate the quality of our products during the software development process. Furthermore, there are lots of other good open source tools available that can help us to further extend and improve this first approach.

## References

*Martin, C. Robert.*: Clean Code, Refactoring, Patterns, Testen und Techniken für sauberen Code 2009

*Osherove, Roy*: The Art of Unit Testing. Deutsche Ausgabe. mitp, Verlagsgruppe Hüthig Jehle Rehm GmbH 2010

Wiest, Simon: Continous Integration mit Hudson. Grundlagen und Praxiswissen für Einsteiger und Umsteiger. 1. Auflage, Dpunkt.verlag GmbH Heidelberg 2011

## Correspondence

Martin Ettl
Forschungseinrichtung Satellitengeodäsie, TU München
Geodätisches Observatorium Wettzell
Sackenrieder Str. 25
D-93444 Bad Kötzting

ettl@fs.wettzell.de

Alexander Neidhardt
Forschungseinrichtung Satellitengeodäsie, TU München
Geodätisches Observatorium Wettzell
Sackenrieder Str. 25
D-93444 Bad Kötzting

neidhardt@fs.wettzell.de

[4] http://www.stack.nl/~dimitri/doxygen/
[5] http://astyle.sourceforge.net/

# Time Transfers and Ranging – The ELT-Mission and the new big Goal at Wettzell

*U. Schreiber, P. Lauber, J. Eckl, S. Mähler, A. Neidhardt, N. Brandl, M. Mühlbauer, G. Herold, R. Motz, R. Dassing*

ABSTRACT
The European Laser Timing (ELT) evolution and mission schedule is depicted briefly. The new big goal at the Wettzell station for time transfers is introduced. The past and current activities concerning time transfers and ranging at the Wettzell station are also described shortly.

## 1. The ELT-Mission

ELT was designed to transfer time from one SLR station to another or a satellite using time transfers of already existing ground-space satellite links. Compared to other time transfer missions, one improved precision and simplicity of the latter. In addition, Wettzell as a prototype ELT SLR ground station meets the mission prerequisites per definition. For the ELT mission, the Pre-Flight validation of the hardware components was carried out at Wettzell. The final results can be found detailed in[1].

The space qualified hardware components will be put on the Atomic Clock Ensemble in Space (ACES) platform of the International Space Station (ISS). From 2015 on, the components should work on the ISS and this will be the ELT mission operated by the ESA. The ground data infrastructure will be set-up much earlier. Mainly due to the lack of the latter currently, the identical proposed space components were not yet selected for an interplanetary mission.

## 2. Time Transfers

### 2.1 The new big Goal at Wettzell

From the physics point of view, especially atomic clock laboratories should be time synchronised on an intercontinental optical basis in the future. As an example connection for such laboratories, the Physikalisch-Technische Bundesanstalt (PTB) at Braunschweig/Germany and the National Institute of Standards and Technology (NIST) at Boulder/US were envisaged. The optical connection should include transfer of an optical time pulse through a fibre from the PTB to the Wettzell SLR station - in particular an optical time distribution at the station - and the time transfer using the usual satellite links. Some more detailed descriptions of the optical link is given in the section 3.

### 2.2 Past and Current Activities

For the time transfer, the Lunar Reconnaissance Orbiter (LRO, NASA) has been used already. The first hits on the LRO detector generated by the Wettzell Laser Ranging System (WLRS) laser were made in 2009. Since the WLRS refurbishment in 2010, LRO is tracked routinely.

Beside the WLRS telescope refurbishment, a new control system called SLR2.0 has been set-up. It is written completely in the programming language C++ and covers almost only new written code. It has been used at the Satellite Observing System Wettzell (SOS-W) already and will replace the good old LabView control system entirely at the WLRS and maybe at the Transportable Integrated Geodetic Observatory (TIGO) in the future too.

It must be mentioned explicitly here that all hard- and software set-ups and/or upgrades consider always - beside the ranging - the time transfer capability.

# 3. Time Transfer around the World

For such a time transfer, the satellite links and the fibre links will already exist. The satellite links will be established at least by the ELT mission. In Germany, some optical fibre links between research institutes already exist. The missing optical fibre link for the complete connection between the PTB and the Wettzell station will be set-up in the near future. By the way, for current time and frequency state-of-the-art optical links see [2] and [3]. The lacking optical time and frequency distribution at the Wettzell station will be set-up in the near future too. A more detailed overview of the optical set-up is shown in Figure 1.

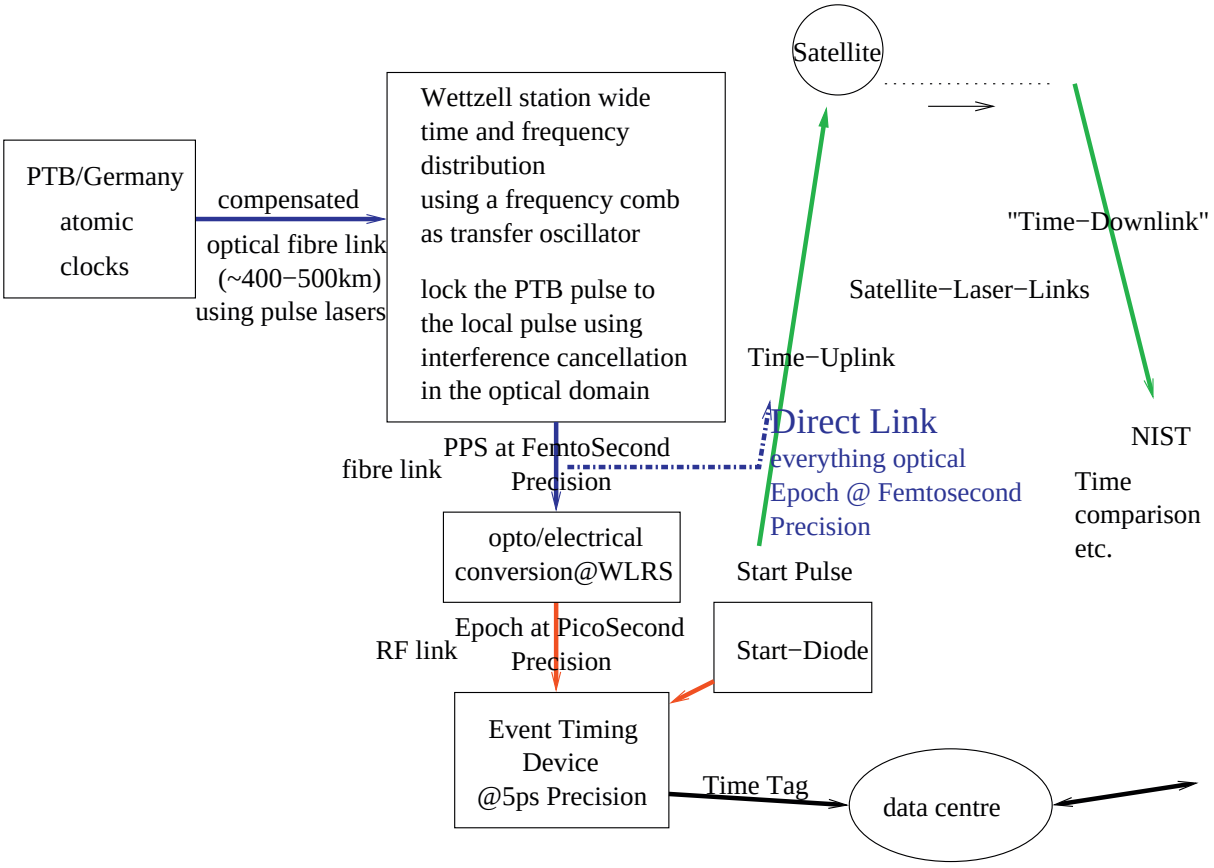


**Figure 1: Intercontinental optical link between atomic clock laboratories.**

Time links base on optical laser pulses having very low time jitters on the rising pulse edges. Currently, time transfers use sub-optimal electrical time links too. The latter should be replaced by their optical counterparts in the future. Instead of using the Radio Frequency (RF) based Global Positioning System (GPS) time references, the time reference should be delivered through a compensated optical fiber link directly from the PTB to Wettzell station. At the station, the optical pulses should discipline a frequency comb which acts as a transfer oscillator. The latter supplies the entire station with locked time and frequency. In the best case, the 10 Pulse-Per-Second (PPS) epoch precision at the satellite uplink is at femto-second level. In the near future unfortunately, some current electrical based components will be used too. In this case, the satellite uplink epoch precision be will at pico-second level only. Currently only electrical based components are used at the ground station. Thus e.g. for ELT, the epoch precision is at about 10 nano-second level only.

## Acknowledgements

For fruitful support, we would like to thank Nicolaus Brandl, Rainer Dassing, Johann Eckl, Martin Ettl, Svetlana Mähler, Günther Herold, Andreas Leidig, Matthias Mühlbauer, Rudolf Motz at the Federal Agency for Cartography and Geodesy (BKG) and Alexander Neidhardt, Ulrich Schreiber, Urs Hugentobler at the Technical University of Munich (TUM) and Lea Schreiber.

## References

[1] *Schreiber, K.U., Prochazka, I., Lauber, P., Hugentobler, U., Schäfer, W., Cacciapuoti, L., Nasca, R.,* 2010: Ground Based Demonstration Of The European Laser Timing (ELT) Experiment, IEEE, Transactions on Ultrasonics, Ferroelectrics, and Frequency Control, Vol. 57 Issue 01, Digital Object Identifier 10.1109/TUFFC.2010 .

[2] *Rost, M., Fujieda, M., Piester, D.,* 2010: Time Transfer through optical Fibers (TTTOF): Progress on calibrated Clock Comparisons, Proc. 24th European Frequency and Time Forum, 13-16 April, Noordwijk/The Netherlands.

[3] *Williams, P. A., Swann, W.C., Newbury, N.R.,* 2008: Practical performance limits on optical frequency transfer over fiber optic links, NIST, IEEE, OSA/CLEO/QELS, OCIS codes: 060.2360, 120.3930 .

## Correspondence

P. Lauber
Geodetic Observatory Wettzell
Sackenrieder Str. 25
93444 Bad Koetzting
Germany

lauber@fs.wettzell.de .

**Mitteilungen des Bundesamtes für Kartographie und Geodäsie**

Band 1, 1998 Geodätische Vernetzung Europas

Band 2, 1999 Arbeitsgruppe Automation in der Kartographie, Tagung 1998

Band 3, 2002 Ansprachen anlässlich der Verabschiedung des Präsidenten und Professors des IfAG, Univ.-Prof. Dr.-Ing. Hermann Seeger und der Amtseinführung seines Nachfolgers Univ.-Prof. Dr.-Ing. Dietmar Grünreich

Band 4, 1999 Automatische Oberflächenrekonstruktion durch digitale Bildzuordnung

Band 5, 1999 3. DFG-Rundgespräch zum Thema Bezugssysteme

Band 6, 1999 EUREF Publication No. 7/I (No. 7/I u. 7/II werden nur gemeinsam verkauft)

Band 7, 1999 EUREF Publication No. 7/II (No. 7/I u. 7/II werden nur gemeinsam verkauft)

Band 8, 2000 Ringlasertechnologie für geowissenschaftliche Anwendungen

Band 9, 1999 Das Deutsche Referenznetz 1991 – DREF 91

Band 10, 1999 Proceedings – 11th International Workshop on Laser Ranging – Volume 1 (Volume I und II werden nur gemeinsam verkauft)

Band 11, 1999 Proceedings – 11th International Workshop on Laser Ranging – Volume 2 (Volume I und II werden nur gemeinsam verkauft)

Band 12, 1999 German and Romanian Activities in the Frame of the CERGOP, Messungen 1996 im Überwachungsnetz Wettzell und Deformationsanalyse

Band 13, 1999 Theorie und Praxis globaler Bezugssysteme

Band 14, 2000 Fortführung von Geoinformationssystemen anhand direkt aufgezeichneter digitaler Bilddaten

Band 15, 2000 Geodetic Applications of the Global Navigation Satellite (GLONASS) and of GLONASS/GPS Combinations

Band 16, 2000 Der Einfluss des Wasserdampfes auf die modernen raumgestützten Messverfahren

Band 17, 2000 Arbeitsgruppe Automation in der Kartographie, Tagung 1999

Band 18, 2000 Endlager chemisch-toxischen Abfälle im Salz – Validierung von Prognoserechnungen zur Standsicherheit

Band 19, 2000 Second International Symposium on Geographical Names GeoNames 2000

Band 20, 2001 Arbeitsgruppe Automation in der Kartographie, Tagung 2000

Band 21, 2003 Modelling of the Gravimetric Effects Induced by Vertical Air Mass Shifts

Band 22, 2002 Arbeitsgruppe Automation in der Kartographie, Tagung 2001

Band 23, 2002 EUREF Publication No. 10

Band 24, 2003 Arbeitsgruppe Automation in der Kartographie, Tagung 2002

Band 25, 2002 EUREF Publication No. 11/I (No. 11/I u. 11/II werden gemeinsam verkauft)

Band 26, 2002 EUREF Publication No. 11/II (No. 11/I u. 11/II werden gemeinsam verkauft)

Band 27, (xxx) Festschrift des BKG (in Vorbereitung)

Band 28, 2003 Training Course on Toponymy

Band 29, 2003 EUREF Publication No. 12

Band 30, 2004 Ein eingebettetes Expertensystem zur Automatisierung der VLBI-Auswer - tung

Band 31, 2004 Arbeitsgruppe Automation in der Kartographie, Tagung 2003

Band 32, 2003 Erdrotation und globale dynamische Prozesse

Band 33, 2004 EUREF Publication No. 13

Band 34, 2005 Arbeitsgruppe Automation in der Kartographie, Tagung 2004

Band 35, 2006 EUREF Publication No. 14

Band 36, 2006 Arbeitsgruppe Automation in der Kartographie, Tagung 2005

Band 37, 2005 Verbesserung des Datenmanagements in inhomogenen Rechnernetzen geo - dätischer Messeinrichtungen auf der Basis von Middlewar e und Dateisys - temen am Beispiel der Fundamentalstation Wettzell

Band 38, 2006 EUREF Publication No. 15

Band 39, 2007 Arbeitsgruppe Automation in der Kartographie, Tagung 2006

Band 40, 2008 EUREF Publication No. 16

Band 41, 2008 Arbeitsgruppe Automation in der Kartographie, Photogrammetrie und GIS, Tagung 2007

Band 42, 2008 EUREF Publication No. 17

Band 43, 2009 Arbeitsgruppe Automation in der Kartographie, Photogrammetrie und GIS, Tagung 2008

Band 44, 2009 Space-Time Reference Systems for Monitoring Global Change and for Precise Navigation

Band 45, 2010 Arbeitsgruppe Automation in Kartographie, Photogrammetrie und GIS Tagung 2009

Band 46, 2010 A User-Oriented Map Design in the SDI Environment; Using the Example of a European Reference Map at Medium Scale; Dissertation von Anja Hopf stock

Band 47, 2011 Arbeitsgruppe Automation in Kartographie, Photogrammetrie und GIS Tagung 2010

Band 48, 2012 Proceedings of the 17th International Workshop on Laser Ranging, Extending the Range